Volume n° 2 - from B16 to B33

Field Trip Guide Book - B28

32nd INTERNATIONAL GEOLOGICAL CONGRESS

THE NEAPOLITAN ACTIVE VOLCANOES (VESUVIO, CAMPI FLEGREI, ISCHIA): SCIENCE AND IMPACT ON HUMAN LIFE

Leader:
G. Orsi

Associate Leaders:
S. de Vita, M.A. Di Vito, R. Isaia

Florence - Italy
August 20-28, 2004

Pre-Congress **B28**

The scientific content of this guide is under the total responsibility of the Authors

Published by:
APAT – Italian Agency for the Environmental Protection and Technical Services - Via Vitaliano Brancati, 48 - 00144 Roma - Italy

Series Editors:
Luca Guerrieri, Irene Rischia and Leonello Serva (APAT, Roma)

English Desk-copy Editors:
Paul Mazza (Università di Firenze), Jessica Ann Thonn (Università di Firenze), Nathalie Marléne Adams (Università di Firenze), Miriam Friedman (Università di Firenze), Kate Eadie (Freelance indipendent professional)

Field Trip Committee:
Leonello Serva (APAT, Roma), Alessandro Michetti (Università dell'Insubria, Como), Giulio Pavia (Università di Torino), Raffaele Pignone (Servizio Geologico Regione Emilia-Romagna, Bologna) and Riccardo Polino (CNR, Torino)

Acknowledgments:
The 32nd IGC Organizing Committee is grateful to Roberto Pompili and Elisa Brustia (APAT, Roma) for their collaboration in editing.

Graphic project:
Full snc - Firenze

Layout and press:
Lito Terrazzi srl - Firenze

Volume n° 2 - from B16 to B33

32nd INTERNATIONAL GEOLOGICAL CONGRESS

THE NEAPOLITAN ACTIVE VOLCANOES (VESUVIO, CAMPI FLEGREI, ISCHIA): SCIENCE AND IMPACT ON HUMAN LIFE

EDITORS:
G. Orsi[1], S. de Vita[1], M.A. Di Vito[1], R. Isaia[1]
AUTHORS:
D. Andronico[5], R. Avino[1], R. Brown[1], S. Caliro[1], G. Chiodini[1], R. Cioni[3], L. Civetta[2], M. D'Antonio[2], F. Dell'Erba[1], P. Fulignati[3], D. Granieri[1], L. Gurioli[3], P. Marianelli[3], R. Santacroce[3], A. Sbrana[3], R. Sulpizio[4]

[1]Osservatorio Vesuviano - INGV - Italy
[2]Università di Napoli - Italy
[3]Università di Pisa - Italy
[4]Università di Bari - Italy
[5]INGV, Catania - Italy

Florence - Italy
August 20-28, 2004

Pre-Congress

B28

Front Cover:
View of the Neapolitan volcanoes from Ischia (P. Fabris - "Campi Phlegraei" of Lord William Hamilton 1776)

Leader: G. Orsi
Associate Leaders: S. de Vita, M.A. Di Vito, R. Isaia

Introduction

A large number of communities as well as megacities have been growing around and even on active volcanoes. Mostly for soil fertility and abundance of volcanic rocks that are good building material, cities on or near volcanoes have grown and continue to grow. If, as is the case of the Neapolitan area, they are in a temperate climate zone, in both commercially advantageous and strategically favourable areas, despite the hazards, humans find good reasons for settlement and development.

The Neapolitan area has been inhabited since Neolithic times (Orsi et al., 2003). The development of an organized society began with the settlement of Greek colonies in the 8th century BC at Ischia and Cuma, in 680 BC on the Megaride islet and called Parthenope, and in 531 BC at Pozzuoli.

Naples is a very suitable site for a field trip devoted to the illustration of the problems of a megacity in an active volcanic area. In fact, together with its surrounding towns, it has been growing between the Campi Flegrei restless caldera and the Somma-Vesuvius, forming a megacity, which we would like to call «Parthenopean Megacity» (Fig. 1).

Figure 1 - Intense urbanization of the Neapolitan area, from satellite imagery.

This megacity, lying on two active volcanic areas and being densely populated, is one of the best examples of high volcanic risk areas in the world.

Regional geologic setting

The Neapolitan area is located within the Campanian Plain, which is bordered by the Southern Apennines (Fig. 2). This mountain chain results from deformation of the African continental margin and is composed of a variety of Mesozoic and Palaeogenic palaeogeographic domains (D'Argenio et al., 1973). The crust is about 25-30 km thick and composed of a pile of tectonic thrusts made up of Triassic to Pliocene sedimentary rocks (Fig. 2) overlying a crystalline-metamorphic basement. From Miocene to Pliocene time, variable compressional tectonic phases have deformed both the sedimentary rocks and their basement terrain. Since Quaternary times, mostly extensional tectonic phases have generated the present setting of the Campanian area.

Figure 2 - Geological sketch map of the Neapolitan area. 1) Quaternary and active terrigenous sediments; 2) Somma-Vesuvius volcanics; 3) Phlegraean District volcanics; 4) Pliocene and Miocene terrigenous sediments; 5) Mesozoic carbonate units; 6) faults; 7) overthrusts; 8) caldera margins.

The Campanian Plain, in which lie the active volcanoes, is composed of 2-3,000 m thick sequences of Plio-Quaternary continental, deltaic, and marine sediments, intercalated with volcanic deposits. It is underlain by a graben formed during activation of NW-SE and NE-SW trending normal faults which, at least during Quaternary times (Brancaccio et al., 1991), have downthrown the western Apennines. The regional stress regime, which has determined the formation of the plain, has also favoured generation and rise of the magmas that have fed the recent and active volcanism. Geophysical data and deep wells have shown the presence of volcanic rocks beneath the sediments filling the plain. These rocks have calc-alkaline composition, while those exposed and overlying the sediments are alkaline. The latter belong to the Somma-Vesuvius composite volcano

Volume n° 2 - from B16 to B33

and the Phlegraean Volcanic District, which includes the Campi Flegrei, Ischia and Procida volcanoes. The active volcanoes are Campi Flegrei, Somma-Vesuvius and Ischia; at the island of Procida the last eruption occurred about 18 ka bp.
The Neapolitan area is mostly made up of volcanic rocks and subordinately of shallow-sea, alluvial, coastal and palustrine sediments (Fig. 2). The oldest dated rocks are exposed at Ischia and yield an age of 150 ka. Historical eruptions have occurred at Ischia (from VII century BC to 1302 AD), Campi Flegrei (1538 AD), and Vesuvius (from 79 to 1944 AD).

Somma-Vesuvius. – The Somma-Vesuvius is composed of an older volcano, Mt. Somma, truncated by a summit caldera, and a more recent cone, Vesuvius, within the caldera (Fig. 3).
The growth of the Vesuvius cone took place, although with some minor summit collapses, during periods of persistent low-energy open-conduit activity, the last of which occurred between 1631 and 1944 (Arrighi et al., 2001). The caldera is an elliptical (Fig. 3) complex structure resulting from several collapses, each related to a Plinian eruption (Cioni et al., 1999).

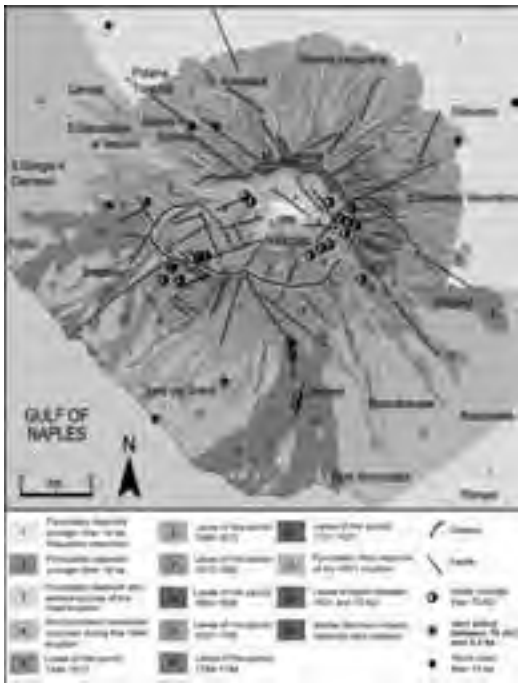

Figure 3 - Somma-Vesuvius geological sketch map (after Orsi et al, 2003. Structural lineaments are after Ventura et al., 1999).

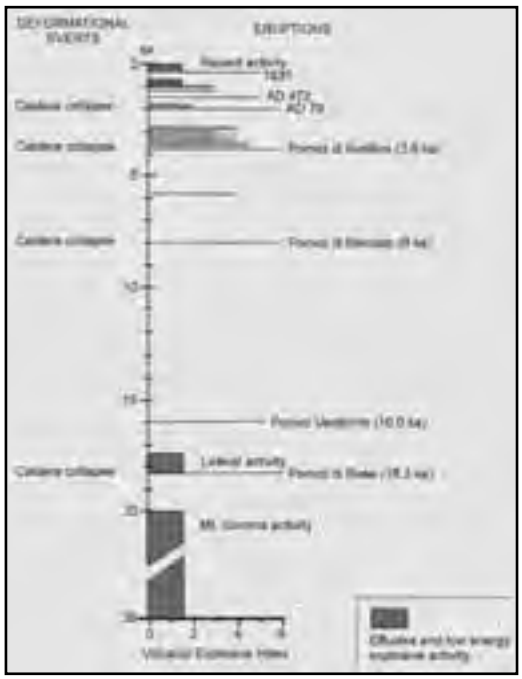

Figure 4 - Chronogram of volcanic and deformational history of Somma-Vesuvius (after Orsi et al., 2003).

The northern portion of the caldera margin is a 300 m high scarp, while the southern portion has been filled by lava flows, which covered the southern slopes of the Mt. Somma as far as the seacoast.
Volcanism in the Somma-Vesuvius area has been active since at least 400 ka bp as testified by volcanic rocks drilled at 1,350 m depth (Brocchini et al., 2001). The Somma volcano formed after the Campanian Ignimbrite eruption of Campi Flegrei (39 ka; De Vivo et al., 2001) (Fig. 4) and its activity was mostly effusive and subordinately explosive, with low energy events (Cioni et al.,1999). The history of the volcano has been characterised either by long quiescence periods, interrupted by Plinian or sub-Plinian eruptions, or by periods of persistent volcanic activity (Fig. 4), with lava effusions and Strombolian to phreato-magmatic eruptions, related to the alternation of closed and open conduit conditions, respectively (Civetta and Santacroce, 1992).
The earliest known Plinian eruption (Pomici di Base; 18.3 ka; Cioni et al., 1999 and references therein) determined the beginning of both the collapse of the Mt. Somma volcano and the formation of the caldera. The Pomici di Base eruption was followed by eruption of lavas that flowed along the eastern slopes

of the volcano, and a quiescent period interrupted 15 ka bp by the sub-Plinian eruption of the Pomici Verdoline (Cioni et al., 2003 and references therein). The subsequent long period of quiescence, during which only two low-energy eruptions took place, lasted until 8 ka bp, when it was broken by the Plinian Mercato eruption (Cioni et al., 1999 and references therein). During the following period of quiescence, interrupted only by two low-energy eruptions, a thick paleosol formed. This paleosol contains many traces of human occupation until the Early Bronze age, and is covered by the deposits of the Plinian Avellino eruption (Cioni et al., 1999 and references therein). This eruption was followed by at least 8 Strombolian to sub-Plinian eruptions, over a relatively short time, and by no less than 7 centuries of quiescence, broken by the Plinian AD 79 eruption (Cioni et al., 1999 and references therein). After this eruption, the volcano generated only two more sub-Plinian events in AD 472 (Rosi and Santacroce, 1983) and 1631 (Rolandi et al., 1993b; Rosi et al., 1993), and low-energy open-conduit activity between the 1st and 3rd, 5th and 8th, 10th and 11th centuries, and 1631 and 1944 (Arrighi et al., 2001). Since the last eruption of 1944, Vesuvius is quiescent, as it has not shown signs of unrest and only moderate seismicity and fumaroles testify its activity.

All Plinian eruptions are characterised by a vent opening, a sustained column and pyroclastic flow and/or surge phases, and are accompanied by volcano-tectonic collapses. Sustained columns, which reach maximum heights of about 30 km, generate widespread fallout deposits (1.5-4.4 km^3, DRE) (Fig. 5).

Pyroclastic currents (0.25 and 1 km^3, DRE) are distributed along the volcano slopes and within the surrounding plains, reaching maximum distances of over 20 km from the vent. In proximal areas, thick breccia deposits are related to caldera collapse. The quiescence periods preceeding the Plinian eruptions last from several centuries to millennia (Fig. 4)

Among the sub-Plinian eruptions of Vesuvius, only the AD 472 and the 1631 events are studied in detail (Rosi and Santacroce, 1983; Rolandi et al., 1993; Rosi et al., 1993). They are characterised by the alternation of sustained columns and pyroclastic flow and/or surge generation. Sustained columns are less than 20 km high and pyroclastic currents travel distances not in excess of 10 km.

Fallout deposits of both Plinian and sub-Plinian eruptions are dispersed to the east of the volcano

Vesuvius is located at the intersection of NW-SE and NE-SW oriented fault systems. The results of seismic investigations, constrained by one deep drilling (Zollo et al., 2002) show that the shallow structure of Vesuvius comprises 1.5-2 km of interbedded lavas and volcaniclastic, marine, and fluvial sedimentary rocks of Pleistocene age. A high velocity body, likely to be a sub-volcanic structure, is under the summit caldera. The top of the Mesozoic limestone basement is at 2.5-3 km of depth. The occurrence of a high-P wave velocity zone beneath the volcano, which extends from about 0.5 to 2-3 km of depth, as well as of local volcano-tectonic seismicity shallower than 6-7 km of depth (Bianco et al., 1998), indicate that it is extremely unlikely that shallow magmatic reservoirs of significant size (>1 km in diameter) occur in the 0-7 km range of depth. Furthermore, the results of a seismic tomography study (Auger et al., 2001) identify a horizontal low-velocity layer with its flat top at about 8 km beneath the volcano. This is interpreted as the top of the present magma

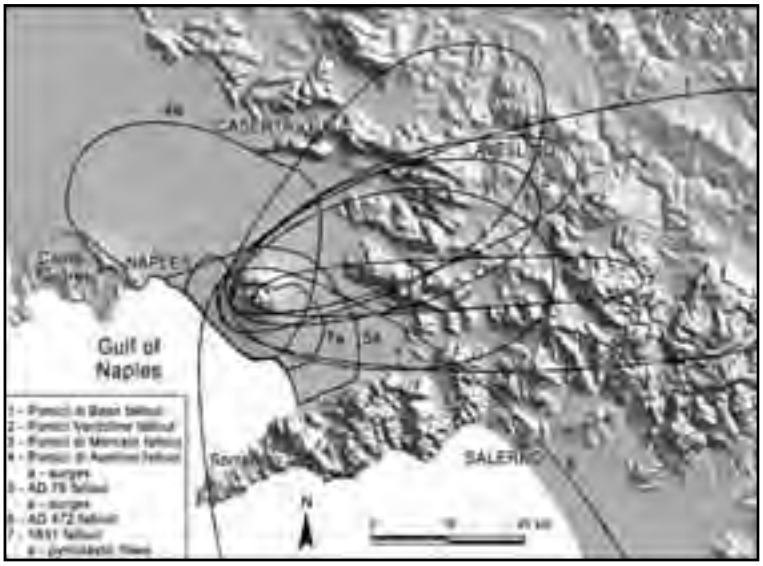

Figure 5 - Distribution of Plinian and sub-Plinian deposits of Somma-Vesuvius eruptions.

reservoir. This depth coincides with the upper portion of a zone of clinopyroxene crystallization, indicated by fluid inclusion data (Belkin et al., 1985; Marianelli et al., 1995; 1999). The Moho discontinuity in the Vesuvius area is at a depth of 29-30 km (Gasparini et al., 2001).

In its history Somma-Vesuvius has erupted about 50 km^3 of magma of varying composition. According to the different degrees of silica under-saturation of the erupted magmas, it is possible to distinguish three periods of activity (Santacroce, 1983). The oldest, from ca. 39 to 11.5 ka bp, is characterised by emission of slightly under-saturated lavas, of variable composition from K-basalt to K-trachyte. The second period, from 8 ka bp to AD 79, is characterised by the emission of products varying in composition from tephrite to phonolite. The products of the last period, from AD 79 to AD 1944, range from leucititic tephrite to leucititic phonolite.

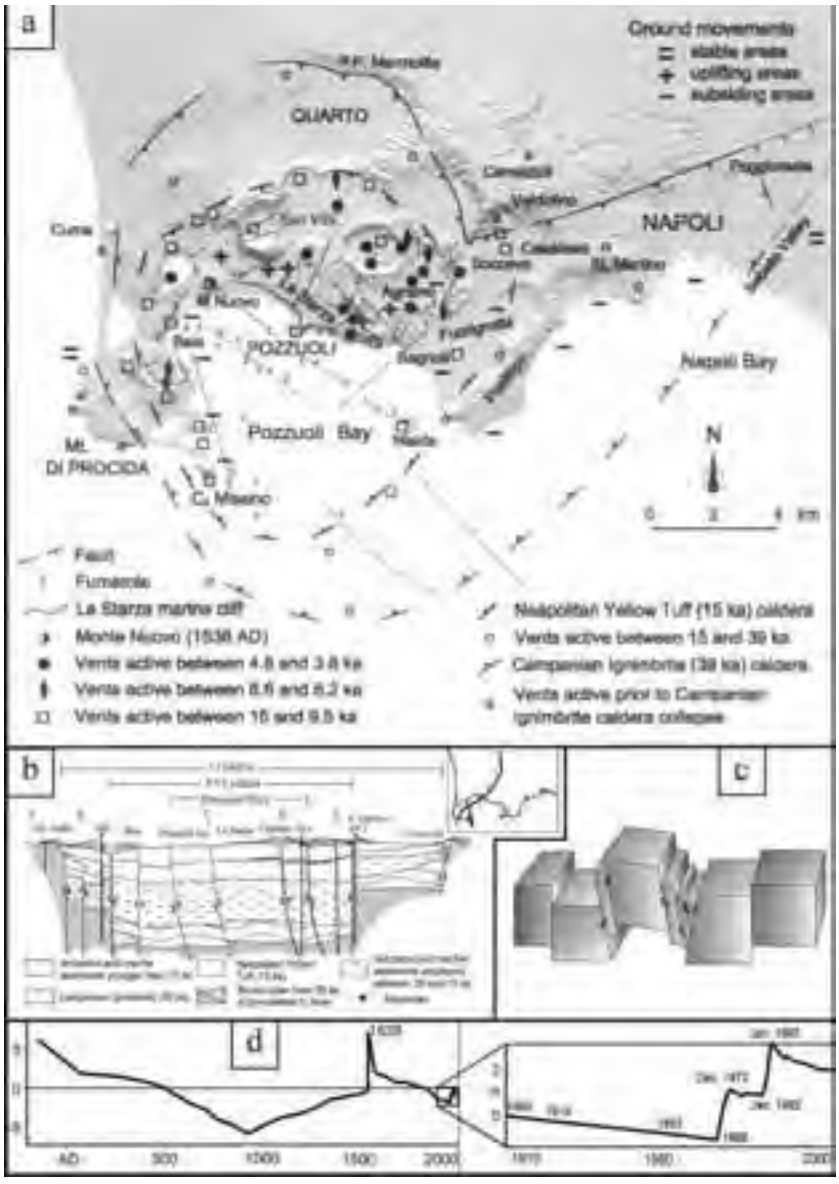

Figure 6 - a) Structural map of the Campi Flegrei caldera; b) SW-NE cross section (location is shown in the insert); c) simple-shearing block resurgence model for the caldera complex; d) vertical ground movements at Serapis Roman market in Pozzuoli.

Sr-Nd-Pb isotopic compositions (D'Antonio et al., 2004 and references therein): $^{87}Sr/^{86}Sr$ ratio ranges between 0.7066 and 0.7080; $^{143}Nd/^{144}Nd$ ratio ranges from 0.5126 to .5124; Pb isotope ratio show smaller ranges (e.g. of values for $\delta^{18}O$ (7.3-11.4‰) is reported (Ayuso et al., 1998 and references therein), whereas $^3He/^4He$ ratios are clustered around 2.4 R/R_a (Graham et al., 1993). Sr and Nd isotopes of the Plinian and Strombolian products show a variation through time, with increasing or decreasing $^{87}Sr/^{86}Sr$ ratio (and the

Figure 7 - Chronogram of volcanic and deformational history of the Campi Flegrei caldera (after Orsi et al., 2003).

opposite for Nd isotopes) from the first to the last erupted magma. Strong isotopic disequilibria occur among minerals and between minerals and glass. The Sr- and Nd-isotopes have been used to investigate the processes in the magma reservoirs. The isotope and geochemical data for Plinian eruption products evidence that the magma chamber(s) feeding Plinian eruptions (3-5 km depth; Barberi et al., 1981) are refilled by isotopically distinct, mafic, high-T (>1150 °C) magma batches rising from depths of 10-20 km (Cioni et al., 1999 and references therein), where mantle-derived magmas stagnate, differentiate and probably are contaminated by continental crust.

The deep magma batches, through crystallization and mixing with the shallow portions of the feeding systems, generate isotopically and geochemically layered reservoirs. On the contrary, during open conduit conditions the deep, volatile-rich magma batches rise to less than 2 km of depth and mix with the crystal-rich, volatile-poor resident magma, triggering eruptions (Marianelli et al., 1999 and references therein).

<u>Campi Flegrei caldera</u> - The Campi Flegrei caldera, the main feature of the Phlegraean Volcanic District, includes a continental and a submerged part. It is a resurgent nested structure (Fig. 6) formed during two major caldera collapses related to the eruptions of the Campanian Ignimbrite (39 ka; Fedele et al., 2003 and references therein) and the Neapolitan Yellow Tuff (15 ka; Deino et al., 2004 and references therein), respectively (Orsi et al., 1996).
The geometry and dynamics of both large calderas, as well as of smaller volcano-tectonic collapses, were deeply influenced by both local and regional stress regimes. Each large collapse affected the structural conditions of the system, and constrained the foci of later volcanism. The age of the beginning of volcanism in the area is not known. The oldest dated volcanic unit yielded an age of 60 ka (Pappalardo et al., 1999) and is related to a volcanism extending beyond the caldera (Fig. 6a)

The Campanian Ignimbrite eruption and caldera collapse was the earliest event to profoundly influence the present geological setting of the area. The Neapolitan Yellow Tuff eruption and caldera collapse was the last dramatic event in the history of the caldera.
After the Neapolitan Yellow Tuff eruption, both volcanism and deformation have been very intense within the caldera (Fig. 6, 7) (Orsi et al., 1999a and references therein). There have been about 70 eruptions, grouped in three epochs of activity (15.0-9.5, 8.6-8.2 and 4.8-3.8 ka), during which eruptions have followed one another at mean time intervals of a few tens of years. The last event was in 1538, after about 3.0 ka of quiescence (Fig. 7), and formed the Mt. Nuovo cone (Di Vito et al., 1987). 64 of these eruptions were phreatomagmatic to magmatic explosive events. Contemporaneous magmatic and phreatomagmatic fragmentation dynamics has been widely recognised and has been demonstrated for the Agnano-Monte Spina eruption (Dellino et al., 2004a and references therein). Only the Pomici Principali (10.3 ka; Di Vito et al., 1999 and references therein) and the Agnano-Monte Spina, occurred during the I and III epochs of activity respectively were of high-magnitude, Plinian eruptions. On the basis of the extent of the area covered by the deposits, considered as indicative of the magnitude, the other explosive events have been subdivided by Orsi et al. (2004) in low- and medium-magnitude eruptions. Fallout deposits of the I epoch covered the north-eastern sector of the caldera and the Camaldoli hill, 15 km from the caldera centre (Fig. 8a). Only beds of the Pomici Principali Tephra are 20 cm thick along the western

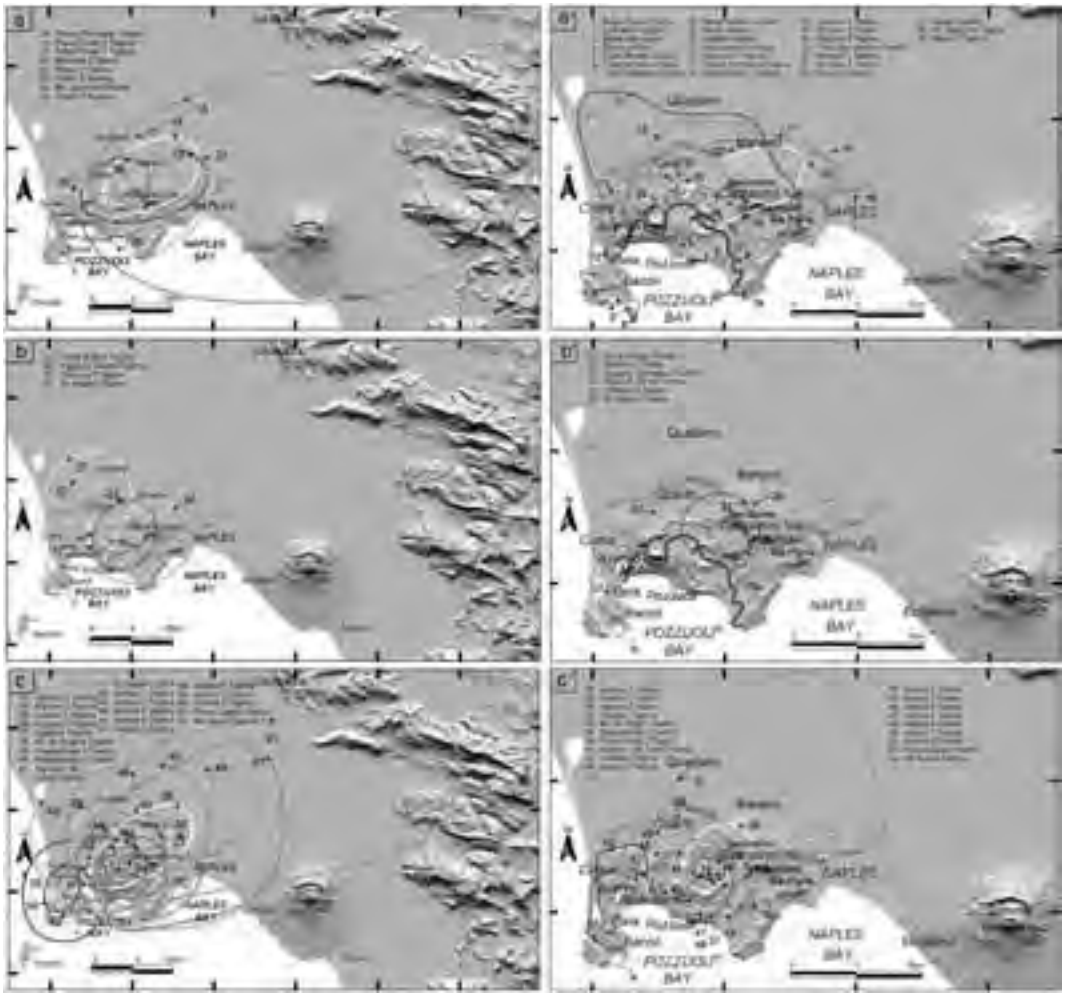

Figure 8 - Distribution of the pyroclastic deposits of the past 15 ka at the Campi Flegrei caldera. a, b and c: 10-cm isopachs of fallout deposits of the I, II and III epoch, respectively; a', b' and c': areal distribution of pyroclastic-current deposits of the I, II and III epoch, respectively.

margin of the Apennines, at about 50 km from the vent. Pyroclastic currents travelled within the caldera floor and reached the Campanian plain. The eruptions of the II epoch were all low-magnitude events. Fallout deposits covered only the caldera and its immediate surroundings, while most of the pyroclastic currents deposited their load within the caldera lowland (Fig. 8b). The fallout deposits of the III epoch and of the Mt. Nuovo eruption covered the caldera floor and its surroundings (Fig. 8c). Only beds of the Agnano-Monte Spina Tephra covered a large area up to the Apennines. Pyroclastic currents travelled across the caldera floor and subordinately over the northern slopes of the Camaldoli hill (de Vita et al., 1999).

The caldera has been affected by structural resurgence through a simple-shearing mechanism (Orsi et al., 1991) that broke its floor in blocks and caused a maximum net uplift of about 90 m at the La Starza marine terrace (Fig. 6) (Orsi et al., 1996). The distribution of the vents active through time (Fig. 6a) is a good tracer of the structural conditions of the caldera. In fact during both the I and II epochs vents were mostly located along the marginal faults of the Neapolitan Yellow Tuff caldera. Whereas the vents of the III epoch were along the normal faults intersecting the north-eastern portion of the Neapolitan Yellow Tuff caldera floor, in response to the simple-shearing mechanism, established not later than 5 ka bp (Orsi

et al., 1999a).

This mechanism generated a compressive stress regime within the south-western portion of the caldera floor, the Pozzuoli bay, and a tensile stress regime within the north-eastern portion, the area between the Agnano and San Vito plains (Fig. 6). Only Averno 1 and 2, and Mt. Nuovo eruptions occurred in the sector where the two fault systems delimiting the resurgent block north-westward, intersect.

During the past 2.0 ka, the floor of the caldera has been affected by ground movement, documented at the Serapis Roman market in Pozzuoli (Fig. 6d). Since late 1960s, unrest episodes have been documented by the monitoring system in 1969-72, 1982-84, 1989, 1994 and 2000, and have generated uplifts of 170, 180, 7, 1 and 4 cm, respectively. Geometry of these short-term deformation events are very similar to that of the long-term deformation. This element, together with the earthquake focal mechanisms, suggest that also the unrest episodes occur through a simple-shearing mechanism. Therefore they are likely to be transient events during the long-term deformation and reflect the stress regime within the caldera, which has not changed at least over the past 5 ka (Orsi et al., 1999a).

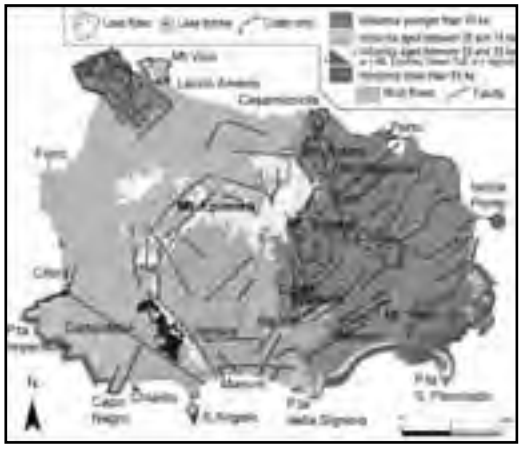

Figure 9 - Geological sketch map of Ischia (after Orsi et al., 2003).

The magmas erupted at Campi Flegrei range in composition from trachybasalt to phono-trachyte, with a predominance of trachyte (D'Antonio et al., 1999 and Pappalardo et al., 1999, and references therein). The less differentiated magmas (trachybasalt and latite) erupted between 10 and 8 ka along NE-SW regional tectonic structures (Orsi et al., 1996).

Seismic data show that beneath the Campi Flegrei caldera, the top of the Mesozoic limestone basement occurs at about 4 km depth (Zollo et al., 2003), above which no evidence of magma reservoirs of significant size has been found. Melt inclusion data indicate zones of clinopyroxene and olivine crystallization between 10 and 20 km depth, suggesting the presence of deep magma reservoirs (Cecchetti et al., 2001), at the same depth of those estimated for Vesuvius. The depth of the Moho below the Phlegraean Volcanic District is of about 25 km (Ferrucci et al., 1989).

The Campi Flegrei rocks exhibit a wide range of $^{87}Sr/^{86}Sr$ (0.7068-07086), but limited ranges of $^{143}Nd/^{144}Nd$ (0.51240-0.51266) and Pb-isotope ratios (e.g. $^{206}Pb/^{204}Pb$: 18.85-19.25; Pappalardo et al., 2002a, b and references therein). Wide ranges of $\delta^{18}O$ (Turi and Taylor, 1976) and $\delta^{11}B$ (Tonarini et al., 2004) have also been measured.

Variations of Sr, Nd and Pb isotope ratios of magmas erupted since 60 ka illustrate the history of the Campi Flegrei magmatic system. $^{87}Sr/^{86}Sr$ increases from 60 to 44 ka, is constant from 44 to 17 ka, increases again at 15 ka, prior to the Neapolitan Yellow Tuff eruption, and then exhibits a wide range, between 0.7073 (value characteristic of Campanian Ignimbrite) and 0.7086. The increase of $^{87}Sr/^{86}Sr$ is associated with a decrease in the Nd isotope ratio. According to the isotopes-time correlation, Pappalardo et al. (2002b) have identified four groups of magmas: 1) trachytic magmas erupted before Campanian Ignimbrite ($^{87}Sr/^{86}Sr$ ca. 07068); 2) Campanian Ignimbrite trachytic magmas ($^{87}Sr/^{86}Sr$ ca. 0.7073); 3) Neapolitan Yellow Tuff latitic to trachytic magmas ($^{87}Sr/^{86}Sr$ ca. 0.70755); 4) shoshonitic magmas erupted for the first time at ca. 10 ka ($^{87}Sr/^{86}Sr$ ca. 0.708) along portions of regional faults. The shoshonitic magmas contain xenoliths and xenocrysts of probable crustal origin, enriched in radiogenic Sr ($^{87}Sr/^{86}Sr$ up to 0.711; Pappalardo et al., 2002b). Mixing/mingling among the four components can explain all the isotopic variations of the post-Neapolitan Yellow Tuff products.

The structure of the magmatic system is, therefore, characterised by a deep reservoir extending between 20 and 10 km depth, where mantle derived magma stagnate and eventually are contaminated by continental crust (Pappalardo et al., 2002b). From the deep reservoir, magmas rise to shallow depth, where they either form large chambers, or reach the surface through regional faults along which they mix with residual melts.

Volume n° 2 - from B16 to B33

Ischia - The island of Ischia, the emerged top of a large volcanic complex rising more than 1,500 m above sea floor, is an active volcanic field that covers an area of about 46 km^2 and is dominated by Mt. Epomeo (787 m a.s.l.). Ischia is composed of volcanic rocks, landslide deposits, and subordinate terrigenous sediments (Fig. 9). The volcanic rocks range in composition from trachybasalt to phonolite; the most abundant are trachyte and alkali-trachyte. Volcanism began more than 150 ka bp (Vezzoli, 1988) and continued until the last eruption of 1302 AD (Fig. 10).

Figure 10 - Chronogram of volcanic and deformational history of Ischia.

The oldest rocks are exposed in the south-eastern part of the island and belong to a partially exposed volcanic complex. The products of the volcanism between 150 and 74 ka bp, are small trachytic and phonolitic domes at the periphery of the island. A poorly defined period of pyroclastic activity followed, predating the large Mt. Epomeo Green Tuff caldera-forming eruption (55 ka). Lacking a detailed stratigraphic and compositional study on the volcanics aged between 74 and 55 ka, volcanism in the past 55 ka has been tentatively subdivided into three periods of activity (Civetta et al., 1991).

The Mt. Epomeo Green Tuff consists mostly of trachytic ignimbrites that partially filled a depression invaded by the sea in what is now the central part of the island. The caldera collapse was followed by the Mt. Epomeo block resurgence, which occurred through a simple-shearing mechanism (Fig. 6c) and determined a net uplift of about 900 m (Orsi et al., 1991). Volcanism continued with a series of hydromagmatic and magmatic explosive eruptions of trachytic magmas up to 33 ka. Most of the vents were located along the present south-western and north-western periphery of the island.

After a 5 ka long period of quiescence, volcanism resumed at about 28 ka with the eruption of trachybasaltic magma along the south-eastern coast, and then continued sporadically until 18 ka. Hydromagmatic and magmatic explosive eruptions along the southern coast mostly erupted alkali-trachytic magmas, while effusive eruptions formed trachytic lava flows.

The most recent period of activity began at about 10 ka. Volcanism has been mainly concentrated in the past 2.9 ka, with almost all the vents in the eastern part of the island (Sansivero, 1999). Only a few were outside this area, along regional faults. They generated a lava field, in the north-western corner of the island, and a pyroclastic sequence in the south-western part. At least 35 effusive and explosive eruptions took place. Effusive eruptions emplaced lava domes and high-aspect ratio lava flows. Explosive eruptions, both magmatic and phreatomagmatic, generated tuff cones, tuff rings and variably dispersed pyroclastic-fall and -flow deposits. Emplacement of landslide and mudflow deposits prior and after these eruptions testifies ground deformation, and are likely to be related to resurgence.

Geological and petrological data, as well as the results of modelling of magnetic data (Orsi et al., 1999b), suggest that the magmatic system of Ischia is presently composed of a deep and poorly-evolved magma reservoir, interconnected with shallower, smaller and more-evolved magma batches, which have fed the recent activity.

The magmas erupted at Ischia have a wide range of isotopic values: $^{87}Sr/^{86}Sr$ ratio varies between 0.7058 and 07073, while $^{143}Nd/^{144}Nd$ ratio varies between 0.51246 and 0.51261 (Civetta et al. 1991b); $^{206}Pb/^{204}Pb$ ratio varies between 18.88 and 19.05 (Arienzo et al., 2004); δO^{18} varies between 6.14 and 6.99. The Sr isotopic ratios are generally less radiogenic than those of Vesuvius and Campi Flegrei, while the Nd, Pb and B isotopic ratios are similar. Geochemical and isotopical variations through time (Civetta et al., 1991) have evidenced that the magmatic system between 55 and 33 ka acted as a closed system. Before the 28-18 ka period of activity, it was refilled by a deeper less-evolved magma, which progressively mixed with the more-evolved resident magma. The last period of activity was preceded by arrival of new magma. Complex mingling/mixing processes operated till the last eruption, as testified by isotopic and mineralogical disequilibria.

Origin of the Campanian magmas - In agreement with geophysical and geological data on the geodynamics of the Tyrrhenian Sea and the structural setting of Neapolitan volcanoes, the isotopic data (Sr, Nd, Pb, B) (Tonarini et al., 2004; Arienzo et al., 2004; Civetta et al., 2004) suggests the involvement of three components in the genesis and evolution of the feeding magmas: 1) the T-MORB asthenospheric mantle, mostly represented by Tyrrhenian seafloor basalts and, in part, by Procida K-basalts; 2) fluids derived from sediments of the Ionian NW-dipping subduction zone, which progressively modify the mantle wedge in relation to Ischia-Procida and Vesuvius-Campi Flegrei; 3) fluids deriving from the continental crust which contaminate the mantle derived magmas. This last process is operative mostly on the post-39 ka Vesuvius and Campi Flegrei magmas, at a depth between 10 and 20 km, where mineralogical and geophysical data indicate the occurrence of discrete magma reservoirs. From these depths, batches of isotopically distinct magmas rise to shallow reservoirs, where they mix with the resident magma, differentiate and, in cases, can trigger an eruption.

Field itinerary

DAY 1

Stop 1:

The 1944 eruption of Vesuvius and the present Crater

Significance. - The 1944 last eruption of Vesuvius. Evolution of the crater after the 1906 eruption. Physical and socio-economical features.

The 1944 eruption. - The 1944 eruption is the last eruption of the Vesuvius. Since then, the volcano has been quiescent, only fumaroles and moderate seismicity testify its activity. The 1944 eruption closed a cycle of persistent activity, begun in 1914 and characterised by mainly effusive central eruptions. 50-100 millions of m^3 of lavas and pyroclasts had almost completely filled the 1906 eruption crater (720 m wide and 600 m deep).

Imbò (1949) reported a detailed description of the eruption, which is here summarised.

On March 13, the spatter cone, emerging from the crater, began to collapse and seismicity increased. A new cone formed between March 13 and 16 and collapsed on March 17.

Figure 11 - Distribution of the 1944 Vesuvius eruption deposits.

The eruption begun on the afternoon of March 18th with Strombolian activity. A lava flow overflowed out of the northern portion of the crater rim at 4.30 pm, and reached the Valle dell'Inferno at 10.30 pm (Fig. 11).

Other lavas overflowed the southern portion of the rim, almost simultaneously, and the western portion at 11.00 pm, reaching the Fosso della Vetrana at 11.00 am of March 19. From the afternoon of March 20 and for the following night, new lava flows overflowed the northern portion of the crater rim. On March 21st, the southern lava flow stopped at about 300 m a.s.l., while the northern flow reached the towns of S. Sebastiano and Massa di Somma between 1.00 and 2.00 am. The 10,000 inhabitants were evacuated and transferred to Portici. Around 5.00 pm a new phase of the eruption which generated 8 spectacular lava fountains, began and lasted till 00.48 pm of the next day. The last fountain, lasted about 5 hours, reached a height of about 1,000 m. Scoriae and ash fallout beds were laid down southeast of the volcano, between the towns of Angri and Pagani. A large amount of incandescent scoriae, due to the ground movement related to intense seismic tremor, generated hot avalanches which reached the foot of the cone.

At 00.48 pm of March 22nd there was a transition from the lava fountain phase to a buoyant column phase (Fig. 12). The convective portion of this column, 5-6 km high, was dispersed towards south-east. Partial collapses generated pyroclastic currents which moved along the slopes of the cone. This eruption phase, during which the crater enlarged progressively, was characterised by intense seismic tremor. On March

Figure 12 - Buoyant column phase of the 1944 Vesuvius eruption.

Figure 13 - Partial column collapse with generation of pyroclastic currents during the 1944 Vesuvius eruption.

23 a new and last phase began. It was dominated by phreatomagmatic explosions with energy decreasing through time. Also seismicity changed from tremor to discrete shocks. The ash-rich columns were directed towards the south-south-west, and small pyroclastic currents flowed on the slopes of the cone (Fig. 13). The eruption ended on March 29.

The 1944 products range in composition from phonolitic tephrite to tephrite. The lower portion of the pyroclastic sequence includes both brownish vesicular and dark dense lapilli juvenile clasts. The two types of clasts, petrographically and chemically similar, differ for vesicularity, matrix colour (yellowish to brownish) and crystallinity. The upper portion of the sequence includes only denser juvenile clasts, rich in clinopyroxene.
Phenocrysts content increases and vesicularity decreases up-section. Clinopyroxene is ubiquitous phenocryst phase and occurs in two varieties, a colourless diopside and a greenish salite. Leucite, plagioclase, biotite and olivine occur as phenocrysts and in glassy groundmass during the whole sequence, in varying proportions. Leucite at the base and clinopyroxene and olivine upward occur as loose megacrysts during the whole sequence.
K-phonotephritic magma was emitted during the effusive phase and the first lava fountain, whereas strongly porphyritic K-tephritic magma was extruded during the most intense fountain. Melt inclusions compositions (major and volatile elements) highlight that the erupted magmas underwent differentiation at different pressures. The K-tephritic volatile-rich magma (up to 3wt.% H_2O, 3.000 ppm CO_2 and 0.55wt. % Cl) evolved to a K-phonotephritic melt through crystallization of diopside and forsteritic olivine at total fluid pressure >300 MPa. This magma fed a very shallow reservoir. The low pressure differentiation of the volatile-poor K-phonotephritic magmas (H_2O less than 1wt.%) involved mixing, open-system degassing, and crystallization of leucite, salite, and plagioclase. The eruption was triggered by intrusion of a volatile-rich magma rising from a depth of 11-22 km into the shallow magma chamber. The lava effusion phase of the eruption partially empted the shallow reservoir, the top of which is within the caldera edifice. The newly arrived magma mixed with that resident in the shallow reservoir and forced the transition to the lava fountain phase.
The pyroclastic deposits contain lithics of skarn and other thermo-metamorphic rocks, grouped in four main lithotypes: metasomatised cumulites, Ca-skarn, Mg-skarn and cornubianites. These rocks, which could result from an interaction between magma and magma chamber sedimentary wall-rocks (limestones, dolomites, marls and siltites), are particular in this 1944 eruption. Their occurrence suggests that the magma chamber was a high aspect ratio structure, reaching the sedimentary basement of the volcano around 3-4 km of depth. The presence of periclase in the Mg-Skarn could suggest hypo-abyssal conditions with maximum pressures of 1,000 bars.
The most relevant effects of the eruption were: twenty-six people dead in the area affected by lapilli and ash fallout, due to a collapse of the roots; two villages partially destroyed by lava flows; three years of missed crops in the downwind area.

The crater - A complete sequence of the 1914-1944 deposits of the last cycle of activity at Vesuvius is exposed along the north-eastern portion of the crater

Figure 14 - View of the north-eastern portion of the Vesuvius crater.

slope (Fig. 14). The sequence is dominated by lavas, the most significant was extruded on 1929, with minor spatter and scoriae beds. It is horizontal, fills the 1906 eruption crater and unconformably covers the sequence of rocks exposed in the 1906 crater. Both sequences are topped by the deposits of the 1944 eruption in parallel unconformity.

A grey massive lava, the basal unit of the 1944 eruption sequence (Fig. 15), is a continuous layer grading into a densely-welded crudely-stratified spatter succession emplaced during the lava fountaining phase. The largest part of this succession was emplaced during the VIII fountain (7.30 am -00.48 pm, March 22), when concomitance of rapid spatter accumulation and strong seismic tremor, caused hot avalanches. The spatter succession is covered in parallel unconformity by another succession of black and grey scoriaceous lapilli and bomb deposits with interlayered coarse ash

Figure 15 - The 1944 Vesuvius eruption deposits along the northern crater wall.

beds. Variation in deposit characteristics is related to the change in fragmentation dynamics at 00.48 pm, with the formation of a buoyant ashy column.
The upper part of the 1944 sequence is composed of intercalated reddish and violaceous lapilli and bomb deposits, and coarse ash beds, and is topped by grey ash deposits rich in lithic fragments, mainly composed of fresh and hornfelsed lavas. It was deposited during the phreatomagmatic final phase of the eruption.
The Vesuvius fumaroles. - Fumarole activity is widespread in the Vesuvius crater area. Fumaroles of the crater rim and of the inner crater slopes

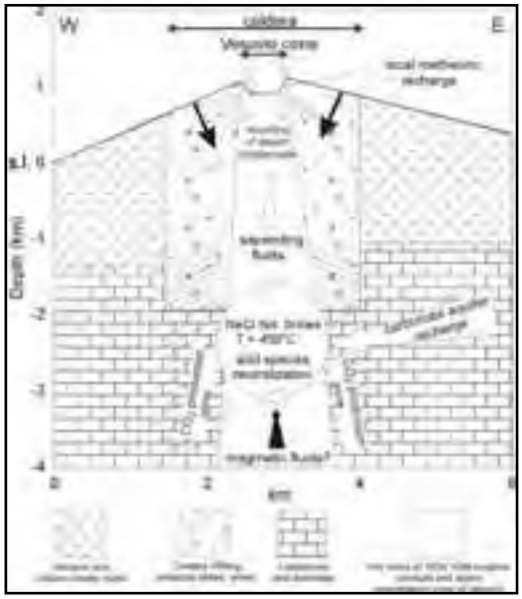

Figure 16 - Geochemical model of the Vesuvius hydrothermal system.

discharge fluids rich in atmospheric gases with outlet temperatures ranging from 60 to 75°C. The fumarolic fluids of the crater bottom (vents FC1, FC2, and FC5) have, instead, typical hydrothermal compositions, with H_2O as a major constituent, followed by CO_2, H_2, H_2S, N_2, CH_4, and CO in order of decreasing concentrations, and undetectable SO_2, HCl, and HF. These fumaroles, whose outlet temperatures have been close to the local water boiling point since 1988, are fed by a hydrothermal system located underneath the crater.
Fumarolic water is either meteoric water enriched in ^{18}O through water-rock oxygen isotope exchange in the hydrothermal environment or a mixture of

Volume n° 2 - from B16 to B33

meteoric and arc-type magmatic water, as indicated by the $\delta^{18}O_{H2O}$ values, suitably corrected for oxygen isotope exchange between H_2O and CO_2, and the δD_{H2O} values. It is equally possible that both water-rock oxygen isotope exchange and addition of magmatic water take place in the hydrothermal system of Vesuvius crater.

Fumarolic CO_2 has a double origin: part of The CO_2 is of deep provenance (magmatic), and part is from metamorphic reactions involving marine carbonates (although addition of a small fraction of magmatic CO_2 cannot be ruled out), as suggested by both the $\delta^{13}C_{CO2}$ values and gas equilibria. The decarbonation reactions result from a local thermal anomaly in the thick carbonate sequence, at >2.5 km underneath the volcano (Chiodini et. al., 2001) (Fig. 16).

Seen the large availability of salts in deep volcanic hydrothermal environments, mainly due to absorption of acid, magmatic gases in deeply circulating ground-

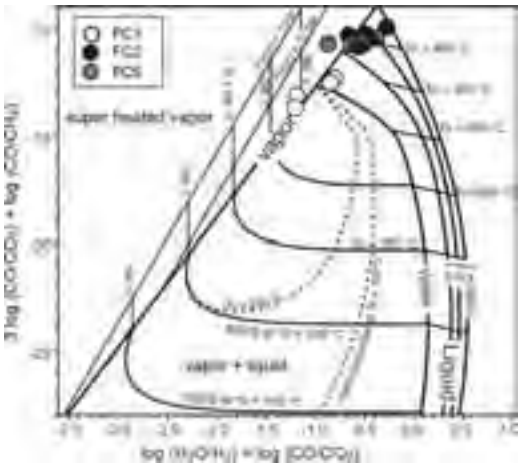

Figure. 17 - Gas equilibria within the H_2O-H_2-CO_2-CO-CH_4 gas system (after Chiodini and Marini, 1998).

waters and the subsequent neutralization of these acidic aqueous solutions through water-rock interaction, it seems likely that NaCl liquids of unknown (probably high) salt content rather than pure water, circulate in the Vesuvius hydrothermal system.

Accepting this hypothesis, gas equilibria was investigated taking into account the solubility of relevant gas constituents in NaCl aqueous solutions of specified concentrations. It turns out that C-H-O gas species equilibrate, probably in a saturated vapour phase, at very high temperatures: 360 to 370°C for vent FC1 and 430 to 445°C for vents FC2 and FC5. The minimum salinity of the liquid phase coexisting with

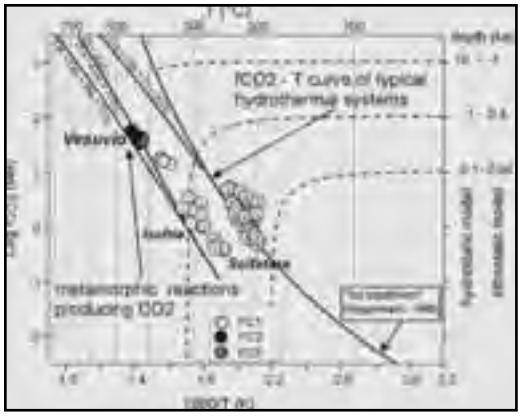

Figure 18 - Carbon dioxide fugacities versus 1000/T (K) diagram. The points of Vesuvius are representative of a very high temperature hydrothermal system (400-500°C). The carbon dioxide fugacity of the Vesuvius hydrothermal system might be controlled by thermo-metamorphic reactions.

the vapour phase is close to 14.9 wt.% NaCl (1 m), whereas its maximum salinity is 49.2 to 52.5 wt.% NaCl (2m and 3m), corresponding to saturation with halite (Fig. 17).

As the salt contents of the aqueous solutions circulating in this system cannot be constrained satisfactorily, total fluid pressures (which are closely approximated by $PH_2O + PCO_2$) in the zones of the hydrothermal system where gases equilibrate, are also poorly constrained. They are 260 to 480 bar for vents FC2 and FC5 and 130 to 220 bar for vent FC1. Based on a simple hydrostatic model (Fig. 18), the hydrothermal reservoirs connected with these fumaroles are at depths of 2.6-4.8 km and 1.3-2.2 km, respectively. Consequently, the deepest hydrothermal reservoir appears to be within the carbonate sequence, which is at depths >2.5 km underneath the volcano, whereas the shallowest reservoir is in the overlying volcanic rocks.

Monitoring the thermodynamic conditions of this hydrothermal system trough the study of the fumaroles chemical composition is of primary relevance in the surveillance of Vesuvius.

A detailed CO_2 flux campaign on the Vesuvius cone, indicates that the degassing process of hydrothermal gases affects most of the slopes and bottom of the crater, and few spots on the slopes of the cone. A total CO_2 output is estimated at 100±20 td^{-1}.

Discussion points. - Transition from lava fountaining conditions to buoyant column reflects different fragmentation conditions in the conduit or modifications of the vent geometry? Non vesiculated juvenile material characterises the lithic dominated Vulcanian deposits suggesting that ground-water entered the conduit, and fragmentation was triggered by magma-water interaction. Hydrothermalised lavas and dykes are subordinate in the deposit suggesting a minor role of hydrothermal fluids in triggering Vulcanian explosions.

Stop 1.2:

The Osservatorio Vesuviano

Significance. The Osservatorio Vesuviano historical building, presently an information centre on volcanic hazards and risk.

The Osservatorio Vesuviano. - The Osservatorio Vesuviano, the oldest volcano observatory in the world, was founded in 1841 by king Ferdinand II of Bourbon. It was inaugurated during the 7th Congress of the Italian Scientists, held in Naples in 1845.

The historical building of the Osservatorio Vesuviano, the elegant work of the architect Gaetano Fazzini, is on the Colle del Salvatore at an elevation of 609 m a.s.l., between Ercolano and Torre del Greco. The position chosen was particularly favourable since the site, hosting already a small church and a hermitage dating back to 1600, had never been damaged by the very frequent eruptions, occurred after the large 1631 event. The first director was Macedonio Melloni, one of the most prominent experimental physicists. The construction was completed in 1848; only a few months later, for political reasons, Macedonio Melloni was dismissed as director. His successor was the physicist Luigi Palmieri, at the time professor of philosophy at the University of Naples, who provided the Osservatorio with a meteorological tower. Luigi Palmieri built the first electromagnetic seismograph, with which he wanted to "make the smallest motions of the ground clear, recording them on the paper or indicating their nature, strength and duration". He first detected harmonic tremor caused by magma oscillation and degassing in the conduit and concluded that such a phenomenon could be used to forecast an eruption. The following directors were Raffaele Vittorio Matteucci and Giuseppe Mercalli. The latter, inventor of the homonymous scale of seismic intensity, drew the first modern classification of volcanic eruptions. Ciro Chistoni and Alessandro Malladra followed Mercalli as directors . In 1937 Giuseppe Imbò was appointed as director. He strengthened the existing instruments on the volcano reaffirming the old objectives of Melloni and Palmieri on forecasting eruptions. He made instruments for seismological, electrical and radioactive observations, hoping to forecast the final eruption of the cycle begun in 1913. Imbò with the aid of a seismograph and observations on the Vesuvius activity, managed to forecast the 1944 eruption and to inform the authorities. He was director until 1970, the year of the first ascending phase of the recent Phlegraean bradyseismic events. In the second half of the 1990s the Osservatorio Vesuviano has gone through the most significant change of its long history. It was transformed into a volcano observatory capable of carrying out research and technical activities aimed at performing long- and short-term forecasting of volcanic eruptions, volcanic hazard assessment and zoning of the territory exposed to the hazards. In such an atmosphere, the historical building of the Osservatorio Vesuviano was transformed in a volcanology museum, with the aim of disseminating information on volcanic hazards and risk. At present the Osservatorio Vesuviano is a section of the Istituto Nazionale di Geofisica e Vulcanologia.

Discussion points. – Volcanic eruption forecasting. Information and education as tools for risk mitigation.

Stop 1.3:

The AD 79 eruption at Herculaneum excavations

Significance. – The most famous Plinian eruption and its effects on land and urban settlements.

The AD 79 "Pompeii" eruption. - On August 24 of AD 79, Vesuvius awakened, and destroyed the towns of Herculaneum, Oplontis, Pompeii and Stabiae. The eruption has been studied by many authors (Lirer et al., 1973; Sigurdsson et al., 1985; Barberi et al., 1989; Cioni et al., 1999; Gurioli et al., 2002) and three major phases have been distinguished: (1) opening phreatomagmatic; (2) main Plinian; (3) caldera-forming with phreatomagmatic surges and flow emplacement. Significant variations of the characteristics of the pyroclastic deposits have allowed the definition of Eruption Units, deposits emplaced by pulses within a phase, with well defined eruptive mechanism. The AD 79 eruption sequence includes 8 Eruption Units, each with distinct areal distribution and lateral variations (Fig. 19, 20).

Volume n° 2 - from B16 to B33

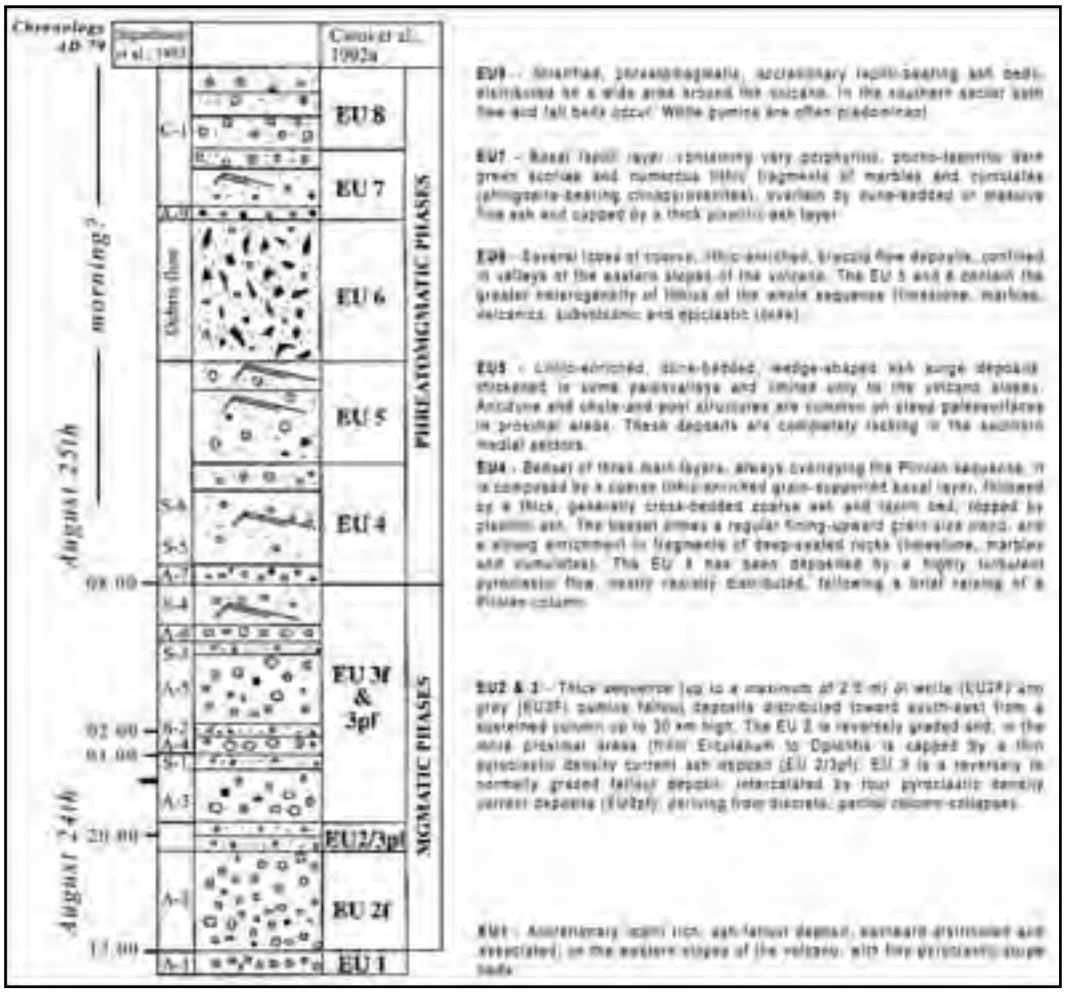

Figure 19 - Generalised sequence of the AD 79 Vesuvius eruption deposits.

An accretionary lapilli-rich ash layer (EU1), the only product of the opening phreatomagmatic phase, is covered by the pumice-fall deposit of the Plinian phase. This latter phase was dominated by an eruption column which reached a maximum altitude of 30 km. The Plinian deposit is composed of white phonolitic pumice (EU2F), locally capped by a thin, whitish ash-flow deposit (EU2/3PF), which passes upwards, with a sharp colour change, to grey, mafic phonolitic pumice (EU3F). The upper part of the deposit contains intercalated ash-flow beds (EU3PF) and is closed by pumice and ash flow deposits in proximal exposures. During this phase, which tapped more than 3 km^3 of magma, thick fallout deposits accumulated on a large area to the southeast, and pyroclastic-current deposits buried Herculaneum to the south. The caldera forming phase began with the most powerful and widespread pyroclastic current (EU4). The strong earthquake and the dark cloud witnessed by Pliny the Younger at Cape Misenum on the morning of August 25th is likely to correspond to this pyroclastic current. The currents of this phase destroyed human settlements along the western and northern slopes of the volcano and devastated the Pompei-Stabia area. The caldera-forming phase continued with the emplacement of the pyroclastic-current deposits of EU5, distributed in proximal areas and confined in valleys of the volcanic edifice. EU5 is covered by very coarse, lithic breccia flow deposits of EU6, extensively exposed along the eastern slopes of Mt. Somma.

Areal distribution as well as lithic types and content

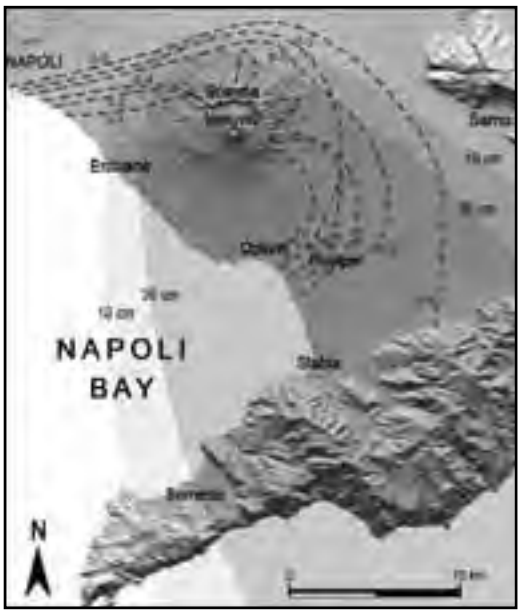

Figure 20 - Distribution of the AD 79 Vesuvius eruption deposits.

of the latter deposits, suggest that they were erupted during the paroxistic events of the caldera-forming phase. The protracted withdrawal of the magma chamber, favoured by magma-water interaction, led to tapping of the more mafic liquid that characterises the juvenile fraction of the widespread EU7. During the waning stage of the eruption, wet, phreatomagmatic, ashy pyroclastic currents (EU8) were generated, showing a sharp compositional reversal towards the more salic compositions of the initial phase of the eruption.

The Plinian deposits (fall and minor flows) range from early phonolitic white pumice to late tephritic-phonolitic grey pumice; the upper phreatomagmatic flow units exhibit larger variations with both grey and white pumice clasts and more abundant mafic crystals in the grey pumice. White pumice results from the withdrawal of phonolitic magma from the top of the chamber. Temperature was evaluated at about 850-900° on the basis of homogenisation temperature of glass inclusions in sanidine and leucite. The grey pumice results from the mixing of three isotopically distinct components: phonolitic white melt, mafic cumulates and a crystal-poor grey magma. The grey magma had high temperature (around 1050° C), very low viscosity and density slightly higher than that of the white magma. These features are consistent with the establishment of a physical discontinuity separating the white from the grey body. The lower portion of the Pompeii chamber was therefore occupied by a homogeneous, phonolitic-tephritic, grey magma which was never erupted without being largely mixed. The grey-white mixing was mainly sin-eruptive, as suggested by variations in magma discharge rate closely linked to the extent of the mixing.

The Herculaneum excavations

Herculaneum Beach. - The grey wall (23 m thick) including at least six units, is the best exposure of the AD 79 pyroclastic-current deposits that buried Herculaneum (Fig. 21).

These deposits lie on the old coastline. Along the waterfront a series of arches form the base of the Sacred Area. Each arch forms a chamber. On the southern part of the waterfront are the Suburban Thermae. The beach and the shoreline consisted of yellow tuff of the Avellino eruption, covered by black sand. The tuff formed a wave-cut platform whose surface was worked to provide a slip-way for large boats.

The first deposit of the eruption is a 35 to 50 cm thick unconsolidated, poorly sorted, massive grey surge layer (EU2/3pf) which extends into the chambers.

Figure 21 - The pyroclastic-currents deposits of the AD 79 Vesuvius eruption at the Herculaneum coast-line.

All the skeletons of the human victims, as well as the skeleton of a horse, occur within this surge layer.
This unit overlies filling material, probably related to the restorations of the earthquake damages preceding the eruption, and is overlain by a lithified, pyroclastic lensoid pumice-flow deposit (EU3pf1). A 8 m long boat, was found in the first pyroclastic flow on the beach. The sequence follows with a fines-depleted, coarse grained, pumice rich layer (up to 200 cm thick) with abundant building material (EU3pf2a), cropping out on the downwind side of buildings, and thinning and fining away from the walls. This layer grades in the overlying massive, consolidated pumice flow deposit (EU3pf2b), <5 m thick, that thins towards the suburban Thermae, maintaining a horizontal upper surface. A fines-poor, discontinuous bed of pumice lapilli and lithic fragments (skarn, marbles and cumulitic rocks) represents the most important discontinuity visible in this area. Its scalloped bottom is clearly related to the deformation effect of ballistic blocks. This bed marks the transition to the thick (up to 15 m) lithic rich flow deposits of the phreatomagmatic phase, correlatable to the basal layer of EU4 in the southern sector of the volcano (EU4). A massive, consolidated pyroclastic flow (s) deposit (yellow tuff), 8 m thick, follows. The last deposit (F4) is a massive, poorly lithified, lithic rich pyroclastic flow, up to 5 m thick.

Palestra. Palestra is a rectangular park surrounded by porticos, and used for gymnastics, sports and games; in the centre of the park is a cross-shaped, 1.2 m deep swimming pool. It is covered by the EU3pf2 and EU4 deposits.
EU2/3pf includes a basal massive unit with a high amount of building material and a stratified upper part. Inside the Bourbon tunnels, it thickens locally up to 1.5 m. Inside the Palestra, EU3pf1 forms lenses, EU3pf2 directly overlies EU2/3pf, and shows a basal fines-poor layer, rich in building debris. EU3pf2 is overlain by EU4 and lithic rich pyroclastic deposits, 7 m thick.

DAY 2

Stop 2.1:

Traianello Quarry: the past 19,000 years of Somma-Vesuvius activity

<u>*Significance.*</u> – A long period of Somma-Vesuvius eruptive history is testified by the products exposed in the quarry. Occurrence of both fall and flow deposits of the Plinian events suggests a scarce control by the topographic barrier of the Mt. Somma caldera wall on their dispersion.

Figure 22 - General view of the Traianello quarry.

<u>*The quarry.*</u> - Traianello quarry (Fig. 22) is on the Mt. Somma slopes, 2 km north of Somma Vesuviana. In a small excavation within the quarry floor a 100-150 cm-thick brownish to reddish scoria deposit is exposed, this is related to eccentrical vents of Mt. Somma. In other parts of the quarry thin lava flows are interbedded with the scoria deposits.

The "Pomici di Base" tephra overlies the scoria bed. It is a compositionally zoned Plinian pumice-fall deposit, composed of a white pumice lower bed, surmounted by a grey banded and a black pumice beds. The upper part of the sequence, a stratified, lithic-rich fall layer surmounted by a dark ash-flow deposit, with sparse lithic and juvenile clasts, records the final phase of the eruption, dominated by phreatomagmatic explosions.
The "Greenish Pumice" Tephra mostly includes fall deposits with contrasting grain-size.
A layer of pedogenised yellowish ash, separates the "Greenish Pumice" Tephra from the Agnano Pomici Principali. The products of this Phlegraean eruption are widely dispersed over the Mt. Somma slopes and constitute an important marker bed.
The "Mercato Pumice" Tephra is well exposed in the central part of the quarry, along a 30 m high scarp. From base upwards it includes a white pumice-fall deposit, interbedded with a layer of pinkish ash, overlain by a thick sequence of pyroclastic-flow

Figure 23 - View from Camaldoli towards the east-southeast.

deposits. The pinkish ash that laterally passes to a pumice flow, with a very sharp lateral transition from faintly laminated to a massive pyroclastic flow. The upper pyroclastic-flow sequence includes several flow units, locally cross-stratified and characterised by a variable content of lithic blocks and juvenile clasts."
The "Avellino Pumice" Tephra partially fills palaeo-valleys. The Plinian fall deposit is characterised by a sharp change in colour from white at the bottom to grey at the top, reflecting a compositional change. An accretionary lapilli-rich ash layer and an overlying massive ash-flow deposit are at the top of the sequence, on the Plinian fall deposits, and are related to variable phreatomagmatic activity. The first can be correlated with a very impressive pyroclastic surge deposit outcropping in the western and north-western part of the volcano, while the second is linked to a less energetic, Vulcanian-type activity that formed an alternance of lithic-rich fall layers and pyroclastic flows, well exposed on the north-western slopes.
The AD 79 eruption, represented by at least four massive ash-flow units with abundant lithic blocks, close the stratigraphic sequence, filling the paleo-valleys partially occupied by the Avellino products.

Discussion points. - Pyroclastic flows of the Plinian eruptions of Somma-Vesuvius: lateral transitions and topographic influence. The effects of a caldera wall on the dispersal of pyroclastic currents.

Stop 2.2:

The Campi Flegrei caldera from the Camaldoli hill

Significance. - A general view of the active portion of the Campi Flegrei caldera.
The caldera. - From south counterclockwise, the island of Capri, the Sorrento peninsula, the Somma-Vesuvius, the city of Naples, the Campi Flegrei caldera, the islands of Procida and Ischia (Figs. 1, 2, 23).
The Sorrento peninsula and the island of Capri are part of the Apennine chain, intersected by NE-SW and NW-SE trending faults, which determine a horst-and-graben type structural pattern. The graben-type structure in the central part of the peninsula is partially filled by the Campanian Ignimbrite, on which is built the town of Sorrento.
A very good view of the Somma-Vesuvius and its relationships with the city of Naples and surrounding towns can be appreciated.The town of San Sebastiano is also well visible and the 1944 lava flow which destroyed it.
The Vomero-Arenella saddle was a preferential pathway for pyroclastic currents erupted in the Soccavo plain during the I epoch (15÷9.5 ka) of the third period of activity of the Campi Flegrei caldera.
The largest part of the morphological boundaries of both Campanian Ignimbrite and Neapolitan Yellow Tuff calderas, are visible. Towards the east, at Casalesio, the horizontally laying Campanian Ignimbrite is cut by a southward dipping high-angle surface, which is part of the Campanian Ignimbrite caldera margin overlain by the Neapolitan Yellow Tuff. The same relationships occur along an ENE-WSW alignment up to Poggioreale, towards the east, and up to Punta Marmolite, towards north-west.

The St. Martino hill is a complex morphology including a lava dome buried by a sequence of pyroclastic-surge deposits, all generated between the Campanian Ignimbrite and the Neapolitan Yellow Tuff eruptions.
The scarp bordering the Posillipo hill towards the northwest, is the only exposed part of the Neapolitan Yellow Tuff caldera margin. The densely urbanized Fuorigrotta-Bagnoli and Soccavo plains, have been the site of eruption vents during the I epoch (15 - 9.5 ka) of the third period of activity.

Figure 24 - The Astroni crater from Camaldoli.

Looking towards the south-west, one can have a view of the almost complete caldera, and of the islands of Procida and Ischia. In the foreground the Agnano plain and the Astroni tuff ring. The former results from a volcano-tectonic collapse during the Agnano-Monte Spina eruption (4.1 ka) which will be discussed at Stop 3.1. Behind the Astroni and Gauro volcanoes, is the Averno-Capo Miseno alignment of tuff cones and tuff rings, which marks the western margin of the Neapolitan Yellow Tuff caldera. All these volcanoes but Fondi di Baia (8.6 ka), formed during the I epoch (15 ÷ 9.5 ka) of the third period of activity of the caldera.
The Astroni volcano, a well preserved elliptical edifice with axes of about 2 and 1 km, (Fig. 24), formed during the III epoch of activity (4.8-3.8 ka) of the Campi Flegrei caldera (Di Vito et al., 1999).

Isaia et al. (2004), on the basis of a stratigraphic study, have defined 7 depositional units, delimited by either thin paleosols or erosional unconformities.
The eruption vents, although confined in the present crater, migrated from NW to SE.
The volcano grew at the north-western edge of the Agnano-Monte Spina volcano-tectonic collapse, (4.1 ka), in the final part of the 4.1-3.8 ka time span. This implies that the 7 eruptions followed each other at very short time intervals. This conclusion is also supported by constancy in archaeological facies of findings within the paleosols between variable Astroni units, in the plain north of the caldera. The sequence of close eruptions makes the Astroni volcano peculiar in the recent history of the caldera. Therefore, the definition of its history is very important in order to understand one of the past phenomenologies of the caldera, and are relevant elements for forecasting its behaviour.

<u>Discussion points.</u> - Campanian Ignimbrite and Neapolitan Yellow Tuff calderas. Volcanism within the Neapolitan Yellow Tuff caldera. Volcanic hazard and risk of a megacity inside an active caldera.

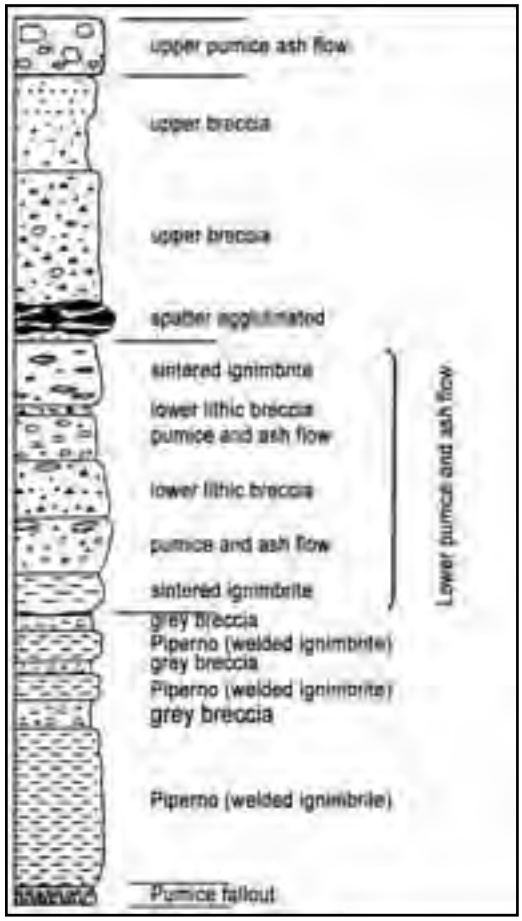

Figure 25 - Generalised eruption sequence of the proximal Campanian Ignimbrite (modified after Rosi et al., 1996).

Stop 2.3:

Verdolino quarry

<u>Significance.</u> - The caldera forming eruptions. Geometrical relationships among Campanian Ignimbrite, Neapolitan Yellow Tuff and interposed deposits.

<u>The Campanian Ignimbrite.</u> - The Campanian Ignimbrite catastrophic eruption occurred in the Phlegraean area and was accompanied by a caldera collapse (Rosi et al., 1999; Orsi et al., 1996; Ort et al., 2003; Pappalardo et al., 2002; Polacci et al., 2003). The collapsed area, about 230 km^2 (Fig. 6), includes the present Phlegraean Fields, the city of Naples, the bay of Pozzuoli and the north-western sector of the

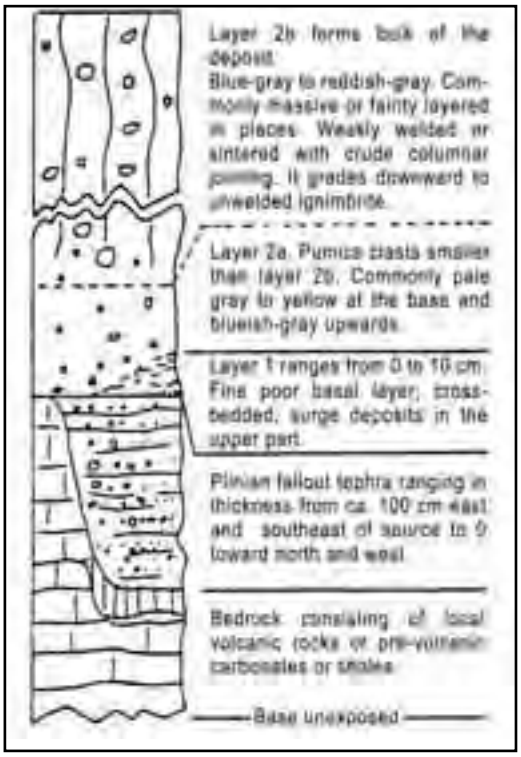

Figure 26 - Generalised eruption sequence of the distal Campanian Ignimbrite (After Fisher et al., 1993).

bay of Naples (Orsi et al., 1996).
The Campanian Ignimbrite sequence includes a basal Plinian fallout deposit surmounted by pyroclastic-current units, which in proximal areas are intercalated by densely welded ignimbrite (Piperno) and lithic-rich breccia units (Museum Breccia) (Fig. 25). The basal Plinian deposit (Rosi et al.,1999, Polacci et al., 2003), dispersed towards the east, consists of a well sorted and reversely graded lower portion, followed by a well to poorly sorted and crudely stratified upper portion. The pyroclastic-current deposits, which covered an area of about 30,000 km^2, show homogeneous sedimentological characteristics in medial and distal areas (10 to 80 km from the source) (Fisher et al., 1993).

From the base upwards, they include a very thin, discontinuous, fines-poor layer, above which lies the bulk of the ignimbrite (Fig. 26). They are partially welded to non-welded (greyish), although they can be lithified by zeolites (yellowish). These deposits, which underlie much of the Campanian Plain, also occur in isolated valleys in the Apennines, in the area of the Roccamonfina Volcano, and in the Sorrento Peninsula.
A stratigraphic and compositional study of a core drilled in the city of Naples, which includes four superposed pyroclastic-current units, has given to Pappalardo et al. (2002a) a unique opportunity to define the compositional features of the magma chamber, the timing of magma extraction, the withdrawal dynamics and the timing of the caldera collapse.

Pumice fragments range in composition from trachyte to phonolitic trachyte. Their phenocryst content decreases from the least evolved (10 vol%) to the most evolved (<3 vol%) samples. Phenocrysts are alkali-feldspar with subordinate plagioclase, diopside and salite clinopyroxene, biotite, magnetite and apatite. The stratigraphically uppermost Unit 4 contains the less evolved trachytic pumice, while the basal Units 1 and 2 contain the most evolved, alkali-trachytic to phonolitic fragments. Pumice fragments of Unit 3 have intermediate chemical composition. Major elements composition of glass from pumice fragments has a bimodal distribution. CaO content shows two modes, which correspond to the composition of the most and least evolved rocks, respectively. The composition of the glass from pumice fragments of Unit 3 comprises both modes. The geochemical variation detected in the cored units matches well those of the distal rocks, proximal breccia deposits and basal fallout beds (Pappalardo et al., 2002a and references therein). The degree of evolution of the erupted magma increased during the Plinian phase and decreased during the pyroclastic-current phase. The least evolved composition has been detected in the latest erupted magma and in glass inclusions hosted in clinopyroxene from the lower portion of the basal fallout deposit. Variation in major and trace element concentrations and constancy of Sr, Nd, Pb and B isotopic ratios, suggest that the eruption was fed by a trachytic magma chamber which included two co-genetic magma layers separated by a compositional gap (Pappalardo et al., 2002a). The upper layer was more evolved and homogeneous, whereas the lower layer was less evolved and zoned. During the course of the eruption, the two magma layers were extruded either individually or simultaneously producing the hybrid magma detected in Unit 3 of the core.
The eruption probably began with phreatomagmatic explosions, followed by the formation of a sustained Plinian column, which reached a maximum height

of about 44 km (Rosi et al., 1999) and was fed by simultaneous extraction of the two magma layers present into the chamber. Due to upward migration of the fragmentation surface, reduction of magma eruption rate, and/or formation of fractures, an unstable pulsating column was formed and fed only by the most evolved magma. The maximum height reached by this column was of about 40 km (Rosi et al., 1999).

This Plinian phase was followed by the beginning of the caldera collapse and the generation of expanding and initially over-pressurized pyroclastic currents fed by the upper magma layer. The currents moving northward, surmounted the Roccamonfina Volcano (>1,000 m a.s.l.) at 50 km from the source, while the southward currents reached the Sorrento Peninsula, over seawater. During the following major caldera collapse, the maximum mass discharge rate was reached and both magma layers were contemporaneously tapped as the intermediate composition magma, generating further expanding pyroclastic currents which travelled radially from the vent and deposited ignimbrites at distances in excess of 80 km. Towards the end of the eruption, only deeper and less differentiated magma was tapped, producing less expanded and less mobile pyroclastic currents, which travelled short distances within the Campanian Plain without crossing the Apennines or reaching the Sorrento Peninsula.

Figure 28 - Geographic distribution of the Campanian Ignimbrite deposits.

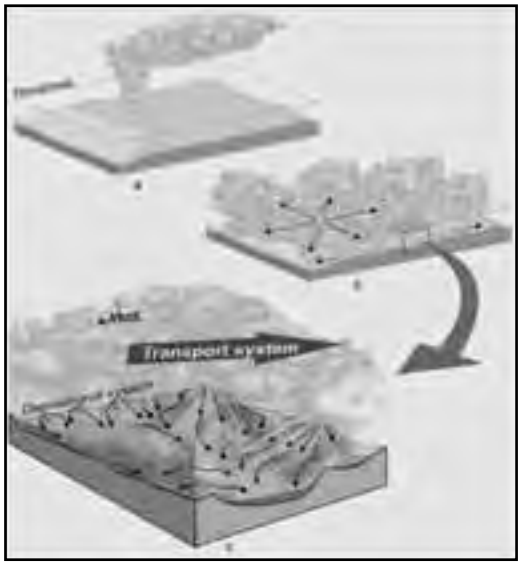

Figure 27 - The Campanian Ignimbrite eruption: main phases (a, b) and model of the transport and depositional systems of the pyroclastic currents (c) (After Fedele et al., 2003).

Fisher et al. (1993) and Ort et al. (2003) suggested that the pyroclastic currents which surmounted high mountain ranges and travelled over seawater were characterised by distinct transport and deposition systems (Fig. 27). Initial pyroclastic currents were expanding gas-particle mixtures that moved over the landscape as dilute currents. The transport system moved outward from source and was thicker than the highest relief. It was kept turbulent by the significant surface roughness. As the currents travelled away from the vent, they stratified continuously with respect to density, forming the deposition system in their lower part. This system, blocked by morphological obstacles and decoupled from the transport system, drained off ridges and down valleys in directions dictated by slope direction.

Ash layers related to the Campanian Ignimbrite eruption are known from cores in the Mediterranean Sea. The Y5 ash layer recognized from the Ionian Sea to the eastern Mediterranean and correlated with an oxygen isotope date of ca. 38,000 yr bp (Thunnel et al., 1979) has the same composition of the most evolved and intermediate Campanian Ignimbrite erupted magmas. Campanian Ignimbrite ash layers were also rec-

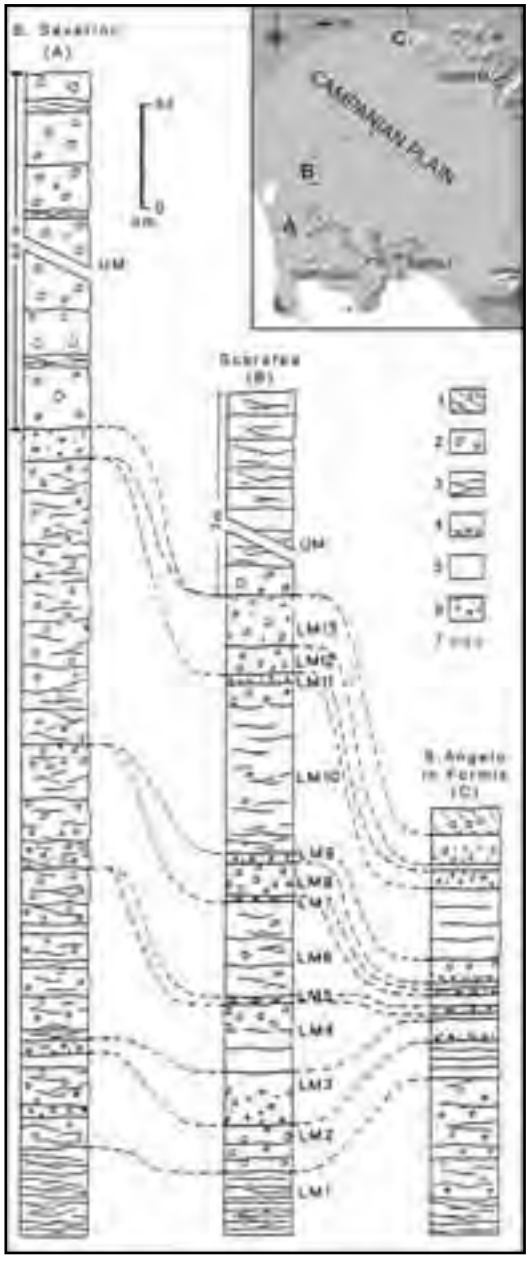

Figure 29 - Outcrop area and stratigraphic sections of the proximal (St. Severino), intermediate (Scarafea), and distal (Sant'Angelo in Formis) facies of the Neapolitan Yellow Tuff. 1: reworked deposits; 2: pyroclastic flow deposits; 3: pyroclastic surge deposits; 4: pumice-and-ash fallout deposits; 5: ash fallout deposits; 6: debris flow; and 7: accretionary lapilli. (after Orsi et al., 1992)

ognized in Greece (Seymour and Christanis, 1995) as well as in northern and central Italy, Bulgaria, and the former USSR (Narcisi and Vezzoli, 1999 and references therein) (Fig. 28). Fedele et al. (2004) estimated that the co-ignimbrite ash cloud rose in the atmosphere at a height of at least 30 km, and suggested that the ash layer could result from particle deposition within either the umbrella cloud of the Plinian columns or the transport system, of the pyroclastic currents. The latter, likely controlled by wind both at low altitude (<10 km) and in the stratosphere, laid down particles over a very large area. Furthermore, considering the sequence of phenomena, the characteristics of the pyroclastic currents, and the volume estimates for the variable portions of the eruption, the authors suggested that the erupted magma was >200 km^3 (DRE).

Fedele et al. (2004) evidenced the occurrence of the eruption during a time interval characterised by bio-cultural modifications in western Eurasia, including the Middle to Upper Palaeolithic transition and the supposed change from Neanderthal to "modern" Homo sapiens anatomy, a subject of continuing investigation and controversy. At several archaeological sites of south-eastern Europe, the ash separates the cultural layers containing Middle Palaeolithic and/or "Earliest Upper Palaeolithic" assemblages from those with Upper Palaeolithic industries. At the same sites the tephra coincides with a long interruption of occupation. The palaeoclimatic records show that the eruption occurred just at the beginning of Heinrich Event 4 (HE4), characterised by extreme climatic conditions, compared to the other HEs. The authors hypothesised a positive climate-volcanism feedback triggered by the co-occurrence of the eruption and HE4 onset.

The Neapolitan Yellow Tuff. - The Neapolitan Yellow Tuff is the second largest pyroclastic deposit of the Campanian area. Conservative estimates of the area covered by the tuff and volume of erupted magma are 1,000 km^2 (Fig. 29) and about 40 km^3 (DRE), respectively. The deposit, generally grey and poorly lithified in distal areas, in the proximal Neapolitan-Phlegraean area is zeolitised and yellow, from which the name. The tuff has attracted the interest of many geologists since the 19th century. Orsi et al. (1992; 1995) and Wohletz et al. (1995) reconstructed in details its stratigraphic and chemo-stratigraphic sequence, the eruption mechanisms, the feeding magmatic system, and the relationships among eruption dynamics, magma

Volume n° 2 - from B16 to B33

withdrawal, and timing of caldera collapse. Orsi et al. (1996), reconstructed the structural boundary of the area collapsed during the eruption (Fig. 6).

The Neapolitan Yellow Tuff sequence was divided into a Lower Member (LM) and an Upper Member (UM) (Fig. 29), on the basis of textural characteristics, dispersal and occurrence of an angular unconformity. LM is the product of the largest known trachytic phreato-Plinian eruption. Its thickness varies from 11 m in the most proximal exposures, to 85 cm at Sant'Angelo in Formis, at the foot of the Apennine mountains, 35 km from the vent area. In contrast, the characteristics of UM are typical of a phreatomagmatic eruption. Its thickness varies from about 100 m in the Quarto Plain, to 7 m at Scarafea, in the Caserta Plain (Fig. 29).

LM includes 13 layers, designated LM1 through LM13 from base upward. Layer LM1 occurs over the entire outcrop area and is composed of many ash to coarse ash, millimetres to centimetres thick, surge beds; lapilli-sized components occur only in proximal areas. Often it shows cross laminations and erodes the underlying paleosol. Layers LM2, LM4, LM6, LM8, LM10 and LM12 include variable beds, composed of ash with high amount of accretionary lapilli, and few scattered pumice and hornfelsed lithic clasts. The beds vary from undulating and cross laminated to massive and plane-parallel with distance from vent, suggesting that in proximal area they were deposited dominantly by erosive surge clouds while in distal areas deposition was mostly due to ash fallout. Layers LM3, LM5, LM7, LM9, Lm11 and LM13 are pumice- and ash-fallout beds.

The basal pumice fallout contains a significant amount of ash and variable amount of lithic clasts. Size of pumice and lithic fragments not always decreases with distance from the vent. The upper ash fallout contains millimetre-sized pumice fragments and a large amount of accretionary lapilli.

UM is a sequence of pyroclastic-flow and -surge deposits which shows considerable variation with both distance from the vent and azimuth around the caldera. Pyroclastic-flow deposits dominate within the caldera, while pyroclastic-surge beds are the most abundant outside the caldera. Likely UM was generated by multiple fracture vent eruptions and pyroclastic currents were transformed (Fisher, 1983) across the caldera scarps.

The Neapolitan Yellow Tuff composition varies from latite to alkali trachyte. Phenocrysts (<3% by volume) are sanidine, plagioclase, clinopyroxene, biotite,

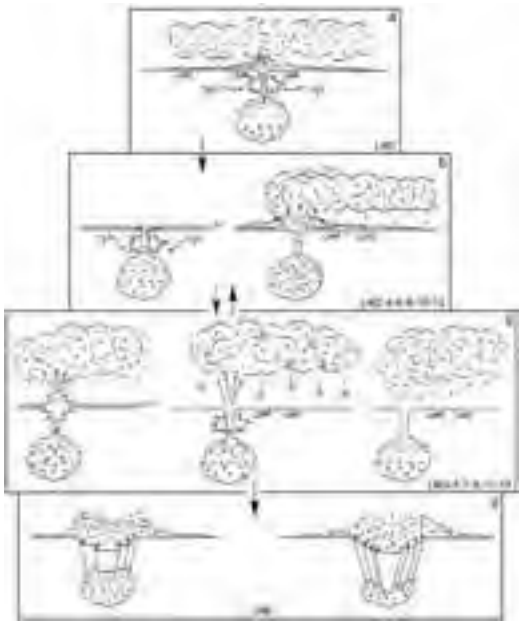

Figure 30 - Illustration of magma chamber withdrawal and eruption column behaviour during the Neapolitan Yellow Tuff eruption. The three magma types in the chamber are: alkali trachyte (dashes), trachyte (dots), and trachyte to latite (x) (after Wohletz et al., 1995).

magnetite, in order of decreasing abundance, and rare apatite. Sanidine in latite, anorthitic plagioclase in trachyte and alkali trachyte, reversely zoned plagioclase and two clinopyroxenes (diopside and salite) are evidence of mineralogical disequilibrium.

Compositional variation of pumice fragments, allows a fourfold distinction of the sequence, from the base upward in: LM alkali trachyte (LMat), LM trachyte (LMt), UM alkali trachyte (UMat) and UM alkalitrachyte-to-latite (UMt). Glass shards from the trachytic pumice-and-ash fallout beds of LM, show all the chemical compositions displayed by the pumice fragments of the whole sequence. Trace element, K_2O, Na_2O, SiO_2 and P_2O_5 contents distinguish the two trachytic groups, whereas the two alkali trachytic groups are distinguished by their stratigraphic position. LMat pumice has a fairly homogeneous composition. LMt pumice becomes progressively less differentiated up-section. LMt and LMat pumice are separated by a compositional gap. A compositional gap separates UMat from the underlying LMt. Umt includes alkalitrachytic to latitic pumice progressively less differentiated upsection, without any compositional gap with the underlying UMat. The stratigraphically lowermost

alkali trachytic sample of this group, enriched in Sr, Ba, K_2O and P_2O_5 and depleted in Na_2O, Zr, Nb, Th, REE with respect to the underlying UMat, marks the arrival of a new magma in the chamber. Pumice clasts from the least differentiated UMt sample, have latitic (dark) and trachytic (white) compositions, suggesting magma mingling, probably during extrusion.

The magma chamber was composed of three discrete layers: an upper alkali trachyte (magma 1), an intermediate trachyte (magma 2) and a lower alkali trachyte to latite (magma 3), separated by compositional gaps (Orsi et al., 1995). The three magmas, characterised by similar Sr-isotope ratio, are not related to crystal fractionation processes, and represent distinct magma batches originated from a similar deep source. Syneruptive mingling is documented by the occurrence of glass shards of variable composition in the same bed. The eruption was likely to have been triggered by the arrival of magma 3 into the chamber, and began (Fig. 30a) with explosions driven by efficient water/magma interaction that produced LM1. These explosions were fed by the uppermost, compositionally evolved, volatile- and likely bubble-rich, LMat layer of magma. After LM1, the character of the explosions abruptly changed.

The vesiculated LMt magma interacted with water and fragmented very efficiently, producing highly energetic phreato-Plinian explosions which generated LM2 (Fig. 30b). These explosions apparently flushed the water out of the conduit so that the following rising magma, which generated LM3, did not encounter a significant amount of water until it reached the sea floor. Only the upper part of this magma interacted efficiently with the sea water and was disrupted in fine particles, while the lower part was mainly fragmented by exsolution of the magmatic gases. Alternation of phreato-Plinian (LM2, LM4, LM6, LM8, LM10, LM12) and mostly magmatic (LM3, LM5, LM7, LM9, LM11, LM13) explosions was repeated six times after eruption of LM1. The phreato-Plinian explosions gave rise to surge emplacement in proximal areas and ash fallout in both proximal and distal areas. Accretionary lapilli were abundant due to a high amount of steam. In contrast, phreato-Plinian to magmatic explosions (Fig. 30c) generated sustained columns that dispersed downwind plumes of pumice laden with fine ash and steam experiencing premature ash fallout and formation of accretionary lapilli. Each phreato-Plinian explosion tapped all three magma layers, whereas the phreato-Plinian to magmatic explosions only drained the intermediate trachytic layer. Increase in withdrawal depth, evidenced by commingling of the three layers of the chamber, could result from a dramatic pressure decrease on the magma in correspondence of the conduit and/or from a large increase in eruptive mass flux, both consequences of the water/magma interaction efficiency during phreato-Plinian explosions.

A time break occurred after LM eruptions, and then activity resumed with very different characteristics in UM explosions (Fig. 30d). The time break is marked by initiation of a caldera collapse and a change from central-vent to ring-fracture eruptions. This change in vent character caused an overall pressure decrease on the chamber that allowed the previously trapped magma in the chamber top (UMat) to be erupted. The eruption then continued with the extraction of the deepest magma in the chamber (UMt). Water/magma interaction during UM eruptive phases was not as efficient as during LM phases. Explosions fed pyroclastic flows and surges. The caldera likely continued to collapse also after the end of the eruption, as suggested by the absence of any outcrop of Neapolitan Yellow Tuff in the central part of the Phlegraean Fields.

Wohletz et al. (1995) attempted to evaluate the physical parameters of the eruption. Calculations based on magma chemistry show an increase in magma density, a decrease followed by an increase in viscosity, and a general decrease of gas fraction during both LM and UM eruptive phases. From a depth of 400 m, calculated fragmentation depths gradually rise during each phase. Application of sequential fragmentation/transport analysis to granulometric data shows an average ratio of phreatomagmatic to magmatic components of 70:30 for LM and 80:20 for UM. However, computed water/magma interaction ratios generally decrease from about 0.65 to 0.05 and are fairly constant at about 0.1 during eruption of LM and UM, respectively. Furthermore, surge/flow run-out distances and estimates of eruptive velocities from R values show that column collapse heights were extremely high (6 to 7 km) during the first phase and were substantially lower during the second phase (2 to 3 km). Vent radii required for calculated eruption velocities of 180 to 370 m/s are between 70 and 300 m, suggesting a cumulative eruption duration of over 10 hours, perhaps spanning of one to several days.

The quarry. - In an old quarry dug at the mouth of the Verdolino valley, in the Soccavo plain (Figs. 6, 31), the oldest exposed rocks are Piperno and Breccia

Figure 31 - View of the Verdolino valley from the south-west. CI: Campanian Ignimbrite; TB: Tufi Biancastri; VRa-e as in figure 32; NYT: Neapolitan Yellow Tuff.

Museo deposits of the Campanian Ignimbrite. They are overlain by pyroclastic deposits, named Tufi Biancastri (Whitish Tuffs), whose stratigraphic sequence, reconstructed by Orsi et al. (1996), is reported in figure 32.

Units VRa, VRb and VRd were generated by eruptions dominated by phreatomagmatic explosions

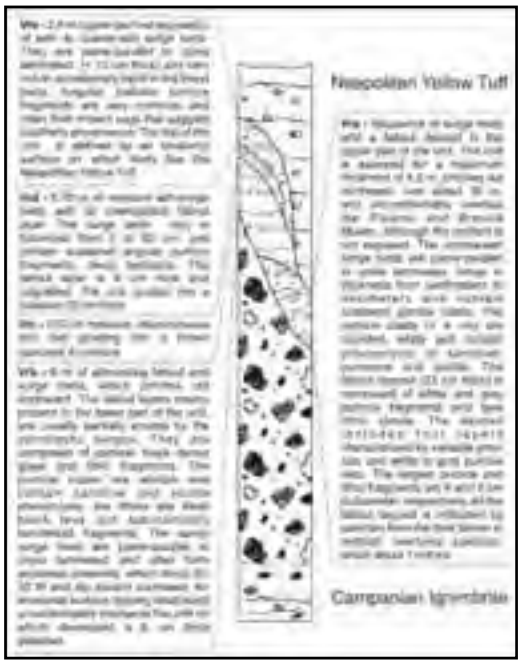

Figure 32 - Verdolino quarry stratigraphic sequence (after Orsi et al., 1996).

with minor magmatic events from vents located not far from the outcrop area. Unit VRc is a very thin and discontinuous ash bed. Unit VRe is the proximal deposit of a phreatomagmatic eruption whose vent was to the south of the Verdolino valley. The stratigraphically highest unit is the Neapolitan Yellow Tuff, which is deeply zeolitized throughout the area.
The sequence of Piperno and Breccia Museo, whose top is at about 200 m a.s.l., dips of about 6° towards the north and is intersected by an erosional surface dipping about 35° southward. Units VRa and VRb unconformably mantle this surface and die out toward its upper part. Both units are cut by an erosional surface, which dips about 30° southward and is mantled by Units VRc, VRd and VRe. All the exposed sequence up to unit VRe, is crosscut by a third erosional surface whose dip increases southward. This surface is mantled by the Neapolitan Yellow Tuff, whose thickness of about 100 m increases towards the Soccavo plain and whose base, at about 240 m a.s.l. at the top of the surface, is 170 m a.s.l. at its foot.

The erosional surface between Units VRb and VRc was likely to have been generated by an intense erosion during the Würmian sea level low stand (17-14 ka).

Discussion points. - Implications of deposit attitude and their geometrical relationships on caldera collapse features and morphological evolution.

DAY 3

Stop 3.1:

Pianura, Torciolano natural section - The Agnano-Monte Spina eruption

Significance. - Agnano-Monte Spina Tephra, the deposit of the highest magnitude eruption of the Campi Flegrei caldera in the past 5 ka.

The Agnano-Monte Spina eruption. - The Agnano-Monte Spina eruption history, including geometry and timing of the accompanying volcano-tectonic collapse, has been recently reconstructed by de Vita et al. (1999). The authors have also constrained its age to 4,100±50 y using ^{14}C (AMS) and $^{40}Ar/^{39}Ar$ methods. Variation of lithological features and occurrence of a well-defined erosional unconformity were used by the authors to subdivide the whole sequence into six members named A through F, which represent as many eruption phases. Details for each member are reported in figure 33. Dellino et al. (2001; 2004a),

Figure 33 - Agnano-Monte Spina Tephra type section (after de Vita et al., 1999).

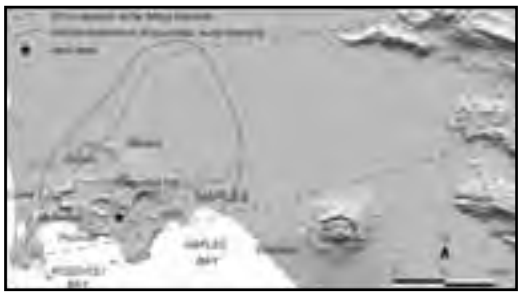

Figure 34 - Distribution of the Agnano-Monte Spina Tephra.

have discriminated the role of variable fragmentation dynamics operating in each eruption phase. The sequence alternates pyroclastic-current and -fallout beds, distributed over an area of about 1,000 km^2. The fallout beds are dispersed towards the north-east (Fig. 34). High particle concentration pyroclastic currents were confined in the Agnano depression, while lower concentration currents overtopped the morphological boundary of the caldera and travelled at least 20 km over the surrounding plain. Thickness of the tephra varies from a maximum estimated value of about 70 m in the Agnano plain, the inferred vent area for the eruption, to a few centimetres over a distance of about 50 km. Analysis of lateral facies variations and vertical facies associations of correlated layers reveals that during some eruption phases (layers B2, D2 and E2) the contrasting eruptive dynamics were almost contemporaneous (Dellino et al., 2004a). The phreatomagmatic origin of the pyroclastic-current deposits, which contrasts with the magmatic origin of fallout beds, suggests that the pyroclastic density currents did not result from eruption column collapses. They were most likely related to radially spreading clouds which were contemporaneous with fallout activity but issued from distinct zones in the vent area. Turbulence and high expansion made the base surges capable, under certain conditions, of passing over high topographic obstacles, with hazardous effects in distal areas. Dellino et al. (2004b), using a physico-sedimentological model, reconstructed both velocity and density of pyroclastic currents of layer E2 and calculated a dynamic pressure of the flow of about 3.1 kPa.

The Agnano-Monte Spina Tephra range in composition from trachyte to alkali-trachyte. Pumice and scoria fragments are porphyritic, with phenocrysts of feldspar, clinopyroxene, black mica, apatite and opaques in order of decreasing abundance. Olivine is present only in few samples. Clinopyroxene generally is green salite, very rarely is diopside. Feldspar phenocrysts are both normally or reversely zoned bytownitic plagioclase and homogeneous sanidine. Black mica is a Mg-biotite, fluor-apatite often forms inclusions in Mg-biotite and salite crystals, and opaque is a Ti-magnetite.

Pumice clasts of the lower portion of the stratigraphic sequence are more evolved (alkali-trachyte), those of the upper portion are less evolved (trachyte), whereas those of the middle part of the sequence have intermediate composition. Furthermore, beds with texturally and chemically variable pumice fragments also occur in the middle portion of the sequence. Sr-isotope ratio in the alkali-trachyte is about 0.70748, while for trachyte it ranges from 0.70750 to 0.70756. The alkali-trachyte of the lower portion of the stratigraphic sequence contains mineral phases in isotopic equilibrium. Conversely the trachyte of the upper portion shows isotopic disequilibrium among whole-rock and some mineral phases.

The isotopical and geochemical data suggest the existence of a stratified reservoir containing two isotopically distinct magma layers. The upper layer was slightly less-radiogenic and alkali-trachytic, while the lower layer was more-radiogenic and trachytic in composition. The two layers partially mixed during the course of the eruption. The occurrence of xenocrysts of olivine, An-reach plagioclase and Mg-reach clinopyroxene suggests that also a mafic magma might have been involved in the eruption. The detected Sr-isotope range is similar to that of the Neapolitan Yellow Tuff suggesting that the magma which fed the eruption could be differentiated residues of the Neapolitan Yellow Tuff magmas still present into the Phlegraean system.

The Agnano-Monte Spina is the highest-magnitude eruption occurred over the past 5.0 ka years within the Campi Flegrei caldera. A volume of magma of about 2.4 km^3 (D.R.E.) was extruded through a vent located in the sector of the resurgent after, affected by NW-SE fault systems related to an extensional stress regime (Orsi et al., 1996).

The eruption began with explosions driven by efficient water/magma interaction and generation of a highly expanded ash cloud which deposited the thin and widely dispersed basal part of layer A1. As a consequence of these explosions, water was driven out of the conduit, and the next explosion was magmatic and

generated a relatively low (about 5 km) column, which deposited the upper fall-out bed of layer A1. Phreatomagmatic and magmatic explosions, generated the pyroclastic-surge and -fallout deposits of layer A2. During this phase the upper alkali-trachytic batch of magma was tapped. The second phase began with magmatic explosions generating a pulsating column which reached a maximum eight of about 23 km and deposited the fallout layer B1. The basal beds of layer B2 were deposited by pyroclastic currents, generated by explosions which tapped the upper alkali-trachytic batch of magma. At this stage a network of fractures, foreshadowing a volcano-tectonic collapse, likely formed and became the site of scattered vents. Opening of fractures allowed ground water to access variable parts of the reservoir. Therefore, the following explosions were triggered by variable magma-water interaction efficiency and produced pyroclastic surges and Strombolian fallout. Fragmentation surface deepened and tapped a magma resulting from mingling between the alkali-trachytic and the trachytic magma batches. Such a mingling was likely favoured by pressure lowering on the reservoir. A pause in the eruption, and heavy rains caused diffuse erosion along steep slopes. Magmatic fine ash settled down, also favoured by rain flushing, to form Member C. Increase in fracturing of the roof rocks caused a lowering of the lithostatic pressure on the reservoir, at this stage containing only the trachytic magma batch. Pressure lowering determined volatiles exsolution in the trachytic magma and its migration towards surface. This rising magma interacted with the geothermal system, causing its flashing. The following phreatomagmatic explosions marked the renewal of the eruption and the beginning of the third phase with deposition of the D0 base surge deposits. Again the pressure wave drove the water out of the conduit. The following explosions were magmatic and generated an eruption column about 27 km high, that deposited layer D1. Activation of faults along the margins of the present Agnano plain produced the main episode in the volcano-tectonic collapse. The collapsed area, corresponding to the present Agnano Plain, has a polygonal shape and is bordered by NW-SE and NE-SW trending high-angle scarps (Fig 35). These rectilinear features, many of which include triangular facets, were generated by the activation of new faults and partial re-activation of pre-existing faults.

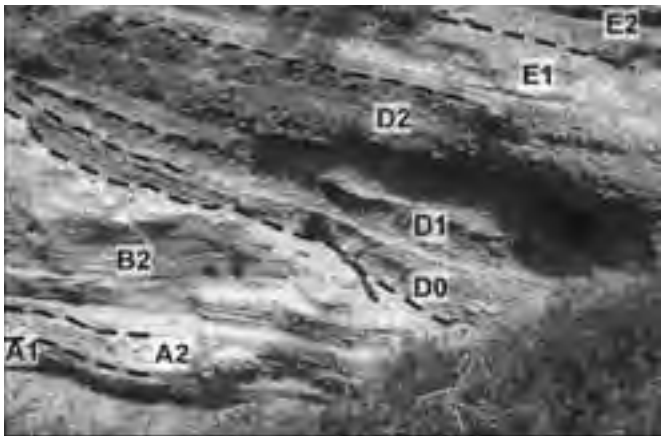

Figure 36 - The Agnano-Monte Spina Tephra at Torciolano.

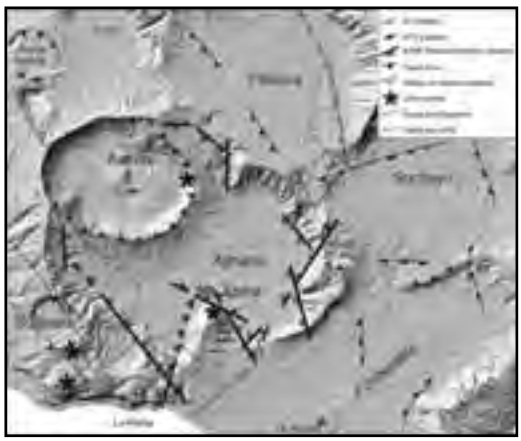

Figure 35 - Structural map of the Agnano plain.

The collapsed area is about 6 km^2 and the collapse was about 60 m, on average. Related to this collapse pyroclastic currents were generated within the caldera depression (layer D2). New vents opened along the faults and erupted pyroclastic surges that overtopped the northern sector of the morphological boundary of the caldera and flowed into the plain. Variation of the structural setting of the Agnano area allowed a large amount of ground water and geothermal fluids to access the reservoir. The following phreatomagmatic explosions marked the beginning of the fourth phase of the eruption, during which highly expanded ash cloud were erupted through vents along the structural boundary of the volcano-tectonic collapse. During the fifth and last phase of the eruption, magma supply

was discontinuous and progressively decreasing. A series of discrete phreatomagmatic explosions generated the ash beds of Member F. Settling of particles suspended in the atmosphere, likely favoured by rainfall, marked the end of the eruption.

The Torciolano exposure. - A sequence of the Agnano Monte Spina Tephra is exposed along the north-eastern side of the relict of the Pisani volcano, between Pianura plain and Camaldoli hill (Fig. 35). The exposure is a typical sequence of this tephra at intermediate distance from the vent area (Fig. 36).
Discussion points. - Magmatic vs phreatomagmatic explosions. Lithological and petrological evidences for volcano-tectonic collapse. A Plinian eruption in a densely populated area.

Figure 37 - The Solfatara crater.

Stop 3.2:

The Solfatara volcano

Significance. - A low-magnitude explosive eruption of the Campi Flegrei caldera in the past 5.0 ka. Crater geometry versus structural lineaments. Geochemical monitoring of active volcanoes.
The volcano. - The Solfatara volcano (Fig. 37), about 2 km east-northeast of Pozzuoli, is characterised by a sub-rectangular (0.5x0.6 km) crater, shaped by NW-SE and SW-NE trending faults (Fig. 35).
The Solfatara Tephra (Di Vito et al., 1999) overlies the Monte Olibano and Accademia lavas, both younger than Agnano-Monte Spina Tephra (4.1 ka) and underlies the Astroni Tephras (3.8 ka), from which it is separated by a thin paleosol containing many charcoal fragments. It is distributed over a small area (<1 km^2), and comprises a phreatomagmatic coarse breccia overlain by a sequence of pyroclastic-surge deposits, alternating with pumiceous fallout beds. The breccia contains large blocks of green tuff, altered lavas and dark scoriaceous bombs engulfed in an hydrothermally altered matrix. It is overlain by stratified, dune-bedded deposits composed of accretionary lapilli-bearing ash layers and thin, well-sorted, rounded pumiceous lapilli beds. The juvenile

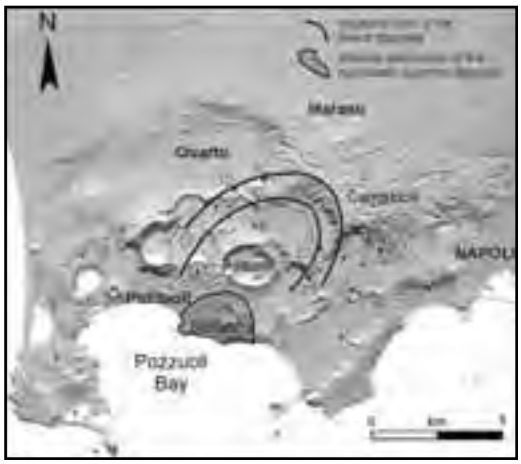

Figure 38 - Distribution of the Solfatara Tephra.

fragments are porphyritic scoriae (basal breccia) and crystal-poor to subaphyric pumice (upper sequence). The scoriae contain crystals of sanidine, plagioclase, clinopyroxene, biotite and Fe-Ti oxides, in order of decreasing abundance. Rare crystals of leucite converted to analcime are also present. The late erupted pumice fragments are alkalytrachytic in composition and contain rare crystals of plagioclase. A thin layer exposed at Cigliano, Torre Caracciolo and Verdolino is likely a distal counterpart of the Solfatara Tephra (Fig. 38) (Di Vito et al., 1999).
This layer, grey to yellowish in colour, is massive and consists of fine-to-coarse ash with scattered pumice clasts and interbedded pumice beds. It is a fallout deposit dispersed towards the north-east with a minimum measured thickness of 5 cm at Verdolino, about 7 km from vent. The sedimentological characteristics of the Solfatara Tephra suggest that the eruption was dominated by phreatomagmatic, with subordinate magmatic explosions.

The geothermal system. - The crater of the Solfatara has been the site of an intense hydrothermal activity

since Greek times. It is the most impressive manifestation of the present hydrothermal activity of the caldera, which includes both focused vents, with a maximum temperature of about 160°C (Bocca Grande fumarole), and large areas of hot steaming ground. The average molar composition of the fluids is H2O about 82 %, CO2 17.5%, H2S 0.13% and minor amounts of N2, H2, CH4 and CO. The isotopic compositions of H2O, CO2 and He suggests the involvement of magmatic gases in the feeding system of the fumaroles (Chiodini et al., 1997). Subsequently the original magmatic gases are condensed by an aquifer system as suggested by the absence of the soluble acid gases SO2, HCl and HF, typical of the high-temperature volcanic gas emissions. Boiling of this heated aquifer(s) generates the Solfatara fumaroles.

At present the Solfatara is the main object of the geochemical surveillance of the caldera. In particular both the chemical compositions of the fumarolic fluids and CO2 fluxes from the soil of the crater are monitored.

The hydrothermal system can be simplified in three main zones:

zone 1) - a heat source represented by a relatively shallow (few kilometres deep) magma chamber;

zone 2) - an aquifer located above the magma chamber. The magma body transfers to the aquifer(s) mainly heat, causing an intense boiling process;

zone 3) - the shallower part of the system is characterised by the presence of superheated vapour produced by boiling of the aquifer. In 1982, temperature and pressure, estimated on the base of gas composition, were close to the conditions of maximum enthalpy of the steam (236°C, 31 bar).

Since the 1982 unrest, systematic geochemical monitoring began providing 175 samples (from 1983 to 2003) for the hottest vent (Bocca Grande, T = 150–164°C), that is considered representative of the entire fumarolic field of Solfatara. Strong variations involving both main and minor gas species were observed during the bradyseismic crises in 1982–1984, 1989, 1994, and 2000. A physical modelling was recently applied to explain these recent bradyseismic crises (Chiodini et al., 2003). The model hypothesizes periodic injections of hot CO2-rich fluids at the base of a shallow hydrothermal system (Fig.1), consistent with the observed chemical variations. Moreover the model predicts an average increase in pore pressure and temperature within the system, suggesting potential effects on ground deformation. Interestingly, compositional peaks systematically follow the corresponding maximum uplift, with a delay of the order of few hundreds days (Fig. 39).

Systematic measurements of the soil CO2 fluxes from the Solfatara crater began in 1995. The measurements are done with the accumulation chamber 'time 0' method which allows one to perform quick and reliable punctual measurements (Carapezza and Granieri, 2004).

The evolution in time of the degassing process is monitored through the following 3 different types of measurements:

- detailed campaigns covering most of the floor of the Solfatara crater (4-5 per year). Soil CO_2 flux and soil temperature (20 cm depth) at 200 points regularly spaced, are measured during each campaign . Therefore three specific campaigns (400 measurement points), covering the entire anomalous area of the Solfatara, were carried out in March-April 1998, in July 2000 and in July 2003. The results are impressive: the area degas about 1000-1500 ton/d of CO_2. This amount is of the same order of magnitude or higher than the amount of gas released from an erupting volcano;

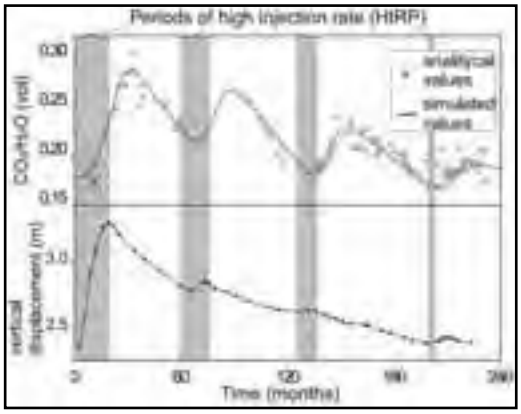

Figure 39 - (a) Comparison between observed (open dots) and simulated (solid line) gas composition expressed as CO_2/H_2O (molar ratio). The shaded area highlights periods of enhanced fluid injection (HIRP); (b) Ground deformation.

- quick campaigns (50-70 per year). Sixty selected, fixed, points are weekly measured in order to investigate the seasonal variations of the degassing process;
- continuous measurements. Since October 1997

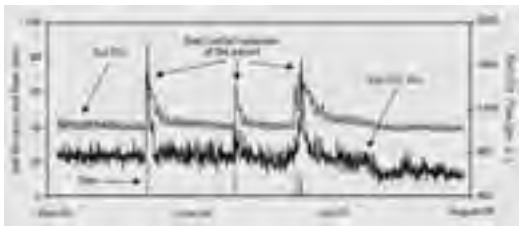

Figure 40 - Soil relative humidity, soil ∀CO2 and rainfall chronograms at Solfatara site from May to August, 1999. The positive anomalies of the soil humidity, due to rainfall episodes, produce a growth in the soil ∀CO2.

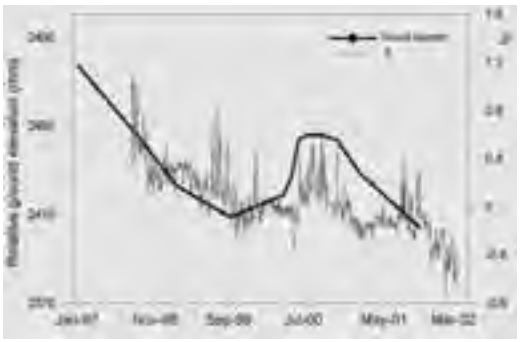

Figure 41 - Long-term trend of the filtered soil CO_2 signal (Xt) and soil deformation chronograms at Solfatara site. The best correlation is obtained by back-shifting the Xt series by three months.

an automatic station measures soil CO_2 fluxes and environmental parameters (air temperature, air humidity, air pressure, wind speed, soil temperature and soil humidity) (Fig. 40). The measurements are performed every 2 hours. The statistical analysis of dataset showed that (1) the highest frequency fluctuations are due to variations of environmental parameters (particularly soil humidity and air temperature) and (2) the long-term trend of the filtered data is correlated with the ground deformation (Granieri et al., 2003) (Fig. 41).

Discussion points. - A volcano in a fumarolic stage within a densely populated area. Does a low-magnitude explosive eruption generate hazards in urban areas?

Stop 3.3:

Averno lake

Significance. - Averno 1 and 2, and Mt. Nuovo eruptions, the only eruptions within the north-western sector of the Campi Flegrei caldera in the past 5 ka.

The volcano. - Averno 1 (4.5 ka), Averno 2 (3.7 ka)

Figure 42 - Stratigraphic sequence of the Averno 2 Tephra

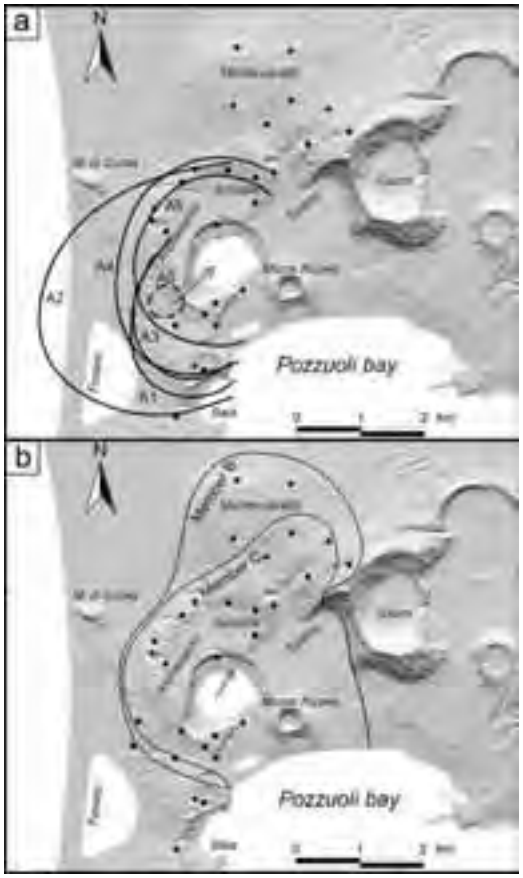

Figure 43 - Distribution of the Averno 2 Tephra. a: isopachs of the fallout deposits of Member A, arrow indicates direction of vent migration; b: pyroclastic-currents deposits of Member B and C.

and Mt. Nuovo (1538 AD) are the only three eruptions over the last 5 ka in the northwestern sector of the Campi Flegrei caldera, at the intersection of NE-SW and NW-SE fault systems, bordering towards the north-west the most uplifted portion of the resurgent block within the Neapolitan Yellow Tuff caldera floor (Orsi et al., 1996).

The Averno 2 eruption was characterised by magmatic and phreatomagmatic explosions which produced a sequence of pyroclastic-fall and -surge deposits. The whole sequence has been subdivided into three members named A through C (Fig. 42; Di Vito et al., 2004).
Member A was emplaced during the first phase of the eruption by prevailing magmatic explosions which generated six fallout beds deposited by columns reaching a maximum height of 10 km.
The subsequent phases of the eruption generated explosions driven by variably efficient water-magma interaction with formation of wet to dry surges, which emplaced Member B and C, respectively. Isopachs and isopleths maps of fallout deposits, as well as areal distribution of both ballistic fragments and facies of surge beds (Fig. 43), suggest a vent migration during the course of the eruption from south-west to north-east, likely along the NE-SW fault system. This migration contributed to the irregular shape of the crater, elongated towards the south-west, and presently filled by a perennial lake. The erupted magma was about 0.05 km^3 (DRE).

Pumice fragments show variable vesicularity and porphyricity. Texture varies from aphyric to porphyritic and glomero-porphyritic, with groundmass mostly holohyaline. Porphyricity ranges from less than 1 to about 9 vol. % of plagioclase, alkali-feldspar, biotite and clinopyroxene. The first erupted rocks are weakly peralkaline alkali-trachyte, while the last erupted are alkali-trachyte. Sr- and Nd-isotope ratios are constant throughout the sequence; slightly more radiogenic values have been detected in fallout layers 3 and 4 of Member A.
Variation of major and trace elements content suggests that during the eruption two distinct magma layers were tapped. The most evolved, peralkaline, uppermost magma layer was tapped during the first phase, while the least evolved, lowermost magma layer was extruded during both last magmatic phases of Member A, and last phreatomagmatic phases of the eruption. The slightly peralkaline character of the magma, as well as of those feeding the other eruptions occurred in the western sector of the Campi Flegrei caldera over the past 5 ka, suggests that only in this sector small batches of magmas can stagnate at shallow depth for a time long enough to drive their chemical character toward peralkalinity. Furthermore, a slight though significant change in the geochemical and isotopic characteristics of the products occurred during emplacement of Member A, contemporaneously with the first migration of the vent. Thus, the eruption demonstrates that a close relationship may exist between structural setting and magma composition and variation, even in a very small magmatic system.

<u>Discussion points.</u> – *The* relationships among deformation dynamics, eruption vents location and magma composition in a resurgent caldera.

Stop 3.4:

Serapeo Marketplace and bradyseismic events

Significance. - Short-term deformation in a resurgent caldera.

The Serapeo. - Ground deformation in the Neapolitan Yellow Tuff caldera over the past 2 ka, is documented at the Serapeo roman monument in Pozzuoli (Parascandola 1947). The Serapeo (Fig. 44), located few tens of meters inland at Pozzuoli, was first supposed to be a temple devoted to the Egyptian god Serapis, from which the name. Only at the beginning

Figure 44 - The Serapeo marketplace at Pozzuoli.

of last century was recognized as a marketplace. Excavation of the monument began in 1750, by order of Charles of Bourbon the king of Naples, in an area called "the vineyard of the three columns" because three marble columns were coming out of the ground. After excavation, the columns showed lythodomes holes up to 7 m above the floor of the monument, testifying the maximum subsidence of the area (Fig. 44).

The monument, constructed between the end of the I and the beginning of the II century AD, was restored at the beginning of the III century AD because sea water had invaded its floor. Since then the ground was subsiding until the X century AD when it began to uplift (Fig. 6d). This uplift lasted until the 1538 Monte Nuovo eruption. Since the beginning of the XVI century AD there was an acceleration of the uplift as testified by royal edicts with which newly-formed land was ceded to the town of Pozzuoli. In the last few days before the Monte Nuovo eruption an uplift of 5 to 8 m took place in the vent area (Parascandola, 1947). After the eruption the ground has subsided until 1969 (Fig. 6d).

Issel (1883) coined the word bradyseism (from the greek bradi = slow and seism = movement) to mean slow subsidence or uplift of the ground. The word is in use in the volcanological literature on the Campi Flegrei caldera since the beginning of last century to mean the vertical ground movements in historical times.

Two major unrest episodes (bradyseismic events) have occurred between 1969 and 1972, and 1982 and 1984 (Fig. 6d) (see Orsi et al. 1999a for references). The maximum ground uplift was about 170 and 180 cm, respectively. Since 1984 the ground has been generally affected by subsidence interrupted by small episodes of inflation in 1989 (7 cm), 1994 (<1cm), and in 2000 (4 cm), with maximum ground deformation always in the area of Pozzuoli. Only 85 cm of the net uplift has been recovered.

Orsi et al. (1999a) performed detailed analyses of short-term ground deformation and seismicity of the 1982-84 unrest episode. The shape of the deformation despite its amount and versus, is invariant in time and space. Furthermore, the analysis of the vertical ground movement carried out along three alignments radially distributed around the area of maximum deforma-

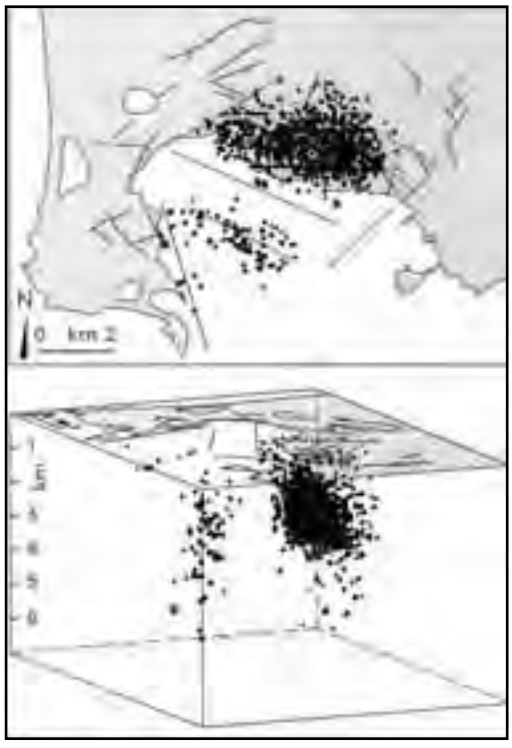

Figure 45 - Plan and 3D view from south-east of the hypocentres of earthquakes occurred in the 1982-84 unrest episode.

tion, showed significant breaks in slope, independent from amount and versus of the ground movement, in correspondence of known structural discontinuities. Seismicity was concentrated mostly in the area of the maximum vertical movement and subordinately in the western part of the bay of Pozzuoli. The depth of the hypocentres varied from a few meters to about 5 km (Fig. 45).

The hypocenters of the events occurred along the Averno-Capo Miseno and Mofete-Banco di Nisida alignments, span from very shallow depth to 5 km. Those of the events occurred along the faults systems bordering the seismogenetic area towards the north-west and the south-east, were at intermediate depth. Focal mechanisms showed four main solutions: normal, normal/strike-slip, strike-slip and reverse/strike slip. Most of the events occurred between the San Vito-Agnano alignment and the Pozzuoli coast showed normal-type solution. The events that occurred along the Mofete-Nisida alignment were characterised by reverse/strike-slip and strike-slip solutions.
This short-term deformation has been interpreted by Orsi et al. (1996, 1999a, c) as the result of the interplay of a ductile and a brittle component. The authors have suggested that both components are generated by a pressure and temperature increase in the shallow magma reservoir due to the arrival from depth of small magma batches, less evolved and hotter than the resident magma. The ductile component could result from the expansion and migration of geothermal fluids due to temperature increase. The brittle component could be generated by a slip along fault planes in the shallow crust above the magma reservoir. Ground deformation data and both epicentres and hypocentres location of the earthquakes occurred during the bradyseismic events and show that the deformed area has a polygonal shape defined by fault systems of the resurgent block inside the Neapolitan Yellow Tuff caldera (Orsi et al., 1999a). This geometry is also well constrained by SAR interferometry data (Lundgren et al. 2001). The striking similarity between ground deformation geometry occurred during the recent bradyseismic events and that of the III epoch, suggests that the resurgence dynamics is not changed since the quiescence period between the II and III epoch. The similarity in shape between long- and short-term deformation corroborates the hypothesis that the former results from the summation of many short-term deformation events (Orsi et al., 1996).

Discussion points. - Relationships between long- and short-term deformation in a resurgent caldera. Hazards related to unrest episodes. Relationships between unrest episodes and eruptions.

DAY 4

Stop 4.1:
Ischia

Significance. - A circumnavigation of the island, devoted to the illustration of its stratigraphical, volcanological, structural and geomorphological features.
From Ischia Porto to Carta Romana. - The Ischia harbour was made in 1853-54 by cutting a narrow strip of land, separating a crater lake from the sea (Fig. 46). The deposits related to this crater are

Figure 46 - The Ischia harbour crater: view from north.

alkalitrachytic scoria fallout layers and surge beds, which overlay a paleosol containing archaeological findings of the VI-V century BC (see Sansivero, 1999 for references).
Out of the harbour, the area comprised between Costa Sparaina and Mt. Rotaro is well exposed south-westward (Fig. 47). Costa del Lenzuolo is a half moon shaped ridge that degrades toward the morphological heights of Bosco dei Conti to the east. Its morphology results from lava domes covered by pyroclastic deposits younger than the XI century AC The morphological heights toward west are the Mt. Maschiata-Montagnone complex. The superimposition of the Montagnone dome (the northernmost height) over the remnant of the Mt. Maschiata dome is clearly visible (Fig. 47).
The pine-wood extending from the coast south-westward, grows on the lava flows of the 1302 AD Arso eruption (Fig. 47), the last on the island.. The flows, erupted from a vent located 2.7 km inland, have a maximum width of 1 km, a thickness of 40-50 m and vary in composition from trachyte to latite.

The islet on which the Aragonese Castle is built is an

Figure 47 - View from NE of the area between C. Sparaina and Mt. Rotaro.

alkalitrachytic lava dome (130 ka). The northern cliff is a section through the central part of the dome along which its feeding conduit and internal structure are well exposed (Fig. 48).
Beyond the islet a well exposed steep scarp is the morphological evolution of a NE-SW trending regional fault that downthrown the northern part of the Mt. Vezzi block (Fig. 49). The rocks that compose this block, the oldest outcropping on the island, are exposed along the cliffs of the south-eastern coast. The flat lowland to the north-west of Mt. Vezzi is bordered toward west by a series of differentially displaced blocks, whose uplifting is maximum for the Mt. Epomeo. Most of the vents active in the past 10 ka are in this area, which is under an extensional stress regime due to the simple-shearing mechanism of resurgence.
At Carta Romana there are many subaqueous thermal springs whose alignment follows a regional tectonic trend.

Figure 48 - The northern slope of the Aragonese castle lava dome (130 ka).

<u>From Carta Romana to Punta della Signora.</u> - At the southern end of the Carta Romana beach, a sea cliff extends along the south-eastern coast up to Punta della Signora. From Carta Romana to II Porticello bay, the base of the cliff is composed of alkalitrachytic lavas of the Parata unit (73 ka). These lavas are overlain by pyroclastic-fall and -flow deposits belonging to variable units. Pyroclastic-fall deposits erupted either at Procida or at the Campi Flegrei caldera, occur in this sector of the island. They overlay products older than 75 ka. At Punta della Pisciazza, erosion has dissected a dome and a scoria cone (>75 ka), both alkalitrachytic. The feeding system of the dome is well exposed. The sea floor between the islands of

Figure 49 - View from NE of the Torone-Mt. Cotto alignment, bordering toward north a flat lowland.

Ischia and Procida is characterised by morphological features, likely remnants of volcanic cones.
A section through a trachybasaltic scoria cone and its feeding system is well exposed at Grotta di Terra (Fig. 50). The cone lies on a NE-SW trending fracture, parallel to the already described regional fault system. Its eruption marked the beginning of the 28-18 ka period of activity. The succession exposed in the sea cliff includes from top to bottom: pyroclastic deposits of the last period of activity (<10 ka); the scoria deposit and the feeding dyke of the Grotta di Terra cone (28

Figure 50 - Grotta di Terra. 1: lavas older than 75 ka; 2: pyroclastic deposits aged between 75 and 55 ka; 3: pyroclastic deposits of the 55-33 ka period of activity; 4: trachybasaltic Grotta di Terra dyke and scoriae (28 ka); 5: pyroclastic deposits of the past 10 ka.

ka); pyroclastic deposits of the 55-33 ka period of activity; pyroclastic deposits aged between 75 and 55 ka; lava flows older than 75 ka.
In the central part of the II Porticello bay, pyroclastic deposits overlay the Parata lavas, while in the western part, up to Punta della Cannuccia, they overlay lava flows of the Mt. Vezzi complex (126 ka). The oldest rocks on the island are exposed in this area, behind the Spiaggia di San Pancrazio. The San Pancrazio promontory is composed of a sequence of lavas of

Figure 51 - View of the eastern part of the Scarrupata di Barano cliff. 1: lava flows older than 75 ka; 2: pyroclastic deposits aged between 75 and 55 ka; 3: Mt. Epomeo Green Tuff sequence; 4: pyroclastic deposits of the 28-18 ka period of activity; 5: pyroclastic deposits of the past 10 ka.

the Mt. di Vezzi volcanic complex, intercalated with pyroclastic deposits. The upper part of this sequence includes the Mt. Epomeo Green Tuff.

The Scarrupata di Barano is a sea cliff that extends from Punta San Pancrazio to La Guardiola promontories (Fig. 51). Along this cliff the stratigraphic relationships among the products of the oldest activity are discernible, as they are little deformed by tectonics. The massive yellow-white ignimbrite, which forms most of the top of the cliff (marked at its base by a black scoria layer), has previously been correlated with the Mt. Epomeo Green Tuff. Work is currently being undertaken on the Mt. Epomeo Green Tuff stratigraphy and on earlier erupted deposits (Brown et al., 2004).

The La Guardiola, Capo Grosso and Punta della Signora promontories are composed of alkalitrachytic lavas (147 ka) overlain by this yellow-white ignimbrite and by later pyroclastic units, which are mainly composed of pyroclastic-fall and -flow deposits.

From Punta della Signora to S. Angelo promontory.

The Lido dei Maronti is a beach between Punta della Signora and S. Angelo promontories. At its eastern termination we will cross again the fault bordering the Mt. Vezzi block. Coastal exposures are the products of the dismantling of the Mt. Epomeo block, which are composed of very recent landslides and mud-flows, and older catastrophic debris avalanches that travelled as far as 40 km toward south (Chiocci et al., 1998). At the base of the S. Angelo promontory an alkalitrachytic lava dome (100 ka) is overlain by block-and-ash-flow and pyroclastic-fall and -flow deposits belonging to explosive volcanism that preceeded the Mt. Epomeo Green Tuff eruption (Brown et al., 2004). This is overlain by pyroclastic deposits aged between 55 and 20 ka. The youngest pyroclastic unit (20 ka), mostly composed of pyroclastic-surge deposits, lies unconformably over the older rocks. The S. Angelo village is built on mud flows that overlay these pyroclastic deposits.

From S. Angelo promontory to Punta Imperatore.

- The cliff between S. Angelo and Punta Chiarito is eroded into the surge deposits forming the top of the S. Angelo promontory.The Punta Chiarito promontory (Figs. 52, 53) is composed of alkalitrachytic lava flows, unconformably overlain by the youngest pyroclastic unit of the S. Angelo sequence. The uppermost deposits are the products of superficial gravitational movements.

In the bay between Punta Chiarito and Capo Negro, a NNE-SSW trending fault downthrows the eastern side bringing into contact the unit overlying the Punta Chiarito lavas with a pyroclastic sequence, likely of the 55-33 ka period of activity (Fig. 52).

The Capo Negro promontory is composed of alkali-

Figure 52 - View of the Chiarito bay. 1: lava domes older than 75 ka; 2: pyroclastic deposits of the 55-33 ka period of activity; 3a, 3b and 3c: pyroclastic deposits of the 28-18 ka period of activity.

Figure 53 - View between Capo Negro and P. Chiarito. 1: lava domes older than 75 ka; 2: pyroclastic deposits of the 55-33 ka period of activity; 3: pyroclastic sequence aged between 28 and 20 ka; 4: pyroclastic deposit aged at 20 ka

trachytic lava flows overlain by the same pyroclastic unit, which is in turn overlain by two thick pyroclastic units; the youngest of which is dated at 20 ka (Fig. 53).

The rocks exposed between Capo Negro and Punta Imperatore belong to the 28-18 ka period of activity.
The cliff between Capo Pilaro and Grotte del Mavone includes alkalitrachytic lavas with minor welded-scoria layers of the Pilaro complex, overlain by a sequence of alternating welded-scoriae and pumice-fall layers of the Scarrupo di Panza complex, and two younger pyroclastic units.

At the base of the Grotte del Mavone promontory, alkalitrachytic lavas (28 ka) are exposed.
In the cliff between Grotte del Mavone promontory and Punta Imperatore, a section through the Scarrupo di Panza volcano is well exposed. The section in its middle part is composed of a thick sequence (ca.100 m) of intensely welded scoriae, while at Grotte del Mavone, towards the south, and at Punta Imperatore, towards the north, it includes alternating layers of pumice-fall and welded scoriae interpreted by Rittmann (1930) as the products of a lava lake. In the bay between Grotte del Mavone and Punta dello Schiavo, this sequence is overlain by alkalitrachytic lavas (24 ka) and by two pyroclastic units composed of pyroclastic-fall and -surge deposits. Therefore the Scarrupo di Panza eruption must have occurred between 28 and 24 ka bp.
The base of Punta Imperatore promontory is composed of alkalitrachytic lavas (117 ka) covered by a pyroclastic breccia erupted prior to the Mt. Epomeo Green Tuff (Brown et al., 2004). This lithic breccia is overlain by a thick (c. 40 m) pumice-fall breccia with several intercalated scoria layers. A white ignimbrite, which may relate to the Mt. Epomeo Green Tuff eruption, fills a small valley cut into this thick fall deposit (Fig. 54). On the southern slope of the promontory this sequence attains a maximum thickness of 50 m and is unconformably covered by the products of the Scarrupo di Panza eruption that are in turn unconformably overlain by the pyroclastic units of the 28-18 ka period of activity. Along the northern side of the promontory, beneath the products of the Scarrupo di Panza eruption, is the Pietre Rosse pyroclastic unit (46 ka), which pinches out at the western end of the slope. This unit overlies the Mt. Epomeo Green Tuff and the sequence of pyroclastic units separated by paleosols that along this side of the promontory, pinches out eastward.
<u>*From Punta Imperatore to Zaro*</u>. –The Citara beach extends between Punta Imperatore and Pietre Rosse . Along the cliff behind the Citara beach, the Pietre Rosse unit is well exposed and contains

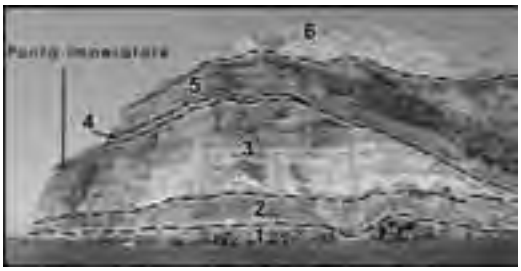

Figure 54 - Punta Imperatore promontory. 1: lava flows older than 75 ka; 2: breccia deposit at the base of the sequence aged between 75 and 55 ka; 3: pyroclastic sequence aged between 75 and 55 ka; 4: Mt. Epomeo Green Tuff sequence; 5: deposit of the Scarrupo di Panza volcano; 6: pyroclastic deposit of the 28-18 ka period of activity.

U-shaped channels. This tuff can be followed from Punta Imperatore to Pietre Rosse and represents the remnant of a tuff-ring whose vent was very likely located in this stretch of sea. A good section of this tuff is exposed at Pietre Rosse (Fig. 55). From its base upwards the sequence includes an ignimbrite deposit surmounted by a succession of surge beds with intercalated pumice-fall deposits.
From Pietre Rosse to Zaro the coast is low and formed by piles of landslide and debris-flow deposits derived from the Mt. Epomeo block. From this position it is possible to have a good view of the western slope of the Mt. Epomeo block (Fig. 56).
It is bordered by inward dipping, high angle reverse

Figure 55 - Pietre Rosse promontory. Natural section of the exposed pyroclastic sequence.

faults, whose directions vary from N40E to NS and N50W, from the north-western to the south-western parts of the block, testifying a compressional stress regime. These features are cut by late outward dipping normal faults due to gravitational readjustment of the slopes (Marotta, 2001). The north-eastern and south-western sides are bordered by vertical faults with right transtensive and left transpressive movements, respectively (Marotta, 2001).

Rione Bocca is the only locality within the resurgent area where the base of the Mt. Epomeo Green Tuff is exposed. Here, it overlies several metres of marine sediments, which in turn overlie an alkalitrachytic lava (133 ka). Recent work has shown that the Mt. Epomeo Green Tuff, as exposed at Rione Bocca, comprises two flow-units, each comprising a coarse heterolithic breccia at their base that passes up into a massive crystal and pumice rich ignimbrite (Brown et al, 2004). These flow units are separated by several metres of reworked, slumped and convoluted sediments. Towards Ciglio and Serrara the contact between yellowish pyroclastic deposits (33 ka) dipping at high angle south-westward, and the Mt. Epomeo Green Tuff is exposed. The contact is defined by a high-angle reverse fault generated by the Mt. Epomeo block resurgence. The high dip of the pyroclastic deposits is due to tilting produced by faulting. This geometrical relationships is an evidence that resurgence is active at least since 33 ka bp.

Sailing northward, beyond the Forio village there is the Zaro promontory, composed of a discrete number of superposed lava domes and flows, likely emplaced in a short time-span, along a complex network of N45E, N50W and subordinately E-W trending fractures. The vents for this volcanism are among the very few of the last period of activity located outside the eastern sector of the island.

Figure 56 - The western slope of Mt. Epomeo block between Ciglio and Capo dell'Uomo.

<u>*From Zaro to Ischia Porto.*</u> - Doubled the Zaro promontory we will find ourselves in the San Montano bay which is delimited by the Zaro lava domes and flows and the Mt. Vico promontory. The basal part of Mt. Vico promontory is composed of phonolitic lavas (75 ka). On these lavas, in small morphological depressions, is a sequence of pyroclastic-fall deposits of unknown provenance separated by paleosols. On the eastern slope of the Mt. Vico promontory, the lavas are unconformably covered by deposits attributed to the Mt. Epomeo Green Tuff that are in turn overlain by a succession of pyroclastic-surge and minor -fall beds (San Montano unit; 33 ka). On the upper part of the promontory, above a paleosol containing archaeological findings of roman age, is a pyroclastic deposit of uncertain provenance. Between Mt. Vico and Casamicciola the coast is cut into landslide and debris-flow deposits

derived from the Mt. Epomeo block, whose northern slope is well visible. This slope is an E-W trending section through the block and shows its asymmetrical shape with the high angle western slope and the gently degrading eastern slope. From Casamicciola to Ischia Porto the products of the past 10 ka of activity are well exposed. They include lava flows and domes and both magmatic and phreatomagmatic pyroclastic deposits of the Mt. Rotaro and Mt. Montagnone composite volcanoes, older lava flows and domes and the remnant of some tuff-cones, aged between the XIII and the VIII century BC.

Discussion points. - Relationships among magmatism, tectonism, volcanism, volcano-tectonism and surface processes.

References cited

Arienzo, I., Civetta, L., D'antonio, M. and Tonarini, S. (2004). Mantle and crustal component for the genesis of phlegraean volcanic district. Earth Planet. Sci. Lett., submitted.

Arrighi, S., Principe, C. and Rosi, M. (2001). Violent Strombolian Eruptions at Vesuvius During post-1631 Activity. *Bull. Volcanol.* 63, 126-150.

Auger, E., Gasparini, P., Virieux, J. and Zollo, A. (2001). Seismic Evidence of an Extended Magmatic sill Under Mt. Vesuvius, *Science*, 9918.

Ayuso, R.A., De Vivo, B., Rolandi, G., Seal Ii, R.R. and Paone, A. (1998). Geochemical and isotopic (Nd-Pb-Sr-O) variations bearing on the genesis of volcanic rocks from Vesuvius, Italy. *J. Volcanol. Geotherm. Res.* 82, 53-78.

Barberi, F., Bizouard, H., Clocchiatti, R., Metrich, N., Santacroce, R. and Sbrana, A. (1981). The Somma-Vesuvio magma chamber: a petrological and volcanological approach. Bull. Volcanol. 44, 295-315.

Barberi, F., Cioni, R., Rosi, M., Santacroce, R., Sbrana, A. and Vecci, R. (1989). Magmatic and phreatomagmatic phases in explosive eruptions of Vesuvius as deduced by grain-size and compositional analysis of pyroclastic deposits. *J. Volcanol. Geotherm. Res.* 38, 287-307.

Belkin, H.E., De Vivo, B., Roedder, E. and Cortini, M. (1985). Fluid inclusion geobarometry from ejected Mt. Somma-Vesuvius nodules. *Am. Mineral.* 70, 288-303.

Bianco, F., Castellano, M., Milano, G., Ventura, G. and Vilardo, G. (1998). The Somma-Vesuvius stress field induced by regional tectonics: evidences by seismological and mesostructural data. *J. Volcanol. Geotherm. Res.* 82, 199-218.

Brancaccio, L., Cinque, A., Romano, P., Rosskopf, C., Russo, F., Santangelo, N. and Santo, A. (1991). Geomorphology and Neotectonic Evolution of a Sector of the Tyrrenian Flank of the Southern Apennines, (Region of Naples). *Z. Geomorph N. F.* 82, 47-58.

Brocchini, D., Principe, C., Castradori, D., Laurenzi, M.A. and Gorla, L., (2001). Quaternary evolution of the southern sector of the Campanian Plain and early Somma-Vesuvius activity: insights from the Trecase 1 well. *Mineral. Petrol.* 73, 67-91.

Brown, R. J., Orsi, G., de Vita, S. and Civetta, L. (2004). Multiple caldera collapse episodes on Ischia. in prep.

Buchner, G. (1986). Eruzioni vulcaniche e fenomeni vulcanotettonici di età preistorica e storica nell'isola d'Ischia. *In* «Tremblements de terre, eruptions volcaniques et vie des hommes dans la Campanie antique» (Centre Jean Bérard, Institut Français de Naples Ed.), 7, 145-188.

Carapezza, M.L and Granieri, D. (2004). CO_2 soil flux at Vulcano (Italy): comparison of active and passive methods and application to the identification of actively degassing structure. *Applied Geochemistry*, 19/1: 73-88..

Cecchetti, A., Marianelli, P. and Sbrana, A. (2001). A deep magma chamber beneath Campi Flegrei? Insights from melt inclusions. GNV Framework Program 2000-2002, I year results: 59-65.

Chiocci F.L., Sposato A., Martorelli E. e gruppo di ricerca TIVolI (1998). Prime immagini TOBI dei fondali del Tirreno centro-meridionale (settore orientale). Geologica Romana 34, 207-222.

Chiodini, G. and Marini, L., (1998). Hydrothermal gas equilibria: the H_2O-H_2-CO_2-CO-Ch_4 system. *Geochim. Cosmochim. Acta* 62, 2637-2687.

Chiodini, G., Frondini, F., Magro, G., Marini, L., Panichi, C., Raco, B., and Russo, M. (1997). Chemical and isotopic variations of Bocca Grande fumarole (Solfatara volcano, Phlegrean Fields). *Acta Vulcanologica* 8 (2), 228-232.

Chiodini, G., Marini, L. and Russo, M., (2001). Geochemical evidence for the existence of high-temperature hydrothermal brines at Vesuvio volcano, Italy. *Geochim. Cosmochim. Acta* 65 (13), 2129–2147.

Chiodini, G., Todesco, M., Caliro, S., Del Gaudio, C., Macedonio, G., and Russo, M. (2003). Magma degassing as a trigger of bradyseismic events: the case of Phlegrean Fields (Italy). *Geophys. Res. Lett.* 30, 1434.

Cioni, R., E. Corazza, and L. Marini, (1984). The

gas/steam ratio as indicator of heat transfer at the Solfatara fumaroles, Phlegrean Fields (Italy). *Bull.Volcanol*. 47, 295–302.

Cioni, R., Santacroce, R. and Sbrana, A. (1999). Pyroclastic Deposits as a Guide for Reconstructing the Multi-Stage Evolution of the Somma-Vesuvius Caldera. *Bull. Volcanol.* 60, 207-222.

Cioni, R., Sulpizio, R. and Garruccio, N. (2003). Variabilità of the eruption dynamics durino a Subplinian event: the Greenish pumice eruption of Somma-Vesuvius (Italy). *J. Volcanol. Geotherm. Res*. 124, 89-114.

Civetta, L. and Santacroce, R. (1992). Steady state magma supply in the last 3400 years of Vesuvius activity. *Acta Vulcanologica* 2, 147-159.

Civetta, L., D'Antonio, M., De Lorenzo, S., Di Renzo, V. and Gasparini, P. (2004). Thermal and geochemical constraints to the "deep" magmatic structure of Mt. Vesuvius. J. Volcanol. Geotherm. Res., in press.

Civetta, L., Gallo, G. and Orsi, G. (1991a). Sr- and Nd- isotope and trace-element constraints on the chemical evolution of the magmatic system of Ischia (Italy) in the last 55 ka. *J. Volcanol. Geotherm. Res.* 46, 213-230.

D'Antonio, M., Civetta, L., Arienzo, I., Carandente, A., Di Renzo, V., Di Vito, M.A., Giordano, F. and Orsi, G. (2004). Magmatic history of Mt. Vesuvius on the basis of new geochemical and isotopic data. *J. Petrol.,* in press.

D'Antonio, M., Civetta, L., Orsi, G., Pappalardo, L., Piochi, M., Carandente, A., de Vita, S., Di Vito, M. A., Isaia, R. and Southon, J. (1999). The present state of the magmatic system of the Campi Flegrei caldera based on the reconstruction of its behaviour in the past 12 ka. *J. Volcanol. Geotherm. Res.* 91, 247-268.

D'Argenio, B., Pescatore, T. S. and Scandone, P. (1973). Schema geologico dell'Appennino Meridionale. *Acc. Naz. Lincei, Quad*. 183, 49-72.

de Vita, S., Orsi, G., Civetta, L., Carandente, A., D'Antonio, M., Di Cesare, T., Di Vito, M.A., Fisher, R.V., Isaia, R., Marotta, E., Ort, M., Pappalardo, L., Piochi, M. and Southon, J. (1999). The Agnano-Monte Spina eruption (4.1 ka) in the resurgent, nested Campi Flegrei caldera (Italy). *J. Volcanol. Geotherm. Res.* 91, 269-301.

De Vivo, B., Rolandi, G., Gans, P.B., Calvert, A., Bohrson, W.A., Spera, F.J. and Belkin, H.E. (2001). New constraints on the pyroclastic eruptive history of the Campanian volcanic Plain (Italy). *Mineral. Petrol.* 73, 47-65.

Deino, A.L., Orsi, G., Piochi, M. and de Vita, S. (2004). The age of the Neapolitan Yellow Tuff caldera-forming eruption (Campi Flegrei caldera – Italy) assessed by $^{40}Ar/^{39}Ar$ dating method. *J. Volcanol. Geotherm. Res.,* in press.

Dellino, P., Isaia, R. and Veneruso, M. (2004b). Turbulent boundary layer shear flow as an approximation of pyroclastic surge: implication for hazard assessment at Phlegraean Fields. *J. Volcanol. Geotherm. Res.*, in press.

Dellino, P., Isaia, R., La Volpe, L. and Orsi, G. (2001). Statistical analysis of textural data from complex pyroclastic sequence: implication for fragmentation processes of the Agnano-Monte Spina eruption (4.1 ka), Phlegraean Fields, southern Italy. *Bull. Volcanol.* 63, 443-461.

Dellino, P., Isaia, R., La Volpe, L. and Orsi, G. (2004a). Interference of particles fallout on the emplacement of pyroclastic surge deposits of the Agnano-Monte Spina eruption (Phlegraean Fields, Southern Italy). *J. Volcanol. Geotherm. Res.*, in press.

Di Girolamo, P., Ghiara, M.R., Lirer, L., Munno, R., Rolandi, G.and Stanzione, D. (1984). Vulcanologia e petrologia dei Campi Flegrei. *Boll. Soc. Geol. It.* 103, 349-413.

Di Vito, M. A., Isaia, R., Orsi, G., Southon, J., de Vita, S., D'Antonio, M., Pappalardo, L. and Piochi, M. (1999). Volcanic and deformational history of the Campi Flegrei caldera in the past 12 ka. *J. Volcanol. Geotherm. Res.* 91, 221-246.

Di Vito, M. A., Lirer, L., Mastrolorenzo, G. and Rolandi, G. (1987). The Monte Nuovo eruption (Campi Flegrei, Italy). *Bull. Volcanol.* 49, 608-615.

Di Vito, M., D'Antonio, M., Braia, G., Carrol, M., Civetta, L., Isaia, R., Orsi, G., Piermattei, M. (2004). The Averno 2 eruption (Campi Flegrei caldera, Italy): influence of structural setting on magma evolution and eruption history. In prep.

Dubois, C. (1907). Pozzuoles Antique; Historie et topographie. Paris, Albert Fontemoing, 249-268.

Fedele, F., Giaccio, B., Isaia, R. and Orsi, G. (2003). The Campanian Ignimbrite eruption, Heinrich Event 4, and Palaeolithic change in Europe: a high-resolution investigation. *In* "Volcanism and Earth's Atmosphere", (A. Robok and C. Oppenheimer Ed.). AGU book, 139, 301-325.

Ferrucci, F., Gaudiosi, G., Pino, N. A. and Luongo, G. (1989). Seismic detection of a major moho upheaval beneath the Campania volcanic area (Naples, southern Italy). *Geophys. Res. Lett.* 16, 1317-1320.

Fisher, R.V. (1983). Flow transformations in sediment gravity flows. *Geology* 11, 273-274.

Volume n° 2 - from B16 to B33

Fisher, R.V., Orsi, G., Ort, M. and Heiken, G. (1993). Mobility of large-volume pyroclastic flow – emplacement of the Campanian Ignimbrite, Italy. *J. Volcanol. Geotherm. Res.* 56, 205-220.

Fulignati, P., Marianelli, P., and Sbrana,A. (1998). The 1944 eruption. *In* "Cities on volcanoes Field Excursion Guidebook" (G. Orsi, M.A. Di Vito and R. Isaia, Ed.), pp. 86-96. Osservatorio Vesuviano, Naples.

Giggenbach, W.F. (1987). Redox processes governing the chemistry of fumarolic gas discharges from White Island, New Zealand. *Applied Geochemistry* 2, 143-161.

Graham, D.W., Allard, P., Kilburn, C.R.J., Spera, F.J. and Lupton, J.E. (1993). Helium isotopes in some historical lavas from Mount Vesuvius. *J. Volcanol. Geotherm. Res.* 58, 359-366.

Granieri, D., Chiodini, G., Marzocchi, W., and Avino, R. (2003). Continuous monitoring of CO_2 soil diffuse degassing at Phlegraean Fields (Italy): influence of environmental and volcanic parameters. *Earth Planet. Sci. Lett.* 212, 167-179 .

Gurioli, L., Cioni, R., Sbrana, A. and Zanella, E. (2002). Transport and depositino of pyroclastic density currents over an inhabited area: the deposits of the AD 79 eruption of Vesuvius at Herculaneum, Italy. *Sedimentology* 49, 929-953.

Imbò, G. (1949). L'attività eruttiva vesuviana e relative osservazioni nel corso dell'intervallo intereruttivo 1906-1944 ed in particolare del parossismo eruttivo del marzo 1944. *Annali Oss. Vesuviano* serie V, 185-380.

Isaia, R., D'Antonio, M., Dell'Erba, F., Di Vito, M. A. and Orsi, G. (2004). The Astroni volcano: the only example of close eruptions within the same vent area in the recent history of of the Campi Flegrei caldera (Italy). *J. Volcanol. Geotherm. Res.,* in press.

Issel, A. (1883). Le oscillazioni lente del suolo o bradisismi. *Atti R. Univ. Genova*, IV:1-210.

Lajoie, J., Boudon, G. and Bourdier, J.L. (1989). Depositional mechanics of the 1902 pyroclastic nuée-ardente deposits of Mt. Pelée, Martinique. *J. Volcanol. Geotherm. Res.* 38, 131-142.

Lirer, L., Pescatore, T., Booth, P. and Walker, G. P. L. (1973). Two plinian pumice-fall deposits from Somma-Vesuvius, Italy. *Geol. Soc. of Am. Bull.* 84, 759-772.

Lundgren, P., Usai, S., Sansosti, E., Lanari, R., Tesauro, M., Eonaro, G. and Berardino, P. (2001). Modeling surface deformation observed with synthetic aperture interferometry at Campi Flegrei caldera. *J. Geophys. Research.* 106, 19355-19366.

Marianelli, P., Metrich, N. and Sbrana, A. (1999). Shallow and deep reservoirs involved in magma supply of the 1944 eruption of Vesuvius. *Bull. Volcanol.* 61, 48-63.

Marianelli, P., Metrich, N., Santacroce, R. and Sbrana, A. (1995). Mafic magma batches at Vesuvius: a glass inclusion approach to the modalities of feeding stratovolcanoes. *Contrib. Mineral. Petrol.* 120, 159-169.

Marotta, E. (2001). Processi deformativi all'interno di caldere risorgenti: analisi strutturale dell'isola d'Ischia e comparazione con altre aree risorgenti. PhD Thesis, pp 214. University of Naples, Italy.

Narcisi, B. and Vezzoli, L. (1999). Quaternary stratigraphy of distal tephra layers in the Mediterranean – an overview. *Global Planet. Change* 21, 31-50.

Orsi, G., Civetta, L., D'Antonio, M., Di Girolamo, P. and Piochi, M. (1995). Step-filling and development of a three-layers magma chamber: the Neapolitan Yellow Tuff case history. *J. Volcanol. Geotherm. Res*. 67, 291-312.

Orsi, G., Civetta, L., Del Gaudio, C., de Vita, S., Di Vito, M. A., Isaia, R., Petrazzuoli, S., Ricciardi, G. and Ricco, C. (1999a). Short-Term Ground Deformations and Seismicity in the Nested Campi Flegrei Caldera (Italy): an example of active block resurgence in a densely populated area. *J. Volcanol. Geotherm. Res.* 91, 415-451.

Orsi, G., D'Antonio, M., de Vita, S. and Gallo, G. (1992). The Neapolitan Yellow Tuff, a large-magnitude trachytic phreatoplinian eruption: eruptive dynamics, magma withdrawal and caldera collapse. *J. Volcanol. Geotherm. Res.* 53, 275-287.

Orsi, G., de Vita, S. and Di Vito, M. (1996). The restless, resurgent Campi Flegrei nested caldera (Italy): constraints on evolution and configuration. *J. Volcanol. Geotherm. Res.* 74, 179-214.

Orsi, G., de Vita, S., Di Vito, M., Nave, R. and Heiken, G. (2003a). Facing volcanic and related hazards in the Neapolitan area. *In* "Earth Sciences in the Cities: A Reader" (G. Heiken, R. Fakundiny, J. Sutter, Eds), pp. 121-170. Am. Geophys. Un., Sp. Publ. Series, Vol. 56, Washington.

Orsi, G., Di Vito, M.A. and Isaia, R. (2004b). Volcanic hazard assessment at the restless Campi Flegrei caldera. *Bull. Volcanol.,* in review.

Orsi, G., Gallo, G. and Zanchi, A. (1991). Simple shearing block resurgence in caldera depressions. A model from Pantelleria and Ischia. *J. Volcanol. Geotherm. Res.* 47, 1-11.

Orsi, G., Patella, D., Piochi, M. and Tramacere,

A. (1999b). Magnetic modeling of the Phlegraean Volcanic District with extension to the Ponza archipelago, Italy. *J. Volcanol. Geotherm. Res.* 91, 345-360.

Orsi, G., Petrazzuoli, S. and Wohletz, K. (1999c). The interplay of mechanical and thermo-fluid dynamical systems during an unrest episode in calderas: the Campi Flegrei caldera (Italy) case. *J. Volcanol. Geotherm. Res*. 91, 453-470.

Ort, M., Orsi, G., Pappalardo, L. and Fisher R.V. (2003). Anisotropy of magnetic susceptibility studies of depositional processes in the Campanian Ignimbrite, Italy. Bull. Volcanol. 65, 55-72.

Pappalardo, L., Civetta, L., D'Antonio, M., Deino, A., Di Vito, M. A., Orsi, G., Carandente, A., de Vita, S., Isaia, R. and Piochi, M. (1999). Chemical and isotopical evolution of the Phlegraean magmatic system before the Campanian Ignimbrite (37 ka) and the Neapolitan Yellow Tuff (12 ka) eruptions. *J. Volcanol. Geotherm. Res.* 91, 141-166.

Pappalardo, L., Civetta, L., de Vita, S., Di Vito, M., Orsi, G., Carandente, A., and Fisher R.V. (2002a). Timing of magma extraction during the Campanian Ignimbrite eruption (Campi Flegrei caldera). *J. Volcanol. Geotherm. Res.* 114, 479-497.

Pappalardo, L., Piochi, M., D'Antonio, M., Civetta, L. and Petrini R., (2002b). Evidence of multi-stage magmatic evolution deduced from Sr, Nd and Pb isotope data: the past 60 ka Campi Flegrei (Italy) history. *J. Petrol.* 43, 1415-1434.

Parancandola, A. (1947). I fenomeni bradisismici del Serapeo di Pozzuoli. Genovesi, Napoli.

Polacci, M., Pioli, L. and Rosi, M., (2003). The Plinian phase of the Campanian Ignimbrite eruption (phlegrean Fields, Italy): evidence from density measurements and textural characterization of pumice. *Bull. Volcanol.* 65, 418-432.

Rittmann, A. (1930). Geologie der Insel Ischia. Z. f. Vulkanol. Erganzungsband, 6.

Rittmann, A. (1950). Sintesi geologica dei Campi Flegrei. *Boll. Soc. Geol. It*. 69, 117-177.

Rolandi, G., Mastrolorenzo, G., Barrella, A. N. and Borrelli, A. (1993b). The Avellino Plinian Eruption of Somma-Vesuvius (3760 y.B.P.): the Progressive Evolution From Magmatic to Hydromagmatic Style. *J. Volcanol. Geotherm. Res.* 58, 67-88.

Rosi, M. and Santacroce, R. (1983). The A.D. 472 "Pollena" eruption: volcanological and petrological data for this poorly known plinian-type event at Vesuvius. *J. Volcanol. Geotherm. Res.* 17, 249-271.

Rosi, M. and Santacroce, R. (1984). Volcanic hazard assessment in the Phlegeran Fields: a contribution based on stratigraphic and historical data. *Bull. Volcanol.* 47(2), 359-370.

Rosi, M. and Sbrana, A. (1987). Phlegraean Fields. CNR Quad. de "La ric. sci." 114(9), pp. 167, Roma.

Rosi, M., Principe, C. and Vecci, R. (1993). The 1631 eruption of Vesuvius recunstructed from the review of chronichles and study of deposits. *J. Volcanol. Geotherm. Res.* 58, 151-182.

Rosi, M., Vezzoli, L., Castelmenzano, A. and Grieco, G. (1999). Plinian pumice fall deposit of the Campanian Ignimbrite eruption (Phlegraean Fields, Italy). *J. Volcanol. Geotherm. Res.* 91, 179-198.

Sansivero, F. (1999). Assetto stratigrafico ed evoluzione vulcanologica del settore orientale dell'isola d'Ischia negli ultimi 10 Ka. PhD Thesis, pp. 203, University of Naples, Italy.

Santacroce, R. (1983). A general model for the behavior of the Somma-Vesuvius volcanic complex. *J. Volcanol. Geotherm. Res.* 17, 237-248.

Seymour, K. and Christanis, K. (1995) Correlation of tephra layer in western Greece with a Late Pleistocene eruption in the Campanian province of Italy. *Quaternary Research* 43, 46-54.

Sigurdsson, H., Carey, S., Cornell, W. and Pescatore, T. (1985). The eruption of Vesuvius in 79 A.D.. *National Geographic Res.* 1, 332-387.

Tedesco, D. and Scarsi, P. (1999). Chemical (He, H_2, CH_4, Ne, Ar, N_2) and isotopic (He, Ne, Ar, C) variations at the Solfatara crater (Southern Italy): mixing of different sources in relation to seismic activity. *Earth and Planet. Sci.*171, 465– 480.

Thunnel, R., Federman, A., Sparks R.S.J. and Williams, D. (1979). The origin and volcanological significance of the Y-5 ash layer in the Mediterranean. *Quaternary Research* 12, 241-253.

Tonarini, S., Leeman, W.P., Civetta, L., D'antonio, M., Ferrara, G. and Necco, A. (2004). B/Nb and δ^{11}B systematics in the Phlegrean Volcanic District (PVD). *J. Volcanol. Geotherm. Res.*, in press.

Turi, B. and Taylor, H.P. (1976). Oxygen isotope studies of potassic volcanic rocks of the Roman Province, Central Italy. *Contrib. Mineral. Petrol.* 55, 1-31.

Vezzoli, L. (1988). Island of Ischia. CNR Quaderni de "La ricerca scientifica" 114 (10), pp. 122.

Wohletz, K., Orsi, G. and de Vita, S. (1995). Eruptive mechanisms of the Neapolitan Yellow Tuff interpreted from stratigraphic, chemical and granulometric data. *J. Volcanol. Geotherm. Res.* 67, 263-290.

Zollo, A., Judenherc, S., Virieux, J., Makris, J., Auger, E., Capuano, P., Chiarabba, C., De Franco, R.,

Nichelini, A. and Musacchio, G. (2003). Tomographic imaging of the Campi Flegrei, Southern Italy, Caldera structure by high resolution active seismics. *EGS-AGU-EUG Joint Assembly*, Nice, France 6-11 April 2003, abstract.

Zollo, A., Marzocchi, W., Capuano, P., Lomax, A. and Iannaccone, G. (2002). Space and time behavior of seismic activity at Mt. Vesuvius volcano, Southern Italy. *Bull. Seism. Soc. Am.* 92, 625-640.

Back Cover:
field trip itinerary

FIELD TRIP MAP

32nd INTERNATIONAL GEOLOGICAL CONGRESS

Edited by APAT

Volume n° 2 - from B16 to B33

32nd INTERNATIONAL GEOLOGICAL CONGRESS

THERMO - MECHANICAL EVOLUTION OF THE ALPINE BELT, FROM THE ENGADINE WINDOW TO THE MATTERHORN

Leader: G. Gosso

Associate Leaders: M. Engi, F. Koller, J.M. Lardeaux, R. Oberhaensli, M.I. Spalla

Field Trip Guide Book - B29

Florence - Italy
August 20-28, 2004

Pre-Congress **B29**

The scientific content of this guide is under the total responsibility of the Authors

Published by:
APAT – Italian Agency for the Environmental Protection and Technical Services - Via Vitaliano Brancati, 48 - 00144 Roma - Italy

Series Editors:
Luca Guerrieri, Irene Rischia and Leonello Serva (APAT, Roma)

English Desk-copy Editors:
Paul Mazza (Università di Firenze), Jessica Ann Thonn (Università di Firenze), Nathalie Marléne Adams (Università di Firenze), Miriam Friedman (Università di Firenze), Kate Eadie (Freelance indipendent professional)

Field Trip Committee:
Leonello Serva (APAT, Roma), Alessandro Michetti (Università dell'Insubria, Como), Giulio Pavia (Università di Torino), Raffaele Pignone (Servizio Geologico Regione Emilia-Romagna, Bologna) and Riccardo Polino (CNR, Torino)

Acknowledgments:
The 32nd IGC Organizing Committee is grateful to Roberto Pompili and Elisa Brustia (APAT, Roma) for their collaboration in editing.

Graphic project:
Full snc - Firenze

Layout and press:
Lito Terrazzi srl - Firenze

Volume n° 2 - from B16 to B33

32nd INTERNATIONAL GEOLOGICAL CONGRESS

THERMO - MECHANICAL EVOLUTION OF THE ALPINE BELT, FROM THE ENGADINE WINDOW TO THE MATTERHORN

AUTHORS:
G. Gosso (University of Milano - Italy)
M. Engi (University of Bern - Switzerland),
F. Koller (University of Wien - Austria),
J.M. Lardeaux (University of Nice - France),
R. Oberhaensli (University of Potsdam - Germany),
M.I. Spalla (University of Milano - Italy)

Florence - Italy
August 20-28, 2004

Pre-Congress

B29

Front Cover:
Alpe Albion, Southern Steep Belt, Central Alps
(Ticino, Switzerland)

Leader: G. Gosso
Associate Leaders: M. Engi, F. Koller, J.M. Lardeaux, R. Oberhaensli, M.I. Spalla

Introduction

This field trip illustrates the advances in investigation strategies and the definition of tectonic processes which took place at various stages of the Alpine orogeny; recent results are summarised in a data base supporting the new tectonic and metamorphic map of the Alps (see T12.03 topical symposium). About a century ago, a progressive shortening episode was envisaged to have generated the thickened crust of the Penninic nappe belt, a multiply deformed stack of continental and oceanic materials, constructed during the Africa-Europe convergence and elimination of interposed sedimentary and ophiolitic basins (Figure 1, a and b).

In the last thirty years, crustal thickening processes have been envisaged to be more complex than previously thought: in this period, nappe formation was demonstrated to be polyphased, and was revealed, in the continental crust (and/or ophiolites), by the tectono-thermal signatures of P-T regimes, related to lithosphere-scale tectonic events of pre-orogenic rifting, subduction, or collision. Contrasting P-T imprints and tectonic coupling/decoupling of the units were recognised within continental or oceanic crustal slices (and related Permian-Mesozoic to Lower Tertiary sedimentary covers) of the Alpine nappe stack. This interpretation of the nappe formation process is nowadays, however, under thorough revision, in accordance with the tectonic mechanisms of plate dynamics; the comparison of tectono-metamorphic imprints of continental and oceanic basements and covers, have added constraints to reconstructions of nappe formation, and to the role of crustal blocks in forming the lithospheric frame of the belt (Adriatic, Apulian, or African outer margin=Southern Alps block; Austroalpine block; Penninic block; and the European inner margin=Helvetic-Dauphinois-Provençal block).

In this excursion, the nature, origin and timing of sedimentary, igneous or metamorphic protoliths, and their contribution to the unravelling of the tectonic

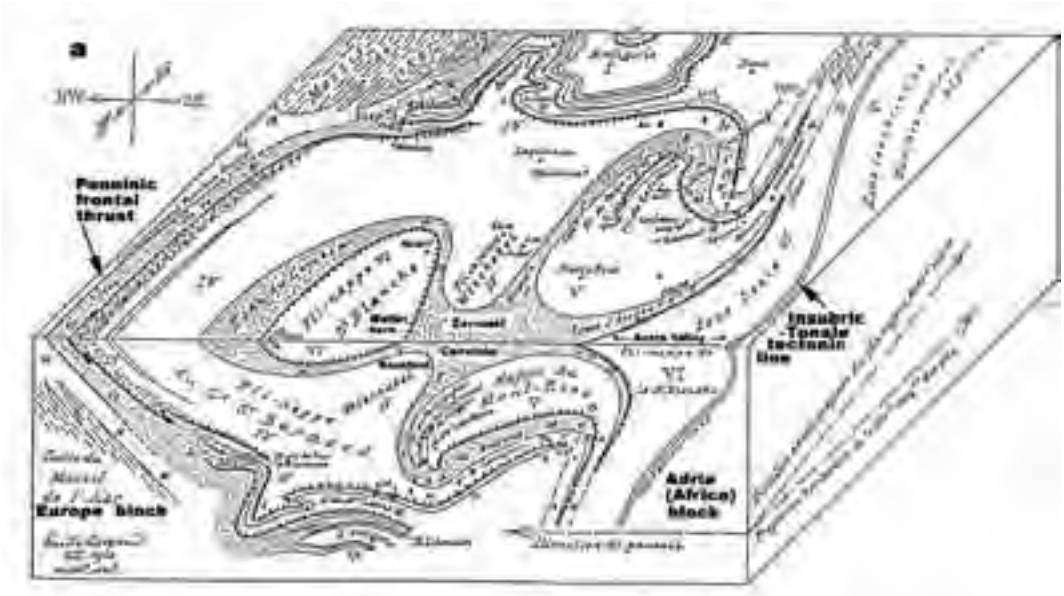

Figure 1 - a: block diagram of the central western Alps, illustrating the oceanic suture zone (Penninic nappes) between the European and African continental margins, located in the axial part of the belt; the tectonic structure is traced by the pre-Alpine crustal rocks (unornamented), and Mesozoic sediments+ophiolites (shadowed); it shows the regional scale complexity of the nappe implications, as reconstructed by Argand (1911), applying the principle of down dip projection of orientation of structures at the surface. The plunge of the fold axes of the nappe structure towards the front face (along the Aosta Valley), is shown to expose the topmost structural element of the pile (Dent Blanche, with the Matterhorn-Cervino); axes culminate to the northeast. The historical names of the pre-Alpine continental crust nappes, from I to VI, are respectively: Antigorio, Lebendun, Monte Leone (Simplon-Ticino, lower Pennine nappes), Grand St.Bernard, Monte Rosa, Dent Blanche (upper Pennine nappes); the intervening nappes consist of Mesozoic materials.

Volume n° 2 - from B16 to B33

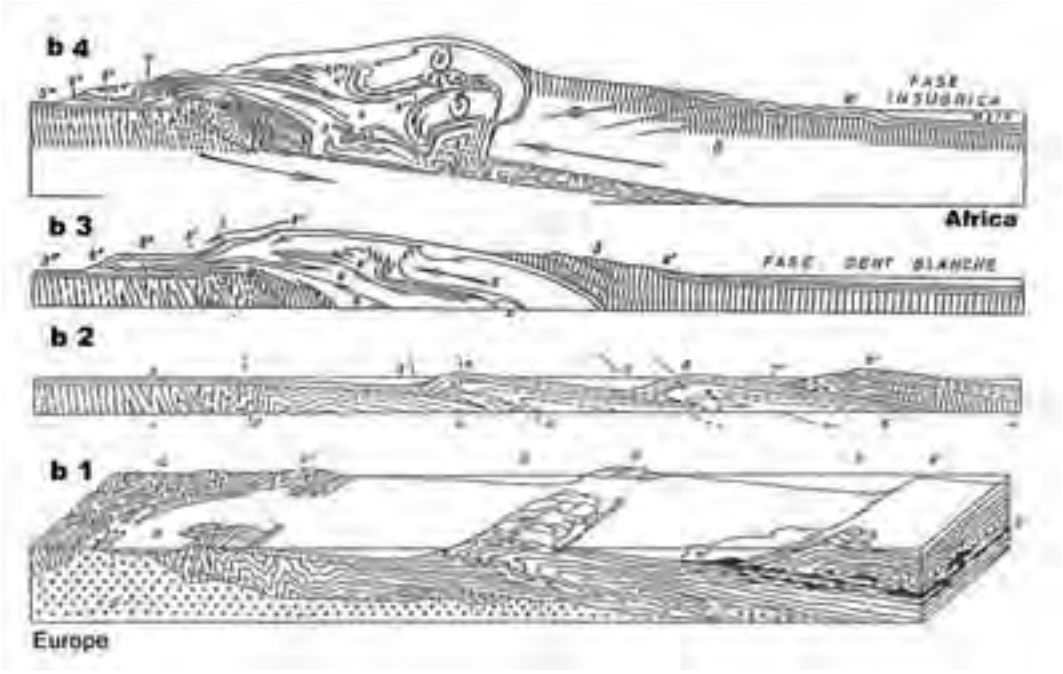

Figure 1 - b: four (b1 to b4) progressive stages of the tectonic development of the fold nappes, as depicted by Argand's (1911) "embryotectonic" kinematic interpretation of the Alpine orogeny; crustal thickening derives from implication within recumbent fold stacks of a pre-orogenic lithostratigraphy, consisting of: a thin pre-Alpine continental crust flooring the Penninic ocean (crosses in b1), its Mesozoic sedimentary sequences (folded lines), hosting interlayered ophiolites (black). In the final stage, corresponding to the front face of Figure 1a, the continental margins of Europe and Africa are closer facing, on each side of the ocean basin's suture.

history, will be discussed as we visit key localities to study the rocks, and to admire structural views, through an eight-day trip from Milano to the Swiss-Austrian border in the Engadine, and back to the Tessin and Aosta regions, ending at Mt. Cervino, (on the Italian side of the Matterhorn), and finally back to Florence.

During the field trip, the significance of differences in the structural, metamorphic, and time evolution of nappes, from three of the four main tectonic blocks forming the wide scale tectonic frame of the belt, will be discussed, along three cross sections (see localities visited in days 1-2-5-6, 3-4 and 7-8 in Figure 6).

The Southern Alps, Austroalpine and Penninic blocks will be visited (see also the tectonic map of Figure 2); only the Helvetic domain (European margin) will not be crossed. An outlook to the pre-orogenic rock associations of the continental and of the oceanic crusts will be delineated when we visit the well preserved rocks of the Lake Como (day 1) and of Bürkelkopf – Flimspitze and Piz Mundin (days 3-4: otherwise only day 3; still better: south vs. north Penninic domain). Only Alpine rocks will be studied on days 2, 5-6 and 7-8.

Regional geologic setting

The present-day structure of the Alpine belt has been investigated over the last 25 years by the Ecors-Crop, NRP20, and the TransAlp deep seismic exploration traverses, fanning respectively from the West to the East of the belt; new geological interpretations were constructed to interpret geophysical models (seismic, gravimetric, and magnetic) of the collisional suture (axial belt), and the multiply indented continental crustal margins of Europe and Adria (Apulia or Africa) (e.g. Roure et al., ed., 1990; Pfiffner et al, ed., 1997; TransAlp Conference Abstr., 2003).

Although velocity models might appear complex (Figure3), objectively the Moho depth reflects well the distinction of the belt into sectors of coherent geological history (Figure4). The Alps are subdivided geologically, from top to bottom and from the internal to the external side, in the following elements (see Figure 2 and 6, and cross sections of Figure 5): (1) the Po river plain hinterland, which represented also the Cretaceous – to Recent fore-land of the

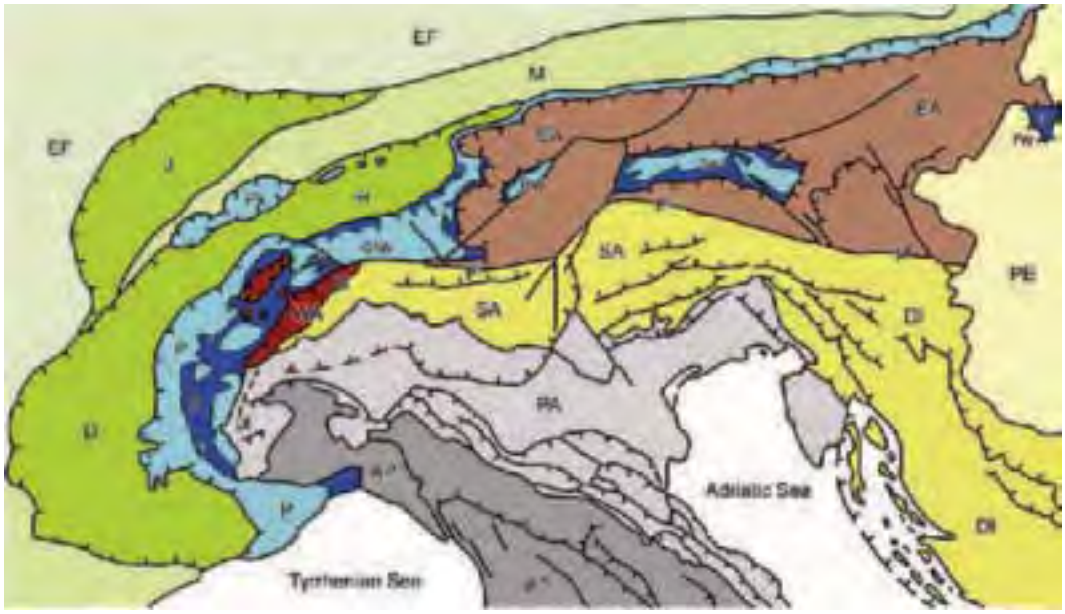

Figure 2 - Tectonic map of the Alps - (1) Europe-vergent collisional belt: i) Western (WA) and Eastern (EA) Austroalpine; ii) Penninic domain: continental and ophiolitic (o) nappes in the western Alpine arc, (P) and tectonic windows (otw: Ossola-Ticino window; ew: Engadine w.; tw: Tauern w.; rw: Rechnitz w.; Prealpine klippen: (Pk); iii) Helvetic-Dauphinois-Provençal (H-D) domain; iv) Molasse foredeep (M); v) Jura belt (J). (2) Southern Alps (SA), bounded to the north by the Periadriatic lineament (pl), Pannonian Basin (PB), European (EF) and Po Valley-Adriatic (PA) forelands, and the Dinaric (DI) and Apenninic (AP) thrust-and-fold belts. From Dal Piaz et al., 2003.

Southern Alps; (2) the South-vergent nappe system of the southern Alps, conventionally bounded to the north by the neogene Peri-adriatic (Insubric-Tonale) fault system; (3) the Europe-vergent Alpine nappe system, including: (a) Austroalpine cover and basement nappes, (b) Piedmont/Ligurian ophiolitic units, and their central and eastern Alpine equivalents (Platta-Arosa, Malenco-Avers, Glockner, Rechnitz), (c) the upper Penninic Monte Rosa/ Gran Pradiso/ Dora-Maira, Suretta, and Tauern basement nappes, (d) the middle Penninic Grand St. Bernard and Tambò cover and basement nappes, (e) the lower Penninic basement nappes of the Simplon-Tessin core, (f) the ophiolite-poor Valais calcschists, and the external north-Penninic flysch units of the Sion-Courmayeur to the Rheno-Danubic border zones; (4) the Helvetic basement and cover units, and related décollement nappes, overlain by (5) the Prealpine pile of décollement sheets; (6) the Swiss-Austrian molasse foredeep; (7) the Jura thrust belt, and (8) the European fore-land. The vertical crustal structure, interpreted from surface geological data, across the over 1000 km-long Alpine arc is shown in the cross-section fan of Figure 5; the crustal wedge delimited by the Periadriatic Lineament (or Tonale-Insubric-Canavese line, PL), and the Penninic Front (PF) records the syn-metamorphic subduction- and collision-related tectonic evolution at deep structural levels, and contains the ophiolitic suture.

The deep geological interpretation of the present-day structure of the Alps does not substantially diverge from that envisaged by Argand, (1911) (Figure1a). The interpretation of continental basement-mesozoic sediments and ophiolites nappe architecture, made nearly a century ago, is impressive indeed; however, the earliest authors were not able to envisage a realistic kinematic picture of nappe formation during lithospheric convergence, because a previously held tenet of ocean basins evolution was the imposition of a thin continental crust as the ocean basement: the continental crust flooring the Penninic ocean would on this premise, therefore, have nourished the crustal fragments of the recumbent fold-nappes of the axial Alpine zone (e.g. the classic Pennine nappes, see the "embryotectonic" history of nappe formation in Fig 2b). The nomenclature of continental nappe sheets, introduced at the beginning of 1900s (large-scale

Volume n° 2 - from B16 to B33

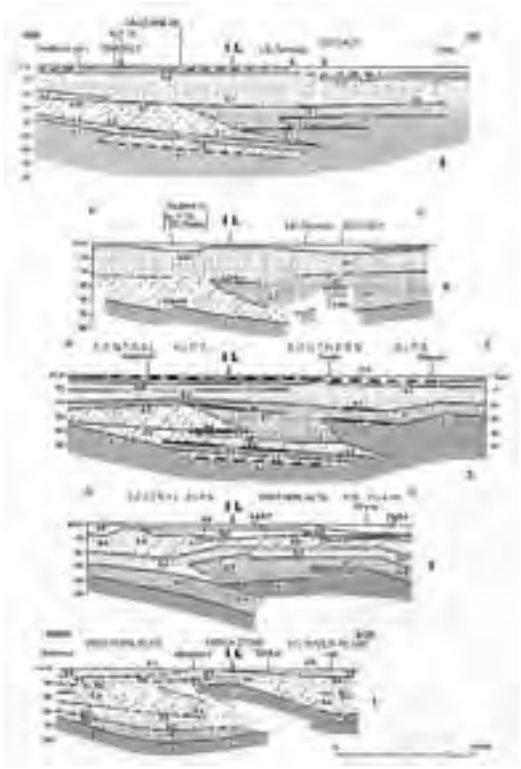

Figure 3 - Comparison of velocities and Moho depths after recent DSS, WARR, and NVR seismic sounding experiments in five stripes across the Alps, compiled by Cassinis and Scarascia (2003); a fan profile is localised in Figure 4.

recumbent folds, known as "Penninic-style nappes"), is still in use; their kinematic history may now be interpreted in accordance with tectono-thermal imprints of tectonic mechanisms active during pre-Alpine roifting, subduction, continental collision, and orogenic denudation.

The present day discriminatory ability of the effects of various superposed lithosphere-scale tectonic processes, however, generates new, and somewhat transversal, definitions of units, (tectono-metamorphic u., thermally-characterized and structurally distinct), with a marked physical (thermo-tectonic) connotation; corresponding tectonic histories are now credited to lithologic associations, carrying equivalent mineralogical, structural, and chronological signatures.

The new regional inventory of peak mineral assemblages– the first numerical inventory of Alpine metamorphic and tectonic stages (see the map presented at T12.03 topical symposium of this World Conference)– may support and consolidate this trend. The new regional inventory is implemented locally, with information on the relationships between the metamorphic history and the evolution of successive structural imprints. This is an approach which exploits the full structural and mineralogical memory of metamorphic tectonites, (assemblage evolution vs. syn-metamorphic foliations, regional cleavage and fold belts, shear, and mylonitic zones), and will eventually be illustrated during the trip. The tectono-thermal study, supported in several Alpine cases, defines orogenic terrains into tectonic units, which are noticeably different in shape and size in relation to the ones defined by litho-stratigraphic affinities (i.e. litho-tectonic units) (Spalla, 1996; Spalla, 2000, and references therein). A first result of such criteria is the separation of subducted from non-subducted tectonic units.

Field itinerary and schedule of the excursion

First day: Wed, 11 Aug 2004. Leave from Malpensa International Airport – Milano, at 15.00, taking our bus to Valtellina (Central Alps, Italy). A short roadside stop on the northeastern bank of Lake Como: tectono-metamorphic history of pre-Alpine rocks of the Southern Alps basement (protoliths of the alpinised continental crust). Maps of the tectono-metamorphic history. Hotel overnight in Tirano, lower Valtellina, Italy.

Second day: Thurs, 12 Aug 2004. Transfer to

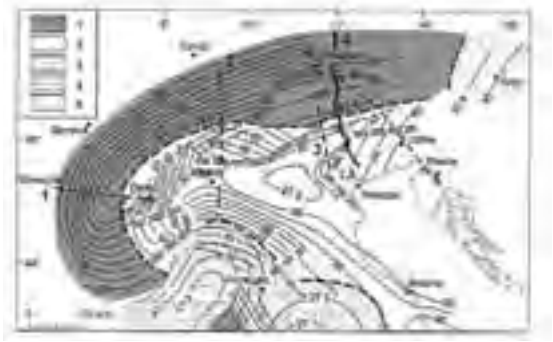

Figure 4 - Moho depth contours in the whole Alpine and North Italian region (from Cassinis et al., in press). Five crustal types are interpreted: 1=European; 2=Adriatic; 3=Transitional peri-Tyrrhenian; 4=Suboceanic; 5=Western corner of the Pannonian basin. Traces 1 to 5 of the five profiles of Figure 5 are located.

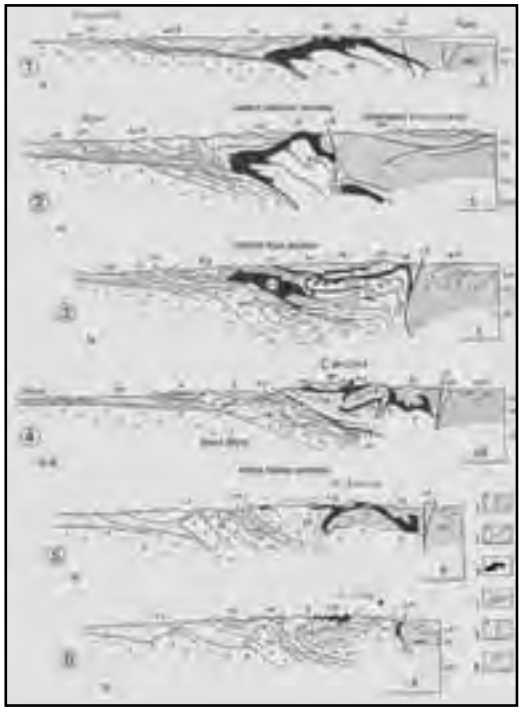

Figure 5 - (a) Popular, multi-authored, and generally credited, simplified cross sections across the Eastern (1), the Central (2), and the Western Alps (3). Legend: 1= Penninic nappe system, mainly deriving from continental crust; 2= Austroalpine system: (a) cover units and (b) mainly basement units; 3= ophiolites and related flysch and mélanges; 4= flysch décollement units, mostly Cretaceous in age; 5= Tertiary European (a) and Po River plain (b) molasses; 6= Late Alpine plutons of Eocene-Oligocene age (45-25 Ma); 7= Southern Alps thrust system, unaffected by high-P Alpine metamorphism. Black stars indicate the position of Alpine UHP rocks. Labels: AD= Adula-Cima Lunga nappe, AU= Austroalpine basement and cover system, TW= Tauern window, CA= Canavese zone, DB= Dent Blanche nappe, Austroalpine, GO/TV/AAR/MB= Gotthard, Tavetsch, Aar, Mont Blanc Helvetic-Dauphinois cover units, HE= Ultra-helvetic, Helvetic and Dauphinois cover units, LPN= Simplon Tessin lower Penninic nappes, NCA= northern Calcareous Alps, Austroalpine, P= Prealpine décollement nappes; PA/GL/MA/PI/AN= Platta-Arosa, Glockner, Malenco-Avers, Piedmont and Antrona ophiolitic units, TN/SU/TA/MR/SB/GP/DM = Tauern, Suretta, Tambò, Monte Rosa, Grand St. Bernard, Gran Paradiso, Dora Maira Penninic basement nappes, SA= Southern Alps, SL= Sesia Lanzo zone, Austroalpine, VA= Valais ophiolitic and flysch units, PF= Penninic thrust front, PL= Periadriatic Lineament.

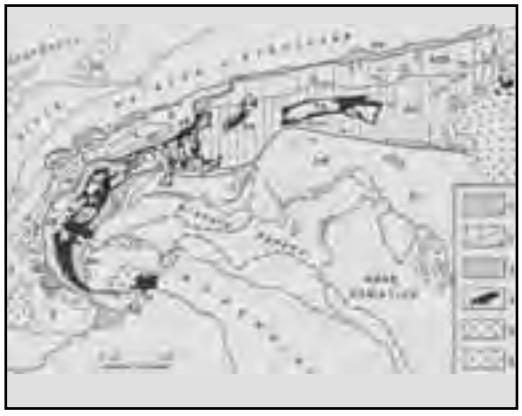

Mortirolo Pass (1900 m, Italy) - road-side geology with very short walks (light shoes). Continental rocks of the Austroalpine units of the Southern Steep Belt, located right north of the Insubric-Tonale regional tectonic Line, separating the Southern Alps block from the Austroalpine. Permian intrusives with Alpine metamorphic imprint in the Austroalpine. Maps of the tectono-metamorphic history. Transfer to Samnaun, Switzerland, by bus and hotel overnight.

Third day: Fri, 13 Aug 2004. Transfer from Samnaun (Switzerland) to the Idalm area (Austria) by cable car. High altitude hiking, between 2800-2400 m (mountain shoes), on the Engadine window South-

Figure 6 - Location of itineraries progressively visited during the excursion (day numbers with short line segments), in a tectonic scheme of the Alpine chain, with some essential metamorphic and sedimentary features. 1: distribution of blueschist and eclogitic metamorphism in the continental units of the western and central Alps (undistinguished in ophiolitic units); 2: very low grade (a) and HP-LT, greenschist and amphibolite facies assemblages (b) in the eastern Austroalpine cover and basement units; 3: Cretaceous to Eocene flysch deposits and Gosau beds; 4: undifferentiated ophiolitic units (with eclogitic-blueschist imprint in the western Alps and Tauern-Rechnitz windows); 5: main Oligocene (-Eocene in Southern Adamello) plutons along the Insubric-Tonale-Pusteria-Gailtal fault system; 6: perialpine and intramontane Oligocene and Miocene basins (Po valley molasse not indicated). A: Adula nappe; Ad: Adamello pluton; AU: eastern Austroalpine cover and basement nappes; B: Bergell pluton; D: Dinarides; EW/TR/RW: Engadine, Tauern, and Rechnitz tectonic windows; HE: Ultrahelvetic, Helvetic, and Dauphinois Provençal units; LPN: lower Penninic nappes; MR/GP/DM/S: upper Penninic Monte Rosa, Gran Paradiso, Dora-Maira and Suretta nappes; NCA: northern calcareous Alps; PF: Penninic front; SA: southern Alps; SB: Grand St. Bernard nappe; SC: Subalpine chains; SL/DB: western Austroalpine and Dent Blanche nappes.

Penninic units, up to the overlying Austroalpine Silvretta nappe, in Austria. The Swiss-Austrian border will be crossed by hiking: please do not forget your passport. Hotel overnight in Samnaun.

Fourth day: Sat, 14 Aug 2004. Transfer from Samnaun (Switzerland) to Martina by private bus, and from Martina to Alp Tea with shuttle; 1,5 hrs. high altitude (2300-2700 m; mountain shoes) hiking to Piz Fot. in the Engadine tectonic window North-Penninic units. Descent to Martina by shuttle. Transfer from Martina to Roveredo by bus; ascent from Roveredo with shuttle to Capanna Gesero and overnight in simple mountain cabin.

Fifth day: Sun 15 Aug 2004. Full day mountain hike (mountain shoes): Alpe Gesero-Passo San Jorio-Alpe Albion-Alpe Gesero. Transect through SSB: fragmentation of (sub)oceanic and supracrustal bodies in TAC (Tectonic Accretion Channel); deformation and magmatism along the Insubric Line.

Sixth day: Mon, 16 Aug 2004. Transfer with shuttle to Val d'Arbedo (deformation, migmatites) (light shoes); Castione calschists and metabasics. Alpe Arami-Gorduno: Garnet Peridotite, eclogites; decompression history. Descent to Arbedo with shuttle. Transfer to Breuil-Cervinia (Italy) by private bus and hotel overnight.

Seventh day: Tue, 17 Aug 2004. Transfer from Breuil-Cervinia (2000 m, Italy) to Plateau Rosa (3500m, Swiss border) by cable car: tectonic landscape on the Alpine nappe pile. 2 hrs. easy down-walk (mountain shoes), from 2900 to 2500 m, on the eclogitised oceanic rocks of Zermatt Saas unit. Hotel overnight in Breuil-Cervinia.

Eighth day: Wed, 18 Aug 2004. Transfer from Breuil-Cervinia to the Lower Aosta Valley by bus: road side geology with very short walks (light shoes) on the eclogitised continental crust of Sesia Lanzo Zone. Departure by bus to Florence at 14.00 h.

DAY 1

The pre-alpine metamorphic basement of the southern alps (piona peninsula - como lake - valtellina, italy)

***Guido Gosso*[1], *Maria Iole Spalla*[1], *Gian Bartolomeo Siletto*[2]**

[1] University of Milano - Italy

[2] Geological Survey of Regione Lombardia - Italy

The Southalpine thrust belt represents the African (Adria) deformed plate margin, involving thick-skin pre-Alpine basement and Permian-Mesozoic cover slices, and is the hinterland of the Alpine arc. The Southalpine domain is limited from the Penninic-Austroalpine north-verging nappe system by the Periadriatic tectonic lineament (Insubric-Tonale line), and was only locally affected by very low- to low-grade metamorphism (Colombo, 2001). The Southalpine basement of Lake Como consists of two Alpine slices (the Musso unit, Val Colla-S.Marco unit) separated by cataclasites (Musso Alpine fault zone Schumacher, 1996). The Musso Fault Zone (MFZ) represents a pre-Alpine greenschist facies mylonitic belt (Bertotti, 1991; Bertotti, 1993; Gosso, 1997; Heitzmann, 1983; Siletto, 1990), reworked during Alpine times. The shallow Musso Alpine unit of Schumacher and Laubscher (1996), displays a homogeneous metamorphic pre-Alpine evolution (di Paola, 2000; di Paola, 2001), and coincides with the Domaso-Cortafò Zone (DCZ) described by Fumasoli (1974) and Bocchio, (1980). Conversely, the lithologically homogeneous Val Colla-S.Marco unit of Schumacherand Laubscher (1996) consists of portions recording heterogeneous pre-Alpine metamorphic evolutions, namely the Dervio-Olgiasca and Monte Muggio Zones (DOZ, MMZ) (e.g. Gosso, 1997; Spalla, 2000). The boundary between the northern (DOZ) and southern (MMZ) units is the Liassic syn-sedimentary Lugano-Val Grande normal Fault Zone (LVGFZ), a greenschist mylonitic belt, overprinted by a pre-Alpine cataclasis (Bertotti, 1993; Siletto, 1991).

The pre-Alpine metamorphic basement consists of similar lithologic associations in all three zones: gneisses and micaschists (local names: Morbegno and Stabiello Gneisses), with interlayered amphibolites, quartzites, marbles, calcschists, and metagranitoids; pegmatites occur exclusively in the Bt- and Sil-bearing schists of the DOZ, representing the only difference in the litho-stratigraphy of the three zones. Protoliths of metapelite have been interpreted as Early Palaeozoic in age (Mottana, 1985). Relationships with the non-metamorphic Permo-Mesozoic sedimentary cover differ in the three zones: i) deposits of the Verrucano Lombardo Fm. non-conformably overlie the leucocratic metagranitoids of MMZ; ii) slices of Permo-Mesozoic dolostones, conglomerates, and siltstones are separated by tectonic boundaries (MFZ, IL) from the DCZ basement; iii) no Permo-Mesozoic sediments are in contact with the DOZ basement.

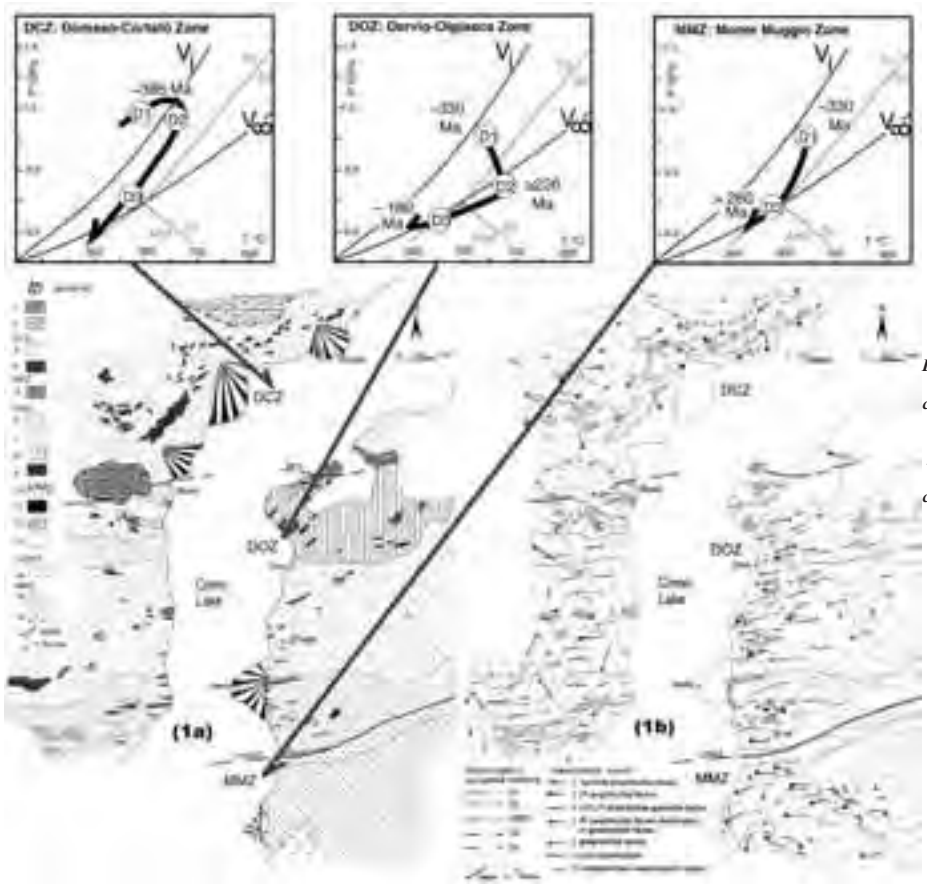

Figure 1.1 - a : Geologic map of Domaso-Cortafò, Dervio-Olgiasc,a and Monte Muggio tectono-metamorphic units (DCZ, DOZ, and MMZ respectively on the map,) separated by the greenschist mylonites defining the Musso Fault Zone (MFZ) and the Lugano-Val Grande Fault Zone (LVGFZ). Legend: 1= Dolomia Principale (Norian): re-crystallised massive dolostones, locally cataclastic; 2= massive medium to fine-grained and calcareous breccias at the contact with the micaschists (sedimentary slices along the Insubric Line). DCZ: 3= metapelites with BtII, MsII, Pl, Grt, ±St, and ±Ky defining the S2 foliation reactivated during D3; Chl, opaque minerals, MsIII, BtIII, and Ab define S3. Relics of S1 are underlined by BtI, MsI, and Cld; 4= amphibolites with HblII, Pl, ±Ilm, ±Qtz, defining the S3 is underlined by Ep, Chl, and Ttn. HblI and Grt occurs as porphyroclasts in S2. MFZ: 5= mylonites with Chl, Ms, Ab, and ribbon Qtz, locally with ultramylonitic texture. s-c structures and extensional crenulation cleavages are widespread. DOZ: 6= micaschists and gneisses with Chl and Ms underlining S3, in places with mylonitic textures, or s-c cleavages; Grt and Bt relics are preserved; the modal amount of Chl increases towards the LVGFZ; 7= Grt-St-bearing micaschists and minor gneisses containing MsI, BtI, GrtI, and St contemporaneous with S1; S2 crenulation cleavage is defined by BtII, MsII, GrtII, ±Si; Chl and MsIII grow during D3; 8= Sil-Bt-bearing micaschists and minor gneisses with Ms, BtII, GrtII, Sil, Pl, ±Kfs mark S2; BtII and Sil define s-c structures and extensional crenulation cleavages; relics of GrtI, Ky, and St are locally preserved. Centimeter-sized and poikiloblasts grow during late D2; 9= amphibolites with Pl, HblII, ±Qtz, ±Grt, ±Bt, ±Ep, and relics of HblI; amphibolites with Hbl, Di, Pl, ± Ttn; S2 is defined by the HblII and Pl compositional layering, or by the SPO of Hbl and Di; rare hornblendites with Chl, Ttn, Ilm, show coronitic textures; 10 a= metagranitoids with Ms and Chl, containing relics of Bt and Grt. Compositional layering defines S2; 10b= fine-grained mylonitic metagranitoids, with Ms and Chl, containing millimeter-sized Kfs porphyroclasts; 11= Qtz, Kfs, Ms, tourmaline, ±Grt-bearing pegmatites. Generally with undeformed cores and foliated (S2) margins; 12= quartzite layers of centimeter to meter thickness, containing Chl, Bt and Ms; 13= fine-to medium -grained, white to light grey marbles, locally containing amphibole and pyroxene; silicate-rich layers are constituted by Zo, Tr, Tlc, and Chl. LVGFZ: 14= mylonitic micaschists and gneisses with Qtz, Ms, Chl, and Ab underlining S3; shear-zones with s-c structures and extensional crenulation cleavages, and dark coloured ultramylonites are widespread; cataclastic feldspar, sericite- bearing gneisses, with granular texture; S3 is well-developed at the boundaries with the mylonites. MMZ: 15= metapelites with Chl, Ab, MsII, ±Mrg underlining S2 foliation. Relics of Grt, Bt, St, Pl, and Ky, developed during D1. Grt-amphibolites rarely occur as meter-sized lenses elongated in S2; rare quartzite layers of centimeter to meter thickness, containing Chl, Bt, and Ms have compositional layering parallel to S2; 16= metagranitoids with Ms, Chl, ±Bt; mineralogical layering defined by alternating quartz-feldspar and sheet silicates layers is parallel to S2.

P-T-d-t trajectories of DCZ, DOZ, and MMZ rocks located in the tectono-metamorphic map of the Lake Como pre-Alpine basement. The metamorphic evolutions and relative radiometric ages are discussed in the text. The unperturbed (V_i) and maximally relaxed geotherm (V÷) are after England and Thompson (1984); Aluminum silicate triple point after Holdaway (1971). Legend: 1= Penninic nappes; 2= Austroalpine nappes; 3= Bergell pluton; 4= Domaso-Cortafò tectono-metamorphic unit; 5= Dervio-Olgiasca tectono-metamorphic unit; 6= Monte Muggio tectono-metamorphic unit; 7= greenschist belts, mainly with mylonitic fabric; 8= slices of Carboniferous conglomerates; 9= Permo-Mesozoic sedimentary cover units; 10= faults: IL= Insubric Line; LVGFZ= Lugano Val Grande Fault zone; MFZ= Musso Fault zone; OL= Orobic tectonic line.

b : Foliation map of DCZ, DOZ and MMZ tectono-metamorphic units. MFZ and LVGFZ correspond respectively to Musso Fault Zone and Lugano Val Grande Fault Zone. The lithological boundaries are shown for reference; the mineralogical assemblages related to successive fabrics in each rock type are listed in the legend of Figure 1 a. The information on the relative chronology of superposed foliations, and on the metamorphic environments in which they developed, are specified respectively by relative ages and metamorphic imprints symbols. In the DCZ, the D2/D3 foliation symbol is used to discriminate S_2 foliation reactivated during D_3. Keys of the metamorphic imprint symbols: 1= epidote amphibolite-facies; 2= intermediate pressure amphibolite-facies; 3= low pressure amphibolite-granulite -facies (corresponding to the HT-LP metamorphic imprint of the text); 4= intermediate pressure amphibolite-facies reactivated in greenschist-facies; 5= greenschist-facies; 6= non metamorphic; 7= undetermined metamorphic imprint. (Stop 1.1)

Volume n° 2 - from B16 to B33

Different P-T-d-t evolutions (Figure 1.1) are recorded in three zones that therefore represent three different tectono-metamorphic units (Spalla, 2002):
DCZ: the earliest metamorphic imprint in epidote-amphibolite facies conditions (TA 550°C), developed during the formation of D1 planar fabric; during D2, rocks re-equilibrated under amphibolite facies conditions (T= 560-650°C and P= 0.7-1.1 GPa); during D3, greenschist facies minerals assemblages developed (T<550° C and P< 0.6 GPa). The D1-D2 portion of the inferred P-T loop (Figure 1) has been interpreted as the thermal record of eo-Variscan subduction and mid-Variscan continental collision; the available K-Ar age of ˜385 Ma fits this tectonic outline (di Paola, 2000; di Paola, 2001);
DOZ: the earlier metamorphic assemblage grew in amphibolite-facies conditions (T= 530-630°C and P = 0.7-1.2 GPa), during the development of D1 structures, re-equilibrated at T = 650-750°C and P = 0.4-0.55 GPa during D2 deformation, and finally underwent greenschist facies conditions (T< 500°C and P = 0.2-0.3 GPa), during the formation of D3 structures (di Paola, 2000; Diella, 1992). An age of ˜330 Ma may be proposed during D1, by comparison with the analogous syn-D1 thermal state of MMZ. Timing of D2 is constrained at ˜226 Ma (Rb-Sr and K-Ar mineral ages; (Sanders, 1996) by syn-D2 pegmatite emplacement, and the D3 greenschist retrogression may be related to Liassic normal faulting along the LVGFZ (e.g, Gosso, 1997). The inferred P-T loop for DOZ (Figure 1.1), has been interpreted as the result of deep-seated Variscan crust exhumation during Permo-Triassic rifting (e.g. Diella, 1992; Spalla, 1999);
MMZ: the earlier metamorphic imprint, contemporaneous with D1 deformation, developed under amphibolite facies conditions (T = 560-600°C and P = 0.8-1.1 GPa); during D2 fabric development, rocks re-equilibrated under greenschist facies conditions (T< 500°C and P< 0.4 GPa) (Bertotti, 1993; Spalla, 2002). A K-Ar age of ˜330 Ma may be attributed to the syn-D1 amphibolite facies metamorphic imprint (Mottana, 1985). Syn-D2 greenschist retrogression predates the deposition of the Verrucano Lombardo sedimentary sequences in Late Permian times (B260 Ma). This tectono-metamorphic evolution (Figure 1.1), has been considered to be the result of the thickened continental crust exhumation, during the thermal relaxation induced by Variscan continental collision (Spalla, 2000).
The foliation trajectory map (Figure 1.1) shows the finite strain field by means of the planar fabrics configuration, and the systematic information on the mineral re-equilibration steps in relation to microfabric changes: location, thickness (less than 5 km), and areal extent of each unit are here confidently constrained. On this map, the association of relative fabric age and metamorphic environment is not univocal across the whole area; actually an independent use, either of the relative chronology of superimposed fabric, or of the different metamorphic imprints, would have induced us to correlate syn-metamorphic structures actually developed in different times and in different geodynamic environments. For example, fabric D2 in DOZ, that developed in LP-HT metamorphic conditions at about 226 Ma, cannot be correlated with fabric D2 in MMZ, which was developed in greenschist metamorphic conditions and predates the deposition of Permian sedimentary covers (and is therefore older than 260 Ma). Conversely, as discussed above, greenschist re-equilibration in DCZ, DOZ, and MMZ took place in different times and under different geodynamic environments.

Stop 1.1:

Locality: Piona Peninsula, north-eastern shoreline of the Como Lake. Map: 1:200.000 scale Road Atlas of the Italian Touring Club.
Topics: Permo-Triassic tectono-metamorphic imprint in Southalpine metapelites and pegmatite emplacement; pre-Alpine protoliths outside the deep-seated Alpine collisional belt (i.e. south of the Insubric Tectonic line). Illustration of the use of foliation maps to unravel the tectono-metamorphic history of polydeformed metamorphic basements.
Equipment and program: road geology, with a 5+5 min. walk on a forest path (light shoes).
The only stop of the first day is reached by following the highway Lecco-Colico (S.S. n°36) to the Piona exit, eastern shoreline of the Como Lake; drive backwards on the road (S.P. n°72) to the Piona peninsula, and cross the village of Olgiasca. Stop some hundred meters before the Piona Abbey, in a parking area. Excursion stop is located in Figs. 1.1 and 1.2. Short walk (10 min.) through a holly wood, up to a small abandoned quarry, where a pegmatite was emplaced along a Sil-Bt-bearing shear zone. Pegmatite contains Qtz, Tur, Ms, Ab, Kfs, minor Bt, and Grt; accessory minerals are monazite, uraninite, zircon, beryl, chrysoberyl, pyrite, arsenopyrite, etc. The grain-size decreases from the undeformed core to the foliated margins. The Sil-Bt shear bands, widespread in the northern part of DOZ (Figure 1.3),

Figure 1.2 - Geographic location of Day 1 Stop on Lake Como, and panoramic view of the Piona peninsula and Musso fault zone. (Stop 1.1).

dipping to S-SSW, show a dextral sense of movement along the sub-horizontal stretching lineation. The composite s-c foliation (s = 176-195/60-75; c = 198-210/80-87), lies at a low angle to the pegmatite (185/70; Figure 1.3 c, e, f). Microstructural analysis evidentiates that cleavage asymmetries are compatible with extension (Figure 1.3 d). These observations indicate a syn-D2 pegmatite emplacement. High-T shear bands dominate the fabric of small outcrops along the road and downhill. Fibrolite and BtII intergrowths define a marked stretching lineation and both shear and foliation planes of D2 (Figure 1.3 d). Fibrolite and prismatic Sil grew contemporaneously in different microstructural sites: fibrolite underlines shear and foliation planes and prismatic Sil occupies microlithons. Grt is incompletely pseudomorphosed by aggregates of fibrolite and BtII (Figure 1.3 a), which occupy also asymmetric pressure shadows. Relict white mica is rarely preserved, is overgrown by small needles of fibrous Sil, and commonly has lobate margins (Figure 1.3 b). Locally S2 grades into sigmoidal domains (up to centimetric), of polygonal Qtz aggregates, Pl, minor K-fs, and red-brown Bt with lobate margins, bounded by s and c planes.

DAY 2

Eo-Alpine HP metamorphism on the Permian intrusives and their country rocks in the Austroalpine units within the Southern Steep Belt, right north of the Insubric tectonic line (Mortirolo Pass, on the Valtellina - Upper Val Camonica watershed, Italy). Illustration of the use of foliation maps to individuate tectono-metamorphic units in polycyclic (poly-orogenic) metamorphic terrains

In spite of the widespread and well documented HP-LT eo-Alpine metamorphic imprint in Austroalpine units, from the western and eastern Alps (e.g. Dal Piaz, 1972; Compagnoni, 1977; Hoinkes, 1991; Thoeni, 1993), in the Austroalpine domain of the central Central , Western and Eastern Alps are toponyms, not just adjectives Alps, records of this tectono-metamorphic stage are scanty (Vogler, 1981), and localised in the Southern Steep Belt, due north of the Insubric Line. Abundant eo-Alpine eclogites, even if heterogeneously distributed, in the uppermost structural level of the Alpine nappe pile (Spalla, 1996, and refs. therein), invalidates the idea that the Austroalpine domain represents a unitary and homogeneous tectonic system, and indicates two types of Austroalpine units: i) units unaffected by the eo-Alpine subduction metamorphism (the Alpine orogenic lid); ii) units deeply involved in the subduction zone, such as the ophiolitic and Penninic continental basement nappes. At a regional scale, a sharp continuous boundary between them has not yet been defined. In the Austroalpine units, exposed along the upper Val Camonica – Valtellina ridge, Permian diorites and granitoids constitute discriminating tools to detect Alpine tectono-metamorphic histories.

The Upper Austroalpine units of the central Alps include the Languard - Campo Nappe (LCN), and

Volume n° 2 - from B16 to B33

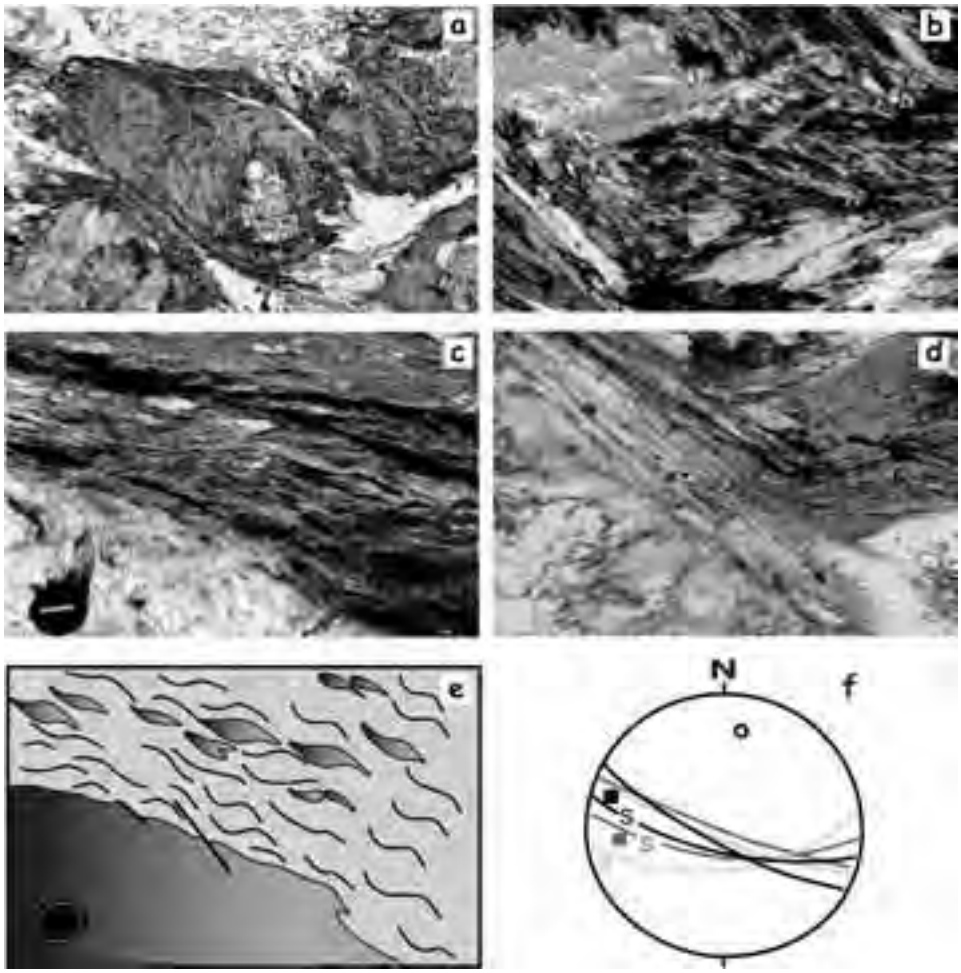

Figure 1.3 - Photomicrographs of microstructural relationships between critical minerals and mesoscopic structures of rocks from the Dervio-Olgiasca tectonometamorphic unit (DOZ). (Stop 1.1 on Lake Como). a) garnet porphyroblasts replaced by sillimanite-biotite intergrowths. Fibrous sillimanite and biotite mark both shear and foliation planes and occur in asymmetric garnet pressure shadows. Granoblastic domains contain mainly quartz and plagioclase, with minor K-feldspar and red-brown biotite – plane-polarized light, long side of photomicrograph = 15 mm; b) white mica, biotite I and plagioclase, partly replaced by a fine aggregate of fibrolite and biotite II – cross-polarized light, long side of photomicrograph = 0.8 mm;

c) Pegmatite near the Piona Abbey, showing "s-c" structures at the rims: shear and foliation planes developed during deformation D2, at pegmatite margins and in biotite-sillimanite gneiss.

d) shear and foliation planes, marked by sillimanite and biotite II intergrowths. Biotite II displays a Ti content higher than that of relict biotite I (Diella et al., 1992), indicating T-increment during D_2. Plane-polarized light, long side of photomicrograph = 2.5 mm.

e) Interpretation of structural patterns of figure c): pegmatite emplacement is assisted by an extensional effect, contemporaneous with a s-c cleavage. Diameter of black disc is 5 cm long.

f) In a Schmidt plot (lower hemisphere), s-c planes are shown together with Sill-bearing mineral lineation. O = pole to pegmatite bedding; S = foliation planes; squares = sillimanite-bearing lineation. (Stop 1.1, near the Piona Abbey on Lake Como).

the Tonale Series (TS), both consisted of a poly-metamorphic rock association. LCN and TS display a generally steeply dipping attitude immediately north of the Insubric line (Southern Steep Belt,Schmid, 1996). LCN represents the highest unit capping the Lower Austroalpine (Margna, Sella, and Bernina nappes) in which thin tectonic elements with ophiolitic affinity (Corvatsch and Platta) are interlayered (Figure 2.1 b).

In the literature, LCN has been distinguished from TS on lithological grounds, and, consequently, on the depth of crustal derivation. According to Venzo, (1971, and refs. therein), LCN comprises low to medium grade muscovite-, Bt- and minor St- gneisses and micaschists, with interlayered amphibolites, marbles, quartzites, and pegmatites, whereas TS is formed by

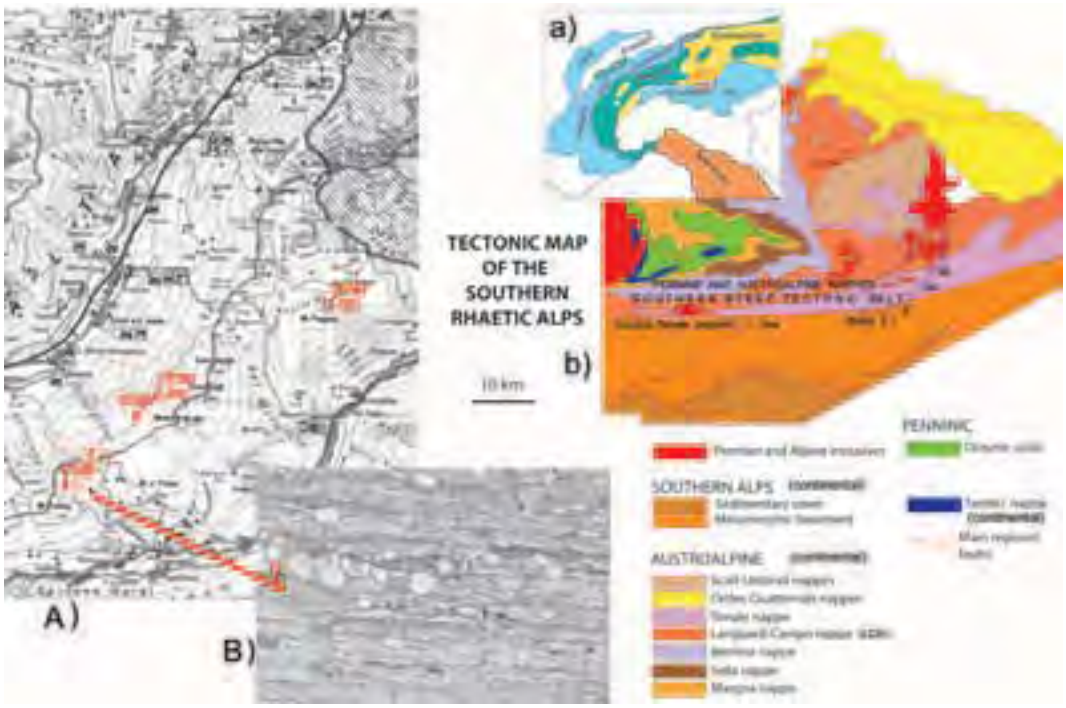

Figure 2.1 Location of Day 2 stops, near Passo del Mortirolo, on the Valcamonica-Valtellina ridge (inset A); tectonic map of a portion of the Central Alps (=Southern Rhaetic Alps, with legend, insets a and b), and a microstructure of a mylonite from the Insubric-Tonale tectonic line (inset B). Day 2 stops are also located in the oblique polygon inside inset B) reporting the detailed map location of Figure 2.2. In inset b), the Insubric-Tonale tectonic line (related mylonites shortly visited at Stop 2.1), separates the continental and oceanic Alpine nappe belt generated at depth during subduction and collision tectonic episodes (Austroalpine and Pennine nappes of the southern steep tectonic belt, North of this tectonic line) from the continental upper crustal thick-skin (basement+covers) overthrusts of the Southern Alps (South of this tectonic line); the Southern Alps thrust belt is south-verging and tectonic units are bounded by EW and SW-NE trending overthrust faults of Alpine age (see Southern Alps block in legend of inset b); it developed under very low – to low metamorphic conditions. B) shows a typical microstructure of greenschist facies–dominated mylonites, with feldspar porphyroclasts and fine-grained chlorite+white mica in the foliation planes.

Figure 2.2. - a): Simplified geological map reporting lithostratigraphy and km-scale strain (fabric) gradients within Permian-age metaintrusives. Legend: grey=undifferentiated country rocks of the Permian intrusives; Red=Grt-bearing pegmatites. Gradients of colour shading identify the fabric gradients, from coronitic to normally foliated (tectonitic) and mylonitic, within metagranodiorites (yellow to orange), and metadiorites (pale blue to dark blue). The LCN (Languard-Campo nappe) extends from top north to the red dashed line, also corresponding to the Mortirolo tectonic line; TS (Tonale series) extends from south to the dashed red line. STS=Scisti del Tonale series; CRS=Cima Rovaia series; PRS=Pietra Rossa series (Bonsignore & Ragni, 1966; 1968). b): P-T-d-t paths of the Languard Campo Nappe - Tonale Series (after Gazzola et al. 2000; Zucali, 2001); inset c): pre-Alpine and Alpine P-T paths compared with the stable geotherm (Vi).

Volume n° 2 - from B16 to B33

higher grade Sil-bearing gneisses and micaschists, Grt- and Bt-bearing amphibolites, marbles, and pegmatites. In both these units (Figure 2.1b), post-Variscan intrusives (granitoids, diorites, and minor gabbroids) commonly occur (Tribuzio, 1999,and refs.) with mineral ages clustering in two groups: the first, ranging from 298 to 224 Ma, is interpreted as magmatic cooling ages (Tribuzio, 1999), whereas the second, ranging from 125 to 78 Ma, is considered as the effect of Cretaceous reactivation during Alpine tectonics (Del Moro, 1981). LCN and TS have been considered as inhomogeneously affected by an Alpine metamorphic imprint, never exceeding greenschist facies conditions (e.g. Bockemuehl,1985), until new petrological and structural data attributed higher pressure conditions to this metamorphism (Spalla, 1995; Gazzola, 2000; Zucali, 2001). Permian intrusives represent a time reference which has been utilized to separate Alpine from pre-Alpine structural and metamorphic characters. Pre-Alpine structures consist of sets of pre-D2 fabrics, marked by contrasting mineral assemblages in the metapelites (pre-D2a: St + Grt + BtI + MsI + Qtz + Pl ± Ky; pre-D2b; Grt + Bt + Sil + Pl + Qtz). D2 structures include the most prominent pre-Alpine folds and related foliation; they are synchronous with the emplacement of Permian diorites and granodiorites (260-280 Ma), and are underlined by BtII + Sil ± Grt ± Crd ± Kfs + Pl + Qtz in metapelites. And + MsII overgrew S2. During Alpine times, three groups of superposed structures overprint the pre-Alpine syn-metamorphic fabrics and deform Permian intrusives. HP assemblages developed during D3 in metapelites (GrtII + MsIII + Qtz + Ab ± Cld ± Ky ± Ts), and in metaintrusives (Grt + Ab + Qtz + Zo/Czo + Phe ± AmpII). S3 maxima occur at 162/55 and 355/87. Two groups of large-scale fold systems (D4 and D5), are associated with greenschist facies re-equilibration, during which Alpine Bt grew (120-80 Ma; (Del Moro, 1981); joint sets and Chl/Kfs-bearing fracture systems overprint D5 structures. The quantitative P-T-d-t path of Permian intrusives, and their country rocks, corresponding to the described pre-Alpine and Alpine evolution, is summarised in Figure 2.2 b.

The goal of the second day field trip is to show that the different lithostratigraphic units, in which this Austroalpine basement has been subdivided, reflect an Alpine strain gradient, coinciding with a metamorphic transformation gradient; in addition, these lithostratigraphic units belong to a single tectono-metamorphic unit during Alpine evolution. This is easily perceived in Figure 2.2a), where planar fabric gradients (in metaintrusives), foliation ages, and related evolving metamorphic conditions are represented together on a single map.

Stop 2.1:

Locality: Monte Padrio, Valle di Guspessa (Valtellina – Val Camonica ridge, near Mortirolo Pass). Map: 1: 200.000 scale Road Atlas of the Italian Touring Club.
Topics: Mylonitic belt, marking the Insubric Line.
Equipment and program: mountain road geology, with a 10+10 min. walk offroad (light shoes recommended).

The first stop of the second day is reached by following the road from Aprica to Mortirolo Pass; drive backwards on the road up to Monte Padrio, and park along the road where some outcrops of mylonites of the Insubric tectonic line are located (Figure 2.1 b and B). South of the mylonitic belts, the pre-Alpine metamorphic rocks of the southern Southern is a geological term in this case (a paleogeographic domain!) Alps thrust belt are exposed; they consist mainly of metapelites, with interlayered quartzites which underwent a polyphase Variscan metamorphic evolution from intermediate pressure amphibolite facies, to greenschist facies (Spalla, 1999). Alpine tectonic evolution occurred under very-low to low grade metamorphic conditions. North of the Insubric-Tonale mylonitic belt poly-cyclic (poly-orogenic) Austroalpine metamorphic rocks, that will be studied in detail at the next stops, are exposed.

Stop 2.2:

Locality: Mt. Motto della Scala western slope (Valtellina – Val Camonica ridge). Map: 1:200.000 scale Road Atlas of the Italian Touring Club.
Topics: Tonale Series metamorphic rocks (Tonale Series=part of Tonale nappe of Figure 2.1 b) with a dominant high grade pre-Alpine metamorphic imprint; low strain Alpine deformation zone.
Equipment and program: mountain road geology, with a 10+10 min. walk offroad (light shoes).
The second stop (2.2), is reached following the road towards Mortirolo Pass up to Alpe Troena, at the foot of Mt. Motto della Scala; parking along the road, where some outcrops of high grade metapelites with interlayered marbles and amphibolites occur (Figure 2.1). In these high-grade Bt-Sil gneisses and schists, with interlayered Grt- and Bt-bearing amphibolites, marbles and pegmatites, the dominant fabric is foliation S2, a high temperature pre-Alpine mineral layering. D2

structures consist of tight to isoclinal folds from centimeter to kilometer scale; relics of foliation S1 are locally preserved (Figure 2.2 a and 2.3). In metapelites, S2 foliation films are defined by Sil and red-brown Bt, whereas Grt, Pl and prismatic Sil occupy the microlithons; locally Kfs and Crd occur. In granoblastic metabasics, foliation S2 is a mineral layering in which Hbl-bearing layers alternate with An-rich Pl and Scp-bearing layers. Bt from Ca-rich metapelites have Ti and Al^{VI} contents, indicating a T-range of 650°-750°C. Hbl is generally zoned: Ti content in Amp cores indicates 730°<T<820°C, whereas Ti content in the faded rims is 550°<T<600°C, according to Otten (1984). For these two T-intervals, the coexistence of amphibole with An-rich plagioclase and Grs-Adr-rich garnet suggests P≤ 0.5 GPa. During Alpine deformation, foliations are poorly pervasive, and concentrated in narrow zones, actually pre-Alpine fabrics and mineral assemblages are widely preserved. In this case Alpine minerals develop as reaction rims (Fig 2.3).

Stops 2.3:

Locality: *Stop 2.3a* - Il Boschetto, western slope of Cima Cadì (Valtellina – Val Camonica ridge);

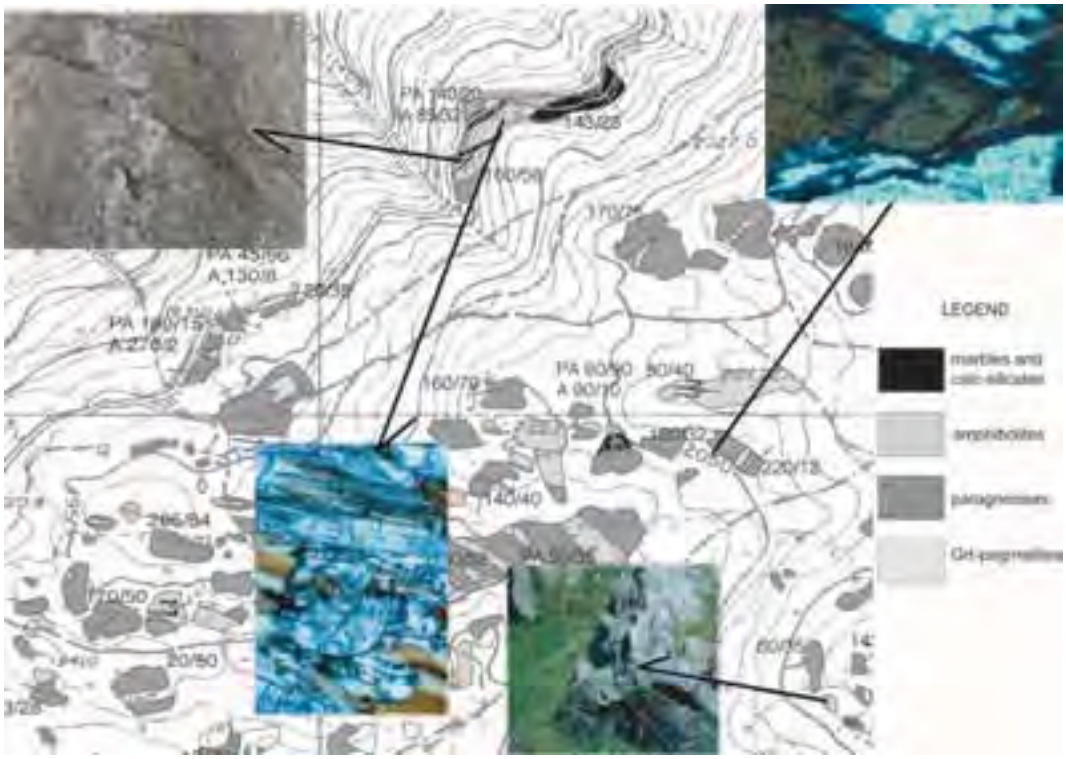

Figure 2.3. - Map of high grade metapelites with interlayered marbles and amphibolites at the foot of Monte Troena; the dominant granular scale fabric (S2) of all rocks is pre-Alpine; it is overprinted in the metapelites, by Alpine corona-texture transformations (with no strain associated). D2 folds deform the lithologic layering.
Lower left photomicrograph: S2 foliation in metapelites, marked by biotite and sillimanite preferred dimensional orientation (PDO), with pre-Alpine garnet porphyroblasts and ilmenite included; crossed polars (CP), lower side of photograph(LSP) = 4 mm.
Lower-right photograph: garnet pegmatites deformed by D2 folds. LSP = 2 m.
right photomicrograph: strain-absent corona metamorphic transformations of Alpine age, generate tschermakitic amphibole at the rims of pre-Alpine biotite grains, within high grade metapelites (kinzigites), that macroscopically do not appear to have been reactivated; crossed polars (CP), LSP = 3 mm.
Upper-left photomicrograph: Amphibolites with pre-Alpine mineral scale foliation S2 parallel to lithologic layering (Sl), within the pre-Alpine high grade metapelite-marble-amphibolite sequence; LSP = 45 cm. Stop 2.2

Stop 2.3b Pianaccio (Valle di Grom) at the base of Monte Pagano northern slope (Valtellina – Val Camonica ridge).

Topics: Permian intrusives and their country rocks, affected by Alpine HP metamorphism; high strain Alpine deformation zone.

Equipment and program: mountain road geology, with a 10+10 min. walk offroad.

In both stops, Permian intrusives (diorites) and their country rocks show various type of Alpine deformations and metamorphic transformation patterns (Figure 2.4). Metadiorites still preserve igneous textures and mineral associations across meter-size volumes: igneous textures are defined by mm to cm-size dark Amp, displaying euhedral to subhedral shape; Pl is interstitial. Alpine metamorphic minerals occupy extremely small volumes within the texture of undeformed

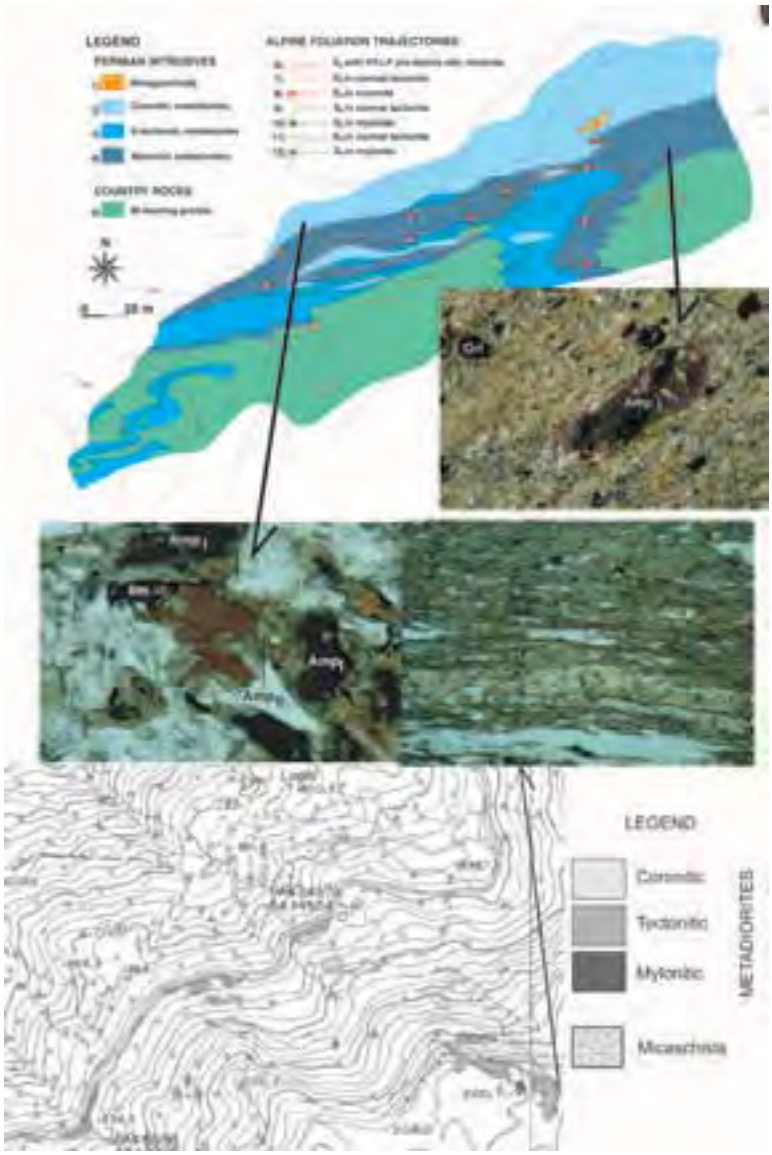

Figure 2.4. - Top image: form surface map of the Monte Pagano Permian diorite, deformed during Alpine polyphase metamorphism. States of increasing strain in Permian intrusives are mapped with trajectories of the Alpine superposed foliations; their relative chronology is shown by the number of dots. The metamorphic conditions, under which successive fabrics developed, are specified by different colors: red= HP eo-Alpine (epidote-amphibolite facies) imprint; green= green-schist facies imprint. Where metadiorites are undeformed, metamorphic minerals mimic the igneous fabrics (coronitic texture).

Top photomicrograph: mylonitic foliation in metadiorite, which wraps garnet porphyroblasts (Grt) and igneous amphibole porphyroclasts (AmpI), is defined by a fine-grained aggregate of amphiboleII, white mica and clinozoisite. AmpI shows subgrains and new grains of amphibole II at the margins; crossed polars (CP), LSP = 3 mm.

Lower-left photomicrograph: coronitic tschermakitic amphibole (AmpII) develops at the boundary of dark igneous hornblende (AmpI) and biotite (BtI), in an undeformed metadiorite; plane polarised light, low side of image = 2 mm.

Lower-right photomicrograph: S3 foliation is marked by the shape preferred orientation of light green alpine amphiboles, quartz ribbons and white mica + garnet-rich layers; ppl, lsi = 8 mm.

Lower map: 1:10.000 original map of Alpe Boschetto region, with partitioning of strain in Permian intrusives, which were deformed during eo-Alpine metamorphic re-equilibration.

metadiorites (i.e. *coronitic* domains): Alpine reactions produce corona-like growth of white mica, Grt and pale-blue Amp in the lack of new planar or linear fabric. In *tectonitic* (i.e. normally foliated) and *mylonitic* domains, the newly grown Alpine minerals (pale-blue Amp, Grt, white mica, Pl, and Zo/Czo) mark foliations and lineations developed during D3 Alpine deformation; in tectonitic domains, relics of igneous minerals are still preserved as mm-size porphyroclasts within the S3 foliation; in mylonitic domains, relics of igneous assemblage are no longer visible, and the mylonitic foliation S3 is exclusively marked by Alpine pale-blue Amp, white mica, Zo/Czo, and Pl (albite), Grt (Figure 2.4). In country rocks, new Alpine minerals define D3 fabrics (white mica, Cld, Mg-rich Chl and Grt) where tectonitic and mylonitic texture developed and randomly replace the pre-Alpine assemblage in coronitic domains. D4 and D5 deformations developed under greenschist facies conditions; they mainly consist of m- to dm-scale shear zones or fold systems. The newly-formed foliations are marked by the SPO of white mica, Chl, Ab and Ep ± BtII in metadiorites; and by white mica, Chl and Qtz in micaschists.

DAYS 3 - 4

The Engadine Window at the border of the eastern and western Alps

R. Bousquet[1] and R. Bertle[2], B. Goffé[3], V. Höck[5], F. Koller[1] and R. Oberhänsli[4]

[1] Department of Earth Sciences University of Basel, Switzerland
[2] Institute for Geological Sciences University of Vienna, Austria
[3] Geological department ENS Paris, France
[4] Institute for Geological Sciences University Potsdam, Germany
[5] Institute for Geology and Palaeontology, University of Salzburg, Austria

Introduction:

When, in 1904, for the first time, Pierre Termier described the geology of the lower Engadine as a window, he qualified it as *"de plus bel exemple que l'on puisse citer"* ("the most beautiful example we may cite"), due on the one hand to the straight contacts between the different units, and on the other hand to the mapping evidence (Figure 3. 1).

The Engadine window is an antiform trending NE-SW

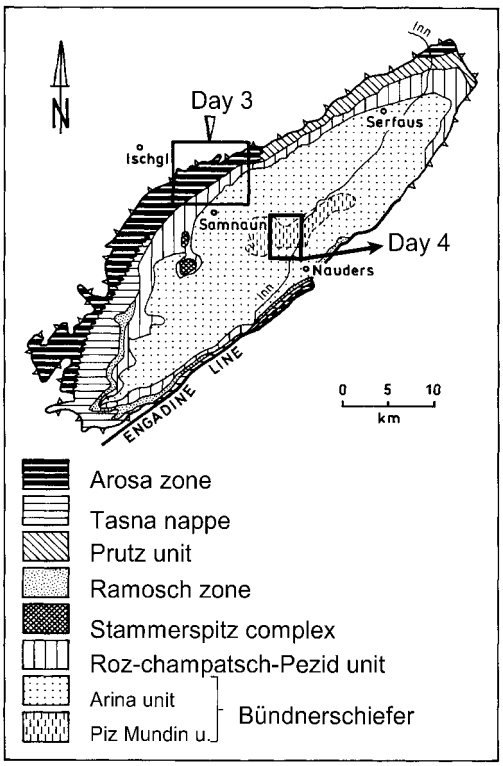

Figure 3.1 - Tectonic sketch map of the Engadine tectonic wondow, with location of areas visited in days 3 and 4.

(Klay, 1957), situated between the Eastern and Central Alps. It exposes a stack of Penninic nappes, overlain and framed by Austroalpine nappes (Figure 3.2). The rocks of the Engadine window can be subdivided into several distinct units (Hammer, 1921; Cadisch *et al.*, 1968; Trümpy, 1975; Oberhäuser, 1980); from top to base, they are as follows:

The Arosa zone ***(that will be visited on the third day)*** is a highly tectonized ophiolite-bearing unit, a few tens to more than a thousand m thick (Ring *et al.*, 1990). It includes an ophiolite series, mostly composed of serpentinites and gabbros (Höck & Koller, 1987), and a sedimentary series of radiolarian cherts, pelagic limestones and black shales of Hauterivian-Aptian age (Weissert & Bernoulli, 1985), and flysch deposits. The Arosa zone in the eastern part of the Grisons continues southward in the Platta nappe, with similar compositional and paleogeographic features (Dietrich, 1976; Frisch *et al.*, 1994). It is likely also correlative with the Matrei zone in the Tauern window (Frisch *et al.*, 1987), that was interpreted as part of an imbricated thrust stack formed by the overriding

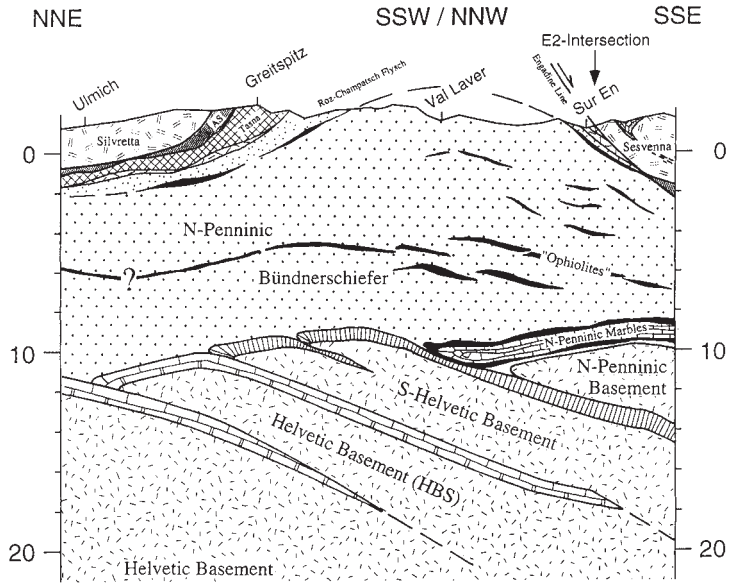

Figure 3.2 - Geological cross-section across the Engadine tectonic window.

of the Austroalpine units, that can be compared to an accretionary prism (Ring, 1992) (Figure 3.2).

The Tasna nappe is a continuous sedimentary sequence from the Permo-Triassic to the Upper Cretaceous, locally associated with slices of continental basement (Waibel & Frisch, 1989). The Lias-Cretaceous sequence is composed mainly of turbidites with associated debris flows and pelagic limestones. However, recent studies in the Tasna nappe basement (Florineth & Froitzheim, 1994), revealed a preserved transition from the continental crust of the Briançonnais terrain to the oceanic crust of the Valais basin.

The Ramosch Zone represents the transition between a continental unit (Tasna nappe) and an oceanic domain (Valaisan ocean) (Florineth & Froitzheim, 1994). The main unit is of a serpentinized peridotite-body associated with ophicarbonates and serpentinite breccias (Vuichard, 1984). Metagabbros are lenticular within. and adjacent to the serpentinite body. Directly underlying the serpentinite along an Alpine, top-north directed thrust fault, pillow basalts represent a part of the Valais ocean (Froitzheim *et al.*, 1996).

The Bündnerschiefer ***(that will be visited on the fourth day)*** underlies the Engadine window (Hitz, 1994), with up to 10 km of calcschists interbedded with shales and quartzites. It grades upward into flysch deposits that are lithologically very similar to the Bündnerschiefer, and are dated as Upper Cretaceous to Eocene (Ziegler, 1956). Some mafic bodies are intercalated within the schists, particularly in the core of the window. These bodies are mainly composed of pillow basalts and hyaloclastites associated with metaradiolarites, where geochemical criteria suggest an oceanic basement (Dürr *et al.*, 1993). This unit is the remnant of the northern Penninic ocean, the Valais basin (Trümpy, 1980; Stampfli, 1993). The metapelites are metamorphosed at blueschist facies (Goffé & Oberhänsli, 1992; Oberhänsli *et al.*, 1995) while metabasites have a greenschist (crossite, lawsonite) metamorphic overprint (Leimser & Purtscheller, 1980).

The LEW is overthrust by the Silvretta crystalline unit, consisiting of medium to high grade metamorphic augen-gneisses, biotite bearing paragneisses, and micaschists, as well as amphibolites and even eclogites. Occasionally, small wedges at the base of the Silvretta unit are found, consisting of slightly metamorphosed sandstones, dolomites, and limestones.

The exposure of Penninic units in the window is not only due to erosion of the Austroalpine nappes, but also to the movement along the Engadine line, which runs along the southeastern border of the window. The Engadine line is a tectonic lineament along which oblique slip and block rotation took place in Late

Tertiary times (Schmid & Froitzheim, 1993). It acted in this area as a southeast-dipping oblique normal fault, so that the Penninic units were uplifted relative to the Austroalpine nappes in the southeastern block (Hitz, 1994). The vertical throw is estimated to be approximately 4 km (Schmid & Haas, 1989).

DAY 3

Fimber unit and the Idalp ophiolite (South Pennic unit, Lower Engadine Window; Austria-Switzerland)

V. Höck[1], F. Koller[2], R. Bertle[2] and R. Bousquet[3]

[1] Institute for Geology and Palaeontology, University of Salzburg, Austria

[2] Institute for Geological Sciences, University of Vienna, Austria

[3] Department of Earth Sciences, University of Basel, Switzerland

Introduction

The northwestern and western part of the Lower Engadine Window (LEW) is formed by two units, the lower Tasna nappe, believed to be of Middle Penninic (Brianconnais) origin, and the higher Arosa zone, which is assigned to the South Penninic (Ring et al 1990, Bousquet et al. 1998). Occasionally, a Fimber unit is delineated containing elements of the South Penninic Arosa zone and parts of the Middle Penninic Tasna nappe (Fuchs and Oberhauser, 1990, Bertle 2000). In the following descriptions, we will distinguish between the Idalp Ophiolite and the Fimber unit, the former being in a higher tectonic position.

The LEW is overthrust by the Silvretta crystalline unit, consisting of medium to high grade metamorphich augen-gneisses, biotite-bearing paragneisses and micaschists, as well as amphibolites, and even eclogites. Occasionally, small wedges at the base of the Silvretta unit are found, consisting of slightly metamorphosed sandstones, dolomites and limestones. They are termed "Subsilvrettide zone" (Dauerer 1980, Oberhauser 1980).

Fimber zone

The stratigraphic sequence in the Fimber zone starts, apart from blocks of granitic and metamorphic rock, as well as dolomites and limestones, with the Upper Triassic Keuper beds, which contain sandstones, quartzites, limestones, rauhwackeys, variegated shales, and gypsum. They are overlain by the Liassic Steinsberg limestone. Its biostratigraphic classification is based on ammonites, brachiopods, bivalves, and microfossils. The limestone is overlain by Posidonia shales, and the Doggerian Idalp sandstone. The Jurassic formations end with Malmian limestone breccias and limestones similar to the Aptychus Limestones. The Lower Cretaceous is represented by bluish to greyish calcschists with microbreccias (Neocomian Flysch), and the Tristel beds middle Lower Cretaceous fine-grained limestone breccias. They are followed in turn by sandstones interbedded with micro- and macro- breccias of the late Lower Cretaceous (Alb). The overlying Couches Rouges with Globotruncanae are most likely of Late Cretaceous age (Campan to Santon). The uppermost section is formed by the "variegated Bündnerschiefer", consisting of sandstones, breccias and shales. Based on the occasional findings of foraminifera, their stratigraphic age ranges from Late Cretaceous to Eocene.

Metamorphism of all formations mentioned above is badly constrained. First of all, fluid inclusion investigations, from late metamorphic discordant veins (Bertle & Goetzinger 2003), clearly demonstrate an alpine HP-event in Triassic carbonates just south of Greitspitz. P_{max} was estimated with 4.25 kbar for pure aqueous fluid inclusions at a trapping temperature of ca. 200 °C. Secondly, age dating of detrital micas from the Idalpsandstone shows the influence of alpine heating, at low temperature steps in the Ar-release diagram (Bertle 1999). Deformation lamellae of calcite from Tristelschists indicate deformation at temperatures above 200 °C.

The Idalp Ophiolite

The Idalp ophiolite displays the uppermost unit of the LEW and is overlain to the north and northwest by the Austroalpine Silvretta unit, and the "Subsilvrettide zone" (see above) At its southern border,, the ophiolite body rests tectonically on Mesozoic sediments of the Fimber zone. The ophiolite body itself is subdivided into two independent units called Flimsspitze nappe (southern part) and Bürkelkopf nappe (northern part) by Daurer (1980). They are separated by a tectonic slice, consisting of diaphtoritic micaschists, gneisses, and amphibolites, known as the "Flimjoch wedge", which originated from the Silvretta unit.

The reconstructed columnar section of the Idalp ophiolite can be seen in Figure 3.3. The ophiolite sequence starts with 60-80m thick serpentinites They contain some small inclusions of rodingites (metagabbros). The serpentinites are separated by a tectonic contact from the overlying isotropic gabbros, which are intruded by rare diabase dikes. The volcanic

Volume n° 2 - from B16 to B33

section has a tectonic contact at its base, and starts with pillow lavas intercalated with several layers of massive diabase, and with some hyaloclastites that increase in abundance towards the upper levels. At the stratigraphic top, tuffs with radiolarian schists are deposited. The whole volcanic pile (including the sediments) has a thickness of 250 to 300 meters.

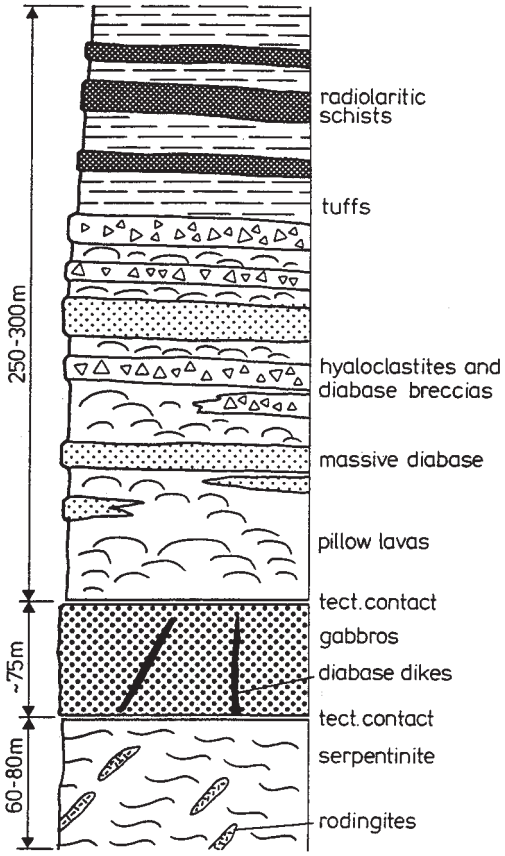

Figure 3.3 - Interpretative lithostratigraphy of the Idalp ophiolite.

The two tectonic subunits of the ophiolite complex have the same tectonic style, which consists of, firstly, a serpentinite-gabbro association with a maximum thickness of 150 m at its base; and resting on this, but tectonically separated, a large recumbent fold overturned towards the north, consisting of a small serpentinite-gabbro body in the core, surrounded by massive lava-flows and pillows. The hyaloclastites, tuffs and radiolarites form the outermost part of the fold (Figure 3.4).

The metamorphism of the ophiolites is twofold; an older HT oceanic metamorphic event can be separated from a younger HP imprint. Evidence for the former comes from the replacement of gabbroic clinopyroxenes by amphiboles (pargasite, magnesian-hornblende to actinolite) formed at relatively high temperatures. This, together with some metasomatic changes of the bulk geochemistry (mainly Na enrichment), and some local strong oxidation, argues for this hydrothermal event. Remnants of the E-W striking oceanic high temperature deformation planes in the gabbros, show black amphibole formation in their vicinity, as a common indication of H_2O infiltration (Figure 3.5). The cores of these amphiboles in the altered gabbros, still contain high Cl contents, of up to 4000 ppm. In the hyaloclastites and pillow breccias, the hydrothermal influence locally causes ~E-W striking epidote-rich veins, and high oxidation with an intense red color.

The Alpine metamorphic grade of the Idalp ophiolite sequence belongs to the low-temperature conditions at the transition between greenschist and blueschist facies, with 7-9 kbar at ~300°C. The mineral assemblages are defined by pumpellyite + chlorite + albite. The

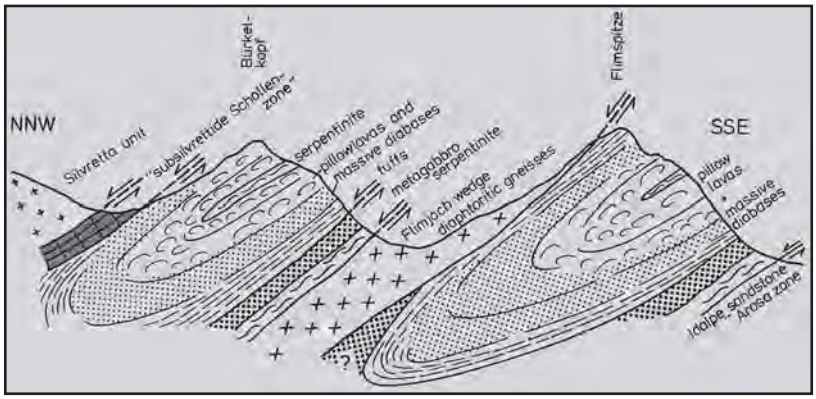

Figure 3.4 - Geologic cross-section of the Silvretta Austroalpine and Idalp ophiolite units, between Flimspitze and Bürkelkopf, showing the two tectonic units of Flimspitze and Bürkelkopf nappes.

Figure 3.5 - Hydration reactions in the Idalp gabbros.

pumpellyite of the metagabbro is Mg-rich, the green pumpellyite of the diabases with a Fe^{tot} / (Fe^{tot}+Al) range between 0.11-0.15. Prograde replacements by epidote are rare. In the metabasite, a high phengitic mica, with an Si of 3.6, was locally found.

The Idalp ophiolite is typical among many ophiolitic occurrences in the Alps: it is highly dismembered and displays a very small ultramafic-mafic cumulate section; its lateral extension is a few kilometers only, with a thickness of several hundred meters. Metabasalts and metatuffs are closely comparable to N-type MORB, derived from a depleted mantle by partial equilibrium melting, with a subsequent crystal fractionation resulting in highly evolved Ti-, Zr-, and V-rich magmas. From a geochemical point of view, the Idalp ophiolite is very similar to ophiolites from the Hohe Tauern (Höck 1983, Höck and Koller 1989, Koller and Höck 1990), and to same ophiolitic rocks of the Rechnitz window at the easternmost end of the eastern Alps (Koller, 1985).

Excursion log 3rd day (Idalp Area)
Riding up to Viderjoch from Samnaun by cable-car
Part 1: walking from Viderjoch – Flimspitz northern and western ridge – Pardatschgrat back to Viderjoch
Part 2: walking from Viderjoch to Greitspitz and back to Viderjoch
Back to Samnaun by cable-car

Part 1: Trip from Viderjoch to Pardatschgrat: guided by F. Koller and V. Höck, R. Bousquet

Stop 3.1:

Pillow lavas

The basaltic unit of the ophiolite consists of low grade metamorphic equivalents, of pillow lavas, pillow breccias, hyaloclastites, and fine-grained tuffs as well as of massive basalt flows, locally with large pyroxene phenocrysts. In general, all these rocks show a very fine-grained matrix. Primary structures, such as ophitic, intersertal plagioclase and flow textures are well-preserved. All glassy areas and fragments are replaced by a dark-green chlorite mass.
The fine-grained basaltic groundmass is partly replaced by a metamorphic assemblage, containing albite, epidote, calcite, rare pumpellyite, actinolite, and lesser amounts of quartz, haematite, and sphene.
The metabasalts and metatuffs are tholeiitic in chemistry, resembling abyssal tholeiites. The K_2O contents are very low, the concentration of TiO_2 as well as the content of trace elements, such as Zr, Y, V, Cr, and Nb, are in the range of typical MOR basalts, but some may reach values more typical of a within-plate environment (ocean island basalts).

Stop 3.2:

Basaltic Dikes in Gabbros

Isotropic gabbros cross-cut by E-W-striking basalt dikes with MORB composition. Their chemical composition is relatively less evolved with respect to the pillow lavas of stop 3.1 (Figure 3-3).

Stop 3.3:

Isotropic gabbros and gabbro pegmatites

The plutonic sections consist mainly of a clinopyroxene-plagioclase gabbro, which is poor in iron oxide minerals. The grain size shows a strong variation (from 5 mm up to 10cm), in pegmatitic areas. Among the primary magmatic minerals only clinopyroxene has survived, and may be sheared and deformed or has partly reacted to form amphiboles. The former plagioclase is only a form relict, and has been replaced by a fine-grained brown mass of epidote-clinozoisite, or pumpellyite and albite. In the few ferrogabbroic dykes, form relicts after ilmenite and titanium-magnetite were also found, replaced mainly by sphene and haematite. Amphiboles deriving from the clinopyroxenes show a complex mineralogical history. They consist of an older brown magnesium-hornblende, or a green hornblende. These older phases were replaced by a greyish-green or blueish-green actinolitic amphibole and, later on, by newly-formed, weakly-colored actinolite needles. The metamorphic mineral assemblages of the gabbros are the same as those of the extrusive rocks. In gabbroic dykes inside the serpentinites, rodingitization has taken place, with a new formation of hydrogrossular or idocrase.

Stop 3.4:

Hyaloclastites and radiolarites

Hyaloclastites are heterogeneous breccias of lava fragments and devitrified glass components, sometimes with sediment participation, often red-coloured due to finely-dispersed haematite. Tuffs and tuffites are heterogeneous mixtures of minerals, lava and glass re1ics without vo1canic textures, and with variable participation of sedimentary material. Sedimentary interca1ations are rich in carbonate, muscovite, and quartz, with decreasing vo1canogenic participation. Radiolarites occur mainly in the Bürke1kopf nappe, forming layers of some meters thick. They are red, extreme1y fine-grained, sometimes banded rocks, with questionable re1ics of Radio1arians.

Stop 3.5:

"Subsilvrettide zone"

Dolomites, banded and partly-folded calcareous slates of uncertain Triassic or Jurassic age. An isolated block of dolomite within the Flimspitze Nappe belongs to this zone, too.

Stop 3.6:

Silvretta crystalline rocks, including "pseudo-tachylites"

Ortho- and paragneisses, micaschists, amphibolites. In the area of the "Subsilvrettide Schollen", the rocks are well-preserved, and almost not retro-metamorphosed. Immediately above the thrust plane, pseudotachylites (ultramylonites resembling fine-grained dike rocks), cut the crystalline rocks. Going westwards, retro-metamorphic transformations increase.

Retro-metamorphic two-micaschists and amphibolites tectonically separate the ophiolite nappes. Pseudotachylites in the micaschists are strong arguments for the tectonic imbrication of Silvretta Crystalline unit.

Part 2:Trip from Viderjoch to Greitspitze (2871 m), guided by R. Bertle

Stop 3.7:

Bunte Bündnerschiefer: Lens between two slices of ultramafic rocks:

Outcrop of typical breccias of "Bunte Bündnerschiefer" of Upper Cretaceous age, as indicated by age-constraining planktonic foraminifera. Components of breccia are mainly carbonates, but also minor volcanics and metamorphic rocks (micaschists).

Stop 3.8:

Bunte Bündnerschiefer – Palombini type:

The outcrop exposes typical Palombini-type Schistes lustrés of South Penninic origin: sandstones with intercalated dark phyllites, both intensely folded together. Heavy mineral investigations show chromite as an accessory mineral, which is assumed to be an index mineral for Cretaceous South Penninic sediments. The age is given by *Globigerina archaeocretacea* (Early Cretaceous; Bertle, 2002).

Stop 3.9:

Grenzstein 5 - Tristelformation:

Typical rocks of the Middle Cretaceous Tristelformation are exposed – carbonatic microbreccias, containing well-preserved index microfossils of Barremian to Aptian age: *Dictyoconus* sp., *Palorbitolina lenticularis* Blumenbach, *Salpingoporella* sp., etc. The Tristelformation will also be visited on the next day, at Piz Mundin. The source of the breccias can be located in the Tasna microcontinent (Schwizer, 1983; Oberhauser, 1983, Bertle, 2002)

Stop 3.10:

Greitspitze – Peak:

The peak of the Greitspitze consists of limestones of the "Steinsberger Lias". It can be classified as grainstone after Dunham, however intense recrystallisation took place during alpine metamorphism. Nevertheless, index ammonites of Liassic age can be found: *Paltechioceras* sp. of *raricostatum*-Zone (Sinemurian). Small outcrops of "Posidonienschiefer" and "Idalpsandstein" can also be found. The age of the Idalpsandstein is given by *Hammotoceras insigne* of Toarcian age; the age of the underlying Posidonienschiefer outcrops is given by their position between Idalpsandstein and "Steinsberger Lias".

DAY 4

HP/LT metamorphism within the North Penninic ocean (Lower Engadine Window; Austria-Switzerland)

R. Bousquet[1] and R. Bertle[2], B. Goffé[3], F. Koller[1] and R. Oberhänsli[4]

[1] Department of Earth Sciences University of Basel, Switzerland

[2] Institute for Geological Sciences University of Vienna, Austria

[3] Geological department of ENS Paris, France

[4] Institute for Geological Sciences University of Potsdam, Germany

Ferro- and magnesio-carpholite: an index mineral of HP-LT metamorphism in the metasediments

The name carpholite derives from the Greek word carphos, meaning "hair of fire", due to the yellow-colored needles of the mangano-carpholite (Werner, 1871) found in the Ardennes massif. Ferroan and magnesian carpholite form a continous solid solution from the pure-iron end-member, Fe-carpholite {0.5 < XFe = Fe/(Fe+Mg) < 1} to pure-magnesium end-member, Mg-carpholite {0.5 < XMg = Mg/(Fe+Mg) < 1}. These two minerals were discovered relatively recently: De Roever found first the Fe-carpholite in Sulawesi Island in 1951, and Goffé et al. (1973) described the Mg-carpholite in the western Alps (Vanoise massif). Since the beginning of the 1980s, these minerals have been intensively studied, and so they have become the index-mineral for the HP-LT metamorphism of the metasediments. The stability field (Figure 4.1) was experimentally determined by Vidal et al. (1992). Since then, many occurrences have been discovered in the Tethyan mountain belts all over the world: in the Western Alps (Goffé & Chopin, 1986, Goffé et Bousquet, 1997), Central Alps (Goffé & Oberhänsli, 1992), in Corsica (Daniel *et al.*, 1996), the Apennines (Theye et al. 1997,), Calabria (De Roever et al., 1967), the Betics (Goffé et al., 1989,), Rif (Bouybaouène et al., 1995), Crete and the Peloponnese (Theye et al., 1992), Turkey (Oberhänsli et al., Rimmele et al., 2003); Oman (Goffé et al., 1988), and in New Caledonia (Black et al., 1993).

These minerals occur practically in all kinds of HP-LT metasediments, which previously contained mineral association with kaolinite and chlorite or chlorite and illite, but these metasediments are always deprived of feldspar and plagioclase. We can find (Fe, Mg)-carpholite in metabauxites, pelitic schists, calcschists, or conglomerates. So it appears in three different ways:

Well-preserved, as macroscopic curved fibers up to 30 cm in length, in quartz or calcite veins. These metric-sized veins are often stretched and parallel to the main schistosity. Then (Fe, Mg)-carpholites can also occur in the rock itself as centimetric rosettes.

Partially-retrograded, but always visible to the naked eye, as small fibers in disaggregated quartz veins. (Fe, Mg)-carpholite are replaced by associations composed of sheet silicates (micas, chlorite, pyrophyllite). In this case, no relic can be found in the country rocks.

In relic, as small needles (between 0.5 µm to around 50 µm length), only recognizable with a microscope in old sheared quartz veins.In some case, all relics can disappear, and vestiges of (Fe, Mg)-carpholite can be recognized due to the fibrous and woody aspect of the quartz.

All these various kind of (Fe, Mg)-carpholite correspond to different tectono-metamorphic evolutions during subduction and exhumation processes.

(Fe, Mg)-carpholite in the Engadine window

In the north Pennine metasediments of the Engadine window, two units display distinct metamorphic histories (Bousquet et al., 1998; Bousquet et al., 2002).

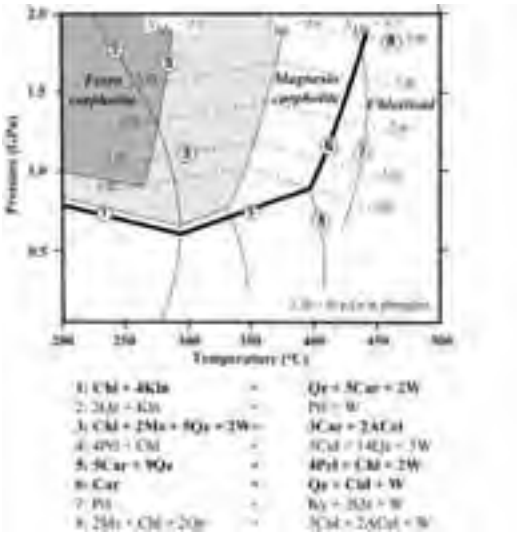

Figure 4.1 - P-T stability field of carpholites, according to Vidal et al., 1992.

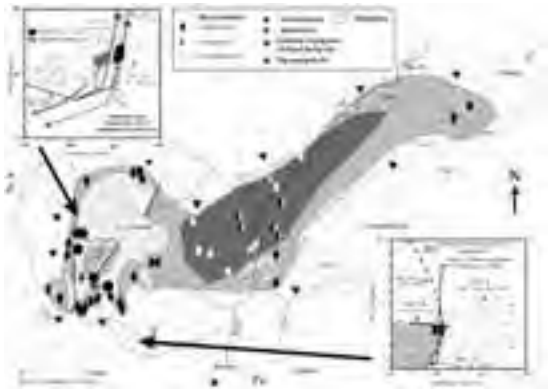

Figure 4.2 - Field occurrences of critical metamorphic minerals.

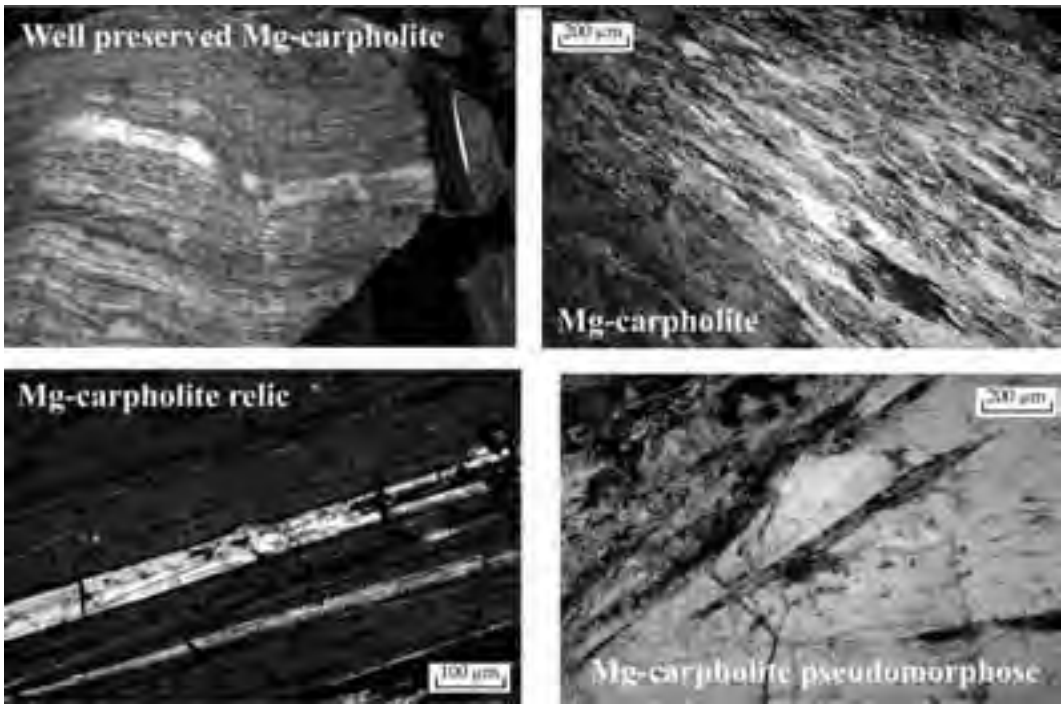

Figure 4.3 - Field and microscopic appearances of carpholite occurrences at Piz Fot (Piz Mundin).

The structurally lower unit (Mundin unit) has a clear HP-LT history, whereas the upper unit (Arina unit), does not show obvious HP-LT mineral assemblages. (Fe,Mg)-carpholite in metapelites (Figure 4.2) and glaucophane in metapillows are exclusively found in the central part of the window (i.e., the Mundin unit), forming the core of a late anticline.

In the overlying Arina unit, evidence for HP metamorphism is scarce. However, crossite and lawsonite occur in metabasites (Leimser & Purtscheller, 1981), and Mg-pumpellyite and associations with Chl - Alb – Phg, occur in metapelites of the Arina unit. In the core of the Mundin unit antiform, carpholite appears as relics (Figure 4.3). In contrast, in the upper part of the same unit, immediately below the contact with the Arina unit, carpholite is well preserved. For the Mundin unit, *P-T* estimates range between 11 and 13 kbar for a temperature around 350-375°C (Bousquet et al., 2002). The PT conditions for the Arina unit range around 6 kbar, 300°C (Figure 4.3). However, the composition of mica in this unit is quite variable. In particular, the pyrophyllite to alumino-celadonite proportions increase with increasing distance from the Mundin unit. Such a variation is consistent with pressures decreasing upwards in the Arina unit, i.e. with increasing distance from the HP (Mundin) unit. The pressure gap between both units is at least 5 kbar.

Carpholite fibers within quartz lenses and between boudins, mark a consistent northwest-southeast mineral lineation. Later stretching increments, in the same direction, reworked the carpholite fibers, which are boudinaged, and finally opened cracks filled only with quartz. This late deformation was also less ductile and less penetrative than the first event, which occurred during the HP metamorphism. Observations in the *X-Z* plane reveal chiefly top-to-the-northwest sense of shear, localized preferentially in a major shear zone, called the Mundin shear zone (Figure 4.4; Bousquet et al., 1998).

Above the Mundin shear zone, deformation in the carpholite-free zone is characterized by the same stretching direction, although strain is much less penetrative and intense. The most common structures are northwest-verging folds, whose axial planes tend to be less oblique in relation to the regional foliation of the Mundin shear zone. The folds change from open folds, far from the contact between both units, to sheath folds, with axes parallel to the stretching

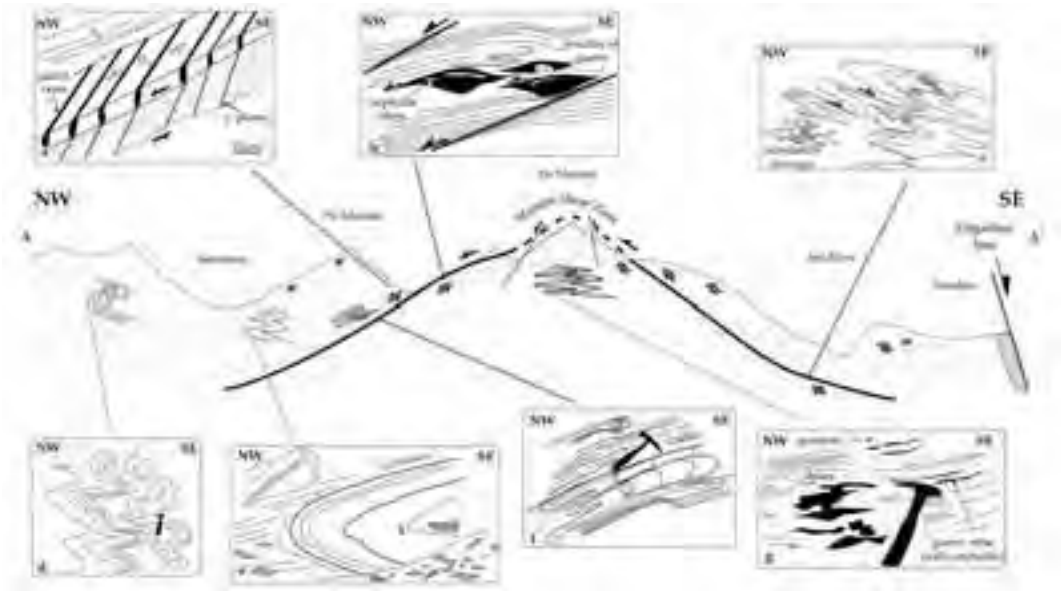

Figure 4.4 - Geological profile across the Piz Mundin area in the Engadine window Bündnerschiefer.

lineation near the contact (Figure 4.4). This change suggests that the shearing was distributed in the whole upper part of the Bündnerschiefer, though shear strain was greatest in the Mundin unit (Bousquet et al., 1998; Jolivet et al., 1998).

Field itinerary

Stop 4.1:

Costa Bella – Contact basalts-sediments.
First view of the metamorphism. Contacts between MOR-basalts and sediments (stratigraphic or in the accretionary wedge?) can be seen. Metasediments and metabasalts show the same metamorphic evolution:

Mineralogy of the metasediments in the Mundin unit

Carpholite occurs in synfolial segregations of quartz and calcite as green-white colored fibers up to 20 cm in length. This aspect is typical for carpholite in metapelites throughout the Alps (Goffé & Chopin, 1986; Goffé & Bousquet, 1997). Carpholite fibres are always elongated in the same direction, and show kinking. Two types of carpholite can be clearly distinguished: relics of carpholite and pseudomorphs, after carpholite in the core of the Mundin unit (lower part), and a fresh carpholite at the edge (upper part). Fresh carpholite forms rock-forming fibers 200-300 mm thick, or microfibers, 10 to 100 mm long, and 0.5 to 10 mm thick, trapped in quartz and calcite crystals. XMg ranges from 0.52 - 0.72. Pseudomorphs after carpholite are composed of Mg-rich chlorite and white mica, whereas relics appear as microfibres in quartz. Any sudoite, pyrophyllite, or kaolinite occur in the pseudomorphs after carpholite. The fluorine content shows a very large variation from 0.3 to 4.6 wt. % (Goffé & Oberhänsli, 1992), with a mean around 2-3 wt. %. F-rich carpholite is always well-preserved, but F-poor carpholite appears also as fresh fibres in the upper part of the Mundin unit.
White micas are fine-grained phengite and paragonite, in which there is relatively high Na-content in phengite and K-content in paragonite; both phases are finely intergrown. The mean Si^{4+} content of phengite in the lower part is higher (3.32 with 3.40 as maximum) than the mean in the upper part (3.22 with 3.34 as maximum, Si p.f.u).

Mineralogy of the metabasalts in the Mundin unit

Na-amphiboles of two types occur rarely in the mafic body of Piz Mundin (Bousquet et al., 1998): glaucophane with albite, tremolite, chlorite, and epidote, as a rock-forming assemblage in metapillows, and riebeckite in association with epidote, chlorite, stilpnomelane, and albite, (Oberhänsli, 1978) in crosscutting veins. Glaucophane is extensively retrogressed and appears as fine needles in less deformed zones or in the core of large crystals of

Volume n° 2 - from B16 to B33

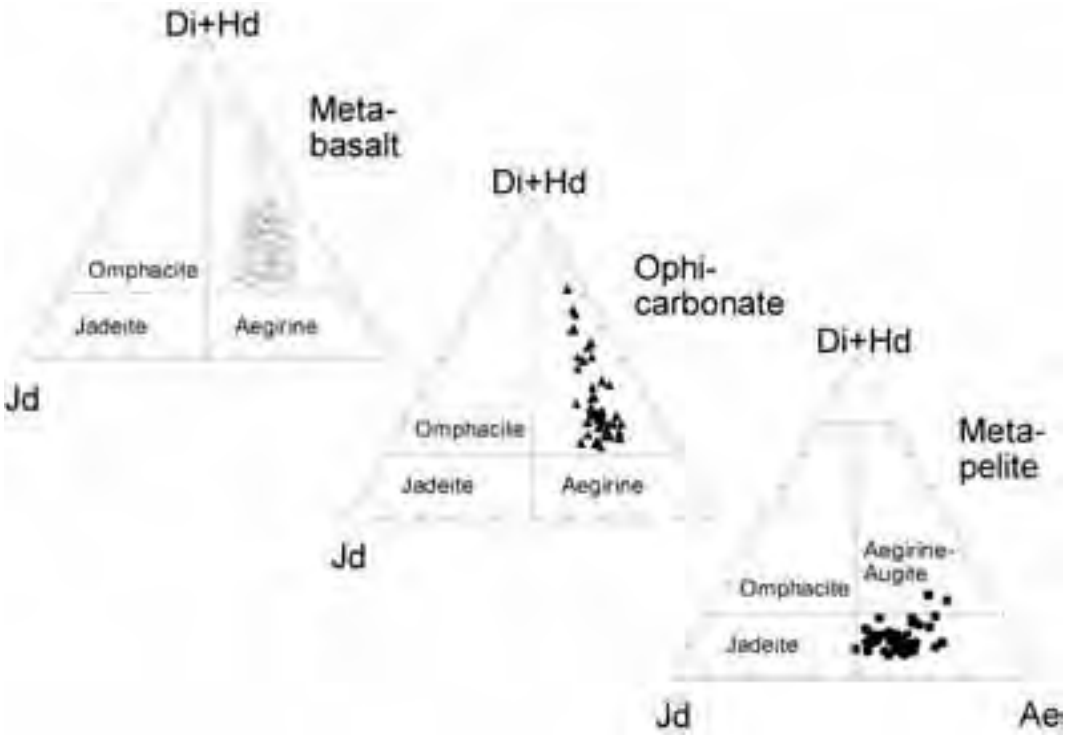

Figure 4.5 - Compositions of high-pressure-related clinopyroxenes in the Costa Bella metaophiolites of Piz Mundin.

green actinolite.

Na-pyroxene can be found in the following three types of samples, 1) in metabasites, 2) in ophicarbonates, and 3) in graphite-bearing metapelites close to the metabasites. It must be noted, that all Na-pyroxene-bearing samples underwent, prior to the pyroxene formation, alterations through oceanic metamorphism, or through interaction with oceanic fluids. From this influence a higher oxidation stage, and sometimes Na excess in the rock is common. In metabasite and ophicarbonates, all Na-pyroxenes are green aegirine-augite, with a 12-20 % Jd component in the metabasitesl and 10-20 in the ophicarbonates (Figure 4.5). In the rare pyroxene bearing metasediments, the Na-pyroxene composition is close to the join aegirine-jadeite, with a 25-45 % jadeite component (Figure 4.5). The following mineral assemblages can be described:

Metabasite: *Aegirine-augite ± Mg-riebeckite + chlorite + epidote + haematite + quartz*

Ophicarbonates: *Aegirine-augite ± Mg-riebeckite + calcite/aragonite + chlorite + clinozoisite/epidote ± stilpnomelane*

Metapelites: *Aegirine-jadeite ± Mg-riebeckite + quartz + phengite + chlorite + graphite ± haematite*

Most of the blue amphiboles of the Na-pyroxene assemblages are riebeckite to Mg-riebeckites, and seem to replace the pyroxenes.

Aragonite was found as a relict in the Na-pyroxene bearing assemblages, partly or strongly replaced by calcite.

In this stop S-C-fabrics may be observed; they indicate a to-the- northwest sense of shear, and some isoclinal folds. The stretching lineation, oriented NW-SE, is formed by the carpholite fibers. On the way to stop 2, axinite might be found, as well as large blocks of blueschists.

Stop 4.2:

Costa Bella – Pillow-basalts

Beautiful and well-preserved pillow basalts can be seen. These pillows are greatly deformed and stretched in the same direction as the carpholite fibers. In these pillow-basalts, some relics of magmatic structures can be found. Blue amphibole is present in thin sections. Geochemical data show MOR-characteristics for these basalts (Dürr et al., 1997).

Stop 4.3:

Piz Fot – Mega-needles of carpholite

Pitz Fot is the best outcrop for carpholite in the Engadine window: elongated needles of more than 50 cm are found here.

The sediments occurring here never underwent HP/LT conditions. In these sediments, the following minerals can be found:

White micas, as in the Mundin unit, are phengite and paragonite. Analyses of paragonite give results that are close to the end-member composition. There are two types of phengites: large crystals, with no preferential orientation, showing numerous aspects of alteration, are probably detrital and newly grown. In fine-grained micas in the foliation, in association with Chl and Alb, the Tschermak substitution varies from 3.05 - 3.35 (Si p.f.u), with a deficit in the interlayer site, which can be important (K^++Na^++ Ca^{2+}=0.75 to 0.95). In these phengites, the Tschermak substitution decreases with distance from the Mundin unit.

Pumpellyite was found in one sample of schists in the Arina unit as small brown-colored twinned prisms, associated with chlorite, is Mg-rich (XMg = 0.82).

Kaolinite occurs as unoriented lamellae in the youngest veins, synchronous with D2, in association with albite and phengite in one sample of the Arina zone.

Albite only occurs in the metapelites of the Arina unit, in the mineral association, or as veins. Large grains of albite contain inclusions of phengite (that can contain up to 5% Ba).

DAYS 5 - 6

The southern steep belt of the central alps

Martin Engi and Alfons Berger (University of Bern, Switzerland)

Fifth day – *A section of the Southern Steep Belt, between Alpe Gesero and Passo San Jorio (Swiss - Italian border): High-strain mélange sequence, metamorphosed in upper amphibolite facies, with abundant partial melting, cut by the Jorio-Tonale segment of the Insubric Line, delimiting the Central Alps to the Southern Alps (unaffected by Alpine metamorphism).*

The Southern Steep Belt (SSB), terminates the collisional core complex of the Central Alps against the northern margin of the Adriatic (=Apulian) plate. A segment of the Insubric Line, the Jorio-Tonale Line (Cornelius & Furlani-Cornelius, 1930), forms the steep E-W trending fault contact between the Southern Alps and the SSB (Figure 5.1). The role of the SSB has long been enigmatic. It was classically regarded as the "root zone" from which the Pennine and lower Austroalpine nappes (Argand, 1911) were supposed to have emerged. However, detailed field work (e.g. Knoblauch et al., 1939; Knup, 1958; Fumasoli, 1974; Bächlin et al., 1974; Milnes et al., 1981), failed to support such an interpretation. Knoblauch (1939) had found, on the basis of meticulous mapping in the Bellinzona-Jorio area,

Figure 5.1 - Schematic tectonic map of the Central Alps. Units shaded in gray are mélange units with HP-fragments, considered part of the Alpine TAC (tectonic accretion channel: CL – Cima Lunga unit, Or – Orselina zone, So – Someo zone, SSB-TAC – collection of TAC-fragments making up the bulk of the Southern Steep Belt. IL: Insubric Line. Swiss coordinate network labelled in km.

that he could not distinguish individual thrust sheets corresponding to the crystalline nappes further north. Instead he proposed various "zones", in order to group the extraordinary variety of rock types found in the SSB, but the tectonic significance was left open. It proved impossible, prior to the concept of plate tectonics, to account for the great variability of rock types and late-orogenic magmatism found within the SSB, and to comprehend the relation of this high-strain complex to the basement nappes which make up most of the Lepontine Alps.

This part of the field trip aims to present and discuss the evidence that lead Engi et al. (2001a) to interpret the major portion of the SSB as an exhumed Tectonic Accretion Channel. This TAC is thought to have initiated early during convergence, along the plate interface (Figure 5.2), where the tectonic mélange unit is likely to have been fed by tectonic slivers from both

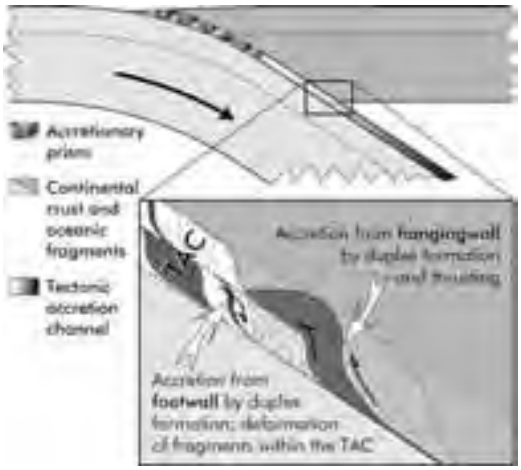

Figure 5.2 - Schematic cross-section through the convergent margin to Asthenospheric depth, showing the position of the TAC (tectonic accretion channel) at the plate interface. Inset: Cartoon of mechanisms feeding the TAC, both during subduction and collision/extrusion

plates. Continued evolution of this unit during and following the collision stage, and the particular significance of the TAC to the tectonometamorphic characteristics of the Central Alps, will be the main theme of this field trip (5th and 6th day). Special emphasis is placed on discussing petrological and geochronological data, in the context of results from numerical simulations, in order to understand the processes responsible for (a) the rapid extrusion of HP-relics from Mantle depths, (b) the high-temperature Barrovian (medium pressure) regional metamorphism in the Lepontine, (c) the origin and character of the migmatite belt linked with the TAC, and (d) possible implications on paleo-geographic reconstructions.

Base maps: Regional topography (1:100,000) on Swiss sheet "Sopraceneri"; detailed maps (1:25,000) are "Passo S. Jorio" (sheet #1314) for the 5th day, and "Bellinzona" (sheet #1313) for the 6th day. These are *essential* for geologists willing to go on the hikes on their own! An equally detailed geological map is available only for the 6th day (Bächlin et al., 1974), whereas the Jorio map sheet (Knoblauch et al., 1939), is unfortunately out of print.

Regional geologic setting

The Lepontine belt of the Central Alps reveals a type example of a collisional orogen, characterized structurally by a stack of crystalline thrust sheets (Figure 5.1) derived from the Penninic area. Some 82% of the (pre-Quaternary) units surfacing in the Lepontine have witnessed one or more pre-Alpine orogenies. Evidence of polymetamorphism is thus widespread, with relics from the Variscan (ΞHercynian), Caledonian, and even Pre-cambrian orogenies, having been recognized. The Alpine overprint is quite variable, especially in the northern Lepontine, a fact that has plagued early efforts in documenting regional metamorphic patterns (Niggli,

Figure 5.3 - Metamorphic mineral zones and isograds in the Central Alps (after Frey & Ferreiro Mählmann, 1999, and sources therein). Abbreviations as in Figure 5.1

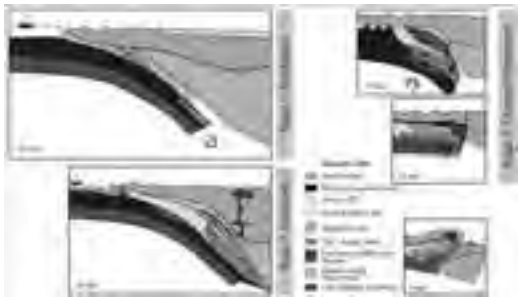

Figure 5.4 - Schematic scenario of the tectonic evolution of the Central Alps (simplified from Pfiffner et al., 2000)

1974). Through the study of the metamorphic grade of post-Permian sediments, i.e. post-Hercynian protoliths, the now well-established metamorphic zonal pattern could be deciphered (Figure 5.3, 5.5). Mineral zone boundaries and isograds form a fairly regular concentric pattern, which appears to cross major nappe boundaries. This indicates that the regional metamorphic overprint, at least at its peak conditions, must have been reached *after* thrusting

had essentially ceased. The Insubric Line is younger yet, as it transects the zone of highest Barrovian metamorphism in the Central Alps, whereas the adjacent Southern Alps are but minimally affected by Alpine heating (Colombo & Tunesi, 1999).

However, the tectonometamorphic evolution of the Central Alps (Figure 5.4) is not as simple as the above scenario might suggest. Firstly, the quantitative metamorphic field gradient of the classic Barrovian (medium-pressure) belt is odd: whereas the *isotherm map* (Figure 5.5) shows a pattern similar to the metamorphic isograds, with the Insubric Line cutting through the core of the thermal dome, the *isobar map* shows two maxima in the center of the Lepontine. This delineates two structural domes: the Leventina dome (E), and the Verampio dome (W) which are separated by the synformal Maggia nappe, trending NNW. Secondly, the thermal conditions mapped in Figure 5.5 are certainly *diachronous*, as mineral formation ages (Figure 5.6) indicate a protracted metamorphic evolution. This is confirmed, thirdly, by the range of P-T paths documented from several units, as well as the occurrence of high pressure relics in the Lepontine – Alpine eclogite relics appear to be entirely restricted to remnants of the TAC (Figure 5.1); relic blueschist facies conditions are known from (post-Variscan) Valaisan units. Recent age data indicate that the HP stage is Eocene throughout. Fission track data for the Lepontine indicate cooling age patterns with little resemblance to Barrovian T_{max} and formation ages.

Figure 5.5 - Metamorphic isotherms and isobars (updated from Engi et al., 1995; Todd & Engi, 1997); these data are thought to reflect conditions near T_{max} and P at/near T_{max} for each sample. The pattern is substantially diachronous across the orogen.

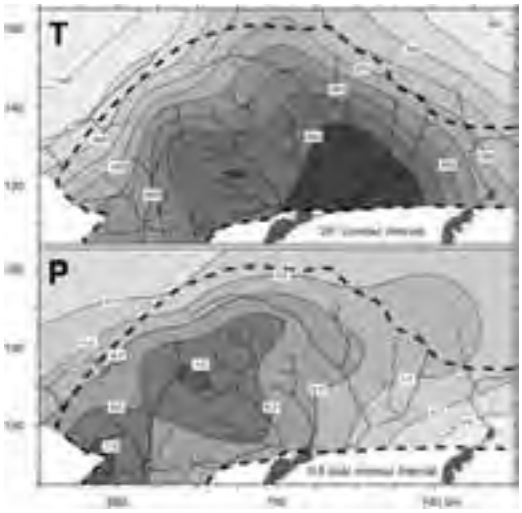

These observations constrain models of how the Alpine nappe stack was assembled, i.e. how deeply each unit had been subducted prior to being assembled, and in what sequence the thrust sheet contacts were (re-)activated during stacking. To the best of our present knowledge, TAC fragments were the only units in the Central Alps to have reached depths >30 km in the Eocene, around 40 Ma ago, with P_{max} >28-30 kbar. In the SSB, the calcalkaline magmatism (e.g. Jorio tonalite), migmatite formation, and thermal overprint in upper amphibolite facies overprint, have been dated at 32-29 Ma, with pressures at the time of T_{max} near 5.5-6 kbar.
These constraints, combined with a wealth of

Figure 5.6 - Three age belts in Lepontine: Map of select age data interpreted as mineral formation ages formed during Alpine Barrovian overprint (Köppel & Grünenfelder, 1975; 1978; Köppel et al., 1981; Vance & O'Nions, 1992; Schärer et al., 1996; Gebauer, 1999; Engi et al., 2001b).

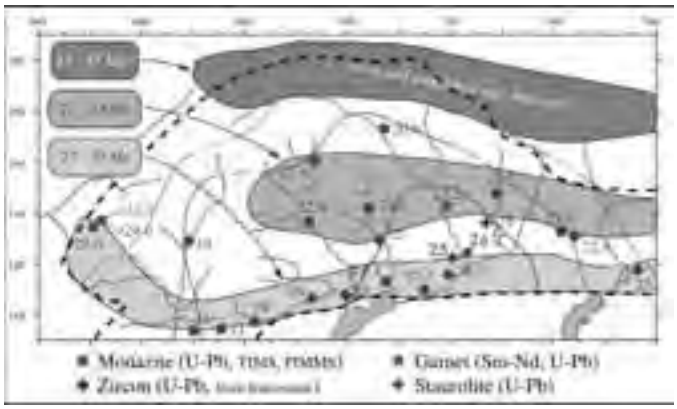

Three age belts in Lepontine: Map of select age data, interpreted as mineral formation ages formed during Alpine Barrovian overprint (Köppel & Grünenfelder, 1975, 1978; Köppel et al., 1981; Vance & O'Nions, 1992; Schärer et al., 1996; Gebauer, 1999; Engi et al., 2001b)

Three age belts in Lepontine: Map of select age data interpreted as mineral formation ages formed during Alpine Barrovian overprint (Köppel & Grünenfelder, 1975; 1978; Köppel et al., 1981; Vance & O'Nions, 1992; Schärer et al., 1996; Gebauer, 1999; Engi et al., 2001b).

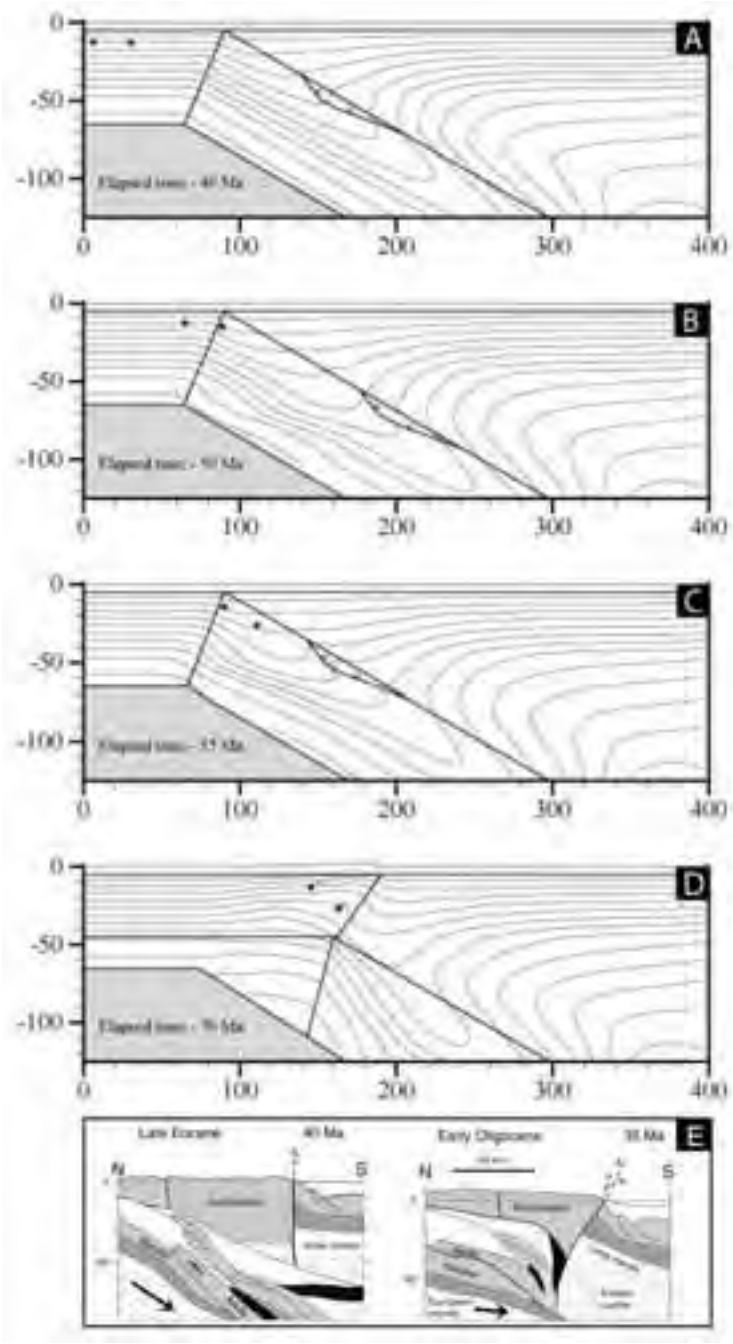

Figure 5 - Results of numerical modelling: Computed time slices through the model orogen. Note location of tracking points that move with the deforming grid. A: Late subduction stage, with the mobile tectonic fragment (scaled to the current dimension of the Adula thrust sheet), descending into the subduction channel at the same velocity (v(z) = 0.8 cm yr^{-1}) as the subducting plate; B: Maximum pressure stage for the tectonic fragment (v(z) = 0 cm yr^{-1}), but with subduction continuing (v(z) = 0.5 cm yr^{-1}); C: Extrusion stage of fragment (v(z) = -0.8 cm yr^{-1}), depicted at a level just prior to its juxtaposition with an underlying unit (mimicking the Simano nappe) that is still subducting at v(z) = 0.5 cm yr^{-1}; note shape of isotherms at base of TAC-fragmen,t due to the combined effects of advection and shear heating; D: Final exhumation stage of entire nappe stack, kinematically described by several channels, mimicking uplift and retroshear displayed by the Insubric Line (labelled IL in E), with a high erosion rate (approx. 0.25 cm yr^{-1}) specified to keep the evolving topography below 4 km in depth; E: Tectonic model sections (slightly simplified from Pfiffner et al., 2000) for two stages of the orogenic evolution of the Central Alps. The Late Eocene situation corresponds approximately to the model stage shown in C, whereas the Early Oligocene situation depicts the kinematics just prior to the stage shown in D.

other geophysical, tectonic, petrological, and geochronological data, have been integrated to construct thermal models of collisional orogeny (Roselle et al., 2002), on the basis of the geometry, large-field kinematics, and actual material properties for the Central Alps. Results of such simulations (Figure 5.7, 5.8), provide a basis by which to interpret the dynamics of the thermal evolution, and to address the effects of individual factors such as partial melting.

Field itinerary

1. Hike to Alpe d'Albion

Start: Swiss coord. 729.9/115.9/1775 m

We start our hike towards the north, along the road from Gesero to Cadinello; stops are not numbered, since observation may be continuous along the path. A subvertical series of massive gneiss slabs, trending E-W, form the steep 400 m flank to the crest north of Corno di Gesero. This series is

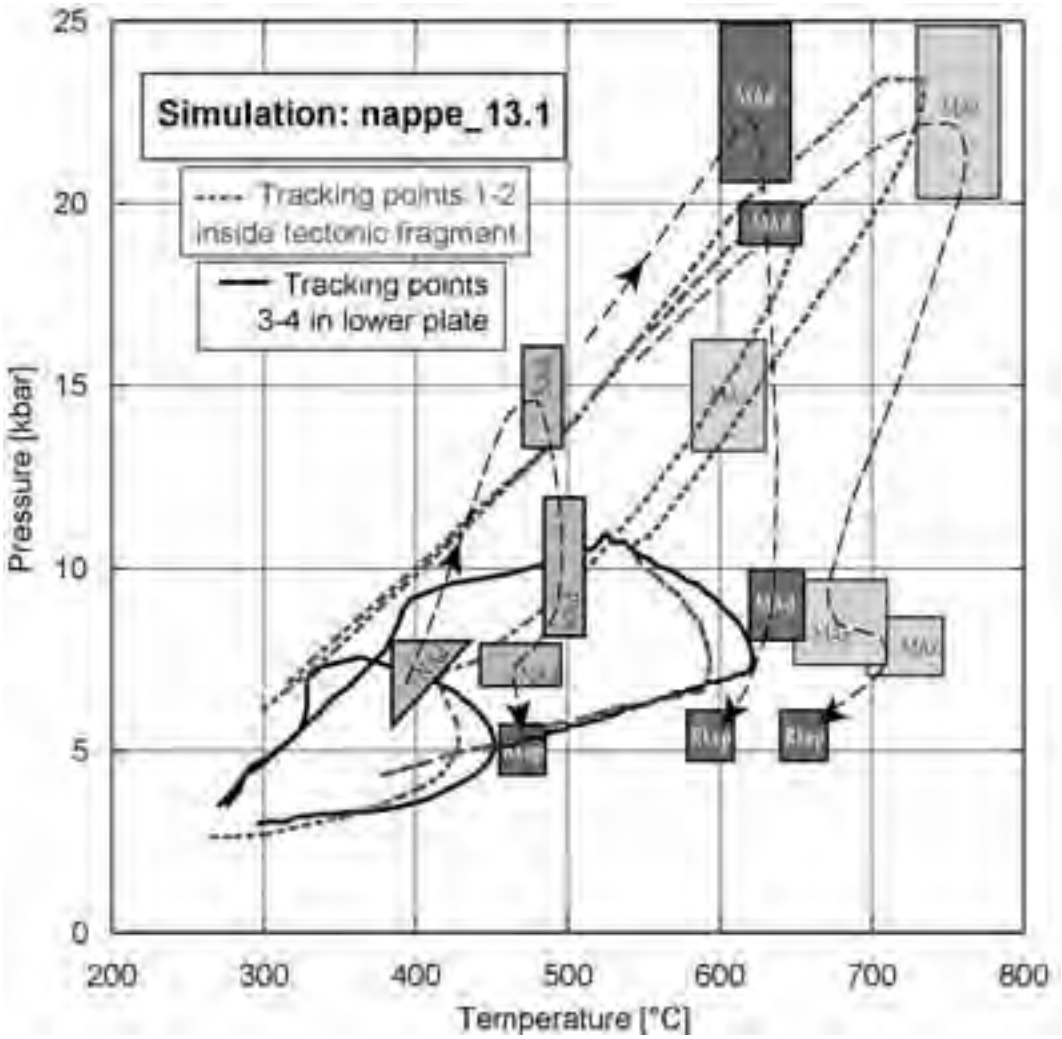

Figure 5.8 - PTt-paths in the Lepontine. Comparison for groups of samples documented along a N-S profile (Figure 5.1b), with numerical simulations for corresponding locations (Engi et al., 2001a; Roselle et al., 2002). The latter are shown as asterisks (subducted plate), and open circles (TAC fragment) in Figure 5.7 (A-D). Thermobarometric data and P-T paths for samples from northern Adula (NAd: Heinrich, 1983; Löw, 1987), Middle Adula (MAd: Partzsch & Meyre, 1995; Meyre et al., 1997; Nagel, 2000), Mergoscia-Arbedo zone (MAz: Tóth et al., 2000; Brouwer & Engi, 2004), regional Lepontine conditions (RLep: Todd & Engi, 1997).

part of the Bellinzona-Dascio zone, a sequence of TAC that is quite uniform in structure: subparallel bands of leucocratic alkalifeldspar-rich to mesocratic biotite-plagioclase gneisses alternate with pyroxene-amphibolite layers (commonly only cm to dm thick), with layers of pelitic schist and lenses of diopside marble, calc-silicate and ultramafic rocks. Considering the high metamorphic grade (sillimanite-Kspar zone), most lithotypes are surprisingly fine-grained. This is attributed to continued recrystallization during strong transpressional deformation. This gneiss package shows many of the regionally typical features, including mylonitic banding, isoclinal folds with both steep and flat E-W axes, rootless hinges, and a few microlithons resisting the strong flattening strain. Crosscutting and conformable pegmatites occur (dm- to m-thick), the latter commonly show boudinage or pinch-and-swell structures.

Volume n° 2 - from B16 to B33

On clear days, Alpe di Cadinello offers a splendid view towards the west: Between densely forested knobs of the SSB and the Monte Rosa massif in the distance, the Insubric Line first runs E-W to the Magadino delta, then bends to the SW, following the shoreline north of Lago Maggiore. To the south, pre-Alpine basement units – notably the Ceneri gneiss of the Southern Alps – emerge, whereas to the north, massive gneiss slabs outline the Verzasca antiform, which bends the flat-lying Pennine nappe stack of the central Lepontine into a subvertical position. Thus the highest unit of that stack, the Maggia nappe, resting on TAC-remnants and the Simano nappe, reaches the lowlands just north of the Magadino plain.

From Cadinello we begin our hike (trail –> SE) up towards Cima da Cügn. Excellent exposures along the trail display the variability of rock types in the mélange sequence, showing sillimanite-Kspar grade metamorphism, with evidence of partial melting, and fabrics due to strong high T (dextral) transpressive deformation. Along the way to Alpe Albion, vistas to the north and east continue our panorama geology: low down in the broad Mesolcina valley, the Simano nappe is topped by the main mass of the Adula thrust sheet, composed largely of TAC material. It forms most of the middleground as well as the main peaks visible to the north (Pizzo di Groven, Adula) and west (Cima di Paina). Looking north, an axial dip ~20° E is evident within the Adula unit; this post-nappe folding (D_3, D_4), affected the entire nappe stack, and formed the Leventina dome.

At Alpe Albion, the buff colors of several ultramafic lenses enclosed in the gneiss package stand out (note the flora change). The largest mass (~120*50 m), is *harzburgitic,* and its main assemblage is spinel-chlorite-enstatite-olivine. A polyphase evolution can be inferred: (1) early (mantle-origin?) structures (dunite bands, with seams or aggregates of chromite, opx layers, or veins); (2) intrusion of gabbroic and sparse plagiogranitic dykes, cpx veining; (3) hydration to serpentinite and associated metasomatism (rodingite formation); (4) prograde metamorphic dehydration, isoclinal folding, metasomatism (blackwall formation), and late hydrothermal veining (antigorite+talc stable). Spectacularly zoned *metarodingite* veins and pods are abundant, as are hydrothermal veins with olivine, talc ± anthophyllite, and pennine. In the Central Alps, metarodingite veins are not rare in ultramafic rocks (Trommsdorff & Evans, 1980), and their observation is critical, for they indicate a metasomatic origin, linked to serpentinization of peridotite. Metarodingite in high-grade (spinel or garnet) peridotite thus demands a shallow hydration prior to subduction. SHRIMP dating of zircon from plagiogranite veins, indicates a Jurassic magmatic age (146 Ma, Stucky, 2001) and has been interpreted to show an origin from the Piemonte cean for the Alpe Albion ophiolite rocks.

Neither garnet peridotite nor eclogite have been reported from the Bellinzona-Dascio zone, but these do occur (Fumasoli, 1974) in other TAC zones adjacent to the north (e.g. Mergoscia-Arbedo zone; cf. 6th day of excursion), and in southern parts of the Adula thrust sheet to the east (Monte Duria).

2. Hike to Passo S. Jorio

Start: Swiss coord. 729.9/115.9/1775 m

From Alpe Albion, we take the steep trail up to the crest just north of Corno di Gesero, follow the exposed ridge to Cima da Cügn, and then descend to Passo San Jorio; stops are not numbered, since observation may be continuous along the path. The heterogeneous Bellinzona-Dascio zone is in steep contact with the Jorio tonalite body. The fabric in this Oligocene intrusive is rarely magmatic, much more typically gneissic and banded the mineral quartz is banded (at the microscope of course) oligoclase / andesine, dark green hornblende, and biotite dominate, with minor magmatic epidote (±allanitic core), titanite, and zircon. Hornblende barometry indicates pressures of ~8.5 kbar (Schmidt, 1989), some 2.5-3 kbar higher than documented for the regional metamorphic overprint (Todd & Engi, 1997), which reached its peak temperatures in the SSB ~28±1.5 Ma ago (Engi et al., 1995). Hence, the Jorio tonalite entered the TAC at a time when the southern Lepontine belt was undergoing prograde metamorphism while decompressing. It is likely that migmatite formation in the Arbedo and Bellinzona zones also peaked in that interval, although a few aplites and tonalites crosscut the tonalite. Syn- and postmagmatic deformation is evident in the tonalite along the path up to Cima da Cügn, as is some hydrothermal veining and greenschist facies overprint.

As in the adjacent gneisses, numerous aplite, pegmatite and granite dikes cross the Jorio tonalite. Mylonites and other high-T strain effects are common, but low-T cataclastic effects occur as well. The southernmost band (Melirolo augengneiss: dark and pervasively foliated, with porphyroclasts of andesine), is in steep contact with the greenschist facies Tonale series, which comprises micaschist, retrogressed albie-epidote amphibolites, and very minor carbonates.

The surface expression of the major tectonic contact

with the Southern Alps is strongest at the margin between the Tonale series, and the virtually non-metamorphic Triassic carbonates, hence this is where the classic Jorio-Tonale line has been mapped. However, the Apulian plate margin is strongly affected by cataclastic deformation, with a complex fault pattern, cutting up both the Hercynian basement and its sedimentary cover, producing a chaotic series in a belt of 1-2 km width (Reinhard, 1939). The Triassic (Anisian-Norian) is poorly exposed near Passo San Jorio; lower parts of Val Morobbia offer better exposures, also of the deformation associated with the late-Alpine exhumation of the Central Alps along the Jorio-Tonale line.

Return from San Jorio to Capanna Gesero for dinner and rest. Overall, the intensity of deformation diminishes, and the strain becomes more localized as we move away from the Insubric Line. A system of Riedel shear bands is oriented some 20-30° to the pervasive banding and foliation in the tonalite.

Castione, Gorduno and Alpe Arami, then return to Arbedo. Mid-afternoon transfer to Breuil-Cervinia (Italy) by bus.

Problems linked to the formation, characteristics, and role of the TAC (Tectonic Accretion Channel), as introduced on the 5th day, remain a focal point of today's program.

Regional geologic setting

The emplacement of *HP fragments* into collisional orogens is not well understood, despite the significance commonly attributed to the occurrence of eclogites. In the Central Alps it has long been clear that this orogen has not, as a whole, undergone eclogite facies metamorphism. HP relics appear to be restricted to localities in tectonic mélange units, such as the Adula thrust sheet (e.g. Jenny et al., 1923; Heinrich, 1986; Trommsdorff, 1990; Meyre & Frey, 1998; Meyre et al., 1999), the Cima Lunga unit (e.g. Evans & Trommsdorff, 1978; Pfiffner

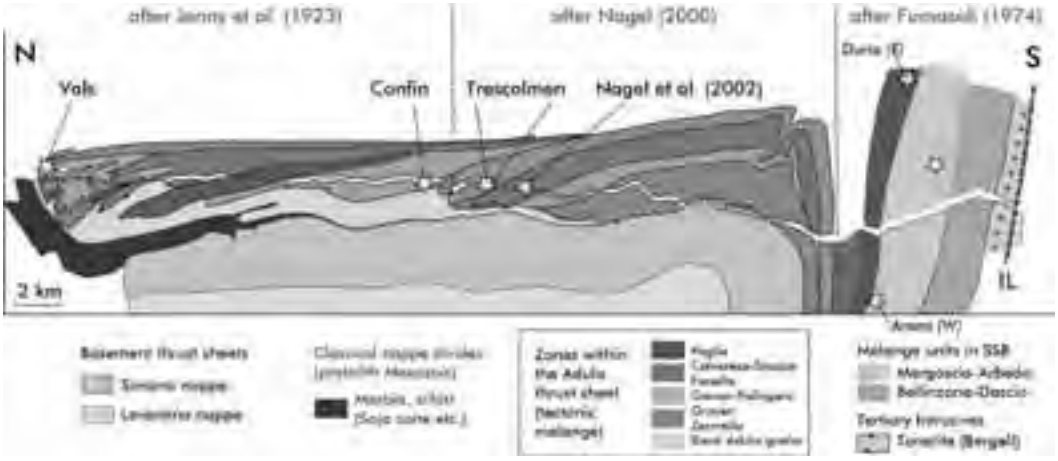

Figure 6.1 - Cross-section through the Adula thrust sheet and TAC-zones in the SSB, showing imbricate structure. Asterisks denote principal locations of HP relics (mostly eclogite).

Hydrothermal alteration under greenschist facies conditions is closely linked to these discrete deformation zones, in which epidote, chlorite, albite, sericite, and minor carbonate occur.

DAY 6

Emplacement of Eocene high-pressure rocks (eclogite, garnet, peridotite), and calc-silicate marbles in the Southern Steep Belt; decompression history and Oligocene Barrovian overprint, formation of orogenic migmatites during transpression.

By minibus from Alpe Gesero via Val d'Arbedo to

& Trommsdorff, 1998), certain zones in the SSB (Southern Steep Belt), such as the Mergoscia-Arbedo zone, and equivalent zones further west, such as the Someo zone (Figure 5.1). Taken as a whole, the TAC fragments form a spatially coherent belt at the present erosion level of the Central Alps. However, this belt is imbricated internally, with an enormously variable spectrum of lithotypes. Metasedimentary, ophiolitic as well as continental basement rocks occur, but supracrustal rocks (orthogneiss, garnet-micaschist) are volumetrically dominant. Individual TAC zones, consisting of particular associations of rock

types, have classically been mapped (as reviewed by Trommsdorff, 1990), and such zones may form imbricated slices, as in the Adula nappe (Figure 6.1). HP relics within and between such slices commonly occur as stringers of lenses or boudins, enveloped by gneissic and schistose members. Since it is the sum total of these that are viewed here as remnants of the Alpine TAC, and because the Barrovian overprint of the entire Lepontine has lead to the substantial reequilibration of HP rocks under medium-pressure conditions, it is not always easy to delimit TAC units from neighbouring tectonic units, i.e. the crystalline basement nappes.

Most prominent among the HP occurrences in the Central Alps is *Alpe Arami* (e.g. Grubenmann, 1908; O'Hara & Mercy, 1963; Moeckel, 1969; Evans & Trommsdorff, 1978; Ernst, 1977, 1978, 1981), a garnet peridotite body with a partial eclogite rim, located within the SSB. There has been a heated debate over the significance of the mineralogical remnants discovered by Dobrzhinetskaya et al. (1996), the validity of various barometers (estimates from ~80 to >300 km having been forwarded for the depth of equilibration), and the speed of exhumation (e.g. Green et al., 1997; Hacker et al., 1997; Brenker & Brey, 1997; Bozhilov et al., 1999; Nimis et al., 2000; Trommsdorff et al., 2000; Risold et al., 2001; Paquin & Altherr, 2001; Risold et al., 2003; Olker et al., 2003). The overall significance to the evolution of the TAC is not yet clear, but a two-stage process is conceivable, by which the Alpe Arami body was first emplaced from the (Asthenospheric) mantle into a deep portion of the TAC, and that extrusion along the suture set in after that. Slab-breakoff (von Blanckenburg & Davies, 1995) has been proposed as a mechanism that may have triggered such a scenario (Olker et al., 2003).

The interpretation of the HP localities known in the Lepontine has long been hampered by the uncertainty regarding their age. Until recently, evidence of HP metamorphism between ~43 and 37 Ma has been restricted to Alpe Arami and Cima di Gagnone (Gebauer, 1996; Becker, 1993), but a systematic Lu-Hf study, undertaken to date eclogite remnants from several other TAC localities, confirms Eocene HP conditions (Brouwer et al., 2003).

The widespread occurrence of migmatites, including the classic "Injektionsgneiss", within the SSB – in a belt shaped by strong transpressional deformation – poses several important questions: What is the dominant mechanism leading to partial melting (e.g. dehydration or fluid-assisted melting)? What mechanical and thermal effects are evident? What spatial-temporal relation is there to the regional Barrovian metamorphism in the Lepontine? These shall be addressed in the first part of today's field trip.

Base maps: See 5th day. Guidebook for Alpe Arami: Pfiffner & Trommsdorff (1998).

Field itinerary

1. Roadside outcrops in Valle d'Arbedo

Start at Swiss coord. 729.9/115.9/1775 m

Descending from Capanna Gesero towards the town of Arbedo (NE of Bellinzona), the private road offers sections through two zones of the SSB, both interpreted as TAC remnants, i.e. the Bellinzona-Dascio zone, and the Mergoscia-Arbedo zone. Stops at good outcrops in both zones to study orogenic migmatite (not numbered).

Leucosomes typically make up 20-30% in metaclastic and metagranitoid rocks, and much smaller fractions of quartz-feldspar veining occur in amphibolitic gneiss and biotite-plagioclase gneiss of basic-to-intermediate composition. Leucosomes range from concordant and folded together with their host rocks, to slightly discordant and either massively or weakly foliated, to completely undeformed types which may be weakly discordant or crosscutting the steep, regional E-W banding and foliation. Locally-generated veinlets predominate, but minor coalescence phenomena are common, as are quartz-feldspar veinlets a few cm across, and dikes up to 2-3 m in width. The geometry and abundance of leucosomes, their paucity in aluminous phases (chiefly sillimanite), and microstructural observations, all indicate that dehydration melting accounts for but a small fraction of the leucosomes. Partial melting must have been triggered to a major extent by fluid-assisted melting. The integrated flux of hydrous fluid required to explain the observed leucosome volume fraction is estimated as 25±10 m^3/m^2. Feedback mechanisms of enhanced fluid migration, transpressional deformation, partial melting, and melt separation are likely to have been important during protracted tectonic activity at mid-crustal conditions. Examples of repeated fluid access, formation of local melts, and variable deformation of earlier leucosomes (Figure 6.2), are abundant in several lithotypes. For example, quartz-rich tonalitic mesosomes are commonly crosscut by hornblende-bearing granitic dikelets, which required external fluid to drive the reaction

bio + $plag_1$ ($An_{\sim 35}$) + fluid –> hbl + Kspar + $plag_2$

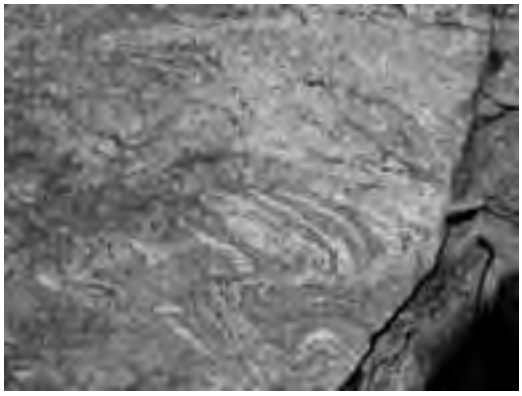

Figure 6.2 - Migmatite outcrop in central Val d'Arbedo: Multiple formation of granitic partial melt, veining, and variable deformation of leuco-, mesosome, and restite stress the role of feedback mechanisms between fluid migration, partial melting, and deformation during mid-crustal extrusion of TAC units in the SSB.

Ma, and uplift in the southern Lepontine is known to have been particularly rapid in the Oligocene (Hurford, 1986), partial melting appears to be linked and indeed restricted to that period of active retro-thrusting (Pfiffner et al., 2000) and channel exhumation.

2. Castione quarry

Swiss coord. 723.60/121.41/240m

After traversing the floor of the overdeepened glacial valley (Figure 6.3) at the eastern end of the Magadino plain, we visit a series of quarries some 3 km to the north of Bellinzona, the proud capital of the canton (=Swiss province) of Ticino.

At Castione, a metacarbonate sequence is in subvertical position; classical maps position these metasediments between gneisses of the Simano nappe at their footwall (surfacing to the N), and the Adula unit in the hangingwall (to the S). Whereas the Simano nappe is a classic Pennine thrust sheet,

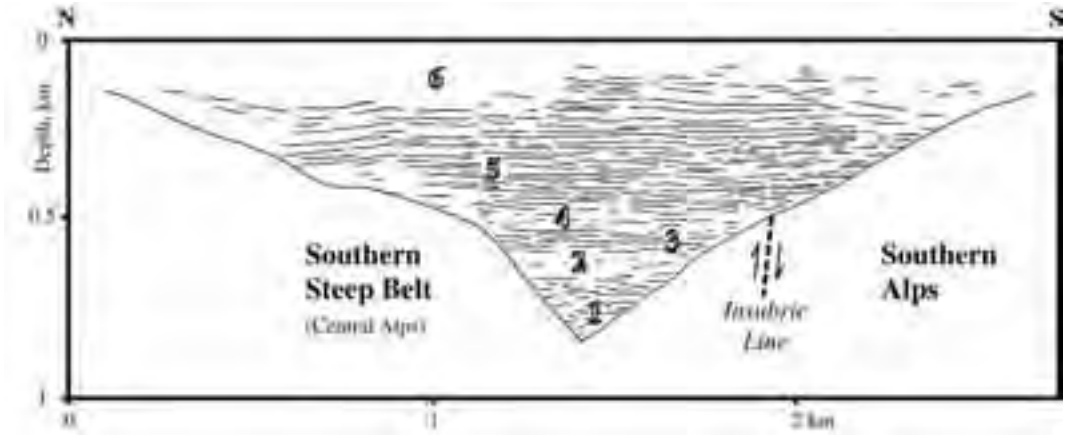

Figure 6.3 - Incision and backfilling in the central Magadino plain. Results of NRP 20 (Pfiffner et al., 1997). Sediment types: 1 Fluviatile deposits; 2 Coarse fluviatile sediments; 3 Fine grained lacustrine deposits; 4 Coarse fluviatile sediments; 5 Lacustrine sediments (Lago Maggiore); 6 Recent alluvial deposits.

Incision and backfilling in the central Magadino plain. Results of NRP 20 (Pfiffner et al., 1997). Sediment types: 1 Fluviatile deposits; 2 Coarse fluviatile sediments; 3 Fine grained lacustrine deposits; 4 Coarse fluviatile sediments; 5 Lacustrine sediments (Lago Maggiore);6Rec entalluvial

($An_{\sim 7}$)

Thermobarometry on restites and *in situ* leucosomes indicates 9-5 kbar for migmatites in the SSB, i.e. a depth interval of 28-16 km for partial melting. As monazite age data from restites consistently yield ~29

the Adula unit is not, as it represents an internally imbricated stack of tectonic slivers (Fig 6.1) attributed to the Alpine TAC.

Three stops inside the quarry are planned (*and will be undertaken if we have time*):

- Stop A: Start at the north end of the Ambrosini quarries: A 150 m wide sequence of carbonaceous metaclastics is mined for road gravel in this quarry. The rock type here (named "Castione nero" for its dark color), is likely to be a highly metamorphic equivalent of *Bündnerschiefer* (a heterogeneous sequence of largely Jurassic sediments, predominant in variably clastic and carbonate contents). Thick sequences of Bündnerschiefer, comprising several units, form part of the Alpine accretionary prism in northern parts of the Central Alps; thin trails of these metasediments (and/or their Permotriassic base), can

be followed over some 15-25 km southwards from the Pennine front, marking the tectonic contacts between flat-lying crystalline nappes. In some cases, such *nappe divides* show a fairly intact internal stratigraphy; indeed, in the northern part of the Lepontine the basal units are locally in stratigraphic contact with their pre-Alpine substrate. Further south, however, trails of metasediments cannot be linked with certainty to larger parts of the accretionary prism. This is the case for the Castione metasediments, for which no continuous connection to classic nappe divides exists. Nonetheless, regional correlation had lead earlier investigators to conclude that the "root zone of the Adula nappe" may be located between the two carbonate units found at Castione (Codoni, 1981; Bächlin et al., 1974). However, such correlations are hampered by discontinuous outcrops and strong polyphase deformation. Large isoclinal folds are visible, e.g. in amphibolite-marble intercalations, at the margin of the quarry.

Apart from its tectonic interest, Castione offers particularly rich *mineral assemblages*, notably in metapelitic and metamarly rocks. All three alumosilicates occur together in segregations with quartz. Textural evidence indicates the sequential overgrowth of commonly kinked blue kyanite by pink andalusite, with partial or complete replacement of both of these by greenish-grey sillimanite (fibrolite). Whereas andalusite occurs only in quartz-rich segregations, kyanite+sillimanite occur in the pelitic matrix as well, with fibrolite mats commonly growing at the direct margin of corroded kyanite laths. In dark marly host rocks garnet+diopside prevail next to calcite+quartz; scapolite is frequent, and large prisms occur in quartz-rich segregations in the "Castione nero", but without alumosilicates. Whereas the above segregations are aligned in the metamorphic foliation, a discordant variety (containing tourmaline, biotite books, muscovite, and very calcic plagioclase), can be found in large blocks at the south end of this quarry.

- Stop B: ~150 m to SE, at the N end of the next quarry, discordant pegmatites cut the calcsilicate rocks. The best quality "Castione nero" is mined here: It is of marly composition, more homogeneous, and coarser-grained than in the northern quarry. This variety makes an attractive building stone for interior use – its pyrite contents makes it unfit for outside applications.

- Stop C: ~150 m to SE, the southernmost quarry hosts the "Castione bianco", a white marble with darker bands rich in phlogopite. These bands commonly show isoclinal folding. Titanite, scapolite, muscovite, and quartz occur as accessories, locally concentrated.

The provenence of this last siliceous marble unit is controversial. If the "Castione nero" is indeed derived from Bündnerschiefer, the close association with the calcitic "Castione bianco" may suggest that these marbles are of Triassic origin. However, in the Central Alps, Triassic carbonate sequences are predominantly dolomitic, so one needs to explain what kind of metasomatism caused such Mg-loss in the "Castione bianco". Alternatively, spatial proximity does not necessarily imply a close stratigraphic or paleogeographic relation. For example, the spatial associations of different metasediments in TAC units of the Adula thrust is probably due to the tectonic juxtaposition of fragments. It does not seem possible to estimate the amount of total strain within and between the different bodies at Castione, but field relations in high-grade metamorphic terrains certainly indicate substantial tectonic mobility of carbonate-rich units. It thus seems possible that different marble and calcsilicate types found at Castione have been tectonically assembled in the TAC, and may not represent paleogeographic relatives.

The main thermal overprint in the southern Lepontine has been dated using a calcsilicate sample taken at Castione (Vance & O'Nions, 1992); these authors interpreted the Sm-Nd age of 26.7±1.7 Ma, measured in garnet, to be a growth age. This result is in conflict with earlier data by Jäger and coworkers (see Hunziker et al., 1993), but it agrees well with the U-Pb ages for monazite available in the southern Lepontine (Köppel & Grünenfelder, 1975, 1978; Köppel et al., 1981; Engi et al., 2002), and the U-Pb age of staurolite (Nagel, 2000). Also, P-T conditions estimated for that sample 600 ± 40 °C, and 8.6 ± 1.5 kbar, given by Vance & O'Nions (1992) for their Castione sample, are in agreement with the regional pattern (Engi et al., 1995; Todd & Engi, 1997). This indicates that the Castione section was equilibrated during the regional Barrovian metamorphic overprint, and that the climax in temperature was reached in the Miocene, following rapid exhumation (during the Oligocene).

End up at Swiss coord. 723.97/120.95/250m

3. Roadside outcrop above Gorduno

Swiss coord. 722.7/119.9/390m

A lens (ca. 120*30 m) of eclogitic garnet amphibolite surfaces in the open forest, just above the town of Gorduno, along the road to Bedretto and Alpe Arami. Engulfed by highly deformed leuco- to mesocratic

quartz-two feldspar gneisses, this mafic lens shows partial hydration of eclogite, as it is commonly seen in the Mergoscia-Arbedo zone of the TAC. The formation of mm- to cm-size compositional domains reflect local equilibration volumes and retain mineralogical featuresyielding valuable clues the conditions of decompression and late heating associated with emplacement (Tóth et al., 2000).

In the main part of the body, very dark amphibolite preserves a weak foliation which lies almost perpendicular to the pervasive regional E-W fabric, that dominates the all-enveloping gneiss types. This latter foliation is not visible inside the lens, where the amphibolite retains many characteristics of its early high P-T evolution. Garnetiferous varieties prevail, except near the margins of the lens, and in bands that show evidence of higher plastic strain. The core region of the metabasite lens displays a dominant, symplectitic type of retrograded eclogite rich in garnet, whereas a continuous change from meta-eclogite to garnet amphibolite is recognized near and towards the rim of the body, within some 5-10 m from the contact. The rim of the body is totally devoid of garnet. Contacts with the encasing gneisses are poorly exposed; where visible, they do not appear tectonically disturbed.

The main part of the meta-eclogite consists of a fine to medium-grained symplectite matrix, with randomly distributed garnet porphyroblasts (with rutile±ilmenite), rimmed by a corona rich in plagioclase (An_{40-60}), and pale green hornblende. Omphacite relics are very rare, and low-Na salite is common. Some domains contain Al-rich phases (corundum, kyanite, hercynite, or staurolite), and pseudomorphs after lawsonite have been identified (Brouwer & Engi, 2004). Assemblages from this and adjacent mafic lenses indicate an evolution (Tóth et al., 2000; Brouwer, 2000; Grandjean, 2001) from HP-conditions, that differs from one locality to the next, within the Mergoscia-Arbedo zone of the TAC, but their final exhumation paths (Figure 6.4) for P < 7 kbar, are similar. This indicates that these bodies may have followed different HP histories, but became part of a coherent unit following extrusion to mid-crustal levels.

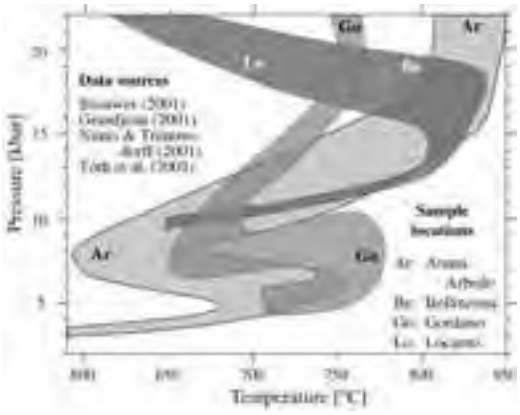

Figure 6.4 - P-T paths of ultramafic and mafic HP relics found in the SSB. Note the very different temperatures near P_{max} and in a first stage of decompression, converging to rather similar paths at mid-crustal levels. Although the low-T parts are poorly constrained, such a pattern is consistent with individual fragments having coalesced into a coherent(?) TAC only during extrusion. Data and P-T paths from (Brouwer, 2000; Nimis et al., 2000; Tóth et al., 2000; Engi et al., 2001a; Paquin & Altherr, 2001); conflicting thermobarometric results for Alpe Arami are under debate (see text).

4. Alpe Arami

The starting point of an easy 30 minutes hike to this classic location, known for its beautiful Mantle rocks, is the hamlet of Bedretto (Swiss coord. 720.15/120.8/1283m). The gravel road climbs gently to the S, then W and NW along outcrops of veined gneisses, fibrolite-garnet-biotite-Kspar schists (with cordierite in local biotite restite), and pyroxene amphibolite, with granitic dikes intruding the steeply S-dipping sequence.

At Alpe Arami, outcrops of garnet peridotite prevail, eclogite occurs principally at the poorly exposed margin of the lens (Figure 6.5). The HP assemblages are partially hydrated in some parts of the lherzolite, with garnet being rimmed by amphibole-spinel kelyphite, which in turn is progressively replaced by chlorite knobs. In other parts of the lens, porphyroclastic garnet grains are fresh and bright red (~66.5% pyrope, 19% almandine, 13.7% grossular). Garnet coexists with grass-green chromian diopside, minor grey enstatite (locally kinked) and amphibole (pargasit-edenite), and two generations of olivine (~90% forsterite), one of them porphyroclastic (Ø 2-3 mm), the second one recrystallized to small subhedral grains. It is in the earlier type of olivine that topotactic chromite and ilmenite ($FeTiO_3$) rods were discovered by Dobrzhinetskaya et al. (1996), who interpret b-$FeTiO_3$ to be the result of exsolution from perovskite, which implies depths of ~300 km. These inferences and thence the ultrahigh pressure origin have been questioned by Risold et al. (2003), who explain the microstructural evidence differently and favor depth estimates based on multi-equilibrium thermobarometry, indicating

Volume n° 2 - from B16 to B33

32±3 kbar, 833±34 °C, i.e. depths of just over 100 km. These rest on preserved thermodynamic equilibria, and are in conflict with disequilibrium considerations raised by Brenker & Brey (1997), Paquin & Altherr (2001), and Olker et al. (2003), who conclude that subduction reached depths of 180 km (59±3 kbar, 1180±40 °C), and that extrusion rates for an initial phase (to ~800°C) were B1.5 cm/a. Consensus among the various proponents does not appear immanent, but

Figure 6.5 - Simplified geological map of Alpe Arami (from Moeckel, 1969)

the data sets, taken at face value, seem compatible with Alpe Arami being a sliver of subcontinental mantle which was tectonically incorporated into the Alpine TAC, following slab breakoff between 43 and 36 Ma ago, based on zircon SHRIMP data by Gebauer (1996; 1999). After amalgamation with subducted supracrustal TAC fragments, extrusion to mid-crustal levels followed along the subduction fault system. Quite conceivably, accretion into what is now observed as the Mergoscia-Arbedo zone continued during this phase, though the flow mechanisms are not well constrained. The final phase involved retrothrusting (Pfiffner et al., 2000) along a Proto-Insubric Line, and rapid tectonic denudation of the Central Alps (e.g. along the Simplon detachment, Merle, 1994), during the Oligocene and arly Miocene a loose use of stratigraphic terms is compulsory in the crystalline basement Stratigraphy in the foreland and hinterland basins of the Alps (Schlunegger et al., 1997) correlates well with such erosional fluxes from the evolving orogen.

Field itinerary

1. Fresh garnet peridotite

Swiss coord. 719.15/121.22/1460m

By following a small trail from the huts of Alpe Arami, ~250 m to the NNW into a steep, narrow valley, the northern margin of the ultramafic lens is reached. Buff weathering blocks and outcrops of fresh garnet peridotite can be sampled. Bright green Cr-diopside occurs frequently near garnet porphyroclasts. In many samples, garnet is rimmed by kelyphite, a fine symplectic intergrowth of amphibole and spinel, and further hydration may have converted these into silver-grey chlorite. Minor serpentine occurs principally along brittle fractures and shear planes in this peridotite.

1. Variably retrogressed peridotite and eclogite

Swiss coord. 718.85/121.1/~1700m

After returining to the huts of Alpe Arami, climb gently WNW along a fading trail through the open timber of Pianca Grande. Towards the western margin of the lens, observe blocks and outcrops of peridotite, with spinel-amphibole preudomorphs after garnet and with opx+sp+hbl replacing cpx. Occasional layers of garnet pyroxenite are found, and eclogite at the margin occurs both fresh and progressively hydrated to garnet amphibolite. Garnet-free black amphibolite is found in contact with biotite-plagioclase gneiss surrounding the peridotite lens, much the same as the eclogite lens above Gorduno.

A more massive band of clinopyroxenite outcrops at ~1650 m, and marks the SW border of the Alpe Arami lens.

Conclusions, Outlook

The two days in the Southern Steep Belt of the Central Alps have focussed on the role and significance of the TAC. While far from fully understood, three aspects appear pivotal to the evolution of the Alpine collisional orogen:

(1) Made up of highly diverse fragments, comprising rocks from continental to oceanic to Mantle origin, the TAC acted as a conveyer belt along the convergent plate boundary. In view of the strong internal reworking, it seems unlikely that the paleogeographic origin of the fragments can be reconstructed.

(2) In its evolution over a period >20-25 My, this mélange unit underwent dramatic changes. Its thermal state, rheological properties, and fluid budget were crucial to such processes such as the extrusion of HP fragments, partial melting, calcalkaline magmatism, and orogenic exhumation.

(3) Accretion of dominantly upper crustal TAC-fragments, rich in radioactive components, added a substantial source of heat (2.6 μWm^{-3}) along the base of the upper plate (i.e. the Apulian continental margin). Combined with the crustal material accumulated at mid-crustal depth upon collision with the Briançonnais microcontinent, the extruded TAC-units (Figure 5.1) contributed heat essential to generate the Barrovian overprint in the Lepontine dome.

Recent reports indicate that a TAC has played a critical role not only in the Central Alps, but that a similar tectonic element has developed in other collisional orogens (e.g. Ábalos et al., 2003; López Sánchez-Vizcaíno et al., 2003), and perhaps beneath introceanic fore-arcs as well (Cluzel et al., 2001).

Acknowledgments
We thank Fraukje Brouwer, Tom Burri, Igor Villa and Volkmar Trommsdorff for discussions, Capanna Gesero for hospitality, and the Swiss Nationalfonds for support of our research on metamorphic evolution (grant 20-63593.00).

DAYS 7 - 8

Geology of the dent blanche, mesozoic ophiolites and sediments (monte cervino) and the eclogitised continental crust of sesia lanzo zone (lower val d'aosta)

Giorgio Vittorio Dal Piaz[1] , Guido Gosso[2], Maria Iole Spalla[2], Paola Tartarotti[2], Michele Zucali[2], Jean Marc Lardeaux[3]
[1] University of Padova, Italy
[2] University of Milano, Italy
[3] University of Nice, France

2.1. The austroalpine system

Seventh and eighth days – *An overview into the structure, lithostratigraphy and petrology of the western Austroalpine tectonic system (Dent Blanche nappe) and underlying Mesozoic meta-ophiolites (Piemonte zone) and sediments (Combin z.) in the Monte Cervino (Matterhorn) area, and a section of the middle Aosta valley (Italian side of the Western Alps). In this region of the Alps, a significant progress in the kinematic interpretative syntheses has been developed in the last few decades.*

The main tectonic blocks that are interpreted to form the central-western Alpine belt in a lithosphere-scale cross-section, are represented in Figure 7.1 (from Dal Piaz et al., 2003). The oceanic suture zone, recording subduction metamorphism, involves the so-called Penninic domain and the Austroalpine.

The Western Austroalpine system consists of the internal Sesia-Lanzo zone (nappe) and the external Dent Blanche nappe, the latter subdivided by the Aosta-Ranzola fault running along the middle Aosta valley into northern (Dent Blanche, Mont Mary, Pillonet, Etirol-Levaz) and southern klippen (Glacier-Rafray, Tour Ponton, Emilius, Santanel, Chatillon), Figure 7.2 (A) and (B). The Austroalpine system was deformed and metamorphosed from the Cretaceous-

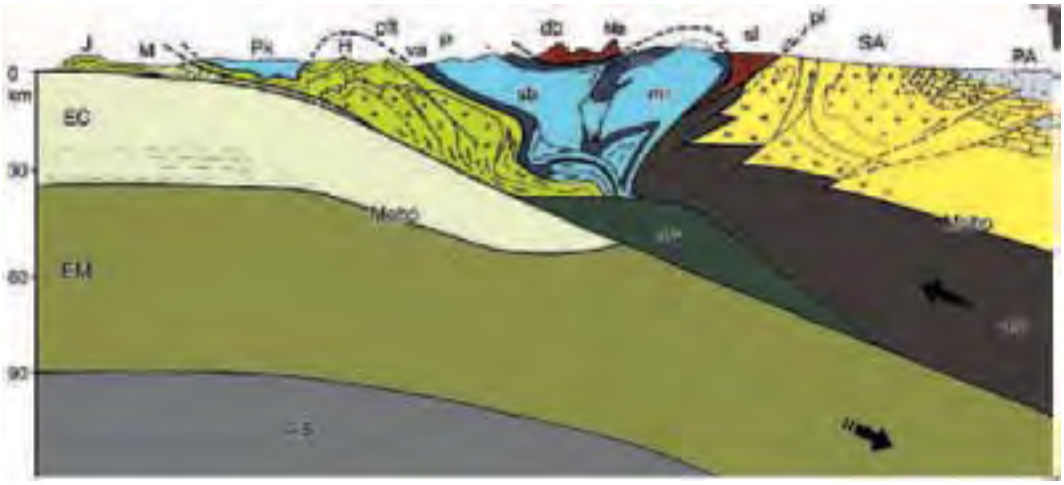

Figure 7.1. Lithospheric section of the central-western Alps (after 150 years of field geology and 35 years of geophysical investigations; no vertical exaggeration) - 1) Western Austroalpine nappe system: Sesia-Lanzo inlier (sl) and Dent Blanche nappe s.l. (db), including Matterhorn (Ma); 2) Penninic domain (P): Piedmont ophiolitic units (po), Monte Rosa (mr) and Grand St. Bernard (sb) nappes, underlain by lower Penninic and outer Penninic Valais zone (va), Penninic klippen (Pk), Penninic frontal thrust (pft); 3) Helvetic basement slices and cover nappes (H); 4) Molasse foredeep (M); 5) Jura belt (J); 6) buried wedge (BW) of European mantle or eclogitized crustal units; 7) European lithosphere: continental crust (EC) and mantle (EM); asthenosphere (AS); 8) Adriatic lithosphere: antithetic belt of Southern Alps (SA) and mantle (AM); Periadriatic Tonale-Insubric-Canavese fault system (pl); 9) Padane-Adriatic foreland (PA). From Dal Piaz et al., 2003.

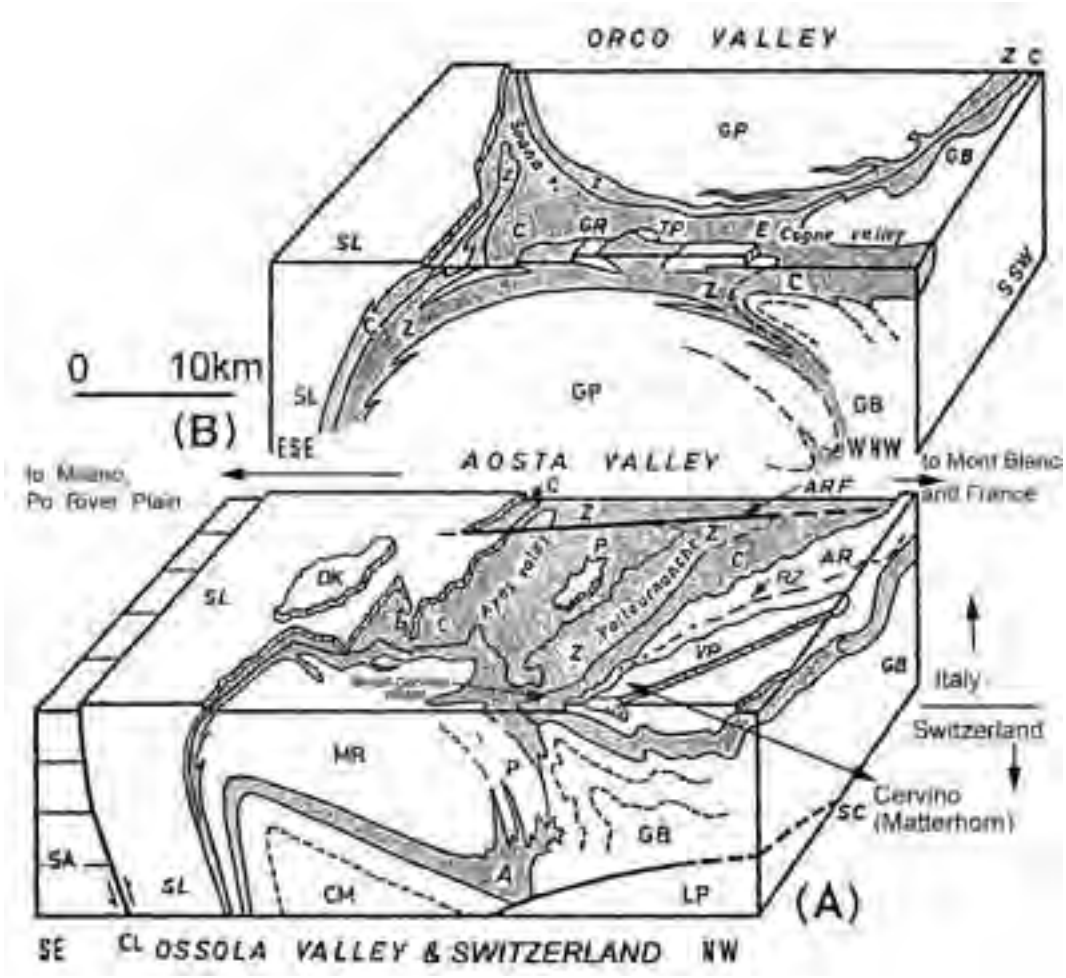

Figure 7.2
Block diagrams of the central-western Alps, across three main Alpine valleys, viewed from Switzerland (=from the North) and displaying the tectonic relationships between the sheets (nappes) of pre-Alpine continental crust and the Mesozoic oceanic crust or Mesozoic sediments of oceanic or continental margin affinities. Compare with Figure 7.1 and 1a (making the effort of reversing east with west); utilize this 3-D diagram to understand the three-dimensional structure of the western Alps, while looking south from the panoramic Stop 7.1 at Plateau Rosa.
Sheets (nappes) of pre-Alpine continental crust: SL=Sesia-Lanzo - Dent Blanche system, DK=II Diorite-Kinzigite zone, MR=Monte Rosa, GP=Gran Paradiso, P=Portjengrat, GB=Grand Saint Bernard, CM=Camughera-Moncucco, LP=Lower Pennine, VP and AR=Valpelline and Arolla series of the Sesia-Lanzo-Dent Blanche system, with infolded RZ=Roisan Zone Mesozoic cover, GR, TP, E, P =Glacier-Rafray, Tour Ponton, Emilius, and Pillonet klippen of the Sesia-Lanzo-Dent Blanche system. Traditionally, as in the rest of the Alps, the continental sheets underlying the Mesozoic oceanic rocks are called Pennine nappes, and the overlying ones Austroalpine.
Sheets (nappes) of Mesozoic oceanic crust or Mesozoic sediments of oceanic or continental margin affinities: Z and A= Zermatt-Saas and Antrona ophiolites, with thin oceanic sedimentary covers; C=Combin Mesozoic covers of continental margin-to slope affinity, including the Frilihorn-Tsaté and Pancherot-Cime Bianche trench sediments.
SA=Southern Alps: a south-verging thick-skin Alpine thrust system located south of the Tonale-Insubric-Canavese tectonic exhumation fault system. SC, ARF =Simplon-Centovalli and Aosta-Ranzola tectonic denudation fault systems.

Paleogene (eoalpine) to the Eocene-Lower Oligocene (mesoalpine) under eclogitic and greenschist facies conditions; the geological history of this unit ends in the Neogene with ductile-brittle deformation of the nappe pile (Dal Piaz et al., 1972, 1983; Hunziker, 1974; Compagnoni et al., 1977; Oberhansli et al.,

1985; Ballèvre et al., 1986; Pognante et al., 1987; Vuichard, 1989; Droop et al., 1990; Polino et al., 1990; Lardeaux and Spalla, 1991; Venturini et al., 1994).

The pre-Alpine protoliths are represented by Variscan paragneisses of high metamorphic grade (kinzigite, felsic granulites), with interbeddings of mafic granulite, amphibolite, and marble, by Permian intrusive granitoids and gabbros, and by minor Mesozoic covers (mainly platform carbonates, rift sedimentary breccias, and flysch; Mont Dolin, Roisan zone, internal Sesia-Lanzo zone) (Compagnoni et al., 1977; Dal Piaz, 1993; Venturini et al., 1994).
The eoalpine subduction metamorphism is largely preserved in the Eclogitic Micaschists complex of the internal Sesia-Lanzo zone (Ballèvre et al., 1986; Droop et al., 1990; Dal Piaz et al., 1993), in the southern Austroalpine klippen as a whole, and in the Etirol-Levaz thrust sheet; peak P-T-conditions of the eclogitic metamorphism are estimated at around 550°C and 1.5-1.8 GPa. With the exception of the Etirol-Levaz sheet (Kienast, 1983), the other northern klippen are eclogite-free, displaying only a few mineral relics of relatively high pressure (aegirine, sodic amphiboles, garnet, and white mica with high Si contents) below a pervasive greenschist facies overprinting (Gneiss Minuti complex, Arolla Gneisses; Dal Piaz, 1976; Ayrton et al., 1982; Pennacchioni and Guermani, 1993). Greenschist-facies-dominated Gneiss Minuti also outcrop along the external side of the Sesia-Lanzo zone, where they locally preserve eclogitic mineral relics (Spalla et al., 1991). The Dent Blanche-Mt.Mary klippen, and the Sesia-Lanzo zone, are structurally composite, both displaying a top unit (known as the Valpelline Series and 2nd Diorite-Kinzigite zone, respectively) formed by lower continental crust rocks with a few slices of mantle peridotite. These lower continental crust rocks are closely similar to lithologies occurring in the Southalpine kinzigitic complex of the Ivrea zone (Stutz and Masson, 1938; Diehl et al., 1952; Dal Piaz et al., 1971, 1972; Compagnoni et al., 1977; Cesare et al., 1989; Vuichard, 1989; Canepa et al., 1990).

2.2. Ophiolitic units

The Alpine ophiolitic units are slices of a Upper Jurassic oceanic lithosphere, generally coupled with Cretaceous trench-derived flysch sequences, and minor mélanges (Bernoulli and Lemoine, 1980; Lagabrielle, 1987; Ziegler, 1988; Dal Piaz and Polino, 1989; Dercourt et al., 1990; Polino et al., 1990; Martin et al., 1994). These units occur as thin sheets, never exceeding 1-2 km in thickness. The thickest units generally consist of tabular bodies of metagabbro and/or serpentinized mantle peridotite, in places directly covered by oceanic metasediments. In other words, the Alpine ophiolites never preserve a complete section of normal oceanic crust (Lombardo and Pognante, 1982; Auzende et al., 1983; Polino et al., 1990), and probably represent slices of topographic highs of the oceanic floor (horst, fracture zones, seamounts, etc.), which were delaminated and scraped off when the ocean floor entered the trench and collided with the active margin. In this view, Alpine ophiolites are fragmented records of the subducting ocean, transferred tectonically to the overriding plate; they were made free to interplay tectonically within the subduction channel, after episodical decoupling from the Tethyan lithosphere consumption at depth. In the Northwestern Alps, the following ophiolitic units are recognized:
1) The Piedmont ophiolitic zone,
a structurally-composite nappe system, sandwiched between the Austroalpine nappes and the underlying Upper and Middle Penninic nappes. From contrasting lithological settings and metamorphic imprints, the Piedmont zone of Aosta Valley and southern Valais is currently divided into two ophiolite-bearing units (Figure 7.1): the overlying greenschist facies-dominated Combin (Tsaté) unit, and the underlying eclogitic Zermatt-Saas unit (Bearth, 1967; Dal Piaz, 1974, 1988, 1992; Dal Piaz and Ernst, 1978; Dal Piaz et al., 1979, 1985; Ballèvre et al., 1986; Sartori, 1987; Vannay and Allemann, 1990).
North of the Aosta-Ranzola fault, the two units are separated by a thin ophiolite-free décollement unit (Pancherot-Cime Bianche-Bettaforca unit: PCB; Figure 7.1), and locally by the Austroalpine Etirol-Levaz eclogitic slice (Ballèvre et al., 1986; Dal Piaz, 1988, 1992). The PCB consists of Permian-Cretaceous cover sequences deriving from a continental basement.
The Combin ophiolitic unit is the tectonic sole of the northern Austroalpine Dent Blanche, Mt. Mary and Pillonet klippen, altogether forming a tectonic multilayer which experienced the same blueschist to greenschist facies metamorphic evolution, whilst southern homologues of the Zermatt-Saas nappe are the tectonic sole of the southern Austroalpine eclogitic klippen (Ballèvre et al., 1986; Polino et al., 1990). As shown in Figure 7.1 and 7.2, the Zermatt-Saas unit and southern homologues lie directly over the Monte Rosa and Gran Paradiso continental

nappes, disappearing to the northwest beneath the inner Gran St. Bernard back folds and back thrusts (from Mischabel, near Zermatt, to Grand Nomenon in the Aosta-Cogne area); by contrast, the Combin zone extends much more externally, being thrust over the outer Grand St. Bernard nappe system (Elter, 1960; Escher et al., 1986).

The Combin ophiolitic sequence consists of carbonate to terrigenous flysch-type metasediments (calcschists *sensu lato*), commonly including multiple interleavings of tabular greenschist facies metabasalts (prasinites), and minor serpentinite slices (Dal Piaz, 1965, 1988; Vannay and Allemann, 1990). Major ophiolitic bodies, with a cover of manganiferous quartzite and other oceanic metasediments, may locally predominate in the upper section of the Combin nappe. They display a peculiar greenschist facies imprint of mid-Tertiary (mesoalpine) age, that predates the
transecting Oligocene (31-30 Ma) andesite-lamprophyre dykes of the Periadriatic magmatic activity (Dal Piaz et al., 1979; Venturelli et al., 1984; Diamond and Widenbeck, 1986). In addition, relatively high-P relics locally occur in metabasalts, metagabbros, and metasediments (blue amphiboles, paragonite, phengite, garnet, and rutile; Dal Piaz, 1976; Ernst and Dal Piaz, 1978; Ballèvre et al., 1986; Polino et al., 1990). These relics may be related to a subduction event of unknown age, probably Late Eoalpine (Paleocene) or Early Eocene.

The Zermatt-Saas ophiolites consist of huge mafic and ultramafic bodies, with minor metasedimentary remnants of the oceanic cover and orogenic deposits (Bearth, 1959, 1967; Dal Piaz and Ernst, 1978). Alpine transposition and metamorphic reworking have pervasively effaced most of the original stratigraphic relations and primary features. Therefore, the reconstruction suggested here is only tentative, being essentially inferred from low strain domains described elsewhere in the Alpine-Apenninic domain, and from present-day oceanic lithosphere. The Zermatt-Saas unit displays this lithological setting:
i) thick basal titanclinohumite-bearing antigorite serpentinites (formerly mantle peridotites), cut by numerous rodingitic gabbro dykes (Dal Piaz, 1969; Dal Piaz et al., 1980) and locally mantled by ophicarbonate breccias (ophicalcites; Driessner, 1993); gigantic ultramafic bodies occur in both sides of the Aosta valley (Monte Avic and Monte Rosso di Verra-Breithorn massifs); ii) Mg-rich and minor Fe-Ti-rich metagabbros and related cumulus ultramafics; iii) metamorphosed massive basalts, pillow lavas, pillow breccias, and hyaloclastites; iv) quartzites and piemontite-spessartine-rich manganiferous metacherts (Dal Piaz et al., 1979; Mottana, 1986), capped by marbles and minor calcschists, a sequence which roughly recalls the supraophiolitic cover (Callovian-Oxfordian radiolarian cherts-Calpionella limestones), capping the Ligurian ophiolites of the Northern Apennines; v) orogenic metasediments and an eclogitic subduction mélange (Riffelberg-Garten complex) consisting of rounded to faceted blocks of eclogitic metabasalts within ankerite-bearing garnet micaschists (Bearth, 1967; Dal Piaz and Ernst, 1978). A transitional to normal-MORB geochemical affinity is reported for
the Combin, Zermatt-Saas and Antrona mafic rocks (Dal Piaz et al., 1981; Beccaluva et al., 1984; Pfeiffer et al., 1989). On the basis of lithological association and geochemical signature, these ophiolites have been so far univocally interpreted as slices of oceanic lithosphere.
The Zermatt-Saas nappe displays an eclogitic imprint of Cretaceous age (90 Ma; Bocquet et al., 1974; Hunziker, 1974; Hunziker et al., 1992). The eclogitic assemblage is particularly well-preserved in the classic Allalin body (Bearth, 1967; Droop et al., 1990), and in minor Fe-gabbro bodies from the Italian side (Baldelli et al., 1985; Benciolini et al., 1988), as well as in some massive and pillow metabasalts. Mineral equilibria in eclogitic gabbros suggest metamorphic conditions of T=450°-650°C for minimal pressures of 1.0-1.5 GPa (Chinner and Dixon, 1973; Ernst and Dal Piaz, 1978; Benciolini et al., 1988; Martin and Tartarotti, 1989; Droop et al., 1990; Dal Piaz et al., 1993). In the northern Aosta valley, temperatures for the eclogitic peak seem to have attained higher values than those for the southern ophiolites (Ernst and Dal Piaz, 1978; Oberhänsli, 1986). Coesite has been recently found within Mn-Mg-rich garnets from the Cignana (Valtournanche) metacherts of the Zermatt-Saas unit, recording peak conditions of T=590°-630°C and P=2.6-2.8 GPa (Reinecke, 1991). The post-eclogitic evolution of the Zermatt-Saas ophiolites is characterized by multiple re-equilibration under decreasing pressure, at first under high-T/blueschist facies conditions (glaucophane-garnet-bearing assemblages), and later, under Ab-amphibolite and greenschist facies conditions (Bearth, 1967; Ernst and Dal Piaz, 1978; Kienast, 1983; Ballèvre, 1988; Martin and Tartarotti, 1989; Reinecke, 1991).

2.3. The penninic basement and cover nappes

1) The Upper Penninic Monte Rosa and Gran Paradiso nappes.

The Monte Rosa and Gran Paradiso nappes occur at the same structural level within the present nappe pile (Figure 7.1 and 2). They consist of Variscan garnet-biotite-sillimanite paragneisses and cordierite-bearing migmatites, with mafic bodies and some marble interbeddings (pre-granitic complex), intruded by Upper Carboniferous porphyritic granites (310 Ma; Hunziker, 1970) and aplite-pegmatite dykes; these rock units are partly preserved at all scales in domains of low strain (Bearth, 1952; Dal Piaz, 1993). The predominating alpine derivatives are represented by various kinds of garnet micaschists, often albite-bearing (Gneiss minuti), and by metagranites to augengneisses, that record an eoalpine eclogitic imprint (400-530°C, 1.0-2.0 GPa), and a mesoalpine greenschist to amphibolite facies overprint (Bearth, 1952; Dal Piaz, 1971; Compagnoni and Lombardo, 1974; Compagnoni et al., 1974; Chopin and Maluski, 1980; Dal Piaz and Lombardo, 1986; Ballèvre, 1988; Biino and Pognante, 1989). Note that the Dora-Maira nappe - the southern homologue of Monte Rosa and Gran Paradiso - displays the first occurrence of coesite found in the Alps (Chopin, 1984). The Monte Rosa and Gran Paradiso basement is locally mantled by décolled remnants of Permian-Mesozoic cover sequences (quartzites, dolostones, marbles, and calcschists). As shown in (Figure 7.1 and 7.2), the Monte Rosa nappe is a huge recumbent fold (post-nappe deformation), resting over the Antrona ophiolites and narrowing down, to the southeast, into the inner steep belt occurring along the Ossola valley (Milnes, 1974; Klein, 1978; Milnes et al., 1981), i.e. into Argand's root zone of the Penninic nappes. By contrast, the tectonic sole of the Gran Paradiso and Dora-Maira nappes, located out of the Ossola-Tessin culmination, is not exposed at the surface.

2) The Middle Penninic Grand St. Bernard nappe system. The Grand St. Bernard system continuously extends from the Gulf of Genoa to the Valais and the Ossola valley; Bigi et al., 1990). From Valais to the northern Aosta valley (Figure 7.2), it is represented by a huge tectonic multilayer, consisting of the capping Mont Fort unit, the Siviez-Mischabel and Ruitor units, the Pontis unit and the basal and external "zone houillère", a thick décollement unit made up of Upper Carboniferous-Permian metaclastic deposits with coal interbeddings (Ellenberger, 1958; Elter, 1960, 1972; Caby et al., 1978; Escher et al., 1987; Escher, 1988). The Grand St. Bernard system displays a penetrative mid-Tertiary metamorphic imprint, ranging from blueschist to later greenschist facies. A pre-Westfalian basement (paraschists with associated igneous bodies generated by a bimodal magmatism), is preserved in the Siviez-Mischabel, Ruitor, and Pontis units. The basement is characterized by a Variscan amphibolite facies regional metamorphism (biotite, garnet, staurolite, kyanite; Frey et al., 1974; Desmons, 1992), and by older (eo-Variscan ?) relict eclogites (Thelin et al., 1993). The Variscan basement was intruded by Paleozoic granites and subvolcanic bodies, and is unconformably covered by Carboniferous-Triassic clastic deposits and volcanics, followed by Middle Triassic-Eocene platform- to deep-water carbonate and clastic deposits (Briançonnais sedimentary cover; Ellenberger, 1958; Marthaler, 1984; Escher, 1988). Basin analysis suggests that the Briançonnais domain operated as a structural high during the early stages of Mesozoic rifting.

DAY 7

Geology of the dent blanche, mesozoic ophiolites and sediments (monte cervino)
(Warm clothes and mountain shoes)

Stop 7.1:

Tectonic view from the terraces of the Plateau Rosa, the uppermost station of the cable car from Breuil-Cervinia. Comments will be made from two outstanding vantage points on the 3-D structure of the ophiolites and Dent Blanche nappe, and on their correlated sedimentary covers, according to the

Figure 7.3
View, from Plateau Rosa, of the Pancherot-Cime Bianche unit on the northern slope of Motta di Pleté (to be connected with 7.4 and 5.)

geologic relationships as described above. These vantage points are as follows: to the west on the Dent Blanche nappe, Combin and Zermatt-Saas zones (Figure 7.3, 4, 5 and 6); and to the north, on the backfold of the Gd. St. Bernard nappe (Figure 7.7, 8 and 9). The significance of the gabbro of Monte Cervino-Collon, and the tectonic implications of mesozoic covers in the partially-rejuvenated pre-Alpine continental crust will be discussed.

Figure 7.6
Explanatory tectonic scheme of Grandes Murailles and Monte Cervino southeastern slope geology (from a previous sketch by Giorgio V. Dal Piaz). See enclosed legend.

Figure 7.4
View of the Mont Blanc du Creton- to Dent d'Hérens chain (=Grandes Murailles) with Dent Blanche (Arolla metagranitoids and Valpelline series-metapelites, marbles and amphibolites. Mesozoic meta-ophiolites and calcschists in the lowermost part of the valley.)

Figure 7.7
View of the Zermatt valley from the north (Plateau Rosa, to be combined with 7.8 and 9). Mischabel backfold of the Gd. St. Bernard nappe on the left slope of the valley.

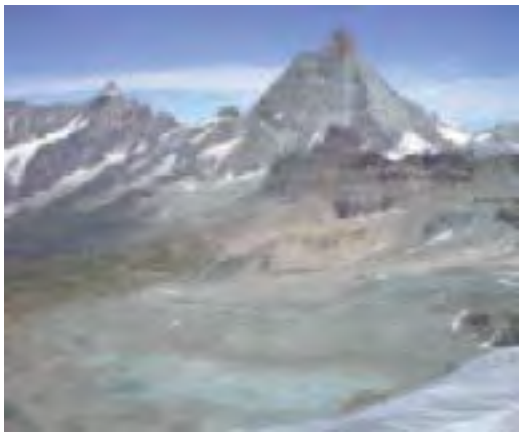

Figure 7.5
Southeastern slope of Monte Cervino (the Swiss Matterhorn). =For explanation see captions for Figure 7.6.

Figure 7.8
Right flank of the Zermatt valley

Figure 7.9
Piccolo Cervino (Lesser Matterhorn) metaophiolites.

Figure 7.10 - Eclogitic mafic layers and boudins included in calcschists of the Riffelberg-Garten sub-unit (Stop 7.3).

Stop 7.2:

Manganiferous metacherts north of Plan Maison. North of the Plan Maison cable-car station, the top of the eclogitic Zermatt-Saas unit consists of partly retrogressed eclogitic metabasalts, with normal-MORB affinity, and with an overlying bed of Mn-rich quartzite, which may be referred to as the Middle-Upper Jurassic base of the supraophiolitic oceanic covers. Metabasalts are characterized by the occurrence of lozenge-shaped aggregates of zoisite-epidote and white micas, replacing pre-eclogitic (prograde) lawsonite, glaucophane omphacite-almandine peak assemblage, and greenschist facies retrogression. The overlying metasediments consist of garnet-phengite quartzites, including thick bands and nodules rich in manganiferous and other minerals, such as piemontite (reddish), spessartine and alurgite (pink), brownite (black), and epidote (yellow). This mineralisation is representative of Alpine polyphase (eclogitic and greenschist facies) recrystallisation of ocean-floor hydrothermal deposits developed during the Mesozoic spreading of the Tethyan Ocean.

Field itinerary

Stops 7.3, 7.4:

"Riffelberg-Garten" Unit. Rocks exposed from the Testa Grigia (Plateau Rosa; see Stop 7.1, 7.2) - Ventina Glaciers to the town of Cervinia are part of the upper Zermatt-Saas ophiolitic unit. The outcrops, mostly covered by moraine deposits, consist of eclogitic metabasalts, serpentinites, and calcschists. At Stop 7.3 (close to the "Cime Bianche" station of the cable railway), boulders polished by the glacier (roche moutonée), expose marble and calchscists, including dm-scale layers and boudins, and cm to dm-scale subspherical to roughly-faceted clasts of metabasalt (Figure 7.10). These rocks make up the so-called "Riffelberg-Garten" sub-unit (Dal Piaz 1965; Bearth, 1967), which extends for a few km^2 between the "Cime Bianche" and "Plan Maison" cable car stations. It also outcrops in the upper part of the Ayas Valley (East of the Valtournanche Valley), and in Switzerland. In the Cime Bianche-Plan Maison area, the host rock of the Riffelberg-Garten sub-unit consists of either calcschist *s.s*, calcschist *s.l*. (micaschist interbedded with micaceous marble), quartz-rich calcschist, micaschist, marble, or carbonate-rich mafic rock (impure basalt? see Stop 7.3). Mafic boudins and clasts show homogeneous mineralogy, and consist of carbonate-rich eclogite. At Stop 7.4, near the Goillet lake (see figure7.10), the Riffelberg-Garten sub-unit is mostly represented by marly calcschists, including mafic boudins of various sizes and shapes.

The origin of these uncommon rocks still remains controversial, altough in the past they have been interpreted as a possible eo-alpine subduction mélange (Dal Piaz, 1965).

Geological Maps

Geologischer Atlas der Schweiz 1:25.000, Blatt 1347 Matterhorn. Office fédéral des eaux et de la géologie.

DAY 8 (morning)

The eclogitised continental crust of Sesia Lanzo Zone and its implications with the Mesozoic oceanic units (Lower Aosta Valley).

In the Western Alps, high-pressure low-temperature (HP-LT) metamorphic imprint widely affects not only the ophiolites and related sedimentary sequences, but also large volumes of the pre-Alpine continental crust. The Sesia-Lanzo Zone (SLZ; Figure 8.1) is the widest portion of the continental crust affected by eo-Alpine eclogite-facies metamorphism of this sector of the chain; its Alpine tectonic evolution, with eo-Alpine ages (130-70) proposed for the HP-LT metamorphic imprint (e.g: Hunziker, 1974; Oberhaensli, 1985; Stockhert, 1986; Rubatto, 1998; Rubatto, 1999), is characterised by a LT eclogite imprint followed by blueschist re-equilibration (Castelli, 1991; Pognante, 1991) and references therein), and a successive LP-greenschist retro-gradation. This evolution is compatible with an uplift during active oceanic lithosphere subduction (Spalla, 1996, Zucali, 2002). The characteristic low T/P ratio facilitated preservation of relict assemblages in rocks, undergoing several successive Alpine re-crystallizations. The pre-Alpine metamorphic evolution of this portion of Austroalpine continental crust, from granulite to greenschist facies conditions, is variably preserved in marbles, meta-pelites, meta-granitoids, meta-gabbros, granulites, and amphibolites (Compagnoni, 1977; Lardeaux, 1991; Rebay, 2001 and references therein). The granulite to amphibolite PT path has been considered to be the result of an extension-related uplift during Permo-Triassic times of the pre-Alpine lower crust (Lardeaux, 1991; Dal Piaz, 1993), an event similar to the one described in the Ivrea Zone (e.g. (Schmid, 1976; Sills, 1984; Mayer, 2000). Relics of the pre-Alpine history are preserved through the three main lithologic complexes of the SLZ (Figure 8.1): i) Gneiss Minuti complex (GMC), ii) Eclogitic Micaschists complex (EMC) and iii) II Dioritic-Kinzigitic Zone (IIDK). IIDK consists of kilometric lenses not recording the eclogitic re-equilibration; EMC and GMC, both pervasively eclogitised, strongly differ in the volume

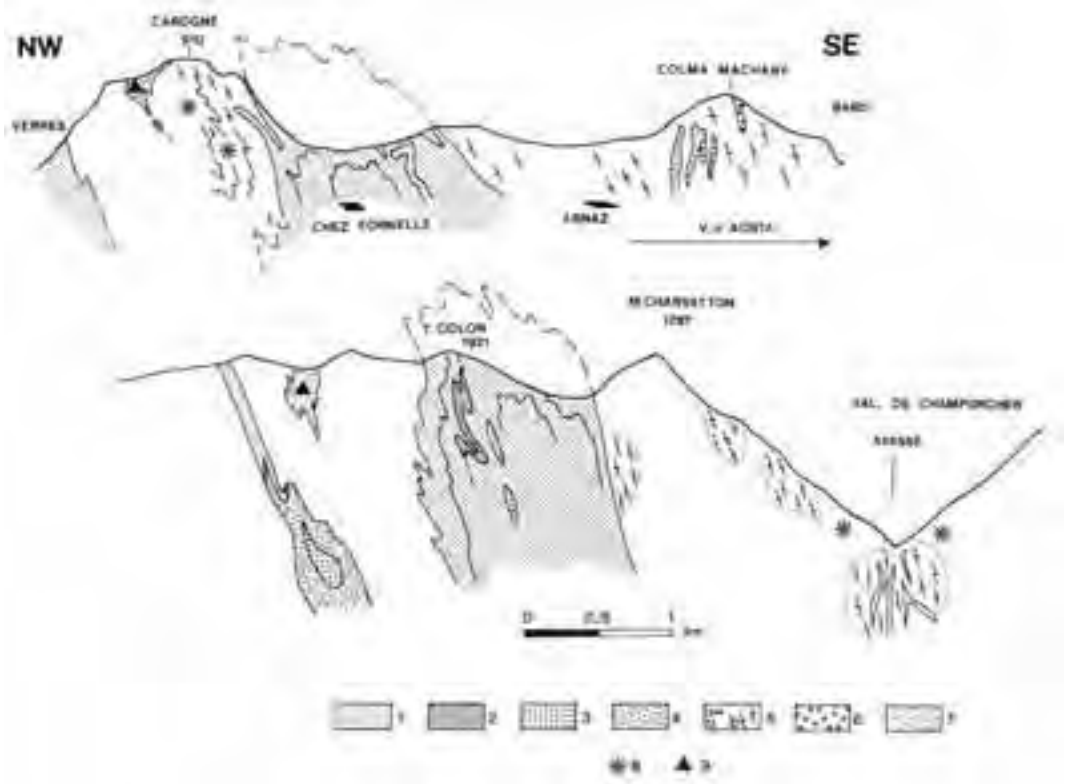

Figure 8.1- Cross section, seen in the natural exposure, of the implication of the external margin of the Sesia-Lanzo zone and the Mesozoic calcschists of the Combin unit. 1=calschists, 2=metabasics, 3=metagabbros, 4=serpentinites, 5=high grade pre-Alpine metapelites with blueschist Alpine overprint, 6=high grade amphibolites associated with 5, 7=quartzites, marbles, and high grade metapelites, 8=eclogites, 9=pre-Alpine granulites.

percentage of greenschist re-equilibration. GMC is widely reequilibrated under greenschist conditions, and marks the continent-ocean tectonic boundary, active during subduction-exhumation processes of the SLZ and the meta-ophiolites of the Piemontese Zone. In GMC, the greenschist imprint is generally associated with mylonitic textures (Stuenitz, 1989; Spalla, 1991). The EMC constitutes the innermost part of the SLZ; here the greenschist overprint is confined to discrete shear zones, more pervasive towards its inner boundary with the Southern Alps. The Alpine syn-metamorphic structures of Sesia-Lanzo Zone are intruded by calc-alkaline and ultrapotassic dikes during Oligocene (Dal Piaz, 1973; Dal Piaz, 1977).
The lower Aosta valley (Figure 8.1), from Borgofranco to Verres, offers a complete section across the Sesia-Lanzo zone, from the EMC (mainly eo-alpine eclogite facies rocks), to the GMC (mainly greenschist facies mylonites).

Stop 8.1:

Locality: Arnad, along highway A5, from Aosta to Torino.
Topics: Panoramic view over kilometer scale isoclinal folds of tectonic contact between GMC continental rocks and the metasediments of the Piedmont ophiolite zone.
The first stop of the eighth day is reached by following the Aosta-Torino highway (A5). The stop is some hundred meters after the Bard gate, in a parking area. The excursion stop is illustrated in Figs. 8.1 and 8.2.
In the natural cross section between Verres and Bard, the continental unit of the external SLZ (GMC) displays an historically known tectonic implication (by a several kilometer-scale fold) with the underlying Mesozoic calcschists and ophiolites. Analysis of

Figure 8.2 - General map of the Sesia-Lanzo zone, and location of Stop 2.
schema Sesia: (B) Simplified geological map of the Sesia-Lanzo-Zone. Legend: 1 = II Dioritic- Kinzigitic zone; 2A = Gneiss Minuti complex; 2B = Eclogitic Micaschists complex; 3A = non-metamorphic Tertiary intrusives; 3B = contact metamorphic aureole; Symbols: a) = metagabbros; b) = metagranitoids; c) = calc-silicate marbles; d) = relict eclogites in the Gneiss Minuti complex. (C) E-W idealized cross-section, in which deformation and greenschist re-equilibration gradients from the Eclogitic Micaschists (East) to Gneiss Minuti (West) complexes are represented by the frequency of greenschist deformation zones (beards). Legend: 1) and 2) meta-ophiolites and calcschists of the Piemonte Zone, respectively; 3) Lanzo ultramafics; 4) Gneiss Minuti and Eclogitic Micaschists Complexes; 5) II Dioritic-Kinzigitic zone; 6) Tertiary intrusives; 7) Ivrea Zone; I.L. = Insubric Line.

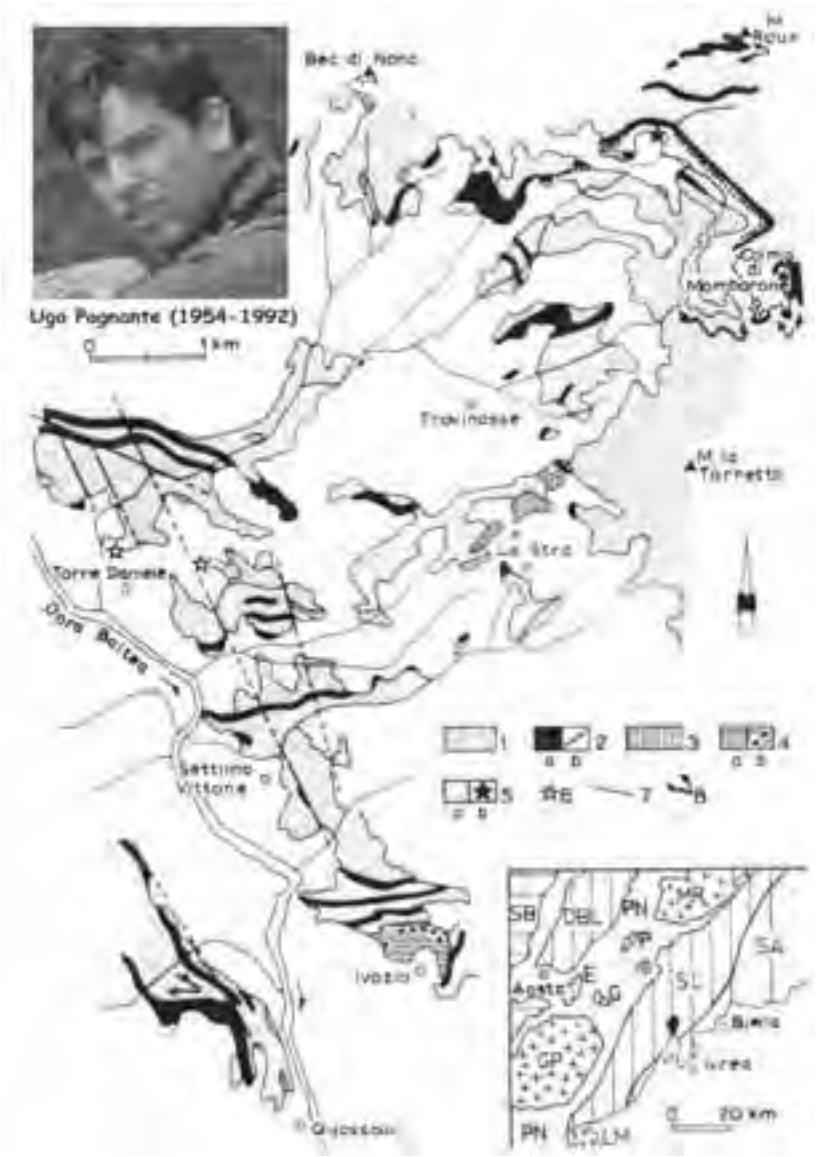

Figure 8.3 - Map of the internal part of the Eclogitic Micaschists complex along the lower Aosta valley (Colma di Mombarone, western slope), by Ugo Pognante (1980). 1) marbles and carbonate schists; 2a) metagranitoids; 2b) jadeite megablastic layers; 3) amphibole eclogites (La Stra); 4a) eclogitic metabasites (Ivozio); 5a) eclogitic micaschists; 5b) kyanite-chloritoid-garnet micaschists; 6) post-metamorphic lamprophyric dikes; 7) faults and fracture zones; 8) main D2 structures; 9) traces of cross sections (see Figure 2 in Pognante et al., 1980); SA=Southern Alps; LM=Lanzo Massif; SL=Sesia-Lanzo zone; DBL=Dent Blanche nappe; G=Glacier-Rafray klippe; E=M.Emilius klippe; P=Pillonet klippe; PN=Piemonte Ophiolite nappe; MR=Monte Rosa nappe; GP=Gran Paradiso nappe; SB=Saint Bernard nappe.

small scale folds and cleavages demonstrates that this fold belt, which is a dominant tectonic feature of the SLZ external margin, over several tens of kilometers, developed under greenschist facies conditions. In spite of the pervasive greenschist overprint, small relics of Alpine eclogite and pre-Alpine granulites are preserved both in the GMC (Figure 8.2), and in the metabasalts associated with the Mesozoic calcschists.

Stop 8.2:

Locality: Montestrutto area, at the boundary between the Valle d'Aosta and Piemonte regions, a few kilometers north of Ivrea.

Topics: coarse-grained polydeformed eclogite facies-rocks of EMC; deformation vs. reaction rate and the role of bulk chemistry.

The second stop of the eighth day is reached

by following the highway Aosta-Torino to the Quincinetto exit and the main road for Ivrea (S.S. n° 20) to Montestrutto village. Stop in parking area along the main road, excursion stop is located in Fig. 8.1. Short walk (10 - 20 min.) along a foot-path in the wood.

The rocks of the region around Montestrutto belong to the EMC (Figure 8.1), and consist of micaschists and gneisses with Qtz, Phe, Grt, ± Na-Cpx, ± Gl, Pg, Zo, Ep, Rt, locally Ky, and Mg-rich Cld. Micaschists and gneisses include layers and lenses, up to 10 meters thick, of mafic rocks (eclogites, amphibole bearing eclogites, glaucophanites and hornblendites), folded or boudinaged during polyphase Alpine deformation, and showing different eclogitic assemblages, depending on their bulk composition and fabric evolution (Figure 8.4). Amphibole-bearing eclogites show the most common mineral assemblage: Omp, Grt, Rt, Gl/Ca-Na Amp, white mica, and Zo. Zo and Pg locally replace Lws in the eclogites of Ivozio (Figs. 8.3). Pure and impure marbles (Cal, Ank, Dol, ± Phe, Grt, Qtz, and Omp), interlayered within micaschists (Figure 8.3), locally show mylonitic texture (Castelli, 1991); leucocratic metagranitoid dykes (Qtz, Na-Cpx, Phe, ±Grt, Gl, and relict Kfs) are folded and transposed in micaschists.

Internal deformation of EMC manifests four generations of Alpine folds (Pognante, 1980; Williams, 1983): D_1 and D_2 developed under HP-LT conditions, as evidenced by Phe and Na-Cpx aligned in the S_1 foliation, and by the recovery sub-structure of the deformed HP minerals during D_2 micro-folding. A pre-eclogite fabric is preserved in the mafic rocks, where Amp, Zo/Czo, white mica, and Rt define a foliation overgrown by Na-Cpx, Grt and Zo (Pognante, 1980); similar patterns have been interpreted, in adjacent areas of SLZ (Valchiusella), as the mineral record of a subduction-related prevailing P-prograde trajectory (Reinsch, 1979). D_3 is synchronous with the re-equilibration under blueschist-facies conditions; D_4 mega-scale folds overprint the previous structures (Williams, 1983).

References

Ábalos, B., Puelles, P. & Gil Ibarguchi, J. I., 2003. Structural assemblage of high-pressure mantle and crustal rocks in a subduction channel (Cabo Ortegal, NW Spain). Tectonics, 22(2).

Argand, E., 1911. Les nappes de recouvrement des Alpes Pennines et leurs prologements structuraux. Matériaux pour la Carte Géologique de la Suisse; nouvelle série, 31.

Bächlin, R., Bianconi, F., Codoni, A., Dal Vesco, E., Knoblauch, P., Kündig, E., Reinhard, M., Spaenhauer, F., Spicher, A., Trommsdorff, V. & Wenk, E., 1974. Geologischer Atlas der Schweiz 1: 25000, Blatt 1313: Bellinzona, Schweizerische Geologische Kommission.

Bearth, P. (1967). Die ophiolite Zone von Zermatt-Saas Fee. Beitr. Geol. Karte Schweiz, 130., 132 pp.

Becker, H., 1993. Garnet peridotite and eclogite Sm-Nd mineral ages from the Lepontine dome (Swiss Alps): New evidence for Eocene high-pressure metamorphism in the central Alps. Geology, 21, 599-602.

Bozhilov, K. N., Green, H. W. I. & Dobrzhinetskaya, L., 1999. Clinoenstatite in Alpe Arami peridotite; additional evidence of very high pressure. Science, 284, 129-132.

Brenker, F. E. & Brey, G. P., 1997. Reconstruction of the exhumation path of the Alpe Arami garnet-peridotite body from depths exceeding 160 km. Journal of metamorphic Geology, 15, 581-592.

Brouwer, F. M., 2000. Thermal evolution of high-pressure metamorphic rocks in the Alps. Unpub. Ph.D. Thesis, Utrecht University, Utrecht.

Brouwer, F. M. & Engi, M., 2004. Staurolite and other high-alumina phases in Apline eclogite: Analysis of domain evolution. Canadian Mineralogist, Carmichael volume, (submitted).

Brouwer, F. M., Engi, M., Berger, A. & Burri, T., 2003. Towards complete PTt paths: Unravelling Alpine eclogite relics. Norsk Geol. Unders. Report, 2003.055, 25-26.

Cluzel, D., Aitchinson, J. C. & Picard, C., 2001. Tectonic accretion and underplating of mafic terranes in the Late Eocene intraoceanic fore-arc of New Caledonia (Southwest Pacific): geodynamic implications. Tectonophysics, 340, 23-59.

Codoni, A. G., 1981. Geologia e petrografia della regione del Pizzo di Claro. Unpub. PhD Thesis, ETH Zürich, Zürich.

Colombo, C. & Tunesi, A., 1999. Alpine metamorphism of the Southern Alps west of the Giudicarie Line. Schweiz. Mineral. Petrogr. Mitt., 79(1), 183-189.

Cornelius, H. P. & Furlani-Cornelius, M., 1930. Die insubrische Linie vom Tessin bis zum Tonalepass. Denkschrift der Akademie der Wissenschaften

Wien, math. naturwiss. Kl., 102. Dal Piaz G.V., 1992. Le Alpi dal M. Bianco al Lago Maggiore. I Volume: 13 itinerari. Guide Geol. Regionali, BE-MA Milano, 311 pp., 181 Figure

Dal Piaz G.V., 1999. The Austroalpine-Piedmont nappe stack and the puzzle of Alpine Tethys. In G. Gosso et al. (Eds): Third Meeting on Alpine Geol. Studies, Mem. Sci. Geol., 51, 155-176.

Dal Piaz G.V., 2001. History of tectonic interpretations of the Alps. J. Geodynamics, 32, 99-114.

Dal Piaz G.V., 2001. Geology of the Monte Rosa massif: historical review and personal comments. Schweiz. mineral. petrogr. Mitt., 81, 275-303.

Dal Piaz G.V., Cortiana G., Del Moro A., Martin S., Pennacchioni G. & Tartarotti P., 2001. Tertiary age and paleostructural inferences of the eclogitic imprint in the Austroalpine outliers and Zermatt-Saas ophiolite, Western Alps. Intern. J. Earth Sci., 90, 668-684.

Dal Piaz G.V., Bistacchi A. & Massironi M., 2003. Geological outline of the Alps. Episodes. september 2003.

Dal Piaz G.V., De Vecchi Gp. & Hunziker J.C., 1977. The Austroalpine layered gabbros of the Matterhorn and Mt.Collon-Dents de Bertol. Schweiz. mineral. petrogr. Mitt., 57: 59-88.

Dal Piaz G.V. & Lombardo B., 1986. Early-Alpine eclogite metamorphism in the Penninic Monte Rosa-Gran Paradiso basement nappes of the northwestern Alps. Geol. Soc. Am. Mem., 164: 249-265.

Dal Piaz G.V., Di Battistini G., Venturelli G. & Kienast J.R., 1979. Manganiferous quartzitic schists of the Piemonte ophiolite nappe in the Valsesia-Valtournanche area (Italian Western Alps). Mem. Sci. Geol., 32: 24 pp.

Dal Piaz G.V., Venturelli G., Spadea P. & Di Battistini G., 1981. Geochemical features of metabasalts and metagabbros from the Piemonte ophiolite nappe, Italian Western Alps. N. Jb. Min. Abh., 142: 248-269.

Cortiana G., Dal Piaz G.V., Del Moro A., Hunziker J.C. & S. Martin S., 1998. 40Ar-39Ar and Rb-Sr dating of the Pillonet klippe and Sesia-Lanzo basal slice, western Austroalpine. Mem. Sci. Geol., 50, 177-194.

Dal Piaz, G.V. (1965). La formazione mesozoica dei calcescisti con pietre verdi tra la Valsesia e la Valtournanche ed i suoi rapporti strutturali con il ricoprimento del Monte Rosa nell'alta Val d'Ayas. Boll. Soc. Geol. It., 84, 67-104.

Dobrzhinetskaya, L., Green, H. W. & Wang, S., 1996. Alpe Arami: a peridotite massif from dephts of more than 300 kilometers. Science, 271, 1841-1845.

Engi, M., Berger, A. & Roselle, G. T., 2001a. Role of the tectonic accretion channel in collisional orogeny. Geology, 29(12), 1143-1146.

Engi, M., Cheburkin, A. & Köppel, V., 2002. Non-destructive chemical dating of young monazite using XRF: 1. Design of a mini-probe, age data for samples from the Central Alps, and comparison to U-Pb (TIMS) data. Chemical Geology, 191(1-3), 223-239.

Engi, M., Scherrer, N. C. & Burri, T., 2001b. Metamorphic evolution of pelitic rocks of the Monte Rosa nappe: Constraints from petrology and single grain monazite age data. Schweizerische Mineralogische und Petrographische Mitteilungen, 81(3), 305-328.

Engi, M., Todd, C. S. & Schmatz, D. R., 1995. Tertiary metamorphic conditions in the eastern Lepontine Alps. Schweizerische Mineralogische und Petrographische Mitteilungen, 75(3), 347-369.

Ernst, W. G., 1977. Mineralogic study of eclogitic rocks from Alpe Arami, Lepontine Alps, Southern Switzerland. J. Petrol., 18, 371-398.

Ernst, W. G., 1978. Petrochemical study of some lherzolitic rocks from the Western Alps. J. Petrol., 19, 341-392.

Ernst, W. G., 1981. Petrogenesis of eclogites and peridotites from the Western and Ligurian Alps. Amer. Mineral., 66, 443-472.

Evans, B. W. & Trommsdorff, V., 1978. Petrogenesis of garnet lehrzolite, Cima di Gagnone, Lepontine Alps. Earth and Planetary Science Letters, 40, 333--348.

Frey, M. & Ferreiro Mählmann, R., 1999. Alpine metamorphism of the Central Alps. Schweizerische Mineralogische Petrographische Mitteilungen, 79, 135-154.

Fumasoli, M. W., 1974. Geologie des Gebietes nördlich und südlich der Jorio-Tonale-Linie im Westen von Gravedona (Como, Italia). Unpub. Dissertation Thesis, Universität Zürich.

Gebauer, D., 1996. A P-T-t-path for an (ultra?) high-pressure ultramafic/mafic rock association and its felsic country-rocks based on SHRIMP-dating of magmatic and metamorphic zircon domains. Example: Alpe Arami (Swiss Central Alps). In: Earth Processes: Reading the Isotopic Code, pp. 309-328, American Geophysical Union.

Gebauer, D., 1999. Alpine geochronology of the

Central and Western Alps: new constraints for a complex geodynamic evolution. Schweizerische Mineralogische und Petrographische Mitteilungen, 79, 191-208.

Grandjean, V., 2001. Petrographical evolution of mafic relics and their interpretation for the geodynamics of the Central Alps. Unpub. Ph.D. Thesis, University of Bern.

Green, H. W., Dobrzhinetskaya, L., Riggs, E. M. & Jin, Z. M., 1997. Alpe Arami: a peridotite massif from the Mantle Transition Zone? Tectonophysics, 279(1-4), 1-21.

Grubenmann, U., 1908. Der Granatolivinfels des Gordunotales und seine Begleitgesteine. Vierteljahresschrift der Naturforschenden Gesellschaft Zürich, 53, 129-156.

Hacker, B. R., Sharp, T., Zhang, R. Y., Liou, J. G. & Hervig, R. L., 1997. Determining the origin of ultrahigh pressure lherzolites. Science, 278, 702-704.

Heinrich, C. A., 1983. Die regionale Hochdruckmetamorphose der Aduladecke. Unpub. PhD Thesis, ETH Zürich, Zürich.

Heinrich, C. A., 1986. Eclogite facies regional metamorphism of hydrous mafic rocks in the Central Alpine Adula nappe. Journal of Petrology, 27(123-154).

Hunziker, J. C., Desmons, J. & Hurford, A. J., 1993. Thirty-two years of geochronological work in the Central and Western Alps: a review on seven maps. Mémoires de Géologie (Lausanne), 13.

Hurford, A. J., 1986. Cooling and uplift patterns in the Lepontine Alps, south-central Switzerland, and an age of vertical movement on the Insubric fault line. Contributions of Mineralogy and Petrology, 92, 413-427.

Jenny, H., Frischknecht, G. & Kopp, J., 1923. Geologie der Adula. Geol. Komm., Bern.

Knoblauch, P., 1939. Gebiet nördlich der Iorio-Tonale-Linie, Wurzelzone. In: Erläuterungen zum Geologischen Atlas der Schweiz 1:25000, Blatt Jorio, pp. 52-69, Geologische Kommission, Bern.

Knoblauch, P., Reinhard, M. & Kündig, E., 1939. Geologischer Atlas der Schweiz 1:25000, No. 11 (Blatt Jorio).

Knup, P., 1958. Geologie und Petrographie des Gebietes zwischen Centovalli-Valle Vigezzo und Onsernone. Schweizerische Mineralogische und Petrographische Mitteilungen, 38, 83-235.

Köppel, V. & Grünenfelder, M., 1975. Concordant U-Pb ages of monazite and xenotime from the Central Alps and the timing of high temperature metamorphism, a preliminary report. Schweizerische Mineralogische und Petrographische Mitteilungen, 55, 129-132.

Köppel, V. & Grünenfelder, M., 1978. The significance of monazite U-Pb ages; examples from the Lepontine area of the Swiss Alps. In: 4th Internat. Conf. on Geochronology, Cosmochronology, and Isotope Geology, pp. 226-227, US Geol Survey, Open File Report, Denver, CO.

Köppel, V., Günthert, A. & Grünenfelder, M., 1981. Patterns of U-Pb zircon and monazite ages in polymetamorphic units of the Swiss Central Alps. Schweizerische Mineralogische und Petrographische Mitteilungen, 61, 97-120.

López Sánchez-Vizcaíno, V., Gómez-Pugnaire, M. T., Azor, A. & Fernández-Soler, J. M., 2003. Phase diagram sections applied to amphibolites: a case study from the Ossa-Morena / Central Iberian Variscan suture (Southwest Iberian Massif). Lithos, 68, 1-21.

Löw, S., 1987. Die tektono-metamorphe Entwicklung der Nördlichen Adula-Decke. Stämpfli & Cie., Bern.

Merle, O., 1994. Syn-convergence exhumation of the Central Alps. Geodin Acta, 7(3), 129-138.

Meyre, C., De Capitani, C. & Partzsch, J. H., 1997. A ternary solid solution model for omphacite and its application to geothermobarometry of eclogites from the middle Adula Nappe (Central Alps, Switzerland). Journal of Metamorphic Geology, 15(6), 687-700.

Meyre, C., de Capitani, C., Zack, T. & Frey, M., 1999. Petrology of high-pressure metapelites from the Adula nappe (Central Alps, Switzerland). Journal of Petrology, 40(1), 199-213.

Meyre, C. & Frey, M., 1998. Eclogite facies metamorphism and deformation of the middle Adula nappe (Central Alps, Switzerland): Excursion to Trescolmen. Schweiz. Mineral. Petrogr. Mitt., 78(2), 355-362.

Milnes, A. G., Greller, M. & Mueller, R., 1981. Sequence and style of major post-nappe structures, Simplon-Pennine Alps. Journal Structur Geology, 3, 411-420.

Moeckel, J. R., 1969. Structural petrology of the garnet-peridotite of Alpe Arami (Ticino, Switzerland). Leidse Geol. Mede., 42, 61-130.

Nagel, T., 2000. Metamorphic and structural history of the southern Adula nappe (Graubünden, Switzerland). Unpub. Ph.D. Thesis, University of Basel, Basel.

Niggli, E., 1974. Metamorphism and Tectonics of the

Volume n° 2 - from B16 to B33

Alps. Mem. Soc. geol. It., 13, 285-289.

Nimis, P., Trommsdorff, V. & Russo, U., 2000. Revised thermobarometry of Alpe Arami and other garnet peridotites from the Central Alps. Journal of Petrology, 42, 103-115.

O'Hara, M. J. & Mercy, E. L. P., 1963. Petrology and petrogenesis of some garnetiferous peridotites. Trans. Royal Soc. Edinburgh, 65, 251-314.

Olker, B., Altherr, R. & Paquin, J., 2003. Fast exhumation of the ultrahigh-pressure Alpe Arami garnet peridotite (Central Alps, Switzerland): constraints from geospeedometry and thermal modelling. J. metamorphic Geol., 21, 395-402.

Paquin, J. & Altherr, R., 2001. New constraints on the P-T evolution of the Alpe Arami garnet peridotite body (Central Alps, Switzerland). J. Petrol., 42, 1119-1140.

Partzsch, J. H. & Meyre, C., 1995. The structural evolution of the Middle Adula nappe (Central Alps, Switzerland). Bochumer geologische und geotechnische Arbeiten, 44, 136-138.

Pfiffner, M. & Trommsdorff, V., 1998. The high-pressure ultramafic-mafic-carbonate suite of Cima Lunga-Adula, Central Alps: Excursions to Cima di Gagnone and Alpe Arami. Schweizerische Mineralogische und Petrographische Mitteilungen, 78, 337-354.

Pfiffner, O. A., Ellis, S. & Beaumont, C., 2000. Collision tectonics in the Swiss Alps: Insight from geodynamic modeling. Tectonics, 19(6), 1065-1094.

Pfiffner, O. A., Heitzmann, P., Lehner, P., Frei, W., Pugin, A. & Felber, M., 1997. Incision and backfilling of Alpine valleys: Pliocene, Pleistocene and Holocene processes. In: Deep Structure of the Swiss Alps (eds Pfiffner, O. A., Lehner, P., Heitzmann, P., Müller, S. & Steck, A.), pp. 265-288, Birkhäuser, Basel.

Reinhard, M., 1939. Gebiet südlich der Iorio-Tonale-Linie, Insubrische Zone. In: Erläuterungen zum Geologischen Atlas der Schweiz 1:25000, Blatt Jorio, pp. 69-81, Geologische Kommission, Bern.

Risold, A.-C., Trommsdorff, V. & Grobéty, B., 2001. Genesis of ilmenite rods and palisades along humite-type defects in olivine from Alpe Arami. Contrib. Mineral. Petrol., 140, 619-628.

Risold, A. C., Trommsdorff, V. & Grobéty, B., 2003. Morphology of oriented ilmenite inclusions in olivine from garnet peridotites (Central Alps, Switzerland). Eur. J. Mineral., 15, 289-294.

Roselle, G. T., Thüring, M. & Engi, M., 2002. MELONPIT: A finite element code for simulating tectonic mass movement and heat flow within subduction zones. American Journal of Science, 302, 381-409.

Schärer, U., Cosca, M., Steck, A. & Hunziker, J., 1996. Termination of major ductile strike-slip shear and differential cooling along the Insubric line (Central Alps): U-Pb, Rb-Sr and Ar-40/Ar-39 ages of cross-cutting pegmatites. Earth Planet Sci Lett, 142(3-4), 331-351.

Schlunegger, F., Matter, A., Burbank, D. W. & Klaper, E. M., 1997. Magnetostratigraphic constraints on relationships between evolution of the central Swiss Molasse basin and Alpine orogenic events. Geol Soc Amer Bull, 109(2), 225-241.

Schmidt, M. W., 1989. Petrography and structural evulation of ophiolitic remants in the Bellinzona Zone, Southern Steep Belt, Central Alps. Schweizerische Mineralogische und Petrographische Mitteilungen, 69, 393-405.

Stucky, A., 2001. High grade Mesozoic ophiolites of the Southern Steep Belt, Central Alps. Unpub. Ph.D. Thesis, ETH Zürich.

Todd, C. S. & Engi, M., 1997. Metamorphic field gradients in the Central Alps. Journal of Metamorphic Geology, 15, 513-530.

Tóth, M., Grandjean, V. & Engi, M., 2000. Polyphase evolution and reaction sequence of compositional domains in metabasalt: A model based on local chemical equilibrium and metamorphic differentiation. Geological Journal, 35, 163-183.

Trommsdorff, V., 1990. Metamorphism and tectonics in the Central Alps: The Alpine lithospheric mélange of Cima Lunga and Adula. Memorie della Società Geologica Italiana, 45, 39-49.

Trommsdorff, V. & Evans, B. W., 1980. High grade rodingites from the central Alps: metamorphism and geochemistry. Areh. Sc. Geneve, 33, 181--184.

Trommsdorff, V., Hermann, J., Müntener, O., Pfiffner, M. & Risold, A. C., 2000. Geodynamic cycles of subcontinental lithosphere in the Central Alps and the Arami enigma. Journal of Geodynamics, 30, 77-92.

Vance, D. & O'Nions, R. K., 1992. Prograde and retrograde thermal histories from the Central Swiss Alps. Earth and Planetary Science Letters, 114, 113-129.

von Blanckenburg, F. & Davies, J. H., 1995. Slab breakoff: A model for syncollisional magmatism and tectonics in the Alps. Tectonics, 14(1), 120-131.

Back Cover:
field trip itinerary

FIELD TRIP MAP

32nd INTERNATIONAL GEOLOGICAL CONGRESS

Edited by APAT

Volume n° 2 - from B16 to B33

Field Trip Guide Book - B30

32nd INTERNATIONAL GEOLOGICAL CONGRESS

THE NEOGENE THRUST-TOP BASINS IN CENTRAL SICILY AND THE NEOGENE VOLCANISM OF THE NORTHERN MONTI IBLEI IN SOUTH-EASTERN SICILY

Leaders:
M. Grasso, R.W.H. Butler, H.U. Schmincke

Florence - Italy
August 20-28, 2004

Pre-Congress **B30**

The scientific content of this guide is under the total responsibility of the Authors

Published by:
APAT – Italian Agency for the Environmental Protection and Technical Services - Via Vitaliano Brancati, 48 - 00144 Roma - Italy

Series Editors:
Luca Guerrieri, Irene Rischia and Leonello Serva (APAT, Roma)

English Desk-copy Editors:
Paul Mazza (Università di Firenze), Jessica Ann Thonn (Università di Firenze), Nathalie Marléne Adams (Università di Firenze), Miriam Friedman (Università di Firenze), Kate Eadie (Freelance indipendent professional)

Field Trip Committee:
Leonello Serva (APAT, Roma), Alessandro Michetti (Università dell'Insubria, Como), Giulio Pavia (Università di Torino), Raffaele Pignone (Servizio Geologico Regione Emilia-Romagna, Bologna) and Riccardo Polino (CNR, Torino)

Acknowledgments:
The 32nd IGC Organizing Committee is grateful to Roberto Pompili and Elisa Brustia (APAT, Roma) for their collaboration in editing.

Graphic project:
Full snc - Firenze

Layout and press:
Lito Terrazzi srl - Firenze

Volume n° 2 - from B16 to B33

32nd INTERNATIONAL GEOLOGICAL CONGRESS

THE NEOGENE THRUST-TOP BASINS IN CENTRAL SICILY AND THE NEOGENE VOLCANISM OF THE NORTHERN MONTI IBLEI IN SOUTH-EASTERN SICILY

AUTHORS:
R.W.H. Butler (Department of Earth Sciences, University of Leeds - U.K.)
M. Grasso (Dipartimento di Scienze Geologiche, University of Catania - Italy)
R. Maniscalco (Dipartimento di Scienze Geologiche, University of Catania - Italy)

Florence - Italy
August 20-28, 2004

Pre-Congress

B30

Front Cover:
Panoramic view of Monte Capodarso showing at the top offlapping succession of prograding calcarenite bodies of Pliocene age.

Leaders: M. Grasso, R.W.H. Butler, H.-U. Schmincke

Introduction

Sicily occupies a key site in the central Mediterranean, recording geodynamic and climatic processes through its unrivalled succession of sedimentary and volcanic rocks. This excursion looks at the Neogene evolution of central and SE Sicily as recorded by these deposits. Themes include:

The interactions between tectonics, sea-level and climate in controlling the record of the Messinian Salinity Crisis; using high resolution stratigraphy to chart tectonic tilting;

Chemical evolution and emplacement mechanisms of subaerial and shallow to deep water volcanics – related to basin evolution.

Regional geologic setting of the Neogene thrust-top basins in central Sicily

Sicily straddles a range of different tectonic structures. The northern edge of the island contains active rift structures associated with opening of the southern Tyrrhenian Basin. The eastern edge of the island contains faults associated with the continental margin into the Ionian sea. The southern side of the island contains the front of the Maghrebian orogenic belt that continues westwards into north Africa (Fig. 0.1). However, part of the orogenic foreland, continuous with the submerged part in the Straits of Sicily, is exposed onland in SE Sicily (the Hyblean block). Yet "foreland" is a misnomer for Hyblea is strongly

Figure 0.1 - Schematic structural map showing the arcuate thrust front in southern Sicily (Gela nappe). Location of sections shown in Fig. 0.2. (after Grasso, 2001).

Volume n° 2 - from B16 to B33

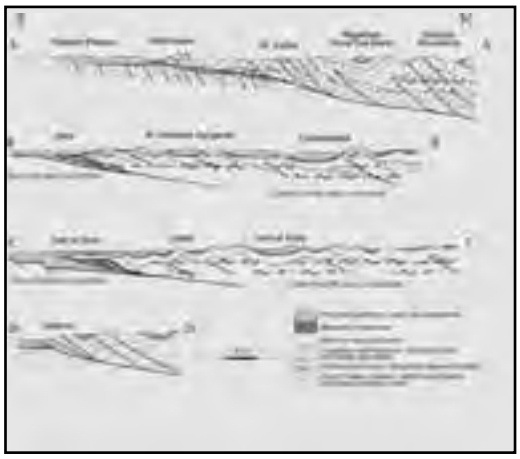

Figure 0.2 - Cross-sections showing the different deformational style affecting the carbonates at Mount Judica and Sciacca imbricates and south-central Sicily where thick clay successions are predominant (after Lickorish et al., 1999): A. Cross section from Mt. Judica to the Hyblean plateau showing thrust imbrication against the platform margin; B and C. Cross sections through the front of the thrust belt (Gela Nappe) in central-south Sicily, showing the dominant structural style characterized by open folding at the surface, with possible thrusts within the basinal succession at depth; D. Cross section through the Sciacca region where the shortening is accommodated by steep-dipping thrusts.

faulted, chiefly by strike-slip and extensional structures. These faults have focussed volcanism through late Neogene and to modern times, with ongoing activity at Etna.

The complexity of the modern tectonic setting is matched by the pre-Neogene palaeogeography of Sicily. While the Hyblean block was only weakly rifted and did not experience substantial vertical movements through Mesozoic and early Tertiary times, the rest of the island bears testimony to substantial rifting, subsidence and subsequent compressional tectonics. Much of the geological history is controversial although most models show a complex passive margin setting that remained largely sediment-starved until earliest Miocene times. The onset of convergent tectonics, the significance of various flysch deposits and the palaeogeography of different units are far from established – and are outside the scope of this excursion. By Neogene times there were substantial compressional structures across which detritus, sourced from the African foreland and from rising parts of the orogen, accumulated. These strata form the fill to the so-called "Caltanissetta Basin" and dominate the geology of central Sicily. To the north are the Madonie and Nebrodi mountains,

Figure 1.1 - Simplified geological map of the north-central part of the Caltanissetta basin. Illustrated is the location of the section line A-B of Fig. 1.2 (modified after Butler and Grasso, 1993).

uplifted largely by Pliocene-age faulting and associated isostatic rebound during Tyrrhenian rifting. This uplift wanes systematically southward, driving regression charted by the southward migration of the Plio-Pleistocene coastline (Butler et al., 1995a). Shallow marine clays and sands of mid-late Pliocene age are found at Enna, at an altitude of 1000 m. (Fig. 0.1).

The Caltanissetta Basin contains the substantial accumulations of Messinian strata (e.g. Decima and Wezel, 1973) making it important for developing models for the Mediterranean Salinity Crisis. In this excursion we will devote one day to this aspect of the geology. These and other strata accumulated across active thrusts and folds. The structures are generally southward vergent and have generated spaced arrays of subsidiary basins in synformal settings. The thrusts and folds at outcrop are believed to detach downwards onto a regional décollement (The frontal structures are termed the Gela Nappe). Well data indicate that this structure has over-ridden the Hyblean-type "foreland" for >>8 km since Mid-Late Pliocene times (Bianchi et al., 1989; Butler et al., 1992, Fig.0.2).
Onland the thrust front is buried by undeformed Pleistocene deposits, indicating that compressional tectonics, at least in east-central Sicily, has ceased.
The "foreland": area to the thrust belt discussed above is the Hyblean plateau. This forms a relatively up-standing block that is faulted not only at its margins but internally too.

DAY 1

Caltanissetta Basin

Messinian strata: onset and end of the Salinity crisis.

The Caltanissetta Basin (Fig. 1.1) is classic ground for the study of Messinian and related strata on Sicily (Decima and Wezel, 1973).

In this first day we will visit sites that collectively display a range of Messinian palaeo-environments and we will relate these to the local structural settings. We shall concentrate on the Corvillo sub-basin, a synformal structure that was tectonically active during and after the accumulation of Messinian deposits (Butler et al. 1995b). Over 300m of halite and K-salts accumulated in the centre of the basin, exploited until the late1980s by Italkali. Only the marginal carbonates and local gypsiferous deposits are preserved at outcrop (chiefly the transgressive Calcare di Base Formation) although mine/well records from Italkali may be used to build up a basin-wide model (Fig. 1.2).

Late Miocene stratigraphy of the Caltanissetta Basin is summarised in Fig. 1.3. The substrata for much of the evaporite complex is the Terravecchia Formation (Upper Tortonian to Lower Messinian). In many places in central-southern Sicily this unit is clay-rich with a fully marine faunal assemblage. The passage of this Terravecchia facies into evaporites has been used

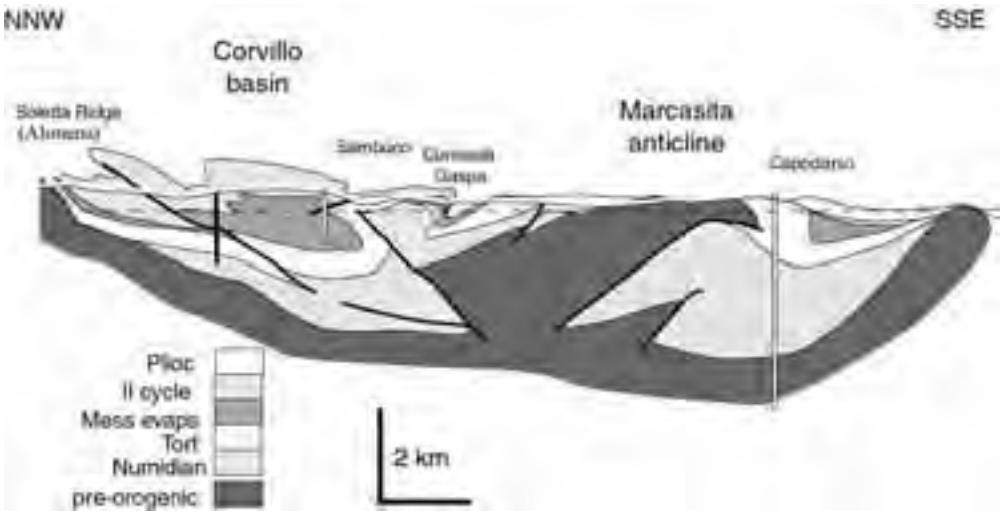

Figure 1.2 - Simplified cross-section (after Butler et al. 1995b) through the Corvillo Basin and Marcasita anticline.

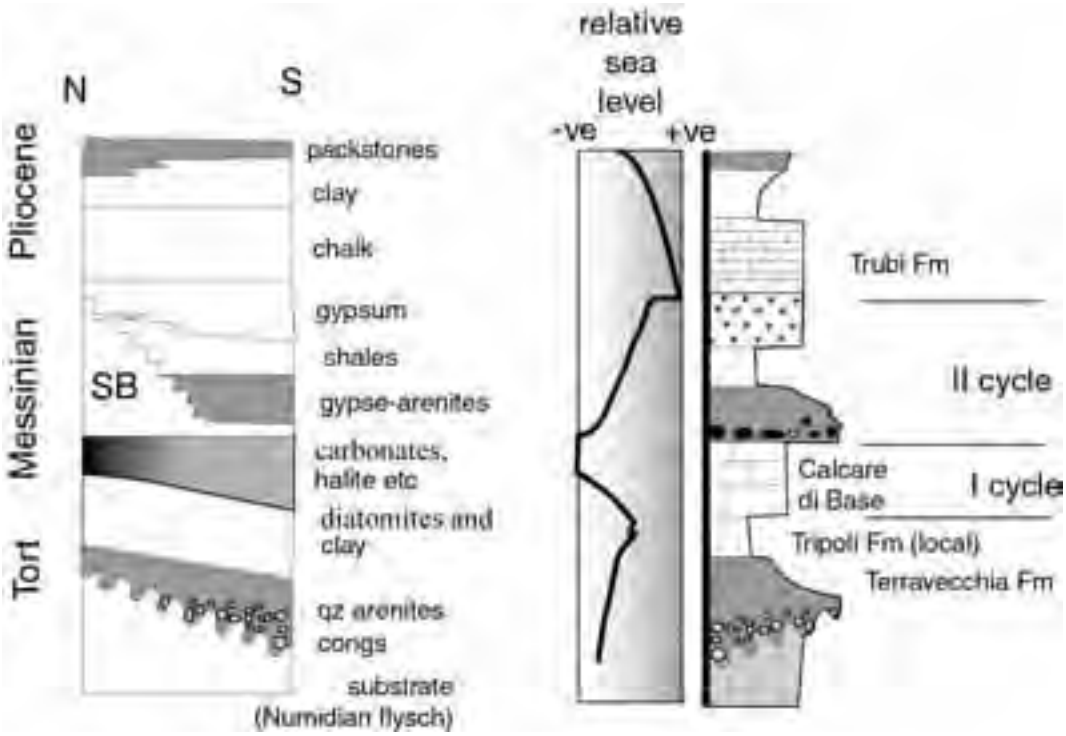

Figure 1.3 - Simplified stratigraphy of Neogene sediments in the Caltanissetta Basin. The left column is a very simplified chronostratigraphy (SB = intra-Messinian sequence boundary) while the right column is an idealized lithostratigraphy - with selected unit names.

to infer a uniformly deep water palaeoenvironment prior to Messinian times. In places the transitional units include diatomitic laminites indicative of increased restriction in marine conditions with transient toxic/anoxic events (the Tripoli Formation). However, in northern Sicily the Terravecchia also includes shallow marine sands (Butler and Grasso, 1993), fluvial conglomerates (Jones and Grasso, 1997) and reef complexes (Grasso and Pedley, 1988).

The distribution of these different palaeo-environments is structurally controlled with thrust-related anticlines forming important barriers to sediment dispersal at this time. Consequently there are many different types of stratigraphic transition upwards into the Messinian evaporites. However, as these evaporites cap all units and overstep onto the pre-Tortonian substrate the whole basin area must have experienced net sea-level rise prior to the dramatic regression in middle Messinian times. This coincides with starvation from clastic sedimentary input. However, the evaporites themselves chart general regression. As the substrate shows differing basin (and presumably palaeo-bathymetric) levels, the onset of evaporite accumulation is expected to have been diachronous, with high-standing areas desiccating sooner than the deeper-water areas (Butler et al., 1995b). This prediction is supported by magnetostratigraphy (Butler et al., 1999).

The basins and thrust-related "highs" set up during Tortonian times continued to influence evaporite accumulation during the Messinian (Butler et al., 1995b). The structural highs are dominated by the Calcare di Base Formation – an autobrecciated carbonate unit that displays bed-by-bed karstification. The basin floors (preserved in the subsurface and known through mining and drilling operations) preserve primary halite and K-salts. There are dramatic lateral thickness changes too that chart the continued deformation of the area. However, the clearest indication of Messinian deformation is shown by the inter-Messinian angular unconformity, charting deformation during Mediterranean-wide

low-stand. The regression as charted by the onset of evaporitic conditions.
The pre-unconformity evaporitic and carbonate units are termed "First Cycle". In the Corvillo Basin the upper Messinian ("Second Cycle") strata are predominantly clastic, reworking earlier deposits including "First Cycle" gypsum and carbonates. Conglomeratic parts of the "Second Cycle" are restricted to inferred incised valleys. These strata pass up into more sheet-like sands that onlap the substrate (chiefly tilted "First Cycle" strata) and in turn show deepening upwards, waning clastic input trends with local lacustrine (Congerie) fauna and primary gypsum deposits.
The Messinian strata were overlain by Trubi Formation chalks of early Pliocene age, charting a return to normal marine conditions across Sicily (and the Mediterranean). These younger rocks are only locally preserved in the Corvillo Basin because deformation continued into Pliocene times. The Calcare di Base is deformed into fold structures clearly visible in the landscape (Keogh and Butler, 1999).

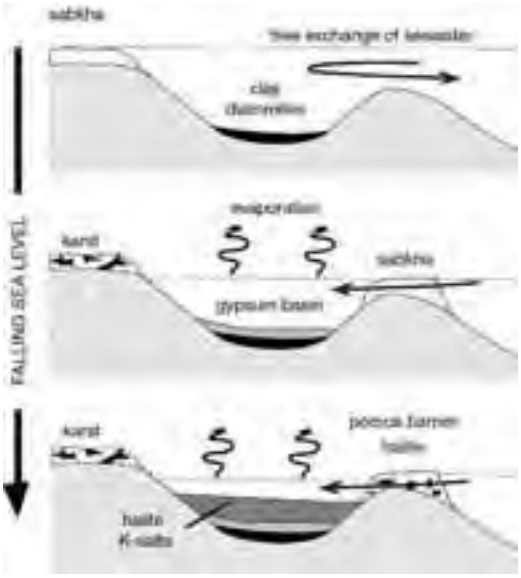

Figure 1.4 - Simplified model for the accumulation of Messinian evaporites and related strata in a thrust-related sub-basin (after Butler et al. 1995b).

Field itinerary

We will depart Catania at 7.30 am and drive west on the motorway, from the foreland area of the Catania basin into the Maghrebian thrust-fold belt. In general most of the structures are buried beneath Neogene syn-tectonic strata. However, the substrate crops out in the craggy massifs of Monte Judica (Day 2), to the south of the motorway. Near the city of Enna (tunnels) we are driving parallel to the structural trend, just ahead of the major Marcasita anticline (Figs.1.1, 1.2). This fold was active through Tortonian to Pliocene times and influenced deposition of sediments of this age. Today we will consider deposition and deformation on the hinterland (northern) side of the Marcasita anticline. The anticline forms the southern edge of the Corvillo Basin. We leave the motorway near Enna and pass through the neighbouring town of Calascibetta. From here the road runs north to our first stop.

Stop 1.1:

Contrada Gaspa

This site displays a section up through Lower Messinian Strata including more than 80m of Tripoli Formation laminites (Grasso et al., 1990; Fig. 1.5A).
This is the greatest development of diatomitic facies in the Caltanissetta Basin. The dominant faunal consituents are planktonic foraminifera, together with diatoms, coccoliths and rare radiolaria, sponge spicules, dinoflagellates and fish remains. Faunal diversity decreases up section (Pedley and Maniscalco, 1999) presumably indicating increased restriction in marine circulation.
The top of the section contains First Cycle evaporites with local halite pseudomorphs and carbonate autobreccia (Calcare di Base Formation). Magnetostratigraphic results indicate onset of evaporite accumulation at end Chron C3Ar (c. 6.5 Ma).

This location is important as it contains the harbingers of the Messinian Salinity Crisis. However, the Gaspa section is a relatively basinal setting, a satellite to the main Corvillo Basin that is the focus of this day's itinerary. The next site lies on a structural high.

Stop 1.2:

Sambuco anticline

A few km NW of Gaspa lies the Sambuco anticline (Figs. 1.1 and 1.2). This structure forms part of an important fold belt that transfers deformation from the Corvillo basin onto the Altesina back-thrust system further east (Fig. 1.6). These folds, including the Sambuco anticline, are readily picked out by the cliff-forming Calcare di Base. At Sambuco this lies on Terravecchia clay without any intervening Tripoli Formation. The core of the fold lies in Numidian

flysch. So the stratigraphy indicates a high-standing position with respect to Gaspa.

The Calcare di Base at Sambuco is of a typical facies flanking the main evaporite basins. It shows bed-by-bed autobrecciation with well-preserved pseudomorphs after halite. The section shows cyclic flooding and emergence, building up only a few metres of section. However, immediately to the north the stratigraphy of Messinian units changes abruptly into the Corvillo Basin. Passing down dip from Sambuco the strata are dominated by halite with K-salts that are strongly deformed. Regretably these rocks are not exposed but we can gain a hint of this lateral variation by skirting the eastern flank of the basin.

Stop 1.3:

Borgo Milletarì - Cacchiamo

The road section from Sambuco crosses the top of the Calcare di Base section which is folded repeatedly around upright structures. These folds represent the western "termination" of the Altesina back-thrust system that increases in importance further east. These structures bring up strata from

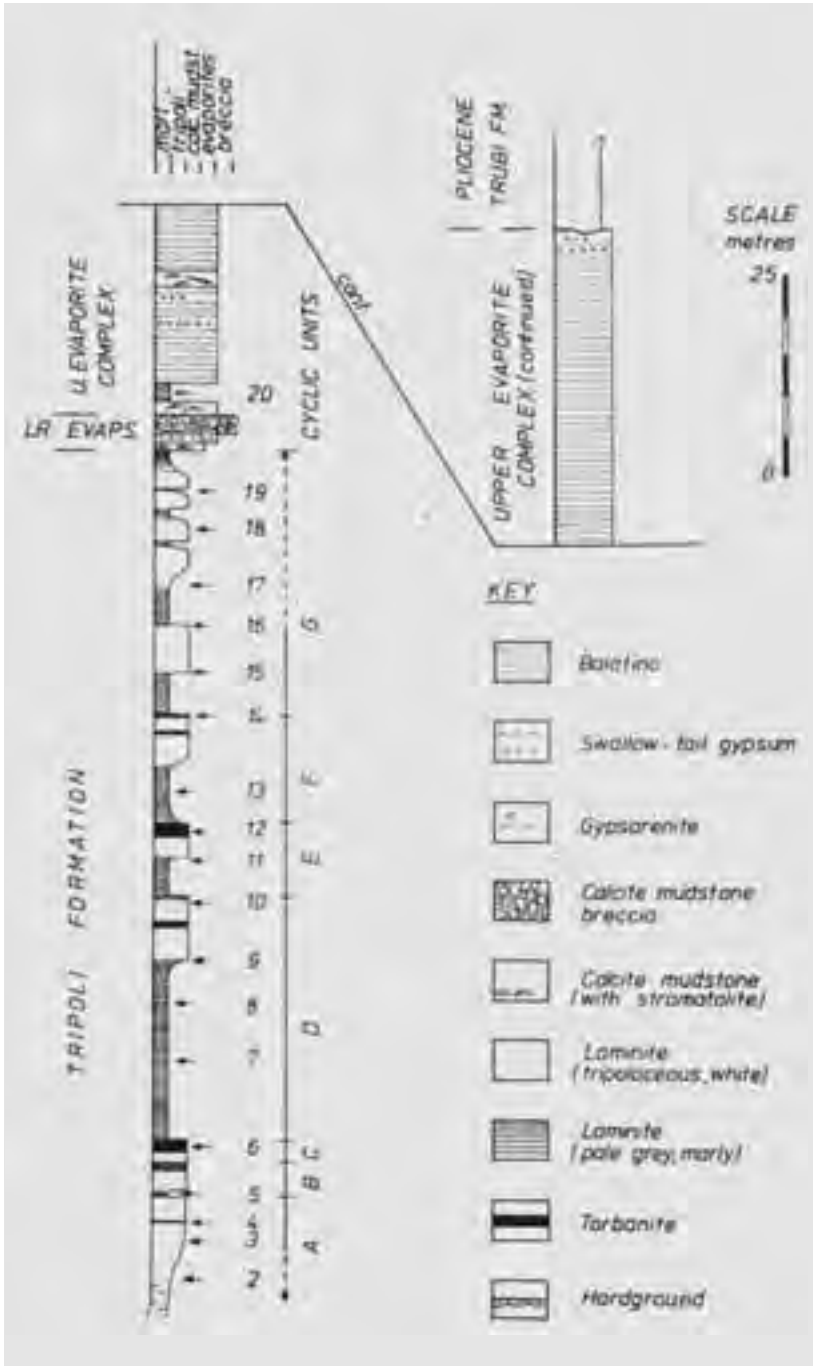

Figure 1.5.A) - Sedimentological log of the Contrada Gaspa road section. Sample points are indicated by numbers and arrows. Cyclic (faunal) subunits of the Tripoli Fm. Are lettered A to G (modified after Grasso et al., 1990).

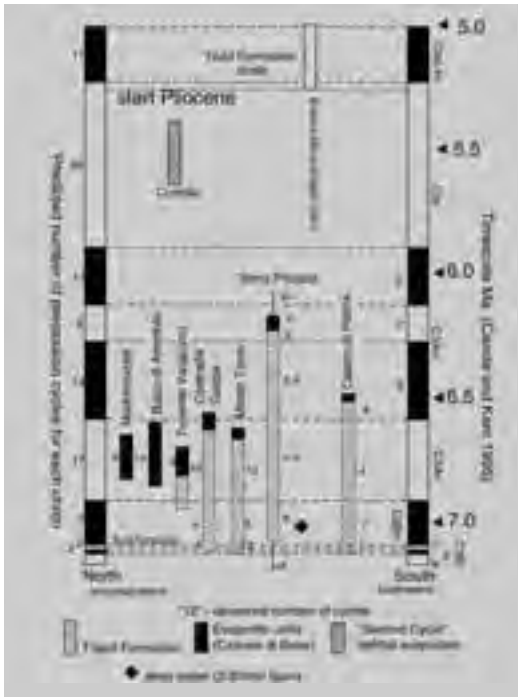

Figure 1.5.B) - Messinian astro-magnetostratigraphy in south-central Sicily (modified after Butler et al., 1999).

eastern flank of the Corvillo Basin. These strata include primary laminated gypsum, seen in the road section 1 km W of Borgo Milletarì village. There are exquisite slump related folds and thrusts in these strata (Fig.1.7).

The key feature here however is the preservation of such features in contrast to the bed-by-bed karstification seen at Sambuco, higher on the southern flank of the basin.
From here we will return to Sambuco and, following the road to Alimena, drop into the core of the Corvillo Basin, passing abandoned mine working that exploited the high order salts. The mine records show more than 300m of stratigraphic thickness of halite and K-salts, with complex deformation including north-vergent folds and shears. At outcrop the geology is represented by clastic Upper Messinian strata (chiefly marls and gypse-arenites) with in general only relatively little deformation. These strata onlap the "First Cycle" Calcare di Base Formation.

Stop 1.4:

Soletta Ridge section (Alimena)

A short walk northwards from the Alimena road gains access to the onlap of Second Cycle gypse-arenites

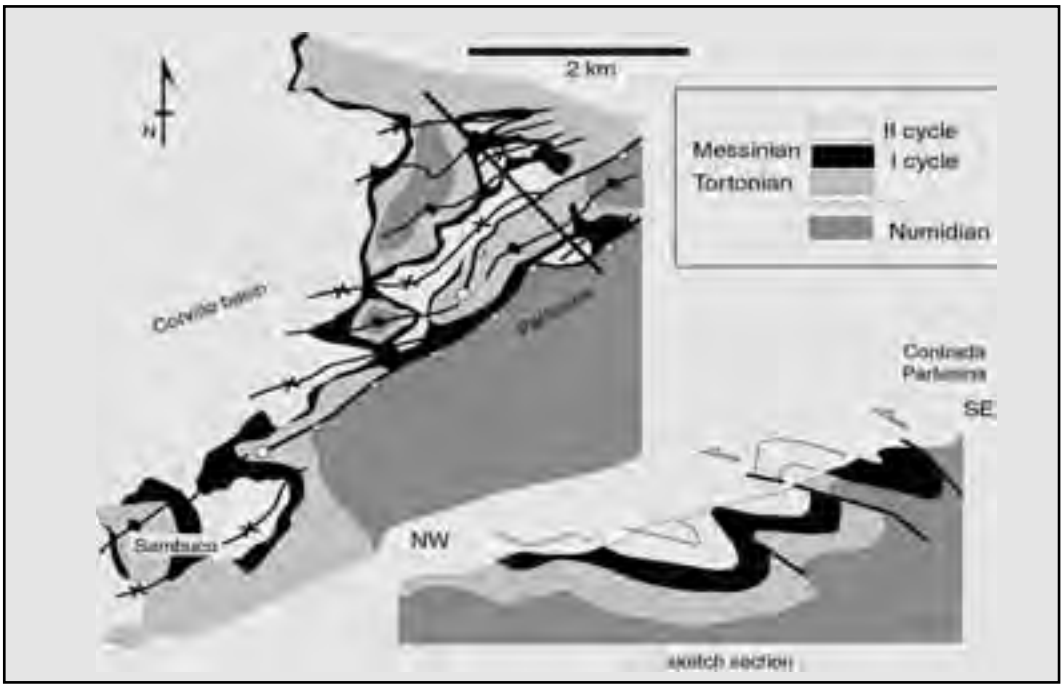

Figure 1.6. - Structural sketch map of the fold belt linking the SE margin of the Corvillo Basin (e.g. Sambuco anticline) with the Altesina back thrust system to the ENE.

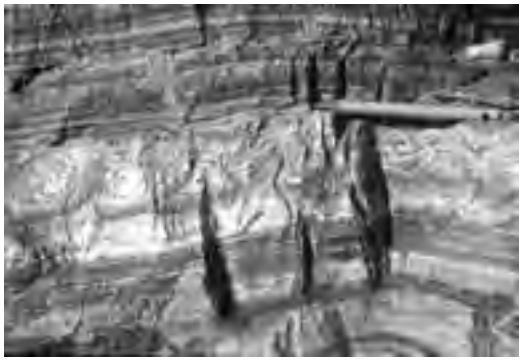

Figure 1.7 - Photograph of micro-slump folds in evaporites at the Borgo Milletarì road section

onto the Calcare di Base. The older rocks are dipping nearly vertically, younging southwards into the Corvillo Basin. In the valley floor these carbonates are incised – a palaeovalley presumed to have contained a major artery of sediment delivery into the Corvillo Basin. The incised valley is filled with conglomerates derived from the mountains to the north. These pass rapidly up into the gently south-dipping gypsarenites (Fig.1.8).

Our plan now is to drive along strike to the west to examine the substrate to the Calcare di Base and another incised valley fill of Late Messinian age. Follow the road to Alimena and continue west to the motorway. Leaving the town of Alimena the road connecting Soletta Ridge to Balza di Rocca Limata runs parallel to the northern edge of the Corvillo basin and flanks the "Calcare di Base" ridge to the main junction with the motorway. To the west of the junction, the road to the village of Resuttano-Balza di Rocca Limata cuts through the pre-Messinian substratum, chiefly made of clays and sands of the Terravecchia Formation. The reef complex at Balza di Rocca Limata lies on such sands and underneath the "Calcare di Base" exposed on the top of Cozzo Terravecchia, where the type-locality of the eponymous formation is located.

Stop 1.5:

Balza di Rocca Limata

These outcrops form a crag-line of reefoidal carbonates within the Terravecchia Formation, (Fig. 1.9) described by Grasso and Pedley (1988). The reef facies here are 45m thick and can be traced for 2 km laterally.

In common with other Late Tortonian – Early Messinian reefs in the Mediterranean, this one is of very low coral diversity. The chief constructional organism is *Tarbellastrea* with local *Porites*. At these outcrops the reef fauna are broadly in situ but pass laterally into breccias (Fig. 1.10A). This is typical of the reef complexes within the Caltanissetta Basin – which are generally just local complexes. This example in common with the others, is anchored on Terravecchia sands and are found exclusively on structural highs.

The Balza di Rocca Limata reef is overlain by clay which passes up in turn into the Calcare di Base, cropping out in the crag lie to the south (Cozzo Terravecchia, 961m above sea level, Fig.1.10B).

This line of carbonate maps eastwards, crossing the Salso valley (with the motorway) and continuing to Alimena and the Soletta ridge. We are therefore on the western continuation of the northern flank of the Corvillo Basin.

Stop 1.6:

Monte Cuticchi

These spectacular outcrops lie within an incised valley fill cutting into the Calcare di Base (Fig. 1.11). The fill is part of the second Cycle Messinian and contains blocks (up to 1m across) of the Calcare di Base. Other clasts include older substrate including Numidian flysch and Mesozoic carbonates. These outcrops are presumed to be the temporal equivalents of the conglomerates at stop 1.4 and they have a similar Late Messinian palaeovalley setting.

From the outcrops a road leads southwards through countryside dominated by the cliff-forming Calcare di Base. We are along strike of the Corvillo Basin here yet the Messinian rocks are only of the marginal facies. This indicates that the Corvillo Basin was doubly-plunging, a presumed requirement for the accumulation of high-order evaporite minerals. The Calcare di Base itself is folded into dramatic structures-chiefly of Pliocene age. These are also seen in the Salso valley from where we rejoin the motorway at the Cinque Archi junction. In detail, the road connecting Monte Cuticchi to Ponte Cinque Archi crosses a large Messinian basin with folded "Calcare di Base". This is overlain by second cycle clastic and evaporitic deposits (Lago Mare gypsum). The road to the motorway passes through S. Caterina Villarmosa village, which is located on the core of a spectacular anticline, and reach the motorway on the southern edge of the Corvillo Basin where is visible

another spectacular fold (Mucciarello anticline, Fig. 1.12).

Just south of the junction we cross the southern flank of the Marcasita anticline (southern barrier to the Corvillo Basin, although it is difficult to pick out in these clay-dominant units). The south-dipping sands visible in the cliff sections either side of the motorway are part of an Upper Tortonian-Lower Messinian sandy deltaic complex. This is the southern limit of shallow-water/subaerial deposition recorded in pre-evaporitic strata. Regretably it is difficult to access these outcrops. The motorway heads east, along the front of the Marcasita anticline. The sands pinch out into Terravecchia clays, indicating that the deltaic complex was only a local feature. Much of the outboard flank of the Marcasita anticline remain sediment starved. We continue to Enna for dinner and overnight stop.

DAY 2

Late Quaternary endorheic basins recording climate changes during Holocene and pre-Holocene times.

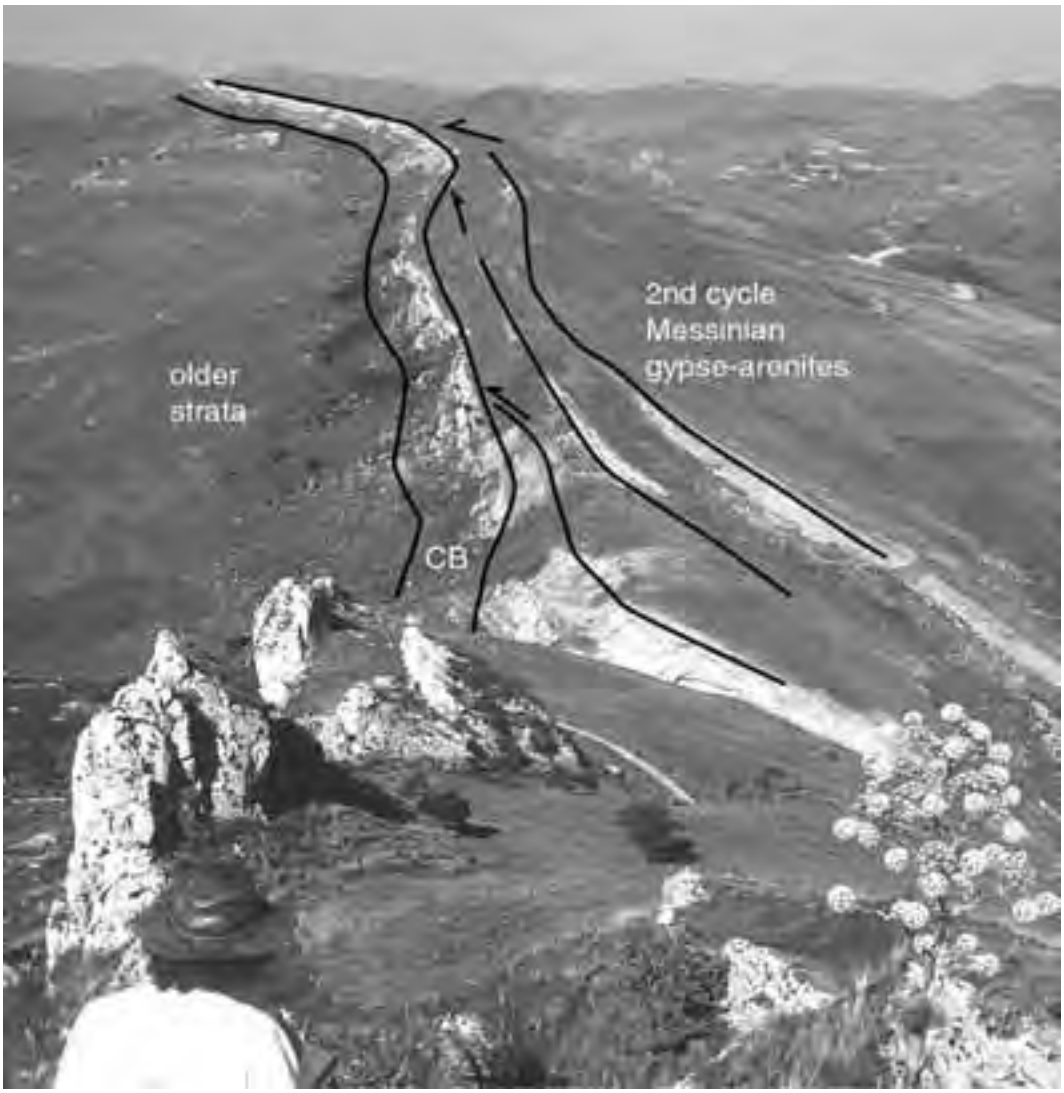

Figure 1.8 - The intra-Messinian unconformity at Soletta, looking east, on the northern margin of the Corvillo Basin.

Results and work in progress

M. Grasso[1], C. Bruchman[2], R. Maniscalco[1], L. Sadori[3], G. Zanchetta[4]

[1] Dipartimento di Scienze Geologiche, University of Catania, Corso Italia 55 – 95129 Catania, Italy

[2] GeoForschungsZentrum Potsdam, Telegrafenberg C322 – D-14473, Potsdam, Germany.

[3] Dipartimento di Biologia Vegetale, Università "La Sapienza", P.le A. Moro,5 - 00185 Roma - Italy

[4] Dipartimento di Scienze della Terra, University of Pisa, Via S. Maria 53-56126, Pisa, Italy

Figure 1.9 - Field photograph of reefoidal carbonates at Balza di Rocca Limata.

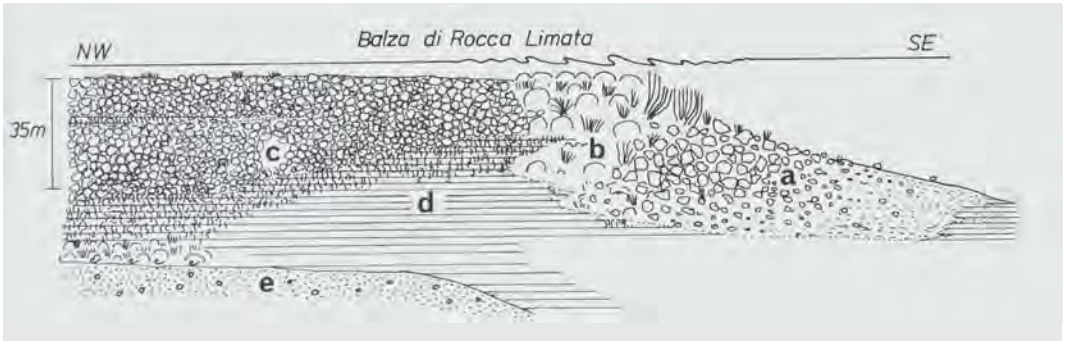

Figure 1.10 - A: a=Sketch illustrating lateral facies variation in the Balza di Rocca Limata reef: a = fore-reef talus fining off basinwards; b= reef core dominated by Tarbellastrea and short cylindrical Porites colonies; organ-pipe Porites growth form and long rods of Tarbellastrea occupying the outer margin; c= back-reef with coarse breccia; d= clay-rich base of reef complex containing vermiform coral growth forms; e= channel base deposits of siliciclastic sands and gravels. (modified after Grasso and Pedley, 1988).

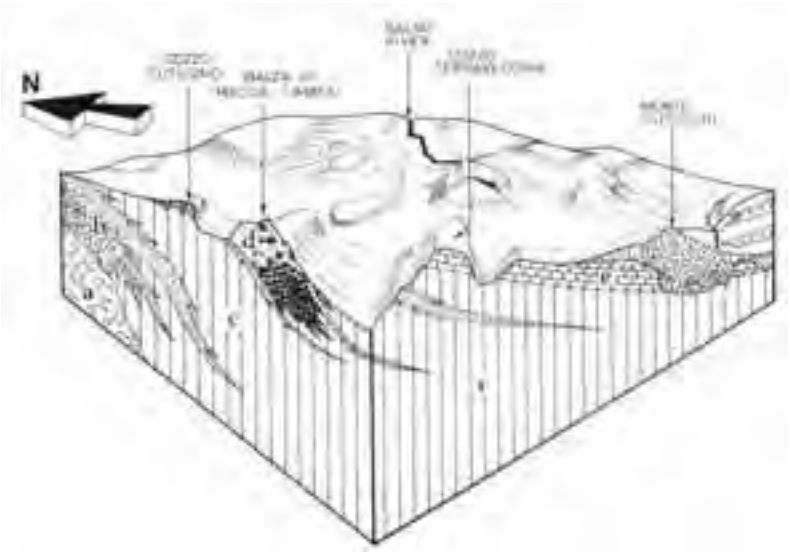

Figure 1.10 B - Relations between the Balza di Rocca Limata reef (late Tortonian), lower Messinian and unconformable upper Messinian successions. a= tectonized substratum. b= siliciclastic sands and conglomerates, and c= Terravecchia Formation clays. d= Balza di Rocca Limata reef complex with basinward dip. e= Calcare di Base (Early Messinian). f=Upper Evaporite Complex (Late Messinian) over a cobble-filled irregular erosion surface (modified after Grasso and Pedley, 1988).

Figure 1.11 - Incised valley fill made of second cycle evaporites into the Calcare di Base at Monte Cuticchi.

Figure 1.12 - Folded Messinian strata within the Corvillo Basin at the Cinque Archi motorway junction, looking east.

Stop 2.0:

Pergusa Lake

The Pergusa Lake is well known in the literature: it was described by Ovid in his "Methamorphoses" (I century AD) and by Claudian in "De raptu Proserpinae" (IV century AD).

John Milton also described the landscape and the myth of the Rape of Proserpine with the following lines:

The birds their choir apply; airs, vernal airs,
Breathing the smell of field and grove, attune
The trembling leaves, while universal Pan
Knit with the Graces and the Hours in dance
Led on th'eternal Spring. Not their fair field
Of Enna, where Proserpina gath'ring flow'rs,
Herself a fairer flow'r, by gloomy Dis
Was gather'd, which cost Ceres all that pain
To seek her through the world; nor thet sweet grove
Of Daphne by Orontes, and th'inspir'd
Castalian spring, might with this paradise
Of Eden strive;…

The Pergusa Lake is located about 5 Km SSE of the town of Enna and occupies a sub-elliptical endorheic basin with an area of 7.22 Km^2. The lake surface is less than 1.4 km^2. The lacustrine sediments have been object of international interest for the central position occupied by the lake in the Mediterranean basin; the Pergusa Lake is the only endorheic lake of Sicily and the only lake of all the Mediterranean islands recording the climate changes occurred throughout the whole Holocene. Sadori (2001) and Sadori and Narcisi (2001) published the results of pollen and tephra analyses carried out on the top 4.60 m of the lacustrine sediments. On the basis of pollen analyses, microscopic characterization of selected samples, AMS radiocarbon dates on macrofossils or bulk sediment, and one tephra layer, they were able to chart the climatic events of the last 11000 uncal. yrs BP. Moist conditions characterized the area since 10700 yrs BP. The onset of the wettest conditions of the Postglacial occurred at about 9000 yrs BP and lasted until 7200 yrs BP. From 7200 yrs onward, aridity started to increase up to reach very arid conditions at about 3000 yrs BP. As the climate had already induced change in the vegetation, the well known human occupancy during the last three millennia did not produce strong effects on the environment. Human impact on vegetation can be surely detected only from about 2800 yrs BP, even if earlier land use cannot be excluded.

New drilling operations were sponsored on August

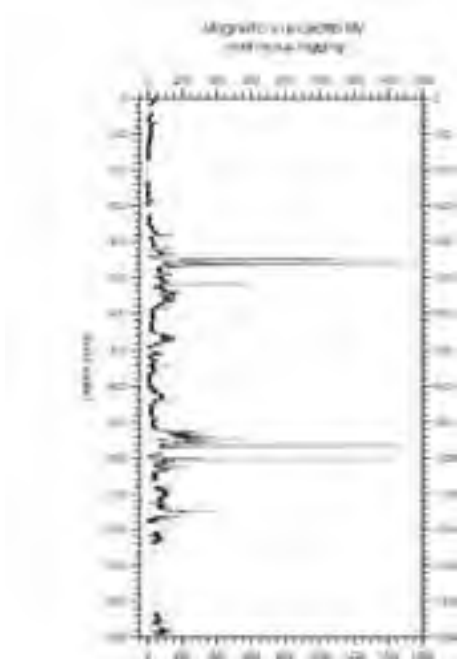

Figure 2.0 - Magnetic susceptibility measured in the topmost 15 m of the core.

2001 by Provincia Regionale di Enna. Coring intercepted a succession of 40 m consisting of lacustrine sediments down to 9 m., and upper Pliocene (MPL6 of Cita, 1975) silty clays from 9 m downhole. A multidisciplinary approach has been applied for the study.

Work by Grasso et al. (2002) is based on radiometric, micropaleontological and pollen analyses on the 40 m of cored succession, with the principal aim of dating the onset of the lake, reconstructing the palaeoenvironment and charting all the climatic events recorded by its sediments. In order to reveal information about changing concentrations of ferrimagnetic particles in the sediment, magnetic susceptibility was measured in the uppermost 15 m (Fig. 2.0).

Higher susceptibility values indicate tephra layers and/or increased erosion in the catchment area due to higher accumulation of magnetic material.

Diatoms were studied so far in the uppermost 80 cm (short core PER 1-1, cored in 1998) using standard methods. The concentration of diatom valves was relatively low and their preservation generally worse. Only littoral diatom species with strongly silicified valves (e.g. *Cocconeis* spp.) were found. As almost all valves were broken and species with finer structures probably dissolved, a detailed diatom analysis is not possible. However, this results suggests a shallow lacustrine environment with drying-out phases and chemical and physical effects of increasing salinity, causing breakage and dissolution of diatom valves.

The lake is mainly fed by local rainfall and ground waters with the isotopic composition of the water body dominated by progressive evaporation. In the years 1988-89 Battaglia et al., (1991) measured a $\delta^{18}O_{SMOW}$ of lake water ranging from +7 to +1 ‰, which is strongly ^{18}O-enriched in respect to isotopic composition of local meteoric precipitation that can be estimated ca -7÷-7.5‰ (Longinelli and Selmo, 2003).

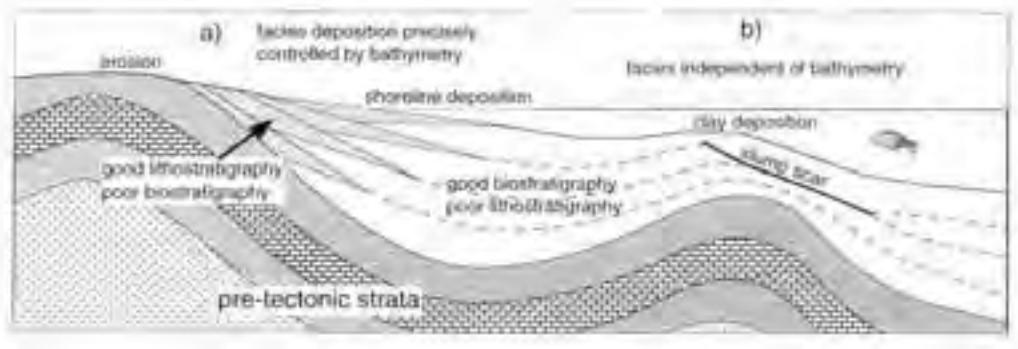

Figure 2.1 - Generalized stratigraphic architecture produced by deposition of syntectonic strata above growing folds. (a) Emergent anticline with shoreline deposition showing generation of well-defined (observable) lithostratigraphic boundaries. (b) Submerged anticline with basinal clay deposition showing preservation of (datable) biostratigraphic boundaries (after Lickorish and Butler, 1996).

Volume n° 2 - from B16 to B33

Figure 2.2 - Detail of the internal geometry of stratal surfaces within the packstone parasequences at Ponte Capodarso. The units are dipping south.

Preliminary isotopic investigation has been performed by Zanchetta G., Borghini A., Bonadonna F.P. (University of Pisa) and A.E. Fallick (SUERC, Glasgow, Scotland) on the first 4 m (preliminary analyses were performed at ca 20 cm intervals) of a 15 m depth core. The first 4 m are mainly made up by marls (mean carbonate content 35%) with the exception of a short interval at ca 3 m where organic fraction dominates and carbonate content decreases to 0%.

The mean $\delta^{18}O_{PDB}$ of bulk carbonate 0.08±0.81‰ suggests that the isotopic composition of lake water was dominated by evaporative processes. Indeed, the $\delta^{18}O_{SMOW}$ of local rainfall suggests that a theoretical carbonate precipitate in equilibrium with lake water should have lower $\delta^{18}O_{PDB}$. However, the role of evaporation changes along the core profile. The upper 1.5 m shows the highest $\delta^{18}O$ values (mean 0.7 ±0.5‰), while from ca 2 to 4 m the $\delta^{18}O_{PDB}$ values are lower (-0.6±0.5‰). The upper part of the isotope profile is in reasonable agreement with carbonate precipitate, with lake water similar to the present time conditions, whereas the lower part is suggestive of $\delta^{18}O$ values of lake water slightly enriched in ^{16}O. This fact may suggest that the effects of evaporation are higher in the topmost part of the core record and lower in the bottom part due to increasing humidity and rainfall. These data are roughly in agreement with pollen data obtained in a nearby core (Sadori and Narcisi, 2001), where wetter conditions seem to dominate in the lower part of the core (up to ca 3 m, estimated age 7200 yr BP) and an aridification trend is recorded in the upper part of the core.

Tectonic controls on parasequence stacking patterns

Butler, R.W.H.[1], Grasso, M.[2], Maniscalco, R.[2]
[1]Department of Earth Sciences, University of Leeds, Leeds LS2 9JT, UK
[2]Dipartimento di Scienze Geologiche, University of Catania, Corso Italia, 55 – 95129 Catania, Italy

Much of the rest of the day is devoted to examining Pliocene strata and the tectonic controls on their depositional architectures. These successions form a generally regressive package that shows ubiquitous large-scale shallowing upwards trends (summarised on Fig. 1.3). The successions are capped by dramatic cliff-forming shelly limestones. These packstone units form the focus of the day. They were deposited at shore faces and therefore track the migration of coastlines through Pliocene times on Sicily. Biostratigraphy in the immediately underlying muds can be used to date coastal migration (Fig. 2.1).

This shows a systematic regression as Sicily has risen, presumably in response to tectonic unloading along the north coast (Tyrrhenian rifting) . However, the long-wavelength, forced regression was modulated by eustatic sealevel fluctuations and by local

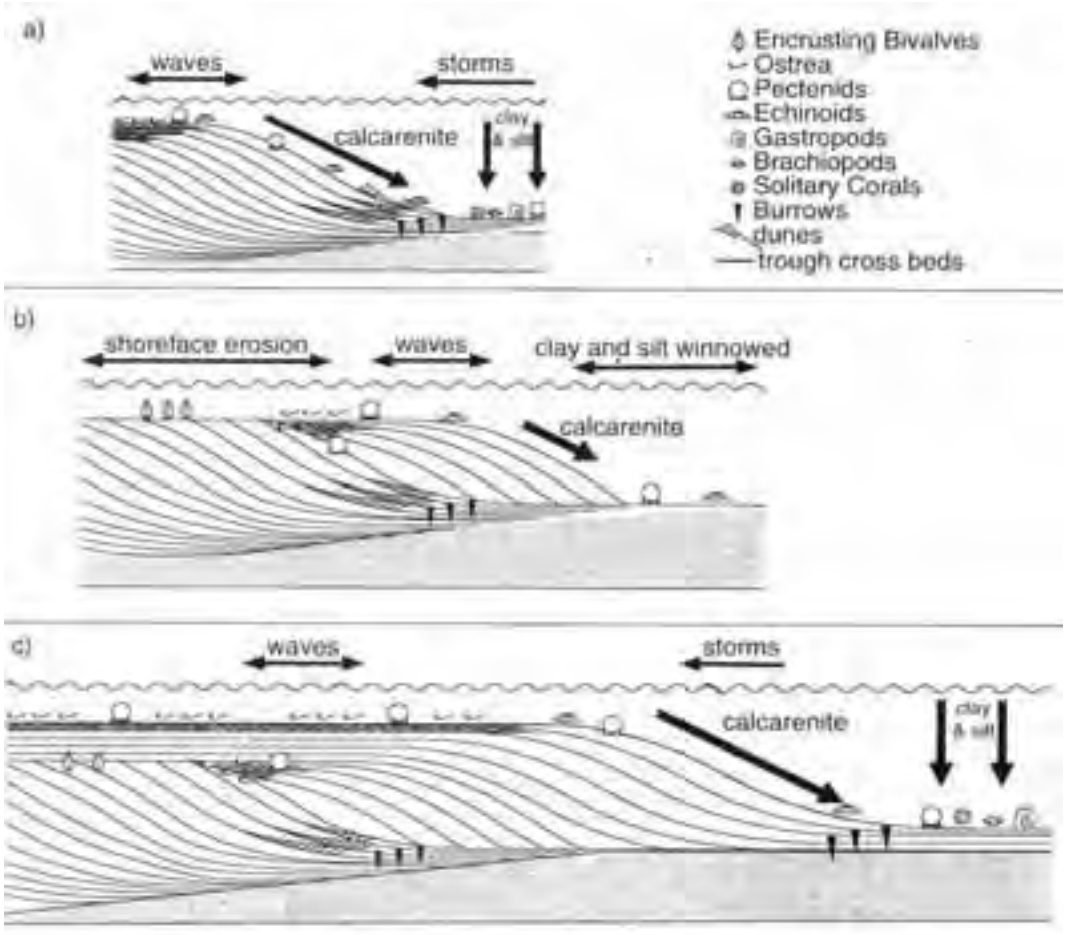

Figure 2.3 - (a) Schematic diagram of normal sedimentary conditions across clinoform. (b) Generation of downlapping package basinward and erosional surface shoreward due to a minor base-level fall. (c) Subsequent onlap after restoration of base-level truncating internal bounding surface (after Lickorish and Butler, 1996).

structural activity. These form the main themes of the morning. Our aim is to examine Pliocene growth strata deposited and deformed on the southern flank of the Marcasita anticline. The strata are important for providing high resolution control on the rates of tilting during folding (Butler and Lickorish, 1997). The structure itself was active through much of the late Miocene into late Pliocene times.

Stop 2.1:

Ponte Capodarso

This site provides an intimate introduction to the Pliocene parasequences (Fig. 2.2).

Each consists of a shallowing-upward package capped by a marine flooding surface. The most dramatic parts of the section are the calc-arenites, units of packstones with dramatic southward-dipping, prograded clinoforms. The evolution of these parasequences is shown in Figure 2.3.

The individual packstone units are mappable for >6km along strike but are <1km in extent down dip. This ribbon shape, together with their internal architecture, fauna and ichnofacies indicate shore-face deposition (Lickorish and Butler, 1996) with the top surfaces being palaeo-abrasion ramps. As these should have syn-depositional slopes of <1º, the whole section has been subsequently tilted.

Volume n° 2 - from B16 to B33

Figure 2.4 - The Monte Capodarso section, looking east.

Stop 2.2:

Necropoli dei Saraceni

The Saracens graveyard on the hillside (c. 700m above sea level) to the west of Capodarso provides a superb vantage point for the Marcasita anticline and, particularly for the stratal relationships on its southern flank. The geometry of the parasequences seen in detail at Ponte Capodarso is well exposed (Fig. 2.4).

Six distinct units can be seen, off-lapping towards the south. There is a gentle decrease in dip (5º) up section. These relationships indicate syn-depositional tilting (Fig. 2.5), forcing local regressive cycles, presumably superimposed upon eustatic sealevel variations.

Biostratigraphy (reviewed by Lickorish and Butler, 1996) and magnetostratigraphy (Butler and Lickorish, 1997) indicate deposition through the Réunion subchron (2.15 Ma) with each parasequence representing one precession cycle (Fig. 2.6). From these, tilt rates of 1º/27.6ka can be estimated.

The central assumption is that the primary depositional cyclicity reflects ordered eustatic sea level variations. The question then is what order of sealevel variation is being recorded. The biostratigraphy linked with magnetostratigraphy strongly suggest that the cyclicity relates to precession time-scales. From the view point we can return to Ponte Capodarso, drive north to the motorway and back over to Enna. Our next target is the Pliocene basin at Leonforte-Centuripe. This depocentre, described by Di Grande et al. (1976) and Butler et al. (1995a) lies in a synformal setting between the Altesina backthrust ridge in the

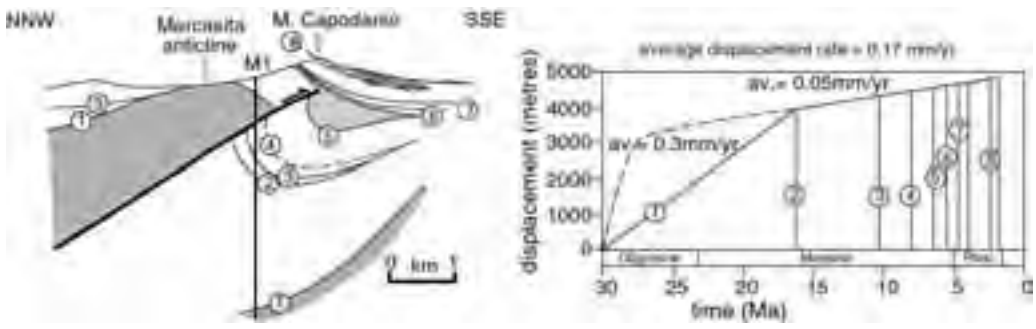

Figure 2.5 - Simplified cross-section through the Marcasita anticline, based on outcrop and well data, used to establish rates of thrusting at this site. The First Cycle Messinian basin (exploited by the Pasquasia mine) and the Pliocene packstones are shaded. The graph shows the incremental evolution of thrusting rates for the structure. Modified after Butler and Lickorish (1997).

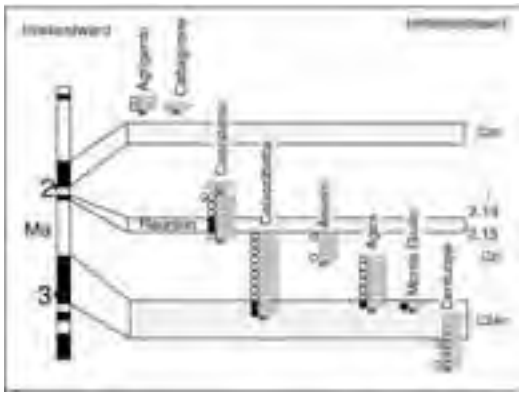

Figure 2.6 - Calibration of Pliocene shallow-water sequences through the Centuripe and Capodarso areas and out to the south coast. The model is based on magnetostratigraphy (linked to published biostratigraphy) with the assumption that each parasequence represents a precession cycle. The general forelandward regression is modulated by local structural growth and eustatic sea-level fluctuations (unpublished data, correlations by W.H.Lickorish).

north and the Monte Judica thrust stack in the south. Much of the basin is filled with Pliocene clays, including olistostromal units shed from the flanks of the structure. The fill is capped by the packstone units that correlate in lithotype with Capodarso. However, they are distinctly older (Fig. 2.6).

We leave the motorway and drive into the Leonforte-Centuripe basin at its southern margin. Here the flank is defined by a prominent crag line of Calcare di Base with a recessive cover of Trubi (lowermost Pliocene). We will stop about 1 km short of the hill town of Agira. The town lies on the NE margin of the basin.

Stop 2.3:

Agira viewpoint

Agira is a hill town built on Pliocene packstones (Fig. 2.7). These units are broadly aggradation, in contrast to the offlapping stacking pattern at Capodarso. However, the units diverge to the SW with increasing structural dips down-section indicating syndepositional tilting. As at Capodarso, the top surfaces of each packstone unit is inferred to represent a palaeo-horizon. Note that the packstones dip less that the underlying Messinian strata (Fig. 2.7). From Agira we return to the motorway (possible brief roadside stop to examine olistostromal clay breccias) en route. We follow the motorway east to Catenanuova and head north into the eastern end of the Leonforte-Centuripe Basin (Fig. 2.8).

Stop 2.4:

Centuripe area

In the hairpins up to Centuripe we can stop to view the southern pinch-out of Pliocene strata onto the Messinian. There is a distinct decrease in structural dip up section, indicating syn-depositional tectonics. The capping Pliocene strata including detrital input, one of the few such sites in the Caltanissetta Basin at this time. This location also gives views south to the Monte Judica thrust stack.

From Centuripe we return to the motorway and cross south to Monte Scalpello.

Stop 2.5:

Monte Scalpello

While the Caltanissetta Basin preserves syntectonic strata very well, the compensating disadvantage is that the structural investigations rely heavily on subsurface data. However, the plunge culmination in thrust structures at Monte Judica gives an insight on structural styles at depth. Here the substrate of Mesozoic units are brought up in a series foreland-

Figure 2.7 - Looking west onto the stacked and differentially tilted packstone parasequences at Agira.

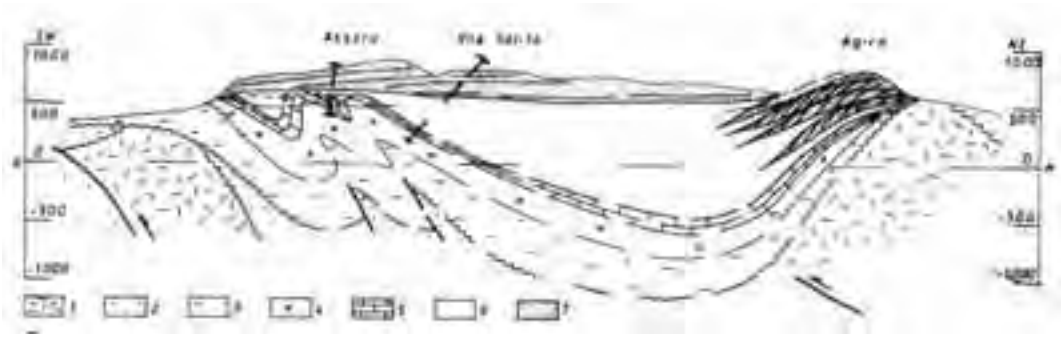

Figure 2.8 - Cross section through the Agira transect of the Leonforte-Centuripe Basin (Butler et al. 1995a). Key: 1 – Eocene and older substrate; 2 – Oligo-Miocene foredeep sediments (Numidian flysch); 3 – Tortonian – Lower Messinian; 4 - Messinian evaporites etc.; 5 – Trubi Formation; 6 – Pliocene clays and deep-water sands; 7 – packstones.

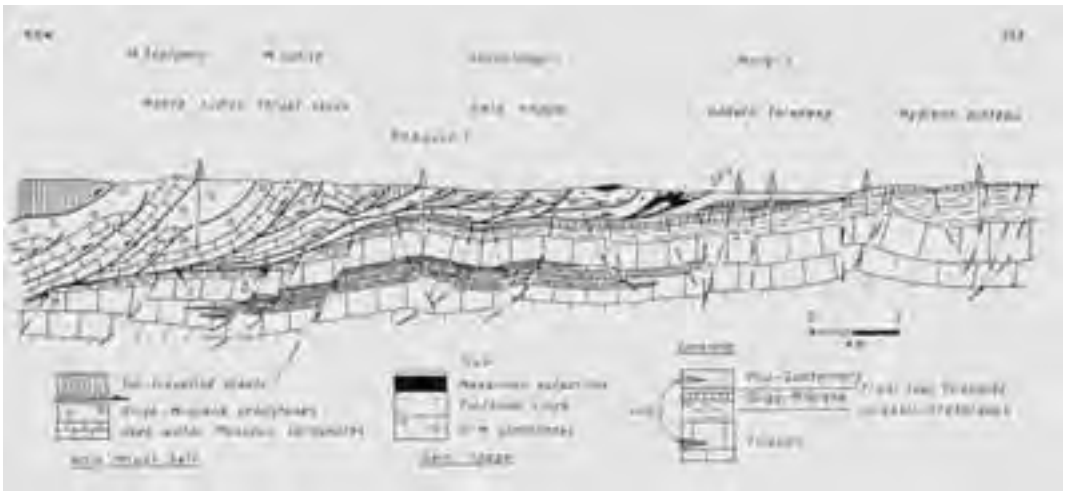

Fig. 2.9 - Simplified cross-section through the frontal thrust structures in eastern Sicily, showing the relationship between the Monte Judica Thrust stack, the Gela Nappe and foreland (after Butler et al., 1992).

vergent imbricate thrusts (Fig. 2.9).

Monte Scalpello is the most hinterlandward of the thrust slices. It also provides panoramic views across eastern Sicily, useful for linking the thrust top basins with the Hyblean foreland. Recent paleomagnetic work by Speranza et al. (2003) show that in M. Scalpello area, 100° and 30° rotation characterize the Eocene-Oligocene and the upper Tortonian sediments respectively, suggesting a 70° rotation occurring between Oligocene and late Tortonian time. When these structures are back rotated by 100°, according to paleomagnetism, they fall within the palaeo-Ionian corridor. Therefore, Speranza et al. (2003) suggest that the whole succession exposed in Monte Scalpello area was deposited over a stretching continental crust during the initial rifting episodes of the Ionian Sea.

THE NEOGENE VOLCANISM OF THE NORTHERN MONTI IBLEI IN SOUTH-EASTERN SICILY

Schmincke H.U.*, Grasso M.**, Sturiale G.**, Suiting I.*

* Geomar Forschungszentrum, Wischhofstrasse 1, D-24148 Kiel, Germany

** Dipartimento di Scienze Geologiche, Corso Italia 55, 95129 Catania, Italy

Regional structural setting of the Iblean Plateau

The Iblean territory comprises the provinces of Siracusa, Ragusa and the southern hinterland of the province of Catania. It is bound by the Channel of Sicily to the south and the Ionian Sea from the Gulf

of Catania to Capo Passero to the east. Its boundaries are the provinces of Caltanisetta and Catania to the northwest. The Iblean (or Hyblean) Mountains (or plateau, or foreland) form a peneplain, just 30 km south of Mt. Etna from which they are separated by the Piana di Catania. The highest point at Monte Lauro near Buccheri has an elevation of 986 m a.s.l.. Characteristic steep valleys form small canyons and gorges. The volcanic-dominated part of the Iblean Mountains covers an area of 350 km^2 in the NE part of the plateau.

The Iblean Plateau occupies the southeast corner of Sicily, south of Mount Etna, and presumably represent the northern edge of the African Plate whose collision with the Calabrian Arc (southern Tyrrhenian Sea) resulted in the Maghrebian thrust belt (Butler at al., 1992). Due to segmentation of the convergence belt along the collision front (Ben-Avraham and Grasso 1990) and the development of a broad rift zone in the Sicily Straits, the collisional processes are complicated. The Iblean Plateau forms a tectonically stable block at the northern edge of the African Plate, not affected by folding or underthrusting below the Eurasian Plate. The African-European plate boundary crosses the Sicilian foreland north of Mount Etna (Barberi et al.,1974). To the east, the Malta Escarpment forms a steep submarine slope that descends into the Ionian Sea down to more than 3000 m (Grasso, 1993). It separates continental crust of the Strait of Siciliy and of the Iblean-Malta Plateau from oceanic crust of the northern Ionian Sea (Grasso and Reuther, 1988). To the north, the Iblean Plateau is bordered by the Piana di Catania halfgraben (Ogniben, 1969). In the southwest the carbonate platform slopes below sea-level to form the Sicily Strait with the central Pantelleria Rift. Representing the emerged northern part of a larger structural unit, the so called Iblean-Malta Platform (Grasso and Reuther, 1988), the Triassic to Miocene carbonate sequences of the Iblean Mountains are characterized by subtropical sedimentation patterns of the northern African shelf in the Tethyan realm. They are intercalated with dominantly submarine hydro- and volcaniclastic units and minor lava flows. Correlation of subsurface data suggests northward migration of eruptive activity that merges with most ancient volcanic episodes at Mount Etna (Longaretti et al., 1991). The geodynamic significance of the Iblean volcanism is not well understood but is basically of intraplate character. The extension-related intraplate magmatism may be described as of a "low-volcanicity-rift" (Schmincke et al., 1997), compositions ranging widely from tholeiitic to extremely alkalic but with a clear separation in time. Large central volcanoes are lacking in the Iblean Mountains, while fissure activity dominated. During the Upper Miocene, a series of diatreme pipes was emplaced in the eastern part of the Iblean Plateau, restricted in time and space.

The Iblean volcanism can be basically divided into three main phases:

1) Middle Triassic to Jurassic volcanic activity is inferred from borehole data around Ragusa.

2) The Cretaceous volcanism is the oldest documented by outcrops.

3) Upper Miocene to Pleistocene volcanic rocks, representing the most widespread episodes of the Iblean volcanism, have been subdivided into several lithostratigraphic units by Schmincke et al., (1997)

Paleogeography of the Iblean Platform during the Neogene

The Miocene carbonates and coral reefs of the Iblean-Malta Platform reflect the transition between open-oceanic conditions and landlocked semi-arid and marginally subtropical environments during the *"Messinian salinity crisis"* (Esteban, 1979, 1996, Hsü et al., 1973). The rising Apenninian-Maghrebian fold belts became increasingly involved in controlling palaeogeography. An overview about the regional palaeogeographic setting of the Iblean- Malta Platform through Neogene times is provided by Pedley (1983). The Iblean- Malta Rise probably existed as a shallow platform throughout the Neogene. To the west, the platform descended gradually into the Central Sicilian Basin, an area of evaporite precipitation during the Messinian. The deep fault boundary to the Ionian abyssal plain was already developing during the late Cretaceus with renewed activities during Tortonian-Messinian interval. The northern coastline of the basin was outlined by mountain ranges that extended continously through northern Sicily and much of the Italian peninsula. As the two areas of patch reef development in Sicily and the Maltese Islands show unusual broad zones and no direct association with terrestrial hinterland, they are interpreted as lying on a threshold between the Central Sicilian Basin and the newly forming Ionian Abyssal Plain of the eastern Mediterranean. A Neogene extension to this threshold, now destroyed due to later block faulting, directly linked the Malta- Sicily area with North Africa. A net eastward sea water flow over the threshold with a considerable volume of water exchange is strongly implied by Pedley (1979, 1981)

and Grasso et al. (1982). Steady replenishment from the Atlantic Ocean with sufficient nutrient supply could permit the growth of a wider patch reef belt than reported from fringe reef locations. The broad platform shelf area was dominated by low diversity coral thickets and small patch reefs. A dominantly miliolid microfauna represents a partly reef-encircled inner shelf environment of less than 40 m water depth. Water depths of only a few meters with a slightly raised salinity are suggested by the widespread occurrence of the foraminifera *Borelis melo melo* in the Carlentini Formation (Grasso et al., 1982). Correlating the Iblean Plateau with the Maltese Islands, Pedley (1983) defines four levels of subaerial features in the Miocene stratigraphy, which seem to prove local emergence by sea level fall produced by oscillations associated with the commencement of the *"Messinian Salinity Crisis"*. Miocene volcanism was locally emergent in a shallow water environment.

Volcanic evolution

The Late Miocene to Pleistocene geological evolution of the northwestern Iblean Mountains between the towns of Militello and Palagonia is marked by a complex interplay of subaerial and submarine volcanism, subsidence and uplift, eustatic sea level changes and shallow water carbonate and clay sedimentation. Volcanic activity occurred in temporally distinct phases, differing drastically in volume, chemical composition, eruptive and depositional sites and eruptive mechanisms. Volcanism is basically of intraplate character and occurred in at least 4 major phases differing in magma composition, eruptive and depositional sites and eruptive and depositional mechanisms (Schmincke et al., 1997).

Phase I: Tortonian-Messinian subaerial to submarine chiefly nephelinitic lavas and volcaniclastics including the volcanics of the Carlentini Formation to the east. The diatremes in the eastern part of the Iblean Plateau around Sortino were emplaced during this time.

Phase II: Basanitic late Lower Pliocene submarine (approximate water depth of emplacement 100 - 300 m) Poggio Pizzuto and Poggio Inzerillo Formation lavas, followed an apparent period of volcanic quiescence of ca. 1-2 million years.

Phase III: Dominantly subaerial widespread tholeiitic lavas (Militello Formation) began to erupt after a relatively brief period of repose, possibly beginning with a shallow submarine stage. Later lava flows entered the sea, forming lava deltas characterized by foreset-bedded pillow and pillow fragment breccias with intercalated collapse breccias. These flows had advanced from emerged eruptive centers in the south-southeast subaerially and over some areas in shallow water. The flows entered deeper water along a coastline southeast of Militello. Lava deltas migrated southwestward on top of earlier pillow breccia debris flow deposits intertongued with soft Trubi marls and chalks. Lava delta formation characterized by foreset bedded pillow and pillow fragment breccias was repeatedly interrupted by partial collapse or local subsidence of isolated blocks (up to >1 km^2), resulting in the deposition of submarine pillow breccias on top of submerged subaerial lavas. Hyaloclastites formed by brittle fracturing during lava delta-forming processes and debris flows. True submarine tholeiitic eruptions (Monte Caliella Formation) simultaneously produced densely packed pillow piles up to 250 m thick at greater water depth to the west-northwest, especially south of Palagonia. The eastern part of a shallow (< ca 300 m) marine basin in which the Lower Pliocene Trubi chalks and marls and thin nephelinitic (Poggio Inzerillo Member) and later nephelinitic to basanitic submarine volcanics (Poggio Pizzuto Formation) had been deposited was filled completely during the Late Pliocene by tholeiitic lavas. Some of the small shallow water submarine volcanic centers north of Vizzini grew above sea level. Inferred water depths based on volcanological and paleoecological criteria of interbedded and overlying calcarenites agree well.

Subsequent alkalic, more explosive Pleistocene volcanic eruptions (Poggio Vina Formation) (Volcanic phase IV) changed from initially submarine to late subaerial indicating growth of edifices above sea level, sea level rise or land subsidence by ca. 50 m after the end of tholeiitic volcanism. They and the latest Militello volcanics are interlayered with minor shallow water calcarenites. The Poggio Vina volcanics were submerged during a second sea level rise amounting to up to 100 m. The sea was generally shallow, i.e. <100 m deep, throughout most of the Late Pliocene and early Pleistocene. The latest and most voluminous of at least four major Poggio Vina volcanic episodes is characterized by a thick sheet of lapillistones grading upwards into agglutinated scoria and lavas. The Poggio Vina volcanism took place prior to the Emilian transgression. The sea level rise might represent a continuation of the subsidence trend that caused the Lower Pliocene Trubi marine basin. Subaerial conditions were reached twice in the approximate time interval 1.9 to 1.6 Ma during phases of voluminuous volcanism that outpaced subsidence.

The northward extent of the subsurface tholeiitic products beyond the present northern margin of the Iblean Plateau is reflected in a large magnetic anomaly in the southern Catania Plain (Grasso and Ben Avraham, 1992) and by drilling data by AGIP (Longaretti et al. 1991). Torelli et al. (1998), recognized a major late Pliocene tectonic event that affected the northern margin of the Iblean Plateau, related to the extrusion of the tholeiitic volcanics. The alkalic Poggio Vina Formation lavas spread over a much longer time span than the preceding tholeiitic volcanism (1.54 to 1.98 Ma).

Uplift of some 600 m (Palagonia) to 986 m (Monte Lauro) occurred subsequent to emplacement of the Pleistocene alkalic volcanics. Bioclastic carbonates deposited concurrently with uplift drape a major fault scarp east of Palagonia with uplift rates in excess of 0.5 mm/a provided most uplift occurred during ca 1 Ma. Basinning continued beneath the half graben of the present Piana di Catania where volcanics several 100 m thick - at least some of them alkalic in composition - occur at a depth of approximately 500-1500 m below the present surface. Quaternary uplift of the northwestern Iblean Plateau may have been due to a major phase of underplating, diapiric mantle rise or lithosphere isostatic readjustment.

Composition of the volcanic rocks, total volume and mass eruptive rates are well correlated. The volumetrically very minor highly mafic Messinian nephelinites may have formed in response to Messinian lithosphere unloading following draining of the Mediterranean resulting in very low degree partial melting. The nephelinitic to basanitic Poggio Inzerillo and Poggio Pizzuto pillow lavas may herald a major mantle decompression event, possibly the rise of a mantle diapir. The remarkably homogeneous bronzite-bearing, relatively SiO_2-rich Militello tholeiites, representing a very short-lived but voluminous eruptive phase, resemble E-MORB and reflect a major high degree partial melting event, possibly the main phase of diapir decompression. The lack of differentiation trends in the tholeiites indicates rapid rise during a very short-lived, but voluminous, magmatic phase. The Pleistocene Poggio Vina alkali basalts to nephelinites resemble the late stage alkalic phase in intraplate magmatic systems (OIB). There is no evidence of simultaneous or randomly alternating eruption of tholeiitic and alkali basaltic magmas at least in the northwestern Iblean Mountains during the Pliocene and early Pleistocene, both groups being clearly separated in time.

The episode of a brief but intense phase of widespread tholeiites followed by primitive alkali basaltic volcanism of much smaller volume is repeated to some degree about 1 million years later at Etna volcano suggesting a northward migration of the main magmatic source and volcanic focus. Here, a succession of widespread basal tholeiites up to about 0.5 Ma old was followed by less than 0.3 million years of – more evolved - alkali basaltic volcanism suggesting similar mantle processes. The difference lies in the establishment of a magma chamber system beneath Etna volcano and greater degrees of differentiation contrasting with the very primitive composition of the Pleistocene northern Iblean alkalic volcanics. The proximity of the Etna volcano-magma system to the edge of a subducting slab and the implications for magma production rates and compositions precludes drawing of a closer analogy, however.

Aim of the field trip

We focus on several types of subaerial and submarine lava flows and clastic volcanic rocks emplaced between Mineo, Militello and Palagonia to the west and a diatreme at Sortino in the east. Especially interesting – and classically developed in the Iblean Plateau - is the complex interplay of subaerial and submarine volcanism, tectonism and shallow water biogenic and volcaniclastic sedimentation. Most importantly, the character of shallow water volcanism, the gradation from true subaqueous to subaerial emplacement and interaction and mixing of lavas and sediments will be the main theme of the trip. Moreover, the volcanic rocks contrast greatly in chemical composition ranging from tholeiites to melilite nephelinites, having been erupted during well-defined episodes and showing greatly contrasting mass eruption rates.

Field Itinerary

DAY 3

Stop 3.1:

The Costa Giardini diatreme (Sortino area)

The morphological depression (about 800 m across and 100 m deep) of *"Costa Giardini"* characterizes the eastern outskirt of the town of Sortino in the eastern Iblean mountains (northern part of the province of Siracusa). The morphology of the area has been shaped by an interplay of volcanic and regional tectonic processes. The highest elevation is 553m a.s.l.; the lowest points at the Anapo River

valley south of Costa Giardini are 140 m a.s.l.. In the southern area, the "Costa Giardini" diatreme forms a semicircular steep morphological depression opening to the south, with walls sloping from 450 m to 150 m a.s.l. in the Anapo River valley. In the north, the morphology changes into a gentle hilly area (420 m- 520 m a.s.l.). The area surrounding Sortino is extensively used for cattle grazing. Intense agricultural use is only possible within the diatreme, where the fertility of the diatreme`s filling is shown by the lush *Citrus sinensis*, *Citrus limon* and *Olea europaea* plantations.

The "Costa Giardini" diatreme is one of at least 11 morphological depressions with vent characteristics in the eastern Iblean Mountains (Carbone and Lentini, 1981, see also the geological maps by Lentini et al.1984 1:100.000 scale and Lentini et al. 1986 1: 50.000 scale). The stratigraphic subdivision of the diatreme`s bedrocks and its external volcaniclastic facies follows the definition of the Sortino Group of Grasso et al. (1982). The rocks in the map area comprise three geological units: (1) a lower shallow water limestone, which forms the walls of the volcanic conduit and the base of the volcanic apron (Monti Climiti Formation); (2) the volcaniclastic sediments and rocks of the diatreme with two intercalated biohermal levels (Carlentini Formation) and (3) a cover of exclusively non-volcanic sediments (Monte Carruba Formation). These strata are of late Miocene age and well-correlate with the "Tripoli" beds and the Messinian evaporites near Licodia Eubea (Grasso et al., 1982) on the western margin of the Iblean Plateau.

Volcaniclastic deposits of the Costa Giardini Diatreme (Carlentini Fm) can be subdivided into extra-diatreme and intra-diatreme facies, each comprising characteristic deposits. Volcaniclastic deposits of the extra-diatreme facies cover an area of ~3km^{2}~ mainly north of the diatreme. These represent relict parts of a former semicircular tephra ring at least 80 m high which surrounded the northern part of the "Costa Giardini" volcano (Fig. 3.1 a-e). Mantle xenoliths are common in the volcaniclastic sediments. At Costa Giardini only the top bioherm of the two intervening biohermal horizons (Intermediate and Top Bioherm) is exposed. The former existence of the Intermediate Bioherm is only proven by layers in the succession. The intra-diatreme facies comprises reworked volcaniclastic deposits (Fig. 3.1 f) with varying degree of carbonatic matrix and deposits of exclusively primary magmatic particles (Fig. 3.1 h).

Tephra ring:

Stop 3.1-a:

(Fig. 3.1): Sortino main Road (495 m a.s.l.)

Lava flow (up to 10 m thick) at the base of the succession is exposed behind the houses. In this stop there are also lava flows connected to the diatreme. The nephelinitic composition of the lava flow corresponds to that of most dikes and volcanic clasts in the intradiatreme facies.

Stop 3.1-b:

(Fig. 3.1) Monticelli (495 m a.s.l.) street section at the beginning of the main switchback road from Sortino to Solarino.

Volcaniclastic sediments of the tephra ring in medial facies (Fig. 3.2) with antidune deposits (Fig. 3.3), impact structures, mantle xenolith-rich layers (X1-X4 in Fig. 3.2), synvolcanic faults.

The matrix is carbonatic to a varying degree. Clasts comprise the whole spectrum of the diatreme`s bedrock fragments. Some tuffs consist entirely of armored lapilli. The largest impact structure (Fig. 3.4) is underlain by a bed extremely rich in armored lapilli (L17 in Fig. 3.2).

These have a core of coralline limestone with a thin rim of carbonatic material plastered onto it. Armored lapilli are 0,5 -3cm in diameter. A ~ 2m thick layer representing relicts of the Intermediate Bioherm can be found behind the bend (lefthand side walking downwards). Some tuffs consist entirely of accretionary lapilli

Stop 3.1-c:

(Fig. 3.1): Monticelli (500 m a.s.l.).

At the beginning of the main switch back road from Sortino to Solarino; top of the hill below the house.

Well-exposed contact of volcaniclastic sediments and underlying limestones. Top Bioherm (Grasso et al., 1982) with paleosoil and in situ coral stocks close to the house are exposed. Many well-preserved fossils such as *Clypeaster* sp. and many different types of snails (e.g. *Strombus* sp.)

Stop 3.1-d:

(Fig. 3.1): Main switchback road from Sortino to Solarino (440 m a.s.l.)

In the inner side of the bend (right hand side walking downwards): basal contact of volcaniclastic sediments and limestones of Mt. Climiti Fm. Left hand side of the road: some meters above the actual

contact in the volcaniclastic sediments there is a patch of homogeneous carbonate containing lava clasts, which are "standing on the edge", as if they had fallen into still soft carbonatic mud (Fig. 3.5).

Stop 3.1-e:

(Fig. 3.1): Main switch back road from Sortino to Solarino, left of the small cave-like stable (420 m a.s.l.)

"Mega-breccia" with lava-clasts up to 1.50 m in diameter, Limestone and Porites-clasts occurs below several tens of meters big carbonate olistolith (house is build on the olistolith) (Fig. 3.6).

Diatreme:

Stop 3.1-f:

(Fig. 3.1): main switch back road from Sortino to Solarino

A limestone olistolith several hundreds of meters in diamater occurs blacktop road, which connects to the main switch back road in the bend, excellent slump structures in the surrounding clastic sediments. Walking down all around the big olistolith. Further lies a several m-thick volcanic dike and different facies of the diatreme`s filling. The road returns to the main switch back road where a small Maria statue is in a small alcove.

Stop 3.1-g:

(Fig. 3.1): Main switch back road from Sortino to Solarino (310 m a.s.l.)

Smooth inclined surfaces of the diatreme`s wall and contact to the volcaniclastic filling. All surfaces dip between 20° and 40° towards the center of the diatreme. Two limestone olistoliths are incorporated in the volcaniclastic filling.

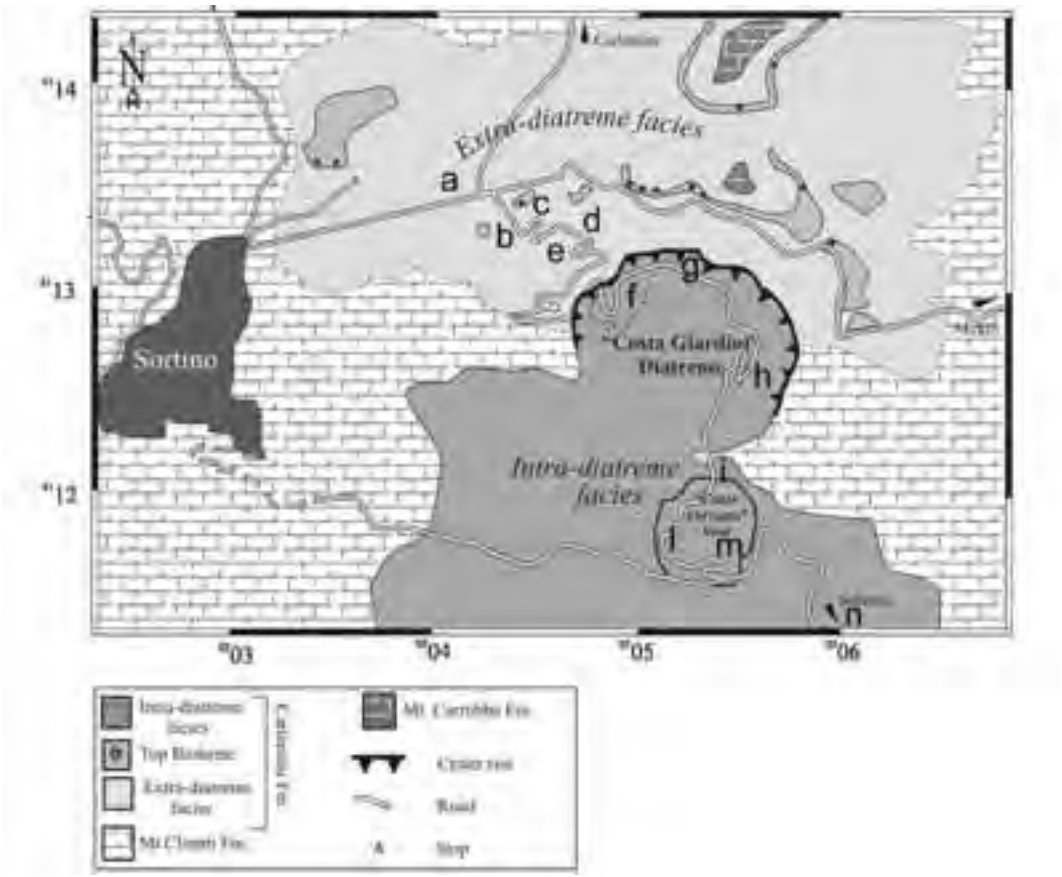

Figure 3.1 - Geology of the Costa Giardini diatreme and surronding area; letters a to n indicate stops.

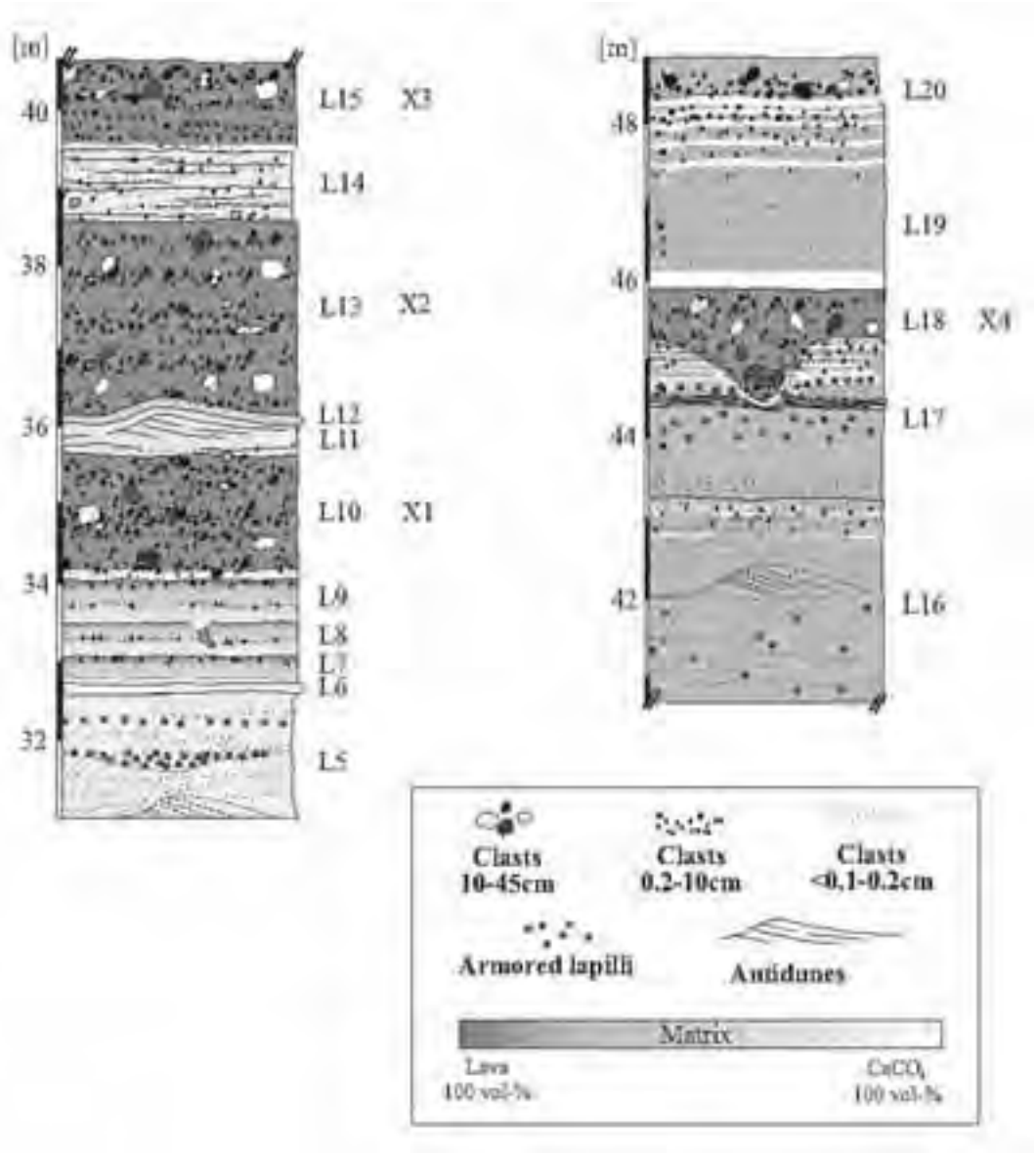

Figure 3.2 - Monticelli street-section shows volcaniclastic deposits of the tephra ring in medial facies. (L = volcaniclastic layer; X = xenolitic – rich deposits)

Stop 3.1-h:

(Fig. 3.1): Main switchback road from Sortino to Solarino (310 m a.s.l.)

Relicts of a hyaloclastite cone. Layered deposit of angular primary volcanic clasts in a carbonatic / zeolitic matrix. Carbonate olistolith has intruded into the deposit.

"Cozzo Ferrante" Vent

The Cozzo Ferrante Vent is a small scoria cone south of Costa Giardini consisting exclusively of lapilli (Fig. 3.1 i), scoria , dikes (Fig 3.1 m), and minor lava flows. It is apparently connected to the Costa Giardini volcanic system. In the crater a small basin was filled with reworked sediments, diatomites (Fig. 3.1 l) and limestones.

Stop 3.1-i:

(Fig. 3.1): Main switch back road from Sortino to Solarino N of an abandoned house (243 m a.s.l.).
Contact of Mt. Climiti Fm and lapillistone with sometimes fresh glassy particles. The lapillistone lacks a carbonatic matrix. Strike and dip of the contact is repeated by faults in the limestone, which result in parallel erosion surfaces 10 m above the contact.

Stop 3.1-l:

(Fig. 3.1): Main switchback road from Sortino to Solarino (215-220 m a.s.l.).
Transitional contact from reworked volcaniclastic deposits to papershale diatomite (fig. 3.7) defined by alternating layers of diatomites and volcaniclastic material.

Diatomites contain fish bones, fish scales, shark teeth and tree leaves on the bedding plains. They represent part of the filling of a small basin in the center of Cozzo Ferrante Vent. The base is characterized by a dm thick layer of red paleosoil (Fig.3.8).

A strongly weathered lava flow crops out next to the abandoned door to a private property.

Stop 3.1-m:

(Fig. 3.1): Main switch back road from Sortino to Solarino (190-215 m a.s.l.).
At the eastern bend of the switchback road there is an excellent outcrop of slightly red oxidized agglutinated scoria and lava bombs (Fig. 3.9) that appear to have formed in an open space environment.
Single pieces of scoria are up to 5 cm thick and several tens of cm wide (Fig. 3.10). Bombs are 20-30 cm in diameter. This area is bordered to the west by a dike several m thick.

Stop 3.1-n:

(Fig. 3.1): Road from Sortino to Solarino, east of the diatreme in the Anapo River valley (150 m a.s.l.).
Debris flow deposits in proximal and distal facies. Deposit comprises many types of volcaniclastic and bedrock fragments of the filling of the diatreme. Matrix is strongly carbonatic. Up the small blacktop road up the hill, an unconformity between debris flow deposit and Pleistocene terrace conglomerate is well-exposed.

Stop 3.2:

Monte Carrubba section
The Monte Carrubba section exposed along the Carlentini-Sortino road shows lavas intercalated with marine sediments; the section precisely stratigraphically constraining the dating of the Upper Miocene volcanism of the Iblean Plateau. The basal tuff rests on a brecciated Siracusa Limestone member surface (Fig. 3.11 a). Highly altered vesicular lavas (5.5 m) complete this lowest volcanic level. Pale brown packstones and wackestones (1.3 m) rest on the volcanics and frequently penetrate downwards into the lava top (Fig. 3.11 b). Faunas in the carbonate level are sparse, except for scattered thickets and solitary colonies of *Porites* sp. and *Tarbellastraea* sp.; *Clypeaster* sp is common. This is the Intermediate Bioherm level. Over 5 m of tuff and lava (Fig. 3.11 c) overlie the planar-topped intermediate bioherm. The volcanics in turn are overlain by a second carbonate level, the top Bioherm level (Fig. 3.11 d). It consists of an upper and lower bed, each 1.3 m thick. About 1 m of volcanic breccia (Fig.3.11 e) separates the two. The lower bed is largely identical to the intermediate bioherm level, except for common brecciation. The upper bed is diagenetically altered, contains no macrofauna and is intensely brecciated. A 28 m-thick lava and volcaniclastic breccia sequence (Fig. 3.11 f) overlies the planar top of the upper bed.
The stratigraphic succession described represents the Carlentini Formation of Grasso et al. (1982). Stratigraphically well-defined sites from all three volcanic horizons in the Carlentini Formation are all normally magnetized. As the Carlentini Formation is known to be of Late Tortonian age Grasso et al. (1982), suggest that it corresponds to magnetic interval 7 McElhinny (1978) in which the directions of magnetization are predominantly normal. The absence of reversed directions, particularly in the lower volcanic horizon suggest that it does not extend below interval 7.
The Carlentini Formation is overlain by 34 m thick of micrite-grade carbonates and subordinate grainstones (Monte Carrubba Formation, Grasso et al. 1982). It may be subdivided at a prominent horizon of synsedimentary faulting into a upper and lower association. The lower association consists (Fig. 3.11 g) of 11 m of biomicritic rock containing a normal marine fauna of small aragonitic bivalve moulds and pectinids. Massive cream wackestones (1.2 m thick units) occur at the base but become progressively more thinly bedded towards the top. Two 0.5 m

Figure 3.3 - Base surge deposits (antidune structure) is sandwiched between two layers rich in mantle-xenolits (L 10 – L 13 in fig. 3.2)

thick, brownish marl levels occur in the sequence and contain *Ostrea* sp. together with *Pecten aduncus* and possibly *P.vigolenensis*. Bivalves are infrequent in the upper, thinner bedded levels. The upper association (Fig. 3.11 h) occurs with marked hiatus upon the faulted lower succession. It consist of about 21 m of cream and white wackestones. Initially they are thinly bedded, 0.5-2 cm thick beds, but later massive bedded, gray wackestones occur. Faunas are locally abundant but are low diversity. The massive bedded strata are apparently without macrofauna and may give way to ooidal grainstone development. The wackestones rarely contain pectinids but *Euxinicardium* sp and *Didacna* sp. are abundant and form lumachelle horizons: barren white micrites occur at the top of the succession and are truncated sharply by overlying Pliocene lavas.

Stop 3.3:

Vallone Loddiero

The Loddiero section represents an excellent place to examine stratigraphic relationships between Plio-Pleistocene tholeiitic (Militello Formation) and alkalic lavas (Poggio Vina Formation). The section is exposed in a quarry on the left bank of Vallone Loddiero, 3 km southwest of the town of Scordia. (Fig. 3.12). For literature see Pedley et al (2001) and Pedley and Grasso, (2002)

The base of the Loddiero section is represented by pillow breccias (pillow fragments in a hyaloclastite matrix) and lesser amounts of closely packed pillow lavas 7.5 m thick, the succession dipping 25-30° toward the east. Pillow lavas are concentrated near the top below grey overlying 7 m thick subaerial lavas, the contact being fairly horizontal. The apparent bedding of the breccias is most evident in the inclination of larger, elongate pillows, but also in the variations in grain size and lithology. Glassy crusts about 1 cm thick are common. The palagonitized hyaloclastites are orange-yellow. The subaerial lavas comprise pahoehoe flow units 1 to 2 m thick. The erosional surface on top of the subaerial lavas is irregular with up to 0.6 m of relief and is filled with a fining-upward

Figure 3.4 - Impact structure with shattered lava block (L 17, L 18 in Figure 3.2)

Figure 3.5 - Homogeneus limestone pactch containing lava clasts

Figure 3.7 - Papershale diatomite in the crater of "Cozzo Ferrante" vent

succession of bioclastic packstones and lava pebbles (Fig. 3.13). Some pebbles are coated with coralline algae.

The basal conglomerate grades upwards into 3 m of packstones (Loddiero subunit), the carbonates being topped by 2 thin dark gray tuff layers possibly representing the onset of the alkalic Poggio Vina Formation. Foraminifera and nannofossils indicate an early Pleistocene age (Emilian). The overlying columnar jointed dark lava flow (Poggio Vina Formation) locally begins with basal pillows intruded into the soft carbonate sediments (Fig. 3.14). The lava flow in the quarry is about 10 m thick while the interval of alkalic lavas exceeds 100 m in the western Loddiero valley.

Figure 3.6 - Mega-breccia at base of the succession directly below 10 m thick olistolith

The top of the Loddiero section is represented by lower Pleistocene calcarenites (Poggio Spica Formation). They contain foraminifer and nannofossil associations of *Globigerina cariacoensis* Zone and of the "*Large Gephyrocapsa Zone* respectively.

DAY 4

Palagonia area

The Palagonia area is a very important place for understanding different types of basaltic submarine volcanic deposits: Sartorius von Waltershausen (1845) recognized the predominantly submarine nature of the Iblean volcanic rocks and applied the term "palagonite" to what he thought to be a hitherto unrecognized mineral.

Stop 4.1:

Road cut just east of Monte Serravalle

Outcrop on both sides of country road between Monte Serravalle on the west side and Monte Casale di San

Figure 3.8 - Base of diatomite with layer of red paleosoil

Basilio on the east side towards the small hamlet Castellana. Along the road massive hyaloclastite, completely palagonitized with carbonate matrix, olivine phenocrysts still fresh. About 2 m above road 10-15 m thick bedded hyaloclastites changing from 10-20 cm bedding to 1 cm bedding in the upper part. This unit is overlain by about 2 m of partly palagonitized hyaloclastite breccia with angular gray blocks of highly vesicular basalt, possibly cliff breccia from subaerial flows overlying the subaquaeous section. The lower 2 m of this breccia are overlain by a thin lens of pillow lavas about 5 m thick, pillows being extremely well-developed with transverse fractures, budding etc. The upper several 10 m are composed mostly of coarse breccias and debris flow deposits that thin towards the plain and thicken towards the south, probably all delta deposits from flows that entered the sea.

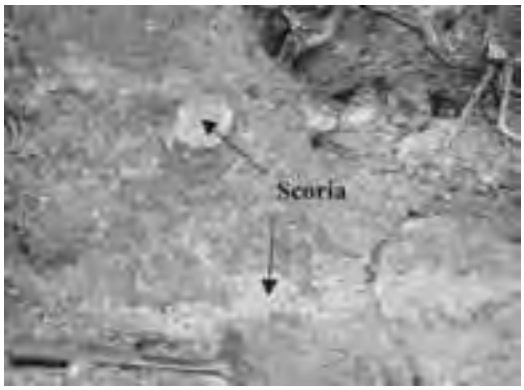

Figure 3.10 - Scoria southside of Cozzo Ferrante vent

Stop 4.2:

Front of escarpment near Palagonia (Santa Febronia section)

Front of escarpment along the road going up to Santa Febronia and Colle del Croce: overall stratigraphy and growth fault landslide breccias.

The section is exposed along the road that link the S.S. 385 with Colle della Croce. The section is exposed on the northern flank of the large volcanic edifice east of Palagonia. At the base of the scarp, densely packed tholeiitic pillow lavas at least 20 m thick overlie massive hyaloclastites (10-15 m thick unit 1 Fig. 4.1) correlated with the Militello volcanics farther south. Moving uphill toward the Santa Febronia scarp, the pillows grade laterally (and possibly vertically) into massive lapilli tuffs with minor pillow fragments and intercalations of

Figure 3.9 - Volcanic bomb southside of Cozzo Ferrante vent

fine-grained bedded tuffs (unit 2 Fig.4.1). Tholeiitic dikes cut the lower sequence and were probably feeders to minor pillow lavas while deposition of the hyaloclastites was continuing, resulting in lens-like occurrences of pillow lavas within the tuffs. Upwards, the tuffs grade into carbonate sediments containing abundant volcanic clasts (unit 3 fig. Fig. 4.1). These in turn are overlain by coarse-grained tuffs (unit 4 Fig. 4.1), a thin horizon of carbonate sediments mixed with volcaniclastics (unit 5 Fig. 4.1), and another sequence of bedded tuffs (unit 6 Fig. 4.1). The entire sequence, taken as representing one eruptive cycle with several interruptions marked by sedimentary intercalations, is overlain by calcarenites (unit 7 Fig. 4.1). The presence of *Globorotalia inflata* implies that

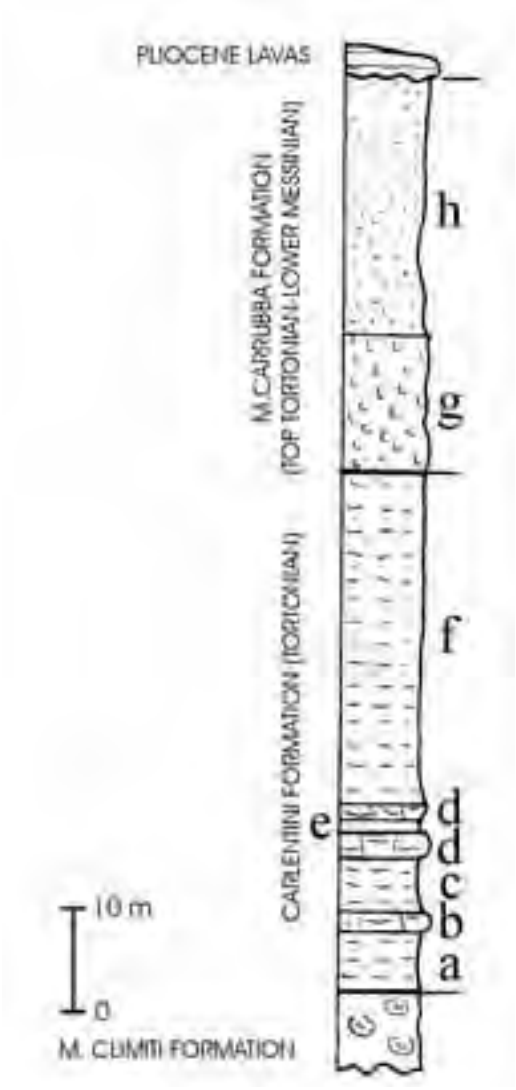

Figure 3.11 - Stratigraphic column of Monte Carrubba section (from Grasso et al. 1982, modified)

this horizon is not older than Late Pliocene.

The uppermost Pliocene horizon is unconformably overlain by calcarenites that pinch out toward the south (Fig. 4.1; Fig. 4.2; Fig. 4.3), thus resting laterally on the northern shoulder of the pre-existing volcanic edifice. The presence of *Pseudoamussium septemradiatum* (Muller), in an intercalated muddy bed, clearly indicates Early Pleistocene. The Pleistocene calcarenites are overlain by approximately 15-20 m of palagonitized bedded shallow submarine alkali basaltic lapilli tuff which decrease in thickness toward the southeast where they are overlain by approximately 3 m of alkali basaltic lava. The top of the Santa Febronia section is represented by lower Pleistocene (Emilian stage) calcarenites.

Overview at cross

Stop 4.3:

Dirt road below Contrada Croce peak, on east slope of Catalfaro valley. 1 km west of road Palagonia-Militello

Going down road on the westside excellent stratigraphic section. At the top several m of calcarenite underlain by a few m of hyaloclastite covering a thin horizon of megapillows with different types of gabbroic and peridotite nodules and olivine phenocrysts overlying carbonate. Down the road in the first curve there is a fault lowering this section against the brownish hyaloclastites which are well-bedded and interlayered with several layers of carbonate and finally a marl horizon underlain at the main curve by tholeiitic Militello pillow breccia and pillows with excellent glass. This sequence unconformably overlies a pillow breccia.

Militello area

Stop 4.4:

Outskirts of Militello/Vallone Lembasi: pillow lavas, hyaloclastites, drained pillows and blocks of subaerial lavas in pillow-hyaloclastite breccia (table 1)**.**

The outcrops along the road from Militello to Vizzini at the outskirts of Militello offer an extremely impressive record of a pillow-hyaloclastite complex formed where lava flows entered a water body, as well as of the transition to subaerial lavas. The transition to the subaerial facies will be studied more conveniently in a quarry about 2 km north of Vizzini (stop 4.10). The outcrop extends from the last houses at the southern ouskirts of the town – note fault at curve of road -, passing a water fountain where cars can park and extending along the road for about 300 m. The outcrops next to the last houses show coarse-grained, relatively well-sorted hyaloclastites with scattered isolated and partly broken pillows, some with central cavities. The deposits are coarsely bedded, the relatively constant dip to the southwest changing little along the road. All pillow (fragments) show excellent thick rims of fresh black sideromelane (basaltic glass). The hyaloclastites consist dominantly of lapilli-sized (2-64 mm) angular fragments of glass,

Figure 3.12 - Tholeiitic Militello Formation lavas showing a change from submarine (a) into subaerial (b) deposition. Alkalic lavas of Poggio Vina Formation at the top (c).

apparently formed when lava entered a water body and became fragmented by various processes. At least one of the fragmentation processes becomes obvious

Figure 3.13 - Top of the Militello Formation showing an erosional surface filled by conglomerate

in an outcrop about 200 m along the road from the water fountain. Here, elongate stringers of drained pillow tubes show collapse structures (implosion), partial fragmentation of the pillow tube walls and quenching of the interior. This clearly indicates that water entered the pillow tube during its formation, accompanying implosion and fragmentation and was able to quench the still hot interior of the draining tube. Further along the road, some structures show incipient remobilization of the pillow-sideromelane foreset breccia and some incorporation of brownish oxidized blocks of vesicular lava, apparently broken from a lava platform covered by subaerial lavas. This shows that the water body had been filled to the brim, the later lavas being emplaced on largely dry ground. It also demonstrates that the effusion rate of lava was high, continuous supply of lava -probably from some distance - allowing to build an entire delta of pillow-hyaloclastite breccia in a very short time.

Stop 4.5:

Contrada Quadarazza

a) Contrada Quadarazza I

At Contrada Quadarazza I the Militello lavas are represented by alternating bedded and massive tuffs and pillow breccias and occur within the Pliocene marls, but the bulk overlies them. The unit becomes progressively richer upward in a chaotic mixture of broken pillows with minor blocks of subaerial lava and rare nonvolcanic rocks. These are exposed at a cliff along the front of lava deltas and of emergent volcanic edifices whose submarine portions consisted of pillow lavas and breccias capped by subaerial lava flows or tuffs. Deposits of pillow fragments, a few centimeters to tens of centimeters in diameter, set in a marly matrix, are thought to represent debris flow deposits derived from eruptive centers in the south or southeast as shown by an increase in the diameter of the clast and of breccia units toward the south and southeast. The debris flows apparently ploughed into, and became thoroughly mixed with, the soft muds explaining the diffuse nature of the stratigraphic boundary between the Trubi marls and the volcanics. Other units consist of extremely vesicular lapilli and what appear to be bomb and spatter fragments and likely represent strongly explosive shallow-water eruptions grading into emergent subaerial volcanics. The presence of blocks of subaerial lava

Figure 3.14 - Contact between alkalic lava flow (Poggio Vina Formation) and underlying packstones

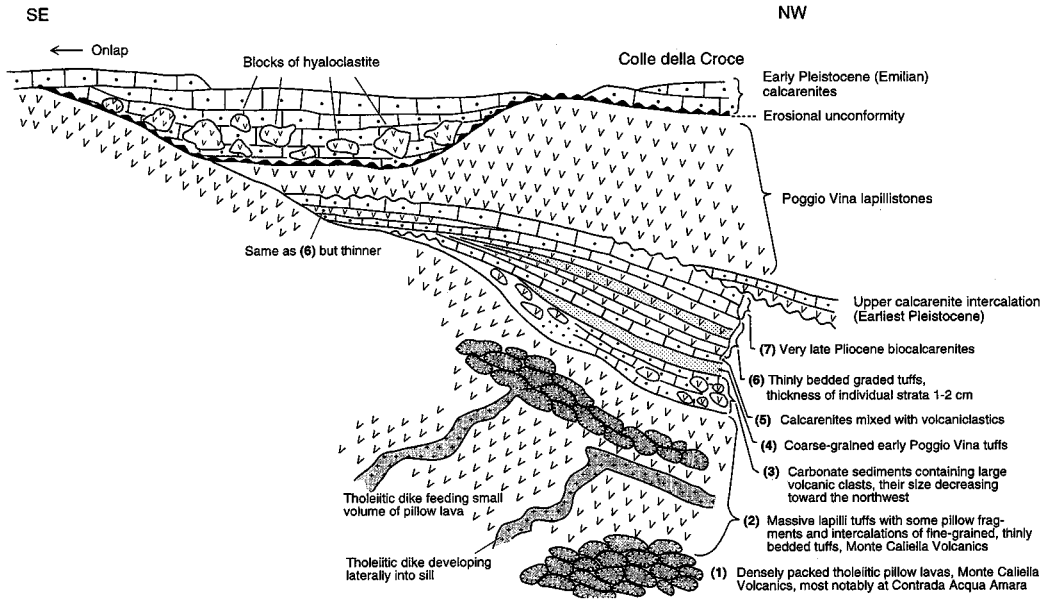

Figure 4.1 - Generalized profile of the Santa Febronia scarp. Note general dip to the right, toward the foredeep adjacent to the northern Iblean margin.

in the topmost of Militello unit suggests that, by the time of their emplacement, very shallow-water to emergent conditions prevailed allowing subaerial lava flows to form, as also suggested by the presence of irregular horizons of fossil rich marls near the top of units. Strong disturbance of the marly horizons indicates that they were emplaced in a highly unstable environment, probably on steep, and frequently collapsing, submarine scarps. The Militello unit is covered with 2 to 5 m thick upper Pliocene marly sediment rich in Pecten jacobeus; reworked Militello pillow fragments and blocks of subaerial lava forming an intercalation within these sediments approximately 3 m thick. They were most probably emplaced after the onset of sedimentation when part of a marine cliff in the Militello volcanics collapsed.

b) Contrada Quadarazza II

In this section a twofold alternation of submarine volcanics (pillow lava and pillow breccia) and subaerial lavas, both related to Militello unit, occur. The contact surface between the submarine flow-foot breccia and the overlying flows indicates the position of the sea-level at the time of the volcanic activity. The repetitive change from subaerial to submarine

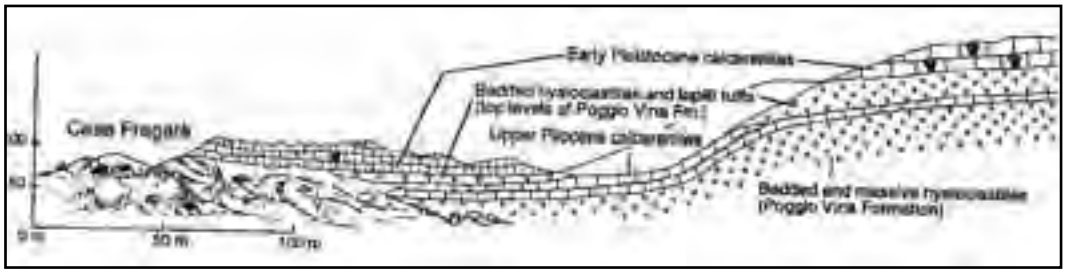

Figure 4.2 - Field sketch illustrating the occurrence of the Plio-Pleistocene boundary on the ridge at Casa Fragalà. The lowermost calcarenite intercalation is of the latest Pliocene, whereas the overlying intercalation marks the beginning of the Pleistocene. Note that this horizon pinches out toward the south (upslope) due to regression caused by the northward growth of the volcanic edifice (from Schmincke et al. 1997)

Volume n° 2 - from B16 to B33

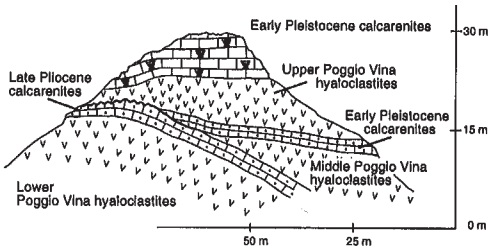

Figure 4.3 - Field sketch showing the occurrence of the upper Pliocene and lower Pleistocene calcarenite intercalations on the northwest side of the Santa Febronia scarp. Lower Pleistocene regressive horizon pinches out toward the southeast. Uppermost calcarenites are of the Emilian transgression (from Schmincke et al. 1997)

A

B

C

D

E

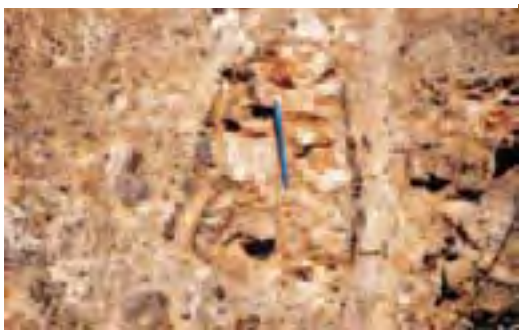

F

environment was not caused by rise of the sea level during a lull in volcanic activity. Most likely, the top of the unstable lava delta fluctuated while sea level remained constant.

Thus, collapse, gradual sinking and subsidence of the entire lava delta, caused by the load of accumulated lavas, could simulate a rise of sea level. The original subaerial part of the delta may subside by several within weeks to months below sea level, carrying the marker line with it. The recognition of repeated lava delta subsidence has significant implications not only for establishing the correct stratigraphy and the definition and chronology of distinct events, but also for time estimates. A sea level rise of at last 30 m between two episodes of tholeiitic volcanism would represent a relatively long period of volcanic repose, probably in the range of tens to hundred of thousands of years. In the model here presented, the time span for the bulk of the tholeiitic eruptive cycle shrinks to a minimum of possibly no more than several decades to a few thousand years, representing one voluminous but extremely brief surge of magma reservoir evacuation.

Stop 4.6:

Stop halfway between Militello and Vizzini Station shortly after road takes off to left toward Francoforte: abandoned quarry in 20 m thick pillow breccia debris flow deposits (table 1)

An abandoned quarry west of the road shows excellent pillow fragment breccias. These occur in the form of debris flow deposits, emplacement units being up to several m thick. The cumulative debris flow units are faulted with offsets to the south. The lithology of the breccias is extremely heterogeneous comprising mostly fragments of pillows ranging from lapilli- to block size but also fragments of brownish oxidized and vesicular blocks of subaerial lava flows.

The section is interpreted as a lower part of a lava delta succession capped by subaerial lavas which had become unstable and was displaced toward the deeper water part of the basin, some faults being normal others listric. Basically the outcrop is thought to represent the continuation of the section along the road at the outskirts of Militello into deeper water.

Vizzini area

Stop 4.7:

Abandoned quarry in small hyaloclastite cone just north of military station and train station

Well-bedded yellowish palagonitized lapillistones and minor tuffs dominate (Fig. 4.6).

Fig. 4.6. Part of shallow water tuff ring .

Lapilli beds are up to 15 cm thick alternating with tuff layers, most only a few cm thick. Clasts are variably glassy and chiefly vesicular. Angular lithic clasts (broken parts of pillows) make up a small percentage of the tephra deposits.

The eruption took place in very shallow water. The outward dipping layers of the tephra ring are capped at the highest point next to the road by some shallow water calcarenite, further evidence that the lapilli cone had formed under water. The cone probably represents the advanced shoaling of true submarine eruptions of Militello Formation tholeiitic lavas.

Stop 4.8:

Hyaloclastite cone with dikes at Vizzini Station. Abandoned quarry just north of major road junction.

On the left side of the road leading to Licodia Eubea a hyaloclastite cone is well exposed. The upper hyaloclastites which consist of highly vesicular thoroughly palagonized glass shards of tholeiitic composition (Militello Formation) are very fine-

Table 1: Different facies of the Militello volcanics in the Militello-Vizzini area.
A: Still intact lava tube with pillow-like cross section of submarine part of tholeiitic Militello Fm. (stop 4.4).
B: Foreset bedding and disconnected lava stringers enclosed in coarse-grained dominantly lapilli-size hyaloclastite breccia (stop 4.4).
C: Interlayered redeposited Militello Formation pillow breccia (lower left and upper right) alternate with collapsed subaerial lava blocks (central part from upper left to lower right), typical of slumped lava delta debris flow deposits (stop 4.6).
D: Drained, partially brecciated pillow tube with external and internal quenching (black glass) of foreset bedded pillow-hyaloclastite breccia (stop 4.4).
E: Thin subaerial tholeiitic lava flow unit overlying foreset-bedded pillow-hyaloclastite breccias. Inclined pipe vesicles at base of upper flow direction from right to left (stop 4.4).
F: Reworked and retransported, poorly sorted pillow-hyloclastite breccias. Militello Formation. Abandoned quarry 1 Km north of Vizzini station.

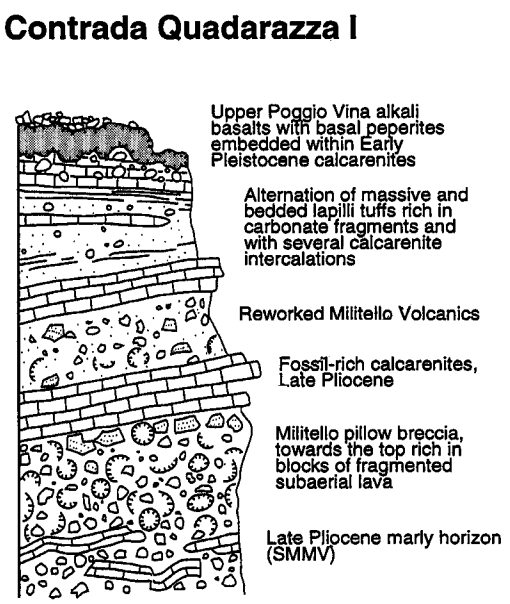

Figure 4.4 - Stratigraphic section of the Contrada Quadarazza I (from Schmincke et al. 1997)

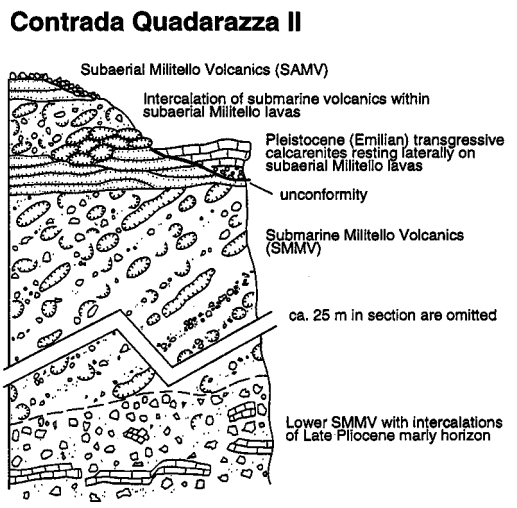

Figure 4.5 - Stratigraphic section of the Contrada Quadarazza II (from Schmincke et al. 1997)

Figure 4.6 - Reworked and retrotransported, poorly sorted hyaloclastite breccia (stop 4.6)

Figure 4.7 - Subaerial pahoehoe lava flow units of the Militello Fm, a few meter above the transition from the underlying submarine facies. The basal and top parts of each flow unit show a higher degree of vescicularity than the massive inner portion..

grained and extremely well-bedded. They are overlain by flat vesicular pillows being transitional to pahoehoe lavas, well-exposed along a path just north of the cone (left side of outcrop). Two dikes about 3 m thick cut the hyaloclastites and show interesting marginal structures which will be discussed on the field trip.

Stop 4.9:

Small abandoned quarry along road to Vizzini about 300 m north of Vizzini station. Basanitic/ nephelinitic pillow lavas intruded into soft lower Pliocene Trubi marls.

The relatively densely packed dark pillows represent nephelinites probably of the Poggio Inzerillo Formation. The lavas are quite fresh except for a thin alteration crust along the glassy pillow rims and along fractures. Vesicles in the lavas are partly filled with carbonates. Carbonates below pillow basalts contain *Pecten* sp. and corals.

Stop 4.10:

Excellent new deep quarry a couple of km north of Vizzini. Entrance to quarry is in subaerial tholeiitic lavas of the Militello Formation. They "grade" alongside the road descending into main quarry into very shallow submarine and then into deeper submarine lavas

At the moment, the best-exposed and most convenient place to study the transition from basalt lava emplaced into a water body to lava emplaced on dry ground - due to the rapid filling of the shallow water body – is a quarry opened in the 1990ies about 2 km north of Vizzini along the road Vizzini rail station – Vizzini town. At the entrance to the quarry subaerial lava flows about 3 m thick are exposed at right. (Fig.4.7).

The lavas are represented by thin flow units of vesicular pahoehoe, some with red oxidized wrinkled surfaces. As is typical for the particular facies of pahoehoe transitional from subaqueous to subaerial, thin glassy rims may surround thin pahoehoe flow units at the very transition water-land. This change in lava facies is well-exposed left of the road leading into

the main quarry. True pillow-sideromelane breccia facies makes up the walls of the main quarry. Here, complex pillow fragment breccias occur in several coarsely banked units, with sideromelane breccia making up a significant portion of the rock bodies. This contrasts with the pillow lava facies in the pillow gorge section south of Palagonia where sideromelane breccias make up but a minor proportion of the lavas. These lavas represent true submarine eruptions and not subaerial lava flows that entered a water body. In this locality, field work is insufficient to decide whether or not the change from subaqueous to subaerial was due to subaerial lava flows entering a shallow marine basin and filling it to the brim and forming a new land surface or whether a true submarine volcano grew to breach sea level and formed a volcanis island.

References

Barberi, F., Civetta, L., Gasparini, P., Innocenti, F., Scandone, R. and Villari, L. (1974). Evolution of a section of the Africa-Europe plate boundary: paleomagnetic and volcanological evidence from Sicily. Earth Planet. Sci. Lett. 22, 123-132.

Battaglia M., Cimino A., Gottini V., Dongarrà G., Hauser S., Ingrasciotta M.V., Rizzo S., Sacco G., (1991). Indagini geochimiche e geofisiche su un lago endoreico della Sicilia: Pergusa. Bollettino della Società Geologica Italiana 110, 53-63.

Ben-Avraham, Z. and Grasso, M. (1990). Collisional zone segmentation in Sicily and surrounding areas in the Central Mediterranean. Ann. Tectonicae 4, 131-139.

Bianchi, F., Carbone, S., Grasso, M., Invernizzi, G., Lentini, F., Longaretti, G., Merlini, S. and Mostardini, F. (1989). Sicilia orientale: Profilo geologico Nebrodi-Iblei. Mem. Soc. Geol. It. 38, 429-458.

Butler, R.W.H. and Grasso, M. (1993). Tectonic controls on base level variations and depositional sequences within thrust-top and foredeep basins: examples from the Neogene thrust belt of central Sicily. Basin Research 5 137-151.

Butler, R.W.H. and Lickorish, W.H. (1997). Using high resolution stratigraphy to date fold and thrust activity: examples from the Neogene of South-central Sicily. J. Geol. Soc. London 154, 633-643.

Butler, R.W.H., Grasso, M. and La Manna, F. (1992). Origin and deformation of the Neogene-Recent Maghrebian foredeep at the Gela Nappe, SE Sicily. J. Geol. Soc. London 149, 547-556.

Butler, R.W.H., Grasso, M. and Lickorish, W.H. (1995a). Plio-Quaternary megasequence geometry and its tectonic controls within the Maghrebian thrust belt of south-central Sicily. Terra Nova 7, 171-178.

Butler, R.W.H., Lickorish, W.H., Grasso, M., Pedley, H.M. and Ramberti, L. (1995b). Tectonics and sequence stratigraphy in Messinian basins, Sicily: constraints on the initiation and termination of the Mediterranean 'salinity crisis'. Bull. Geol. Soc. America 107, 425-439.

Butler, R.W.H., McClelland, E. and Jones, R.E. (1999). Calibrating the duration and timing of the Messinian Salinity Crisis in the Mediterranean: linked tectono-climatic signals in thrust-top basins of Sicily. J. Geol. Soc. London 156, 827-835.

Butler, R.W.H., Grasso, M. and La Manna, F. (1982). Origin and deformation of the Neogene-Recent Maghrebian foredeep at the Gela Nappe, SE Sicily. J. Geol. Soc. London 149, 547-556.

Carbone, S., Catalano, R., Grasso, M., Lentini, F., and Monaco, C. (1990). Carta Geologica della Sicilia centro-orientale, Società Elaborazioni Cartografiche, Florence.

Cita, M.B. (1975). Studi sul Pliocene e gli strati di passaggio dal Miocene al Pliocene. VII Planktonic foraminiferal biozonation of the Mediterranean Pliocene deep sea record. A revision. Riv. It. Paleont. Strat. 81 (4), 527-544.

Carbone, S. and Lentini, F. (1981). Caratteri deposizionali delle vulcaniti del Miocene superiore negli Iblei (sicilia sud-orientale). Geologica Romana 20, 49-104.

Esteban, M. (1979). Significance of the upper Miocene coral reefs of the Western Mediterranean. Palaeogeogr. Palaeoclimatol. Palaeoecol. 29, 169-188.

Esteban, M. (1996). An overview of Miocene reefs from Mediterranean areas: general trends and facies models. In "Society for Sedimentary Geology, Models for Carbonate Stratigraphy from Miocene Reef Complexes of Mediterranean Regions", SEMP concepts in Sedimentology and Paleontology 5, 2-53.

Decima, A. and Wezel, F.C. (1973). Late Miocene evaporites of the central Sicilian basin, Italy: Initial Reports of the Deep Sea Drilling Project 13, 1234-1241.

Di Grande, A., Grasso, M., Lentini, F. and Scamarda, G. (1976). Facies e stratigrafia dei depositi pliocenici tra Leonforte e Centuripe (Sicilia centro-orientale). Boll. Soc. Geol. Ital. 95, 1319-1345.

Grasso, M. (2001). The Appenninic-Maghrebian orogen in southern Italy, Sicily and adjacent areas. In "Anatomy of an Orogen: the Apennines and Adjacent Mediterranean Basins" (G.B. Vai and J.P. Martini, Eds.), 255-286. 2001 Kluwer Academic Publishers.

Printed in Great Britain.
Grasso, M. and Butler, R.W.H. (1993). Tectonic controls on the deposition of late Tortonian sediments in the Caltanissetta basin of central Sicily. Mem. Soc. Geol. Italiana 47, 313-324 (for 1991).
Grasso, M. and Pedley, H.M. (1988). The sedimentology and development of Terravecchia Formation carbonates (Upper Miocene) of North Central Sicily: possible eustatic influence on facies development. Sedimentary Geology 57, 131-149.
Grasso, M., Pedley, H.M. and Romeo, M. (1990). The Messinian Tripoli Formation of north-central Sicily: palaeoenvironmental interpretations based on sedimentological, micropalaeontological and regional tectonic studies. Paléobiologie continentale 17, 189-204.
Grasso M., Amore C., Maniscalco R., Geremia F., Ingrasciotta V. and Ioppolo S. (2002). Dati preliminari sulle ricerche stratigrafiche e sedimentologiche eseguite nel Lago di Pergusa (Enna). Bollettino Accademia Gioenia Scienze Naturali Catania, in press.
Grasso, M. (1993). Pleistocene structures at the Ionian side of the Plateau Ibleo (SE Sicily): implications for the tectonic evolution of the Malta Escarpment. In "Geological development of the Sicilian-Tunisian platform" (M..D. Max, P. Colantoni, Eds.), UNESCO Rep. Mar. Sci. 58, 49-54.
Grasso, M. and Ben Avrham, Z. (1992). Magnetic study of the nothern margin of the Hyblean Plateau, Southeastern Sicily: structural implications. Ann. Tectonicae 6, 202-213.
Grasso, M., Lentini, F. and Pedley, H.M. (1982). Late Tortonian – Lower Messinian (Miocene) paleogeography of S.E. Sicily: information from two new formations of the Sortino Group. Sediment. Geol. 32, 279-300.
Grasso, M. and Reuther, C.D. (1988). The western margin of the Hyblean Plateau: a neotectonic transform system on the SE Sicilian foreland. Ann. Tectonicae 2, 107-120.
Honnorez, J. (1962). Observations sur les coulees et les centers eruptifs subaeriens constituant une partie def formations volcaniques des monts d'Iblea (sud est de la Sicilie). Bull. Soc. Belge Geol. Paleontol. Hydrol. 71, 297-316.
Jones, R.E. and Grasso, M. (1997). Palaeotectonics and sediment dispersal pathways in North-Central Sicily during the Late Tortonian. Studi Geologici Camerti vol. spec. 1995/2, 279-291.
Keogh, S.M. and Butler, R.W.H. (1999). The Mediterranean water body in the late Messinian: interpreting the record from marginal basins on Sicily. J. Geol. Soc. London 156, 837-846.
Lentini, F., Carbone, S., Grasso, M., Di Geronimo, I., Scamarda, G., Bommarito, S., Iozzia, S., La Rosa, N., Sciuto, F. (1984) – Carta geologica della Sicilia sud-orientale, scale 1:100.000. Società Elaborazioni Cartografiche, Florence.
Lentini, F., Carbone, S., Cugno, S., Grasso, M., Scamarda, G., Sciuto, F., Ferrara, V. (1986). Carta geologica della settore nord-orientale ibleo (Sicilia SE), scale 1:50.000. Società Elaborazioni Cartografiche, Florence.
Lickorish, W.H. and Butler, R.W.H. (1996). Fold amplification and parasequence stacking patterns in syn-tectonic shoreface carbonates. Bull. Geol. Soc. America 108, 966-977.
Lickorish, W.H., Grasso, M., Butler, R.W.H., Argnani, A. and Maniscalco, R. (1999). Structural styles and regional tectonic setting of the 'Gela Nappe' and frontal part of the Maghrebian thrust belt in Sicily. Tectonics 18, 655-668.
Longaretti, G., Rocchi, S., Ferrari, L (1991). Il magmatismo dell'avampaese ibleo (Sicilia orientale) tra il Trias e il Quaternario: dati di sottosuolo della Piana di Catania dal Pleistocene al Miocene medio. Mem Soc. Geol. It. 47, 537-555.
Longinelli A., Selmo E. (2003). Isotopic composition of precipitation in Italy: a fist overall map. Journal of Hydrology 270, 75-88.
Pedley, H.M. and Grasso, M. (1993). Controls on faunal and sediment cyclicity within the Tripoli and Calcare di Base basins (Late Miocene) of central Sicily. Palaeogeography, Palaeoclimatology, Palaeoecology 105, 337-360.
McElhinny, M.W. (1978). The magnetic polarity time scale: prospects and possibilities. In "Contributions to the Geologic Time Scale". Am. Ass. Pet. Geol., Stud. Geol. 6, 57-65
Ogniben, L. (1969). Schema introduttivo alla geologia del confine Calabro-Lucano. Mem. Soc. Geol. Ital. 8, 453-763.
Pedley, H.M. (1981). The sedimentology and palaeoenvironment of the southeast Sicilian Tertiary platform carbonates. Sediment. Geol. 28, 273-291.
Pedley, H.M. (1983). The petrology and palaeoenvironment of the Sortino Group (Miocene) of SE Sicily: evidence for periodic emergence. J. Geol. Soc. London 140, 335-350.
Pedley, H.M., Grasso, M., Maniscalco, R., Behncke, B., Di Stefano, A., Giuffrida, S. and Sturiale, G. (2001). The sedimentology and palaeoenvironment of Quaternary temperate carbonates and their

distribution around the northern Hyblean Mountains (SE Sicily). Boll Soc. Geol. It. 121, 233-255.

Pedley, H. M. and Grasso, M. (2002). Lithofacies modelling and sequence stratigraphy in microtidal cool-water carbonate: a case study from the Pleistocene of Sicily, Italy. Sedimentology 49, 533-553.

Pedley, H.M. and Maniscalco, R. (1999). Lithofacies and faunal succession (faunal phase analysis) as a tool in unravelling climatic and tectonic signals in marginal basins; Messinian (Miocene), Sicily. J. Geol. Soc. London 156, 855-863.

Sadori, L. (2001). Holocene climatic change in Central Sicily (Italy). 6th Workshop of the European Lake Drilling Program "High-resolution lake sediment records in climate and environment variability studies". May 11-16, 2001 Postdam, Germany. Terra Nostra 2001/3, 181-186.

Sadori, L. and Narcisi, B. (2001). The postglacial record of environmental history from Lago di Pergusa, Sicily. The Holocene 11 (6), 655-670.

Sartorius Von Walthershausen, W. (1845). Uber die submarine vulkanischen ausbruche in the Tertiar-Formation des Val di Noto im Vergleich mit verwandten Erscheinungen am Atna. Gottingen Studien Abt. A 1, 371-431

Schmincke, H.-U., Behncke, B., Grasso, M., Raffi, S. (1997). Evolution of the northwestern Iblean Mountains, Sicily: uplift, Pliocene/Pleistocene sea-level changes, paleoenvironment, and volcanism. Geol Rundsch. 86, 637-669.

Torelli, L., Grasso, M., Mazzoldi, G., Peis, D. (1998). Plio-Quaternary tectonic evolution and structure of the Catania foredeep, the northern Hyblean Plateau and the Ionian shelf (SE Sicily). Tectonophysics 298, 209-221.

Speranza, F., Maniscalco, R. and Grasso, M. (2003). Pattern of orogenic rotations in central-eastern Sicily: implications for the timing of spreading in the Tyrrhenian Sea. J. Geol. Soc. London 160, 183-195.

Back Cover:
Field trip itinerary and location of planned stops

32nd INTERNATIONAL GEOLOGICAL CONGRESS

FIELD TRIP MAP

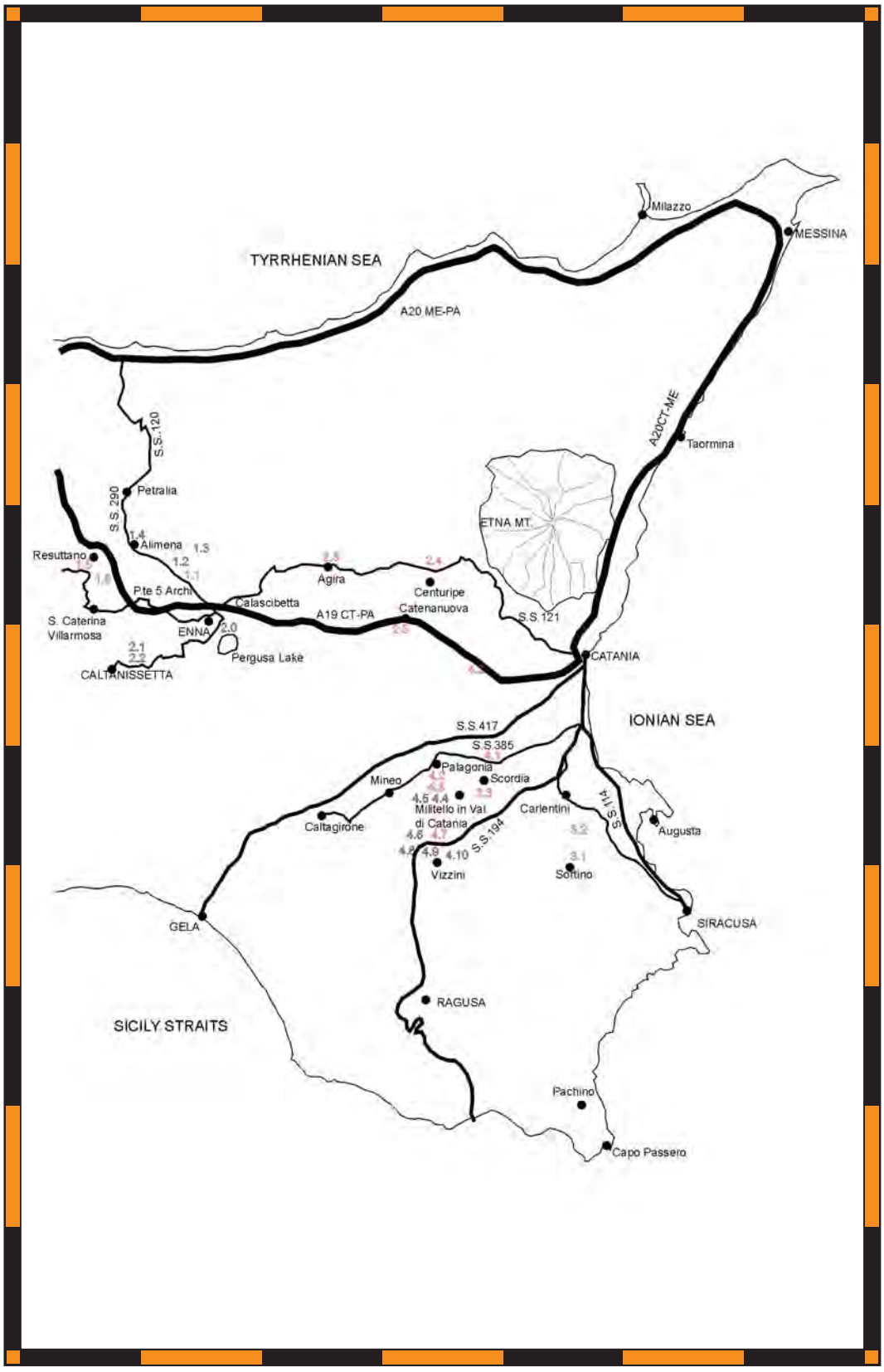

Edited by APAT

Volume n° 2 - from B16 to B33

32nd INTERNATIONAL GEOLOGICAL CONGRESS

CADOMIAN OROGENIC IMPRINTS IN THE BOHEMIAN MASSIF (AUSTRIA, THE CZECH REPUBLIC AND GERMANY)

Leaders:
G. Zulauf, J. Fiala, F. Finger, U. Linnemann

Field Trip Guide Book - B31

Florence - Italy
August 20-28, 2004

Pre-Congress **B31**

The scientific content of this guide is under the total responsibility of the Authors

Published by:
APAT – Italian Agency for the Environmental Protection and Technical Services - Via Vitaliano Brancati, 48 - 00144 Roma - Italy

Series Editors:
Luca Guerrieri, Irene Rischia and Leonello Serva (APAT, Roma)

English Desk-copy Editors:
Paul Mazza (Università di Firenze), Jessica Ann Thonn (Università di Firenze), Nathalie Marléne Adams (Università di Firenze), Miriam Friedman (Università di Firenze), Kate Eadie (Freelance indipendent professional)

Field Trip Committee:
Leonello Serva (APAT, Roma), Alessandro Michetti (Università dell'Insubria, Como), Giulio Pavia (Università di Torino), Raffaele Pignone (Servizio Geologico Regione Emilia-Romagna, Bologna) and Riccardo Polino (CNR, Torino)

Acknowledgments:
The 32nd IGC Organizing Committee is grateful to Roberto Pompili and Elisa Brustia (APAT, Roma) for their collaboration in editing.

Graphic project:
Full snc - Firenze

Layout and press:
Lito Terrazzi srl - Firenze

Volume n° 2 - from B16 to B33

32nd INTERNATIONAL GEOLOGICAL CONGRESS

CADOMIAN OROGENIC IMPRINTS IN THE BOHEMIAN MASSIF (AUSTRIA, THE CZECH REPUBLIC AND GERMANY)

AUTHORS:
G. Zulauf (University of Erlangen-Nürnberg - Germany)
J. Fiala (Department of Geology, Praha - Czech Republic)
F. Finger (University of Salzburg - Austria)
U. Linnemann (State Collections of Natural History, Dresden - Germany)

Florence - Italy
August 20-28, 2004

Pre-Congress

B31

Front Cover:
Field trip itinerary

Leaders: G. Zulauf, J. Fiala, F. Finger, U. Linnemann

Introduction

The Bohemian Massif forms the largest surface 'outcrop' in central Europe where Cadomian (Pan-African) orogenic imprints are well documented (Figure 1). The main goal of the present field trip is to show individual parts of the Bohemian Massif (the Saxo-Thuringian, Teplá-Barrandian, and Brunovistuilian units) where Cadomian imprints are strikingly different. These units are peri-Gondwanan terranes (Armorican Terrane assemblage, ?Avalonia), which also include Florida and the Carolinas in the eastern United States, as well as the Ossa-Morena and Central-Iberian zones of the Iberian Massif. Further remnants of the Cadomian basement occur in the basement units of the Alpine chain, the Carpathians, Turkey, and in the Red Sea surroundings (Murphy et al., 2002, and references therein).

During the field trip Cadomian deformation, metamorphism and igneous activity will be studied at different structural levels, the metamorphic grade of which ranges from very-low to high grade. Major topics are (1) the depositional environment of synorogenic Neoproterozoic and postorogenic Lower Paleozoic rocks, (2) Cadomian igneous activity, (3) Cadomian deformation and related metamorphism, and (4) the geodynamic evolution of the Cadomian belt.

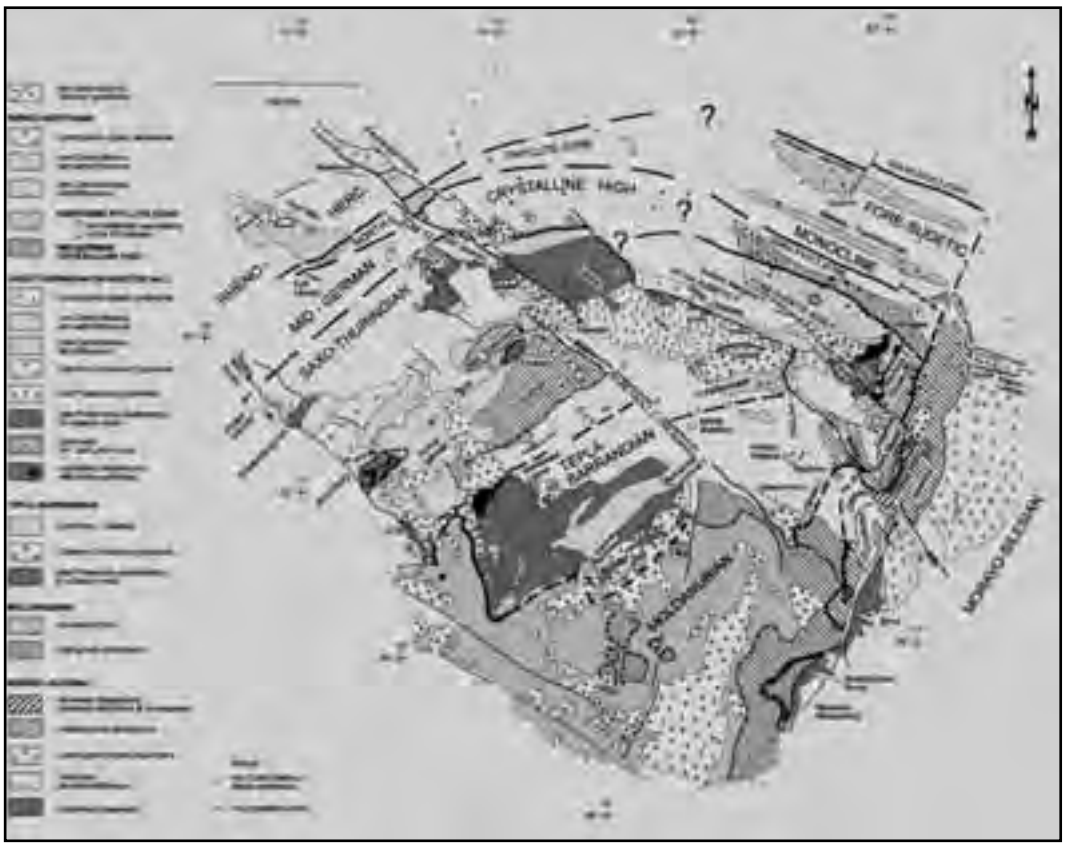

Figure 1 - Geological map of the Bohemian Massif (after Franke and Zelaznewicz, 2002)

The area studied is straddling three major units of the Bohemian massif (the Saxo-thuringian, Tepla-Barrandian and Brunovistulian units) and three different countries (Austria, the Czech Republic and Germany), the latter showing different cultures and history. There are several cities worth seeing, such as Dresden, Prague, Brno and Vienna, all of which will be viewed during the field trip.

Volume n° 2 - from B16 to B33

Regional geological setting

The Saxo-Thuringian unit
(with contributions by R. Romer)

Saxo-Thuringia is a peri-Gondwanan crustal fragment that became incorporated into the Central European part of the Variscan orogenic belt (Figure 2). The oldest volcano-sedimentary rock complexes and plutonic massifs are not older than c. 570 Ma and were formed on the periphery of the West African craton (Linnemann et al., 2000; Linnemann and Romer, 2002). These Late Neoproterozoic to Early Cambrian rock units (ca. 570 – c. 540 Ma) were formed in an active-margin setting by processes that finally led to the build-up of the Avalonian-Cadomian orogenic belt.

In the Saxo-Thuringian part of the Avalonian-Cadomian Arc, subduction-related Cadomian orogenic processes led to the development of Neoproterozoic marginal basins younger than ca. 570 Ma. Tectonically separated remnants of these basins were intruded after the Cadomian orogeny by ca. 540 Ma old plutonic rocks. The Cadomian basement, which involves both sedimentary and magmatic units, was transgressed by Cambro-Ordovician overstep sequences, with depositional gaps during the earliest Cambrian (ca. 540 – 530 Ma) and the Late Cambrian (ca. 500 – 490 Ma), under a passive margin regime (Linnemann, 1995; Linnemann et al., 2000).

"Armorican affinities" (sensu Linnemann et al., 2000), such as the occurrence of a Cadomian unconformity, peri-Gondwanan Cambro-Ordovician faunas, glaciomarine diamictite of the Saharan glaciation during the Hirnantian, and the absence of a Caledonian unconformity, paleogeographically relate Iberia and Armorica, which includes Saxo-Thuringia. Matte (1986, 1991), Tait et al. (1995, 1997), Franke (2000), and Linnemann et al. (2000) demonstrated that the classical "Armorica" of Van der Voo (1979) does not represent a coherent microplate. Therefore, we use the term "Cadomia". Nance and Murphy (1994, 1996) presented a palinspastic reconstruction

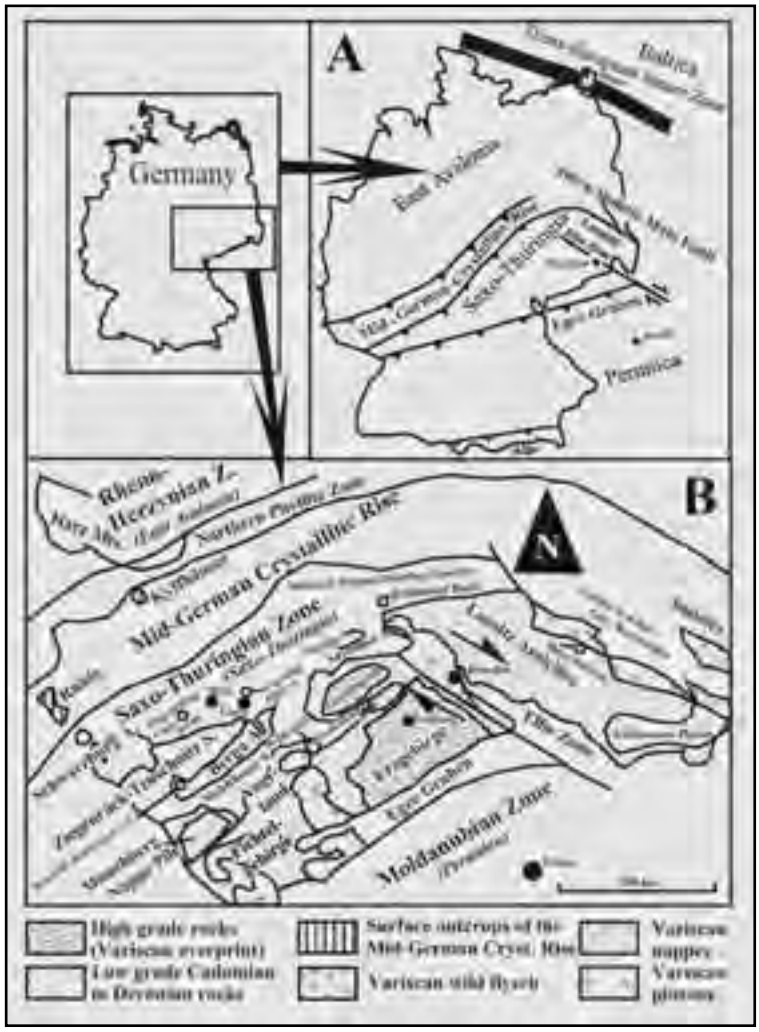

Figure 2 - Location of Saxo-Thuringia; A: present day distribution of Peri-Gondwanan units and their relation to important geological structures in Germany and bordering countries; B: Tectono-stratigraphic units of Saxo-Thuringia and adjoining areas, as well as the position of some deep drillings (circles) and locations mentioned in this paper. Note that the Mid-German Crystalline Rise does not belong to Saxo-Thuringia (from Linnemann et al, 2000).

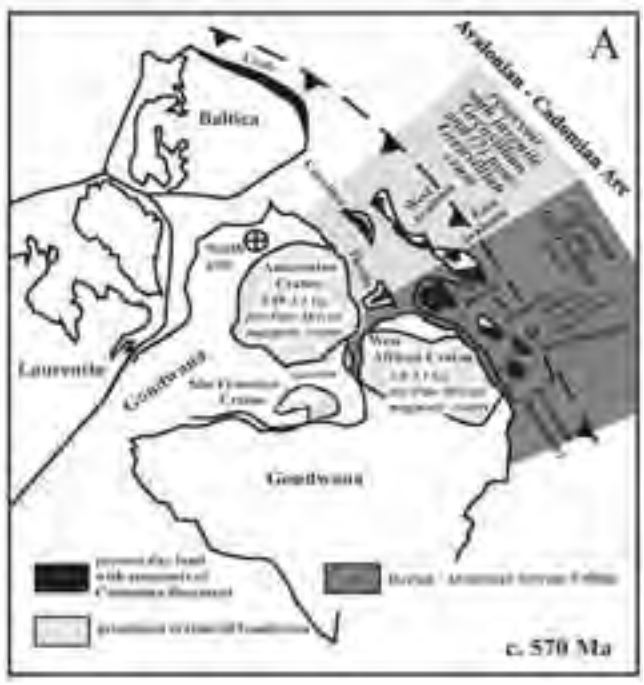

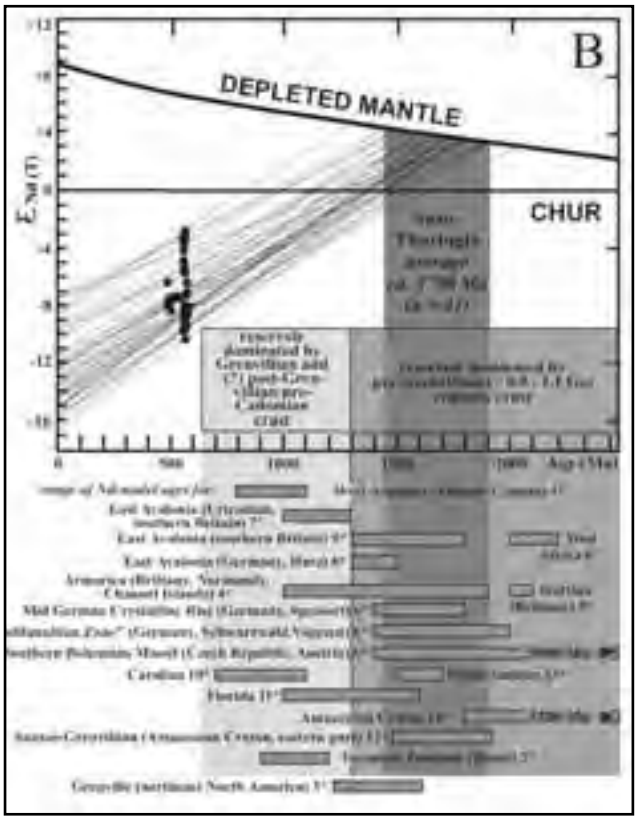

Figure 3 A - Palaeogeography of the Cadomian-Avalonian Arc and related prominent peri-Gondwanan terranes (modified after Nance and Murphy 1994, Linnemann et al., 2000). B. TDM Nd-model ages (DePaolo, 1981) of Saxo-Thuringia.l References of Nd-model ages from other regions, see in Linnemann and Romer, 2002. Depleted mantle curve from DePaolo (1981); CHUR = chondritic uniform reservoir (figure from Linnemann and Romer, 2002).

of the Avalonian-Cadomian Orogenic Belt on the basis of available age data from detrital zircon, initial Nd isotopic compositions, and palaeomagnetic data. This reconstruction was modified from the European point of view by Linnemann et al. (2000), especially due to the addition of basement slivers of the Urals, the change of the position of Iberia, the division of the "classical" Armorica, and the addition of Saxo-Thuringia.

The sedimentary record of Saxo-Thuringia encompasses a time span from the Cadomian arc setting to Early Palaeozoic shelf development, which is representative for large parts of Cadomia. This record not only reflects orogenic crustal growth and recycling within this tectonostratigraphic unit, but also dramatic changes in geotectonic setting and weathering behavior that come along with the uplift and rifting of the Gondwanan margin during the Early Paleozoic. Nd(T) values and resulting model ages of sedimentary rocks and granitoids indicate recycling of old crustal material from the Gondwana mainland. Nd(T) values, furthermore, support paleogeographic reconstructions showing Saxo-Thuringia as a part of the peri-Gondwana margin (Linnemann and Romer, 2002) (Figure 3).

The Neoproterozoic rock units of Saxo-Thuringia were first described in terms of the Cadomian Basement by Linnemann and Buschmann (1995a) after the discovery of the Cadomian unconformity in the core of deep drilling 5507/77 near Gera. The type locality of the Cadomian

Volume n° 2 - from B16 to B33

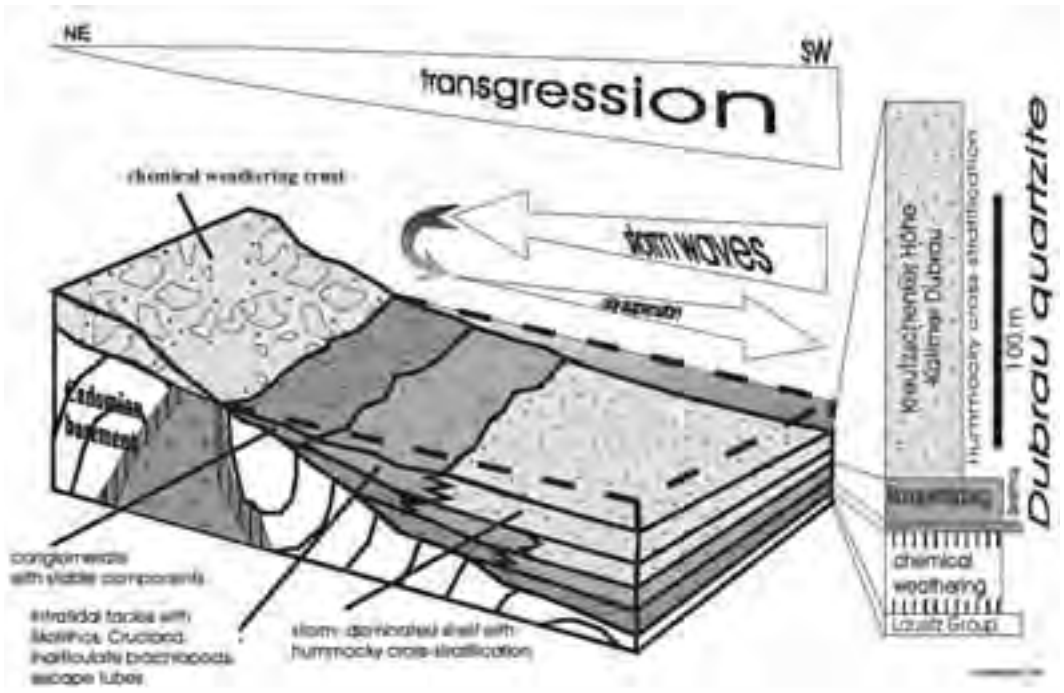

Figure 4 - Model of the Tremadocian transgession in the area of the Monumentenberg and the Hohe Dubrau (from Linnemann and Buschmann, 1995).

unconformity at the surface is located in the area of the Hohe Dubrau at the Monumentenberg, a hill near the village of Gross Radisch in the Lausitz Anticline (Linnemann and Buschmann, 1995b; Linnemann and Schauer, 2000).

The structural complexity of the Neoproterozoic to Lower Carboniferous rock units of Saxo-Thuringia is shown in a simplified geological map (Figure 2). The Cadomian basement of Saxo-Thuringia consists of several back-arc basin remnants that developed on the old Gondwanan basement in a continental arc setting (Linnemann et al., 2000) (Figure 4). The maximum age for sedimentary rocks of the back-arc basins is given by the age of detrital zircon and zircon in ca. 570 Ma granitoid pebbles. One ash layer is dated at ca. 565 Ma (Gehmlich, in Linnemann et al., 2000). The siliciclastic rocks are dominated by graywacke turbidites. In addition, hydrothermal cherts and related effusive volcanic rocks formed during back-arc spreading (Buschmann, 1995). Quartzites derived from the sedimentation of highly mature quartz sands during sea level low stand, and the occurrence of diamictites, show that the Cadomian marginal basins preserved in Saxo-Thuringia were influenced by sea level fluctuations (Linnemann, 1991) and possibly a post-570 Ma Neoproterozoic glaciation, which agrees with a suggested position of peri-Gondwanan crustal units at high latitudes in the southern hemisphere (Scotese et al., 1999).

For parts of the Cadomian basement preserved in Saxo-Thuringia, the continuation of sedimentation in Cadomian marginal basins from the Neoproterozoic up into the Early Cambrian cannot be excluded. Several dated, post-tectonic, granitoid plutons indicate that the Cadomian orogeny ended between 540 and 535 Ma (Gehmlich, in Linnemann et al., 2000).

Archaeocyathids, trilobites, and small shelly fossils (Elicki and Debrenne, 1993; Geyer and Elicki, 1995; Elicki, 1997) demonstrate that the Early Palaeozoic overstep sequence with passive margin signatures overlying the Cadomian unconformity starts post-530 Ma in the Atabanian or Ovetum, respectively. This palaeontological data restricts the time span available for the denundation of the Saxo-Thuringian part of the Avalonian-Cadomian Arc, to a small window between ca. 535 and ca. 530 Ma. Lower Cambrian siliciclastic and carbonate rocks and Middle Cambrian sandstones

overly the Cadomian basement at several places (drill holes; Buschmann et al., 1995). Carbonate sediments, in several levels intercalated with red-bed deposits, and fauna assemblages, indicate a palaeogeographic position of Saxo-Thuringia as a part of the Iberian-Armorican Terrane Assemblage close to the equator (McKerrow et al., 1992; Elicki, 2000). Mafic sills and dykes emplaced in Lower Cambrian deposits formed under conditions of thinned continental crust (Jonas et al., 2000).

After a gap in sedimentation and formation of a chemical weathering crust during the Late Cambrian, which probably was related to block tilting and uplift, the Saxo-Thuringian part of the peri-Gondwana shelf was denuded again (Linnemann and Buschmann, 1995; Linnemann et al., 2000). Most of the Lower to Middle Cambrian deposits were reworked and eroded. Only in areas with originally thick sedimentary successions, such as local graben structures that developed as Cambrian pull–apart basins on the peri–Gondwana shelf (Nance and Murphy, 1991), were Lower to Middle Cambrian basin remnants locally preserved in Saxo-Thuringia.

After this second phase of denudation during the Late Cambrian (500 to 490 Ma), the Saxo-Thuringian shelf was transgressed during the Tremadoc (Linnemann et al., 2000). The disconformity between Lower to Middle Cambrian rocks and Tremadocian Quartzites with a basal conglomerate is only demonstrated in the drillcores Heinersdorf 1 & 2, first described by Wucher (1967). The maturity of Tremadocian quartzites and sandstones, which contain the reworked Upper Cambrian chemical weathering crust, is very high. Ordovician siliciclastic sedimentation on the shelf, and thus, also, shelf-subsidence, reached a maximum during the Tremadoc, when more than 3000 m of sediments were deposited. For comparison, Cambrian (< 1000 m) deposits and Arenig-through-Ashgill deposits combined only reach 500 m in thickness, whereas Silurian (ca. 50 m) deposits are subordinate. This unusually-high sedimentation rate during the Tremadoc is interpreted as reflecting the onset of rifting (Linnemann et al., 2000).

Saxo-Thuringia became a part of the Variscan orogenic belt during the Devonian to Early Carboniferous collision processes (e.g., Matte, 1986, 1991; Franke,

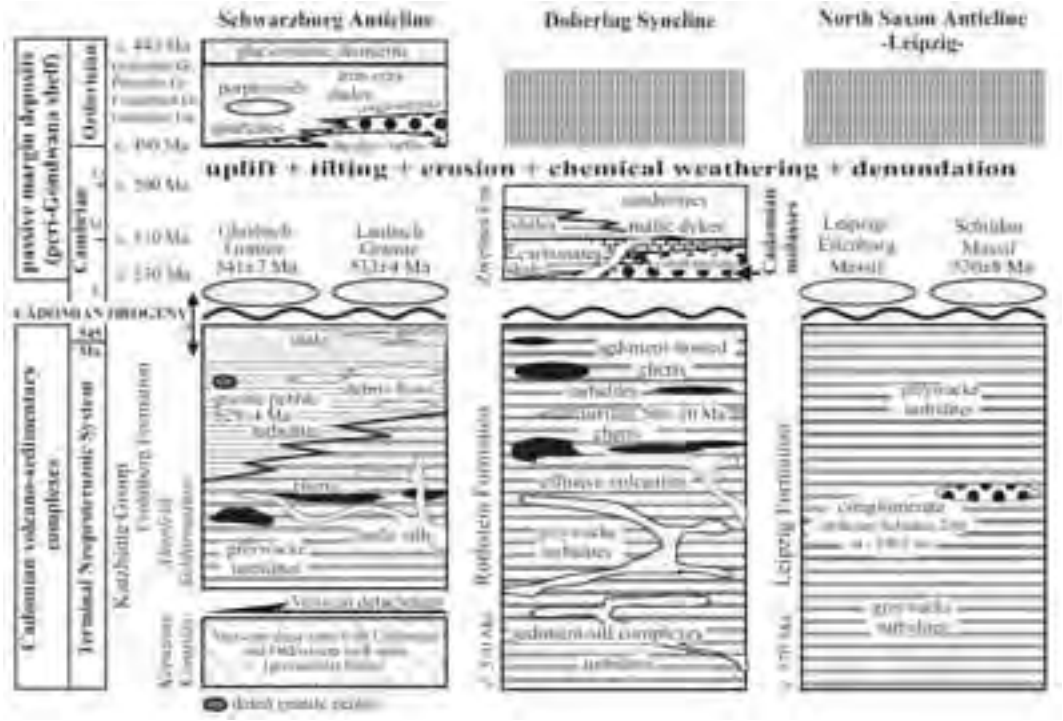

Figure 5 - Tectonostratigraphic columns for Neoproterozoic to Cambro-Ordovician rocks of the Schwarzburg Anticline, Doberlug Syncline, and the Leipzig Complex of the North Saxon Anticline (from Linnemann and Romer, 2002).

Volume n° 2 - from B16 to B33

2000). During the Variscan extensional collapse and transpressional slivering, Saxo-Thuringia was divided into several tectono-stratigraphic units. Low-grade Cadomian to Early Palaeozoic units in Saxo-Thuringia occur in five main outcrop areas, which correspond to main structural units of this region: (1) the Schwarzburg Anticline (the Katzhütte and Frohnberg Groups), (2) the Northsaxon Anticline (the Clanzschwitz Group), (3) the Elbe Zone (the Weesenstein Group), (4) the Lausitz Anticline (the Lausitz Group), and (5) the Doberlug Syncline (the Rothstein Group).
The Lausitz Anticline and the Elbe Zone are objects of this field trip. For completeness, descriptions of the other units are included in this excursion guide.

The Schwarzburg Anticline: The Schwarzburg Anticline is the most complete succession of a volcano-sedimentary rock pile affected by the Variscan orogeny in Germany (Figure 5). The southeastern flank of the structure, originally mapped and described by von Gaertner (1944) and redescribed by many authors, represents the type section of Neoproterozoic to Lower Carboniferous sedimentary rocks in Saxo-Thuringia. The centre of the Schwarzburg Anticline was overprinted under greenschist-facies conditions. The traditional term of von Gaertner for this unit is "Kernzone", which should be translated by "core zone". Usually the "Kernzone" is described as the lowest part of the Neoproterozoic rock pile in a relatively undisturbed succession (e.g. Bankwitz and Bankwitz, 1995). Biostratigraphic data (Heuse, in Estrada et al., 1994), sequence stratigraphy (Linnemann and Buschmann, 1995), and geochronology (Gehmlich, in Linnemann et al., 2000), however, demonstrate gaps in the sedimentary record for the largest part of the Cambrian. Linnemann et al. (1999, 2000) re-interpreted the "Kernzone" as a part of a deeper crustal level that became detached from the low-grade Cadomian basement and the overlying Palaeozoic strata by Variscan transpression. The "Kernzone" consists of a tectonic mixture mostly of predominantly Cadomian (Neoproterozoic) meta-sedimentary rocks and a few Ordovician rock units (Linnemann et al., 1999, 2000).
The low grade part of the Cadomian basement in the Schwarzburg Anticline consists in its lowest part (Katzhütte Group) of graywacke turbidites accompanied by dark shales and hydrothermal cherts and associated mafic sills. The Frohnberg Group in the upper part is dominated by graywacke turbidites and dark shales. The youngest member is a quartzite related to a sea-level low-stand. The Cadomian sedimentary rocks were intruded after Cadomian deformation by several granites, dated at 541±7 Ma and 533±4 Ma (Gehmlich in Linnemann et al., 2000). The Ordovician overstep sequence starts with a 490-Ma-old rhyolite (Gehmlich in Linnemann et al., 2000), tuffites and conglomerates, which were described by von Gaernter (1944) as "Konglomeratische Arkose" (= "conglomeratic arkose"). The nearly 3500-m-thick Ordovician succession is continued by shales, quartzites, subvolcanic porphyroid intrusions, sedimentary iron ores, and the glaciomarine diamictite of the Saharan glaciation (Hirnantian). A mid–Ashgillian limestone layer of only 1 m thickness occurs 2 m below the base of the diamictite. A detailed stratigraphic column of the Ordovician has been published by Linnemann (1998) and Linnemann et al. (2000).

The Berga Anticline: The Cadomian Basement is not exposed in the Berga Anticline. Up to the 1960s only Ordovician to Devonian strata were known. The anticline is bound by Lower Carboniferoious flysch deposits of the Teuschnitz – Ziegenrück Syncline in the northwest and the Mehltheuer Syncline to the southeast. Cambrian sedimentary rocks were discovered unexpectedly in the cores of the drillings Heinersdorf 1 & 2 (Wucher, 1967). The succession is overprinted by greenschist facies metamorphism and consists of quartz phyllites and black to gray marbles. Palaeontological data confirm the Early to Middle Cambrian age of the pre-Ordovician part of the core (Blumenstengel, 1980). The Cadomian basement unfortunately was not reached by the drillings. The most important feature of the Heinersdorf 2 drilling is a disconformity between Lower to Middle Cambrian strata and Ordovician siliciclastics, which clearly documents the Upper Cambrian gap within the succession. The Lower to Middle Cambrian rocks obviously were transgressed during the Tremadoc with a sharp contact and a conglomerate at the base. The lithological spectrum consists only of stable components (quartzites, cherts, and silicified hornfelses) resistant to chemical weathering. The Cambrian rocks in the drill are overlain by the Upper Frauenbach Quartzite (Tremadoc). A number of additional Tremadocian strata present in the Schwarzburg Anticline (e.g. Goldisthal Group) are not found in the Berga Anticline or in the Heinersdorf 2 borehole (Linnemann et al., 2000). This observation demonstrates that the transgression during the Tremadoc was highly diachronous, possibly

documenting a palaeorelief during the Late Cambrian that may be related to block tilting and the formation of grabens and horsts in Saxo-Thuringia, combined with an Late Cambrian tectonically forced regression. Consequently, Lower to Middle Cambrian sedimentary complexes were preserved only in grabens, whereas the rest was eroded. The Heinersdorf 1 and 2 drillings represent relict Cambrian deposit from such a graben filling. The local observations at the Heinersdorf 1 and 2 drillcores most probably reflect the Late Cambrian history which is characteristic of the Saxo-Thuringian peri–Gondwanan basement, since, with the exception of the Doberlug Syncline, all localities with Cadomian basement show Ordovician sediments, whereas Cambrian sediments are not present.

The Doberlug Syncline: This syncline consists of the Cadomian Basement, as represented by the Rothstein Formation and the Zwethau Formation, containing Lower to Middle Cambrian sedimentary rocks (Figure 5). With the exception of the Rothstein Fels, which consists mostly of Cadomian hydrothermalitic cherts, all units are known from drillings only. The Rothstein Formation was described by Buschmann (1995) and Buschmann et al. (1995, 2001). The succession predominantly consists of graywacke turbidites that commonly show soft-sediment deformation. The sedimentary rocks are accompanied by sills and effusive volcanites. The latter ones generally are associated with exhalative hydrothermal cherts. A tuff was dated at 566 ±10 Ma (Buschmann et al., 2001). Cadomian molasses-containing pebbles derived from the Rothstein Formation were described by Buschmann (1995) from drillhole 1706. Lower to Middle Cambrian shallow marine carbonates, shales, and sandstones overlie the Cadomian basement. There Lower Cambrian mafic sills occur (Jonas et al., 2000). Cadomian plutonic and Ordovician sedimentary rocks are not known.

The Northsaxon Anticline: The Northsaxon Anticline is structurally heterogeneous. At its northern border, it is bound by the Doberlug Syncline and parts of the Mid-German Crystalline Rise. The largest part of the anticline consists of Cadomian basement, which in the south is overlain unconformably by Ordovician shelf sediments. To the east, the Cadomian basement of the Northsaxon Anticline continues into the Lausitz Anticline. The Cadomian basement of the anticline consists of two main tectono-stratigraphic complexes, which are different in terms of sedimentary development and other geological observations in the field. Both the Leipzig Complex and the Clanzschwitz Complex are described separately.

The Leipzig Complex consists of graywacke turbidites and intercalated dark gray to black mudstones (Figure 5). The sedimentary rocks are summarized as the Leipzig Group. The only surface outcrop is located in Klein – Zschocher, which is a part of the city of Leipzig. All other parts of the whole area are only known from drillings. From the core of the Schildau 2/66 borehole, a conglomerate composed of predominatly granitoid pebbles is described at a depth of 148.6 m below surface. The well rounded pebbles are 1 to 5 cm in diameter approximately, and are dispersed in the graywacke matrix. The ca. 1-m-thick conglomerate is interpreted as being a debris-flow deposit associated with the turbidites, as there is no evidence for an unconformity within the Cadomian succession. After Cadomian deformation, the Leipzig Group was intruded by the granitoids of the Leipzig–Eilenburg massif and the Schildau Massif, which are only known from drill cores. The age of instrusion of the latter one has been determined at 530 ±8 Ma (Hammer et al., 1999). The Cambro-Ordovician overstep sequence does not exist here, and may have been eroded during post–Variscan denudation.

The second part of the Northsaxon Anticline is presented by the Clanzschwitz Complex. This unit is divided into the Cadomian part of the section, the so-called Clanzschwitz Group, including the Laas Granodiorite, and the Ordovician overstep-sequence (Figure 6). The lower part of the Clanzschwitz Group is composed of mudstones, with a few intercalations of graywacke beds. These rocks are overlain by quartz phyllites and quartzites, around 20 m in thickness, followed by diamictites with a matrix of graywacke and conglomerates. The pebbles within this unit predominately include graywackes, quartzites, and granitoids. One granite pebble was dated by Gehmlich (in Linnemann et al., 2000) at 577 ±3 Ma. There is no consensus concerning the interpretation of the diamictites as glaciomarine deposits or debris flows (see also the sub-chapter entitled "Elbe Zone – Weesenstein Complex"). After the Cadomian deformation, the Clanzschwitz Group was intruded by the ca. 537-Ma-old Laas Granodiorite (Gehmlich, in Linnemann et al., 2000). The Ordovician overstep-sequence is presented by the quartzites and conglomerates of the Collmberg and the Hainichen-Otterwisch Formations. Because of the weathering processes during the Late Cambrian, the conglomerates consist of stable components like pebbles of quartzites, hydrothermal quartz, cherts,

Volume n° 2 - from B16 to B33

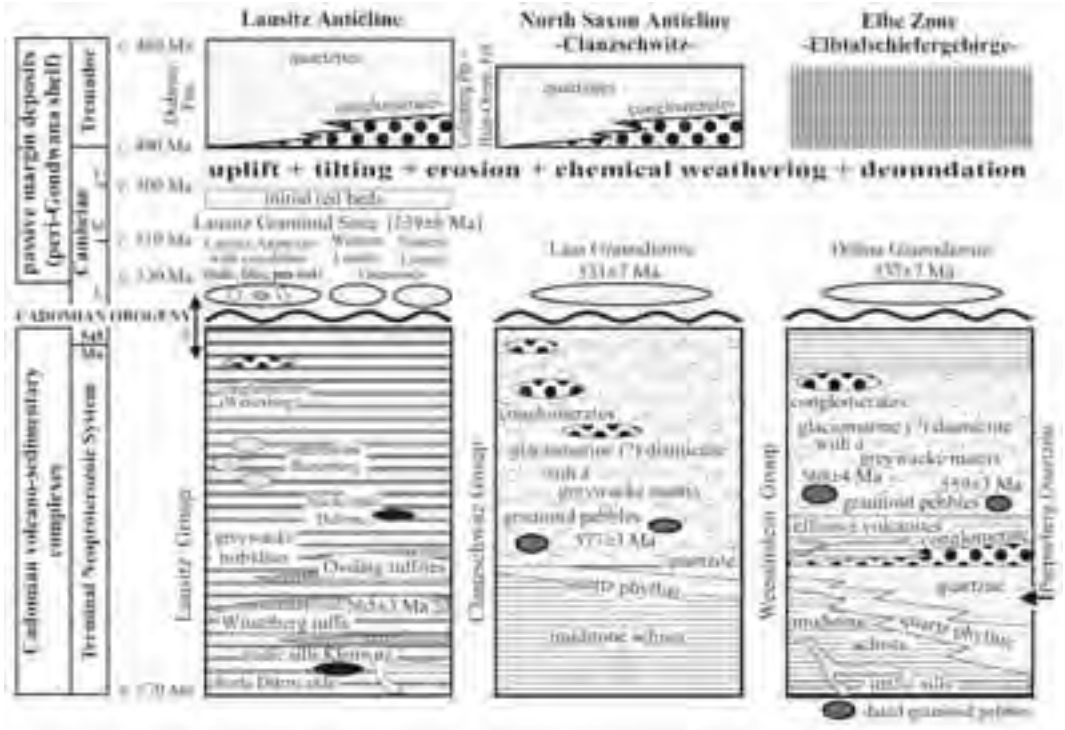

Figure 6 - Tectono-stratigraphic columns for Neoproterozoic to Cambro-Ordovician rocks of the Lausitz Anticline, the Clanzschwitz Complex of the North Saxon Anticline, and the Weesenstein Complex of the Elbe Zone (from Linnemann and Romer, 2002).

and hornfelses. Ichnofossils in the quartzites belong to the Cruziana facies (e.g. Cruziana semiplicata SALTER).

The Lausitz Anticline: The Lausitz area is traditionally described as an anticline, a custom that also is maintained here, although the basement of the Lausitz (from Latin: "Lusatia") represents a horst with a tilted peri-Gondwanan crustal profile (Figure 6). Its deepest units, exposed to the southeast, are dominated by a complex of different plutons. The Cadomian part of the magmatic rock suite is summarised here as the Lausitz Granitoid Suite, which is composed of granodiorites and granites from the western and the eastern Lausitz domains. The outer part of the western Lausitz shows abundant S-type two–mica granodiorite, with locally abundant xenoliths of meta-basalts, felsic remnants of altered volcanic (calc-silicate) rocks, meta-graywackes, and quartzites. The age of the Lausitz Granitoid Suite is disputed. The best estimate for a maximum age at 565 ±3 Ma (Pb/Pb age, Gehmlich, in Linnemann et al., 2000) and 574 ±8 Ma (SHRIMP, Nasdala, in Linnemann et al., 2000) is obtained from an ash layer within the Cadomian graywackes of the Lausitz Group which are intruded by the granitoids. Earlier-reported zircon ages are in part distinctly older. A series of datings yields ages in the range from 540 to 530 Ma (Hammer et al., 1999; Gehmlich in Linnemann et al., 2000), although there are a few younger intrusions, such as the Rumburk Granite (ca. 490 Ma) and Variscan plutons.

Sedimentary units mostly occur in the northwestern part of the tilted horst structure of the Lausitz. The low-grade sedimentary rocks of the Lausitz Group were deformed during the Cadomian orogeny in large open folds, and show a slight contact-metamorphic overprint close to the Lausitz Granitoid Suite. The sediments are dominated by monotonous graywacke turbidites with a few intercalations of dark-gray shale. A number of light gray to gray-green tuff layers, partially altered to calc-silicate rocks, are known from Wüsteberg, near Kamenz, and from a large quarry close to the village of Ossling. The graywacke turbidites locally show early diagenetic concretions,

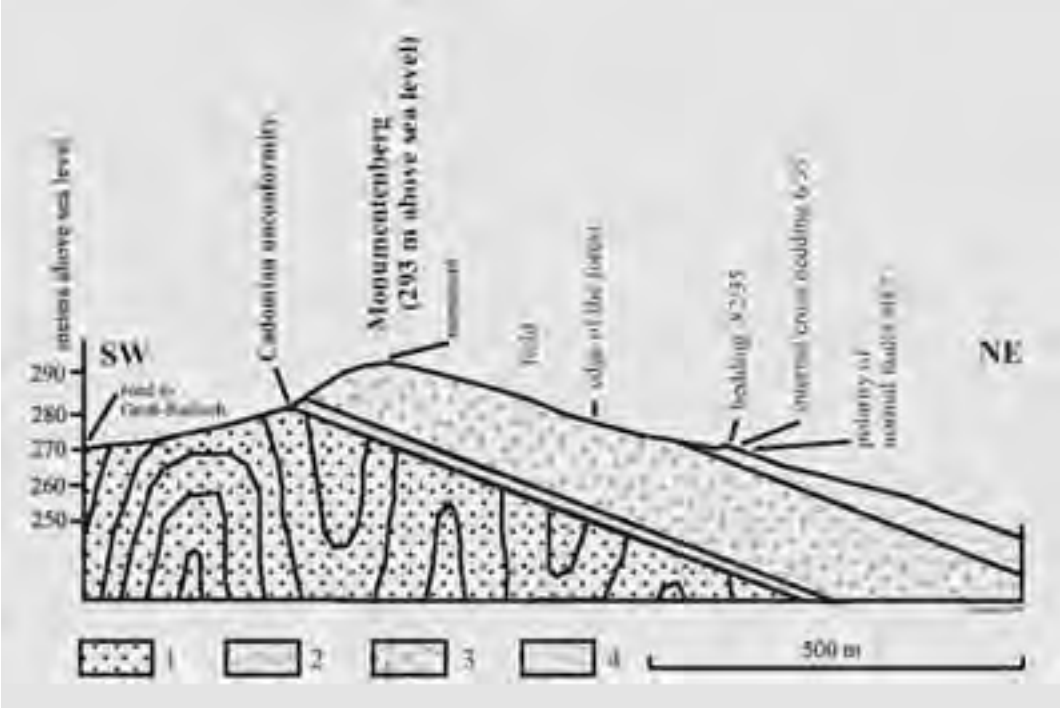

Figure 7 - Cross-section of the type locality of the Cadomian unconformity at the Monumentenberg: 1 - Cadomian graywacke, 2 - basal conglomerate, 3 - intratidal facies with Skolithos, Cruciana, Brachiopods, 4 - storm-dominated facies with HCS (from Linnemann and Schauer, 1999).

which are altered to calc-silicate rock, around rip-up clasts of shale (e.g. the Butterberg quarry, near Kamenz). Fine-grained conglomerates (pebbles < 5 mm) occur in the Wetterberg quarry, near Ebersbach. The clasts are dominated by graywacke, chert, and quartzite, although there are rare clasts of mafic and high-grade metamorphic rocks. There is no evidence of Cambrian sediments resting directly on the Cadomian basement of the Lausitz.

The post-Cadomian overstep-sequence of the Lausitz Anticline, including the type locality of the Cadomian unconformity for Saxo-Thuringia (Linnemann and Buschmann, 1995), is represented by the Dubrau Formation, which is only preserved in the area of the Hohe Dubrau, near Gross Radisch, approximately 40 km to the northwest of Görlitz (Figs. 4 and 7). Inarticulate brachiopod fossils place the c. 200-m-thick Dubrau Formation in the Tremadocian. The basal conglomerate resting unconformably on the Cadomian basement (Linnemann and Schauer, 1999) is composed of weathering-resistent pebbles of quartzite, quartz, and a schorl-cemented breccia. The conglomerate is overlain by variably-silicified sandstone quartzite, with well-preserved primary sedimentary structures. In the lower part, dominantly tidal deposits contain Scolithos sp. and brachiopod shells (Westonisca arachne BARRANDE), as well as poorly preserved specimens of Cruziana sp. In the upper part, the silicified sandstones are characterised by tempestite deposits, such as hummocky cross-stratification and gutter casts. This unit is interpreted as having been deposited in a storm-dominated open shelf (Linnemann and Buschmann, 1995). The top of the section is eroded.

Red beds (denoted as initial red beds in the column) overlying the Cadomian graywacke are preserved only at two locations near Oberprauske (Hohe Dubrau). Their age is only poorly constrained by field data. These red sandstones and shales are younger than the Cadomian basement and older than the conglomerates and quartzites of the Dubrau Formation, i.e., they cover a range from the Lower Cambrian and the lowermost Tremadocian. By analogy with Cambrian red sediments elsewhere in Saxo-Thuringia, we handle these problematic deposits as Lower Cambrian rocks.

Volume n° 2 - from B16 to B33

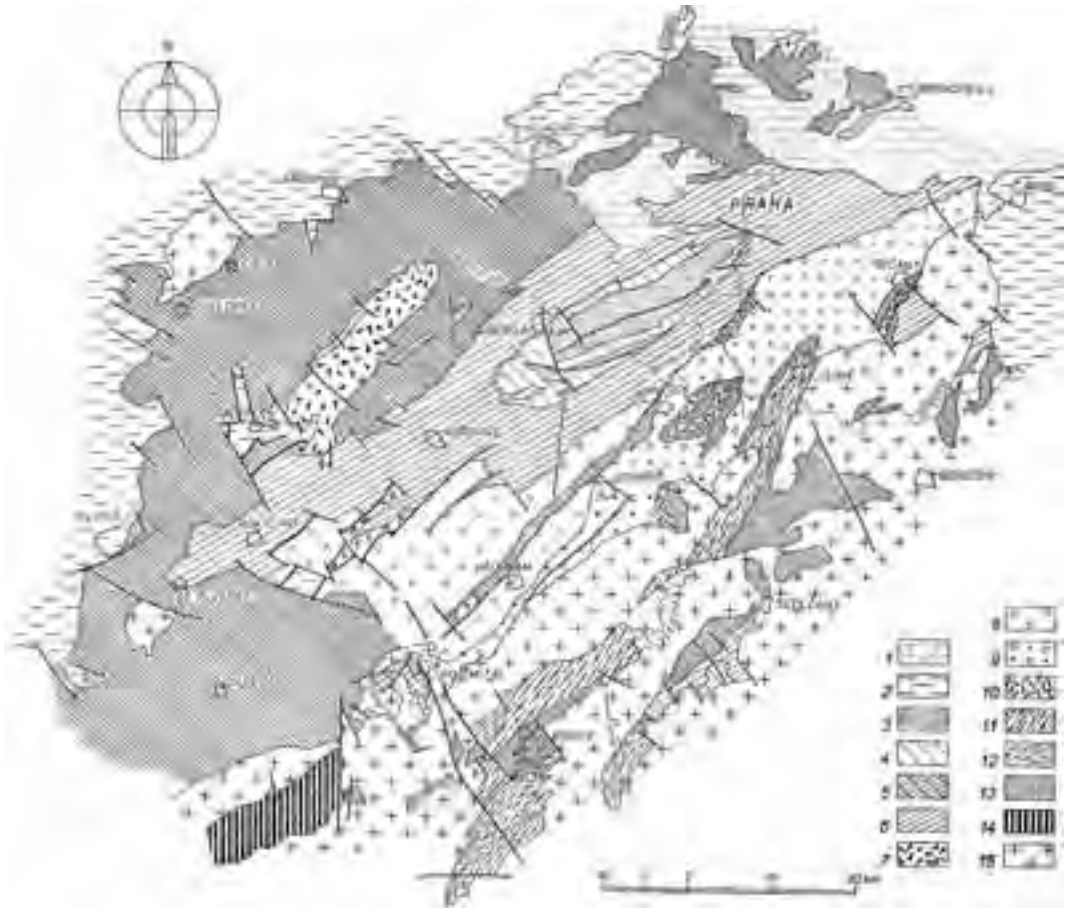

Figure 8 - Geological map of the Barrandian syncline (after Svoboda et al., 1966). 1 = Upper Cretaceous, 2 = Permo-Carboniferous, 3 = Devonian, 4 = Silurian, 5 = Silurian and Ordovician near Ro_mitál, 6 = Ordovician, 7 = K_ivoklát-Rokycany and Strašice volcanics, 8 = Cambrian, 9 = Proterozoic rocks (the Št_chovice group), 10 = Porphyry, 11 = the Jílové zone, 12 = Orthogneiss, 13 = Proterozoic rocks (the Kralupy-Zbraslav group), 14 = Moldanubian zone, 15 = Granitoids

The Elbe Zone: The Elbe Zone is a NW-SE striking major Variscan shear zone with more than 80 km of dextral displacement (e.g., Linnemann, 1995; Linnemann and Schauer, 1999) (Figure 2). The shear zone was active during Early Carboniferous times and separates the high-grade overprinted rocks of the Erzgebirge from the very-low-grade Lausitz Anticline. During Variscan strike-slip movements along the Elbe Zone, three major segments were separated from one originally united remnant of Cadomian basement, which had special features (Linnemann, 1995). These fragments are the Clanzschwitz, the Rödern, and the Weesenstein Complexes, though it should be noted that the Clanzschwitz Complex today is a part of the Northsaxon Anticline. The distinctive feature of the three complexes is the intercalation of diamictites, which may be due to a post-570 Ma Neoproterozoic glaciation or to debris flows. For an interpretation of the diamictites as debris flows, turbidites should be accompanied by turbidites. Turbidites, however, are not known from the Cadomian complexes of the Elbe Zone. Furthermore, the matrix of the diamictites is a diamictite itself, showing very angular clasts of quartz and feldspar.

The Rödern Complex lies within the Elbe Zone, between the Lausitz Anticline and the Meissen Massif (a large, Variscan, granitoid pluton). The Rödern Complex is poorly exposed. It consists of Cadomian graywackes with locally-intercalated pebble–bearing horizons (Schmidt, 1960) and is intruded by the 537

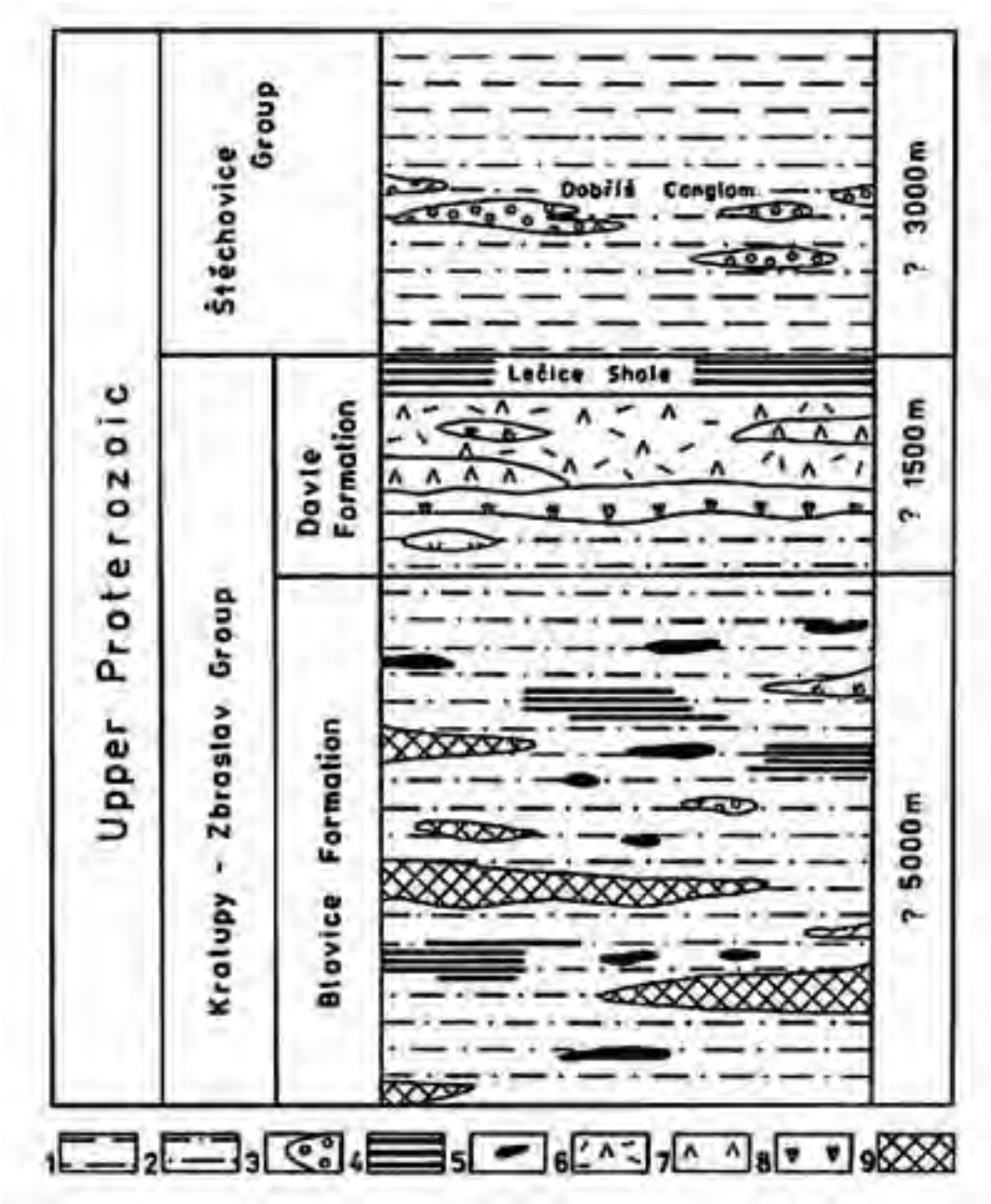

Figure 9 - Proterozoic stratigraphy in the Tepla-Barrandian unit (after Chlupá_, 1993). 1 = siltstone, shale, 2 = siltstone, greywacke, shale, 3 = conglomerate, 4 = black shale, 5 = chert, 6 = pyroclastics of acid and intermediate volcanics, 7 = acid volcanics, 8 = intermediate volcanics, 9 = basic volcanics (predominating).

±7 Ma old Grossenhain Orthogneiss (Gehmlich, in Linnemann, 2000).

The well-exposed Weesenstein Complex crops out about 20 km southeast of Dresden. It is traditionally referred to as "Elbtalschiefergebirge". The excellent outcrop-situation allows an insight into the Elbe ("shear") Zone. The metasedimentary part of

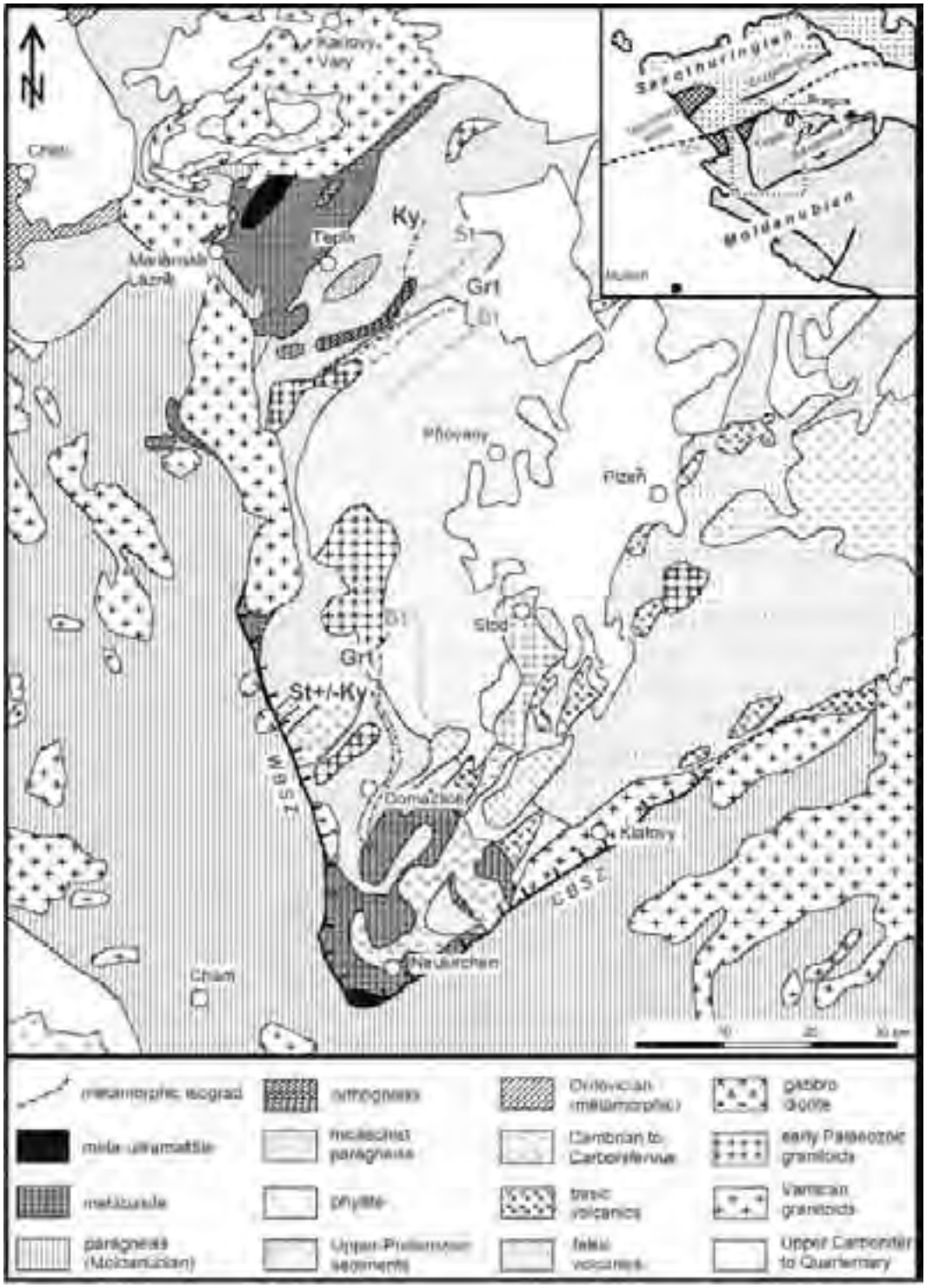

Figure 10 - Geological map of the western part of the Tepla-Barrandian unit (after Zulauf, 1997, and references therein).

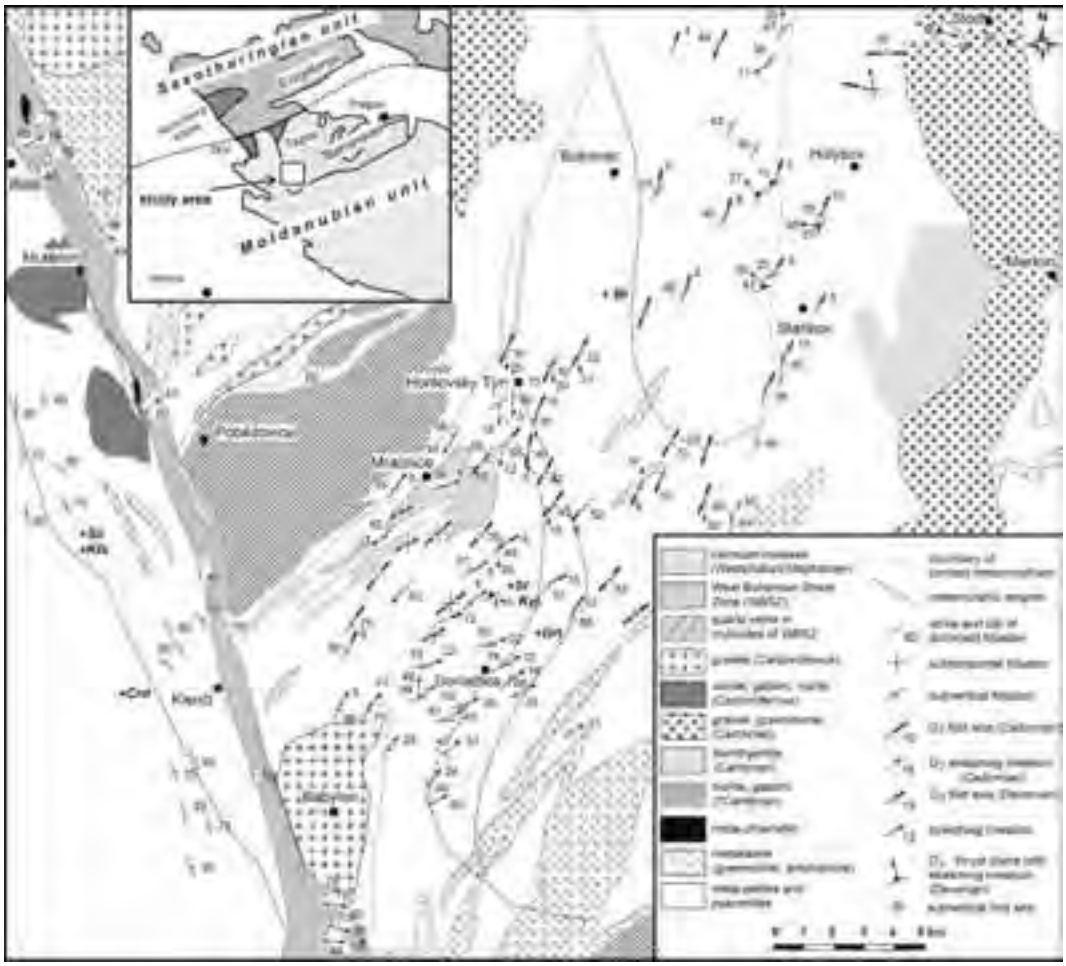

Figure 11 - Geological map of the Doma_lice crystalline complex (after Vejnar, 1982; Zulauf, 1997, and references therein).

the Weesenstein Complex is represented by the Weesenstein Group (Linnemann, 1991), which consists of mudstone schists in the lower part and, higher up, in the section of diamictites with a matrix, of graywackes. Both units are divided by the Purpurberg Quartzite, which shows quite well-preserved primary sedimentary structures. These features characterize the quartzite, accompanied by quartz phyllites at its base, and a conglomerate at the top as deposits that formed during sea level low stand (Linnemann, 1991). The conglomerate consists of weathering-resistant components, like quartz and hornfels pebbles. The quartzite within the Clanzschwitz Complex is interpreted as a more distal equivalent of the Purpurberg Quartzite. Two granite pebbles from the diamictite in the upper part of the Weesenstein Group were dated at 568 ±4 and 559 ±3 Ma (Gehmlich, in Linnemann et al., 2000). At a few locations, the pebbles from the diamictite were enriched as conglomerates, with pebbles derived from granitoids, pegmatites, graywackes, quartzites and felsic as well as mafic volcanites (Schmidt, 1960). In the lower part of the Weesenstein Group mafic sills occur, whereas from the upper part effusive mafic volcanics are known. The Weesenstein Group was intruded after the Cadomian deformation by the 537-±7 Ma old Dohna Granodiorite (Gehmlich in Linnemann et al., 2000).

The Teplá Barrandian unit
(with contributions by W. Dörr and Z. Vejnar)

The Teplá Barrandian unit (TBU) forms an

Volume n° 2 - from B16 to B33

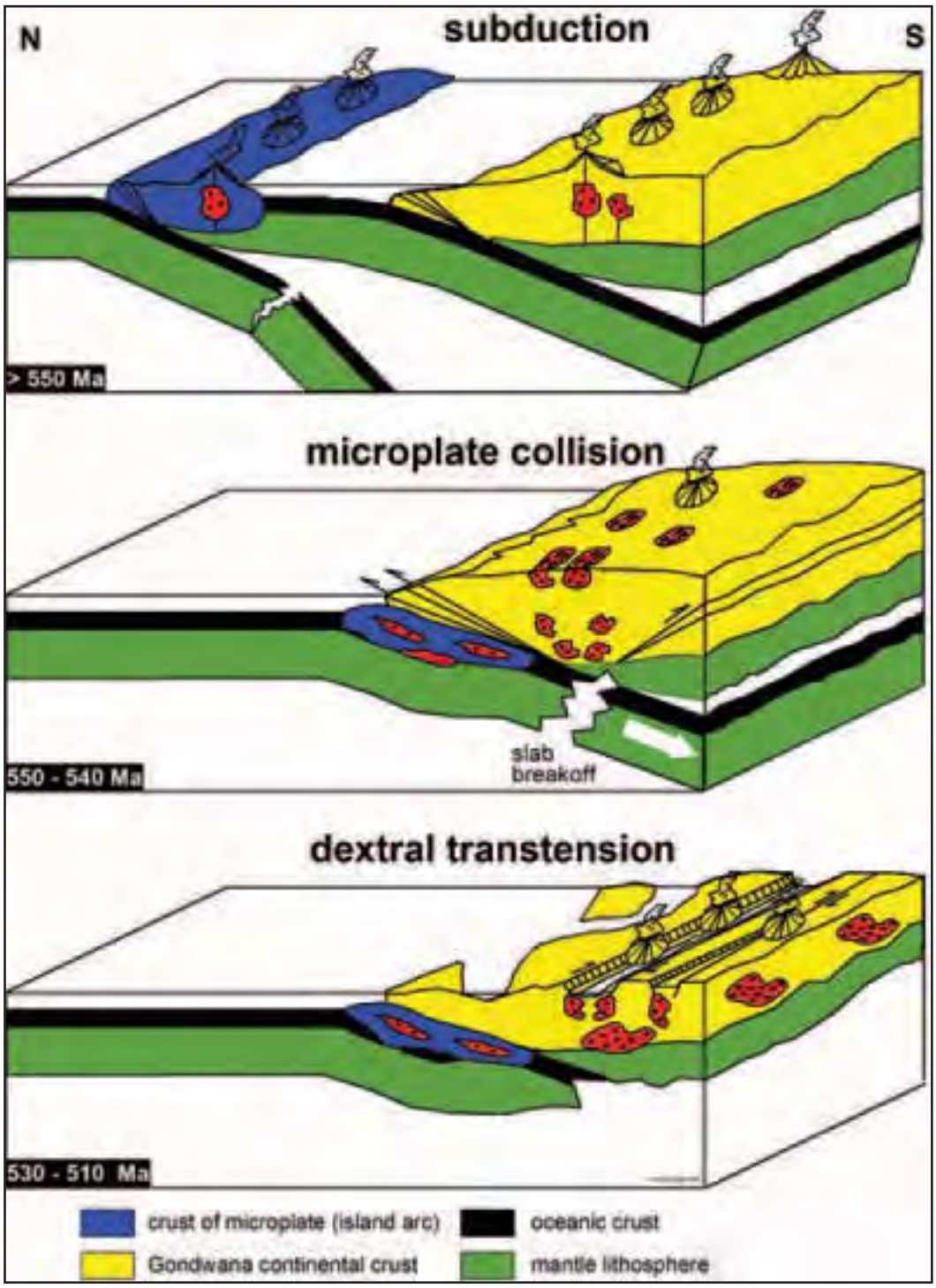

Figure 12 - Geodynamic model for the Cadomian orogeny in the Tepla-Barrandian unit (after Zulauf et al., 1999; Dörr et al., 2002).

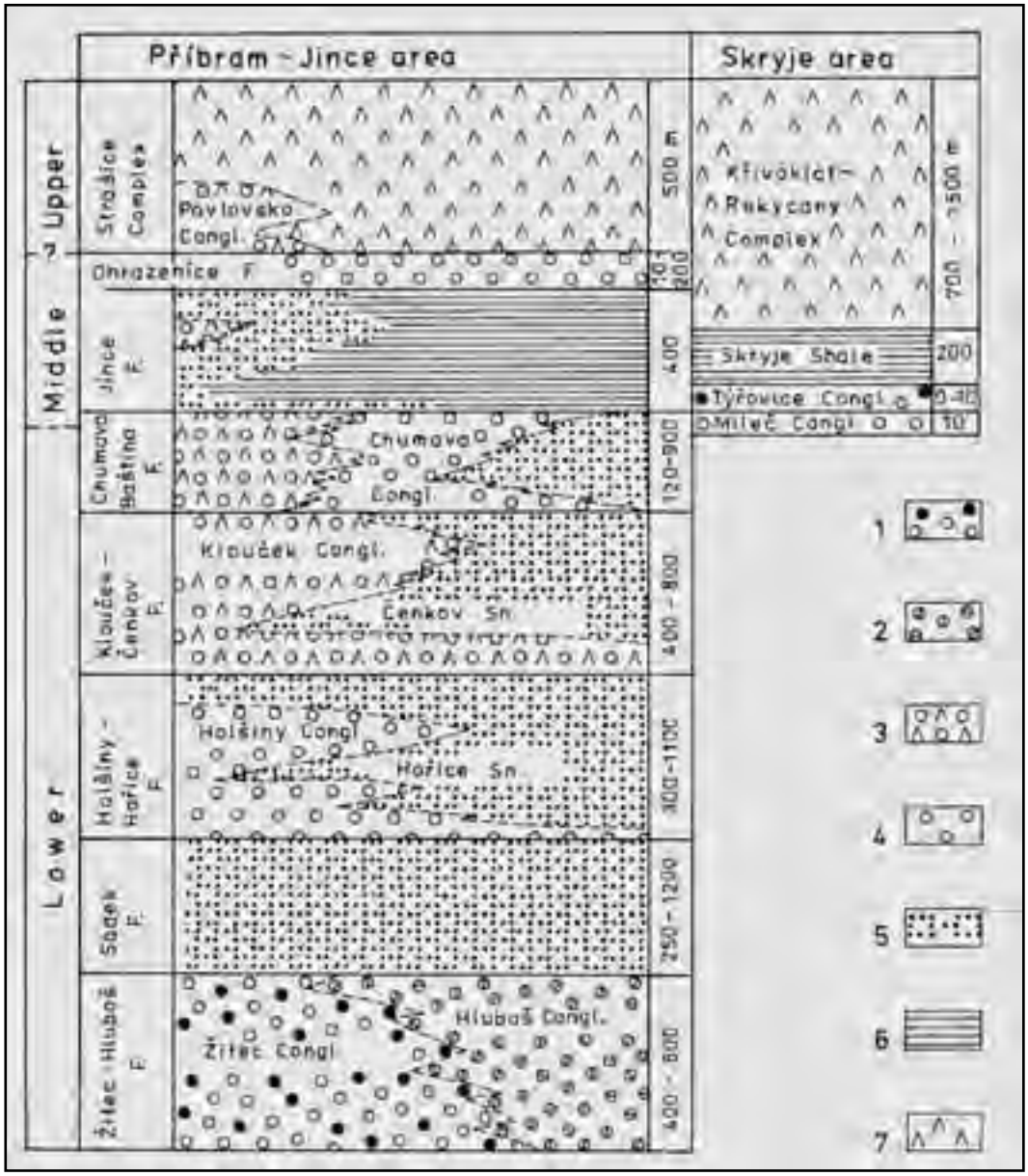

Figure 13 - Cambrian stratigraphy in the Tepla-Barrandian unit (after Chlupá_, 1993, and references therein); 1 = petromictic grey-green conglomerate, 2 = reddish petromictic and oligomictic conglomerate, 3 = conglomerate with volcanic material, 4 = white and grey quartzose conglomerate, 5 = sandstone and greywacke, 6 = siltstone and shale, 7 = effusive volcanics.

exceptional, largely supracrustal complex within Variscan Europe (Figure 1). In contrast to the surrounding units (the Moldanubian and Saxo-thuringian), the TBU was hardly affected by Variscan deformation and metamorphism. This is the reason why the records of Neoproterozoic to Cambrian (Cadomian) imprints are well preserved.

In the Barrandian syncline, located between Prague and Plzeò, unmetamorphic Cambrian to Middle Devonian sediments and volcanics rest unconformably

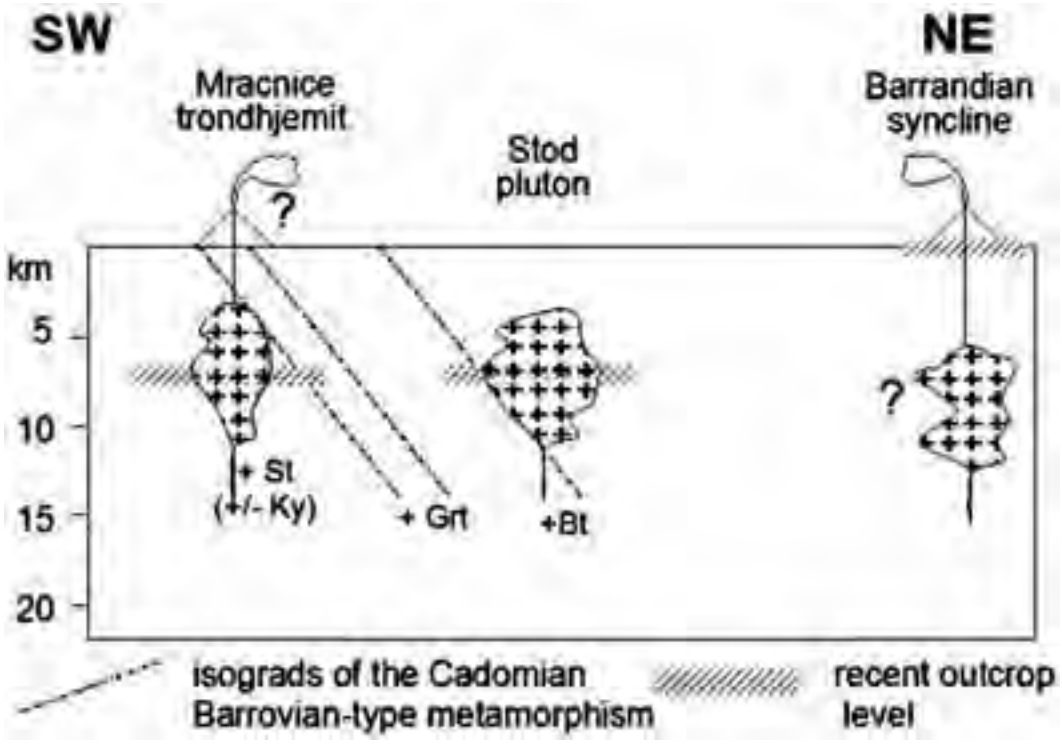

Figure 14 - Cambrian plutons intruded into a tilted crustal profile (between the West Bohemian shear zone and the Barrandian syncline) as is indicated by the tilted metamorphic isograd planes (after Zulauf, 1997).

on a Cadomian basement (Figure 8).

The Neoproterozoic rocks of the TBU can be subdivided into two members (Figure 9). The older *Kralupy-Zbraslav group* (Mašek and Zoubek, 1980) includes the rocks of the Blovice and Davle Formation. The Kralupy-Zbraslav group is present in the northern and western part of the TBU. There are meta-greywackes and –siltstone with intercalations of metavolcanics, as well as cherts and black shales. Mircrofossils suggest a late Riphean to Vendian age of sedimentation (Fatka and Gabriel, 1991). This age is compatible with a K-Ar whole-rock age of volcanics south of Plzeò which yield ca. 630 Ma (Pták and Wartha, 1966; recent decay constant is used). The composition of the volcanics suggests both MORB and subduction-related protoliths (Waldhausrová, 1993).

The *Štìchovice group* is present in the eastern part of the TBU, particularly in a NE-SW trending zone south and east of the Barrandian Paleozoic rocks. It consists of metagreywackes and metasiltstones with intercalated metaconglomerates. Subduction-related magmatism has been dated using magmatic pebbles of these metaconglomerates: 609 +17/-19 Ma, 585 ±7 Ma, and 568 ±3 Ma (U-Pb on Zirkon, Dörr et al., 2002).

Metamorphism in the basement increases from the Barrandian syncline (prehnite-pumpellyite facies, Cháb et al. 1995) towards the W and NW (amphibolite facies, Vejnar, 1982; Žáèek and Cháb, 1993).

Investigations of the crystallization-deformation relationships in the contact aureoles of several Cambrian plutons, described below, allowed separation of Cadomian from Variscan tectonometamorphic imprints. This holds for both the Domažlice crystalline complex (DCC, Figs. 10 and 11), located in the south (Zulauf, 1997; Zulauf et al., 1997), and the Teplá crystalline complex (TCC, Figure 10), located in the northwestern part of the TBU (Dörr et al., 1998; Zulauf, 2001).

There are at least two penetrative *Cadomian* deformation phases, D_1 and D_2, in the TBU. Garnet, staurolite and kyanite, which reflect Cadomian Barrovian-type metamorphism in the TCC and DCC, grew between D_1 and D_2. Quartz veins with pronounced crack-seal fabrics indicate elevated pore fluid pressures and unstable movements during

D_1. During D_2, E-W trending folds developed in the greenschist facies crustal level (west of Stod), whereas a penetrative mylonitic foliation developed in the amphibolite facies part. The D_2 mylonites mainly result from top-to-the-N movements, and late increments of these movements are portrayed by sillimanite that grew in pressure shadows of garnet.

Subsequent to the D_2 stage, a pronounced phase of low-pressure static annealing followed at deeper structural levels. This phase was stronger in the DCC than in the TCC. A similar distribution pattern shows the Cadomian low-pressure metamorphism that is related to D_2. This stage is also stronger in the DCC. Microprobe datings of monazites in amphibolite-facies greywackes of the DCC yield 540 ±16, 542 ±23, and 551 ±19 Ma (Zulauf et al., 1999). Although this age reveals a large uncertainty; it roughly reflects the time of late low-pressure/high-temperature metamorphism in the DCC at T = ca. 600 °C.

The D_2 kinematic data, the distribution of granitoid pebbles within the Upper Proterozoic flysch, and the N-S gradient with respect to the intensity of the D_2-related low-pressure metamorphism and post-D_2 static annealing, indicate a Cadomian magmatic arc located towards the S of the recent TBU (Figure 12).

The thickened Cadomian crust of the TBU collapsed close to the Proterozoic/Cambrian boundary. Normal faulting led to tectonic denudation and to the exhumation of the amphibolite facies rocks of the DCC. This exhumation was associated with a pronounced 'crustal tilting', that is particularly responsible for the present metamorphic isograds of the DCC (Vejnar, 1982; Figure 11). Apart from tectonic denudation, erosive removal of upper crustal levels has contributed to the exhumation of the deeper levels of the DCC. This is documented by the early Cambrian molasse-like sediments of the Barrandian basin (Figure 13). Thus, the Cadomian orogeny ceased no later than the Early Cambrian.

During the late Early Cambrian the Mra¹nice (523 +4/-5 Ma) and the Stod pluton (522 ±2 Ma), and probably also the Pob+žovice pluton, intruded into the tilted crust of the DCC at a depth of ca. 7 km (Zulauf et al., 1997; Figure 14). Similar ages have been derived for plutons of the Neukirchen-KdynÆ crystalline complex, located south of the DCC (Věepadly granodiorite, 524 ±3 Ma; Smézovice tonalite, 523 ±3 Ma; Smézovice gabbro, 523 ±1 Ma; Orlovice gabbro, 524 ±1 Ma; Dörr et al., 2002).

Marine sediments of Middle Cambrian age indicate that during this time the Cadomian relief was largely removed. However, the magmatic activity continued. The Lestkov metagranitoid and the Teplá orthogneiss yield upper-intercept U-Pb zircon ages of 513 +15/-1.3 Ma and of 513 +7/-6 Ma, respectively; the ^{207}Pb / ^{206}Pb age of 516 ±5 Ma of a nearly concordant zircon of the Hanov orthogneiss is a good estimation of its emplacement time (Dörr et al., 1998). Intrusion of associated magmatic dikes continued until early Ordovician times (Košler et al., 1994, Glodny et al. 1998). Despite their emplacement within thinned, extending Cadomian crust, both the plutons and the dikes are mainly of kalkalcalic affinity (Dörr et al., 1998). Most of them intruded into NE-SW- to ENE-WSWtrending, transtensive shear zones (Zulauf and Helferich, 1997). Along these shear zones the metamorphic isograds of the DCC, and probably also the Stod pluton, have been dextrally displaced by ca. 6 km (Figure 11).

The melt temperature of the Cambrian plutons varies, according to their composition, between 750 °C (trondhjemite) and 850 °C (diorite). Thermal modelling indicates that the cooling of the plutons was relatively slow. Thus, high-temperature low-viscosity deformation could occur in the synkinematically emplaced plutons for relatively long periods, from ca. 0.2 to ca. 1.5 m.y. (Zulauf, 1997). The synkinematic dikes were partly sheared under very high temperatures within periods of a few hours to a few days. In one particular case, a minimum strain rate of $2.8 * 10^{-6}$ s^{-1} has been calculated (Zulauf and Helferich, 1997). These phenomena indicate that the melts markedly softened the crust during Cambrian transtension.

The Cambrian transtension introduced the large-scale Ordovician rifting that led to the separation of the TBU from Gondwana, forming a part of the Armorican terrane assemblage (ATA, Tait et al., 2000). The northern drift of Armorica was associated with both production and destruction of oceanic lithosphere. From ?Silurian to Early Devonian times the lithosphere below the Saxo-thuringian ocean was subducted towards the SE beneath the Cadomian basement of the TBU. This *Variscan subduction* is well documented in the eclogite-bearing Mariánské-LáznÆ complex (MLC), situated at the boundary between the Saxo-Thuringian and the TBU (Figure 10). U-Pb zircon dating of gabbropegmatite yields an upper, nearly concordant intercept in the concordia diagram at 496 +/- 1 Ma interpreted as magmatic intrusion age (Bowes and Aftalion, 1991), which reflects initial rifting. Comparable eclogite-bearing

Figure 15 - Geology of the Brunovistulian block, as far as is known from drillings and the exposed basement massifs. Mainly after Dudek (1980) and official maps of the Czech Republic. Inset shows the presumed extent of the Brunovistulian (horizontally hatched), according to Dudek (1980), and its position in the tectonic framework of the Central European Variscides.

complexes, with protoliths, metamorphic records, and cooling ages similar to those of the MLC, have been found in the Münchberg klippe and in the Erbendorf Vohenstrauss zone (ZEV; Figure 1). The eclogites of all these crustal domains are interpreted as resulting from Silurian to Devonian southeastward subduction of 'Saxo-thuringian ocean' lithosphere beneath the Teplá Barrandian plate (Matte et al., 1990; Franke, 2000).

Variscan continent-continent collision of the Teplá Barrandian and Saxo-Thuringian units started during the early Late Devonian (Franke et al., 1995). During this time the intensity of the collapse of the overthickened wedge increased, promoting further extensional faulting and the exhumation of the deeply subducted rocks. Extensional movements led to strong crustal tilting, as is indicated by the metamorphic isograds in the TCC (Figure 10).

Along with the continent-continent collision, the convergent movements migrated towards southeast affecting also the Paleozoic cover of the Barrandian syncline. The F_3 folding in the Stod-Holýšov area started at ca. 370 Ma (Zulauf, 1997) which is close to the break in sedimentation of the Barrandian basin. Finally, the NW-SE compression, which persisted over several million years, led to an Upper Devonian mega-pop-up structure that includes NW vergent folds and thrusts in the northwestern part, including the TCC, and SE vergent folds and thrusts in the southeastern part of the TBU, including the DCC. There is a remarkable time gap of more than 10 M yrs. between the development of the structures in the N and those in the S.

Although Cadomian Barrovian-type mineral assemblages are present in the TCC, there is clear evidence that the major Barrovian imprint occurred during the Variscan cycle: (1) northwest of the staurolite isograd the Cambrian granitoids have been pervasively deformed and changed into mylonitic orthogneiss (Teplá and Hanov orthogneiss; Dörr et al., 1998; Zulauf, 1997), whereas the Lestkov granitoid, largely situated in the garnet zone, does not show a pervasive mylonitic fabric; (2) Variscan garnet developed in pressure shadows behind Cadomian garnet (Zulauf, 1997); (3) andalusite of early Ordovician pegmatites is replaced by Variscan kyanite (Žáèek, 1994); (4) cordierite in the northern contact aureole of the Lestkov pluton is replaced by staurolite (Cháb and Žáèek, 1994), indicating that the staurolite isograd reflects the Variscan cycle; (5) ^{39}Ar-^{40}Ar and K-Ar dating of hornblende and white mica from the TCC yield 383 Ma and 366-371 Ma, respectively (Dallmeyer and Urban, 1998; Wemmer and Ahrendt, unpublished data.; Kreuzer et al., unpublished data). The hornblende ages suggest a Devonian temperature of more than ca. 500° C for the northwestern part of the TCC, assuming a closure temperature of 500° C for the K-Ar isotopic system of hornblende.

Investigations of the crystallization-deformation relationships in the TCC indicate that the biotite and garnet isograd of Cháb and Žáèek (1994) (Figs. 1 and 3) reflect the Cadomian cycle, whereas the staurolite, and probably also the kyanite isograd reflect the Variscan cycle (Dörr et al., 1998; Zulauf, 2001). Variscan biotite and garnet appear just northwest of the Cadomian garnet isograd. Southeast of the garnet isograd, the Variscan deformation occurred under retrograde metamorphic conditions compared to the older Cadomian fabrics.

Enhanced Variscan collapse of the overthickened crust during the Early Carboniferous was related to the activity of the Bohemian shear zone (BSZ). Elevator-style movements along the BSZ led to the sinking of the TBU, as upper crustal level, into its hot substratum (Moldanubian, Saxothuringian). The bendings of the BSZ are used to subdivide it into the North Bohemian shear zone (NBSZ, Zulauf et al., 2002b), the West Bohemian shear zone (Zulauf et al., 2002a), the Hoher Bogen shear zone (HBSZ, Bues et al., 2002), and the Central Bohemian shear zone (CBSZ, Scheuvens and Zulauf, 2000). Elevator-style tectonics along the BSZ can be explained by overthickened crust that was weakened from below.

The Brunovistulian unit

Considerable amounts of well-preserved Cadomian crust are also present in the Moravo-Silesian Zone at the eastern termination of the central European Variscides (Brunovistulicum; Dudek, 1980). At the surface these Cadomian rocks can only be studied in relatively small massifs in the western parts of Moravia and Silesia (Thaya Dome, Svratka Dome, Brno Massif, Keprník and Desná Dome). Most of the Brunovistulian unit is hidden beneath younger sediments. However, thanks to dense oil and gas drilling in the Carpathian foredeep between Brno and Ostrava, and on the basis of additional geophysical data, Dudek (1980) was able to compile a geological sketch map for this subcrop part of the Brunovistulian (Figure15). Unfortunately, little information is available about the crystalline basement beneath the thick Devonian and Carboniferous Silesian sediments

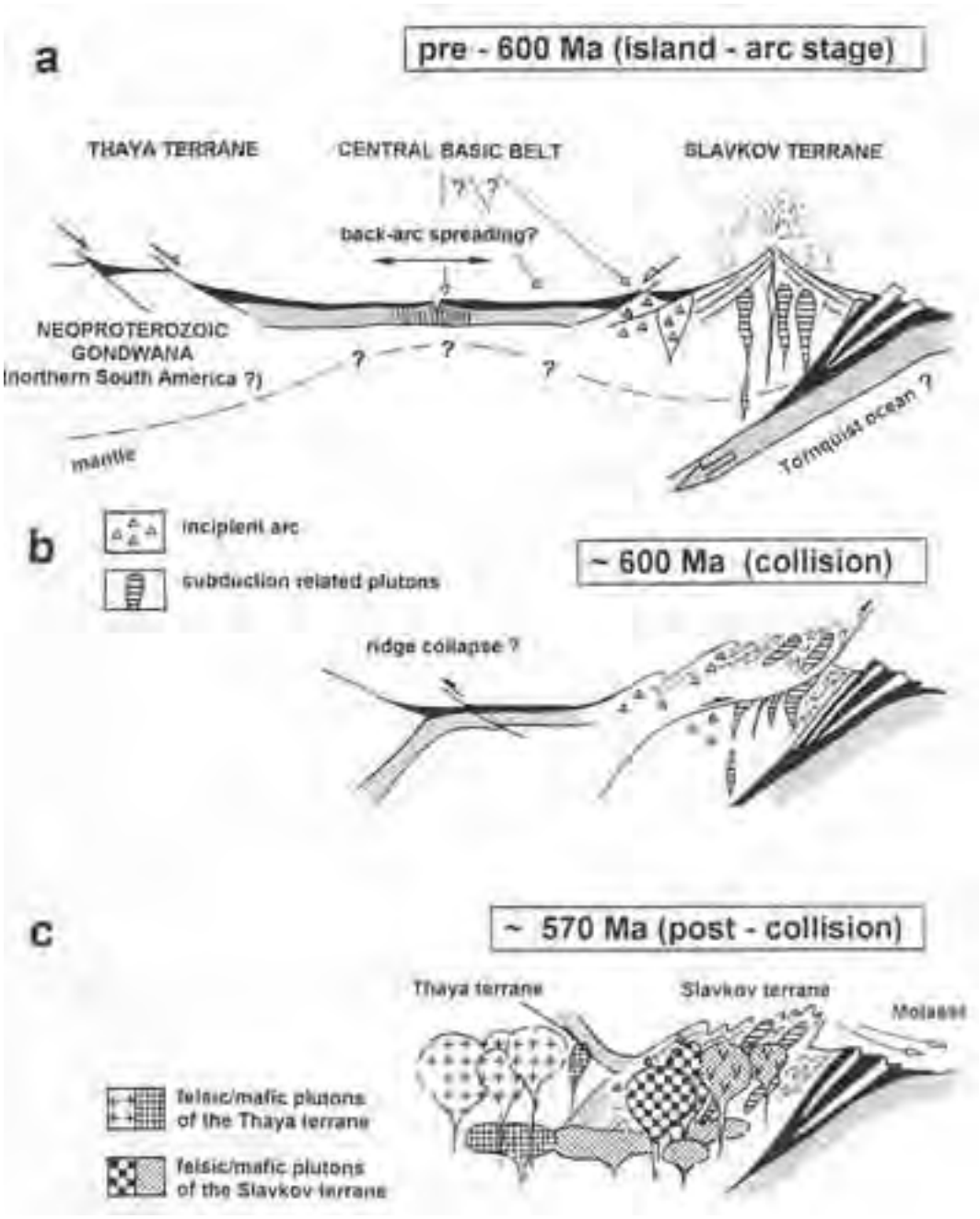

Figure 16 - Tentative geodynamic model for the evolution of the Brunovistulian (see text for explanation).

north of the Neogene Molasse basin. However, since Cadomian rocks outcrop again in the Hrubý Jeseník Mountains (Desná Dome), Dudek (1980) proposed that the whole Moravo-Silesian zone rests upon the same Cadomian-consolidated basement block.

In the Early Carboniferous, during the Variscan orogeny, the western parts of the Moravo-Silesian Zone (=Brunovistulian plus its Early Palaeozoic cover) were overthrust by the Moldanubian unit, the high-grade metamorphic core zone of the Variscan orogen. Due to the increasing Variscan deformation and metamorphism towards the Moldanubian boundary (Frasl 1970, 1991; Schulmann, 1990; Fritz et al., 1996), there is some uncertainty about the actual western limitation of the Brunovistulian Cadomian basement. Most geologists believe that the strongly-sheared granitoid pencil gneisses of western Moravia and Silesia (Bittesch Gneiss, Keprnik Gneiss) still represent parts of the Brunovistulian, although the bodies are probably more or less dislocated from the main basement block in the east. Some authors have argued that even some bodies of granitoid gneisses of the Moldanubian Unit in Lower Austria (Dobra Gneiss, Spitz Gneiss) might represent Variscan reworked and overthrust parts of the Brunovistulian plate (Matura, 1976; Finger and Steyrer, 1995). This concept is, however, still a matter of controversy (see e.g. Fuchs, 1998).

Figure15 illustrates how the Brunovistulian essentially consists of a large metamorphic complex, with mainly paragneisses in the (north)east, and a large granitoid complex in the (south)west (Brno Batholith, Thaya Batholith). The name Thaya Batholith is traditionally used for the granitoids in the Thaya Window, i.e. the area between Eggenburg and Znojmo, although the separation of the Thaya Batholith from the Brno Batholith is presumably a simple result of Permian sinistral strike slip along the Diendorf-Boskovice fault system. Near Brno, a striking narrow belt of metamorphosed basic and ultrabasic rocks passes through the Brno Batholith in a roughly north-south direction (Central Basic Belt).

The large abundance of *Cadomian granitoids* is one of the most outstanding features of the Brunovistulian block, and these rocks have been the subject of several detailed petrographical and geochemical studies (Dudek, 1980; Finger et al., 1989; Jelínek and Dudek, 1993; Leichmann, 1996; Hanžl and Melichar, 1997). All these studies conclude that the Brunovistulian granitoid terrane is essentially an I-type granitoid terrane. However, Finger et al. (1995) have additionally pointed out a pronounced east-west zoning of granite types, with the plutons east of the Central Basic Belt being relatively primitive in composition, resembling island arc magmas (Hbl-granodiorites, tonalites, quartzdiorites), whereas those in the west are mainly high-K granodiorites and granites. The magmatic zonality in the Brunovistulian granitoids is very clearly expressed in the Sr and Nd isotope values (Finger et al., 1995; Finger and Pin, 1997 and in prep.). These are generally primitive in the eastern province ($^{87}Sr/^{86}Sr_{580}$ mostly 0.704 – 0.705, εNd_{580} -1 to +3), and mostly in the typical crustal range in the western granitoids ($^{87}Sr/^{86}Sr_{580}$ 0.708 – 0.710, εNd_{580} –4 to –7). Intermediate initial ratios (0.705-0.707, -1 to -2) have been found in the rare diorite/tonalite bodies west of the Central Basic Belt, and in one distinct subalkaline granite pluton in the southern Thaya Batholith near Eggenburg (Finger and Riegler, 1999). Samples of Bittesch Gneiss yielded generally very mature isotope values (εNd_{580} –10 to –11; see also data in Liew and Hofmann, 1988), while the Keprnik Gneiss has εNd_{580} values of around –5 to –6 (Hegner and Kröner, 2000).

Regarding the magma sources, it is quite obvious from the isotope data that the western high-K granites and granodiorites, including the Bittesch and Keprnik Gneiss, are mainly crustal derived, with cratonic components involved in the melting process. Friedl et al. (2000) reported abundant Mesoproterozoic-inherited zircon cores from the Bittesch Gneiss. However, the additional occurrence of some isotopically more primitive tonalites and diorites in the western province indicates the presence of another magma source (mantle or juvenile crust).

The granitoid magmas east of the Central Basic Belt either formed through the melting of young calc-alkaline crust or contain a significant mantle component. Due to the dominance of felsic granitoids, a great importance is attributed to melting processes in the crust, although in some cases (e.g. basic massifs of Rusava and Jablunkov) the presence of mantle melts seems to be clear.

Geochronological data provide increasing evidence that most of the Brunovistulian granitoids formed during a relatively short plutonic episode at around 570 – 590 Ma. In addition to a number of zircon ages from granitoids of the western province, which all fall in this time span (Finger et al., 2000b), an Ar-Ar hornblende age of c. 590 Ma has been reported for one of the eastern granitoids (Fritz et al., 1996).

Volume n° 2 - from B16 to B33

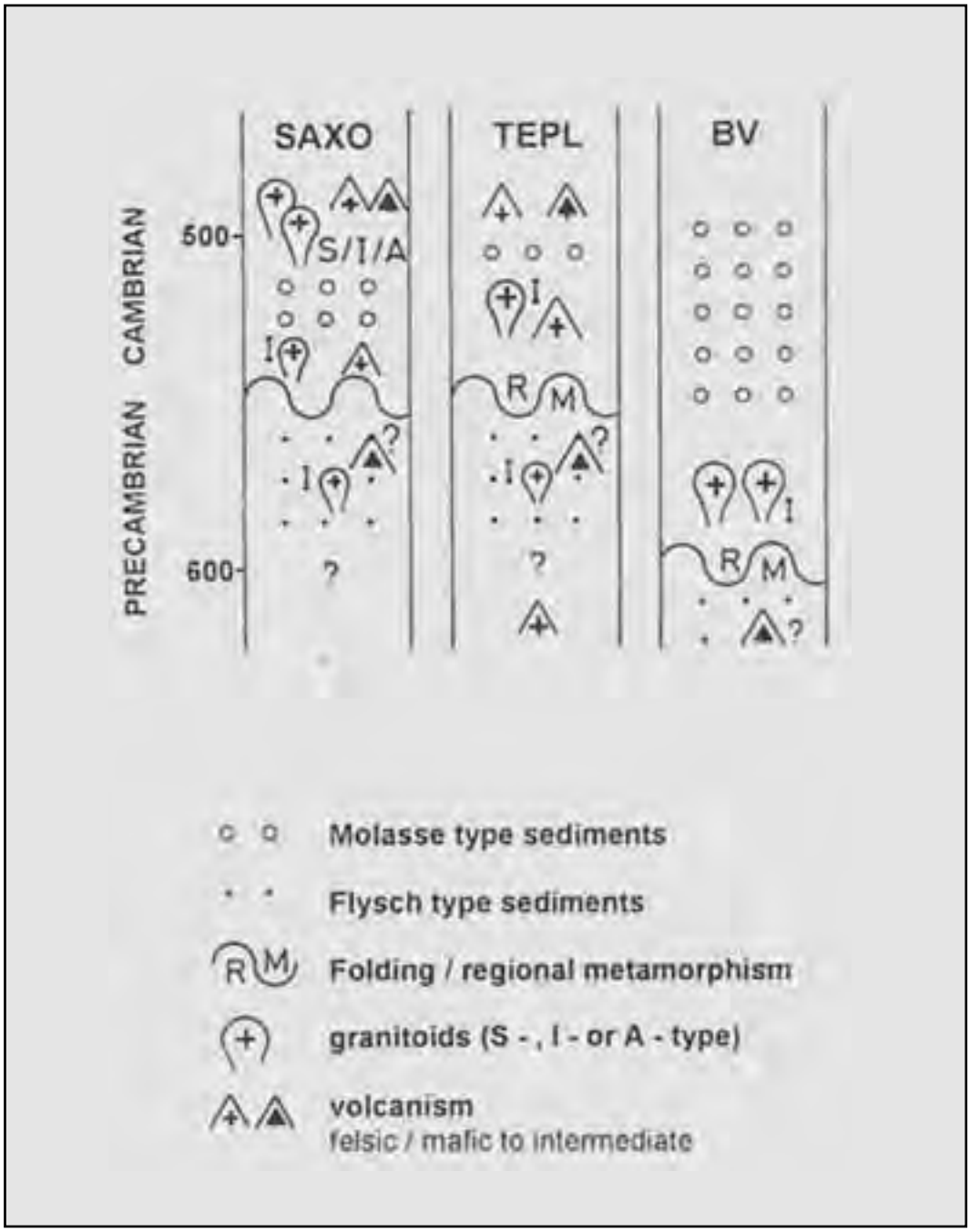

Figure 17 - Schematic comparison of the Cadomian/ Cambrian stratigraphy in the Saxo-Thuringian, Teplá-Barrandian and Brunovistulian, using data from Dörr et al. (1998, 2000, and pers. comm.), Zulauf et al. (1999), Linnemann (1995), Linnemann et al. (1998), Tichomirowa et al. (1997).

Possible candidates for late Cadomian intrusions are the gabbroic massifs in the eastern Brunovistulian; in the contact aureole of the Jablunkov massif (Figure15), Th-U-total Pb monazite ages of c. 550 Ma have been obtained (Finger et al., 1999).

Because of their overall I-type nature, and on the basis of Pearce-type diagrams, the Brunovistulian granitoids were previously mostly interpreted as subduction-related (Finger et al., 1989; Jelínek and Dudek, 1993; Hanžl and Melichar, 1997). Based on the striking east-west zoning of plutonism, a westward dipping Cadomian subduction geometry has been inferred (Finger et al., 1995). However, the pulsed nature of plutonism, subsequent to a phase of regional metamorphism, may suggest a collision event. An arc-continent collision in a Pacific-type tectonic setting is considered as a potential model (see below).

A comprehensive description of the *metamorphic complex* in the eastern half of the Brunovistulian was given by Dudek (1980, 1995). Most of these rocks are derived from flyschoid clastic sediments, mainly greywackes, siltstones and psammites with subordinate pelitic layers. In the area south and southeast of Olomouc, the metasediments contain abundant layers of metavolcanic rocks, mainly metabasalts and meta-andesites.
Regional metamorphism mostly reached medium-pressure amphibolite facies grade. In some cases, partial melting occurred. Microfabrics sometimes provide evidence of two metamorphic phases, with a younger phase of contact metamorphism related to the intrusion of the granitoids (Dudek, 1980; Hanžl et al., 1999). During the Variscan orogeny, parts of the Cadomian metamorphic complex were subjected to penetrative retrograde shearing under greenschist facies conditions.
Dudek (1980) has already emphasized the relatively Al_2O_3-poor character of the metasediments in the eastern Brunovistulian, implying a calc-alkaline (volcanic arc) source area. New trace element and isotope data (Finger and Pin, in prep.) point in the same direction, indicating a young, chemically and isotopically little-evolved island arc-type source. $^{87}Sr/^{86}Sr_{580}$ and εNd_{580} values of the metasediments are generally very similar to those of the adjoining granitoids (0.704-0.706; -1 to +2). This shows that not only the granitoids, but the whole continental crust in the eastern part of the Brunovistulian, were primitive throughout.
In the western part of the Brunovistulian, Cadomian metamorphic rocks are much less abundant. However, paragneiss relics from the roof of the Thaya Batholith and the western Brno Batholith are chemically and isotopically more evolved (εNd_{580} –3 to –7) than the paragneisses in the east. The detritus of these western metasedimentary units obviously derives from much older, cratonic crust (Finger and Pin, in prep.).
Based on the evidence presented from the granitoids and paragneisses, it is unequivocal that the continental crust west of the Central Basic Belt is completely different from that in the east. The Central Basic Belt obviously marks an important terrane boundary. Finger and Pin (1997) have introduced the terms "Slavkov Terrane" for the eastern province and "Thaya Terrane" for the western province.
Kröner et al. (1999) and Hegner and Kröner (2000) have presented Nd isotope data from a number of metasedimentary and metagranitoid rocks from the Jeseníky mountains. This data suggests that the Desná Dome can be correlated with the Slavkov Terrane, while the Keprnik Dome has the isotopic characteristics of the Thaya Terrane.
No precise geochronological information is available for the timing of Cadomian regional metamorphism in the Brunovistulian. K-Ar hornblende and mica ages (Dudek and Melkova, 1975) and Th-U-total Pb monazite ages (Finger et al., 1999) broadly constrain its age between 610 and 580 Ma, suggesting that regional metamorphism and plutonism are related to one single Cadomian tectonothermal cycle. A zircon evaporation age of 599 ±2 Ma was obtained by Kröner et al. (1999) for migmatites from the Desná Dome.
Little is known regarding the age of the volcanic arc material present in the metasedimentary complex of the Slavkov Terrane. The generally-primitive isotope compositions suggest a Neoproterozoic age. For volcanic arc-type granitoid gneisses in the Desná Dome, Kröner et al. (1999) have determined formation ages of 612 ±2 and 684 ±1 Ma. Inherited magmatic zircons in a metagreywacke from the Desná Dome, probably representing volcanic arc detritus, gave evaporation ages of 629 ±2, 642 ±3 and 665 ±1 Ma (Kröner et al., 2000). Unlike in the Thaya Terrane, no evidence for Meso- or Palaeoproterozoic zircons has been found in the Precambrian basement of the Desná Dome.

The *Central Basic Belt* consists of metagabbros, metadiorites, some ultramafics, tholeiitic metabasalts and metarhyolites. In the exposed Brno Massif, a mainly plutonic subzone in the west can be distinguished from a mainly volcanic subzone in the east. Since contacts are generally tectonic, it is unclear if both formed during the same event or represent independent units. The metamorphic overprint of the Central Basic Belt was polyphase (Cadomian and

Variscan), but did not overstep low to moderate P-T conditions (greenschist to lower amphibolite facies; Leichmann, 1996).

Petrographic and geochemical data for rocks of the Central Basic Belt are given in Štelcl and Weiss (1986), Hanžl et al. (1995), Leichmann (1996), Hanžl and Melichar (1997), Finger et al. (2000). Evaluation of this data shows that in the volcanic zone the melts are mainly basaltic and derived from depleted to mildly-enriched mantle sources. According to Leichmann (1996), the degree of enrichment increases towards the north. The metagabbros and –diorites of the plutonic zone have mostly cumulate compositions. They show high LREE/HREE ratios and seem to be derived from a separate mantle source (Finger et al., 2000a).

It has been often suggested that the Central Basic Belt, or parts of it, might represent relics of an ophiolite (Mísaø, 1979; Leichmann, 1996). However, the relative abundance of rhyolites and diorites distinguishes the assemblage lithologically from normal mid-ocean-ridge crust. Alternatively, the belt could be interpreted as part of an ensimatic arc, or as related to back-arc basin extention.

Recently, the first geochronological data from the volcanic zone of the Central Basic Belt have been obtained. A zircon evaporation age of 725 ±15 Ma for a tholeiitic rhyolite suggests that this zone is much older than the granitoids (Finger et al., 2000a). Leichmann (1996) has reported field observations which show that the Central Basic Belt is intruded by granitoids of the Slavkov Terrane at its eastern margin, as well as by granitoids of the Thaya Terrane at its western margin. This means that at ca. 580 Ma the present-day assembly of the Central Basic Belt, the Slavkov and the Thaya Terrane may have been basically established. Nevertheless, during the Variscan orogeny the section was certainly shortened. Parts of the Central Basic Belt were thrust eastwards onto Devonian strata (Hanžl et al., 1999). Sinistral strike-slip tectonics led to a further disturbance of the original Cadomian relationships (Hanžl and Melichar, 1997). **A** *geodynamic evolution model* **for the Brunovistulian has to accommodate the following geological observations:**

- Presence of a distinctly zoned crust with an island arc-type chemical and isotopic signature in the east (Slavkov Terrane) and a continental signature in the west (Thaya Terrane).
- Remnants of an ensimatic basic belt between the Thaya and the Slavkov Terrane.
- Deposition of large masses of flyschoid, arc-derived sediments in the eastern Slavkov Terrane, probably mainly between 600-700 Ma.
- Cadomian deformation and regional metamorphism at ca. 600 Ma, followed by extensive post-kinematic granitoid plutonism.

Finger et al. (2000b) assumed that the starting situation was some kind of island arc–back arc basin setting (Figure16), which had formed in the Neoproterozoic in the subduction realm of the Tornquist ocean, outboard of the Gondwana continent. Similar "Pacific-type" orogenic settings have been proposed for most other Peri-Gondwanan terranes of the Avalonian-Cadomian chain at that time (see Nance and Thompson, 1996). The existence of a pre-600 Ma volcanic arc is mainly inferred on an indirect basis: firstly, from the sedimentation of Neoproterozoic calc-alkaline material prior to 600 Ma in the eastern Brunovistulian, and, secondly, from the fact that large volumes of I-type granitoids of the Slavkov Terrane probably represent a remolten meta-igneous arc-type crust. Original volcanic-arc igneous rocks seem to be preserved under the Upper Moravian Basin (metabasalts and -andesites; see Dudek 1980) and in the Desná Dome (e.g. Ludvikov Gneiss: 684 ±1 Ma; Kröner et al., 2000).

The geological evidence for the proposed back-arc basin is still weak. As mentioned above, the rocks of the Central Basic Belt may equally well represent primitive parts of an ensimatic arc, and it cannot be excluded that this arc formed more or less adjacent to the Gondwana continent margin. However, since, during the Neoproterozoic, the northern Gondwana margin was a long-lived active margin (Nance and Thompson, 1996), the presence of island arcs and back-arc basins is quite likely. Furthermore, it remains open to discussion whether the inferred back-arc basin between the Slavkov and the Thaya Terrane consisted of remnant crust of the Tornquist ocean, or contained a new spreading centre. All this can only be a matter of speculation, until a much more detailed chemical and geochronological data set is available for the rocks of the Central Basic Belt.

Due to the deformation and regional metamorphism, which affected the Brunovistulian at ca. 600 Ma, it can be assumed that the arc system was in a state of compression at that time (Figure2b). It has been suggested that parts of the Central Basic Belt were obducted onto the Thaya Terrane, so that they could be later intruded by crustal granitoids.

Judging from its episodic nature following regional

metamorphism, the ca. 580-590-Ma-old granitoid plutonism in the Brunovistulian can be viewed as post-collision plutonism, rather than as normal subduction-related plutonism. There is no need to claim that subduction of the Tornquist ocean still continued during this stage. For example, post-collisional slab break-off, or delamination of mantle lithosphere (see e.g. Henk et al., 2000), would also provide a suitable tectonothermal mechanism for triggering voluminous mantle and crustal melting. In fact, such a "catastrophic" scenario would better account for the pulsed nature of plutonism than continous subduction activity and water-induced melting in the mantle wedge. The chemical zoning of plutonism may reflect simply the pre-existing crustal heterogeneity and the different source rock composition of the Slavkov and the Thaya Terranes. In the model in Figure16 it is assumed that in the Slavkov Terrane much of the previous arc building was flooded by granitoid melts or remolten at that time.

Based on the SHRIMP age spectrum of inherited zircons found in the Bittesch gneiss, Friedl et al. (2000) have proposed that the Brunovistulian is derived from a Grenvillian cratonic province, and not from Africa, like the Teplá-Barrandian and Saxo-Thuringian terranes (i.e. the Armorican terrane assembly). It has been suggested that the Brunovistulian is a fully-independent peri-Gondwanan terrane, which was situated in the realm of the Amazonian cratonic province by the late Precambrian, comparable to the Avalonian terranes of North America and the United Kingdom (Finger et al., 2000b; Friedl et al., 2000; Winchester et al., 2002).

Figure17 illustrates that also the recorded Cadomian events in the Brunovistulian are significantly distinct from those in the Teplá-Barrandian and the Saxo-Thuringian.

A first important difference is that the Brunovistulian does not show evidence for Eocambrian regional metamorphism and tectonics, nor for Early to Mid-Cambrian granitoid plutonism or related volcanism, whilst Dörr et al. (1998, 2000) have pointed out that these two events are widely recorded throughout the Armorican terrane assembly, from central Europe over Brittany to Spain. In the case of the Teplá-Barrandian Unit, Zulauf et al. (1999) have interpreted these Eocambrian/Cambrian tectonothermal events as part of the process of microterrane accretion to the Armorican sector of the Gondwana margin (see above). At the same time, a non-orogenic, broadly Molasse-like overstep sequence is documented on the Polish side of the Brunovistulian (Bula et al., 1997) and also in a few boreholes in southern Moravia (Jachowicz and Pøichystal, 1997).

Secondly, the Brunovistulian apparently lacks evidence for the plutonic/volcanic event at ca. 500 Ma, which is widely documented in the Armorican parts of the Bohemian Massif (von Quadt, 1994; Tichomirowa et al., 1997; Kröner and Hegner, 1998; Glodny et al., 1998) and mostly interpreted as marking the time when Armorica started to rift from main Gondwana (Pin, 1990; Tait et al., 1997; Floyd et al., 2000). On the other hand, there is as yet no evidence for ~ 600 Ma high-grade regional metamorphism in the Armorican parts of the Bohemian Massif.

Field trip itinerary

DAY 1

(Arrival in Dresden, Introduction to the field trip, Dresden Sightseeing)

DAY 2

(Lausitz and Elbe area)

Stop 2.1:

Quarry Kindisch, 500 m W of the village of Kindisch, near Kamenz

Lower Cambrian granodiorite of the Lausitz Anticline (ca. 540 Ma).

Large areas of the Cadomian basement of the Lausitz Anticline are occupied by Cadomian granitoids that intruded into deformed Cadomian siliclastic rocks (mainly greywackes). Most of these granitoids are granodiorites. Traditionally, two petrographic types of Cadomian granitoids have been distinguished in the Lausitz Anticline: (1) Two-Mica-Granodiorite and (2) Biotite-Granodiorite. Furthermore, all transitional stages between anatexites and Cadomian meta-greywackes (the source rocks of the anatexites) can be recognized. In samples of the Two-Mica-Granodiorite, the large amount of recycled meta-sedimentary rocks is reflected by a high content of rounded zircon. The Cadomian magmatism in the Lausitz Anticline is interpreted as being subduction-related.

At the Kindisch quarry (Hartsteinwerke Kindisch GmbH), a Cadomian Biotite-Granodiorite is cropping out. The intrusion contact with the surrounding Cadomian greywackes (Lausitz Group) is exposed at the northern edge of the quarry. There occur some granodioritic dikes and apophyses within the

greywackes. North-south striking basic dykes of unknown age penetrate the granodiorite. Greywacke xenoliths are distributed within the granodiorite, reflecting the position of the quarry close to the contact between the intrusion and the greywackes.
The intrusion age of the granodiorite was analysed by SHRIMP – U/Pb dating (Linnemann et al., in prep.) at ca. 540 Ma.

Stop 2.2:

Butterberg Quarry, 2.5 km N of Kamenz, near the village of Bernbruch

Neoproterozoic greywacke and shale from the Lausitz Group (Lausitz Anticline) with rare tuffogeneous intercalations.
The greywackes of the Lausitz Anticline represent Neoproterozoic turbidites of a back arc basin. The thickness of the entire sedimentary unit (Lausitz Group) is estimated at exceeding 3000 m. A subdivision is problematic due to the lack of key beds.
The facies scheme for the Lausitz Group corresponds to the Bouma turbidite intervals Ta - e. Its characteristics can be observed in the outcrop. Monotonous greywackes are dominated by the fine sand Ta-b interval, and siltstone and shale beds of Tc - e. The thickness of the sequences ranges from the decimetre to the decametre scale.
The age of sedimentation is determined at ca. 570 Ma by Pb/Pb and SHRIMP U/Pb dating (Linnemann et al. 2000, Buschmann et al. 2001). This age was obtained for an ash layer intercalated in the graywacke beds at Wüsteberg, near Kamenz.
The geochemical signatures of the sedimentary rocks of the Lausitz Group indicate deposition in an active-margin setting (Linnemann and Romer, 2002). The Nd-model ages range from ca. 1.5 Ga to ca.1.8 Ga (Linnemann and Romer, 2002). SHRIMP-U/Pb-data of detrital zircons give age intervals of ca. 570-800 Ma, ca. 1.9-2.2 Ga and 3.0-3.4 Ga (Linnemann et al., in prep.). These age groups and the Nd-model ages are typical features that suggest a highly probable West African provenance.

Stop 2.3:

Monumentenberg, 500 m E of the village of Groß-Radisch

Tremadocian conglomerates, quartzites (Dubrau quartzite) and silty shales of the Lausitz Anticline.
The area of the Hohe Dubau constitutes the type locality of the Cadomian unconformity of Saxo-Thuringia. Tremadoc conglomerates, quartzites, and silty shales are overlying tectonically deformed Cadomian greywackes. The succession is poorly exposed. Nevertheless, the Hohe Dubrau area represents the one and only surface outcrop of Saxo-Thuringia with a definite angular unconformity between the Cadomian basement and the superimposed Lower Palaeozoic sedimentary rocks. Therefore, the Monumentenberg hill in the area of the Hohe Dubrau, near Groß-Radisch, was suggested as type locality of the Cadomian unconformity in Saxo-Thuringia by Linnemann and Buschmann (1995).
The Tremadoc succession is divided into three units (from base to top):
- conglomerates, only consisting of stable components (quartz- and tourmalinised hornfelses);
- intratidal facies with Skolithos- and Cruziana-type trace fossil community and inarticulate brachiopods (Westonisca arachne), mud cracks and, very rarely, HCS;
- storm-dominated shelf facies with HCS;

Only one specimen of Cruziana ”dispar” has so far been described by Schwarzbach (1934). Unfortunately, this single slab has disappeared. Some new specimens of Cruziana sp. were discovered by R. Winkler, M. Röthel and U. Linnemann (Museum of Mineralogy and Geology of Dresden) in July 1997.

Stop 2.4:

Water-filled abandoned quarry of Kunnersdorf, ca. 10 km NW of Görlitz; north bordered by the Kunnersdorf rubbish dump

Early Cambrian (upper Marianian) carbonates and claystone/siltstone of the Charlottenhof Formation, Ludwigsdorf Member (Görlitz Syncline).
In the quarry of Kunnersdorf limestones and red shales of Early Cambrian age are exposed. A large part of the quarry is waterfilled. A short visit to the outcrop is included to give an impression of typical peri-Gondwanan Cambrian rocks that are involved in the Variscan structures of the Central European Variscides. The Cambrian of the Görlitz Syncline is interpreted as representing large olistoliths in a Lower Carboniferous wild flysch matrix. The Görlitz Syncline is the neighbouring structural unit at the northern flank of the Lausitz Anticline.
The sedimentary rocks of the outcrop belong to the Ludwigsdorf Member of the Charlottenhof Formation. A special feature is the so-called “Zebra”-limestone. The biostratigraphic age of the sedimentary succession is determined as Higher

Lower Cambrian. The environment is interpreted as a shallow marine calcimicrobial mudmound sequence (Elicki, 1997, 2000).

Stop 2.5:

Cliffs in the forest near the railway station of Weesenstein, ca. 1 km S of the village of Weesenstein (200 m E of the station)

Late Neoproterozoic pebbly mudstones and diamictites of the Weesenstein Group (Elbe Zone).

The Elbe zone is the neighbouring structural element at the southern flank of the Lausitz Anticline and is interpreted as a mega-shear zone established at ca. 330 Ma during Variscan orogenic processes. This structural element contains several slivers of rock units with distinctly different geological histories. One of them is the Weesenstein Group. The maximum age of the deposition, ca. 570 Ma, is given by SHRIMP-U/Pb data from detrital zircon (Linnemann et al., subm.). The northern part of the Weesenstein Group is intruded by the Dohna Granodiorite, which is dated at c. 540 Ma (Linnemann et al., 2000). This age represents the minimum age of sedimentation of the Weesenstein Group. The main lithologies of the sedimentary unit are diamictites, graywackes, and shales. The rock complex is overprinted under greenschist facies conditions and, in part, extremly sheared at around 330 Ma. Granitoid pebbles from the diamictites gave Pb/Pb and SHRIMP-U/Pb ages of ca. 570 Ma (Linnemann et al., 2000, Linnemann et al., in prep.). Because of the geochronological data, the Weesenstein Group is interpreted as being part of the Cadomian basement. The geochemical "fingerprint" of the sedimentary rocks imply an active margin setting. The Nd-model age is around 1.8-2.0 Ga (Linnemann and Romer, 2002). The sedimentary environment of the diamictites and the related sedimentary rocks are interpreted as being glaciomarine (Linnemann and Romer, 2002).

DAY 3

(Travel from Dresden to Prague, View of Prague, View of outcrops in the Barrandian Syncline, Travel to Plzen)

Stop 3.1:

Quarries at Zábì hlice, near Praha-Zbraslav

Quarries on the left bank of the river Vltava, 2 km S of Praha–Zbraslav, expose a thick sequence of Neoproterozoic rocks of the uppermost part of the Kralupy–Zbraslav Group, the Davle Formation, interpreted now as a pre-Cadomian volcanic arc complex. The following description is according to Chlupáè (1993), although slightly modified.

In the large, active quarry, and mainly in its southern vicinity, the Davle Formation is developed as layers and thick banks of grey-green volcano-sedimentary tuffaceous rocks, alternating with markedly coarse-grained volcaniclastics – agglomerates and breccias. Fragments of lighter intermediate to acidic volcanics of andesite, dacite and rhyolite composition (originally bombs and angular lapilli) are accumulated in grey-green tuffaceous groundmass. Layers with a larger amount of sedimentary material are obviously thinner-bedded and darker in colour.

These rocks are products of explosive, mostly submarine volcanic activity, which produced large amounts of pyroclastics, often dominating over the extrusives proper. The volcanics are intermediate to acidic, calc-alkaline types differing markedly from those of the Kralupy–Zbraslav Group in the NW flank of the Barrandian syncline.

All Proterozoic rocks are deformed. They are gently folded, the folds showing large wavelengths and amplitudes (up to km) and cut by many faults and fissures, mostly striking NW-SE. Anchimetamorphism under conditions of a prehnite-pumpellyte zone, and marked autometamorphism of volcanic rocks, are characteristic. Numerous secondary veins are mineralised with quartz, carbonates and uncommon axinite. The whole sequence is dipping towards the SE, and our further stops will be in younger parts of the sequence.

Behind the office building north of the active quarry, a thick sill of altered andesite is exposed. This rock, composed of albitic plagioclase, quartz, augite, chlorites, leucoxene, calcite and accessories, was taken to be an integrate part of the Davle Formation. The preliminary zircon U-Pb study of this rock, however, supplied a much younger Late Devonian intrusive age (W. Dörr, personal communication).

Stop 3.2:

Outcrops in the Vltava Valley, between Strnady and Vrané

Outcrops in the lower part of the Neoproterozoic Štìchovice Group (Cadomian flysch) on the roadside between Strnady and Vrané, especially near the bus station (description according to Chlupáè, 1993, slightly modified).

The dominant rock types are dark-grey shales (consolidated claystones and siltstones), with

subordinate pale-grey to grey-green laminae, and interbeds of siltstones and greywackes. The sediments are interpreted as distal turbidites deposited in a rather deep sedimentary basin. Rocks are markedly affected by post-Cadomian deformation, exhibiting both brittle (fissures of different strike) and ductile (local schistosity overprinting the bedding) characteristics. This so-called "Jílové schistosity", most probably of Variscan origin, strikes usually NNE – SSW, steeply dipping to ESE.

Just above the bus station a distinct, about 2 – 3-m-thick interval of shales dipping SE exhibits typical slump structures: complex, small-scale, and discontinuous, asymmetrical, and even recumbent folds, lenses and small tongues, all well marked by colour contrast between dark shales and lighter coarser greywacke and siltstone laminae. Slump structures pass locally into convolute structures. Submarine slides could have been triggered by earthquake shocks within the mobile basin floor.

On the opposite, right bank of the river Vltava, magnificent outcrops expose the profile of the Štìchovice Group. The thick sequence of alternating siltstones, shales and greywackes shows a small- and even large-scale cyclicity, typical of the flysch deposits. The structure is monoclinal with a moderate dip towards the SE.

The underlying Davle Formation (see Stop 3.1) occurs some 400 m to the W of the present locality. Above the car-repair service there is exposed the terminating member of the Davle Formation - the Leèice Shale. The Leèice Shale here forms an about 60-m-thick layer of the typical black shale, with a higher content of organic carbon (but less than 1%) which causes its black colour. The monotonous development without coarser greywacke interbeds and without coarser effusive material is characteristic (volcanic material, however, is present as fine tuffaceous admixture). Rocks are commonly silicified and may laterally pass into dark silicites (cherts); disseminated or even clustered pyrite is common. The geochemistry can be characterised by increased contents of Zn, Cu, Ni, Mo, V and U, which are typical of anoxic environments (metallic components occur mostly as sulfides). The Leèice Shale is, therefore, interpreted as sediment of anoxic, low energy, and a rather deep marine environment. Organic carbon evidently derives from abundant phytoplankton (algae); recognizable globular microfossils belong mostly to Acritarcha (Bavlinella). Weathering of pyrite resulted in the production of sulphuric acid, which negatively influenced the vegetation.

Stop 3.3:

The Jezírko quarry at Dobøíš

The Jezírko quarry is situated at the southern periphery of the town of Dobøíš, 200 m W of highway 4, going from Praha to Pøíbram. It is the type locality of the Dobøíš conglomerate within the Neoproterozoic Štì chovice Group.

The dominant rock-type of the exposed upper part of the Štì chovice Group is flysch-like sediments, distinguished by the alternation of grey siltstones, greywackes and shales, with typical graded bedding and small-scale cyclicity (usually tens of cm). A 9- to 14-m-thick disorganised conglomerate is embedded in the above-mentioned sequence, well exposed, particularly on the western face of the quarry. They are typical petromictic conglomerates with unsorted boulders of various size (1 to 110 cm in diameter), mostly well rounded, irregularly distributed in greywacke groundmass. The boulders consist of about 60% fine- to coarse-grained greywackes (containing clasts of quartzite and cherts) and of about 25% acidic volcanics (rhyolites, trachytes) and volcaniclastic rocks (tuffs, tuffites). Less common are siltstones and shales (about 5%), intermediate and basic extrusive rocks, black cherts and rather rare granitoids. No boulders of the Moldanubian-type high-grade metamorphic rocks occur (according to Clupáè, 1993, slightly modified)

The Dobøíš conglomerate is a typical intraformational (not basal) conglomerate, constituting tongues and lens-like bodies within the middle and upper parts of the Štì chovice Group. According to Röhlich (1964) the conglomerate boulders were first rounded by river transport and then deposited in a near-shore marine environment; they were later redeposited by mudflows and fluxoturbidites, filling the channel of a submarine fan.

Rocks exposed in the quarry are monoclinally dipping westwards (40 – 60°); slump structures (irregular folds) are observable in beds closely under- and overlying the conglomerate. Sedimentary structures – flute casts preserved mostly on lower bedding planes of greywacke layers in the sequence underlying the conglomerates -- indicate NE–SW current direction. The source region of conglomerates, situated probably SE of the locality, largely consists of Neoproterozoic rocks of the Kralupy – Zbraslav Group, namely of its presumably younger member – the Davle Formation. Some of the pebbles show deformation which pre-

dates erosion and deposition (Zulauf, 1997)
Dörr et al. (2002) published radiometric U-Pb zircon ages of two boulders of acidic volcanics from this locality. The first one is a rhyolite containing small phenocrysts of quartz and feldspar in a fine-grained matrix. The major element composition is: SiO2 = 72.8%, Al2O3 = 14.6%, CaO = 0.62%, Na2O = 5.1% and K2O = 2.7%. Pyroxene and chlorite are rare.The second one is a crystal tuff of rhyolitic major element composition: SiO2 = 74.3%, Al2O3 = 12.9%, CaO = 0.49%, Na2O = 2.8% and K2O = 5.6%. Lapilli, phenocrysts of quartz, feldspar and hornblende are embedded in a fine-grained matrix. The rhyolite and crystal tuff supplies ages of 585 ±7 Ma and 568 ±3 Ma, respectively. These values are interpreted as extrusion ages of the Kralupy–Zbraslav Group volcanics.
According to the evolutionary model by Dörr et al. (2002), the Kralupy – Zbraslav Group may represent a back-arc volcano-sedimentary complex at the northern margin of the Late Proterozoic Gondwana. The Davle Formation then demonstrates the K-poor magmatism associated with the corresponding island arc. The following accretion, uplift and erosion of volcanic island arc (expressed in the proper Cadomian orogeny) are thus documented by the Dobøíš' conglomerate origin. The youngest sequence – the Štìchovice Group – is then interpreted as the Cadomian flysch.

Stop 3.4:

Outcrops of the Èertova skála rock

Rocky outcrops of Èertova skála on the left bank of the Berounka river, 8 km SW of Køivoklát, supply one of the most instructive occurrences of the Neoproterozoic Kralupy–Zbraslav Group's volcanic rocks. The description follows Chlupáè (1993) with slight modification.
The roadside outcrops and cuttings expose basaltic-type basic rocks known in the literature as "spilites". These are typical pillow-lavas showing globular and lenticular "pillows" of more than 1 m in diameter. Their characteristic structure originated due to rapid cooling of the flowing lava at contact with seawater during extrusion. In cross-section, the individual "pillows" show typical concentric zoning: a fine-grained hypocristalline and rather thin marginal zone, with occasional amygdaloid structures, and an internal part marked by coarser grain-size with intersertal and intergranular texture, enriched with Na2O (cooled more slowly; crystals well developed). The space among pillows was filled with volcanic glass, later palagonised and chloritised. The primary basaltic rocks were affected by autometamorphic (spilitisation), hydrothermal and metamorphic processes: basic plagioclases were replaced by the more acidic ones (oligoclase, albite), and augite, together with other dark minerals, were at least partially replaced by chlorite and/or other metamorphic minerals. The slight regional metamorphism linked with the Cadomian orogeny is documented by the prehnite-pumpellyite zone grading into the chlorite zone towards the NW. All Proterozoic rocks were twice deformed: first in the Cadomian, and later, with lesser intensity, in the Variscan cycle. The effects of tectonics and metamorphism are more intense than at the SE flank of the Barrandian syncline at Vrané.
The spilites of this locality belong to the main volcanic belt of the NW flank of the Barrandian syncline. This is distinguishable in metabasalts of the tholeiitic type, characteristic of oceanic magmatism. In the model by Dörr et al. (2002), these occurrences correspond to peri-Gondwanan back-arc basin geotectonic settings.

Stop 3.5:

Proterozoic–Middle Cambrian angular unconformity N of Týøovice

About 600 m upstream from Stop 3.4, a roadside exposure shows the angular unconformity between the Proterozoic shales of the Kralupy–Zbraslav Group and the transgressive Middle Cambrian strata. On this outcrop, grey silty Proterozoic shales, strongly tectonised and phyllitised and dipping strongly northwards (on the right side of the outcrop), are sharply overlain by gently SE dipping, markedly less-tectonically-affected Middle Cambrian shales (with several beds of greywacke and polymictic conglomerate at the base). The Middle Cambrian age of overlying beds is constrained by findings of trilobite Hydrocephalus careens (Barr.). A marked difference between the strongly deformed and even metamorphosed Proterozoic, and the less tectonised and non-metamorphosed Middle Cambrian, documents the effects of the Cadomian orogeny, which acted here prior to the Middle Cambrian (Chlupáè, 1993).

Stop 3.6:

Exposures on the right bank of the river Berounka, N of Skryje

One of the most famous paleontological localities

in the Middle Cambrian of Skryje is situated on the hillside facing the bridge, across the river Berounka, near the settlement of Luh. It is the place where many of the large paradoxidid trilobites housed in many of the world's collections were found.

The gently eastward-dipping Skryje Shale, cropping out in natural as well as artificial exposures dug by collectors, is developed as grey to grey-green richly fossiliferous silty shales. The principal trilobite species, whose fragments occur in all larger rocks fragments, is the large paradoxidid trilobite Hydrocephalus careens (Barr.), which may be found even as almost complete exoskeletons. The list of less abundant trilobites and other fossil species from this locality can be found in Chlupáè (1993).

On the left side of the road from Luh to Skryje, about 300 m NW of the paleontological locality, there are instructive outcrops in basal Middle Cambrian clastic deposits. In the lower part of the exposure (before the bend of the road) is the Mileè Conglomerate, which transgressively overlies the Proterozoic rocks of the Kralupy–Zbraslav Group below the road (contact not exposed). The quartzose conglomerates are pale-grey to yellow, monomictic, medium-grained with locally very thin claystone intercalations. The exposed thickness is about 5 m, the total thickness is 10 – 11 m.

Above thick banks of conglomerates, markedly thinner bedded sandstones with thin clayey interbeds occur, passing upwards into thicker beds of brownish coloured greywackes. These so called "Orthis Sandstones" exhibit larger amounts of unstable components (feldspars, etc.) and common brachiopods preserved as internal moulds. The orthid Pompeckium kuthani (Pomp.) is the predominant species.

The uppermost rock exposed in this outcrop belongs to the next lithostratigraphic unit – the Conglomerate. It is a typical petromictic and less sorted conglomerate with pebbles of very diverse rocks: Proterozoic shales, greywackes, dark silicites (cherts), spilitic metabasalts, Cambrian sediments (even large blocks of shales) and quartz. The rounding of the pebbles is fair in Proterozoic rocks, which may point to redeposited fluvial material mixed with products of submarine erosion and sedimented as mudflow deposit. The lower limit of the Týøovice Conglomerate is here expressively sharp, and connected with erosion of the underlying "Orthis Sandstone".

After Kukal (1971) the exposed sequence illustrates the transgressive Middle Cambrian deposits, indicating a successive and stepwise deepening of the basin. The Mileè Conglomerate represents marine beach sediments; the "Orthis Sandstone" points to a somewhat deeper environment (possibly below wave base). The Týøovice Conglomerate may be interpreted as flexoturbidites deposited in a rapidly subsiding basin at greater depth and under conditions of a rapid erosion than the source areas. The overlying Skryje Shale is a typical basinal deposit.

DAY 4

(Western part of the Tepla-Barrandian unit, Travel to Brno, Visit of Brno)

Stop 4.1:

Open quarry at Šibeni¹ní v., at the southeastern margin of Stod.

Brittle deformation and basic dikes in Cambrian Stod pluton.

The northeastern part of the quarry of Šibeni¹ní shows biotite granite of the Stod pluton that is locally strongly decomposed and weathered. Most parts of the weathered granite have been exploited as building material. The more or less intact biotite granite consists of quartz, plagioclase, K-feldspar, biotite (partly altered to chlorite), and accessories (apatite and zircon). There are also microscopic xenoliths consisting of strongly foliated country rock (metagreywacke). Overgrowth of magmatic biotite on the xenoliths postdates the stretching of quartz, the latter occurring as lenses within the metagreywacke material of the xenoliths.

There is a large number of deformation stages in the biotite granite, ranging from brittle-ductile to brittle. We are not able to resolve the complete deformation history by taking into account the observed cross-cutting relationships. The following sequence has been found: (1) early steep, normal and strike-slip faults, (2) low-angle thrust faults, and (3) late steep, normal faults. Similar to the normal faults, the strike-slip and reverse faults are themselves polyphase.

The strike-slip faults include: (1) N-S directed sinistral, (2) E-W directed dextral, and (3) NE-SW directed dextral types, the latter being related to the emplacement of lamprophyre dikes (spessartite) that show the same direction of strike as the dextral strike-slip faults (NE-SW). The quartz fabrics in the granite adjacent to the dike suggest shearing in the brittle ductile regime. There are fractures, subgrains (oriented parallel to the prism planes), and evidence for strain-induced grain boundary migration,

including incipient bulging recrystallization. At the direct contact with the basic dike, plagioclase of the granite has been partly replaced by actinolite and sericite. Biotite has been transformed to chlorite.

As the brittle-ductile quartz fabrics are strongly restricted to the direct contacts of the lamprophyres, a synkinematic intrusion of the dike is suggested. The heat of the basic melt progressed into the adjacent granite, supporting thermally-activated deformation mechanisms, such as strain-induced grain boundary migration and bulging recrystallization. The lamprophyre itself shows a distinct magmatic foliation by shape-preferred orientation of hornblende phenocrysts and unhomogeneously-distributed opaque phases. Most of the hornblende phenocrysts occur as pseudomorphs that have been changed to chlorite. Microscopic extensional veins in the lamprophyre are mineralized with chlorite and laumontite and are cut by late shear planes. As the formation of laumontite is generally restricted to T < ca. 250 °C (Liou et al., 1987), the formation of the veins as well as the late strike-slip movements must have occurred at T< ca. 250 °C.

The data presented above suggests that the spessartite dike intruded into an existing brittle strike-slip fault, which was active until the dike had solidified and cooled down to ambient temperatures. An upper age limit for the origin of the spessartite dike is given by the age of the Stod pluton. A concordant U-Pb zircon age of 522 ±2 Ma has been determined for the T+šovice granite, located south of the present locality (Dörr et al., 1997). This age is compatible with an ^{39}Ar-^{40}Ar biotite age (518 ±5 Ma, Kreuzer et al., 1990), the latter suggesting granitic melt emplacement at supracrustal levels (ca. 7 km depth, Zulauf, 1997) and rapid cooling to the K-Ar blocking temperature of biotite still during the Cambrian. A lower, but more speculative, age limit for the spessartite emplacement is given by the following observation. Lamphrophyre dikes of the Barrandian syncline, which are similar to those of the Stod and Domažlice area, cut through the Mid-Cambrian sediments, but are themselves truncated by Ordovician strata (Pato¹ka et al., 1994).

The younger SE-directed thrusts of the outcrop probably reflect Variscan (Late Devonian) shortening. Similar thrust planes are described in the outcrop of the Radbuza valley, between Holýšov and Ohu¹ov.

Stop 4.2:

Railway cut north of Stéelice

The outcrop shows the contact between Stod granite and metagreywacke, the latter being changed to hornfels. The granitoid consists of quartz, plagioclase, K-feldspar, muscovite, and biotite. The metagreywacke (hornfels) is made of quartz, plagioclase, white mica, biotite, and prismatic sillimanite. There is evidence for at least two pre-plutonic deformation stages in the wall rock. Cadomian D_1 is indicated by a first generation of quartz veins that have been folded. Only at the direct contact to the pluton, the F_2 fold axes and S planes are subvertical, suggesting that the rising melt contributed to changing the attitude of the Cadomian structures. The contact metamorphic heating led to the striking static equilibration of almost all minerals (e.g. 120° triple junctions in quartz) and to the growth of 'oblique' biotite and muscovite. K-Ar dating of muscovite from the hornfels yields 483 ±10 Ma. The intrusion depth of the Stod pluton has been determined at ca. 7 km, using phengite barometry and petrogenetic considerations of the country rock (e.g. andalusite has been found in adjacent outcrops).

Stop 4.3:

Outcrop in the Radbuza valley,
between Holýšov and Ohu¹ov.

Cadomian deformation and Devonian brittle-ductile top-to-the-ESE displacement along the Holýšov thrust (chlorite-sericite zone).

The map-scale structural inventory within the Upper Proterozoic rocks SW of Stod is characterized by ESE-vergent folds and related thrusts, that show top-to-the-ESE displacement. This type of folds and thrusts (Holýšov thrust) affect phyllites, metagreywackes and quartzites of the present outcrop. They result from a third (Devonian) deformation stage (D_3). Mineral phases observed in the above metasediments include quartz, sericite, chlorite, biotite, plagioclase, K-feldspar and opaque phases.

Relics of a first (Cadomian) deformation stage (D_1) are quartz veins and S_1 fabrics, the latter occurring between the S_2 planes of competent metagreywackes (only visible in thin sections). The S_1 planes are characterized by oriented sericite and a weak shape-preferred orientation of quartz and feldspar grains.

Cadomian D_2 deformation led to the dominant, tight foliation (S_2) that is characterized by the shape-preferred orientation of sericite and chlorite and by local, but strong, enrichment of opaque phases. At some places quartz veins have formed parallel to S_2. F_2 isoclinal folding, on the other hand, affects quartz veins that opened parallel to S_1. There is

also evidence of non-coaxial deformation during D_2 (e.g. asymmetric pressure shadows of recrystallized quartz and mica behind plagioclase porphyroclasts). However, due to the Variscan D_3 deformation, which in most cases influenced the older fabrics and erased the D_2 stretching lineation, the sense of D_2 shearing determined is not very reliable.

Post-D_2 static growth of biotite and white mica, as well as the static recrystallization of quartz, is related to the contact heating of the Stod pluton that is only 4 km apart from the present outcrop (Figure 11).

Late Devonian F_3 folding of Cadomian S_2 foliation led to ESE-vergent, overturned to recumbent folds that show thickened hinges and thinned limbs. The associated axial-plane cleavage (S_3) is a widely spaced fracture or crenulation cleavage, depending on the mechanical properties of the rock.

The top-to-the-ENE mylonites are some cm wide and strongly foliated. The S_3 foliation of these mylonites results from shape-preferred orientation of synkinematic sericite, chlorite, stretched quartz grains and an unhomogeneous distribution of opaque phases. D_3-related deformation mechanisms of quartz include incipient bulging recrystallization, pressure solution and fracturing, all of which suggest a brittle-ductile regime, compared to the mechanical behavior of quartz. The distribution of quartz-c-axes suggests dominant <a> slip along the basal planes (Zulauf, 2001). The metamorphic conditions during D_3 were retrograde with respect to the Cadomian and Late Cadomian imprints. Biotite has been bent and chloritized. These metamorphic reactions, together with the quartz deformation fabrics, suggest lowermost greenschist facies conditions during D_3 deformation. D_3 top-to-the-ESE shear-sense indicators include mica fish, asymmetric pressure shadows of mica and quartz behind feldspar porphyroclasts (⇑ clasts), SC and shear-band fabrics (Zulauf, 1997).

The Si-content of the sericite of the D_3 mylonites ranges from 3.25 to 3.38. As the critical paragenesis for phengite barometry is present, these values suggest a metamorphic pressure between 4 and 5 kbar at T = 300 - 350 °C for the D_3 thrusting event.

K-Ar dating of synkinematic sericite, separated from the D_3 mylonites, yield 371 ±8 Ma (Wemmer and Ahrendt, unpublished data). As the sericite probably grew below the blocking temperature for the K-Ar isotopic system of white mica, this age is interpreted as the formation age of the syn-D_3 sericite, and thus as the age of the D_3 thrusting event. The Cadomian white micas of the wall rock of the D_3 mylonites yield a K-Ar age of 400 ±9 Ma (Wemmer and Ahrendt, unpublished data). This age is interpreted as a mixing age, meaning that the Cadomian age signature has been slightly influenced by the Variscan thermal imprints. Due to the low temperature and low D_3 strain, the age of the Cadomian sericite has not been completely reset to Devonian ages.

The Late Devonian radiometric age for the D_3 shortening event in the Stod-Holýšov area is compatible with the fact that the sedimentation in the Barrandian basin changed at the Eifelian/Givetian boundary from limy to siliciclastic, and finally ceased close to the Middle/Upper Devonian boundary (Chlupáè, 1993).

Stop 4.4:

Open quarry of NÆmèicky Les, SE of Mraènice.

The outcrop shows Mraènice trondhjemite that is cut by N-S trending pegmatite veins. U-Pb zircon dating of this trondhjemite yields an upper and lower intercept at 2017 +181/-168 and 523 +4/-5 Ma, respectively (Zulauf et al., 1997). The lower intercept is interpreted as the emplacement age. The upper intercept should result from inherited zircons of the pre-Cadomian basement, which is typical for the Armorican Terrane Assemblage (e.g. Icartian gneiss of northern Brittany). The intrusion depth of the Mra¹nice trondhjemite has been constrained at ca. 7 km using phengite barometry and petrogenetic considerations for the contact aureole (Zulauf et al., 1997).

Major minerals of the trondhjemite are plagioclase, quartz, muscovite and biotite. The strain geometry of quartz is of the constrictional type, with the long axis of the finite strain ellipsoid, *X*, trending ENE-WSW. Internal crystal plastic strain in quartz is indicated by shape-preferred orientation and boudinage of rutile needles (stretch = ca. 1.25). The quartz fabrics are further characterized by high-temperature (T > ca. 600 °C) chessboard patterns which result from subrain boundaries aligned parallel to the prism and basal planes. As these chessboard patterns do not occur in the gneiss and micaschist of the country rock, they are explained by being the result of subsolidus constrictional deformation during the initial cooling phase of the synkinematic pluton. The melt temperature of the trondhjemite has been determined at ca. 750° C. Thermal modeling suggests that the 500° C isotherm was reached after a cooling period of 350,000 years (Zulauf, 1997).

Stop 4.5:

Quarry of Hvízdalka at the northeastern margin of Domažlice.

Cooling history, strain and strain rate of a synkinematic trondhjemitic dike within a Cambrian strike-slip fault (staurolite/kyanite zone).

The outcrop shows highly-sheared, retrograded paragneiss (phyllonite) that has been intruded by Cambrian synkinematic trondhjemitic dikes. Results of detailed investigations about the kinematics, crystallization/deformation relationship, wall rock and melt temperature, and cooling history have been described by Zulauf and Helferich (1997). The age of the dike should be close to that of the nearby Mra¹nice trondhjemite (523 +4/-5 Ma, see Stop 4.4). This is supported by the following facts: i) the similarity in mineralogy and geochemistry between the Mra¹nice pluton and the trondhjemitic dikes (Vejnar, 1984), ii) the trondhjemites are cut by late Cambrian to early Ordovician pegmatites, iii) in the quarry U baldovske Kaple (N of Domažlice), the trondhjemitic dikes are affected by Devonian thrusts and folds (Zulauf, 1997). Rb-Sr whole rock and K-Ar dating of white mica of the dike yield ages between 362 and 371 Ma (Zulauf et al., 2002a). These ages are comparable with those of the adjacent metasediments of the Domažlice area and thus are interpreted as cooling ages. They suggest that the K-Ar and Rb-Sr isotopic systems were still open during the Variscan cycle. This is compatible with greenschist facies conditions obtained for the Devonian imprints.

Far from the dike the country rocks are not affected by contact metamorphism. The phyllonites result from pervasive shearing along east-northeast trending transcurrent shear zones that cut the entire quarry under retrograde metamorphic conditions. They display a pronounced stretching lineation (pressure shadows behind garnet, elongated grains of quartz and feldspar, fishes of mica and chlorite) that plunges 20 to 30° east-northeast, mostly on steeply north-northwest dipping planes. Macroscopic shear sense indicators like S-C and shear band fabrics indicate a dextral displacement that was also confirmed under the microscope using drag structures in micas as well as asymmetric pressure shadows of chlorite behind rigid porphyroclasts of garnet, sillimanite, muscovite and biotite.

Within the sheared phyllonite the primary minerals of the paragneiss are strongly altered. Garnet is replaced by biotite, and sometimes both minerals are altered into green chlorite. Plagioclase, sillimanite and staurolite are sericitized. In high-strain domains, garnet and staurolite display pervasive fracturing. Micas are also broken but usually rather show bending and kinking. Deformation features in quartz include subgrain boundaries, aligned parallel to the prism planes, and grain boundary migration, marked by local dynamic recrystallization. Plagioclase is deformed by fracturing and cataclasis.

The trondhjemitic melt emplaced at T = 750 °C into the active low-temperature (ca. 350 °C) east-northeast trending dextral transcurrent shear zone. Thermal modeling indicates that the rheologically critical melt fraction and the solidus of the dike were achieved after 1 and 3 days of cooling, respectively. The major part of the shearing occurred within 8 days after the melt emplaced (Zulauf and Helferich, 1997).

The zonation of the dike, in strain magnitude, mineralogy and geochemistry, can be explained by the laterally varying rheology (from margin to centre) during cooling and shearing. The deformation was volume-constant, and the strain data plot in the apparent constrictional field, suggesting a transtensional tectonic setting during the Cambrian. The unusually high value of the calculated longitudinal strain rate ($> 2.8 * 10^{-6}$ s^{-1}; equivalent to a displacement rate of > 2 cm h^{-1}) is probably related to the intruding melt that 'lubricated' the shear zone and thus enhanced its displacement velocity.

Stop 4.6:

Cliffs at the top of Hrdek, SW of jezd.

The Cadomian basement of the Domažlice crystalline complex (DCC) is exposed at the Hr?dek hill in the form of paragneiss and sheared Late Cambrian/Early Ordovician pegmatite, both of which are situated in the staurolite + kyanite zone. The outcrop is further located within the contact aureole of the Lower Carboniferous Babylon granite. The main foliation of the paragneiss dips steeply (60-80°) ESE. Parts of the pegmatites intruded subparallel to this foliation and are sheared along the foliation planes. The stretching/mineral lineation is almost horizontal, trending NE-SW.

Paragneisses consist of quartz, plagioclase, muscovite, biotite, garnet, staurolite, kyanite, and sillimanite. Quartz is characterized by static fabrics (120° triple point patterns) which might result from contact metamorphic heating of the Babylon pluton. Cadomian Barrovian-type minerals (garnet, staurolite, kyanite) are deformed by fracturing and bending. Kyanite shows margins consisting of

sericite. Silliminate, on the other hand, is hardly deformed. It appears along the foliation planes and is included in quartz and muscovite.

Quartz of the pegmatite shows relics of chessboard patterns that result from two sets of subgrains, one with boundaries parallel to the prism planes, the other with boundaries parallel to the basal planes. The latter suggest c-slip in quartz at T > ca. 600° C (Mainprice et al., 1986), which could be explained by synkinematic emplacement of the pegmatite. T > 600° C is further consistent with the fact that the plagioclase of the pegmatite is partly recrystallized. There are some asymmetric structures, such as asymmetric pressure shadows of biotite behind garnet, which, however, do not indicate an unequivocal sense of shear.

U-Pb dating of monazite, separated from paragneiss, yields ages at ca. 490 Ma (Timmermann, pers. commun.) which is close to the age of the DCC pegmatites (Glodny et al., 1998). K-Ar dating of muscovite and biotite yield 350 ±7 and 306 ±6 Ma (Zulauf et al., 2002). The K-Ar ages might have been influenced by the intrusion of the nearby Babylon pluton. The distance from Hr«dek hill to its northern margin is only ca. 1 km. White mica of gneisses from the DCC, situated remote from the Babylon pluton, yield Ar-Ar and K-Ar ages at ca. 362 Ma (Dallmeyer and Urban, 1998, Zulauf et al., 2002).

DAY 5

Field trip to the Brunovistulian unit
(with contributions by P. Hanžl)

Stop 5.1:

Cadomian island-arc-type crust of the Slavkov terrane: The Blansko granodiorite pluton

Cliffs and large fresh blocks of a mafic facies of the Blansko granodiorite pluton can be studied in a small valley at the eastern margin of Blansko, along the Blansko–Tìchov road (19 km NNE of the centre of Brno). Most of the exposed rocks represent medium-grained biotite-hornblende tonalites. Microdiorite enclaves can often be seen.

The rocks experienced slight alteration at greenschist facies conditions. Epidote is a common secondary mineral. Primary accessory minerals are zircon, apatite, sphene, allanite and magnetite. As most granitoids of the Slavkov terrane, the Blansko granodiorite has a particularly high magnetic susceptibility (Hrouda, 1980).

Geochemistry: The Blansko granodiorite is a normal-K, I-type granitoid with A/CNK ratios slightly below 1. Typical are low Nb (< 10 ppm) and low Th values (< 5 ppm). Chondrite-normalized REE patterns are steep with La/Lun ~10 (La Ξ20 ppm) and show no significant Eu anomalies. $^{87}Sr/^{86}Sr$ initial ratios are very low (~0.704) and, together with εNd_i values of around 0, indicate an immature source (Finger et al., 2000b).

Geochronology: Fritz et al. (1996) reported Ar-Ar hornblende ages of ca. 590 Ma for one sample of the Blansko granodiorite. This age is considered to approximately date the formation of the pluton.

Further reading: Hanžl and Melichar (1997).

Stop 5.2:

Early Cadomian metavolcanic rocks of the Central Basic Belt: quarry at Opálenka

The abandoned quarry at the northern slope of the Opálenka Hill, 2 km E of the railway station in Kuøim (13 km NNW of the centre of Brno) exposes three types of metavolcanic rocks. Dominant are metabasalts, which probably represent former lava flows. Metarhyolites form layers and up to 10-m-thick dikes within the metabasalts. Additionally, lense-shaped bodies of metadolerites occur.

The metabasalts are aphanitic to fine-grained with an ophitic to intersertal or microglomerophyric texture. The metadolerites are similarly mafic, but with a coarser texture, containing mm-sized plagioclase and light-green amphiboles. The metarhyolite dikes are aphanitic to fine-grained rocks, sometimes with a porphyritic texture.

Greenschist facies metamorphism caused a significant alteration of the entire igneous rock assemblage of the quarry. This alteration includes the growth of actinolite, chlorite, epidote, sericite, and albite, and was most severe in the mafic rocks.

Geochemistry: Both metabasite types are olivine-normative and have trace-element compositions similar to MORB. The metadolerite may contain a certain cumulate component (low REE contents!). The metarhyolite displays a fractionated REE pattern with La/Lun of c. 3 (La Ξ25 ppm) and a pronounced, negative Eu anomaly. The MORB-normalized trace-element patterns show negative Sr, P, and Ti anomalies, very probably as a result of plagioclase, apatite, and magnetite fractionation. Chemical and isotopic data (εNd_i: around +7) indicate that the metarhyolite represents a mantle-derived magma, which is cosanguinous with the surrounding MORB-type metabasites.

Geochronology: The metarhyolite was dated by

means of the zircon evaporation method at 725 ± 15 Ma (Finger et al., 2000a). The metabasalts and metadolerites are considered to be of the same age and represent the oldest MORB-type metabasites currently known in Central Europe. The rocks are interpreted as having formed in an incipient arc or a back arc basin setting at the active northern Gondwana margin (see introduction).
Further reading: Leichmann (1996), Hanzl et al. (1999), Finger et al. (2000a)

Stop 5.3:

The Plutonic zone of the Central Basic Belt: the quarry at Želešice

The quarry at Želešice (9 km SSW of the centre of Brno) contains several different rock-types: Hornblendites and medium-grained gabbrodioritic rocks, variably sheared and retrogressed, belong to the plutonic subzone of the Central Basic Belt. The mafic rocks were intruded by medium-grained granitoids of the Thaya terrane and stocks and dykes of brown-red granite porphyries, which are probably genetically related to the granitoids. Fine-grained olivine-basalt dykes represent the youngest magmatic event.
Geochemistry: The older mafic rocks (hornblendites and metagabbros) have MORB-like compositions with low REE contents and flat- to slightly-LREE-depleted REE patterns. As opposed to this, other gabbros of the plutonic subzone of the Central Basic Belt show high LREE/HREE ratios, indicating that at least two different magmatic series are involved (Finger et al., 2000a). For the gabbros of Želešice a depleted mantle source is indicated by positive εNd_{600} Ma values in the range of + 5. The granite porphyries and granitoids have crustal isotopic signatures (εNd_i ~ -2 to -5). The youngest olivine-basalt dikes have mildly-enriched trace-element and REE patterns.
Geochronology: Nd model ages for the amphibolites and metagabbros would be compatible with an early Cadomian (~ 700 Ma) formation, coeval with the volcanic rocks of the Central Basic Belt. Granitoids and granite porphyries are presumably of the same age as the Thaya terrane granitoids (~ 580 Ma). For the olivine basalt dikes a Silurian age has been suggested, based on Ar-Ar data (Hanžl et al., 1999).
Further reading: Hanžl et al. (1999)

Stop 5.4:

A Cadomian high-K diorite from the Thaya terrane: the quarry at Dolní Kounice

In the active quarry between the villages of Moravské Bránice and Dolní Kounice, on the left bank of the Jihlava river (18 km SW of the centre of Brno), diorites (quartzdiorites, quartzmonzodiorites) of the Thaya terrane are exposed. Compared to the mafic plutons in the Slavkov terrane, these mafic rocks are isotopically and chemically more evolved. In the quarry, mixing phenomena between different magmas can be studied. The main type of diorite is medium-grained. It carries amphibole, plus variable amounts of biotite, as mafic constituents, and is typically ilmenite-bearing (resulting in a lower magnetic susceptibility compared to the Blansko granodiorite). Further accessory minerals are zircon, apatite, titanite and allanite.
Geochemistry: The diorites from Dolni Kounice are high-K I-type granitoids. They have enriched REE patterns (La/Lun ~ 8) and relatively high Sr, Ba, Rb, Zr, Nb and Th contents. $^{87}Sr/^{86}Sr_i$ isotope ratios are intermediate (~ 0.705-0.707), εNd_i values are negative (-2), indicating an enriched mantle source or a crustal contamination.
Geochronology: The main diorite was dated by Van Breemen et al. (1982) at 584 ±5 Ma (upper intersect zircon age). Fritz et al. (1996) published a hornblende Ar-Ar age of 599 ±1 Ma for the same diorite from another locality (Anenský Mlýn).
Further reading: Leichmann (1999).

Stop 5.5:

Cadomian, high-K, I-type granodiorite of the Thaya batholith: a quarry near Retz

In an abandoned quarry near Retz (ca. 10 km SW of Znojmo), on the southern slope of the Gollitsch hill, a Cadomian, medium-grained biotite-granodiorite can be studied. The rock shows a slight Variscan deformation of greenschist-facies grades involving the recrystallisation of quartz and the growth of secondary green biotite. Slightly metamorphosed granodiorites of this type are very abundant in the Thaya batholith and are termed “Hauptgranit” (“main granite”) in the literature.
Geochemistry: The chemical composition of the rock is high-K, calc-alkaline. The A/CNK ratio is pivoting around 1.1, but it is probably partly increased due to metamorphic alteration. Little-deformed variants have A/CNK values between 1 and 1.1. Therefore, the granodiorite represents rather an I-type than an S-type magma. This interpretion is also supported by generally-high Sr contents. $^{87}Sr/^{86}Sr_i$ ratios of around 0.709 (Scharbert and Batik 1980) and negative εNd_i values of -4 to -7 (Finger et al., 2000b) suggest that

old (meta)igneous crust served as magma source.
Geochronology: No precise ages are presently available for this rock. An Rb-Sr errorchron gave an age of 610 ± 54 Ma (Finger and Riegler, 1999). Other, subalkaline variants of the Hauptgranite with distinctly high Zr contents have been recently dated at 567 ± 5 Ma (SHRIMP zircon age, Friedl et al. 2004).
Further reading: Finger et al. (1989), Finger (1999)

Stop 5.6:

Overprinted Cadomian Basement close to the Moldanubian thrust: The Weitersfeld pencil-gneiss

The small abandoned quarry near the church of Weitersfeld (ca. 20 km WSW of Znojmo) provides an example of how strongly the western part of the Brunovistulian unit was overprinted during the Variscan orogeny. The grey, mylonitized granite displays a horizontal foliation with a striking NE-trending lineation. K-feldspar augen sometimes show primary Karlsbad twinning; the matrix consists of biotite, muscovite, quartz and plagioclase.
Geochemistry: The exposed pencil gneiss has the composition of a felsic high-K granite. $^{87}Sr/^{86}Sr_{600}$ Ma ratios are high (~ 0.713), εNd_{600} Ma values are strongly negative (-11). Generally, it can be stated that the deformed granitoids at the western margin of the Brunovistulian plate have the most evolved isotope composition of all Brunovistulian granitoids, and are apparently derived from very old cratonic crust (maturation of crust from east to west!).
Geochronology: An Ar-Ar muscovite age of 326 ±1 Ma (Dallmeyer et al., 1990) dates the cooling stage of the Variscan regional metamorphosis. Electron-microprobe-based monazite dating (Finger, unpubl.) revealed a relict population of ca. 600 Ma old monazites.
Further reading: Finger et al. (1989)

Stop 5.7:

Roof rocks of the Cadomian granitoids:
The Fugnitz calcsilicate schists (quarry at Raisdorf, ca. 17 km NW of Eggenburg)

In some places the older roof of the Cadomian granitoids of the Thaya terrane is preserved. This comprises various micaschists (Libowitzky, 1989) as well as distinct, banded fine-grained calcsilicate schists, the sedimentary protoliths of which are considered Late-Proterozoic in age (Frasl, 1991). In the quarry of Raisdorf these rocks display a Variscan, amphibolite-facies metamorphic mineral paragenesis with diopside, hornblende, clinozoisite, quartz and plagioclase (strong inverse zoning with oligoclase cores and labradorite rims), additionally some K-feldspar, biotite, calcite and titanite. Aplitic and pegmatitic layers in the rocks are interpreted as being related to the Cadomian granitic plutonism. Frasl (1991) considered the calc-silicate rocks as having initially experienced Cadomian contact metamorphism.
Further reading: Frasl (1968), Bernroider (1989), Libowitzky (1989)

Stop 5.8:

The Bittesch gneiss: A deformed Cadomian granite with abundant Mesoproterozoic zircon relics (active quarry 1 km NW Harmansdorf, 6 km SW of Eggenburg)

The Bittesch gneiss is a felsic, biotite-muscovite augen-gneiss with granitic to granodioritic composition. It forms an elongated orthogneiss body immediately below the Moldanubian thrust, which accompanies the western margin of the Moravo-Silesian unit over more than 100 kilometres. Microscopic structures and textures display top-to-the-N thrusting.
Geochemistry: A characteristic geochemical feature of the Bittesch gneiss is its relatively high Sr content (~ 300 ppm) and low Rb/Sr ratio (~ 0.5), at a generally high SiO_2 content of 70-75 wt %. The rock is believed to represent a low-T, crustally-derived I-type granite magma (Finger and Sturm 1994). $^{87}Sr/^{86}Sr$ initial ratios are in the range of 0.712 - 0.714, the εNd_i values are strongly negative (-11 to -12).
Geochronology: Ar-Ar muscovite ages of ca. 329 Ma date the cooling of the rock after Variscan regional metamorphism (thrusting of the Moldanubian unit over the Brunovistulian plate). SHRIMP zircon dating has provided magmatic formation ages of 584 ±6 Ma and 578 ±7 Ma for two samples of Bittesch gneiss (Friedl et al., 2004). Furthermore, many inherited zircons with Mesoproterozoic and Early Palaeoproterozoic ages of c. 1.2 Ga, 1.5 Ga, 1.65-1.8 Ga have been found. This has been taken as evidence that the Brunovistulian terrane is derived from a Grenvillian cratonic province, and not from north Africa. A Late Precambrian position close to the Amazonian craton has been inferred (Friedl et al. 2000), comparable to the Avalonian terranes of North America and the United Kingdom.
Further reading: Finger et al. (1989), Friedl et al.

(2000, 2004)

DAY 6

(Departure in the morning for Vienna, visit of Vienna, and travel on to Florence)

References cited

Bankwitz, P. and Bankwitz, E., 1995. Proterozoikum/ Schwarzburger Antiklinorium. In: G. Seidel (Editor), Geologie von Thüringen. E. Schweitzerbart´sche Verlagsbuchhandlung, Stuttgart, pp. 46-77.

Bowes, D.R. and Aftalion, M., 1991. U-Pb isotopic evidence for early Ordovician and late Proterozoic units in the Mariánské Lázné Complex, Central European Hercynides. N. Jb. Miner. Mh., 1991: 315-326.

Bues, C., Dörr, W., Fiala, J., Vejnar, Z. and Zulauf, G., 2002. Emplacement depth and radiometric ages of Paleozoic plutons of the Neukirchen-KdynÆ massif: Differential uplift and exhumation of Cadomian basement due to Carboniferous orogenic collapse (Bohemian Massif). Tectonophysics, 352: 225-243.

Bula, Z., Jachowicz, M. and Pøichystal, A. 1997. Lower Palaeozoic deposits of the Brunovistulicum. Terra Nostra 97/11: 32-38.

Buschmann, B., 1995. Geotectonic facies analysis of the Rothstein Formation (Neoproterozoic, Saxothuringian Zone, Germany). Unpublished Ph.D. Thesis, Bergakademie Freiberg, 122 pp.

Buschmann, B., Linnemann, U., Schneider, J. and Süss, T., 1995. Die cadomische Entwicklung im Untergrund der Torgau-Doberluger Synklinale. Z. geol. Wiss., 23: 729-749.

Buschmann, B., Nasdala, L., Jonas, P., Linnemann, U. and Gehmlich, M., 2001. SHRIMP U-Pb dating of tuff-derived and detrital zircons from Cadomian marginal basin fragments (Neoproterozoic) in the northeastern Saxothuringian Zone (Germany). N. Jb. Geol. Paläont. Mh., 6: 321-342

Cháb, J., Suchý and Vejnar, Z., 1995. Metamorphic evolution. In: Dallmeyer, R.D., Franke, W. and Weber, K. (eds.). Pre-Permian Geology of Central and Eastern Europe, pp. 404-410; Springer-Verlag, Berlin, Heidelberg.

Cháb, J. and Žáèek, V., 1994. Metamorphism of the Teplá Crystalline Complex. KTB Report, 94-3. 33-37.

Chlupáè, I., 1993. Geology of the Barrandian. A Field Trip Guide, 163 pp.; Waldemar-Kramer, Frankfurt a.M.

Dallmeyer, R.D. and Urban, M., 1998. Variscan vs Cadomian tectonothermal activity in northwestern sectors of the Tepl -Barrandian zone, Czech Republic: constraints from 40Ar/39Ar ages. Geol. Rundsch., 87: 94-106.

DePaolo, D.J., 1981. Neodymium isotopes in the Colorado Front Range and crust-mantle evolution in the Proterozoic. Nature, 291: 193-197.

Dörr, W., Fiala, J., Vejnar, Z. and Zulauf, G., 1998. U-Pb zircon ages and structural development of metagranitoids of the Teplá crystalline complex - evidence for pervasive Cambrian plutonism within the Bohemian massif (Czech Republic). Geol. Rundsch., 87: 135-149.

Dörr, W., Zulauf, G., Fiala, J., Franke, W. and Vejnar, Z. 2002. Neoproterozoic to Early Cambrian history of an active plate margin in the Tepl« Barrandian unit – a correlation of U-Pb Isotopic-Dilution-TIMS ages (Bohemia, Czech Republic). Tectonophysics, 352: 65-85.

Dudek, A. 1980. The crystalline basement block of the Outer Carpathians in Moravia: Bruno-Vistulicum. Rozpravy Ceskoslovenské Akademie Vìd Øada matematických a pøirodních Vìd, 90/8: 3-85.

Dudek, A. 1995. Metamorphic evolution of the Moravo-Silesian basement. In Dallmeyer et al. (eds) Pre-Permian Geology of Central and Eastern Europe. Springer, Berlin, pp. 508-511.

Dudek, A. and Melkova, J. 1975. Radiometric age determination in the crystalline basement of the Carpathian Foredeep and of the Moravian Flysch. Vìstnik Ústøedního ústavu geologického, 50: 257-264.

Dvoøák, J. 1995. Stratigraphy of the Moravo-Silesian zone. In: Dallmeyer et al. (eds), Pre-Permian Geology of Central and Eastern Europe. Springer, Berlin, 477-489.

Elicki, O., 1997. Biostratigraphic data of the German Cambrian - present state of knowledge. Freib. For. Hft., C 466: 155-165.

Elicki, O., 2000. Die kambrische “Görlitz-Fauna”: Charakteristik und Bedeutung für die stratigraphische und paläogeographische Rekonstruktion Mitteleuropas. Z. geol. Wiss., 28: 11-32.

Elicki, O. and Debrenne, F., 1993. The Archaeocyatha of Germany. Freib. For. Hft., C 450: 3-40.

Fatka, O. and Gabriel, Z., 1991. Microbiota from siliceous stromatolitic rocks of the Barrandian Proterozoic (Bohemian Massif). Cas. Mineral. Geol., 36: 143-148..

Finger, F., Frasl, G., Dudek, A., Jelínek, E. and Thöni, M., 1995. Cadomian plutonism in the Moravo-Silesian

basement. In: Dallmeyer et al. (eds.) Pre-Permian Geology of Central and Eastern Europe. Springer, Berlin, pp. 495-507.

Finger, F., Frasl, G., Höck, V. and Steyrer, H.P., 1989. The granitoids of the Moravian Zone of north-east Austria - Products of a Cadomian active continental margin? Precambrian Research 45: 235-245.

Finger, F., Hanžl, P., Pin, C., Von Quadt, A. and Steyrer, H.P., 2000. The Brunovistulian: Avalonian Precambrian sequence at the eastern end of the Central European Variscides? Geological Society of London, Special Publication, 179: 103-112.

Finger, F. and Pin, C., 1997. Arc-type crustal zoning in the Bruno-Vistulicum, Eastern Czech Republic: A trace of the late-Proterozoic Euro-Gondwana margin. Journal of the Czech Geological Society, 42: 53.

Finger, F. and Riegler, G., 1999. Der Thayabatholith und der kristalline Untergrund des Weinviertels. Arbeitstagung Geologische Bundesanstalt, 1999: 23-31.

Finger, F. and Steyrer, H.P., 1995. A tectonic model for the eastern Variscides: indications from a chemical study of amphibolites in the south-eastern Bohemian Massif. Geologica Carpathica, 46: 137-150.

Finger, F., Schitter, F., Riegler, G. and Krenn, E., 1999. The history of the Brunovistulian: Total-Pb monazite ages from the Metamorphic Complex. Geolines, 8: 21-23.

Finger, F., Tichomirowa, M., Pin, C. and Hanžl, P., 2000. Relics of an early-Panafrican metabasite-metarhyolite formation in the Brno Massif, Moravia, Czech Republic. International Journal of Earth Sciences, 89: 328-335.

Floyd, P.A., Winchester, J.A., Seston, R., Kryza, R. and Crowley, Q.G., 2000. Review of geochemical variation in Lower Palaeozoic metabasites from the NE Bohemian Massif: intracratonic rifting and plume-ridge interaction. Geological Society of London, Special Publication, 179: 155-174.

Franke, W. and Engel, W. 1982. Variscan Sedimentary Basins on the Continent and relations with south-west England. Proceedings of the Ussher Society, 5: 259-269.

Franke, W., 2000. The mid-European segment of the Variscides: tectonostratigraphic units, terrane boundaries and plate tectonic evolution. In: Franke, W., Haak, V., Oncken, O., Tanner, D. (eds.), Orogenic Processes: Quantification and Modelling in the Variscan Belt. Geol. Soc. London, Spec. Publ., 179: 35-61.

Franke, W., Dallmeyer, R.D. and Weber, K., 1995. Geodynamic Evolution.- In: Dallmeyer, R.D., Franke, W. and Weber, K. (eds.), Pre-Permian Geology of Central and Eastern Europe, pp. 579-593; Springer, Berlin, Heidelberg.

Franke, W. and elaÿniewicz, A., 2002. Structure and evolution of the Bohemian Arc. In: Winchester, J.A., Pharaoh, T.C. and Verniers, J. (eds.), Palaeozhoic Amalgamation of Central Europe. Geological Society Special Publication, 201: 279-293.

Frasl, G., 1970. Zur Metamorphose und Abgrenzung der Moravischen Zone im niederösterreichischen Waldviertel. Nachrichten der Deutschen Geologischen Gesellschaft, 2: 55-61.

Frasl, G., 1991. Das Moravikum der Thaya-Kuppel als Teil der variszisch deformierten Randzone des Bruno-Vistulikums – eine Einführung. Arbeitstagung Geologische Bundesanstalt, 1991: 49-62.

Friedl, G., 1997. U/Pb-Datierungen an Zirkonen und Monaziten aus Gesteinen vom österreichischen Anteil der Böhmischen Masse. unpublished PhD Thesis, Salzburg University, 242 p.

Friedl, G., Finger, f., Mcnoughton, N. and Fletcher, I.R., 2000. Deducing the ancestry of terranes: SHRIMP evidence for South American-derived Gondwana fragments in central Europe. Geology, 28: 1035-1038.

Fritz, H., Dallmeyer, R.D. and Neubauer, F., 1996. Thick-skinned versus thin-skinned thrusting: Rheology controlled thrust propagation in the Variscan collisional belt (The southeastern Bohemian Massif, Czech Republic – Austria). Tectonics, 15: 1389-1413.

Fuchs, G., 1998. Kritische Gedanken zur neueren geodynamischen Forschung in der östlichen Böhmischen Masse. Jahrbuch der Geologischen Bundesanstalt, 141/1: 39-43.

Gaertner, H.R., 1944. Die Schichtgliederung der Phyllitgebiete in Thüringen und Nordbayern und ihre Einordnung in das stratigraphische Schema. Jb. Reichsanst. Bodenforsch., 62: 54-80.

Geyer, G. and Elicki, O., 1995. The Lower Cambrian triliobites from the Görlitz Synclinorium (Germany) - review and new results. Paläont. Z., 69: 87-119.

Glodny, J., Grauert, B., Fiala, J., Vejnar, Z., Krohe, A., 1998. Metapegmatites in the western Bohemian massif: ages of crystallization and metamorphic overprint, as constrained by U-Pb zircon, monazite, garnet, columbite and Rb-Sr muscovite data. Geol Rundsch 87: 124-134

Hammer, J., Eidam, J., Röber, B. and Ehling, B.-C., 1999. Prävariscischer and variscischer granitoider Magmatismus am NE-Rand des Böhmischen Maasivs - Geochemie und Petrogenese. Z. geol. Wiss., 27: 401-

415.
Hanžl, P. and Melichar, R., 1997. The Brno massif: a section through the active continental margin or a composed terrane? Krystallinikum, 23: 33-58.
Hanžl, P., Melichar, R. and Leichmann, J., 1999. Field excursion on Brno Massif. Geolines, 8: 80-95.
Hanžl, P., Pøichystal, A. and Melichar, R., 1995. The Brno Massif: volcanites of the northern part of the metabasite zone. Acta Universitatis Palackiane Olomucensis, Geologica, 34: 73-79.
Hegner, E. and Kröner, A., 2000. A rewiev of Nd isotopic data and xenocrystic and detrital zircon ages from the pre-Variscan basement in the eastern Bohemian Massif: speculations on palinspastic reconstruction. Geological Society of London, Special Publication, 179: 113-130.
Henk, A., von Blanckenburg, F., Finger, F., Schaltegger U. and Zulauf, G., 2000. Syn-convergent high-temperature metamorphis and magmatism in the Variscides – a discussion of potential heat sources. Geological Society of London, Special Publication, 179: 387-400.
Jachowicz, M. and Pøichystal, A., 1997. Lower Cambrian sediments in deep boreholes in south Moravia. Vìstník Èeského geologického ústavu, 72/4: 329-332.
Jelínek, E. and Dudek, A., 1993. Geochemistry of subsurface Precambrian plutonic rocks from the Brunovistulian complex in the Bohemian massif, Czechoslovakia. Precambrian Research, 62: 103-125.
Jonas, P., Buschmann, B. and Gaitzsch, B., 2000. Unterkambrischer und unterkarbonischer Vulkanismus der Torgau-Doberlug Synklinale (NE Saxothuringische Zone). Z. geol. Wiss., 28: 157-175.
Kerr, A., Jenner, G.A. and Fryer B.J., 1995. Sm-Nd isotopic geochemistry of Precambrian to Palaeozoic granitoid suites and the deep-crustal structures of the southeast margin of the Newfoundland Appalachians. Canadian Journal of Earth Sciences, 32: 224-245.
Košler, J., Rogers, G., Bowes, D.R. and Hopgood, A.M., 1994. Rb-Sr isotopic evidence for polymetamorphism in the Domažlice crystalline complex from a study of mica-feldspar pairs in a segregation pegmatite near Stráž, western Bohemia. Mitt. Öster. Miner. Ges., 139: 75-76.
Kreuzer, H., Müller, P., Okrusch, M., Patzak, M., Schüßler, U., Seidel, E., Šmejkal, V. and Vejnar, Z., 1990. Ar-Ar conformation for Cambrian, Early Devonian, and Mid-Carboniferous Tectonic Units at the Western Margin of the Bohemian Massif. 6. Rundgespräch Geodynamik des europ. Variszikums, 15. - 18.11.1990; Clausthal-Zellerfeld (abstr.).
Kröner, A. and Hegner, E., 1998. Geochemistry, single zircon ages and Sm-Nd systematics of granitoid rocks from the Gory Sowie (Owl Mts), Polish West Sudetes: evidence for early Palaeozoic arc-related plutonism. Journal of the Geological Society, London, 155: 711-724.
Kröner, A., Štípská, P., Schulmann, K. and Jaeckel, P., 2000. Chronological constraints on the pre-Variscan evolution of the northeastern margin of the Bohemian Massif, Czech Republic. Geological Society of London, Special Publication, 179: 175-198.
Leichmann, J., 1996. Geologie und Petrologie des Brünner Massivs. Unpbulished PhD Thesis, University Salzburg, 118 p.
Liew, T.C. and Hofmann, A.W., 1988. Precambrian crustal components, plutonic associations, plate environment of the Hercynian Fold Belt of central Europe: Indications from a Nd and Sr isotopic study. Contributions to Mineralogy and Petrology, 98: 129-138.
Linnemann, U., 1991. Glazioeustatisch kontrollierte Sedimentationsprozesse im Oberen Proterozoikum der Elbezone (Weesensteiner Gruppe/Sachsen). Zbl. Geol. Paläont. Teil I, 12: 2907-2934.
Linnemann, U., 1995. The Neoproterozoic terranes of Saxony (Germany). Precambr. Res., 73: 235-250.
Linnemann, U. and Buschmann, B., 1995a. Der Nachweis der cadomischen Diskordanz in einer Tiefenbohrung bei Gera und deren Bedeutung für das proterozoisch-paläozoische Standardprofil im Schwarzburger Antiklinorium. Geowiss. Mitt. Thüringen, 3: 1-11.
Linnemann, U. and Buschmann, B., 1995b. Die cadomische Diskordanz im Saxothuringikum (oberkambrisch-tremadocische overlap-Sequenzen). Z. geol. Wiss., 23: 707-727.
Linnemann, U., Gehmlich, M., Heuse, T. and Schauer, M., 1999. Die Cadomiden und Varisziden im Thüringisch-Vogtländischen Schiefergebirge (Saxothuringisches Terrane). Beitr. Geol. v. Thür. N.F., 6: 7-39.
Linnemann, U., Gehmlich, M., Tichomirowa, M., Buschmann, B., Nasdala, L., Jonas, P., Lützner, H. and Bombach, K., 2000. From Cadomian Subduction to Early Palaeozoic Rifting: The Evolution of Saxo-Thuringia at the margin of Gondwana in the light of single zircon geochronology and basin development (Central European Variscides, Germany). In: W. Franke, V. Haak, O. Oncken, and D. Tanner (eds.), Orogenic processes - Quantification and modelling in

the Variscan Belt of Central Europe. Spec. Publ. Geol. Soc. London, 179: 131-153.

Linnemann, U., Gehmlich, M., Tichomirowa, M. and Buschmann, B., 1998. Introduction to the Pre-Symposium Excursion (part I): The Peri-Gondwanan Basement of the Saxo-Thuringian Composite Terrane. In: U. Linnemann, T, Heuse, O. Fatka, P. Kraft, R. Brocke, B.-D. Erdtmann (Editors), "Pre-Variscan Terrane Analysis of Gondwanan Europe - Excursion Guides and Abstracts"-Schr. Staatl. Mus. Min. Geol. Dresden Nr. 9. Staatliches Museum für Mineralogie und Geologie zu Dresden, Dresden, pp. 7-13.

Linnemann, U. and Heuse, Th., 2000. The Ordovician of the Schwarzburg Anticline: Geotectonic setting, biostratigraphy and sequence stratigraphy (Saxo-Thuringian Terrane, Germany). Z. dt. Geol. Ges., 151/4: 471-491.

Linnemann, U., McNaughton, N.J., Romer, R.L., Gehmlich, M., Drost, K., and Tonk, C. (subm.). West African Provenance for Saxo-Thuirngia (Bohmeian Assif): Did Armorica ever leave pre-Pangean Gondwana? – U/Pb SHRIMP zircon evidence and the Nd-isotopic record. Int. J. Earth Sci. (submitted)

Linnemann, U. and Romer, R.L., 2002. The Cadomian Orogeny in Saxo-Thuringia, Germany: geochemical and Nd-Sr-Pb isotopic characterisation of marginal basins with constraints to geotectonic setting and provenance. Tectonophysics, 352: 33-64.

Linnemann, U. and Schauer, M., 1999. Die Entstehung der Elbezone vor dem Hintergrund der cadomischen und variszischen Geschichte des Saxothuringischen Terranes - Konsequenzen aus einer abgedeckten geologischen Karte. Z. geol. Wiss., 27: 529-561.

Linnemann, U., Tichomirowa, M., Gehmlich, M., Buschmann, B. and Brombach, K. 1998. Das cadomisch-frühpalaeozoische Basement des Saxothuringischen Terranes (geotektonisches Setting, Geochronologie, Sequenzstratigraphie). Terra Nostra 98/2, 99-101.

Liou, J.G., Maruyama, S. and Cho, M., 1987. Very low-grade metamorphism of volcanic and volcaniclastic rocks - mineral assemblages and mineral facies.- In: Frey, M. (eds.), Low temperature metamorphism, pp. 59-112; Chapman and Hall, New York.

Mainprice, D., Bouchez, J.-L., Blumenfeld, P. and Tubia, J., 1986. Dominant c-slip in naturally deformed quartz: implications for dramatic plastic softening at high temperatures. Geology, 14: 819-822.

Mašek, J. and Zoubek, J., 1980. Návrh vymezení a ozna¹ováni hlavních stratigrafických jednotek barrandienského proterozoika. VÆst. Ústé. Úst. geol., 55,2: 121-123.

Matte, P., 1986. Tectonics and plate tectonics Model for the Variscan belt of Europe. Tectonophysics, 126: 329-374.

Matte, P., 1991. Accretionary history and crustal evolution of the Variscan belt in Western Europe. Tectonophysics, 196: 309-337.

Matte, Ph., Maluski, H., Rajlich, P. and Franke, W., 1990. Terrane boundaries in the Bohemian Massif: Results of large-scale Variscan shearing. Tectonophysics, 177: 151-170.

Matura, A. 1976. Hypothesen zum Bau und zur geologischen Geschichte des Grundgebirges von Südwestmähren und dem niederösterreichischen Waldviertel. Jahrbuch der Geologischen Bundesanstalt, 119: 63-74.

McKerrow, W.S., Scotese, C.R. and Brasier, M.D., 1992. Early Cambrian continental reconstructions. J. Geol. Soc. London, 149: 599-606.

Mísaø, Z. 1979. Ultrabazika jako indikátory hlubinné, blokové a vrásové stavby na pøíkladì východního okraje Èeského masívu. Zbornik predn konference Smolenice, 1979: 191-210.

Murphy, J.B., Strachan, R.A., Nance, R.D., Parker, K.D.; and Fowler, M.B., 2000. Proto-

Nance, R.D. and Thompson, D., 1996. Avalonian and Related Peri-Gondwanan Terranes of the Circum-North Atlantic. Journal of the Geological Society of America, Special Paper, 304: 1-390.

Nance, R.D. and Murphy, J.B., 1994. Contrasting basement isotopic signatures and the palinspastic restoration of peripheral orogens: Example from the Neoproterozoic Avalonian-Cadomian belt. Geology, 22: 617-620.

Nance, R. D. and Murphy, J. B., 1996. Basement isotopic signatures and Neoproterozoic paleogeography of Avalonian - Cadomian and related terranes in the circum - North Atlantic, In: R.D. Nance and M.D. Thompson (Editors), Avalonian and Related Peri - Gondwanan Terranes of the Circum - North Atlantic. Geol. Soc. Am. Spec. Pap., 304: 333-346.

Nance, R.D., Murphy, J.B., Strachan, R.A., D´Lemos, R.S. and Taylor, G.K., 1991. Late Proterozoic tectonostratigraphic evolution of the Avalonian and Cadomian terranes. Precambr. Res., 53: 41-78.

O´Brien, S.J., O´Brien, B.H., Dunning, G.R. and Tucker, R.D., 1996. Late Neoproterozoic Avalonian and Related Peri-Gondwanan Rocks of the Newfoundland Appalachians. In Nance, R.D. and Thompson, D. (eds.) Avalonian and Related Peri-Gondwanan Terranes of the Circum-North Atlantic. Journal of the Geological

Society of America, Special Paper, 304: 9-28.
Pato¦ka, F., Galle, A., Vavdrová, M. and Vlašímský, P., 1994. Early Paleozoic evolution of the Barrandian Terrane, Bohemian Massif, Czech Republic: Paleotectonic implications of sedimentary, fossil and volcanic record.- J. Czech Geol. Soc., 39, 82-83.
Pin, C., 1990. Variscan oceans: Ages, origins and geodynamic implications inferred from geochemical and radiometric data. Tectonophysics, 177: 215-227.
Pták. J. and Wartha, K., 1966. Fabric analysis and the major fold structure of the Upper Proterozoic in the Plzeò area. Sbor. geol. vìd, Geologie, 11: 33-48.
Scharbert, S. and Batik, P., 1980. The age of the Thaya (Dyje) Pluton. Verhandlungen der Geologischen Bundesanstalt, 1980: 325-331.
Scheuvens, D. and Zulauf, G., 2000. Exhumation, strain localization, and emplacement of granitoids along the western part of the Central Bohemian shear zone (central European Variscides, Czech Republic). Int. J. Earth Sci., 89: 617-630.
Schmidt, K., 1960. Geologie: Die Geröllführung algonkisch-kambrischer Grauwacken des Westlausitzer Zuges. Freib. For. Hft., C 91: 1-98.
Schulmann, K., 1990. Fabric and kinematic study of the Bites orthogneiss (southwestern Moravia): Result of large-scale northeastward shearing parallel to the Moldanubium/Moravian boundary. Tectonophysics, 177: 229-244.
Scotese, C.R., Boucot, A.J. and McKerrow, W.S., 1999. Gondwanan palaeogeography and palaeoclimatology. J. African Earth Sci., 28: 99-114.
Štelcl, J. and Weiss, J., 1986. Brnìnský masív. Universita J.E. Purkyne, Brno. pp. 1-255.
Tait, J., Bachtadse, V. and Soffel, H., 1995. Upper Ordovician palaeogeography of the Bohemian Massif: implications for Armorica. Geophys. J. Int., 122: 211-218.
Tait, J.A., Bachtadse, V. and Soffel, H.C., 1996. Eastern Variscan fold belt: Palaeomagnetic evidence for oroclinal bending. Geology, 24: 871-874.
Tait, J.A., Bachtadse, V., Franke, W. and Soffel, H.C., 1997. Geodynamic evolution of the European Variscan fold belt: paleomagnetic and geological constraints. Geol. Rundsch., 86: 585-598.
Tait, J.A., Schätz, M., Bachtadse, V. and Soffel, H., 2000. Palaeomagnetism and Palaeozoic palaeogeography of Gondwana and European terranes. In: Franke, W., Haak, V., Oncken, O., Tanner, D. (eds.), Orogenic Processes: Quantification and Modelling in the Variscan Belt .Geol. Soc. London, Spec. Publ., 179: 21-34.
Tichomirowa, M., Linnemann, U. and Gehmlich, M., 1997. Zircon ages as magmatic time marks – Comparison of the crustal evolution in different units of the Saxo-Thuringian zone. Terra Nostra, 97/11: 137-141.
Van Breemen, O., Aftalion, M., Bowes, D.R., Dudek, A., Misaø, Z., Povondra, P. and Vrana, S., 1982. Geochronological studies of the Bohemian massif, Czechoslovakia, and their significance in the evolution of Central Europe. Transactions of the Royal Society of Edinburgh Earth Sciences, 73: 89-108.
Vejnar, Z., 1982. Regionální metamõrfoza psamitickopelitických hornin domažlické oblasti.- Sborník geologických vÆd, Geologie, 37: 9-70 (in Czech with English abstract), Prague.
Vejnar, Z. (1984): Magmatismus. In: Vejnar, et al. (eds.), Geologie domažlicke oblasti, pp. 48-83; Ustøedni Ustav Geologický, Prague.
Von Quadt, A. 1994. U-Pb zircon data and Pb-Sr-Nd isotope chemistry from metagabbros from the KTB-borehole. Journal of the Czech Geological Society, 39/1: 87-88.
Winchester, J.A., Pharaoh, T.C.and Verniers, J. 2002. Palaeozoic amalgamation of Central Europe: an introduction and synthesis of new results from recent geological and geophysical investigations. Geological Society of London, Special Publication, 201: 1-18.
Wucher, K., 1967. Ergebnisse der Kartierungsbohrungen Heinersdorf 1/60 und 2/62 (Thüringisches Schiefergebirge). Jb. Geol., 1: 297-323.
Žáèek, V. and Cháb, J., 1993. Metamorphism in the Tepla upland, Bohemian Massif, Czech Republic (preliminary report). VÆstnik ‡eskeho geologickeho Ustavu, 68/3: 33-37, Prague.
Zulauf, G., 1997. Von der Anchizone bis zur Eklogitfazies: Angekippte Krustenprofile als Folge der cadomischen und variscischen Orogenese im Teplá-Barrandium (Böhmische Masse). Geotekt. Forsch., 89: 1-302.
Zulauf, G., 2001. Structural style, deformation mechanisms and paleostress along an exposed crustal section: Constraints on the rheology of quartzofeldspathic rocks at supra- and infrastructural levels (Tepla-Barrandian unit, Bohemian Massif). Tectonophysics, 332: 211-237.
Zulauf, G., Bues, C., Dörr, W. and Vejnar, Z., 2002a. 10 km minimum throw along the West Bohemian shear zone: Evidence for dramatic crustal thickening and high topography in the Bohemian Massif (European Variscides). Int. J. Earth Sci, 91: 850-864.
Zulauf G, Dörr W, Fiala J, Kotková J, Maluski H,

Valverde-Vaquero P, 2002b. Evidence for high-temperature diffusional creep preserved by rapid cooling of lower crust (North Bohemian shear zone, Czech Republic). Terra Nova, 14: 343-354.

Zulauf, G., Dörr, W., Fiala, J., Vejnar, Z. 1997. Late Cadomian crustal tilting and Cambrian transtension in the Teplá-Barrandian unit (Bohemian Massif, Central European Variscides). Geol. Rundsch., 86: 571-584.

Zulauf, G. and Helferich, S. 1997. Strain and strain rate in a synkinematic trondhjemitic dike: evidence for melt-induced strain softening during shearing (Bohemian Massif, Czech Republic). J. Struct. Geol., 19: 639-652.

Zulauf, G., Schitter, F., Riegler, G., Finger, F., Fiala, J. and Vejnar, Z., 1999. Age constraints on the Cadomian evolution of the Teplá Barrandian Unit (Bohemian Massif) through electron microprobe dating of metamorphic monazite. Zeitschrift der Deutschen Geologischen Gesellschaft, 150: 627-639.

Back Cover:
field trip itinerary

FIELD TRIP MAP

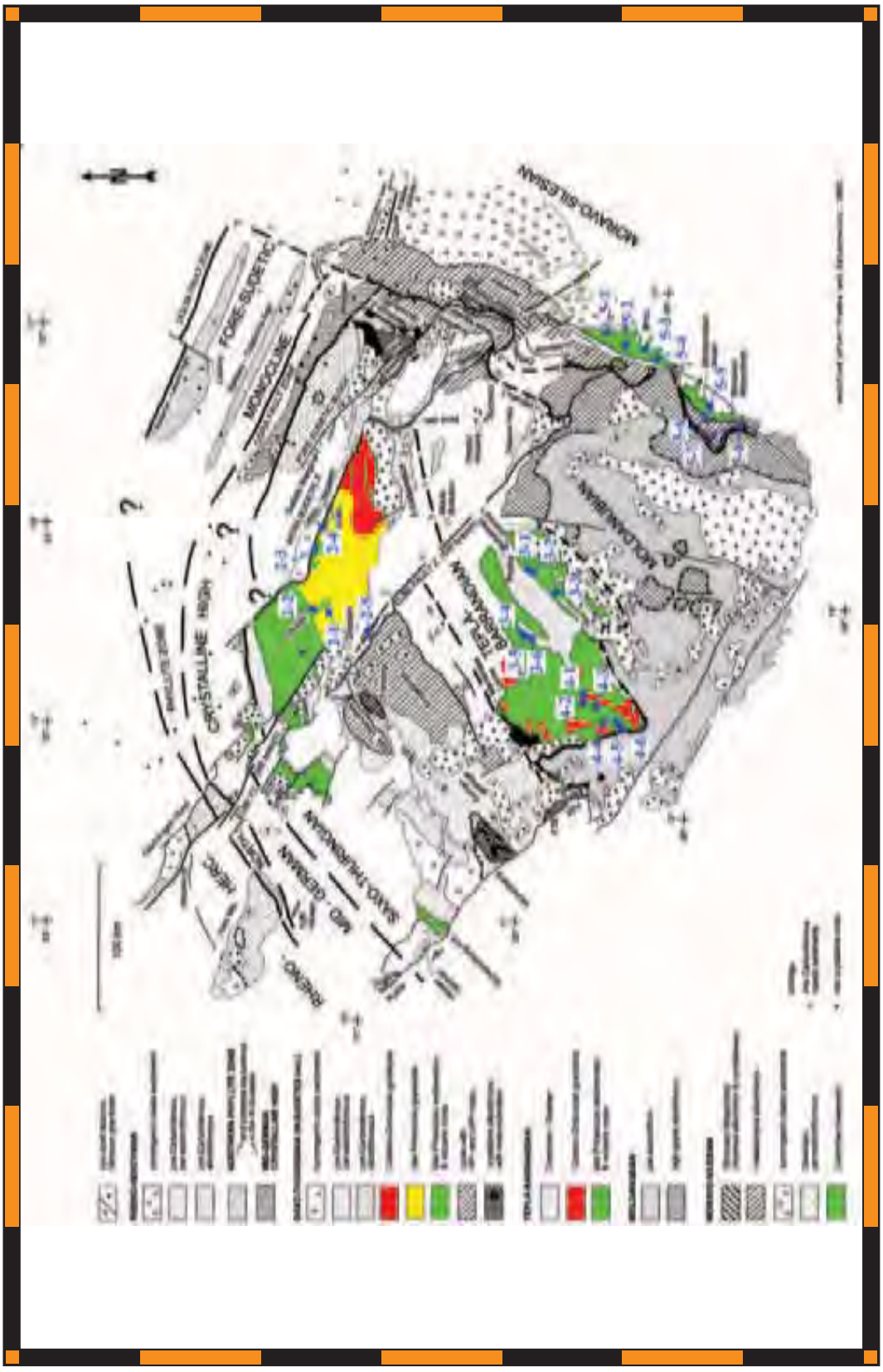

Edited by APAT

32nd INTERNATIONAL GEOLOGICAL CONGRESS

Volume n° 2 - from B16 to B33

32nd INTERNATIONAL GEOLOGICAL CONGRESS

EXHUMATION OF HIGH-PRESSURE METAMORPHIC ROCKS WITHIN AN ACTIVE CONVERGENT MARGIN, CRETE, GREECE

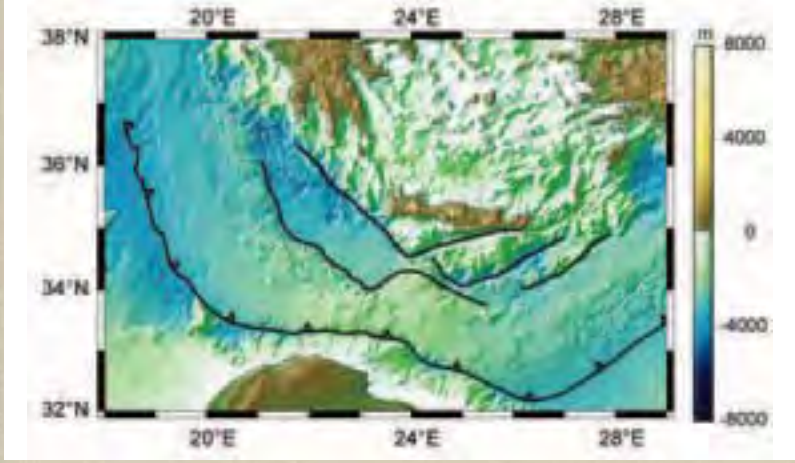

Leaders: J.M. Rahl

Associate Leaders: C. Fassoulas, M.T. Brandon

Field Trip Guide Book - B32

Florence - Italy
August 20-28, 2004

Pre-Congress **B32**

The scientific content of this guide is under the total responsibility of the Authors

Published by:
APAT – Italian Agency for the Environmental Protection and Technical Services - Via Vitaliano Brancati, 48 - 00144 Roma - Italy

Series Editors:
Luca Guerrieri, Irene Rischia and Leonello Serva (APAT, Roma)

English Desk-copy Editors:
Paul Mazza (Università di Firenze), Jessica Ann Thonn (Università di Firenze), Nathalie Marléne Adams (Università di Firenze), Miriam Friedman (Università di Firenze), Kate Eadie (Freelance indipendent professional)

Field Trip Committee:
Leonello Serva (APAT, Roma), Alessandro Michetti (Università dell'Insubria, Como), Giulio Pavia (Università di Torino), Raffaele Pignone (Servizio Geologico Regione Emilia-Romagna, Bologna) and Riccardo Polino (CNR, Torino)

Acknowledgments:
The 32nd IGC Organizing Committee is grateful to Roberto Pompili and Elisa Brustia (APAT, Roma) for their collaboration in editing.

Graphic project:
Full snc - Firenze

Layout and press:
Lito Terrazzi srl - Firenze

Volume n° 2 - from B16 to B33

32nd INTERNATIONAL GEOLOGICAL CONGRESS

EXHUMATION OF HIGH-PRESSURE METAMORPHIC ROCKS WITHIN AN ACTIVE CONVERGENT MARGIN, CRETE, GREECE: A FIELD GUIDE

AUTHORS:
J.M. Rahl[1], C. Fassoulas[2], M.T. Brandon[1]

[1]Yale University - U.S.A.
[2] Natural History Museum of Crete - Greece

Florence - Italy
August 20-28, 2004

Pre-Congress

B32

Front Cover:
topography and bathymetry of the eastern Mediterranean

Leader: J.M. Rahl
Associate Leaders: C. Fassoulas, M.T. Brandon

Introduction

Subduction involves the horizontal convergence of two tectonic plates; however, researchers have long recognized that widespread extensional deformation is a characteristic of many subduction zones (e.g., Royden, 1993). The Hellenic subduction zone is one such region of overall plate convergence and widespread horizontal extension (Figure 1). As the lithosphere of the African plate dips to the north, deformation in the overriding European plate has thinned the continental crust, forming the Aegean Sea. Unlike in some subduction zones (e.g., Japan), extension in the overriding plate is not restricted to the backarc region; thinned continental crust underlies the Sea of Crete outboard of the volcanic arc. Although most of the attenuated continental crust is now submerged, the island of Crete provides a view of extensional deformation in the forearc region. Crete exposes a variety of variably metamorphosed sedimentary and volcanic units juxtaposed by thrust faulting during the Oligocene and later thinned by recent (and still active) normal faults. This tectonic thinning has exhumed high pressure-low temperature metamorphic rocks, which were only recently metamorphosed (~20 Ma) at about 35 km depth above the subducting slab. Thus, the island provides an excellent laboratory to study processes and consequences of syn-convergent extension.

The goal of this field excursion is to examine the tectonic evolution of Crete, including the deformational, metamorphic, thermal, and exhumational history of the rocks. The four day trip will begin in Psiloritis Mountains of central Crete, where we will introduce the major tectonostratigraphic units, and inspect several exposures of the Cretan detachment fault. On the second day, we will examine the thermal and deformational history of the high-pressure, low-temperature metamorphic rocks in Crete. The third day will focus on the development of sedimentary basins in western Crete in response to widespread late Miocene extension. The fourth day will involve a hike through the deeply incised Samaria Gorge, which provides geomorphic evidence of recent rapid uplift of a large footwall block associated with active normal faulting along the south side of Crete.

Essential logistical information:

Crete is very accessible. The island is serviced by two airports, one in Irakleio and the other in Chania. Here, and in the other major cities in Crete, it is possible to rent a car or van. The localities described in the first three days of the field guide are road cuts that are easily reached by automobile. The fourth day of the trip is a hike through the Samaria Gorge in western Crete. To pass the gorge, it is best to take a bus to the village of Omalos. Public buses depart from Chania and Palaiochora. After you hike down the gorge, you will arrive in the village of Agia Roumeli. Here you can purchase a ticket for a boat that will transport you to Chora Sfakion, from where buses will be available for transportation back to Chania or elsewhere.

Field references:

Several relevant field guides have been published that describe the geology of central and western Crete. *Field Guide to the Geology of Crete* by Charalambos Fassoulas outlines 7 days of field stops throughout all of Crete. The book is intended for both the general public and geologists, and is well-illustrated with many color photographs. Another field guide has been written by Meulenkamp and others (1979), who describe a 4 day trip that focuses on the Miocene sediments of western and central Crete.

A good road map is essential for a field trip to Crete, as many of the smaller roads in the interior of the island are unmarked and can be difficult to find. We recommend the series of maps by produced by Road Editions.

The most comprehensive geologic map has been compiled by Creutzberg et al. (1977). A series of more detailed maps has been drafted by the Institute of Geological and Mining Exploration (IGME) of Greece.

Regional tectonic setting

Overview

The Mediterranean Sea represents a vestige of the Tethyan Seaway, an east-west trending ocean basin formed during the breakup of the Pangea. Throughout the Cenozoic, convergence between Eurasia and southern plates of Gondwana (including the African, Apulian, Arabian, and Indian plates) slowly consumed the Tethyan Seaway and led to the formation of the Alpine-Himalayan chain, an orogenic zone that extends for several thousand km from the Alps in southwestern Europe through the Middle East and into the Himalaya.

Volume n° 2 - from B16 to B33

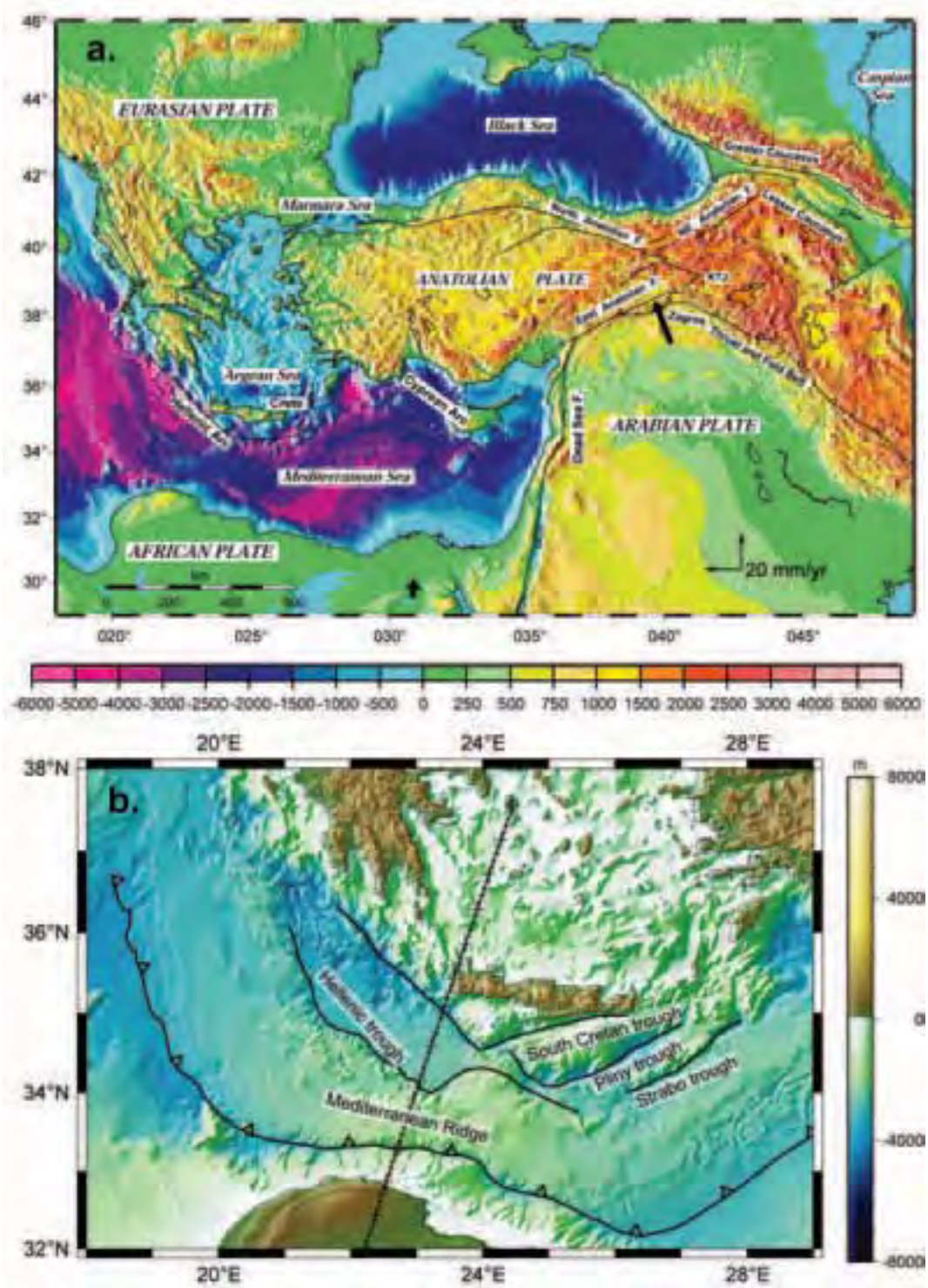

Figure 1 - a) Simplified tectonic map of the eastern Mediterranean region, from McCluskey et al. (2000). Structures are superimposed on topography and bathymetry. Heavy arrows show NUVEL-1A plate motions relative to Eurasia. KTJ – Karliova triple junction. b) Topography and bathymetry of the eastern Mediterranean. Line shows location of cross-section in Figure 2.

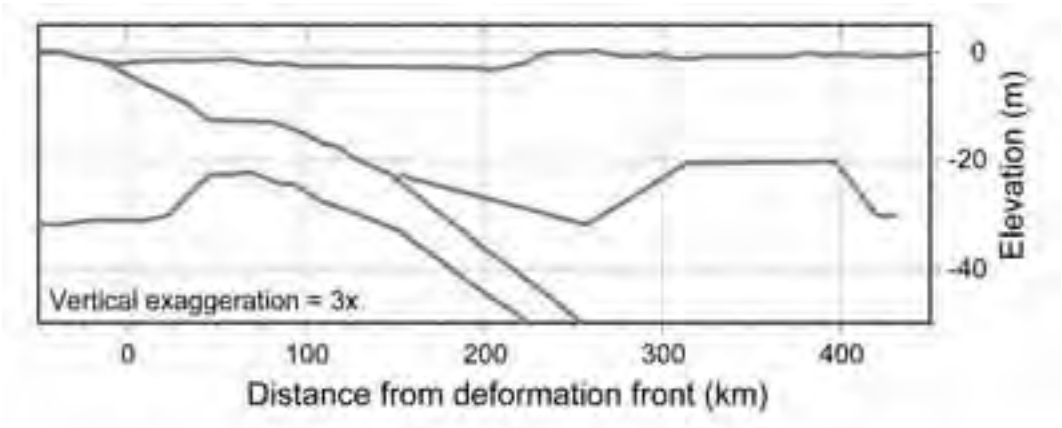

Figure 2 - Cross section through the Cretan wedge, showing variation in topography and depth to the Moho. (Moho from T. Meier et al., unpublished results, 2003).

The Hellenic subduction zone is presently consuming the remnants of Tethyan seafloor, which is subducting northward beneath Crete as part the lithosphere of the African plate (Figures 1 and 2). Crete lies in the forearc of the Hellenic Subduction Zone. Active subduction is indicated by a north-dipping Wadati-Benioff seismic zone extending beneath Crete to a depth of about 200 km (Le Pichon and Angelier, 1979; Knapmeyer and Harjies, 2000). Tomographic studies show that this seismicity corresponds to a cold lithospheric slab that extends through the transition zone and into the lower mantle below Europe (Spakman et al., 1988). At the longitude of Crete, the subduction front in this system is located about 200 km south of the island, just north of the coast of Libya (Kastens, 1991; Kopf et al., 2003) (Figures 1 and 2). Sediments from the downgoing plate have accumulated in the Mediterranean Ridge complex, a broad accretionary wedge positioned between Africa and Crete. Kopf et al. (2003) estimate an accretionary flux of > 17 km^2/myr. Between Crete and the crest of the Mediterranean ridge are a series of east- and northeast-trending depressions or troughs (e.g., Hellenic, South Cretan, Pliny, Strabo in Figure 1b). Early papers considered that these depressions might be the active subduction zone, but subsequent work has shown that the front of the subduction wedge lies along the southern margin of the Mediterranean Ridge (Kastens, 1991). Some authors have suggested that these troughs might mark sinistral strike-slip faults associated with the tectonic escape of Turkey (e.g., Huguen et al., 2001), although direct evidence for the formation of these troughs is lacking.

Crete itself is positioned as an emergent high in the forearc of the subduction system. North of the island, the topography quickly drops off into the thinned continental crust of the Cretan Sea (Figure 2) (Makris and Stobbe, 1984). About 100 km north of Crete lies the volcanic arc of the Hellenic Subduction Zone, represented by the island of Santorini. Like in the Sea of Crete, the crust in the back-arc of the system is also attenuated continental crust (McKenzie, 1978; Le Pichon and Angelier, 1981). North of Santorini, the various islands of the Cyclades expose mid- to lower-crustal metamorphic and igneous rocks exhumed to the surface along low-angle detachment faults (Lister et al., 1984). The exposure of high-pressure metamorphic rocks in the Aegean Sea is one line of evidence that the crust there has been thinned through extensional faulting (Lister et al., 1984; Buick, 1991). This conclusion is confirmed by seismic reflection studies which demonstrate a crustal thickness of 20 to 25 km (e.g., Makris, 1978; Makris and Stobbe, 1984).

Global Positioning System (GPS) studies have provided a detailed view of the modern tectonic motions in the eastern Mediterranean (e.g., McCluskey et al., 2000) (Figure 3). In this region, one important feature shown by the velocity field is the westward migration of the Anatolian block towards the Aegean Sea along the right-lateral North Anatolian fault in northern Turkey. This movement is driven by the ongoing collision between the Arabian block and Eurasia, with Turkey “escaping” as a coherent block to the west (McKenzie, 1972). Escape is though to start sometime between 12 Ma and 4 Ma (McCluskey et al., 2000). The extrusion of the Anatolian block

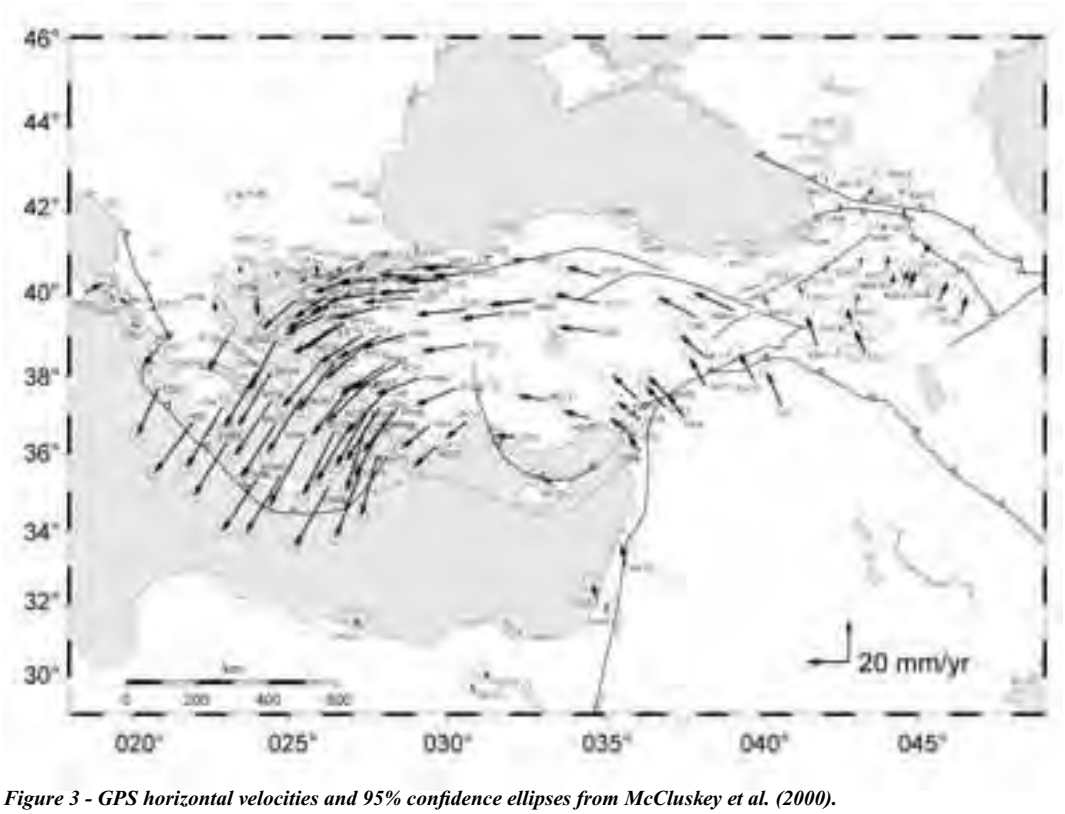

Figure 3 - GPS horizontal velocities and 95% confidence ellipses from McCluskey et al. (2000). Data are in an Eurasia-fixed reference frame for the period 1988-1987.

can be modeled as a counterclockwise rotation (Le Pichon and Angelier, 1979; McCluskey et al., 2000), with both Turkey and the Aegean Sea moving with respect to Eurasia. Both the GPS data and seismic observations (Jackson, 1994) show that Crete and the southern Aegean are moving together at a coherent block. The divergent motion between the Aegean block and mainland Europe is accommodated in a zone of extension in the northern Aegean, with Crete and the Aegean Sea diverging from mainland Europe at a rate of about 30 mm/yr (McCluskey et al., 2000). Studies of global plate motions indicate northward motion of Africa relative to Europe at 10 mm/yr (e.g., Dewey et al., 1989). Thus, the modern net convergence rate across the modern Hellenic subduction zone is about 40 mm/yr.

Southward migration of the Hellenic subduction zone

Subduction at the Hellenic Subduction Zone appears to have been operating continuously since at least 26 Ma, and likely back to 40 Ma (Spakman et al., 1988, Meulenkamp et al., 1988). Cretaceous units in the internal zones in the northern Aegean suggest that earlier subduction zones were probably operating further back in time (e.g., Kilias et al., 1999). Although the subduction process may have been continuous during most of the Cenozoic, it is clear that the significant changes in the geometry and kinematics of the zone have developed in recent geologic past. During the Oligocene, mainland Greece, Crete, and Turkey formed a roughly linear east-west trending belt. During the Oligocene, convergence led to the stacking of a series of sedimentary and volcanic units all along this margin (Le Pichon and Angelier, 1979; Bonneau, 1984). These individual units represent different components of the Tethyan Seaway, including several carbonate platforms and adjacent basins (Robertson et al., 1991). The nappe stacking is commonly taken as evidence of continent-continent collision, but the continuity of the subducting slab beneath Crete suggests that the nappes probably represent the accretion of thin thrust sheets, as is typical of subduction zones, rather than the collision and accretion of lithospheric continental blocks.

Sometime since the Miocene, southward migration of the margin near Crete led to the development of the curvature of the Hellenic arc. Le Pichon and Angelier (1979) argue that the southward migration was related to the initiation of subduction in the region, which they believed occurred at 13 Ma because of the depth of active seismicity. However, the realization that subduction operated for a much longer time (Spakman et al., 1988) has forced a re-evaluation of the timing constraints for the southward migration of the Hellenic arc (see discussion in the Appendix of Kastens (1991)). Paleomagnetic results (Kissel and Laj, 1988; Duermeijer et al., 1998; Duermeijer et al., 2000) show that block rotations in the Hellenic arc were acquired mainly after 5 Ma, suggesting that the formation of the curvature of the Hellenic arc has developed since that time as well.

The southward migration of Crete appears to be related to the extension occurring above the Hellenic subduction zone. North of Crete, the crust beneath the Sea of Crete and the Aegean Sea is continental and typically 20-25 km thick (Makris and Stobbe, 1984). Prior to deformation, the crust of the Aegean Sea has been estimated to be 1.5 to 2 times thicker than the current thickness (McKenzie, 1978; Angelier et al., 1982).

How can widespread extension occur in regions of overall tectonic convergence? Several tectonic processes have been proposed to account for the southward migration of Crete and the formation of the Aegean Sea. One idea focuses on the "Anatolian push" associated with the westward escape of Turkey into the Aegean. The motion of the Anatolian block is proposed to be transmitted to the continental crust of the Aegean region which then spreads and extends southward, causing southward migration of the Hellenic subduction zone (Hatzfeld et al., 1997). This southward motion is sometimes described as overflow of the Aegean over the African plate. However, recent investigations suggest that the "Anatolian push" is probably of secondary importance in controlling the formation of the Aegean Sea. For example, using a finite element model Meijer and Wortel (1997) found that the force applied to the Aegean by the Anatolian block had to be small to get a match to the modern velocity field. The GPS results of McCluskey et al. (2000) also suggest that the westward motion of Turkey does not strongly influence the southward motion of Crete. As described above, the divergence between Europe and the Aegean Sea is accommodated in a zone in the northern Aegean. Thus, extension across the southern Aegean and Crete appears to be related to a "pull" from the subduction zone rather than a "push" from Turkey.

A second idea is that the southward motion of Crete and the formation of the Aegean Sea is related to gravitational collapse of an orogenic topography (Dewey, 1988). The argument is that convergence during the Oligocene led to stacking of thrust nappes and thickening of continental crust. Subsequent thermal relaxation lead to gravitational spreading of the thicken zone. However, as noted by Thomson et al. (1999), there is no evidence for extremely thick continental crust in the Oligocene.

A third idea is that extension in the Aegean Sea is related to rollback of the African plate (Le Pichon and Angelier, 1979). Meulenkamp et al. (1988) showed that subduction had been well-established prior to the formation of the curvature of the Hellenic Arc. They argue that abundant Miocene deformation in Crete is coincident with the initiation of the rollback process. Although tomographic results indicate that the slab is continuous to great depths (in excess of 600 km) at the longitude of Crete, a continuous slab has not been successfully imaged to the west beneath mainland Greece (Spakman et al., 1988; Wortel and Spakman, 2000). These observations have to the hypothesis that the descending slab is torn beneath Greece, forcing the still continuous segment beneath Crete to support the entire load of the downgoing slab. The concentration of the slab-pull force beneath Crete then drives rapid rollback as the African lithosphere sinks deeper into the mantle (Wortel and Spakman, 2000). The importance of rollback in controlling the tectonics of the eastern Mediterranean has been emphasized in finite-element simulations of the region, both for the Aegean Sea (Meijer and Wortel, 1997; ten Veen and Meijer, 1998) and also on the scale of the entire Mediterranean (Jiménez-Munt et al., 2003). In fact, Jiménez-Munt et al. (2003) conclude that it is not possible to match the observed geodetic measurements in the Mediterranean without deep subduction and rapid rollback in the Hellenic Subduction Zone.

Geology of Crete

Most of the geologic units exposed on Crete were initially assembled by thrust imbrication during the Oligocene (Creutzberg and Seidel, 1975; Bonneau, 1984; Hall et al., 1984). That initial sequence was thinned dramatically by normal faulting, starting at ~15 Ma and continuing to the present (Thomson et al., 1998, 1999). Even so, the original nappe sequence formed during Oligocene thrusting is still readily

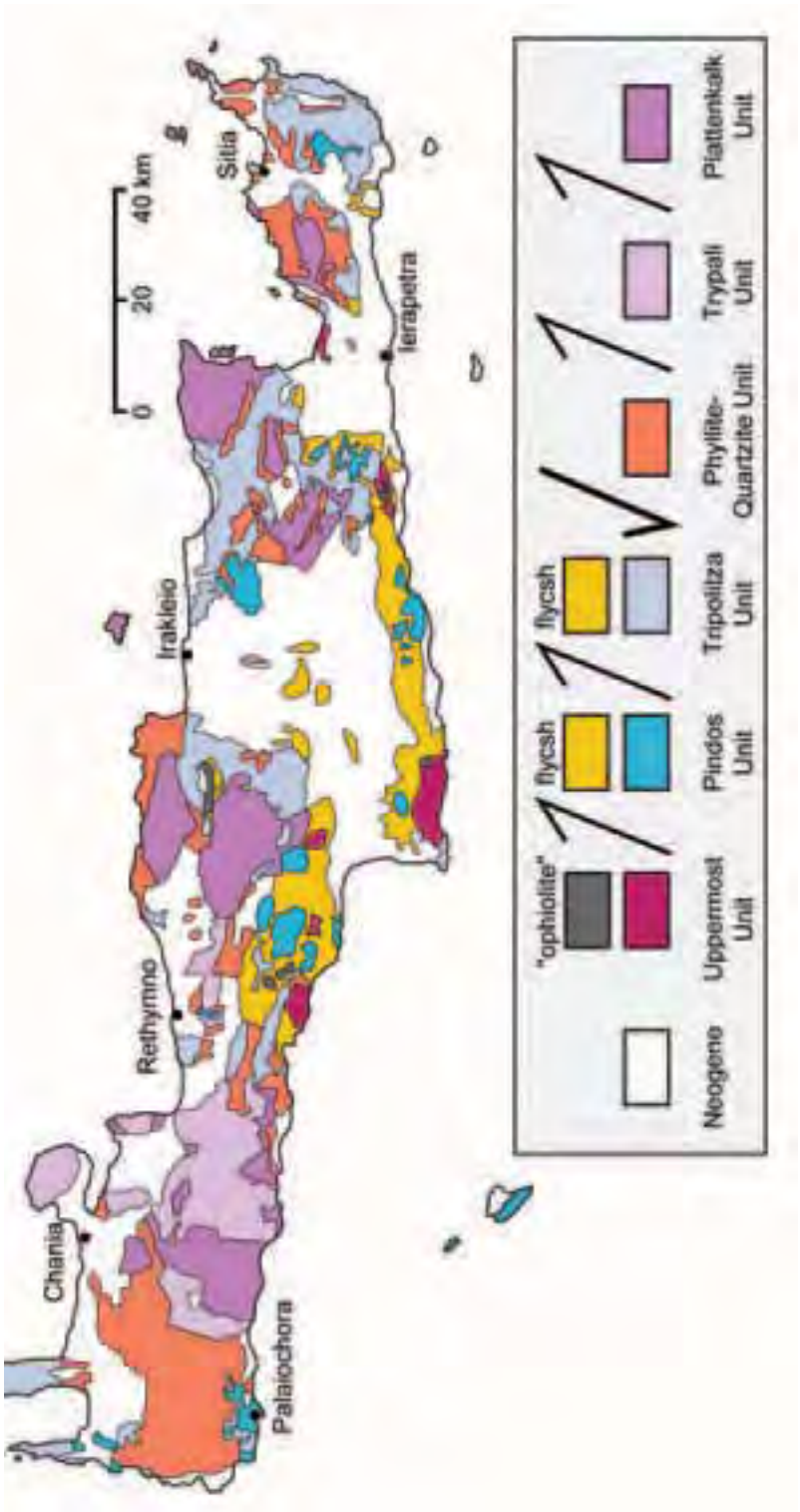

Figure 4
Simplified geologic map of the basement units of Crete and their tectonostratigraphic relationships. After Creutzburg et al. (1977) and Thomson et al. (1999)

apparent, as summarized in Figure 4. The initial assembly of the nappes is widely thought to represent the collision of a microcontinent (known as Adria or Apulia) with the European margin (e.g., Robertson et al., 1991). We have noted above however that this accretion of continental rocks may have been largely thin-skinned in that there is no break observed in the slab beneath Crete. Bonneau (1984) demonstrated that many units in Crete are present to the west and east into mainland Greece and Turkey, respectively. In contrast to other subduction zones, the structural style recorded in Crete is well organized, consisting of imbrication and folding of stratally coherent units. The regional extent of the stratigraphic units indicates accretion of large tectonostratigraphic units, as emphasized in the collisional interpretation of Robertson et al. (1991).

For a start, it is best to view the tectonic sequence in Crete as composed of three parts,

which in increasing structural position are: 1) the *sub-detachment nappes*, 2) the *supra-detachment nappes*, and 3) *syn-extensional sediments*. The *sub-detachment nappes* are defined by a common high pressure-low temperature (HP-LT) metamorphic history, imposed in Oligocene and early Miocene time, shortly after accretion at the Hellenic subduction zone. The stratigraphic units involved are the Plattenkalk, Trypali, and Phyllite-Quartzite (defined below), which consist mainly of carbonates, schists, and quartzites that span in age from Late Carboniferous to Oligocene. This metamorphosed tectonic assemblage is bounded at its top by a one or more low-angle normal faults, which are collectively referred to as the Cretan detachment. It is also important to note that the stratigraphic units that make up the HP-LT footwall of the Cretan detachment are never found above that structural level.

The *supra-detachment nappes* are pre-Miocene accretionary units that lie above the Cretan detachment. Like the *sub-detachment nappes*, this structural assemblage also shows evidence of Oligocene accretion and thrust imbrication, but it contrast it always remained structurally shallow after accretion, as indicated by the absence of Cenozoic HP-LT metamorphism. The stratigraphic units within the *supra-detachment* napes include the Tripolitza, Pindos, and Uppermost units. They are dominated by carbonates, ophiolitic rocks, and some siliciclastic turbidites, with ages spanning from Triassic to Eocene.

The *syn-extensional sediments* correspond to a series of high level sedimentary basins, ranging from middle Miocene to present in age. These basins are intimately associated with late Cenozoic normal faulting in Crete. They provide a detailed record of unroofing of the Cretan nappe sequence, and the emergence of the mountainous subaerial topography associated with modern Crete.

We provide a more detailed review below of Cretan geology, with the discussion moving from the structurally lowest rocks below the Cretan detachment upward to the Late Cenozoic extensional basins. We follow the practice of dividing the nappes in Crete according to their internal stratigraphy and referring to each nappe using the name of the dominant stratigraphic unit in the nappe.

The sub-detachment nappes

Plattenkalk nappe. The structurally lowest unit exposed on Crete is the Plattenkalk (PK) nappe (called Ida nappe by some), which is made up entirely of the Plattenkalk Group. The Plattenkalk Group is commonly overturned, and large recumbent folds are found in some areas. Nonetheless, the unit maintains a coherent well defined internal stratigraphy consisting of stromatolitic dolomite, carbonate breccia, and a distinctive sequence of platy, well-bedded carbonates with chert interbeds (Epting et al., 1972; Seidel et al., 1982; Hall and Audley-Charles, 1983; Krahl et al., 1988). The oldest Plattenkalk consists of shallow marine carbonates with Permian fusilinids (Bonneau, 1984). Younger parts of the section consist of carbonates and cherts that record a transition to deeper water conditions. The thickness of the Plattenkalk is debated, with estimates ranging from 1 and 2.5 km (compare Epting et al., 1972 and Hall and Audley-Charles, 1983). The Plattenkalk is devoid of siliciclastic input except for a thin, 10 – 30 m layer of flysch at the top of the section. In central Crete, foraminifera from this flysch have been dated by Bizon et al. (1976) as Oligocene (29.3 to 28.3 Ma). The Plattenkalk is thought to represent the sedimentary cover of the southern margin of the Adria continental block (sometimes referred to as the Apulia block), which presently underlies the modern Adriatic Sea. The Adria block is being overridden to west by the Apennine thrust belt and to the east by the Dinarides and Hellenides of the western Balkans and Greece. It also continues northward into the Alps, where it forms the highest structural unit in that Alpine collision zone.

Bonneau (1984) correlated the Plattenkalk Group with the carbonates of the Ionian Zone of western mainland Greece. The Plattenkalk is thought to be a fully allochthonous nappe. Although its base is not observed on Crete, the presence of an active subduction zone beneath Crete supports the interpretation that it is an accreted tectonic slice. Furthermore, to the east in Rhodes, the Plattenkalk is found overthrust on a more inboard carbonate platform, associated with the "pre-Apulian domain" from mainland Greece (Bonneau, 1984).

Trypali Nappe. In western Crete, the Plattenkalk nappe is structurally overlain by a small nappe made up entirely of the Trypali Formation, which consists of well bedded dolomite, with peloidal mudstone and detrital carbonate layers (Creutzburg and Seidel, 1975). The age of the Trypali has been reported as upper Triassic (Karakitsios, 1987) or lower Jurassic (Kopp and Ott, 1977). These sediments were deposited primarily in peritidal depositional environments, including sabhkas, tidal

flats, hypersaline lagoons (Pomoni-Papaioannou and Karakitsios, 2002). A distinctive feature of the Trypali is an abundance of brecciated horizons, interpreted to represent submarine fault scarp breccias formed either during an Early Jurassic collapse of the Plattenkalk carbonate platform (Hall et al., 1984) or flexure of the foreland shortly before subduction of the Plattenkalk rocks in the Eocene to Oligocene (Thomson et al., 1999). Recently, Pomoni-Papaioannou and Karakitsios (2002) argue that the carbonate breccias of the Trypali are a recent feature formed by subaerial karst weathering during the late Quaternary.

Phyllite-Quartzite nappe. The next highest nappe is made up of the Phyllite-Quartzite (PQ) group. This nappe, which is widespread throughout Crete, is dominated by quartz-rich siliciclastic sediments, with minor limestone, gypsum, and volcanic rocks (Krahl et al., 1983). In eastern Crete, the sequence also includes slices of Hercynian basement (i.e. upper Paleozoic granitoid rocks) (Seidel et al., 1982). Conodonts define a Late Carboniferous to the Late Triassic age for the sedimentary rocks of the PQ (Krahl et al., 1983). The PQ is found throughout Crete and also in the southern Peloponnesus, where it occupies a similar structural position as on Crete (Theye and Seidel, 1991).

The supra-detachment nappes.

Tripolitza nappe. Above the Phyllite-Quartzite nappe are shallow-water carbonates of the Tripolitza nappe (also known as the Gavrovo nappe). The Tripolitza Group consists of shallow-water marine platform carbonates deposited between the Late Triassic and the middle Eocene. The Tripolitza and the overlying Pindos are correlated with the Triassic to upper Eocene carbonate platform sequence in mainland Greece (Creutzberg and Seidel, 1975; Bonneau, 1984). At the base of the section are the Triassic Ravdoucha beds (Sannemann and Seidel, 1976), which are thought to be equivalent with the Tyros unit in mainland Greece. Higher up section, these shallow marine carbonates grade upwards into calciturbidtes and eventually siliciclastic turbidites (Hall et al., 1984). From the Paleocene to Eocene, the Tripolitza is dominated by flysch deposits thought to be derived from the overriding Eurasian plate (Hall et al., 1984).

Pindos nappe. The Pindos nappe is the next in the structurally sequence, overlying the Tripolitza in thrust contact. The Pindos is characterized by deep water sediments, including pelagic limestones, radiolarites, calciturbidites, and calc-breccias. These oldest parts of the unit are Late Triassic. Like the Plattenkalk and the Tripolitza, the Pindos unit is also capped by a Paleocene to Eocene turbidite sandstones and shales. Bonneau (1984) correlates the Pindos nappe on Crete with the Olonos-Pindos sequence exposed in mainland Greece. The Pindos is interpreted to be a deep basin that formed along the northern margin of the Adria microcontinent (Robertson et al., 1991).

Uppermost nappe. Tectonically above the rocks of the Pindos nappe are a diverse series of rocks that have been grouped into the Uppermost nappe. Although the rocks of the Uppermost nappe are older than the Jurassic, they contain no evidence for metamorphism in the Miocene (Seidel et al., 1976). A variety of rock types are present in the UM unit, including oceanic pillow basalts, gabbros, deep water marine sediments, amphibolites, schists, leucogranites, and an ophiolitic cap of mainly serpentinite (Seidel et al., 1976; Thomson et al., 1998). These rocks are thought to be derived from both the Jurassic to Cretaceous Pindos ocean, as well as the overriding European plate. Some authors (e.g., Bonneau, 1984; Creutzburg and Seidel, 1975) regard the various subunits of the Uppermost nappe as individual and mappable thrust nappes. In contrast, Hall et al. (1984) consider the various rocks (e.g., the Arvi, Miamou, Vatos, Asteroussia nappes) of the UM unit as large blocks in a “Blocky Flysch” that forms a major olistostrome in the upper part of the Pindos units.

Syn-Extensional Sediments

Sedimentation has occurred on Crete since the Miocene, likely beginning in the Serravallian. Meulenkamp et al. (1979) divided the sediments of Crete into six groups of formations, most of which are recognizable over all of Crete.

Prina Group. Dark limestone breccias and brecciocongloмerates that generally have a well-cemented with a calcareous matrix. These sediments were deposited in non-marine to brackish or shallow marine environments.

Tefeli Group. “Non-consolidated” terrige-nous clastic formations deposited on either the sediments of the Prina group or basement rocks. These sediments are predominantly conglomerates, sands, clays and were deposited in fresh-water, brackish, and marine environments

Vrysses Group. This group is composed of bioclastic, commonly reefal, limestones which constitute the lateral equivalent of alternations of laminated and homogenous, shallow-marine marls. In places, the marls contain gypsiferous intercalations. Vrysses group sediments are deposited on the Tefeli Group,

pre-Neogene basement, and occasionally the Prina Group.

Hellenikon Group.
Reddish, fluvio-lacustrine conglomerates, and occasional brackish and lagoonal deposits with gypsum. The Hellenikon conglomerates unconformably overlie the Vrysses Group, older Neogene strata, and locally pre-Neogene basement.
Finikia Group. Open marine marls and clays which commonly display laminated and locally siliceous interbeds. At many places the base of the Finikia Group is formed by a marl breccia. These sediments overlie the Hellenikon Group or the Vrysses Group.
Agia Galini Group. Coarse, generally reddish, non-marine conglomerates and sands that overlie (and are in part the lateral equivalent of) sediments of the Finikia Group. These represent the youngest Neogene rocks on Crete.
Undifferentiated Pleistocene. No formal subdivisions have been made. These marine terraces and continental deposits unconformably overlie Neogene or pre-Neogene rocks.

Metamorphic conditions
The sub-detachment nappes contain clear evidence of HP-LT metamorphism. The Plattenkalk nappe is composed mainly of lithologies unsuitable for thermobarometric work. Even so, a metabauxite horizon near the stratigraphic base of the Plattenkalk in central Crete contains lawsonite, magnesio-carpholite, pyrophyllite and diaspore. Theye et al. (1992) estimate maximum P-T conditions of about 1 GPa and 350°C. HP-LT metamorphic assemblages are more commonly found in the Phyllite-Quartzite nappe. Diagnostic minerals include carpholite, chloritoid, sudoite, phengite, aragonite, and jadeitic pyroxene. Seidel et al. (1982) and Theye and Seidel (1991) estimate that exposed rocks in Crete show an increasing metamorphic grade from 0.6 GPa and 300°C in eastern Crete to 1.0 GPa and 400°C in western Crete.
This HP-LT metamorphism must be late Cenozoic in age since it involves Eocene and Oligocene turbidites in the Plattenkalk and Phyllite-Quartzite napes. K-Ar and Ar-Ar dating of metamorphic white mica gives isotopic ages of 21 to 24 Ma (e.g., Jolivet et al., 1996). We interpret these ages as recording the time of growth of the metamorphic white mica, given that the maximum temperatures during metamorphism were probably less than the partial retention temperatures for white mica (~400°C).

The upper units lack evidence of Miocene HP/LT metamorphism. No high-pressure metamorphic minerals have been described from the Tripolitza and Pindos units, and the few metamorphic rocks in the UM unit are related to an older period of metamorphism and deformation (Seidel et al., 1976). Furthermore, Thomson et al. (1998) showed using apatite fission-track ages that most of the UM unit has been cooler than 120°C since 30 Ma.

The Cretan Detachment Fault and exhumation of the high pressure rocks
The juxtaposition of the HP-LT metamorphic rocks of the PQ unit with the unmetamorphosed rocks of the overlying Tripolitza unit has been taken as evidence for a significant normal fault, the Cretan Detachment (Fassoulas et al., 1994; Jolivet et al., 1996; Thomson et al., 1999). This fault, active in the Miocene, has cut out 20 to 25 km of structural section and is estimated to account for 85 to 90% of the exhumation experienced by the lower plate rocks (Thomson et al., 1999).
The geographic extent of the sub-detachment and supra-detachment units is shown in Figure 5. It is important to note that the original Cretan detachment has been extensively dismembered by younger normal faults. Nonetheless, the offsets on the younger faults are generally a kilometer or less, whereas the Cretan detachment seems to have cut out about 25 to 30 km of the Cretan nappe sequence. As a result, the map scale view shown in Figure 5 probably provides a reasonable view of the original distribution of the sub-detachment and supra-detachment units at the scale of Crete. Some authors have argued that the Cretan detachment formed with a consistent sense of motion, interpreted as top-S by Lister et al. (1984) or top-N by Jolivet et al. (1996). With these interpretations in mind, note that the supra-detachment units are exposed both north and south of the island. Thus, there is no evidence on Crete of a top-N or top-S break-away zone. These features could be located offshore to the north or south. However, as an alternative, we suggest that the Cretan detachment might have formed by slip between a coaxially extending hangingwall (see Fassoulas et al., 1994; Fassoulas, 1999, for a similar coaxial interpretation). In this case, the sub-detachment nappes would have punched upward through the supra-detachment nappes, resulting in a variety of shear-sense directions on the detachment.

Thomson et al. (1999) provide a concise review of the

Figure 5 - Tectonic map showing the distribution of the sub-detachment nappes (in dark grey), which are characterized by Oligocene HP-LT metamorphism, and the supra-detachment nappes (in light grey), which were at shallow crustal levels during the Oligocene. The Neogene sediments are shown in white.

P-T-t evolution of the sub-detachment rocks in Crete (Figure 6). The stratigraphic and thermochronologic constraints for the thermal evolution of these lower plate rocks are summarized in Figure 7. The Oligocene sediments in at the top of Plattenkalk Series demonstrate that the HP-LT tectonic units in Crete were subducted between 32 and 36 Ma. White mica Ar/Ar ages (Jolivet et al., 1996) record metamorphic growth and show peak P-T conditions were achieved between 21 and 24 Ma. Zircon fission-track data show cooling through 240°C at about 18 Ma (Brix et al., 2002). Zircon (U-Th)/He ages obtained by Peter Reiners (Rahl et al., in prep) show that the lower plate rocks cooled below 210°C around 10 Ma. Conglomeratic deposits that contain clasts of PQ indicate the lower plate rocks were exposed at the surface by about 9 Ma (calcareous nannoplankton biozone NN 10) (Frydas and Keupp, 1996).

Extension in the Miocene led to the development of many sedimentary basins throughout Crete (e.g., Meulenkamp et al., 1979; Fortuin and Peters, 1983; ten Veen and Postma, 1999a). The oldest of these basins are thought to be Serravallian, but these units are typically unfossiliferous and difficult to date (Meulenkamp et al., 1979). After a period of subsidence during the Messinian, renewed block uplift led to the formation of widespread basins throughout the island (Meulenkamp et al., 1994).

Active tectonics of Crete

Abundant evidence exists that deformation is still ongoing in Crete. Modern seismicity reveals that Crete is experiencing extension, either radially (Angelier et al., 1982) or oriented east-west (e.g., Armijo et al., 1992). In addition to the continuing sedimentation in fault-bounded basins, many faults have been documented to offset young (Pliocene) sediments (ten Veen and Postma, 1999b; Fassoulas, 2001).

The geomorphology of Crete also indicates a young, actively uplifting landscape. For instance, Crete

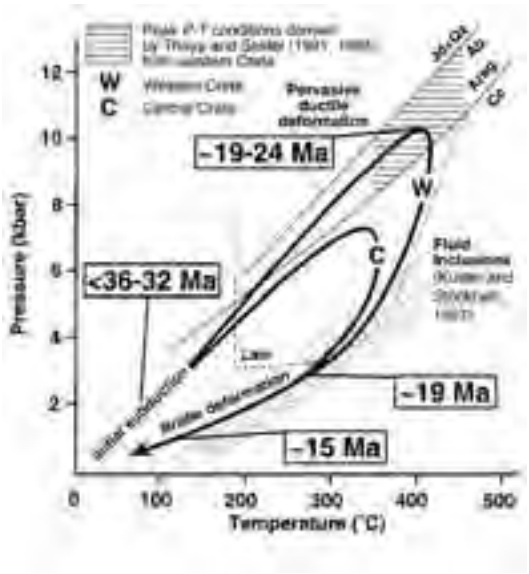

Figure 6 - Pressure-temperature-time (P-T-t) loop of the Phyllite-Quartzite unit of Crete, taken from Thomson et al. (1998). Ab–albite, Arag–argonite, Cc–calcite, Jd–jadeite, Qz–quartz, Law–lawsonite.

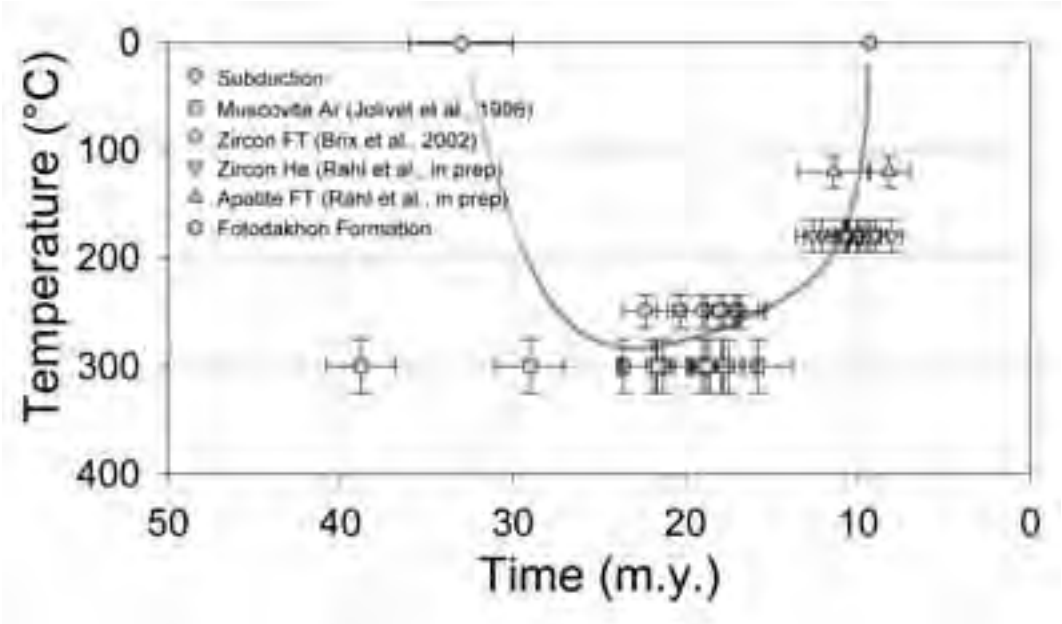

Figure 7 - Time-temperature evolution of the Phyllite-Quartzite unit in central and western Crete. As noted by Thomson et al. (1999), paleogeographic constraints suggest that the Phyllite-quartzite unit entered the subduction zone 4-7 m.y. before deposition of the youngest Plattenkalk sediments. Seidel et al. (1982) and Jolivet et al. (1996) report K-Ar and Ar-Ar dates from white mica which likely record sub-closure temperature growth of mica during metamorphism at depth. Brix et al. (2002) report zircon fission track ages from central and western Crete, indicating cooling through about 240°C at about 18 Ma. New (U-Th)/He data (obtained in collaboration with Peter Reiners) indicate that cooling through about 180°C at about 10 Ma. Apatite fission-track ages (measured by Ray Donnelick) indicate cooling through 120°C also occurred at around 10 Ma. Finally, the observation of cobbles derived from the Phyllite-Quartzite in the sediments of the Fotokadhon Formation indicates that exhumation was complete by 9 Ma.

is famous for several large gorges, such as the Ha gorge in eastern Crete and the Samaria Gorge in western Crete. Messinian deposits are found throughout the island, sometimes at elevations in excess of 1000 m, indicating substantial uplift in the past 5 m.y. (Meulenkamp et al., 1994). In a detailed biostratigraphic study, Meulenkamp et al. (1994) demonstrated that maximum uplift in Pliocene to Recent times in central Crete was on the order of 2000 m. A ^{14}C study of wavecut terraces in western Crete demonstrated that uplift along the south coast is occurring at rates of up to 6 m/yr (Pirazzoli et al., 1982).

What is driving the modern uplift of Crete? Some workers, such as Meulenkamp et al. (1988), emphasize the role that recent reverse faults have played in Crete. In this model, Crete is thickening and uplifting due to horizontal contraction associated with the opening of the Aegean Sea. One attractive alternative, first proposed by Le Pichon and Angelier (1979), is the underplating of subducted sediments beneath Crete, driving tectonic uplift. In addition to explaining the modern uplift, underplating is also consistent with seismic observations. In contrast to the Aegean Sea, the crust beneath Crete is typically 35 to 40 km thick, which is odd given that the late Cenozoic normal faulting should have substantially thinned the crust. Knapmeyer and Harjies (2000) identify low velocity rocks beneath Crete which they interpret as recently underplated sediments. Platt (1986) has argued that underplating can cause extension within a subduction wedge. We suspect that at least some of the extensional faulting observed in Crete is related to underplating, as was also proposed by Fassoulas et al. (1994).

We note that this view contrasts with models that regard Crete as a rigid, non-deforming backstop to the sediments of the Mediterranean Ridge (e.g., Kopf et al., 2003; Le Pichon et al., 2002). Although the rocks of Crete have higher seismic velocities than the unlithified sediments that compose the Mediterranean Ridge, the abundant evidence for active deformation

Volume n° 2 - from B16 to B33

on Crete make it clear that the island is not behaving in a rigid fashion, as required for the backstop interpretation. Thus, we prefer to view Crete as part of doubly vergent wedge (e.g., Willett, 1999), with the north side of Crete corresponding to the back side of this subduction wedge system.

Field itinerary

DAY 1

Psiloritis Mountains, Central Crete

We begin our trip in the Psiloritis (or Ida) Mountains of central Crete. This is an ideal area for a start because nearly all of important tectonostratigraphic units are accessible here. Additionally, the area contains excellent exposures of the Cretan detachment fault. The trip will depart from the village of Anogia, heading southward on the road up to the Nida Plateau.

Drive southward on the road from Anogia towards the Nida Plateau. Pull over at about 3.6 km from the village of Anogia along curve in road.

Stop 1:

Folded Plattenkalk Group

GPS: N 35.26891
E 024.88907

Elevation: 960 m

The deepest tectonostratigraphic unit exposed on Crete is the Plattenkalk Group, a Permian through Oligocene sequence of marbles, dolomites, and platy limestones that represents the sedimentary cover of the southern continental margin of the Adria microcontinent. The Group gets its name from a succession of platy limestones interbedded with chert horizons that make up the bulk of the section. These characteristic beds are can be seen at this locality, along the road from Anogia to the Psiloritis Mountains. Sparse undeformed fossils are present here, indicating that this part of the section was deposited in the Eocene (Bizon et al., 1976).

The Plattenkalk is characterized by tight to isoclinal mesoscale folds. The folds generally have east-west trending axes and are asymmetric with southward vergence. Here, the folded layers of the Plattenkalk generally maintain their thickness, indicating that the folds have developed primarily by flexural shear. Note that the cleavage-bedding intersection is the same on both the upright and overturned limbs, with a geometry consistent with the top-S vergence of the folds. The deformation in the limbs was apparently dominated by an outcrop-scale top-S shearing. Note that this deformation could be due to shear in a limb of larger fold, especially given the fact that folds with amplitudes of 500 m and greater are recognized in the Plattenkalk. Folding must have been younger than deposition of the youngest Plattenkalk (about 29 Ma) and the geometry of the folding is inconsistent with the extensional deformation associated with the Cretan detachment. Thus, this folding is commonly attributed to thrusting during late Oligocene accretion at the Hellenic subduction zone.

Generally the Plattenkalk rocks have a fine grained texture. However, recrystallization and an increase in grain size are commonly observed around cracks and at bedding contacts. These features may mark pathways for fluids that promoted metamorphic recrystallization. The bulk of the Plattenkalk must have been very dry, because there is little evidence for metamorphism in the platy limestone horizons despite the fact that these rocks reached maximum P-T conditions estimated at 0.8 GPa and 350°C (Theye and Seidel, 1991).

Continue to drive southward. As we climb in elevation, we will pass through the detachment and can be seen in the hillslopes to the east and west. The Plattenkalk is platy and more subdued, whereas the Tripolitza, which lies above the detachment, is exposed in rockier outcrops. Pull over along the side of the road after about 11.7 km from Stop 1.

Stop 2:

Oligocene "metaflysch" at the top of the Plattenkalk

GPS: N 35.22268
E 024.87861

Elevation: 1433 m

Following the road southward towards the Nida Plateau, we have moved stratigraphically upsection in the Plattenkalk. Here, we have reached the youngest rocks of the unit, and a facies change occurs from the well-bedded platy limestones with chert interbeds to an approximately 10 m-30 m thick package of metamorphosed turbidite sandstone, or metaflysch as it is locally called.

This metaflysch interval is the youngest part of the Plattenkalk, and is thought to represent an influx of siliciclastic continental material as the Plattenkalk carbonate platform approached the subduction zone. It also provides a useful age datum: Bizon et al. (1976) describe foraminifera (*Globigerina ampliapetura* zone) from this flysch that give an age of 29.3 to 28.3 Ma (Thomson et al., 1999).

The flysch has a weak, gently dipping bedding. A penetrative cleavage dips towards the north, as well as a spaced pressure-solution of cleavage that dips to the south. Minor boudinage in the carbonate layers indicate that the rocks have experience some degree of layer parallel extension.

Continue driving southward. After about roughly 2 km from stop 2, turn left on a small access road that leads to the church of Agios Fanourios. After driving a short distance you will see a driveway on the left side of the road which leads up to the church. Park in the area behind the church.

Stop 3:

The Cretan detachment at the church of Agios *Fanourios*

GPS: N 35.21425
E 024.87474

Elevation: 1395 m

In central Crete, the HP-LT metamorphosed Plattenkalk rocks are tectonically covered by unmetamorphosed limestones of the Tripolitza Group. These units are separated by the Cretan detachment, a significant Miocene normal fault, which has cut out approximately 20 km of structural section. An excellent exposure of the detachment can be found behind the church of Agios Fanourious (Figure 8). The fault zone is nearly horizontal at this location. The footwall is the Oligocene metaflysch of the Plattenkalk (same unit as the last stop), and the hangingwall, Tripolitza limestone.

The relatively weak metaflysch preserves brittle structures that indicate top-S motion at this location on the detachment fault. Brittle, low-angle shear zones dip into the detachment zone. A schistosity has developed parallel to the detachment, and a steep, northward dipping foliation is present in the fault gouge.

Return from the church to the main road. Continue southward towards the Nida Plateau. After about 2.3 km, pull over on the left side of the road at the GeoParks sign which provides a description of the local geology.

Stop 4:

Scenic view of the Cretan detachment and Nida's Plateau

GPS: N 35.21531
E 024.85879

Elevation: 1400 m

This location provides a scenic west-facing view of the Cretan detachment cutting through the landscape (Figure 9). The tallest peaks of the Psiloritis Mountains are visible to the west. Towards the southwest (left side of view), one can see the sharp low-angle contact between the Tripolitza nappe forming the mountainous peaks and the whitish, folded rocks of the Plattenkalk nappe below. This view is cut by a moderately dipping E-side-down normal fault which offsets the nappes and the detachment. Thus, the continuation of the detachment to the north (right side of view) can be found in a lower position near the base of the mountain.

This view also provides a nice view of a large

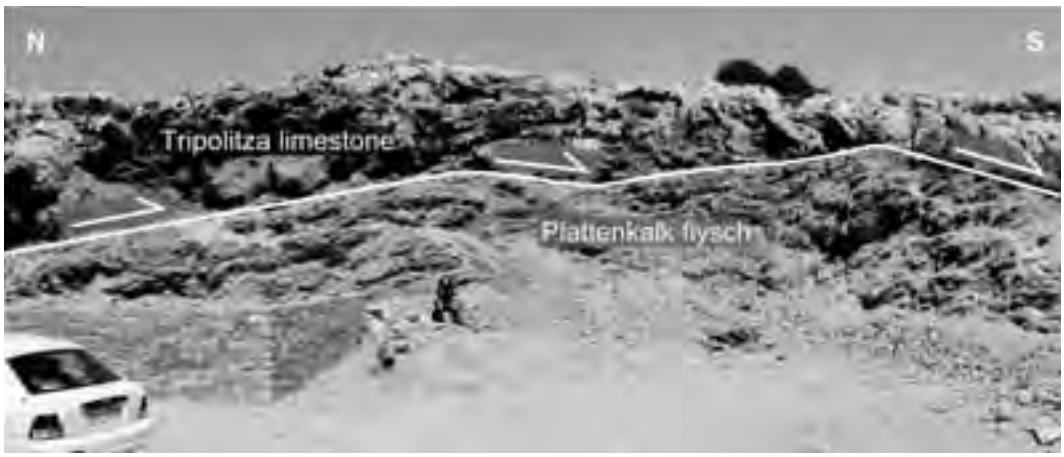

Figure 8 - Panorama of the Cretan detachment fault at the church of Agios Fanourios (Day 1, Stop 3). Here, the detachment fault is nearly horizontal. Limestones of the Tripolitza Group in the hanging wall rest upon the metamorphosed Platenkalk flysch. Brittle shear-sense indicators developed in the flysch indicate top-S motion along this part of the detachment.

Figure 9 - A panorama of the Psiloritis Mountains above Nida's plateau in central Crete. See text (Day 1, Stop 4) for details.

recumbent fold in the Plattenkalk nappe. Although the upper limb of the unit is coherent along most of the top of the ridge, towards the northern end of the view it is folded into a large, asymmetric, south-verging fold. These folds are larger versions of what was observed at stop 1 today. They are also attributed to Oligocene accretion of the nappes.

In the foreground, one can see the Nida Plateau, which formed due to karstic weathering. Several sinkholes are recognized at the northern end of the plateau. The weathering has created an extensive cave system. In the nearby Tafkoura cave, east of the Nida Plateau, the tunnels reach a depth of 950 m below the surface. Furthermore, the Idaion Andro Cave is visible at the the scarp of the normal fault on the northern side of the view. According to legend, this cave is where Zeus was raised (see below).

Continue along the road towards the Nida Plateau for 4.6 km. Park near the taverna at the end of the road.

Stop 5:

Well preserved top-S shear sense indicators (Optional Stop)

GPS: N 35.20684
E 024.83489
Elevation: 1301 m

Just to the west of the taverna at the end of the road is another excellent exposure of the detachment. Fault zone structures are well developed in a 1 to 2 m of zone directly below the stratigraphic break that marks the detachment surface. Again, the structures, including kink folds and S-C structures, are consistent with a top-S motion on the detachment fault.

Cultural note: the Idaion Andro cave

According to legend, Zeus, the most powerful god in the Greek pantheon, was raised here in the Idaion Andro cave in the Psiloritis Mountains. An oracle had prophesized to Zeus' father, Cronus, that he would one day be overthrown by one of his children. In an attempt to avoid this fate, Cronus ate each of his children as they were born so that they would not be able to harm him. His wife, Rhea, grew tired of this, and when she gave birth to her youngest son, Zeus, she secretly hid him at the Idaion Andro cave on Crete. She wrapped a stone in swaddling clothes and presented it to Cronus, who devoured it thinking that it was his son Zeus. Rhea entrusted Zeus to two Nymphs, who cared for the child. Armed youths known as the Kourites performed war dances around the young Zeus' cradle, to drown out the young child's cries. After he matured, Zeus was aided by Gaia (in some versions of the story Metis) and they were able to force Cronus to regurgitate Zeus' five brothers and sisters. Aided by his siblings, Zeus led a revolt that brought the end to the reign of the Titans.

Because of this myth, the Idaion Andro appears to have been the most important religious site in Crete during Minoan and Classical times. Archaeological excavations have revealed abundant, gold, silver, and stone artifacts, today displayed at the Irakleio Archaeological museum.

Return to Anogia, retracing the path that we took up into the mountains. Turn right to leave town, heading towards the east. After about 7 km you should reach the village of Gonies. A road on the right heads uphill out of town, exposing a nearly continuous section about rock. Pull over and stop after continuing up the road for another 1.5 km.

Stop 6:

The supra-detachment nappe sequence

GPS: N 35.28664
E 024.92609
Elevation: 700 m

This road provides an opportunity to view a nearly continuous section that exposes all of the supra-

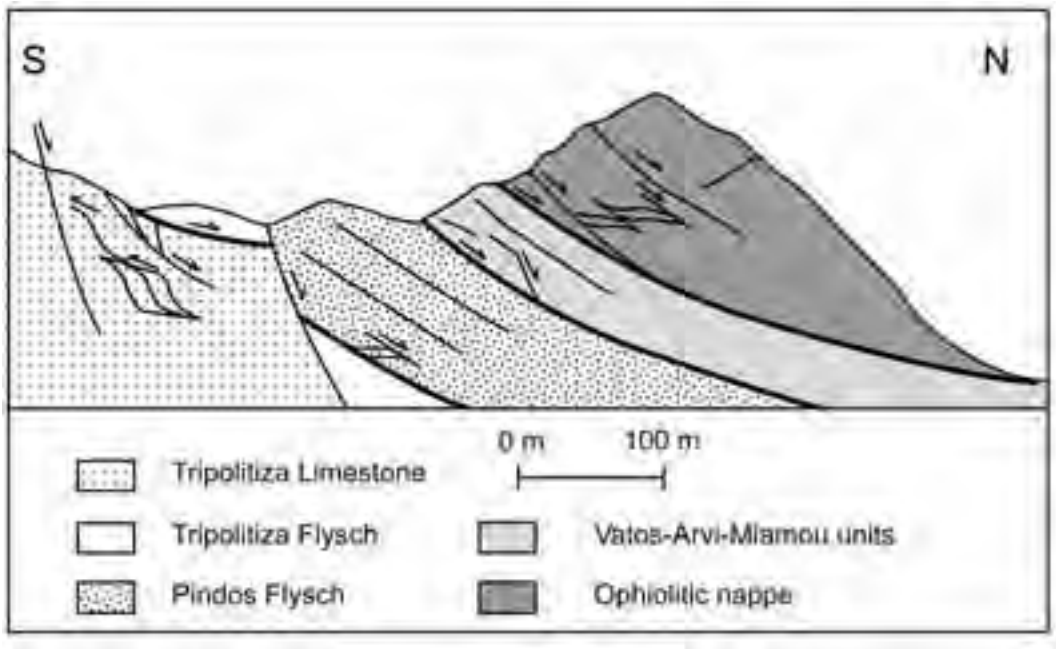

Figure 10 - Schematic cross-section illustrating the structure of the upper-plate units in the area of the village of Gonies (after Fassoulas et al., 1994).

detachment nappes. The traverse, walking downhill along the road, will move upsection through this structural sequence (Figure 10). Note that the section is cut by a number of minor normal faults, which have obscured original contact relations and thicknesses of the nappe units.

Walking down the road, the first outcrops are in limestones of the Tripolitza, which grade upward into Eocene sandstone and minor conglomerate of the Tripolitza flysch. These siliciclastic sediments are thought to represent continental-derived trench-fill deposits, which would have accumulated as the Tripolitza platform approached the Hellenic subduction zone (e.g., Hall et al., 1984). The Tripolitza flysch is much thicker than the flysch at the top of the Plattenkalk, and is typically on the order of 100 to 200 m. The entire thickness of the Tripolitza is about 700 m thick.

Continuing downhill (and upsection), we pass into the Jurassic red ribbon cherts of the Pindos nappe. These rocks contain radiolarites and chert with shale interbeds, and are exposed for about 150 m along the road. At this point, the ribbon cherts grade into the Pindos flysch, which here consists of about 75 m of siliciclastic sandstone, shale, and minor ribbon chert. This unit continues to the break in exposure near the windmill on the west side of the road.

After the windmill is a litholigically heterogenous assemblage of rocks characteristic of the Uppermost nappe. The first exposures are calcareous-siliciclastic sediments of the Vatos member. These are followed by ultra-mafic rocks and the serpentinites. Continue walking towards the left at the split in the road. Exposures of serpentizied ultramafic rocks and subordinate mafic rocks continue for the next several hundred meters where we reach the end of the traverse at the intersection with the main country road.

You will see evidence of several normal faults within this interval. Brittle shear-sense indicators show top-N motion on these faults. They are attributed to widespread late Cenozoic extensional faulting that followed Oligocene accretion of the nappes (Fassoulas, 1994).

Reset the odometer on your vehicle. From the downhill end of this section of road, begin to drive back towards Anogia. A little more than 1 km out of there will be an intersection with a sign pointing towards Aidonochori. Turn right, towards Aidonochori. Past the village of Aidonochori, turn left at the fork in the road onto a gravel road. On your left you should see Miocene sediments. Follow this road to the town of Chonos and take the left road out of town towards Drosia. The outcrops in this area belong to the Plattenkalk Group. After reaching Drosia, turn left out of town, towards

the village of Doxarou. Within this village, turn right towards the Monastery of Timios Stabros. Drive up this road until the odometer reaches about 16.5 km and park along side the road.

Stop 7:

Ductile folds in the Plattenkalk

GPS: N 35.35980
E 024.84586
Elevation: 370 m

Along this north-south road, the Plattenkalk is folded into a large antiform. In its core are the lower parts of the Plattenkalk Group. These strata lack the distinctive platy limestones with chert interbeds that we saw at previous stops. As we walk southward down the slope, we walk upsection and back into the characteristic platy horizons. These strata host spectacular asymmetric, south-vergent folds in the Plattenkalk unit. These folds have roughly east-west trending hinge lines, plunging gently towards the east.

The rocks here apparently experienced higher temperatures than those exposed in the Psiloritis Mountains (Day 1, Stop 1). The hinges of the folds are not as sharp as at other localities. Additionally, changes in layer thickness indicate that the layers have deformed internally.

Drive back to Drosia and continue straight through the town. Turn left on the road that heads to the village of Aloides. Pass through the village. Continue until you have reached roughly about 9 km from the previous stop. Pull over along the side of the road.

Stop 8:

Stratigraphy of the Plattenkalk

GPS: N 35.37925
E 024.88744
Elevation: 400 m

Travelling north along the road towards the northern coast, we pass through a long, continuous section of the Plattenkalk. This section provides an opportunity to view the much of the stratigraphy of the Plattenkalk Group (Figure 11). As we drive towards the north, we are actually driving downsection.

According to Epting et al. (1972), we are driving through the overturned limb of a large, asymmetric, south-vergent recumbent fold. This allows us to move through the entire stratigraphy of the Plattenkalk unit. We begin in the characteristic platy limestones, interbedded with chert deposits. As we move down section we encounter massive, white marbles thought to be lower Jurassic. Finally, lower down we move into the Triassic stromatolitic dolomite. Epting et al. (1972) estimate the entire thickness of the Plattenkalk to be about 2600 m.

Figure 11 - Stratigraphic column of the Plattenkalk Group in central Crete, simplified from Hall and Audley-Charles (1983).

An alternative has been proposed by Hall and Audley-Charles (1983), who argue that rather than consisting of a single recumbent fold, the structure of

the Plattenkalk in this unit is dominated by many tight isoclinal folds that repeat many parts of the section. They also infer the existence of several faults that repeat parts of the section. They infer a maximum thickness for the Plattenkalk Group of about 1000 m.
The Plattenkalk Group sediments record the deepening of a sedimentary basin. The oldest part of the section is composed of shales and massive stromatolitic dolomite, indicating intertidal sedimentation. Upsection, these rocks give way to carbonate breccias and channelled and graded calcarenites. These are interpreted as recording rapid subsidence of the platform following the Triassic (Hall and Audley-Charles, 1983). Farther upsection, the calcarenites grade into finer grained more basinal deposits of the characteristic limestone-chert sequence. Similar deposition is inferred to continue more or less continuously through the Mesozoic and early Cenozoic until the addition of the siliciclastic material of the Oligocene metaflysch at the top of the section.
At the field guide stop, we will see the beautiful Triassic stromatolites. Here, these structures clearly show that the sedimentary section is overturned.
Continue down the road. As we near a bend in the road at about 1 km from the last stop, pull over. The metabauxite horizon is not obvious and can be difficult to find in the outcrop. The GPS coordinates provide the best means of finding the location of the metabauxite.

Stop 8 bis:

Metabauxite horizon within the Plattenkalk (Optional stop)
Elevation: 277 m
N 35.38589
E 024.89451
Continuing down the road, we encounter rocks from deeper in the stratigraphic section. At the base of the stromatolitic dolomite is a metabauxite horizon, significant because it provides the only thermobarometric data from within the Plattenkalk unit (Seidel et al., 1982; Theye et al., 1992; Theye and Seidel, 2001). The assemblage within the metabauxite contains magnesio-carpholite coexisting with pyrophyllite, sudoite, and disapore, leading to an estimate of metamorphic conditions at 0.8 GPa and 350°C.
Continue all the way down until you reach the National Road. Turn right (towards the east) and drive for 4 km. The road will have a large hairpin turn. When you are through this turn and begin travelling on the straight part of the road, immediately pull over on the right side of the road. Fossils of the "Fodele beds" can be seen in the outcrop along the side of the road.

Stop 9:

The "Fodele beds" of the Plattenkalk
GPS: N 35.38406
E 024.91861
Elevation: 115 m
Fossils of the "Fodele beds" of the Plattenkalk Group can be seen in the outcrop along the side of the road. These represent the oldest part of the Plattenkalk Group (Epting et al., 1972). Visible with the naked eye are abundant corals, bryozoa, and brachiopods (Kuss, 1980). Although these rocks experienced high-pressure metamorphic conditions, the fossils show no evidence for deformation or recrystallization. In-filling structures in both corals and gastropods indicate the beds here are overturned.
Turn the car around and head westward. The rest of the stops take place in western Crete, and you will want to drive as far westward as possible before the next day. Both Rethymno and Chania are nice cities to visit for an evening.

DAY 2

Phyllite-Quartzite Nappe In Western Crete

Day two is focused on the Phyllite-Quartzite nappe, the structurally highest of the sub-detachment nappes. This unit has been intensely studied, including its metamorphic, thermochronologic, and deformational history. We will examine the Phyllite-Quartzite Group, discuss both the ductile and brittle deformation in the unit, and consider the processes responsible for its exhumation.
Drive westward along the National Road. As you drive westward past Chania, you will note many exposures of Miocene sediments in large roadcuts. Most of these sediments were deposited in the Pliocene. We will discuss the significance of the Miocene sediments in greater detail tomorrow
Eventually, you will pass over onto the western side of the Rodopos penninsula and to the north the Bay of Kissamos will be visible to the north. Look for the road that leads to Nopigia. Turn right, and follow the road to the coast. When it approaches the coast, this road turns towards the east. Follow it along the western side of the penninsula. The paved road will give way to gravel, and farther along there will be a white church. Drive past the church and over the small crest in the road. Park in the pulloff adjacent to

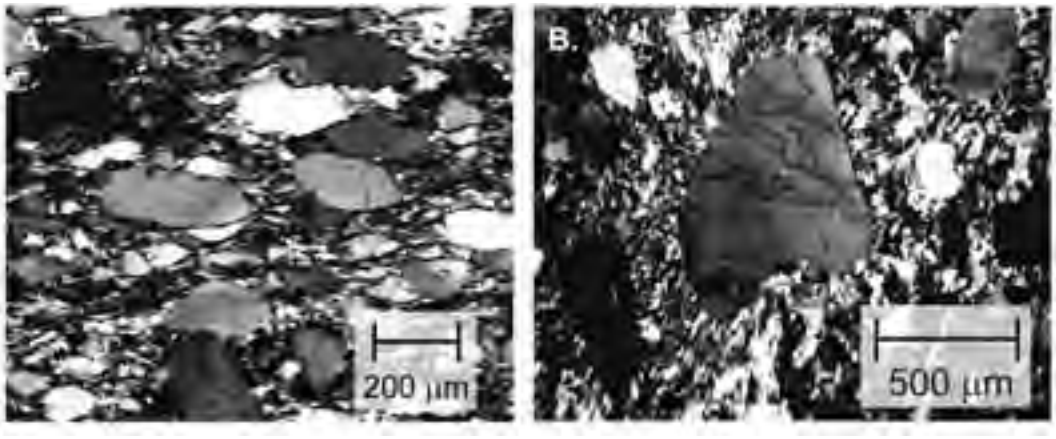

Figure 12 - Photomicrographs illustrating the ductile microstructures common in the Phyllite-Quartzite nappe. X, Y and Z indicate the principal strain directions for maximum extension, intermediate, and maximum shortening, respectively. a) A quartzite thin section illustrating the pressure-solution fabric, with Z oriented in the vertical, and X in the horizontal. The individual quartz grains show little evidence for internal deformation, such as recrystallization or undulose extinction. However, the grains have been shortened in the Z direction by dissolution and extended in the X direction by precipitation of fibrous overgrowths. b) The same sample as in (a) but here observed parallel to cleavage (X-Y section). Note there that the fibrous overgrowths are oriented in all directions indicating a flattening deformation.

several rocky outcrops will be along the coast. This outcrop is about 2.4 km from the intersection with the National Road.

Stop 1:

The Phyllite-Quartzite unit

GPS: N 35.51943
E 023.72288
Elevation: 3 m

The excellent coastal exposures near the village of Nopigia provide a representative view of the Phyllite-Quartzite Group. The section consists of well bedded quartzites and phyllites, with beds ranging from a few cm up to about 1 m thick. Several carbonate-rich layers are also locally present.

Conodont fossils indicate that the Phyllite-Quartzite Group was deposited in a marine setting. The unit has yielded numerous conodont ages ranging from Carboniferous to Triassic (Krahl et al., 1983). The older parts of the section are dominated by siliciclastic sediments, although some carbonates, metavolcanics, and basic intrusives are also present. Carbonate beds become increasingly common in the younger part of the section, as we will see later in the field trip (Day 2, Stop 7).

The Nopigia section shows consistent bedding attitudes throughout indicating that folds were not developed here. We will see mesoscale folds elsewhere in the Phyllite-Quartzite, but such folds are generally not as prevalent as in the Plattenkalk. Microstructural investigations show that these rocks have deformed by pressure solution processes (Figure 12; Schwarz and Stöckhert, 1996; Stöckhert et al., 1999), with material removed from surfaces of detrital quartz grains perpendicular to the shortening direction and redeposited as fibrous overgrowths in the extension direction within the foliation plane. With a hand lens, it is possible to see quartz grains truncated by the cleavage and "beard-shaped" overgrowths oriented parallel to cleavage. Our absolute strain measurements indicate a mass-loss (anisochoric) flattening deformation. Mass-loss is indicated by the fact that the shortening perpendicular to the cleavage is significantly greater than the total extension, which occurs in all directions parallel to the cleavage (Figure 13).

Thin quartz veins are common in this locality and are particularly abundant in the more competent quartzite beds. Schwarz and Stöckhert (1996) argue that these veins formed perpendicular to bedding during diagenesis. The oblique orientation of the views seen at present in the outcrop is attributed to shearing during the pressure-solution deformation.

A brittle shear zone can be seen in the outcrops at the base of the hillslope to the east of the shoreline. The outcrop is composed of thinly-bedded quartzite and phyllite which have been strongly distributed by brittle faulting. Fault zone structures are fairly symmetric, but there seems to be a predominance of

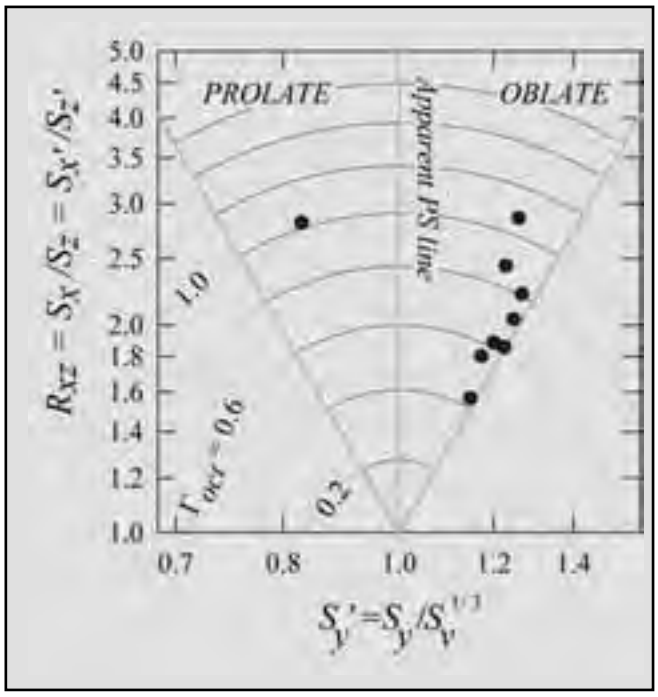

Figure 13 - Nadai plot showing absolute strain data from the Phyllite-Quartzite Unit in western Crete. All samples except one show a flattening strain. Uniaxial shortening was compensated by extension in all directions within the foliation plane.

top-S kinematic indicators.
Farther north along the coast, we can see Miocene carbonates capping the ridge. Farther up, a roughly N-S trending fault drops down rocks to the west. We can see the Miocene sediments near sea level, illustrating the significant offset along this fault. We will return to these north-south trending faults when we discuss the neotectonics of the island.

The Phyllite-Quartzite rocks are useful for studying the metamorphic, deformation, and exhumation history of the HP-LT rocks in the footwall of the Cretan detachment. Unlike the Plattenkalk Group, which is dominated by carbonates, the siliciclastic lithologies of the Phyllite-Quartzite contain assemblages amenable to metamorphic and thermochronologic study. The peak metamorphic conditions for the Phyllite-Quartzite throughout Crete are loosely bracketed to between 0.4-1.0 GPa, and 300-400°C by the co-existence of pyrophyllite, low albite, and lawsonite, plus local aragonite and jadeite (Seidel et al., 1982; Theye and Seidel, 1991; Theye et al., 1992; Brix et al., 2002). Thermobarometry using phengite-muscovite solid solution and exchange between carpholite and chloritoid suggests that metamorphic grade increases systematically from eastern to western Crete, from 0.6 GPa and 300°C in the east to 1.0 GPa and 400°C in west. However, we note that these estimates assume an H_2O activity of unity. If the activity of water deviated from one, the maximum temperatures experienced by the Phyllite-Quartzite could be much less. The preservation of aragonite also suggests lower peak temperatures, since aragonite would have quickly inverted to calcite if the rocks entered the calcite stability field at temperatures significantly greater than about 235°C (Liu and Yund, 1993). K/Ar and Ar/Ar dates from syn-metamorphic white micas in the Phyllite-Quartzite suggest that metamorphism occurred between 21 and 24 Ma (Seidel et al., 1982; Jolivet et al., 1996).

Return to the National Road and travel westward towards Kissamos. Continue through to the town of Platanos. Follow the western coast road towards the village Sfinari. Pull over in a turn off approximately 20.4 km from the intersection of the National Road and the road to Nopigia.

Stop 2:

Brittle deformation and extension

GPS: N 35.44627
E 023.57976
Elevation: 228 m

Park at the pulloff just past one of the tight turns at the north end of the West Coast road. Numerous fresh cuts along this road provide an excellent view of both brittle and ductile structures in the Phyllite-Quartzite nappe. The pressure solution fabric is similar to that observed at the Nopigia locality (Day 2, Stop 1). Anisochoric flattening strains have been measured here as well. Quartz C-axis measurements show no development of a lattice preferred orientation, once again indicating that pressure solution was the dominant ductile mechanism (Schwarz and Stöckhert, 1996). Mesoscale isoclinal folds are locally present at several locations along this traverse.
Throughout Crete, the Phyllite-Quartzite nappe is

Figure 14 - Photo of a well-developed normal-sense fault zone in western Crete (Day 2, Stop 2).

commonly cut by numerous brittle faults (Figure 14). This relationship is well displayed along the West Coast road. These fault zones generally lie at a high-angle to the more gently dipping pressure solution cleavage in the Phyllite-Quartzite. These faults typically have gouge zones that are several cm to several m thick. Brittle kinematic indicators are abundant, usually as Reidel composite structures, with R shears and P foliations most common. We have used these indicators to assess the brittle strain in the Phyllite-Quartzite nappe. In western Crete, almost all of the measured faults show normal-sense offset, with a nearly equal distribution of top-N and top-S indicators (Figure 15). Thus, at the regional scale, the brittle deformation appears to involve N-S coaxial extension within the Phyllite-Quartzite nappe. This brittle deformation overprints the pressure-solution cleavage and likely post-dates the higher temperatures associated with metamorphism. Thus, brittle faulting may be synchronous with late Cenozoic development of the Cretan detachment.

Along this stretch of road, the Phyllite-Quartzite is everywhere overlain by a low-angle fault that separates the Phyllite-Quartzite unit from an unmetamorphosed Miocene(?) conglomerate composed of carbonate clasts (Figure 16). We interpret this low-angle fault as a high-level part of the Cretan detachment (figure 12 in Jolivet et al., 1996 shows a similar interpretation for this structure). At the next ridge down near the next turn in the road is a klippen of this Miocene(?) unit. The conglomerate there is matrix supported and consists mainly of rounded limestone cobbles, which look as if they may have been derived from Tripolitza Group.

A trail goes down from the main road, allowing a view of the fault zone beneath the klippen. Here, in the lowermost part of the fault zone is a breccia that contains angular clasts of Phyllite-Quartzite material. Farther up in the fault zone, the Phyllite-Quartzite clasts disappear, and only limestone clasts are present. We will see a similar Miocene(?) conglomerate later in the trip (the Topolia conglomerate, Day 3, Stop 2). An emerging idea is that these conglomeratic units represent syn-extensional basins that were deposited in the hangingwall of Cretan detachment (e.g., Seidel, 2003). The evidence at Topolia is more convincing, so we will wait until then to more fully develop this idea.

Continue following the western coast road southward to the village of Sfinari. From Sfinari, the next stop is 9.8 km, around a turn just past the village of Kampos.

Stop 3:

Folds in the Phyllite-quartzite nappe

GPS: N 35.38727
E 023.56462
Elevation: 313 m

Mesoscale folds are locally found in the Phyllite-Quartzite nappe (Greiling, 1982; Stöckhert et al., 1999; Thomson et al., 1999). Stöckhert et al. (1999) have recognized two sets of folds in western Crete, both of which can be observed at this location (Figure 17). The older set consists of recumbent isoclinal folds, with fold axes trending NNE-SSW. These folds are associated with a nearly horizontal cleavage and a NNE stretching lineation. The second set of folds have axes that trend approximately E-W. The limbs of these folds are commonly thinned, and more competent quartz-rich horizons are boudinaged. Like the folds in the Plattenkalk, these are also attributed to deformation associated with Oligocene accretion of the Cretan nappes. In our experience, however, folds are not as common in the Phyllite-Quartzite nappe as they are in the Plattenkalk, and the fold geometry observed here may be a local feature. The curve in the

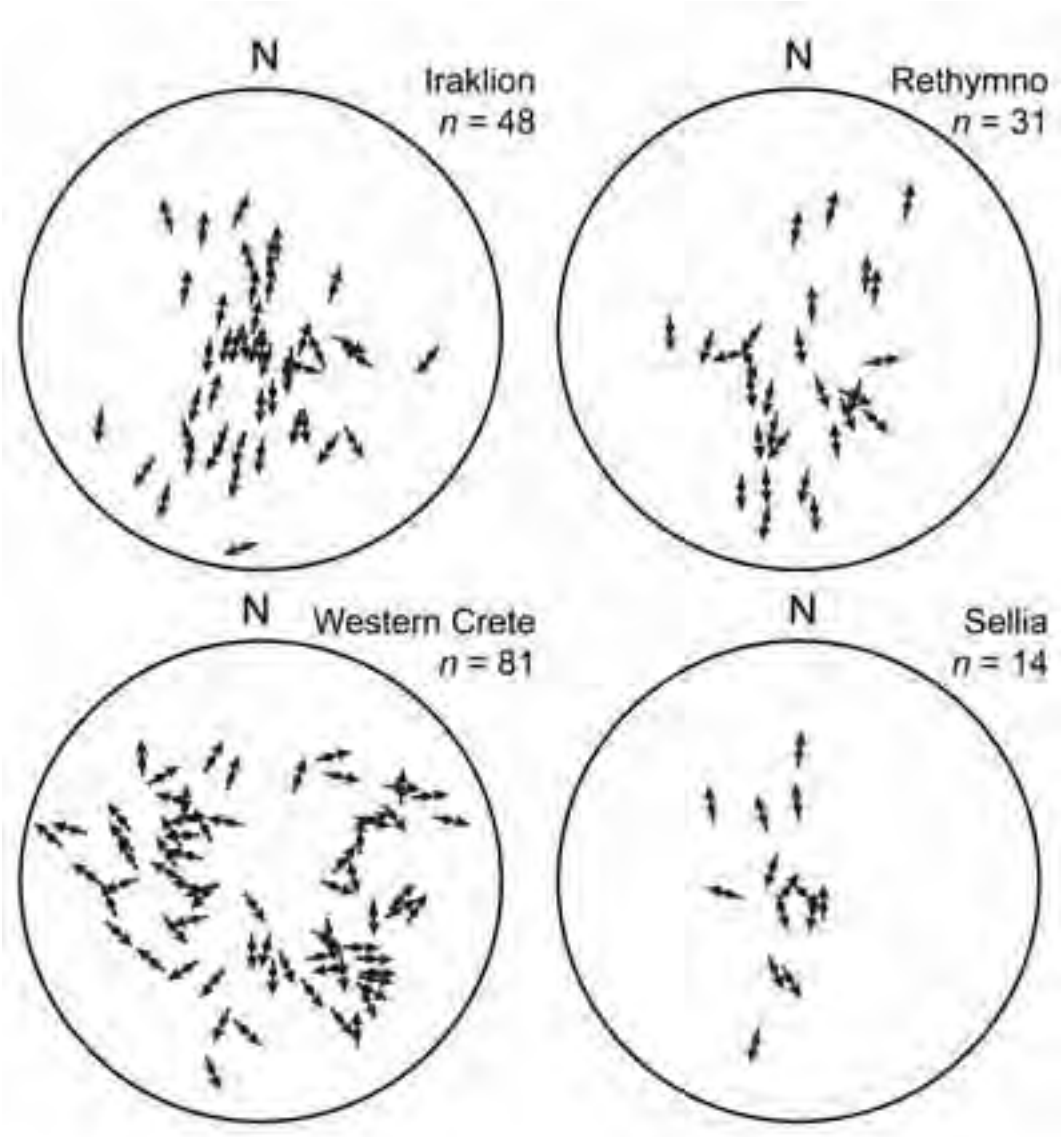

Figure 15 - Lower hemisphere stereonets showing slip-linear data for brittle fault zones within the Phyllite-Quartzite nappe in various areas in western and central Crete. Each square represents the pole to an individual fault plane. The arrow represents the direction of motion of the footwall block relative to a fixed hanging wall block. (Arrows pointing away from the center of stereonet indicate normal-sense slip.) Fault planes show a variety of orientations and nearly all record normal-sense slip.

road here provides a good opportunity to look at these folds in different orientations.

Continue driving southward. Approximately 7.6 km from Stop 3, the road will bend back towards the interior of the island, with a turnoff on the south side of the road. Park your vehicle in the turnoff, and walk along the access road that leads downhill. The evaporites for stop 4 are exposed along the side of this access road.

Stop 4:

Triassic evaporites in the Phyllite-Quartzite nappe (Optional stop)

GPS: N 35.35306
E 023.56938
Elevation: 510 m

Triassic evaporites are present locally in the Phyllite-Quartzite nappe. Here, the evaporites are recrystallized and deformed in a manner similar to the rest of the Phyllite-Quartzite rocks (Fassoulas, 2000). Evaporites of this age are common in Europe and are attributed to rift-related breakup of Pangea.

These Triassic evaporites are near the stratigraphic top of the Phyllite-Quartzite Group. As we will see at a later stop (Day 2, Stop 6), the phyllites and quartzites that characterize the lower part of the section, which is mainly Permian in age, grade upwards to more carbonaceous and evaporitic units.

Thomson et al. (1999) suggest that the Triassic evaporites served as a weak horizon that allowed the Phyllite-Quartzite nappe to detach from its overlying cover and to be deeply subducted. Several workers (Bonneau, 1984; Hall and Audley-Charles, 1983) have speculated that the Phyllite-Quartzite Group was originally overlain depositionally by the Tripolitza Group, which is one of the supra-detachment nappes. They note that there is no known stratigraphic overlap in these two units, with the youngest Phyllite-Quartzite being Triassic in age and the oldest Tripolitza being late Triassic.

Continue along the road, passing through the village of Kefali. Join the road that connects Chania and Elaphonisi, and drive towards Chania. Take the road towards the right that leads to the village of Strovles. Past this village, take the right fork in the road towards the village of Arhondiko and Voutas. After you reach Voutas, continue south towards Pal the road towards Palaiochora. Pull off in the hairpin turn approximately 3.1 km south of Voutas.

Stop 5:

The detachment fault near Voutas

GPS: N 35.27345
E 023.66350
Elevation: 277 m

Near the hairpin turn in the road south of Voutas is an excellent exposure of the Cretan detachment. The approximately 20 m wide fault zone dips towards the south and contains several shear sense indicators consistent with top-S motion.

On the western side of the road, just prior to the sharp turn, a small access road runs downhill. Down this road are several exposures of the supra-detachment Tripolitza nappe. Note tectonic breccia which contains angular clasts of the Tripolitza.

An important question regards the motion along the major detachment fault. Jolivet et al. (1996) argue that extensional deformation in the Phyllite-Quartzite unit is consistently asymmetric, with a dominant top-N sense of shear, whereas Fassoulas et al. (1994) argue for a symmetrical deformation in central Crete. As discussed before, our microstructural evidence suggests that deformation within the Phyllite-Quartzite unit is generally coaxial, at least on the

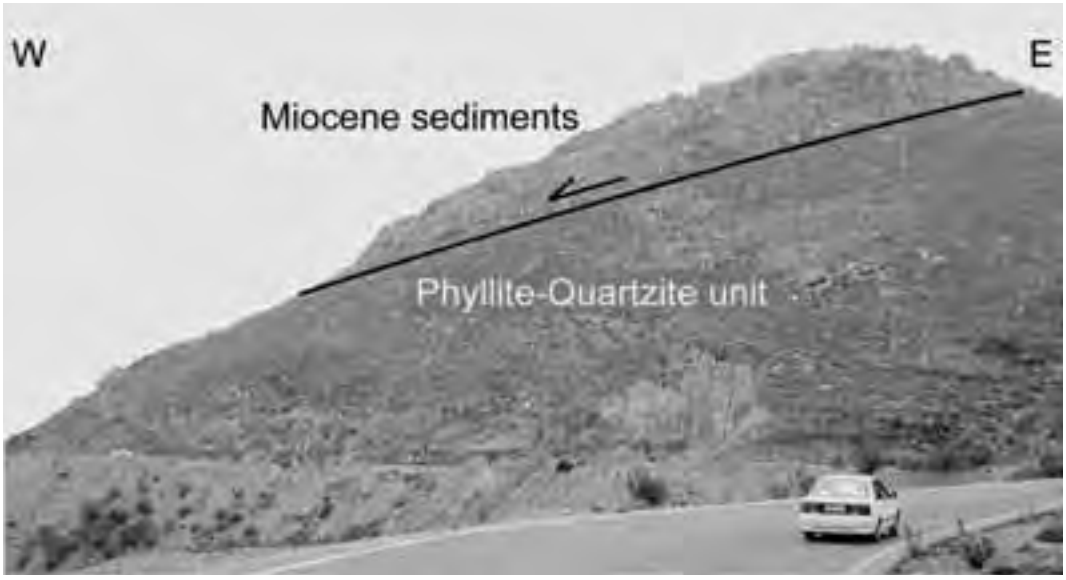

Figure 16 – Photo looking northward, showing the Cretan detachment fault with Miocene sediments in the hangingwall and Phyllite-Quartzite nappe in the footwall (Day 2, Stop 2).

micro-scale. Although Jolivet et al. (1996) admit that the deformation is "partly coaxial" on a small scale, they maintain that mesoscale observations are consistently top-N. However, the detachment here south of Voutas is clearly top-S. Recall that, when visible in the Psiloritis Mountains, the detachment is also top-S.

We agree with Jolivet et al. (1996) that there are many localities in which deformation appears to have a top-N shear sense. However, we do not believe that the deformation is systematically asymmetric. Therefore, we favor a model for the exhumation of the lower plate rocks along two separate detachment faults, one dipping northwards and the other dipping towards the south.

Return to Voutas, and take the road westward out of town towards Sklavopoula. The road to Sklavapoula is very windy and hilly. Upon reaching Sklavapoula, turn left towards Agioi Theodoroi.

Stop 6:

Deformed marbles within the Phyllite-Quartzite nappe

GPS: N 35.29030
E 023.61844
Elevation: 607 m

Between the villages of Sklavapoula and Agioi Theodoroi is a long roadcut that exposes Triassic carbonates of the Phyllite-Quartzite Group. These beds, known as the Kalamos formation, alternate between marbles and metapelites (Theye and Seidel, 1993). The petrology of these rocks has been described in detail by Theye and Seidel (1993). They report that limestones are lawsonite-bearing aragonite marbles, which in many cases have been partly or completely inverted to calcite marbles. The presence of unretrograded aragonite provides an important constraint on the P-T history of these rocks. Work by Carlson and Rosenfeld (1981) and Liu and Yund

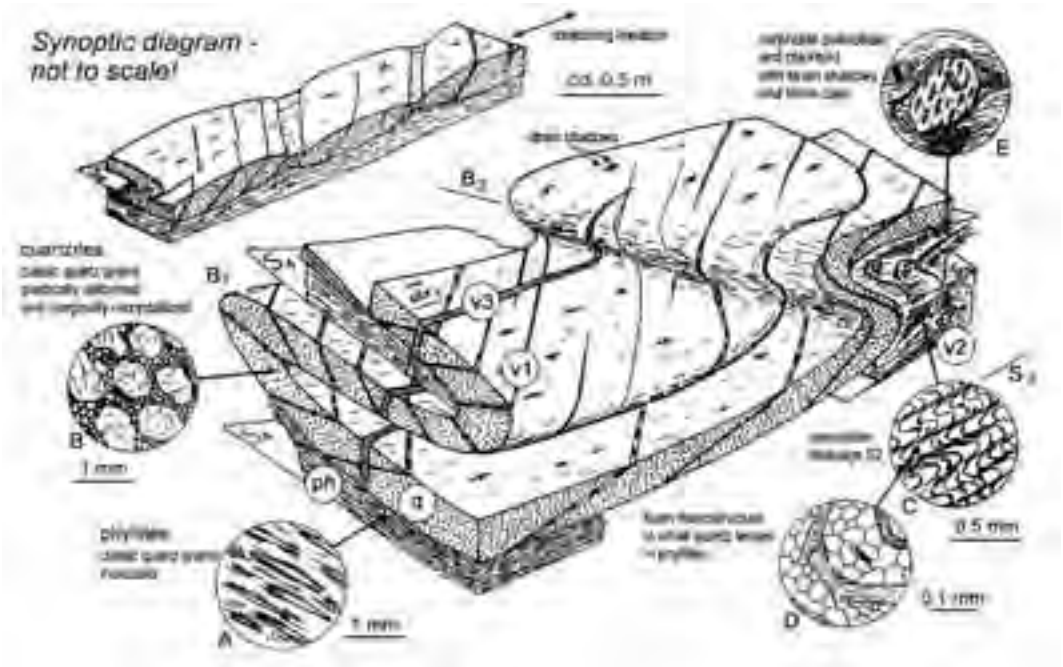

Figure 17 – Synoptic diagram illustrating deformation structures within the siliciclastic rocks of the Phyllite-Quartzite nappe of western Crete, from Stöckhert et al. (1999). B1, S1, str1 denote first-generation fold axis, schistosity, and stretching lineation. B2, S2 denote second generation fold axis and schistosity (crenulation cleavage in phyllites). Ph: phyllites; q: quartzites; v1: veins formed along original joints normal to bedding in sandstone; during deformation these veins were rotated and stretched, with boudinage of the original carbonate filling (black); quartz (white) was precipitated between the boudins; v2: veins formed during HP-LT metamorphism along S1 in phyllites, folded (B2) during progressive deformation and recrystallized; v3: later formed veins crosscutting all earlier structures, undeformed and with original microstructure preserved. Insets A to E reveal characteristic microstructures and their respective positions.

(1993) indicates that aragonite-bearing rocks must enter the calcite stability field at temperatures less than about 235°C for aragonite to survive transport to the surface without regression. This upper limit assumes very fast exhumation rates (~10 km/m.y.). Theye and Seidel (1993) have acknowledged that preservation of aragonite would imply much lower temperatures than the 350°C estimates from their thermobarometry study. This discrepancy is being studied at present by Matthew Manon and Eric Essene of the University of Michigan.

This outcrop is described by Stöckhert et al. (1999). The carbonate sequence is deformed into 100 m to km-scale asymmetric recumbent near-isoclinal folds. The long limbs of the folds have been shortened perpendicular to bedding, creating boudinage structures. Aragonite layers commonly contain veins filled with calcite and quartz oriented nearly perpendicular to bedding, some of which are slightly buckled. The veins are more competent than the aragonite layer, which lead to a characteristic "dog bone" structure during deformation. Stöckhert et al. (1999) describe fossils from these layers that are completely undistorted, demonstrating that even for the carbonate rocks in the Phyllite-Quartzite, the dominant deformation mechanism is pressure solution.

Continue following the road to Palaiochora for the evening.

DAY 3

Basin Development In Western Crete

In the first two days of the field trip, we have emphasized the older history of Crete, focusing on the sub-detachment and supra-detachment nappes. Today we will examine the sedimentary record of exhumation.

Extensional deformation and exhumation started at about 15 to 10 Ma. Coincident with this activity was the development of many local sedimentary basins. The stratigraphic nomenclature for these sequences remains complex, particularly in western Crete. Meulenkamp et al. (1979) has defined six lithostratigraphic units that seem to work well in representing syn-extensional basins throughout Crete. As such, we will use the divisions and terminology of Meulenkamp et al. (1979) in our discussion here, while noting local names where appropriate. Figure 18 shows a composite stratigraphic section for the sediments of western Crete, adapted from Meulenkamp et al. (1979).

Drive westward from Palaiochora along the coast road for about 2 km. Pull over in small lot on the left hand-side of the road.

Stop 1:

Wave-cut terraces along the southern coast at Koundoura beach

GPS: N 35.23722
E 023.66877
Elevation: 2 m

Recent uplift of the southwest coast of Crete can be observed west of Palaiochora at Koundoura beach.

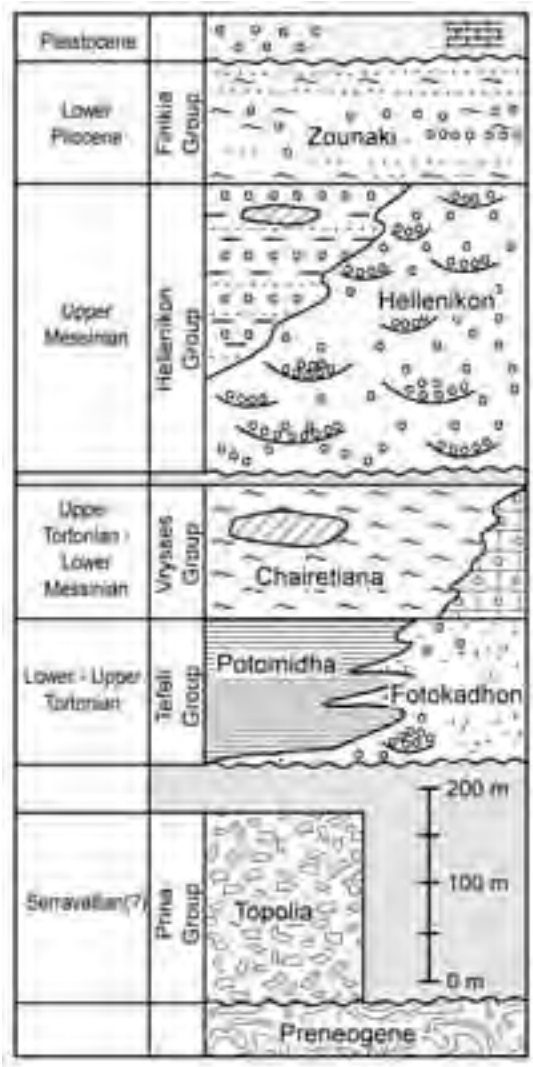

Figure 18 - Composite stratigraphic column for the sediments of western Crete, adapted from Meulenkamp et al. (1979).

You can see there a flight of uplifted wave-cut terraces exposed north of the road. Wave-cut terraces are commonly formed as a result of sea level fluctuations (eustasy) and/or elastic deformation related to the earthquake cycle. The terrace is cut when the rate of uplift of the land matches the rate of rise in sea level. In this case, the surf zone can work for some time to cut the platform. Preservation of the terrace requires that the platform be rapidly uplifted above surf zone. This typically occurs due to coseismic uplift, but a rapid fall in eustatic sea level could produce the same result.

The terraces north of the road locally show a recessed notch that marks the transition from wave-cut platform to the seacliff that use to back the platform. Cemented sand and gravel are locally preserved on the wave-cut surface, and represent remnants of beach deposits. The older terraces would be located higher on the hillslope. These terraces have been eroded away, but at this location they can sometimes be detected by the presence of caves that hosted fresh water streams that drained to sea level.

The youngest uplifted terrace is located on the beach to the south of the road. Look for a low rocky pavement of beach rock exposed just above the modern shoreline. This pavement is composed of cemented conglomerate and sand, and contains cobbles derived from the adjacent Cretan nappes (e.g., Phyllite-Quartzite and Tripolitza). A broad wave-cut platform has been cut into the upper part of this beach rock unit.

Pirazzoli et al. (1982) have dated similar wave-cut terraces in western Crete the using ^{14}C method, and they have demonstrated that uplift is occurring at rates of up to 6 m/yr for over the past 2000 years. We will focus on the modern, continuing uplift in Crete tomorrow.

Return to Palaiochora and follow the main road north out of town. At the village of Plemeniana, turn left on the road towards Dris and Strovles. Continue northward through Strovles. Turn right (towards Chania) when the road reaches an intersection. Drive north for roughly 4.5 km. The valley narrows to the north. Stop just after the memorial on the east side of the road at the bend. Walk south towards the tectonic contact between the Phyllite-Quartzite and the overlying breccia. ***Exercise extreme caution at this locality. The outcrops are exposed along a windy road, so be careful of traffic.***

Stop 2:

The onset of Miocene sedimentation

GPS: N 35.41018
E 023.68315
Elevation: 301 m

Here, we can see the oldest Neogene sediments in western Crete exposed in the cliffs of the Topolia gorge. The Miocene(?) Topolia conglomerate is a poorly sorted, matrix supported conglomerate containing subangular to rounded clasts ranging in size from granules to cobbles. A variety of clasts-types are present, including grey to black limestones, dolomites, recrystallized limestones, radiolarites, calcarenites, and micritic limestone (Seidel, 2003). The conglomerate has been interpreted as an alluvial fan deposit, with debris flow and waterlaid deposits derived from a catchment to the south (Seidel, 2003). The unit is estimated to be about 500 m thick. The coarsest deposits are located in the southern part of the basin, near its base. Higher up-section, the sediments are predominantly debris-flows in the proximal and medial parts of the complex, accounting for 70 to 80%

Figure 19 - Photo of the Topolia breccia in western Crete. The Topolia belongs to the Prina Group, which are the oldest Miocene sediments in Crete. Clasts within the Topolia appear to be exclusively derived from the supra-detachment nappes.

of the alluvial fan.
Importantly, there are no clasts of the lower plate units within this basal unit. The limestones, dolomites, and recrystallized limestones appear to have been derived from the Tripolitza nappe (Figure 19). In fact, Seidel (2003) describes fossils within some of the clasts that correspond with those found in the Tripolitza unit. Other types of cobbles, including radiolarites, calcarenites, and micritic limestone are consistent with derivation from the Pindos unit. However, despite its current close proximity with the Phyllite-Quartzite unit, the Topolia conglomerate does not contain cobbles that may have been derived from this unit. This suggests that during deposition of the Topolia conglomerates, the lower plate rocks of the Phyllite-Quartzite unit were not exposed at the surface. However, the conglomerates were later faulted into directed contact with the Phyllite-Quartzite bedrock.
The age of the Topolia conglomerates is not clear, because a lack of fossils within the complex itself prevents direct dating of the sediments. Sediments stratigraphically above the Topolia have been dated as about 9 Ma (Frydas and Keupp, 1996). Deposition of the alluvial fan may be related to extension associated with the Cretan detachment fault. Exhumation on the Cretan detachment fault is envisaged to have begun between 20 and 15 Ma, suggesting that the Topolia conglomerate was deposited sometime between 20 and 10 Ma (Seidel, 2003). The steep dip of the unit here implies significant rotation caused by uplift since the deposition of these sediments.
Following the road northward, the valley widens as we exit the gorge. Stop near the northern end of the next village, Voulgaro, for a view of the Topolia Conglomerate and the overlying Miocene sediments.

Stop 3:

View of early Miocene sedimentation

Looking towards the east, we have a nice view of the Miocene basin-fill sediments in Crete. Above the Topolia conglomerates are the horizontal sediments of the Tefeli Group (Frydas and Keupp, 1996). The oldest sediments of the Tefeli Group belong to the Fotokadhon Formation and record the initial phases of marine deposition in a shallow water environment. The Fotokadhon (also referred to by some authors as the Roka) is interfingered and overlain by the clays of the Potamida Formation, which contains calcareous nannoplankton indicative of a Tortonian age (NN10 – *Discoaster calcaris*). This demonstrates that in western Crete, the Fotokadhon formation has a depositional age of about 9 Ma.
A sedimentary hiatus followed deposition of the Topolia, as indicated by the presence of an angular unconformity between the Topolia and the overlying sediments of the Miocene Tefeli Group (Figure 20). The Fotokadhon grades both laterally and upsection into the Potamida formation. Above these formations are the well-bedded, sandy marls and interbedded clays of the Chairetiana Formation. The lower part of the Chairetiana of the Vrysses group corresponds to calcareous nannoplankton subzone NN 11a (latest Tortonian), while its upper part belongs stratigraphically to the subzone NN 11b (*Amaurolithus delicatus*), indicating an early Messinian age (Frydas and Keupp, 1996). Gypsum deposits are commonly found contained within the Chairetiana Formation. The consolidated marls of the Chairetiana are distinctive and thus serve as a useful marker horizon throughout northwestern Crete.
Continue driving north until you reach the National

Figure 20 – Panorama looking eastward from the village of Voulgaro, showing the lower Miocene supra-detachment sediments in western Crete. An angular unconformity exists between the Topolia breccia and the overlying sediments of the Tefeli group.

road at the eastern side of the town of Kissamos. Turn right and drive towards the east. Pass the road that heads off towards Nopigia (Day 2, Stop 1) and continue eastward for several km up onto the Rodopos Peninsula. About 10.5 km from Kissamos you will see a low concrete building on the right hand side of the road with "NISSAN" written on it. Turn into the large pullout near this building. There is a large outcrop of Phyllite-Quartzite rocks on the left-hand side of the road. Carefully cross the road and walk towards the east for about 100 m.

Stop 4:

Depositional contact on the Phyllite-Quartzite unit

GPS: N 35.5314
E 023.765

Here, sediments equivalent to the Fotokadhon clearly lie in depositional contact with the Phyllite-Quartzite unit. The contact between the bedrock of the Phyllite-Quartzite and the Miocene sediments is not a flat surface, but rather has an undulating, hummocky nature indicating that it was at the surface at the time. Furthermore, soil horizons also illustrate the depositional nature of the contact between the Phyllite-Quartzite and overlying conglomerate. Walking eastward along the road, we can see that this conglomerate is clearly overlain by the Fotokadhon Formation sediments and the Chairetiana Formation. This clearly illustrates that the Phyllite-Quartzite was exposed at the surface prior to the NN10 Nannozone at about 9 Ma (Frydas and Keupp, 1996).

Walk eastward on the road. Bedding in the Miocene sediments is initially steep but becomes more gentle away from the contact. Continuing eastward for several hundred meters, there is a break in the section across the bridge. After this, the section is still conglomerates, but they fine upward into buff-colored thinly bedded marls of the Potamida Formation. Note on the southern side of the road, we can see that these sediments are capped by the marls of the Tortonian-Messinian Chairetiana Formation.

The presence of cobbles of the Phyllite-Quartzite unit in the sediments can be used to constrain the thermal evolution of the high-pressure, low-temperature rocks of Crete. Here, we summarize the results that we have discussed thus far throughout the trip (Figure 7). This discussion is a modification of the results of Thomson et al. (1999). The Oligocene flysch at the top of the Plattenkalk unit shows that it was still at the surface at ~29 Ma. However, the sediments of the Phyllite-Quartzite are though to have been deposited to the north of the Plattenkalk platform, meaning that the rocks of the Phyllite-Quartzite were deeply subducted prior to 29 Ma. Estimates of the rate of plate convergence during the Oligocene and the inferred paleogeography suggest subduction of the Phyllite-Quartzite sometime between 36 to 32 Ma. White mica Ar-Ar ages, interpreted here as sub-closure crystallization ages, suggest peak metamorphic conditions were reached between 24 and 20 Ma (Jolivet et al., 1996). Previously published

Figure 21 - Photo of depositional contact between the Miocene sediments of the Fotokadhon Formation and Phyllite-Quartzite unit. The Fotodakhon is about 9 Ma based on calcareous nannoplankton, providing a minimum exposure age for the Phyllite-Quartzite nappe in western Crete.

zircon He ages reveal cooling through 240°C at about 18 Ma. New zircon He ages show that the lower plate rocks cooled below 210°C around 10 Ma. Finally, conglomeratic deposits indicate exposure of the HP rocks at the surface at about 8.5 Ma. This suggests that the HP-LT rocks in the footwall of the Cretan were experienced a two -phase exhumation history, with modest exhumation between 20 and 10 Ma, followed by a rapid pulse of exhumation that ultimately led to the exposure of Phyllite-Quartzite bedrock at the surface by 9 Ma.

Drive westward back towards Kissamos. Turn left onto the Old National Road towards Chania (about 1 km before reaching Kissamos). Drive for 0.4 km and then turn right on the road towards Sirikari. Drive another 0.9 km, following the main road. Pull off and park at the hairpin turn in the road.

Stop 5:

The Chairetiana Formation, Messinian evaporite, more recent faulting

GPS: N 35.48585
E 023.67421

Here, laminated marls of the Chairetiana Formation outcrop along the side of the road. At the point in the hairpin turn, a small trail leads towards the west. A few meters from the road, the pavement exposes gypsum associated with the Messinian event. These rocks are exposed at 100 m elevation, thus requiring at least that much uplift since about 5 Ma.

This locality also provides an excellent view of the recent and still active normal faults. In western Crete, these are often oriented N-S. Looking to the north, we can see Kissamos Bay, a north-south oriented waterway bounded by long north-south peninsulas. These are bounded by N-S trending normal faults that have dropped the rocks beneath Kissamos Bay down relative to the rocks of the long peninsulas.

Continue north along the main road for another 0.6 km. Turn right on the road up to Marediana (the sign is only in Greek). Drive for 0.5 km and part at the hairpin turn off on the right-hand side of the road. Walk a short distance along the access road (50 m) to the outcrop.

Stop 6:

Messinian evaporite within Chairetiana formation (Optional stop)

GPS: *N 35.48310*
E 023.67142

Elevation: 105 m

Large (~20 cm) clasts of gypsum crystals can be found in the low outcrops alongside road. The gypsum appears to have been fragmented by depositional reworking. They are found as interbeds in finely laminated marls, indicating a marine depositional environment.

Return to the National Road and drive eastward to Chania for the evening.

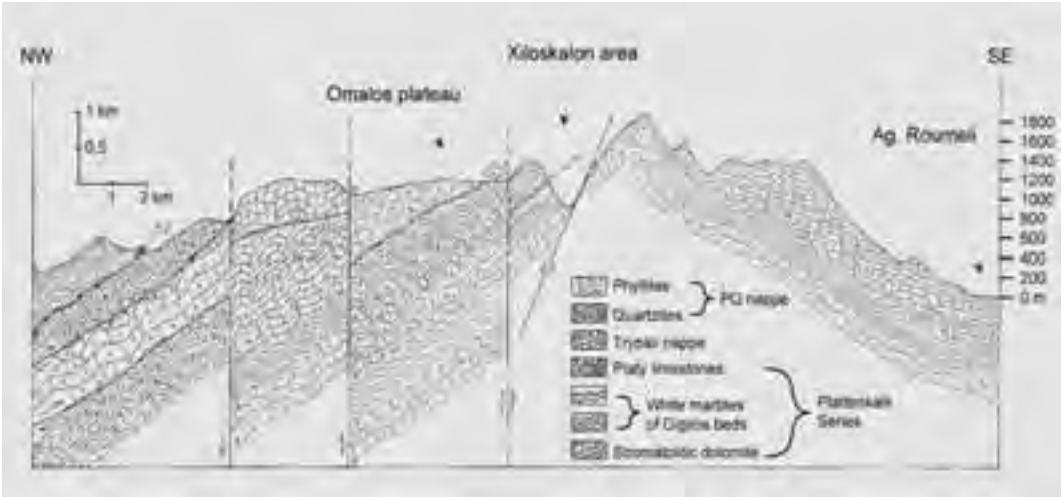

Figure 22 - Cross section of the Lefka Ori Mountains in the Omalos area of western Crete, modified from Fytrolakis (1980) and Fassoulas (2000). The Samaria Gorge begins in the Xiloskalon area and ends at Agios Roumeli.

DAY 4

Samaria Gorge

We will conclude our field excursion with a hike down the beautiful Samaria Gorge. This 16 km gorge is considered the longest in Europe. We will take a bus from Chania to the Omalos Plateau and to the entrance to the Samaria Gorge Park. The hike through the gorge typically takes 4 to 6 hours and ends at the village of Agia Roumeli. From there, we take a ferry eastward to Chora Sfakion where buses will take people back to Chania.

The road to the park passes first through the Phyllite-Quartzite nappe and then into the Trypali nappe after the village of Lakoi. The Samaria Gorge itself is cut into the Plattenkalk nappe. The whitish peaks at the head of the gorge are the Gigilos beds, the massive white marbles in the Plattenkalk that are stratigraphically above the Triassic stromatolitic dolomite but below the typical "platy limestone" horizons (Figure 11). The structure of the Lefka Ori region is depicted in Figure 22, which shows that as we hike down towards the coast we will travel progressively upsection in the Plattenkalk stratigraphy.

The hike begins at an elevation of 1250 m. The surrounding peaks are typically at about 2000 m and reach as high as 2450 m. The first five km of the hike are through the Gigilos beds, the massive white marbles in the Plattenkalk unit that we say at Day 1, Stop 8. The impressive cliffs along the sides of the gorge offer impressive exposures of folds developed in the platy member of the Plattenkalk. The platy rocks drop down to the valley floor about 2 km above the abandoned village of Samaria. For the remainder of the gorge, the platy member is well exposed, revealing numerous south vergent asymmetric folds, similar to the Plattenkalk folds we saw earlier in the trip (Day 1, Stop 7).

The boat trip from Agia Roumeli at the mouth of the gorge to Chora Sfakion provides several views of other south-flowing gorges that have been cut into the southwest flank of Crete. This south slope also has several uplifted wave-cut terraces (Figure 23), similar to the uplifted terraces that we saw east of Palaiochora (Day 3, Stop 1). Many of these terraces have been dated by Pirazzoli et al. (1982), who describe terraces of 8 distinct ages. Throughout western Crete, these are typically uplifted from 3 to 8 m over the past 2000 to 4000 years. If sustained, these values would be equivalent to uplift rate of 0.8 to 4 km/m.y.

Figure 23 - Photograph of uplifted Holocene terraces along the western coast of Crete.

The southwest coast of Crete appears to coincide with a south-dipping normal fault, with the hangingwall offshore to the south. Thus, the southwest coast of Crete represents the footwall of this fault. The uplifted coastal terraces and the deeply incised gorges along the southwest coast indicate that slip on this normal fault seems to be occurring primarily by rise of the footwall, rather than by fall of the hangingwall, as commonly assumed. This distinction is possible here because the geomorphic features allow us to measure displacements relative to sea level. This evidence of footwall rise during normal faulting suggests that horizontal extension may be related to basal accretion

or underplating at depth beneath the island. The HP-LT metamorphism of the sub-detachment nappes indicates that they were accreted by underplating at depths of ~35 km. Continued underplating seems required to account for the 35 km of rock that presently underlie the Plattenkalk and Phyllite-Quartzite units. The record of rapid uplift along the south coast is also consistent with continued accretion through underplating.

Aknowledgments

We benefited from discussions with Jay Ague, Bernhard Stöckhert, and Stuart Thomson. We thank Walter Joyce for assistance with English translations of the German literature on Crete.

Reference cited

Angelier, J., Lyberis, N., Le Pichon, X., Barrier, E., and Huchon, P. (1982). The tectonic development of the Hellenic Arc and the Sea of Crete: a synthesis. *Tectonophysics* 86, 159-196.

Armijo, R., Lyon-Caen, H., and Papanastassiou, D. (1992). East-west extension and Holocene normal fault scarps in the Hellenic arc. *Geology* 20, 491-494.

Bizon, G., Bonneau, M., Leboulenger, P., Matesco, S., and Thiébault, F. (1976). Sur la signification et l'extension des <<massifs cristallins externes>> en Péloponnèse méridional et dans l'Arc égéen. *Bulletin de la Société géologique de France* 18, 337-345.

Bonneau, M. (1984). Correlation of the Hellenic Nappes in the south-east Aegean and their tectonic reconstruction. In: Dixon, J.E., and Robertson, A.H.F., eds. *The Geological Evolution of the Eastern Mediterranean*. Geological Society, London, Special Publications 17, 517-527.

Brix, M.R., Stöckhert, B., Seidel, E., Theye, T., Thomson, S.N., and Küster, M. (2002). Thermobarometric data from a fossil zircon partial annealing zone in high pressure-low temperature rocks of eastern and central Crete, Greece. *Tectonophysics* 349, 309-326.

Buick, I. (1991). Mylonite fabric development on Naxos, Greece. *Journal of Structural Geology* 13, 643-655.

Carlson, W.D., and Rosenfeld, J.L. (1981). Optical determination of topotactic aragonite-calcite growth kinetics: metamorphic implications. *Journal of Geology* 89, 615-638,

Creutzburg, N., Drooger, C.W., Meulenkamp, J.W., Papastamatiou, J., Seidel, and Tataris, A. (1977). General Geological Map of Crete (scale 1:200,000). *Institute of Geological and Mining Exploration (IGME), Athens*.

Creutzburg, N., and Seidel, E. (1975). Zum Stand der Geologie des Präneogens auf Kreta. *Neues. Jb. Geol. Paläont. Abh.* 149, 363-383.

Dewey, J.F. (1988). Extensional collapse of orogens. *Tectonics* 7, 1123-1139.

Dewey, J.F., Helman, J.L., Turco, E., Hutton, D.W.H., and Knott, S.D. (1989). Kinematics of the western Mediterranean. In: Coward, M.P. and Dietrich, D., eds., *Alpine Tectonics*. Geological Society, London, Special Publications 45, 265-283.

Duermeijer, C.E., Nyst, M., Meijer, P.Th, Langereis, C.G., and Spakman, W. (2000). Neogene evolution of the Aegean arc: paleomagnetic and geodetic evidence for a rapid and young rotation phase. *Earth and Planetary Science Letters* 176, 509-525.

Duermeijer, C.E., Krijgsman, W., Langereis, C.G., and ten Veen, J.H. (1998). Post early Messinian counter-clockwise rotations on Crete: implications for the Late Miocene to Recent kinematics of the southern Hellenic Arc. *Tectonophysics* 298, 177-189.

Epting, J., Kudrass, H-R., Leppig, U., and Schafer, A. (1972). Geologie der Talea Ori/Kreta. *Neues Jb. Geol. Paläont. Abh.* 141, 259-285.

Fassoulas, C., Kilias, A., and Mountrakis, D. (1994). Postnappe stacking extension and exhumation of high-pressure low- temperature rocks in the island of Crete, Greece. *Tectonics* 13, 127-138.

Fassoulas, C. (2000). Field Guide to the Geology of Crete. *Natural History Museum of Crete, Publ.,* 104 p., Heraklio.

Fassoulas, C. (2001). The tectonic development of

a Neogene basin at the leading edge of the active European margin: the Heraklion basin, Crete, Greece. *Journal of Geodynamics* 31, 49-70.

Fortuin, A.R., and Peters, J.M. (1984). The Prina Complex in eastern Crete and its relationship to possible Miocene strike-slip tectonics. *Journal of Structural Geology* 6, 459-476.

Frydas, D., and Keupp, H. (1996). Biostratigraphical results in Late Neogene deposits of NW Crete, Greece, based on calcareous nannofossils. *Berliner geowiss. Abh,* E 18, 169-189.

Fytrolakis, N. (1980). The geological structure of Crete: Problems, observations, and conclusions. *Habil. Thesis, Nat. Techn. Univ. Athens*, 143 p.

Greiling, R. (1982). The metamorphic and structural evolution of the Phyllite-quartzite nappe of western Crete. *Journal of Structural Geology* 4, 291-297.

Hall, R., Audley-Charles, M.G., and Carter, D.J. (1984). The significance of Crete for the evolution of the Eastern Mediterranean. *In:* Dixon, J.E., and Robertson, A.H.F. (eds) *The Geological Evolution of the Eastern Mediterranean*. Geological Society, London, Special Publications 17, 499-516.

Hall, R., and Audley-Charles, M.G. (1983). The structure and regional significance of the Talea Ori, Crete. *Journal of Structural Geology* 5, 167-179.

Hatzfeld, D., Martinod, J., and Bastet, G. (1997). An analog experiment for the Aegean to describe the contribution of gravitational potential energy. *Journal of Geophysical Research* 102, 649-659.

Huguen, C., Mascle, J., Chaumillon, E., Woodside, J.M., Benkhelil, J., Kopf, A., and Volskonkaia,k A. (2001). Deformation styles of the eastern Mediterranean Ridge and surroundings from combined swatch mapping and seismic reflection profiling. *Tectonophysics* 343, 21-47.

Jackson, J. (1994). Active tectonics of the Aegean region. *Annual Reviews of Earth and Planetary Science* 22, 239-271,

Jiménez-Munt, I., Sabadini, R., Gardi, A., and Bianco, G. (2003). Active deformation in the Mediterranean from Gibraltar to Anatolia inferred from numerical modeling and geodetic and seismological data. *Journal of Geophysical Research* 108, doi:10.1029/2001JB001544.

Jolivet, L., Goffe, B., Monie, P., Truffert-Luxey, C., Patriat, M & Bonneau, M. (1996). Miocene detachment in Crete and exhumation P-T-t paths of high-pressure metamorphic rocks. *Tectonics* 15, 1129-1153.

Karakitsios, V. (1987). Sur la signification de la série de Trypali dans la région de Sellia en Crète occidentale (Grèce). *CR Acad. Sci. Paris*, 304 (II/3), 123-128.

Kastens, K.A. (1991). Rate of outward growth of the Mediterranean Ridge accretionary complex. *Tectonophysics* 199, 25-50.

Kilias, A., Falalakis, G., and Mountrakis, D. (1999). Cretaceous - Tertiary structures and kinematics of the Serbomacedonian metamorphic rocks and their relation to the exhumation of the Hellenic hinterland (Macedonia, Greece). *International Journal of Earth Sciences*, 88, 513-531.

Kissel, C., and Laj, C. (1988). The Tertiary geodynamical evolution of the Aegean arc: a paleomagnetic reconstruction. *Tectonophysics* 146, 183-201.

Knapmeyer, M., and Harjies, H.P. (2000). Imaging crustal discontinuities and the downgoing slab beneath western Crete. *Geophysical Journal International* 143, 1-21.

Kopp, K., and Ott, E. (1977). Spezialkartierungen im Umkreis neuer Fossilfunde in Tripali und Tripolitzakalken Westkretas. *Neues Jb. Geol. Paläont. Monat.*, 4, 217-238.

Kopf, A., Mascle, J., and Klaeschen, D. (2003). The Mediterranean Ridge: A mass balance across the fastest growing accretionary complex on Earth. *Journal of Geophysical Research*, 108, doi:10.1029/2001JB000473.

Krahl, J., Kauffmann, G., Kozur, H., Richter, D., Förster, O., and Heinritzi, F. (1983). Neue Daten zur Biostratigraphie und zur tektonischen Lagerung der Phyllit-Gruppe und der Trypali-Gruppe auf der Insel Kreta (Griechenland). *Geologische Rundschau* 72, 1147-1166.

Krahl, J., Richter, D., Forster, O., Kozur, H., and Hall, R. (1988). Zur Stellung der Talea Ori im Bau des kretischen Deckenstapels (Greichenland). *Zeitschrift der deutschen geologischen Gesellschaft* 139, 191-207.

Kuss, S.E. (1980). Fuhrer zur Kreta – Exkursion. *Geologisch – Paleontologischen Institue Universitaet Freiburg.*

Küster, M., and Stöckhert, B. (1997). Density changes of fluid inclusions in high-pressure low-temperature metamorphic rocks from Crete: A thermobarometric approach based on the creep strength of the host minerals. *Lithos* 41, 151-167.

Le Pichon, X., and Angelier, J. (1979). The Hellenic arc and trench system: a key to the neotectonic evolution of the Eastern Mediterranean area. *Tectonophysics* 60, 1-42.

Le Pichon, X., and Angelier, J. (1981). The Aegean Sea. *Philosophical Transactions of the Royal Society, London*, 300, 357-372.

Le Pichon, X., Lallemant, S.J., Chamot-Rooke, N., Lemeur, D., and Pascal, G. (2002). The Mediterranean Ridge backstop and the Hellenic nappes. *Marine Geology* 186, 111-125.

Lister, G.S., Banga, G., and Feenstra, A. (1984). Metamorphic core complexes of Cordilleran type in the Cyclades, Aegean Sea, Greece. *Geology* 12, 221-225.

Liu, M., and Yund, R.A. (1993). Transformation kinetics of polycrystalline aragonite to calcite: new experimental data, modelling, and implications. *Contributions to Mineralogy and Petrology* 114, 465-478.

Makris, J. (1978). The crust and upper mantle of the Aegean region from deep seismic sounding. *Tectonophysics* 46, 269-284.

Makris, J., and Stobbe, C. (1984). Physical properties and state of the crust and upper mantle of the eastern Mediterranean Sea deduced from geophysical data. *Marine Geology* 55, 217-254.

McClusky, S. et al. (2000). Global Position System constraints on plate kinematics and dynamics in the eastern Mediterranean and Caucasus. *Journal of Geophysical Research* 105, 5695-5719.

McKenzie, D.P. (1972). Active tectonics of the Mediterranean region. *Geophysical Journal of the Royal Astronomical Society* 30, 109-185.

McKenzie, D.P. (1978). Some remarks on the development of sedimentary basins. *Earth and Planetary Science Letters* 40, 25-32.

Meijer, P.Th. and Wortel, M.J.R. (1997). Present-day dynamics of the Aegean region: A model analysis of the horizontal pattern of stress and deformation. *Tectonics* 16, 879-895.

Meulenkamp, J.E., Dermitzakis, M., Georgiadou-Dikeoulia, E., Jonkers, H.A., and Böger, H. (1979). *Field Guide to the Neogene of Crete.* Publications of the Department of Geology and Paleontology, University of Athens, A, 32.

Meulenkamp, J.E., Wortel, M.J.R., van Wamel, W.A., Spakman, W., and Hoogerduyn Strating, E. (1988). On the Hellenic subduction zone and the geodynamic evolution of Crete since the late Middle Miocene. *Tectonophysics* 146, 203-215.

Meulenkamp, J.E., van der Zwaan, G.J., and van Wamel, W.A. (1994). On Late Miocene to Recent vertical motions in the Cretan segment of the Hellenic arc. *Tectonophysics* 234, 53-72.

Pirazzoli, P.A., Thommeret, J., Thommeret, Y., Laborel, J., and Montaggioni, L.F. (1982). *Tectonophysics* 86, 27-43.

Platt, J.P. (1986). Dynamics of orogenic wedges and the uplift of high-pressure metamorphic rocks. *Geological Society of America Bulletin* 97, 1037-1053.

Pomoni-Papaioannou, F., and Karakitsios, V. (2002). Facies analysis of the Trypali carbonate unit (Upper Triassic) in central-western Crete (Greece): an evaporite formation transformed into solution-collapse breccias. *Sedimentology* 49, 1113-1132.

Robertson, A.H.F., Clift, P., Degnan, P.J., and Jones, G. (1991). Palaeogeographic and paleotectonic evolution of the eastern Mediterranean Neotethys. *Palaeogeography, Palaeoclimatology, and Palaeoecology* 87, 289-343.

Royden, L.H. (1993). The tectonic expression of slab pull at continental convergent boundaries. *Tectonics* 12, 303-325.

Sannemann, W., and Seidel, E. (1976). Die Trias-Schichten von Rawdoucha/NW-Kreta. Ihre Stellung im kreitischen Deckenbau. *Neues Jb. Geol. Paläont. Mh.* 4, 221-228.

Seidel, M. (2003). Tectono-sedimentary evolution of middle Miocene supra-detachment basins (western Crete, Greece). *Ph.D. Dissertation, University of Köln*. 116 pages.

Seidel, E., Okrusch, m., Kreuzer, H., Raschka, H., and Harre, W. (1976) Eo-alpine metamorphism in the uppermost unit of the Cretan nappe system – petrology and geochronology – Part 1. The Lendas area (Asteroussia Mountains). *Contributions to Mineralogy and Petrology* 57, 259-275.

Seidel, E., Kreuzer, H., and Harre, W. (1982). A Late Oligocene/Early Miocene high pressure belt in the External Hellenides. *Geologisches Jahrbuch* E23, 165-206.

Schwarz, S., and Stöckhert, B. (1996). Pressure solution in siliciclastic HP-LT metamorphic rocks - constraints on the state of stress in deep levels of accretionary complexes. *Tectonophysics*, 255, 203-209.

Spakman, W., Wortel, M.J.R., and Vlaar, N.J. (1988). The Hellenic subduction zone: a tomographic image and its geodynamic implications. *Geophysical Research Letters* 15, 60-63.

Stöckhert, B., Wachmann, M., Küster, M., and Bimmermann, S. (1999). Low effective viscosity during high pressure metamorphism due to dissolution precipitation creep: the record of HP-LT metamorphic carbonates and siliciclastic rocks from Crete. *Tectonophysics* 303, 299-319.

Ten Veen, J.H., and Meijer, P.T. (1998). Late Miocene to Recent tectonic evolution of Crete (Greece): geological observations and model analysis. *Tectonophysics* 298, 191-208.

Ten Veen, J.H., and Postma, G. (1999a). Neogene tectonics and basin fill patterns in the Hellenic outer-arc. *Basin Research* 11, 223-241.

Ten Veen, J.H., and Postma, G. (1999b). Roll-back controlled vertical movements of outer-arc basins of the Hellenic subduction zone (Crete, Greece). *Basin Research* 11, 243-266.

Theye, T., and Seidel, E. (1991). Petrology of low-grade high-pressure metapelites from the External Hellenides (Crete, Peloponnese): A case study with attention to sodic minerals. *European Journal of Mineralogy* 3, 343-366.

Theye, T., Seidel, E., and Vidal, O. (1992). Carpholite, sudoite, and chloritoid in low-grade high-pressure metapelites from Crete and the Peloponnese. *European Journal of Mineralogy* 4, 487-507.

Theye, T., and Seidel, E. (1993). Uplift-related retrogression history of argonite marbles in Western Crete. *Contributions to Mineralogy and Petrology* 114, 349-356.

Theye, T., and Seidel, E. (2001). Bauxite in hochdruckmetamorphen Einheiten der externen Helleniden. *Braunschweiger geowiss. Arb.* 24, 225-233.

Volume n° 2 - from B16 to B33

Thomson, S.N., Stöckhert, B., and Brix, M.R. (1998a). Thermochronology of the high-pressure metamorphic rocks of Crete, Greece: implications for the speed of tectonic processes. *Geology* 26, 259-262.

Thomson, S.N., Stöckhert, B., Rauche, H., and Brix, M.R. (1998b). Apatite fission-track thermochronology of the Uppermost Tectonic Unit of Crete, Greece: Implications for the post-Eocene tectonic evolution of the Hellenic subduction system. *In:* Van den haute, P., and De Corte, F. (eds). *Advances in Fission-Track Thermonchronology*, 187-205. (Kluwer Academic Publishers.)

Thomson, S.N., Stöckhert, B. and Brix, M.R. (1999). Micocene high-pressure metamorphic rocks of Crete, Greece: rapid exhumation by buoyant escape. *In:* Ring, U., Brandon, M.T., Lister, G.S. & Willet, S.D. (eds) *Exhumation Processes: Normal Faulting, Ductile Flow and Erosion*. Geological Society, London, Special Publications, 154, p. 87-107.

Willett, S.D. (1999). Rheological dependence of extension in wedge models. *Tectonophysics* 305, 419-435.

Wortel, M.J.R., and Spakman, W. (2000). Subduction and slab detachment in the Mediterranean-Carpathian region. *Science* 290, 1910-1917.

Back Cover:
field trip itinerary

Edited by APAT

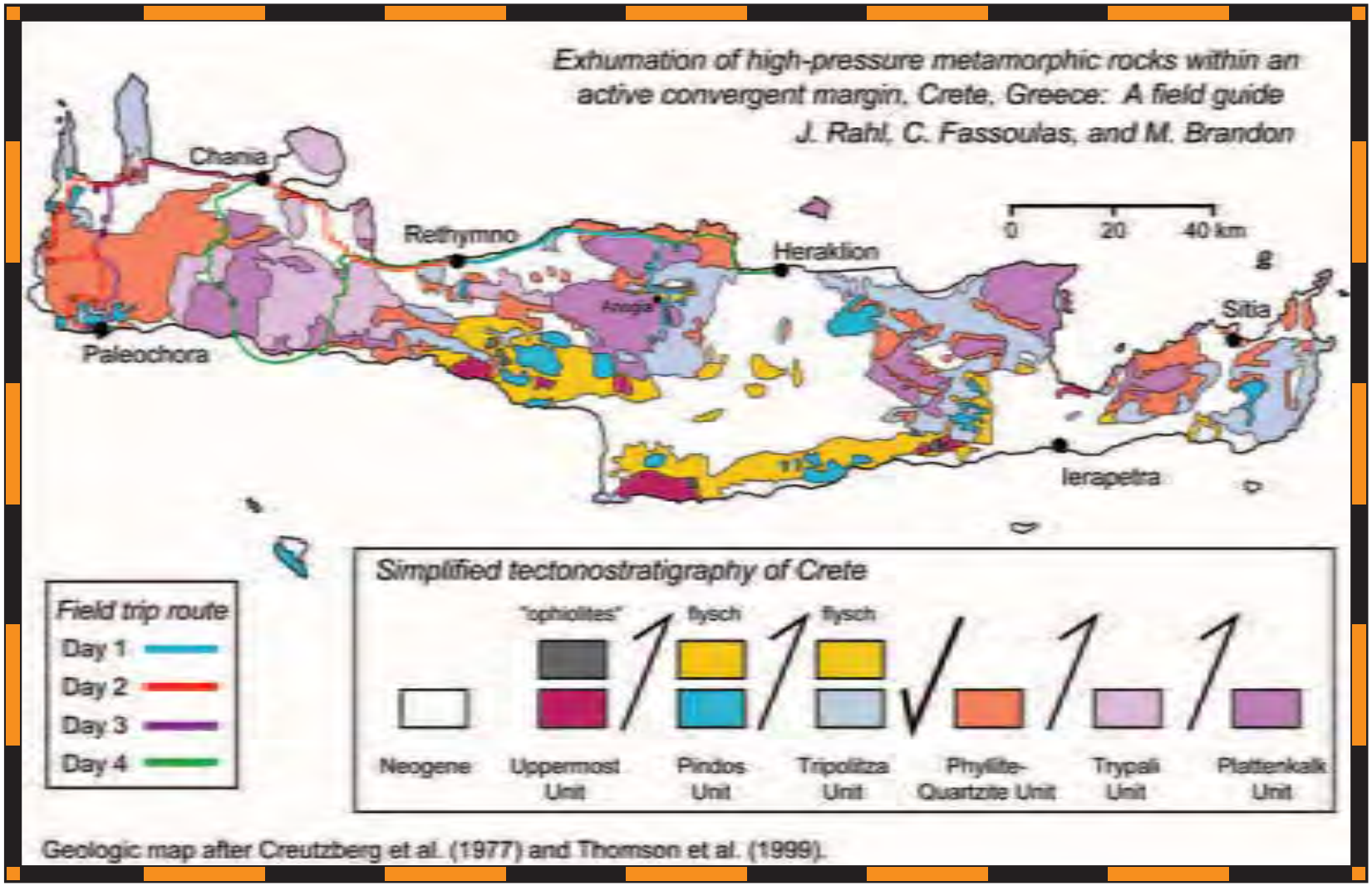

FIELD TRIP MAP

Volume n° 2 - from B16 to B33

32nd INTERNATIONAL GEOLOGICAL CONGRESS

THE CONTROL OF THE MESOZOIC PALEOMARGIN ARCHITECTURE ON THE PLIOCENE OROGENIC SYSTEM OF THE CENTRAL APENNINES

Leaders:
F. Calamita, M. Di Vincenzo,
V. Scisciani, E. Tavarnelli, M. Viandante

Field Trip Guide Book - B33

Florence - Italy
August 20-28, 2004

Pre-Congress **B33**

The scientific content of this guide is under the total responsibility of the Authors

Published by:
APAT – Italian Agency for the Environmental Protection and Technical Services - Via Vitaliano Brancati, 48 - 00144 Roma - Italy

Series Editors:
Luca Guerrieri, Irene Rischia and Leonello Serva (APAT, Roma)

English Desk-copy Editors:
Paul Mazza (Università di Firenze), Jessica Ann Thonn (Università di Firenze), Nathalie Marléne Adams (Università di Firenze), Miriam Friedman (Università di Firenze), Kate Eadie (Freelance indipendent professional)

Field Trip Committee:
Leonello Serva (APAT, Roma), Alessandro Michetti (Università dell'Insubria, Como), Giulio Pavia (Università di Torino), Raffaele Pignone (Servizio Geologico Regione Emilia-Romagna, Bologna) and Riccardo Polino (CNR, Torino)

Acknowledgments:
The 32nd IGC Organizing Committee is grateful to Roberto Pompili and Elisa Brustia (APAT, Roma) for their collaboration in editing.

Graphic project:
Full snc - Firenze

Layout and press:
Lito Terrazzi srl - Firenze

Volume n° 2 - from B16 to B33

32nd INTERNATIONAL GEOLOGICAL CONGRESS

THE CONTROL OF THE MESOZOIC PALEOMARGIN ARCHITECTURE ON THE PLIOCENE OROGENIC SYSTEM OF THE CENTRAL APENNINES

AUTHORS:
F. Calamita[1], M. Di Vincenzo[1], V. Scisciani[1], E. Tavarnelli[2] M. Viandante[1]

[1]Dipartimento di Scienze della Terra, Chieti - Italy
[2]Dipartimento di Scienze della Terra, Siena - Italy

Florence - Italy
August 20-28, 2004

Pre-Congress

B33

Front Cover:

Panoramic view of the E-W trending Gran Sasso thrust front. Dl: Dolomia Principale; CM: Calcare Massiccio; Co: Corniola; Va: Verde Ammonitico; Ce: Calcari bioclastici inferiori; Ma: Maiolica; Sb: Jurassic-Miocene overturned succession; Mcc: Marne con cerrogna; La: Laga Fm.; br: Quaternary cemented breccia; black line: bedding; red line: thrust; blue line: normal fault.
In the insets are reported: a) the Corno Grande Jurassic structural high and thrust ramp trajectory; b) the propagation of the Gran Sasso thrust ramp, and the development of the related fold."

Leader: F. Calamita, M. Di Vincenzo, V. Scisciani, E. Tavarnelli, M. Viandante

Introduction

The Central Apennines of Italy are a well- exposed foreland fold-and-thrust belt, characterized by good outcrop continuity and high vertical relief. Salient geometries of the thrust fronts represent a peculiar feature of the outer zones of this orogenic chain. These reflect the distribution of Mesozoic carbonate platforms and pelagic basins, differentiated during Triassic-Jurassic Tethyan rifting.

The stratigraphic section, and the relationships between tectonics and sedimentation, are well-documented in the numerous foredeep and thrust-top basins, developed in response to the eastward migration of the Neogene thrust fronts.

The proposed field trip focuses on the main geological and structural characteristics of the outer zones of the Central Apennines. A 3-day traverse across the Gran Sasso, Montagna dei Fiori, and Sibillini Mts, will provide an opportunity to illustrate normal faults inherited from Mesozoic rifting and Miocene foreland flexuring events, and to evaluate the influence that these structures played during the subsequent construction of the Apennine fold-and-thrust belt in Late Miocene-Pliocene times. (see: Guide Geologiche Regionali Vols 7 and 10).

Geological and structural studies, carried out in recent decades, across several orogenic belts have shown that pre-existing normal faults, inherited from continental rifting stages, were important in controlling the architecture of younger, superimposed fold-and-thrust systems (positive inversion tectonics). Pre-existing normal faults were reactivated as reverse faults, or were modified, truncated, deformed and passively transported in the hanging-wall blocks of the upward-propagating thrusts. Other studies have outlined that, in the mature orogenic stages, several thrust faults were reactivated as low-angle normal faults, or truncated by high-angle normal faults, as a result of late-, or post-orogenic extension (negative inversion tectonics).

A comprehensive description of the geometry and kinematics of inherited structures, and an illustration of how these structures behaved during two main inversion episodes, both positive and negative, are the main focus of the proposed field trip across the Central Apennines. An analysis of the superpositional relationships of contractional and extensional structures, will provide an opportunity to evaluate the role of inversion tectonics in the construction of the outer parts of the belt. These relationships indicate that the architecture of the Mesozoic passive margin, consisting of alternating pelagic basins and carbonate platforms, was important in controlling the location, geometry and physiography of the subsequent foredeep basins.

Regional geologic setting

The Apennines are a pile of tectonic units which originated in different palaeogeographic domains (Back cover figure). The innermost, i.e. westernmost Liguride/Sicilide units were transported eastwards onto the carbonate Apennine units, which in turn originated at the expense of the Mesozoic Adria continental margin. In the central-southern parts of the belt, the Molise Units are interposed between the Ligurides/Sicilides and the Apennine units. The Ligurides/Sicilides and Molise Units were derived from the oceanic crust of the Alpine and Ionian Neotethys basins respectively. These basins were separated by the Maghrebian or Etrurian continental block, to which the internal carbonate platform units are related (Finetti & Del Ben, 2000; Lentini et al., 2002).

The evolution of the Apennine orogeny started in Tertiary, as a consequence of the closure of the Alpine and Ionian Neotethys basins, and of the convergence of the European and Adria-African continental blocks (Ben Avraham et al., 1990; Finetti et al, 1996; Gattacceca & Speranza, 2002; Lentini et al., 2002).

The Ligurides/Sicilides represent an accretionary prism, connected to the Cretaceous-Eocene subduction of the Alpine Neotethys oceanic crust. This subduction led to the collision of the European and Adria-African continental blocks (Carmignani & Kligfield, 1990). They were involved, from Upper Oligocene onwards, in the deformation of the Northern Apennine Adria paleomargin (Boccaletti et al., 1990). Subsequently, the subduction of the Ionian Ocean, initiated in Middle Miocene time, produced an accretionary prism, formed by the Molise Units and by the external flysch of the Southern Apennines, that, in turn, were thrust eastwards for ca. 100 km onto the Adria paleomargin Apennine Units s.s., formed by the Apulian carbonate platform (Mostardini & Merlini, 1986; Casero et al., 1988; Menardi Noguera & Rea, 2000; Patacca et al., 2000).

The Apennines are arranged in two main arcs (Back cover figure): the Central-Northern Apennine Arc and the Southern Apennine Arc, with NE- and SW-convexity, respectively (Patacca & Scandone,

Volume n° 2 - from B16 to B33

1989). The Lazio-Abruzzi sector (Central Apennines) represents the zone of junction between the two arcs of the Central-Northern Apennines, and that of the Southern Apennines. This sector is bounded by two important tectonic features: the Olevano-Antrodoco line (Parotto & Praturlon, 1975), and the Ortona-Roccamonfina (Locardi, 1982), or Sangro-Volturno line (Ghisetti & Vezzani, 1997); the latter, has long been interpreted as a crustal decoupling zone (Locardi, 1982; Patacca et al., 1990).

In the central sector of the Apennine chain, folds and thrusts with salient geometry involve the Triassic-Miocene carbonate succession of the Adria continental margin and of the foreland and foredeep Neogene-Quaternary basins (Apennine Units s.s.). To the SE of the Sangro-Volturno line, the Molise Allochthonous Units, related to the Neogene-Quaternary closure of the Ionian Neotethys, overthrust the Apennine Units s.s.. In the westernmost zone (Tuscan-Lazio area), the Liguride and Sicilide Units overrode the Apennine Units. In the peri-Adriatic area, the frontal zone of the chain was buried and sealed by Quaternary deposits.

In the Umbro-Marche-Sabina and Lazio-Abruzzi sectors of the Apennine chain, there is an outcropping of the carbonate units related to the deformation of the Adria continental margin (articulated in carbonate platform and pelagic basins, and differentiated, starting from the Upper Triassic rifting process). There is also an outcropping of foredeep siliciclastic deposits, connected with the migration of the orogenic system, which is progressively more recent moving toward the Adriatic foreland.

The main tectono-stratigraphic units, cropping out east of the Quaternary volcanic deposits and the Pliocene-Quaternary deposits of the peri-Tyrrhenian area, are bounded by the Sibillini Mts-Antrodoco-Olevano thrust (Sabine Units), the Gran Sasso thrust (Lazio-Abruzzi Units) and the Morrone Mt. thrust, and by the Teramo and Maiella thrusts (external units of the Messinian and Pliocene foredeeps: Back cover figure).

The architecture of the paleomargin has also controlled the physiography of the Neogene foredeep basins, whose depocenters are located in correspondence with the pelagic palaeobasins.

The Pliocene thrusts located on the Marche-Abruzzi Apennine mountain front (Montagna dei Fiori-Gran Sasso-Morrone Mt., Maiella) accommodate a structural elevation at the top of the carbonate succession of ca. 10 km, an uplift consistent with an estimated amount of total translation of 30 km. Southward, these thrusts are joined to the NE-SW oriented Sangro-Volturno dextral transpressive oblique ramp. A similar kinematic behaviour is found along the Sibillini Mts-Antrodoco-Olevano thrust, that was controlled by the Ancona-Anzio (Auct.) Mesozoic fault.

In the axial zone of the central-northern Apennines, NW-SE trending normal faults, with Quaternary activity, are characterized by a SE-ward increase of displacement of up to 1000 m in the Abruzzi area. They are organized in fault systems with a maximum length of 30-35 km, that bound tectonic depressions (Fucino, Sulmona, Campo Imperatore"Gran Sasso" and L'Aquila intramontane basins), and are associated with an intense seismicity. At depth, these normal faults appear to reactivate pre-existing crustal thrust ramps, as suggested by the seismological data of the 1997 Colfiorito seismic sequence (Boncio et al., 2000; Calamita et al., 2000).

The main geological and structural features of three type sections of the central Apennines (Gran Sasso, Montagna dei Fiori, and the Sibillini Mts), are illustrated. This field trip aims to evaluate the role of the extensional architecture of the Mesozoic Adria passive margin in the subsequent tectonic evolution of the Apennine orogenic system, namely, of the physiography of the foredeep basins and of the structural setting of the fold-and-thrust belt.

The outer zone of the central Apennines

In the Umbria-Marche-Sabine and Lazio-Abruzzi Apennines, different tectonic stratigraphic units are present, and are related to the deformation of the Adria paleomargin. They are also related to arcuate thrust surfaces (salients), whose envelopment defines the central-northern Apennines arc (Back cover figure). The Sibillini Mts, Gran Sasso, and Morrone Mt. thrusts juxtapose the carbonate sequences to siliciclastic deposits of the Messinian-Pliocene foredeep basins, which extensively outcrop in the peri-Adriatic foothills zone (outer units of the Messinian and Pliocene foredeeps).

In general, the minor arcs coincide with the Mesozoic paleogeographic domains, that trend N-S and E-W (Back cover figure). The Sibillini Mts-Antrodoco-Olevano and the Gran Sasso thrusts, correspond to the platform-basin transition zones. These palaeogeographic features are preserved where they trend transverse to the main contractional structures.

Four main tectono-stratigraphic units are recognised:

a) Sabine Units;

b) Lazio-Abruzzi carbonate platform Units;

c) Outer Units of the Messinian and Pliocene

foredeeps;
d) Molise Units: "Allochthonous Ionian Neotethys".

Relationships between the architecture of the adria mesozoic paleomargin, and the geometry of the orogenic system

In the outer zone of the central Apennines, the depocenters of the Neogene foredeep basins (Back cover figure) are located onto Mesozoic-Tertiary pelagic basins of the Adria continental paleomargin, which developed during the rifting and drifting stages that preceded and accompanied the opening of the Ionian and Alpine Neotethys. These basins were flanked by structural highs, located onto pre-existing carbonate platforms. This complicated architecture, in turn, influenced the geometry of the evolving orogenic belt, with thrust ramps developing close to inherited extensional faults (Calamita et al., 2003a, b).

In particular, the depocenter of the Messinian Laga foredeep basin lies on top of the Mesozoic Umbria-Marche pelagic basin; similar relationships are observed further east for younger, Lower Pliocene basins. The northern paleomargin of the Lazio-Abruzzi and Apulian carbonate platforms correspond, respectively, to the areas of structural highs that bounded the depocenters to the south. This is documented by the onlap relationships and by the thickness and facies variations of the siliciclastic deposits, both transversally and longitudinally to the axial development of the depocenters (Maiella, Gran Sasso, Matese Mts).

The salient geometry of the Gran Sasso and the Sibillini Mts-Olevano-Antrodoco thrusts, mimic the paleogeographic architecture of the Mesozoic continental margin, displacing or inverting pre-existing normal faults (Back cover figure).

Field itinerary

First Day: Gran Sasso area (by car). One of the most spectacular examples of thrust fronts in the central Apennines of Italy is magnificently exposed in the Gran Sasso range. Excellent exposures of the Triassic-Miocene succession allows us to observe a wide variety of geological and structural features. In particular, the field trip will focus on:

a) the Gran Sasso thrust front and related folds (Camicia Mt.-Prena Mt., Corno Grande-Montagnone, and Pizzo Intermesoli-Corvo Mt.);

b) pre- and post-thrusting normal faults in the hanging-wall of the Gran Sasso Thrust (Campo Imperatore, Camicia Mt.).

The accommodation is planned in L'Aquila, a town of medieval origins, rich in monuments, and surrounded by spectacular mountains.

Second Day: Prena Mt.-Camicia Mt.-Campo Imperatore. The field trip comprises a ca. 5 hour walk along the southern part of the Gran Sasso thrust front and the Campo Imperatore basin, ranging from 800 to 1800 m in elevation above sea level. The trip will examine:

- The slope-basin Triassic-Miocene succession;
- The Campo Imperatore basin;
- Low-angle and high-angle normal faults (Camicia Mt., Campo Imperatore);
- The tectonic window at "Fornaca", i.e. one of the most spectacular contractional features of the Central Apennines;
- The Prena Mt. thrust.

Accommodation will be in Ascoli Piceno, a small medieval town, located in the southern part of the Marche region, with a well-preserved and picturesque historic center.

Third Day: The Montagna dei Fiori and the Sibillini Mts. Surrounded by siliciclastics of the Messinian Laga Basin, the Montagna dei Fiori thrust-related anticline represents one of the most peculiar structural features of the outer zone of the Central Apennines. The backlimb of the anticline is truncated by a steeply W-dipping normal fault. Excellent exposures along a deep canyon, allow us to observe a complete Mesozoic-Miocene succession, affected by both contractional and extensional deformations. In the first part, the excursion will examine:

-The normal fault in the backlimb of the Montagna dei Fiori anticline (kinematics and relative chronology with thrusting);
-Jurassic normal faults in the core of the Montagna dei Fiori anticline;
-Geometry and kinematics of the Montagna dei Fiori anticline;
-The front of the Montagna dei Fiori thrust.

During the transfer from the Montagna dei Fiori to the Sibillini Mts, the main geological characteristics of the Messinian synorogenic deposits (Laga Fm.), will be examined.

The second part of the field trip will examine the

Volume n° 2 - from B16 to B33

front of the Umbria-Marche Range. A section across the steep gorge of the Fiastrone Valley will make it possible to investigate:
- The geometry and kinematics of the Sibillini Mts thrust front;
- The relationships between Jurassic normal faults and Neogene thrust structures (short-cut geometries);
- Cretaceous-Miocene reactivation of Jurassic normal faults.

Accommodation is planned in Foligno (Perugia). The following day, in the morning, during the transfer to Florence, a tourist visit to Assisi can be organized upon request.

The Gran Sasso salient

The Gran Sasso salient represents the northern mountain front of the Abruzzi Apennines, where the Triassic-Miocene successions of the Lazio-Abruzzi platform and related transition domains are thrust onto the outer units of the Messinian foredeep (Laga Unit: Back cover figure and Figure 1.1).
This salient accommodates a high structural elevation, documented by the occurrence of Triassic successions at ca. 3000 meters a.s.l.. It trends E-W to the north and N-S in the southern sector (Cappucciata Mt.); this thrust juxtaposes the carbonate sequence on the Messinian siliciclastic deposits of the Laga Formation, and the N-S trending structure of the Montagna dei Fiori - Montagnone.
The E-W trending segment of the salient consists of en echelon, overturned anticlines and related thrusts with sinistral transpressional kinematics (Back cover figure and Figure 1.1). A significant thrust displacement, outlined by fault-bounded horses and by the tectonic superposition of Triassic Dolomites onto Jurassic pelagics, to the east, gradually decreases westwards to a tip line at Corvo Mt. (Back cover figure and Figure 1.1). A conservative estimate, constrained by data from the Gran Sasso tunnel, suggest an amount of ca. 6 km of orogenic contraction for the salient (Calamita et al., 2002).
The uppermost thrust surface is antiformally folded, presumably by the growth of a thrust-related anticline in its footwall, a pattern suggestive of a simple piggy-back thrusting sequence in Late Messinian-Early Pliocene times.
Spectacular SW-dipping normal faults, with a maximum displacement of ca. 2500 m, occur in the hangingwall of the Gran Sasso Salient; Calamita et al. (2002, and references therein) recognized:
- Pre-thrusting faults that were rotated during subsequent folding (the Camicia Mt. fault) or that were reactivated during Quaternary time (the Corvo Mt. - Corno Grande fault);
- Faults with mainly Quaternary activity, related to the development of the intermontane basins (Campo Imperatore and Assergi faults).

The Gran Sasso Salient mimics the architecture of the Mesozoic palaeomargin (Back cover figure); the inferred eastward increase in displacement is consistent with paleomagnetic data, that indicate an anticlockwise rotation to the east.
Further east, the Gran Sasso Salient has a N-S trend, parallel to the axial trend of the Cappucciata Mt. anticline, and joins with the Morrone Mt. thrust. These structures represent the carbonate mountain front of the Abruzzi Apennines.
The Gran Sasso–Morrone Mt. thrusts, together with the thrusts related to the Laga and Maiella Units, accommodate a structural elevation of ca. 10 km, which has been estimated using the top of the carbonate succession at a 4000 m elevation in the Gran Sasso Salient, and documented at a depth of about 6000 m in the peri-Adriatic area (Pescara); towards the south, they are joined to the Sangro-Volturno dextral transpressive oblique ramp.

DAY 1

Itinerary by car

The outcropping sequence comprises (Figs 1.1 and 1.2): a) the Upper Trias-Lower Lias *Dolomia Principale* and *Calcare Massiccio* (Corno Grande-Prena Mt. Carbonatic platform succession), coeval to the Upper Triassic *Dolomie Bituminose* and *Dolomie di Vradda,* and to the Lower Lias palaeo-basin succession, here represented by the *Calcari Maculati* and by the *Strati Ammonitici di Vradda* (Vallone di Vradda); b) micritic limestones, calcarenites, and calcirudites with cherts, and marly limestones of the Middle Liassic-Messinian pelagic-hemipelagic sequence (*Corniola-Verde Ammonitico-Calcari bioclastici inferiori* [or *Calcareniti ad Entrochi*]-*Maiolica-Calcari bioclastici superiori* [or *Calciruditi a Rudiste*]-*Scaglia rossa* e *cinerea*-Miocene calcarenites); c) siliciclastic foredeep deposits of the *Laga Fm.* (Messinian); d) thrust-top basin deposits (*Conglomerati di M. Coppe*: Messinian?-Early Pliocene; *Conglomerati di Rigopiano*: Lower Pliocene); and e) Quaternary fluvial-lacustrine deposits (Adamoli *et al.*, 1978; 1990; Bigozzi *et al.*, 1991; Vezzani *et al.*, 1993).

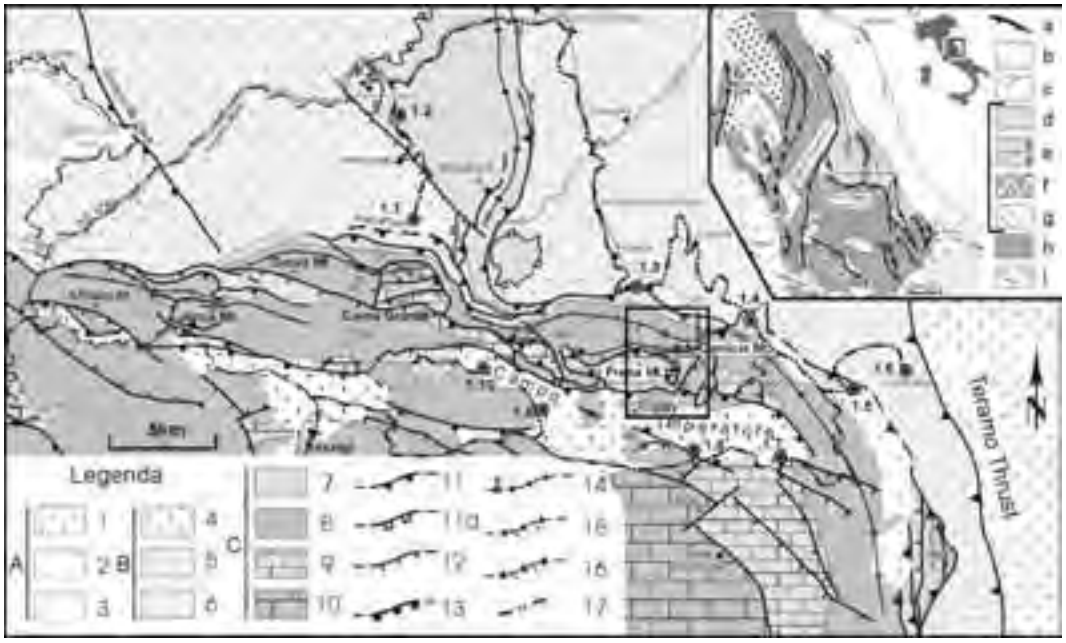

Figure 1.1 - Structural sketch of the Gran Sasso area. The car itinerary from Prati di Tivo to Campo Imperatore is also shown; d) area of the walking itinerary. A) Deposits unconformably overlying the carbonate succession: 1) Continental deposits (Quaternary); 2) Conglomerati di Rigopiano (Lower Pliocene); 3) Conglomerati di M. Coppe (Messinian?-Lower Pliocene); B) Siliciclastic foredeep deposits: 4) Formazione Cellino (Lower Pliocene); 5) Laga Fm. - evaporitic and post-evaporitic members, Marne del Vomano (Messinian- Lower Pliocene); 6)Laga Fm., pre-evaporitic member (Messinian); C) Carbonatic Succession: 7) Hemipelagic and carbonatic ramp deposits (Miocene p.p.); 8) Slope-basin carbonatic succession (Middle Lias-Oligocene); 9) Carbonatic platform succession (Trias-Lower Lias); 10) Carbonatic platform succession (Trias - Cretaceous); 11) Thrust fault; 11a) Laga detachment; 12) Normal fault; 13) Normal fault with dominant Quaternary activity; 14) Anticline - a) periclinal termination; 15) Overturned anticline; 16) Overturned syncline; 17) Itinerary and location of the stops (1.1 – 1.10). PCe: Pizzo Cefalone; PI: Pizzo Intermesoli; CP: Corno Piccolo; MBr: Brancastello Mt.; MC: Coppe Mt.; MS: Siella Mt.; CM: Colle Madonna; PS: Pietra della Spia (Dente del Lupo); MBo: Bolza Mt.. The inset shows the tectonic sketch of the outer zones of the central Apennines: a) Thrust; b) Middle/Upper Pliocene-Pleistocene deposits; c) Quaternary Volcanoclastic deposits; d)Lower Pliocene deposits; e) Messinian siliciclastic deposits pre- (y) and post- (x) evaporitic; f) Tortonian-Messinian siliciclastic deposits; g)Burdigalian-Tortonian siliciclastic deposits; h) Triassic-Miocene carbonate succession; i) Allocthonous Molise unit.

Description of the itinerary

The itinerary passes from Prati di Tivo to Campo Imperatore, and illustrates the structural-geological features of the Gran Sasso front and of its hanging-wall, offset by Quaternary normal faults (Calamita et al., 2003c).

Stop 1.1:

Prati di Tivo 1450 m: Panoramic view of the Gran Sasso "front".

Here we can see the western part of the overturned fold in the hanging-wall of the Gran Sasso thrust (Pizzo d'Intermesoli), that affects the carbonatic succession, and consists of: *Calcari bioclastici inferiori-Marne con cerrogna*. The outcrops of the *Laga Fm.* (Corvo Mt.), stratigraphically overlying the *Marne a Pteropodi Fm*., are outlined by the woods (Figure 1.3).

A thrust surface propagates across the overturned limb of the fold, and this latter roots westwards where it is replaced by the adjacent, en echelon Jenca Mt. anticline.

This stop also affords the front view of the Corno Grande-Corno Piccolo. The cliffs in the background are made up of the Calcare Massiccio of the eastern peak of Corno Grande. The cliffs in the foreground (northern flank of Corno Piccolo), are made of *Calcari bioclastici inferiori,* arranged in N-dipping amalgamated strata. The underlying limestones

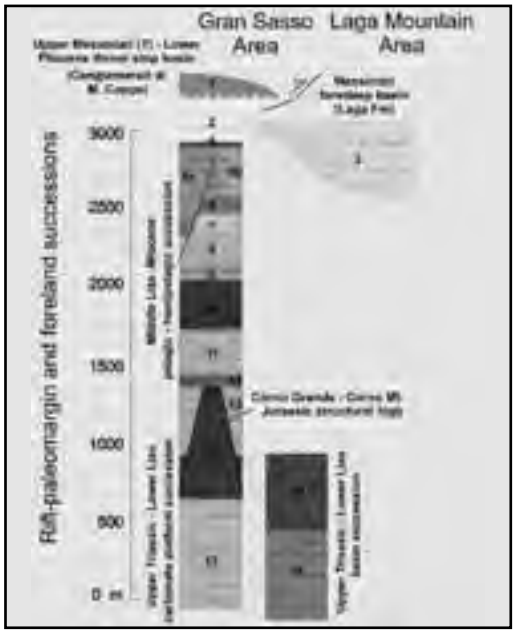

Figure 1.2 - Stratigraphic section of the Gran Sasso and Laga Mountain Area. The thickness of the thrust stop and foredeep basins are not to scale. 1) Conglomerati di M. Coppe; 2) Laga Fm. (Messinian): pre-evaporitic member - pelitic-arenaceous lithosome; 3) Laga Fm. (Messinian): pre-evaporitic member - arenaceous-pelitic and arenaceous lithosome; 4) Marne ad Orbulina ; 5) Marne con cerrogna e Bisciaro (5a) e Calcareniti di M. Fiore (5b); 6) Calcari glauconitici; 7) Scaglia cinerea; 8) Scaglia rossa; 9) Calcari bioclastici superiori; 10) Maiolica; 11) Calcari bioclastici inferiori; 12) Verde Ammonitico; 13) Corniola; 14) Calcari nodulari; 15) Calcare Massiccio; 16) Calcari Dolomitici (Calcari Maculati and Strati Ammonitici di Vradda); 17) Dolomia Principale; 18) Dolomie Bituminose and Dolomie di Vradda.

belong to the overturned *Scaglia rossa-Marne con cerrogna* succession in the thrust footwall.
In the vicinity of the Gran Sasso, the base of the *Laga Fm.* consists of a pelitic-arenaceous lithosome, that grades northwards (Laga Mts) into a more arenaceous facies, reflecting the articulated physiography of the Messinian foredeep basin (see next stop).

Stop 1.2:

Onlap of the Laga Fm. onto the Marne a Pteropodi Fm.

The arenaceous strata of the *Laga Fm.* (La) are in an *onlap* relationship onto the *Marne a Pteropodi Fm.* This relationship was achieved at a foreland ramp during Messinian time, that subsequently evolved into the western limb of the Montagna dei Fiori-Montagnone anticline (Figure 1.4).

The strata of the *Marne con cerrogna* in the Vomano Valley are affected by mesoscopic folds and reverse faults, characteristic of the *Laga Detachment* (Koopman, 1983).

Stop 1.3:

Valico di Santa Maria a Pagliara: Panoramic view of the Corno Grande-Cima Alta.

The Gran Sasso, and the underlying N-S trending Montagnone anticline, are both well exposed (Figure 1.5). The Corno Grande-Corno Piccolo anticline affects the *Dolomia Principale* (DP), the *Calcare Massiccio* "CM" (Corno Grande), the *Corniola - Verde Ammonitico* "CV" (Sella dei due Corni), the *Calcari bioclastici inferiori* (Cbi), and the base of the *Maiolica* "Ma" (Corno Piccolo).
The Corno Grande-Corno Piccolo succession is thrust, along a WSW-dipping thrust, onto Mesozoic-Tertiary limestones and Miocene foredeep siliciclastics (*Corniola-Marne con cerrogna* "Co-Mc"

Figure 1.3 - Panoramic view of the overturned Pizzo Intermesoli – Corvo Mt. anticline (westernmost sector of the E-W trending Gran Sasso salient). Cbi: Calcari bioclastici inferiori; Ma: Maiolica; Cbs:

Figure 1.4 - Valle del Vomano: Laga Fm. (La) in onlap onto the Marne a Pteropodi (MP), overlying the Marne con cerrogna (Mc). The village of Poggiombricchio is built onto the arenaceous beds of the Laga Fm.

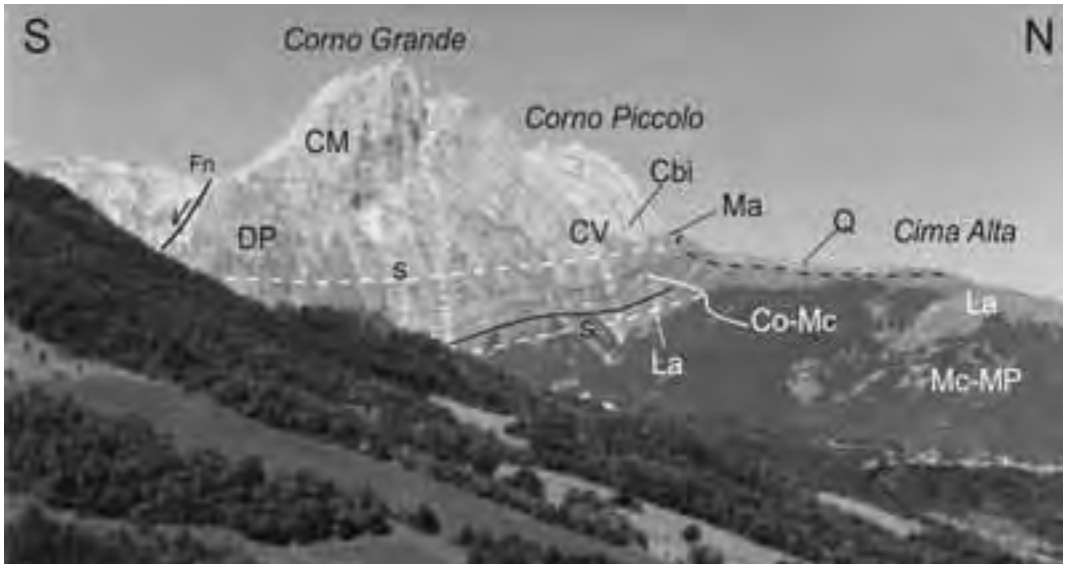

Figure 1.5 - Valico di Santa Maria a Pagliara. Panoramic view of the Corno Grande-Corno Piccolo-Cima Alta group. The frontal Gran Sasso anticline (that affects the Dolomia Principale "DP", Calcare Massiccio "CM", Corniola-Verde Ammonitico "CV", Calcari bioclastici inferiori "Cbi", and the Maiolica "Ma"), the normal fault (Fn) and the two main thrust surfaces (s) are well exposed. These bound the intermediate tectonic wedge (represented by the overturned pelagic sequence Corniola-Verde Ammonitico-Calcari bioclastici inferiori-Maiolica-Calcari bioclastici superiori-Scaglia rossa-Scaglia Cinerea-Marne con cerrogna "Co-Mc", and by the Laga Fm "La"). The footwall of the Gran Sasso thrust exposes the Marne con cerrogna (Mc), the Marne a Pteropodi (MP) and the Laga Fm. Q: Quaternary breccia.

Volume n° 2 - from B16 to B33

- *Laga Fm* "La"). The intermediate tectonic wedge is bounded downwards by another thrust, along which it overrides the *Laga Fm -Marne con cerrogna-Marne a Pteropodi* (Mc-MP) sequence.

cliff exposes the thrust surface (Figure 1.6). The dip of this fault increases northwards, where it defines an antiformal structure that also affects the uppermost tectonic unit, comprising: *Corniola* "Co", *Verde Ammonitico* "Va", *Calcari bioclastici inferiori* "Cbi",

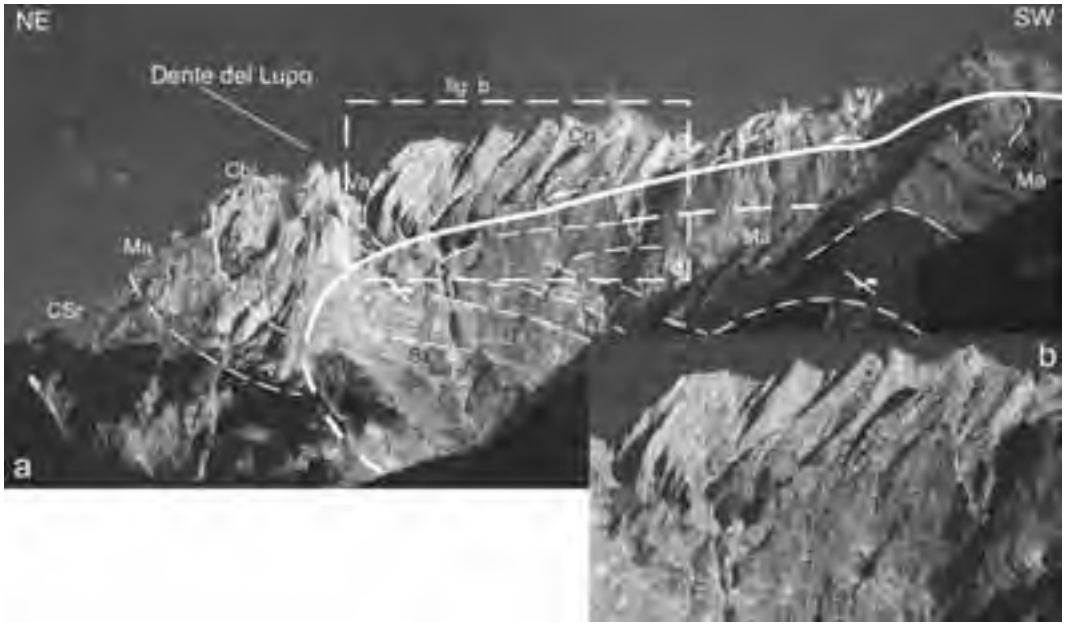

Figure 1.6 - a) Panoramic view of the northern flank of Camicia Mt. "Dente del Lupo": the uppermost Gran Sasso thrust surface (s) is antiformally folded. The Corniola (Co), Verde Ammonitico (Va), Calcari bioclastici inferiori (Cbi), Maiolica (Ma), and Calcari bioclastici superiori-Scaglia rossa (CSr), are exposed in the thrust hanging-wall. The intermediate thrust bounded horse, that affects the intensely folded Maiolica (Ma)-Scaglia rossa (Sr) succession, is also well exposed. b) Detail of Figure 1.6 a.

The Corno Grande corresponds to a Jurassic structural high, outlined by the occurrence of condensed successions (dolomitized Corniola) and by Jurassic-Cretaceous neptunian dykes (Figure 1.2). The normal faults are truncated by a thrust fault, whose upward propagation trajectory defines a short-cut geometry. This thrust is accompanied by the development of an overturned fold within the pelagic succession (Front page figure).

The structural setting of the Gran Sasso is defined by two main superposed tectonic units (the upper Corno Grande-Prena Mt. Unit, and the lower Laga Unit), separated by an intervening tectonic wedge (Prati di Tivo-Santa Colomba Unit). The two main thrusts root towards the west, whereas they become progressively spectacular eastwards.

Looking eastwards from the saddle, the spectacular northern cliff of the Monte Camicia "Dente del Lupo"

Maiolica "Ma", *Calcari bioclastici superiori*, *and Scaglia rossa* "CSr"; the thrust cut-off angle of strata of the uppermost tectonic unit is maintained.

Folds developed within the intermediate, thrust-bounded horse are close and asymmetrical, with sub-horizontal axial surfaces. It seems likely that the uppermost and lowermost thrust surfaces merge within one single tectonic surface, and hence that the thrust-bounded horse terminates eastwards.

Proceeding along the track the junction to Castelli, a village famous for its hand crafted pottery, is reached.

Stop 1.4:

Conglomerati di M. Coppe.

The Miocene *Calcareniti di Monte Fiore*, arranged in thin beds with basal ripple marks, are well

exposed (Figure 1.7). This formation, affected by a spectacular, NW-SE trending mesoscopic fold, is unconformably overlain by the Messinian?-Lower Pliocene *Conglomerati di Monte Coppe*. It is a satellite basin conglomerate, deposited onto consist of mainly carbonatic sub-rounded clasts with subordinate chert, derived from the reworked substratum, and immersed in a calcarenitic matrix.

Figure 1.7 - Angular unconformity between the Conglomerati di M. Coppe (C.MC) and the underlying, intensely-folded Calcareniti di M. Fiore (C.MF).

the already deformed Gran Sasso unit, and in turn affected by further folding and thrusting.

This conglomerate makes it possible to refer the onset of contractional deformation to Late Messinian time. Its clasts are partly sourced by extrabasinal successions of the Liguride Units.

Stop 1.5:

Conglomerati di Rigopiano.

The *Conglomerati di Rigopiano* unconformably overlie the Gran Sasso carbonatic units, and represent the fill of thrust-top basins carried piggy-back onto the siliciclastic deposits of the Laga unit. Similarly to the *Conglomerati di Monte Coppe*, these deposits make it possible to refer the final contractional stage of this part of the Apennine belt to Middle-Upper Pliocene time.

Proceeding for 100 m along the road toward Rigopiano, the *Conglomerati di Rigopiano* are well exposed in locally amalgamated strata. They

Stop 1.6:

Geological Observatory of Farindola.

The Geological Observatory of Farindola, in cooperation with the Department of Earth Sciences of the University "G. D'Annunzio" of Chieti and Pescara, is a seat for teaching, for cultural training, and for scientific documentation and research in the fields of geology, geomorphology and hydrogeology of the area of the Gran Sasso and Laga Mts National Park.

Stop 1.7:

Panoramic view of the Prena Mt. - Camicia Mt. - Tremoggia Mt. - Siella Mt. - San Vito Mt. Group.

The Campo Imperatore tectonic basin is bounded by a system of low-angle and high-angle, S-dipping normal faults. The stratigraphic sequence of the normal fault footwall comprises: the *Dolomia Principale* (DP: Prena Mt.), the *Dolomie Bituminose* "DB", the *Dolomie di Vradda*, the *Calcari Maculati*, the *Calcari ammonitici di Vradda* "DV" and the *Corniola* "Co"

Volume n° 2 - from B16 to B33

(Vallone di Vradda-Tremoggia Mt.); this succession is traced eastwards to Siella Mt. (Figure 1.8).
The stratigraphic succession of the normal fault hanging-wall comprises: the *Corniola* (Co), the *Calcari bioclastici inferiori-Maiolica-Calcari bioclastici superiori* (CbM), and the *Scaglia/ Cretaceous clastic limestones* "CCc" (Camicia Mt. and Colle dell'Omo Morto "COM").
The fluvial-lacustrine deposits, that represent the infill of the tectono-karst Campo Imperatore depression, extensively outcrop in front of the Rifugio San Francesco (San Francesco Refuge).

Stop 1.8:

Panoramic view of the Camicia Mt.- Prena Mt.- Corno Grande group.

The S-dipping normal fault system is well exposed. In particular, the *Dolomia Principale* di M. Prena "DP", that grades laterally into the *Dolomie Bituminose* "DB", and into the *Calcari dolomitici di Vradda,* outcrops extensively. The outcropping stratigraphic sequence of the normal fault hanging-wall consists of *Corniola* "Co"-*Scaglia rossa*/*Cretaceous clastic limestones* of Camicia Mt. "CCc" (Figure 1.9). In particular, the contact produced by a low-angle normal fault (Fn) to the base of the cliffs, among the *Corniola* "Co" and the *Dolomie Bituminose* "DB" (i.e. the white cataclastic belt to the base of the cliffs), can be observed (Figure 1.10).
The hills at the foot of Prena Mt. and Camicia Mt. (Faeto Mt. and Colle Dell'Omo Morto), consisting of the Jurassic-Cretaceous succession, belong to the hanging-wall of the normal fault system. The faults at the base of these hills offset well-developed Late Quaternary conoids, well developed to the edges of the Campo Imperatore depression.

The deep gorge between Prena Mt. and Camicia Mt. exposes the uppermost Gran Sasso thrust surface that bounds, in map view, the Fornaca tectonic window. The thrust surface separates the *Dolomie Bituminose*, in the hanging-wall, from the Jurassic

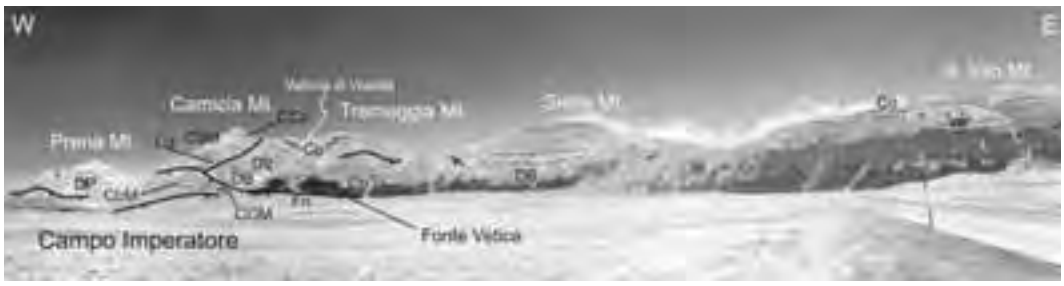

Figure 1.8 - Prena Mt.- San Vito Mt. group, observed from the Rifugio S. Francesco. The E-W trending, S-dipping normal fault system (Fn) is recognised. Normal faults juxtapose the Corniola "Co", Calcari bioclastici inferiori-Maiolica-Calcari bioclastici superiori "CbM", Scaglia/Cretaceous clastic limestones "CCc" (Camicia Mt. and Colle dell'Omo Morto "COM") in the hanging-wall, to the Dolomia Principale "DP", Dolomie Bituminose "DB", Dolomie di Vradda, Calcari Maculati, Calcari Ammonitici di Vradda "DV," and to the Corniola (Vallone di Vradda). Channel fill within the Corniola "cc".

Figure 1.9 - Panoramic view of the Corno Grande- Camicia Mt. group. The main recognized features are the Fornaca tectonic window, the low-angle Camicia Mt. normal fault (Fn) , and the high-angle normal faults that bound the Campo Imperatore depression (F). DP: Dolomia principale; CCc: Scaglia/Cretaceous clastic limestones; DB: Dolomie Bituminose; Co: Corniola; Va-Cbi: Verde Ammonitico-Calcari bioclastici inferiori; Cbs: Calcari bioclastici superiori.

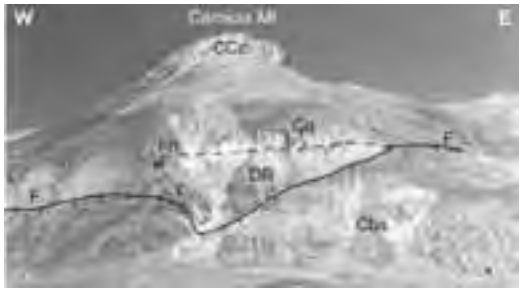

Figure 1.10 - Detail showing the Camicia Mt. low-angle normal fault (Fn), and the Campo Imperatore high-angle normal faults (F). DB: Dolomie Bituminose; Co: Corniola; Cbs: Calcari bioclastici superiori; CCc: Scaglia/ Cretaceous clastic limestones.

Verde Ammonitico "Va", and the *Calcari bioclastici inferiori "Cbi"* of the thrust-bounded horse, in the footwall.

a white cataclastic belt, and located in the northern edge of the depression.

Looking eastwards, the low-angle Camicia Mt. normal fault separates the Jurassic-Cretaceous succession (Corniola- Cretaceous clastic limestones: C-C) in the hanging-wall, from the Dolomie Bituminose, Dolomie di Vradda, Calcari Maculati *and* Corniola *(D-C),* in the footwall.

Stop 1.10:

Western termination of the Campo Imperatore plateau.

From here it is possible to observe the southeastern flank of Corno Grande, where the *Dolomia Principale* "DP", and the *Calcare Massiccio* (CM) crop out extensively; the latter formation is well exposed, and is ca. 600 m thick (Figure 1.12).

Similar to the Triassic succession (Carbonatic platform of Corno Grande-Prena Mt./Vradda Basin),

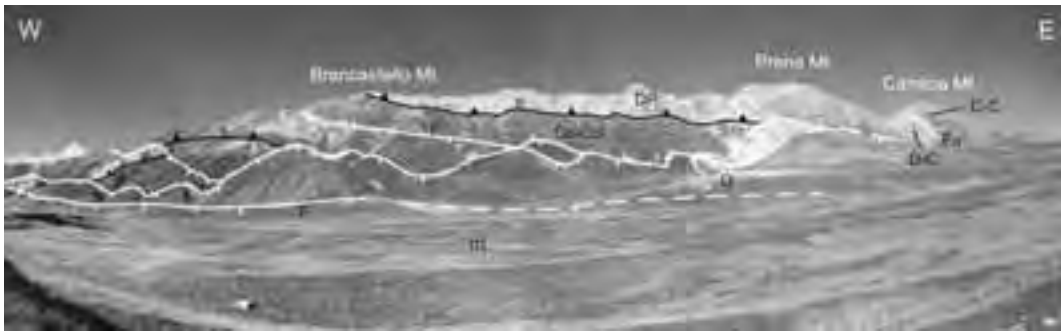

Figure 1.11 - The western flank of the Brancastello Mt.-Prena Mt. group. The uppermost thrust surface (s) is downthrown southwards by the Campo Imperatore boundary faults "F". DP: Dolomia Principale; Co-Cbi: Corniola-Calcari bioclastici inferiori. The low-angle Camicia Mt. normal fault "Fn" is seen to the east. C-C: Jurassic-Cretaceous succession (Corniola, Cretaceous clastic limestones); D-C: Dolomie Bituminose, Dolomie di Vradda, Calcari Maculati, Corniola; m: reworked morrains; Q: Quaternary alluvial conoids.

The main geological-structural features, seen here in panoramic view, will be examined in detail tomorrow.

Stop 1.9:

Panoramic view of the western flank of Prena Mt.-Brancastello Mt..

This panoramic view shows the uppermost thrust surface that separates the *Dolomia Principale*, in the hanging-wall, from the Jurassic succession (*Corniola-Calcari bioclastici inferiori*), in the footwall (Figure 1.11). The surface appears downthrown southwards by the normal fault system. The southernmost fault is the Campo Imperatore boundary fault, outlined by

Figure 1.12 - Panoramic view of Corno Grande. In the normal boundary, Campo Imperatore fault (F) is seen in the foreground. CM: Calcare Massiccio; DP: Dolomia Principale; cb: white cataclastic belt that mimics a pseudo-badland morphology.

the Lower Liassic formations also exhibit remarkable thickness and facies variations. These are represented by the Calcare Massiccio of Corno Grande (ca. 600 m), and by the *Calcari Dolomitici* of Camicia Mt. (ca. 200 m) end-members. Thus, the Triassic deposition basin defined by the *Dolomie Bituminose*, corresponds to the Lower Liassic basin (Figure 1.2).
This stop illustrates the western termination of the Campo Imperatore plateau near Aquila Mt.. Here, too, the normal boundary fault is outlined by a white cataclastic belt "cb", whose weak lithology is reflected by a pseudo-badland morphology. This fault separates the Miocene Calcarenites, outcropping along the road to the Hotel Campo Imperatore, and the Calcare Massiccio of Vado di Corno, inferred from sub-surface data (boreholes and Gran Sasso tunnel excavation: Ghisetti & Vezzani, 1990).
From here the itinerary proceeds to L'Aquila.

DAY 2

Hike itinerary
***(with a contribution by L. Adamoli),* from Campo Imperatore (Miniera di Lignite) to the Prena Mountain.**

It begins in Campo Imperatore, ca. 200 m before the Miniera di Lignite, and follows the n. 7 and 7a CAI tracks, up to the summit of Prena Mt., with a 816 m elevation difference (Figs 2.1 and 2.2). The complete hike itinerary, and return along the same track, can be achieved in ca. 5 hours, excluding the stops (Adamoli et al., 2003).

Stop 2.1:

Starting at Fornaca (1745 m a.s.l.)
From here it is possible to see the Campo Imperatore depression in panoramic view, especially the wide, active alluvial fan at Fornaca, and the southern flank of the Camicia Mt.. Proceeding towards the next stop, the normal fault that separates the "*Calcari bioclastici inferiori-Scaglia*" succession from the "*Dolomie Bituminose-Dolomia Principale*" succession, can be observed. This structure accommodates over 1000 m of displacement (Figure 2.3). Following the track n. 7, one reaches 1965 m elevation in ca. 40 minutes.

Stop 2.2:

1965 m elevation a.s.l.
Upper Triassic *Dolomie Bituminose,* with dolomite olistholites derived from the palaeoplatform (Figs 1.2 and 2.4). Looking westward, the Upper Triassic *Dolomia Principale*, cropping out along the southern flank of Prena Mt., grades laterally into the *Dolomie Bituminose* of Fornaca. Thus, this stop allows us to observe clearly the original relationships between the Palaeoplatform and the Euxinic Palaeobasin (Bigozzi *et al.*, 1991). These formations belong to the Corno Grande-Prena Mt. Tectonic Unit, that overrides, along the uppermost thrust, the thrust-bounded horse. The latter here comprises the *"Verde Ammonitico-Calcari bioclastici inferiori"* succession exposed in the Fornaca tectonic window (Figure 2.5). The base of the *Calcari bioclastici inferiori* consists of brownish finely-bedded micrites.
Ca. 20 minutes are needed to reach the upper part of the Fosso Fornaca (2015 m a.s.l.).

Stop 2.3:

Fosso Fornaca (2015 m elevation a.s.l.).
The uppermost thrust surface that separates the *Dolomie Bituminose* from the Upper Liassic micrites (*Calcari bioclastici inferiori*), belonging to the intermediate thrust-bounded horse (Prati di Tivo – S. Colomba Unit), is well exposed (Figure 2.6).
From here it is also possible to see a NW-SE trending normal fault and its escarpment, that separates Triassic dolomites from Upper Liassic micrites, with a ca. 100 m throw (Figure 2.5).
At higher elevations, along the Coste di Sferruccio, it is possible to see (Figure 2.7), in succession with the *Dolomie Bituminose*, the Upper Triassic *Dolomie di Vradda,* and the overlying, Lower Liassic *Calcari Maculati*.
Proceeding for ca. 45 minutes along the track to Vado Ferruccio (2233 m a.s.l.), it is possible to see in detail the thrust surface that separates the pervasively-foliated *Dolomie Bituminose* from the *Calcari bioclastici inferiori* (Figure 2.8).

Stop 2.4:

Vado di Ferruccio
At Vado Ferruccio, it is possible to see an impressive panoramic overview of the Gran Sasso, Laga Mts, Montagnone, and Montagna dei Fiori. The uppermost thrust surface separates the *Dolomia Principale,* in the hanging-wall, from the intensely folded and overturned *Calcari bioclastici inferiori-Maiolica* succession, in the footwall (Figure 2.9). Looking eastwards, the low-angle Camicia Mt. normal fault can be seen. Its hanging-wall consists of the Jurassic-Cretaceous succession, whereas the *Dolomie Bituminose*, *Dolomie di Vradda*, *Calcari Maculati*

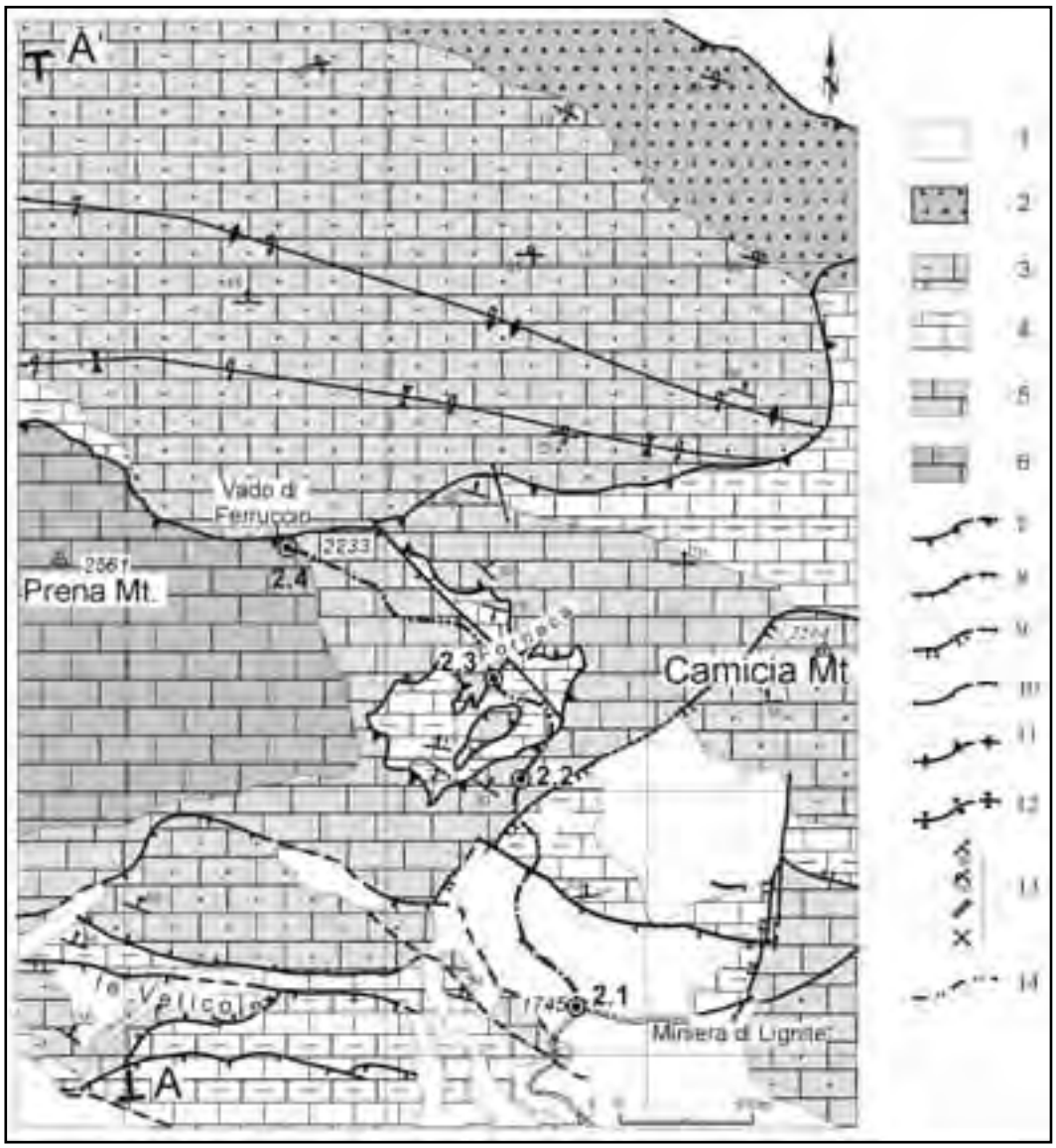

Figure 2.1 - Geological-structural sketch of the Prena Mt.- Camicia Mt. area. The location of the area is shown in Figure 1.1. 1)Quaternary deposit; 2)Calcareniti glauconitiche-Marne con cerrogna (Lower-Upper p.p. Miocene;3)Maiolica-Scaglia Cinerea (Lower p.p. Cretaceous- Middle Eocene); 4) Corniola-Calcari bioclastici inferiori (Middle Lias – Malm); 5)Dolomie Bituminose – Calcari dolomitici (Upper Trias – Lower Lias); 6) Dolomia Principale (Upper Trias); 7) Thrust; 8) Normal fault; 9) Low-angle normal fault; 10) Fault; 11) Anticline; 12) Syncline; 13) Bedding; 14) Itinerary and location of the stops (2.1 – 2.4); A-A': trace of geological section across Prena Mt. (Figure 2.2).

and overlying *Corniola,* are exposed in the footwall (Figure 2.10).

DAY 3

The Montagna dei Fiori and the Sibillini Mts

Montagna dei Fiori

Surrounded by siliciclastics of the Messinian Laga Basin, the Montagna dei Fiori thrust-related anticline is one of the most peculiar structural features of the Laga Unit. This unit represents the common footwall

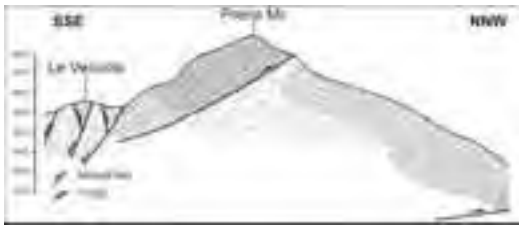

Fig 2.2 - Geological section across Prena Mt.. Symbols as in Figure 2.1. Trace A-A' in Figure 2.1.

of both Gran Sasso and Monti Sibillini Units (Calamita et al., 1998). The stratigraphic succession, affected by anticlinal folding, comprises the Liassic-Miocene carbonaties and overlying Messinian deposits of the Laga Fm (Figs 3.1, 3.2, and Back cover).
The anticline forelimb is overturned and truncated by a thrust surface, whereas the backlimb is truncated by a steeply W-dipping normal fault. An important decollement horizon, indicated as Laga Detachment, affects the pelitic Marne con cerrogna-Scaglia Cinerea succession.
Excellent exposures along a deep canyon allow us to observe the complete Triassic-Miocene succession affected by both contractional and extensional deformations.

Stop 3.1:

The normal fault in the backlimb of the Montagna dei Fiori anticline (kinematics and relative chronology with thrusting).

The normal fault can be traced in outcrop for over 15 km, along the axial culmination of the thrust-related anticline. It separates the Mesozoic-Paleogene succession (Calcare Massiccio-Scaglia) from the Miocene Marne con cerrogna, with a maximum displacement of ca. 1000 m (Figs 3.1 and 3.2).
Here the structure separates the Middle Liassic Corniola from the Miocene Marne con cerrogna (Figure 3.3). The fault trends NW-SE, and dips 70°-80° towards SW. The Marne con cerrogna show an intense shearing (S-C) fabric, with calcite shear veins

Figure 2.3 - Normal fault (Fn) to the foot of the southern flank of Prena Mt., separating the "Calcari bioclastici inferiori-Scaglia (Cbi-S)" succession from the "Dolomie Bituminose (DB)-Dolomia Principale (DP)" succession.

Figure 2.4 - Olistholites of Dolomia Principale (DP) within the Dolomie Bituminose (DB).

and a pervasive cleavage. The inferred kinematics is transtensional, with both dip-slip and left oblique components.
The remarkable thickness and facies variations within the Tortonian-Burdigalian Marne con cerrogna Fm., in the fault hanging-wall and footwall, outlines that this structure was mainly active during Miocene times, when it accommodated a displacement of ca. 1000 m (Figure 3.4).

Stop 3.2:

Normal fault in the western flank of the Montagna dei Fiori.

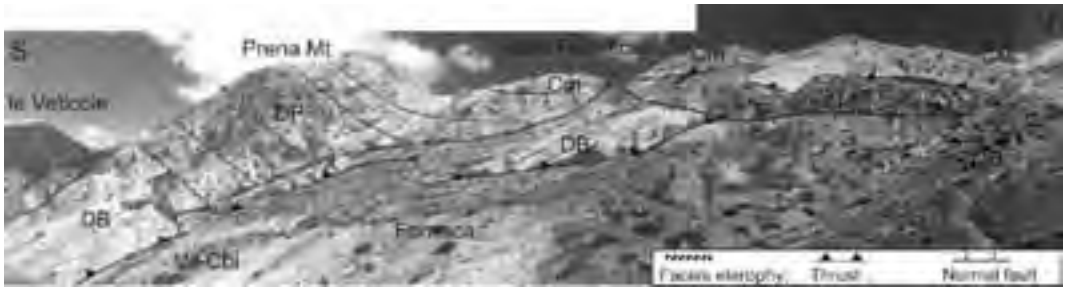

Figure 2.5 - The Fornaca tectonic window. The Dolomie Bituminose (DB), the Dolomia Principale (DP; lateral to the Dolomie Bituminose), and the Calcari Maculati (Cm), are exposed in the thrust hanging-wall. The "Verde Ammonitico-Calcari bioclastici inferiori (Va-Cbi)" succession belongs to the intermediate thrust-bounded horse, and is exposed in the tectonic window.

This stop illustrates another part of the Montagna dei Fiori normal fault. The fault trends N170°E, dips

Figure 2.6 - Detail of the uppermost thrust surface (ss) in the Fornaca tectonic window. The thrust separates the Dolomie Bituminose (DB) from the Calcari bioclastici inferiori (Cbi).

Figure 2.7 - The Upper Triassic-Lower Liassic basin succession outcropping between Vado di Ferruccio and Camicia Mt.. DB: Dolomie Bituminose; Cm: Calcari Maculati.

70° westwards, and juxtaposes the Jurassic Calcare Massiccio-Calcari Nodulari succession (deposited within a Jurassic seamount) with the Cretaceous-Eocene Scaglia Rossa Fm. The latter represents a tectonic sliver between the fault footwall, and its hanging-wall, where the Marne con cerrogna Fm. crops out (Figs 3.1, 3.5 and 3.6). The Scaglia Rossa Fm. is affected by a pervasive cleavage, that is sub-parallel to the fault surface. The cleavage domains, and the fault surface itself, are both overprinted and offset by mesoscopic conjugate reverse faults, that dip 5°-25° toward WNW and 60°-70° towards ESE, respectively. A system of tension veins, that dips 50° toward ESE, is preserved within the Jurassic formations. This system is presumably related to the buttressing of the Miocene normal fault on the subsequent development of the Laga Detachment zone (Figure 3.7).

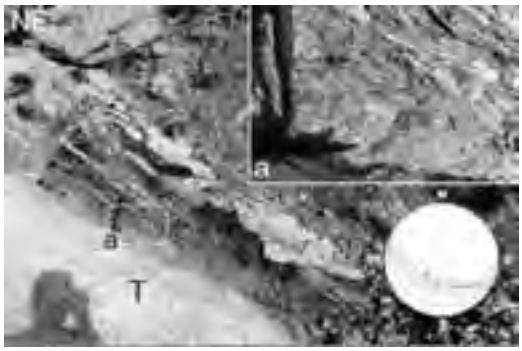

Figure 2.8 - Shear zone, related to upper thrust plane cropping out at the Fornaca tectonic window and involving the Dolomie Bituminose Formation. It is characterized by a pervasive shear plane and centimetric-sized lithones (planar fabric), parallel to the thrust plane (T). (a) Close up showing the planar fabric. The stereonet shows the geometry and kinematics of the thrust.

Figure 2.9 - The uppermost thrust surface (ss), exposed in the vicinities of Prena Mt.. DP: Dolomia Principale; Cbi: Calcari bioclastici inferiori; Ma: Maiolica.

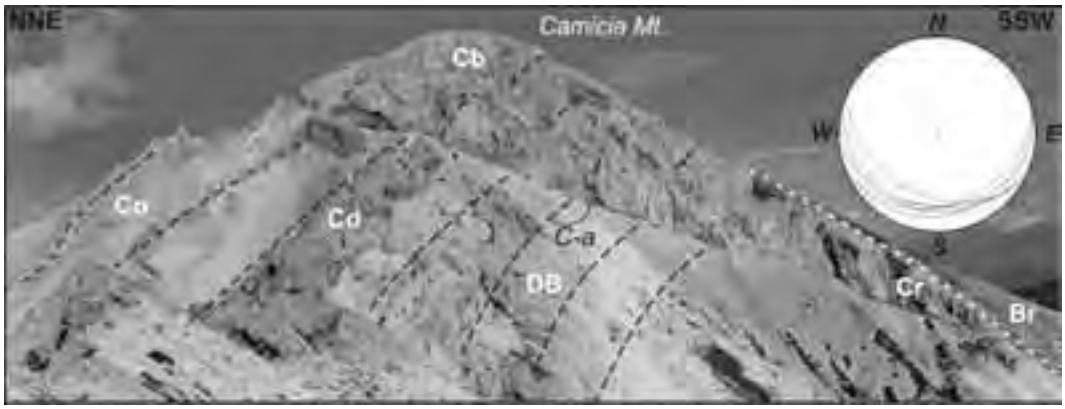

Figure 2.10 - The Camicia Mt. low-angle normal fault and relative synthetic fault planes. DB: Dolomie Bituminose (Upper Triassic); Cd: Calcari Dolomitici (Lower Lias); Co: Corniola (Middle Lias); Cbs: Calciri bioclastici superiori (Lower Cretaceous); Cb: bioclastic Calcarenites (Cretaceous-Oligocene); Br: continental breccia (Quaternary); C-a: Cut-off angle. The stereonet shows the geometry and kinematics of the fault.

Stop 3.3:

The Jurassic Montagna dei Fiori seamount.

The panoramic stop makes it possible to observe a Jurassic structural high, or seamount, that is now exposed in the core of the Montagna dei Fiori anticline. Two main Jurassic faults trend parallel (E-W) and transversal (N-S) to the valley, respectively. These structures bound the seamount, largely made of Calcare Massiccio and an overlying condensed succession. The seamount is flanked by a complete

Figure 3.1 - Structural sketch map of the Montagna dei Fiori. The inset shows the tectonic sketch of the outer zones of the Central Apennines. The key to symbols is in Figure 1.1.: 1) Normal fault; 2) Thrust; 2a) Laga Detachment; 3) Backthrust; 4) Anticline axial trace; 5) bedding; 6) Itinerary and location of the stops (3.1 – 3.5); 7) Quaternary continental deposits; 8) Messinian Laga Fm.; X) Gypsum-arenitic layer; 9) Tortonian-Messinian Marne a Pteropodi Fm.; 10) Burdigalian-Tortonian Marne con cerrogna Fm.; Y) Calcareoclastic deposits; 11) Eocene-Oligocene Scaglia Cinerea Fm.; 12) Lower Lias-Eocene neritic-pelagic succession. A-B Trace of cross-section in Figure 3.2. a) Stratigraphic section of the Umbria-Marche succession.1) Anidriti di Burano (Upper Trias); 2) Calcari e marne a Raethavicula e Calcare Massiccio (Upper Trias-Lower Lias); 3) Corniola, Rosso Ammmonitico and/or Calcari e marne del Sentino (Upper Sinemurian-Aalenian); 4) Formazione del Bugarone (Pleisbachian-Lower Titonian; in the condensed succession); 5) Calcari e marne a Posidonia, Calcari diasprini umbro-marchigiani, Maiolica, Marne a Fucoidi (Bajocian-Lower Cenomanian); 6) Scaglia bianca, rossa e cinerea (Middle Cenomanian-Oligocene); 7) Bisciaro, Schelier, Marne con cerrogna, Marne a pterapodi (Aquitanian-Messinian p.p.); 8) Turbiditic siliciclastic deposits (Burdigalian p.p.-Messinian). The heavy lines represent: Rosso Ammonitico, Marne a Fucoidi and Scaglia cinerea-Marne con cerrogna Fms, from older to younger respectively.

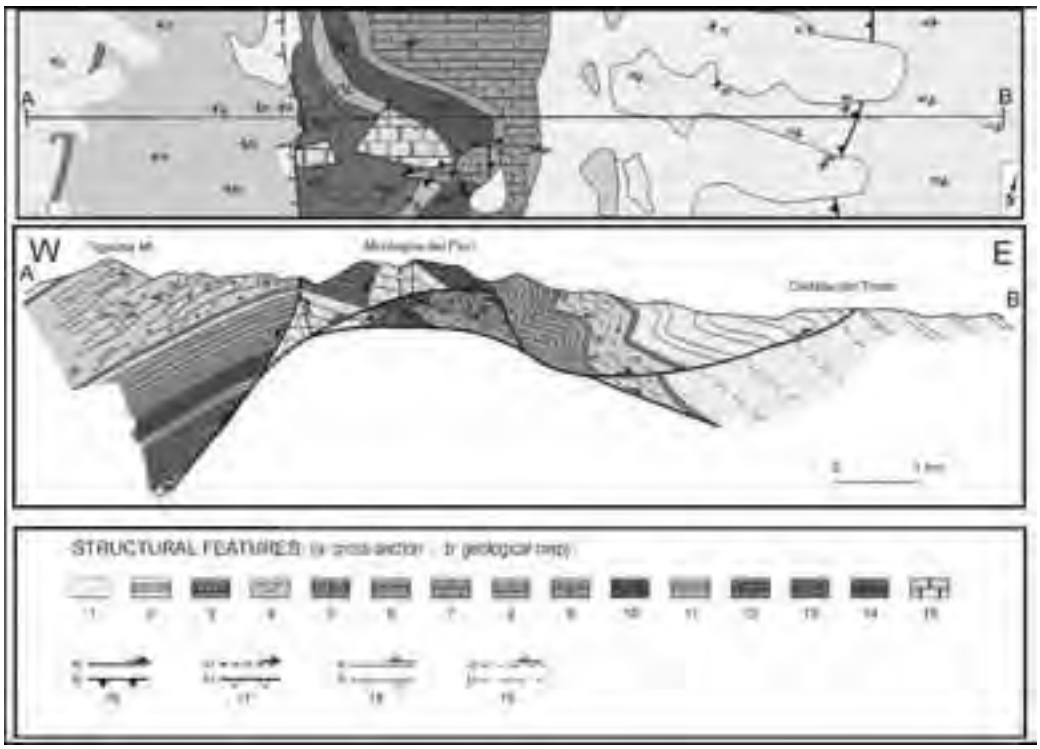

Figure 3.2 - Geological section across the Montagna dei Fiori: 1) Quaternary continental deposits; 2) Laga Fm. (Messinian); 3) Marne a Pteropodi Fm. (Lower Messinian- Tortonian p.p.); 4) Marne con cerrogna Fm. (Tortonian p.p.-Burdigalian p.p.); 5) Bisciaro Fm. (Burdigalian p.p.-Aquitanian); 6) Scaglia Cinerea Fm. (Oligocene-Eocene p.p.); 7) Scaglia Rossa Fm. (Eocene p.p.-Turonian p.p.); 8) Scaglia Bianca Fm. (Turonian p.p.-Cenomanian p.p.); 9) Marne a Fucoidi Fm. (Cenomanian p.p.-Lower Aptian p.p.); 10) Maiolica Fm. (Lower Aptian p.p.-Upper Tithonian); 11) Calcari Diasprini Fm. (Lower Tithonian-Callovian); 12) Rosso Ammonitico Fm. (Bathonian-Toarcian); 13) Corniola Fm. (Pliensbachian p.p.-Sinemurian p.p.); 14) Calcari Nodulari Fm. and Calcari Diasprini Fm. of the condensed succession (Lower Tithonian-Pliensbachian); 15) Calcare Massiccio Fm. (Sinemurian-Hettangian); 16) Thrust; 17) Backthrust; 18) Normal fault; 19) Jurassic normal fault.

Figure 3.3 - Normal fault (Fn) in the western flank of the Montagna dei Fiori. Co (Corniola); Mcc (Marne con cerrogna).

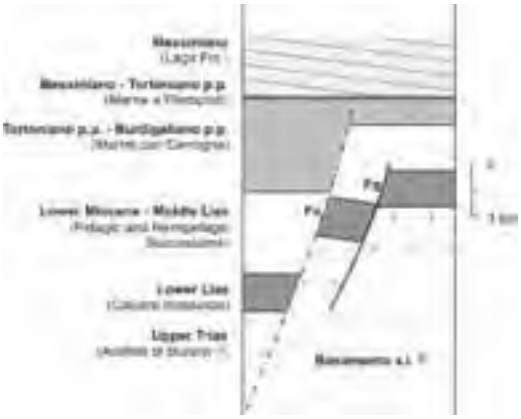

Figure 3.4 - Stratigraphic section of the Montagna dei Fiori succession; Fg: Jurassic fault; Fn: Miocene normal fault.

Figure 3.5 - Normal fault separating the Scaglia Rossa Fm. (Sr) from the Calcari Nodulari (Cn). CM: Calcare Massiccio.

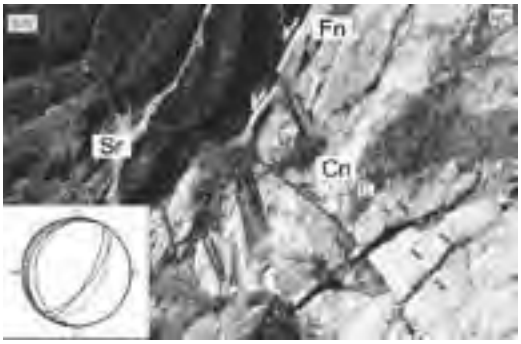

Figure 3.6 - Conjugate system of reverse faults that offsets the normal fault (Fn). Sr: Scaglia rossa; Cn: Calcari Nodulari; C: calcite extension veins. The stereonet shows the attitude of the conjugate system.

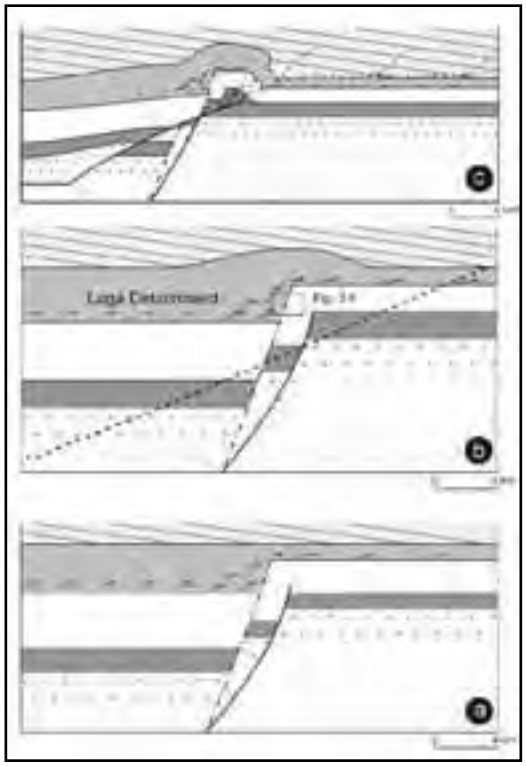

Figure 3.7 - Schematic restored sections across the Montagna dei Fiori structure, showing the main recognized evolutionary steps; see text for explanation. Stratigraphic symbols as in figure 3.4.

Figure 3.8 - Jurassic structural high in the core of the Montagna dei Fiori anticline. Fg- Jurassic faults; CM- Calcare Massiccio Fm.; S- Condensed succesion; Co- Corniola Fm., Rd- Calcari Diasprini/Rosso Ammonitico Fm.; Ma- Maiolica.

Figure 3.9 - The forelimb of the Montagna dei Fiori anticline. The thrust displaces the Jurassic fault and overrides the Calcare Massiccio (CM) and Corniola (Co on the overturned Scaglia rossa (Sr)

Figure 3.10 - The eastern, overturned limb of the Montagna dei Fiori anticline. The thrust fault (T) dips eastwards. Ma- Maiolica Fm.; Mf- Marne a Fucoidi Fm.; Sr- Scaglia Rossa Fm.

succession, consisting of the Corniola (Co), Rosso Ammonitico-Calcari Diasprini (Rd), well exposed in the fault hanging-wall blocks. The normal faults are sealed by strata of the Maiolica Fm. (Ma) and overlying Marne a Fuciodi (Mf) and Scaglia (Sr) formations. These relationships constrain the fault activity to Jurassic time (Figure 3.8).

Stop 3.4:

Western flank of the Montagna dei Fiori: The Montagna dei Fiori thrust.

From here it is possible to observe the cliffs, made of thick, moderately (30°-40°) east-dipping strata of the Calcare Massiccio Fm., and the Jurassic normal fault (Figure 3.9). These structures occur in the hanging-wall of the main thrust (T). The footwall is made of thin, intensely folded strata of the scaglia Rossa Fm. The Jurassic faults were truncated, offset and passively carried piggy-back eastwards by the thrust.

Stop 3.5:

The overturned forelimb of the Montagna dei Fiori anticline.

The eastern limb of the Montagna dei Fiori anticline, to depth, is overturned, and is cored by a blind thrust whose tip is located within the Marne a Fucoidi-Scaglia succession. However, a shear zone within the Scaglia Fm. may be viewed as the distributed continuation of the localised blind thrust. Looking east, the shear zone cuts downsection, a feature probably indicating an attempt at merging with lower, buried thrust faults (Figure 3.10).

The general structural setting of the Montagna dei Fiori is summarized in Figure 3.2, that shows all of the following:

-The Jurassic faults;

-The Miocene normal fault in the anticline backlimb;

-The Laga Detachment within the Marne con cerrogna Fm.;

- The exposed Montagna dei Fiori thrust, and its downward merging with a deeper thrust.

These features, and their overprinting relationships, make it possible to reconstruct the main evolutionary steps, and these may be summarized as follows (Figure 3.7): 1) Jurassic rifting; 2) Miocene foreland flexure, with development of the pre-thrusting normal fault (Figure 3.7a); 3) Messinian onset of contractional deformation, with development of the Laga Detachment (probably the upper flat of a innermost thrust-related fold), and buttressing against the pre-thrusting normal fault (Figure 3.7b); 4) Continued contraction, with propagation of the Montagna dei Fiori thrust, with local downsection trajectories, and development of the thrust-related Montagna dei Fiori anticline (Fig 3.7c).

During the transfer by car from the Montagna dei Fiori to the Sibillini Mts, it is possible to observe several facies associations of the Laga Formation, with particular reference to its Pre-evaporitic Member. It essentially consists of sandstones and siltstones that were deposited within the Messinia foredeep basin (Back cover figure).

The Sibillini Mountains Thrust

The Sibillini Mts Thrust is located along the Umbria-Marche mountain front (Lavecchia, 1985). It is characterized by an arcuate geometry, with changes in trend from NW-SE, in the north, to NNE-SSW, in the south, where it joins the Olevano-Antrodoco

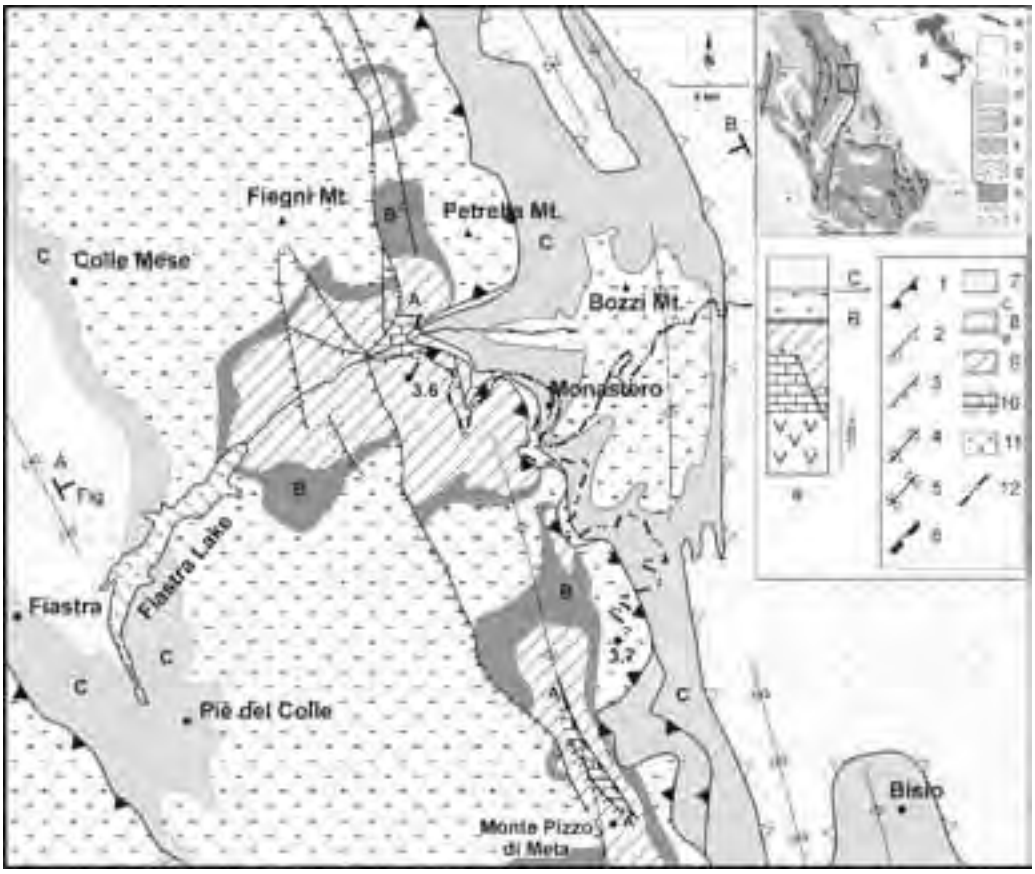

Figure 3.11 - Structural sketch of the Sibillini Mts 1) Thrust; 2) Laga Detachment; 3) Normal fault; 4) Anticline axial trace; 5) Syncline axial trace; 6) Blind up-thrust; 7) Hemipelagic and siliciclastic succession (Upper Miocene): Marne con cerrogna-Laga Fm.; 8) Pelagic and hemipelagic succession (Cretaceous-Oligocene): B- Marne a Fucoidi, C- Scaglia Cinerea; 9) Pelagic succession (Lower Lias-Cretaceous p.p.); 10) Carbonate platform (Lower Lias): Calcare Massiccio Fm.; 11) Evaporites and dolomites (Triassic): Anidriti di Burano Fm.; 12) Itinerary and location of the stops (3.6 – 3.7); A-B: trace of cross-section in Figure 3.12. a) Stratigraphic column: A- Pelagic condensed succession

Figure 3.12 - Geological section across the Sibillini Mts Thrust. A- Pelagic condensed succession. Symbols as in Figure 3.11.

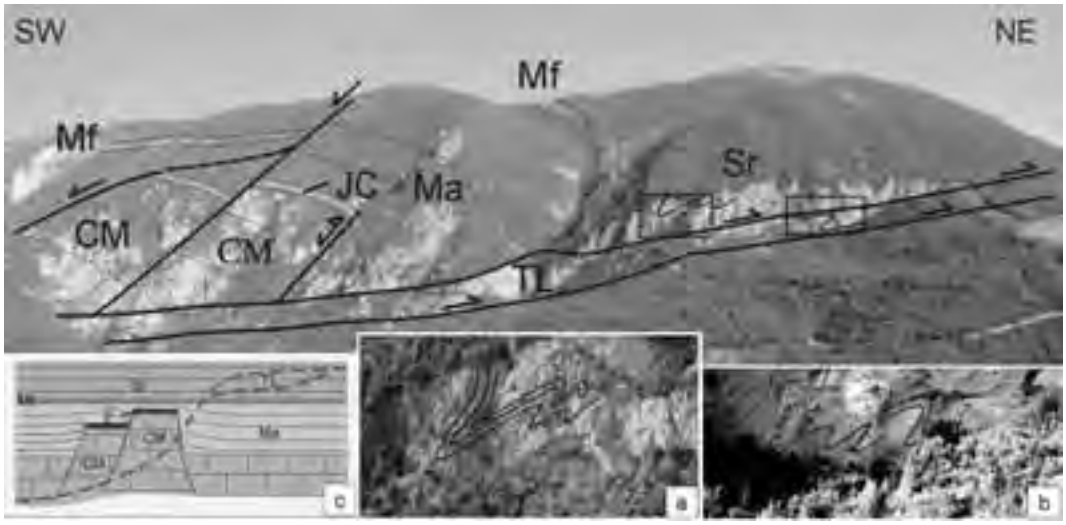

Figure 3.13 - Panoramic view of the Sibillini Mts Thrust. CM- Calcare Massiccio; Jc- Jurassic condensed succession; Ma- Maiolica Fm.; Mf- Marne a Fucoidi Fm., Sr- Scaglia Rossa Fm.; TL- Tectonic sliver of Scaglia Rossa; a, b: details of the structure; c: thrust propagation trajectory across the Jurassic faults, with flat parts located within the Scaglia Rossa, from which the tectonic sliver was detached.

thrust. The latter is localized onto the Jurassic fault that had dismembered the carbonatic platform, whose drowning, to the west, originated the Umbria-Marche pelagic Basin (Back cover figure).

The hanging-wall of the Sibillini Mts Thrust comprises the carbonatic succession (Sabine Units) affected by folding and thrusting, whereas its footwall is represented by the Laga Unit. This is involved in the Acquasanta and Montagna dei Fiori anticlines, that expose the carbonatic succession in their axial culminations. In addition to the Acquasanta and Montagna dei Fiori, another anticline occurs further west, in the foowall of the Sibillini Mts Thrust (Figs. 3.11 and 3.12).

Stop 3.6:

Panoramic view of the Sibillini Mts Thrust.

The panoramic view of the Sibillini Mts Thrust shows a tectonic sliver made up of limestones of the Scaglia Rossa Fm. The eastern limb of the hanging-wall anticline is sub-vertical to overturned, and consists of the Maiolica-Scaglia Rossa pelagic succession. The anticline core comprises the Calcare Massiccio - Jurassic condensed succession. This succession corresponded to a Jurassic high, or seamount, that was bounded westward by a normal fault, whose hanging-wall exposes a coeval, complete Corniola-Calcari Diasprini succession. This Jurassic fault also offsets the Cretaceous Marne a Fucoidi-Scaglia succession, indicating its late reactivation (Figure 3.13).

Looking east, the Jurassic seamount is juxtaposed to the younger, vertical-to-overturned pelagic succession by a blind-thrust. Similar to the Gran Sasso structure (Front page figure), these relationships suggest that the Jurassic normal fault was originally NE-dipping, and that it was later rotated and reactivated as a blind-thrust.

The occurrence of Z-shaped asymmetric minor folds within the Scaglia Rossa Fm. of the thrust hanging-wall, and of the tectonic sliver, make it possible to refer the latter to a flat of the main thrust surface (Fig 3.13a,b,c).

The thrust footwall is affected by the Monte Bozzi anticline. Its western limb parallels the main thrust surface, indicating a flat. The Miocene Marne con cerrogna - Laga *Fm* succession is intensely affected by minor folds and is detached from the underlying Scaglia Cinerea Fm. It seems likely that these structures are related to the Laga Detachment, that represents the upper flat of the Sibillini Mts Thrust localised within the Scaglia Cinerea Fm. A good exposure along the roadcut makes it possible to study in detail the thrust-induced minor folds and shearing fabrics within the Maiolica, Marne a Fucoidi, and Scaglia Rossa succession.

Stop 3.7:

Panoramic view of the Sibillini Mts' Monte Pizzo

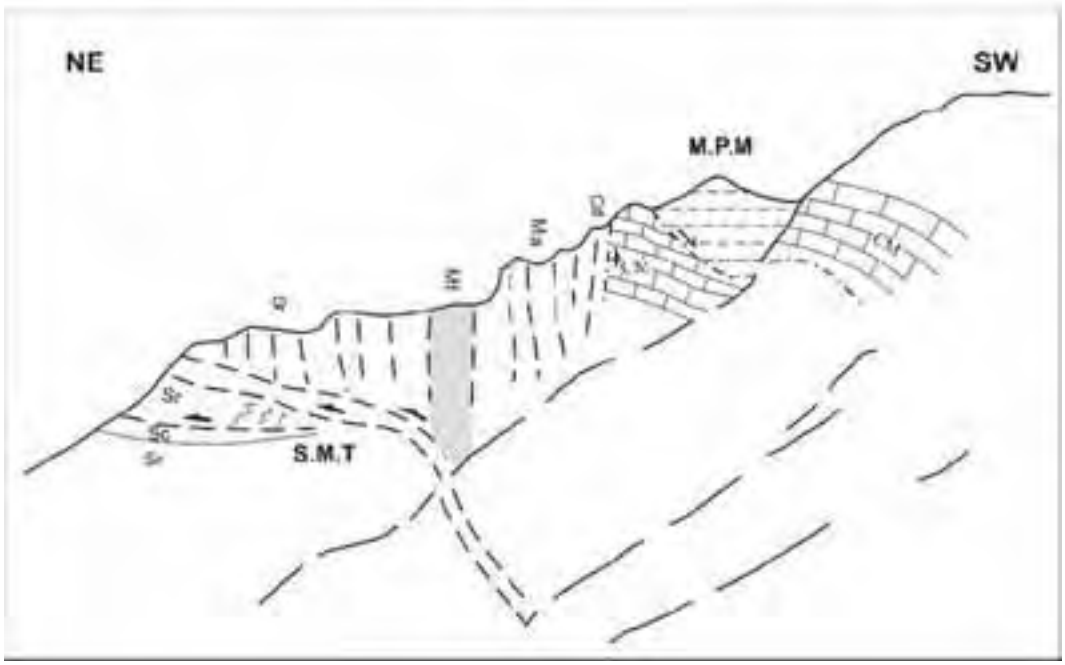

Figure 3.14 - Panoramic view of the Sibillini Mts thrust, looking towards Pizzo di Meta Mt.. CM (Calcare Massiccio); Cd (Calcari Diasprini); Ma (Maiolica); Mf (Fucoidi); Sr (Scaglia Rossa); Sc (Scaglia cinerea).

Volume n° 2 - from B16 to B33

Figure 3.15 - Close up of the figure 3.14, showing the tectonic contact between subvertical strata of the forelimb anticline (Calcari Diasprini-Maiolica: Cd-Ma), and the subhorizzontal Calcare Massiccio beds.

di Meta (M.P.M.).

The thrust structure still comprises the Scaglia Rossa tectonic sliver, in turn embricated at the front, with the development of Z-shaped asymmetric minor folds. The sub-vertical to overturned forelimb of the hanging-wall anticline consists of the Calcari Diasprini-Scaglia Rossa pelagic succession. The tectonic contact between the sub-vertical strata in the forelimb, and the horizontal Calcare Massiccio beds of the core, is accommodated by the blind-thrust. The latter presumably reactivated the Jurassic normal fault that bounded the eastern margin of the Monte Pizzo di Meta structural high (Figs 3.14 and 3.15).

To conclude, this Field Trip has illustrated the main features of the Gran Sasso, the Montagna dei Fiori and the Sibillini Mts ranges, that are among the most characteristic structures of the central Apennines. These structures all shear a short-cut thrust trajectory with respect to pre-orogenic normal faults, most of which were truncated and passively carried piggy-back in the thrust hanging-wall blocks. During the upward migration of the thrust tips, the foreland-dipping normal faults were rotated and reactivated as blind-upthrusts, an evidence inferred from the high angle between the sub-vertical strata of the overturned beds in the forelimb, and the horizontal strata in the anticline core. This high angle is also preserved in the Gran Sasso, where the hanging-wall anticline has been overturned, and the strata of the forelimb dip gently southwestward (Front page figure).

All visited folds and thrusts are arcuate in map view, a geometry that reflects the architecture of the passive margin of Adria, and inherited from Mesozoic rifting and normal fault development. Pre-thrusting normal faults were important in controlling the location, distribution and orientation of the nucleating thrust ramps and related fault-propagation folds during the orogenic events that led to the development of the Apennine belt (Back cover figure).

References

Adamoli, L., Bertini, T., Chiocchini, M., Deiana, G., Mancinelli, A., Pieruccini, U. and Romano, A. (1978). Ricerche geologiche sul Mesozoico del Gran Sasso d'Italia (Abruzzo). II. Evoluzione tettonico-sedimentaria dal Trias superiore-Cretacico inferiore dell'area compresa tra il Corno Grande e S.Stefano Sessanio (F. 140 Teramo). *Studi Geologici Camerti*,

4, 7-17.

Adamoli, L., Bigozzi, A., Ciarapica, G., Cirilli, S., Passeri, L., Romano, A., Duranti, F. and Venturi F. (1990).- Upper Triassic Bituminous facies and Hettangian pelagic facies in the Gran Sasso range. *Boll. Soc. Geol. It*.,109, 219-230.

Adamoli, L., Calamita, F. and Pelorosso, M. (2003). Guide Geologiche Regionali, Abruzzo n° 10. Società Geologica Italiana. BE-MA editrice, 113-120.

Ben-Avraham, Z., Boccaletti, M., Cello, G., Grasso, M., Lentini, F., Torelli, L., Tortorici, L. (1990). Principali domini strutturali originatesi dalla collisione neogenico-quaternaria nel Mediterraneo centrale. *Mem. Soc. Geol. It*. 45, 453-462.

Bigozzi, A., Ciarapica, G., Cirilli, S. and Passeri, L. (1991) – Eteropie di facies nel Trias superiore e nel Lias inferiore del Gran Sasso. *Studi Geologici Camerti, vol. spec.(1991/2), CROP 11*, 115-118.

Boccaletti, M., Ciaranfi, N., Cosentino D., Deiana, G., Gelati, R., Lentini, F., Massari, F., Moratti G., Pescatore T., Ricci Lucchi F. and Tortorici L. (1990). Palinspatic restoration and paleogeographic reconstruction of the peri-Tyrrhenian area during Neogene. *Palaeog. Palaeocl. Palaeoec.*, 77, 41-50.

Boncio, P., Brozzetti, F. and Lavecchia, G. (2000). Architecture and seismotectonics of a regional low-angle normal fault in Central Italy. *Tectonics*, 19, 1038-1055.

Calamita, F., Adamoli, L., Pelorosso, M. and Scisciani, V. (2003c). Guide Geologiche Regionali, Abruzzo n° 10. Società Geologica Italiana. BE-MA editrice, 81-101.

Calamita, F., Coltorti, M., Piccinini, D., Pierantoni, P.P., Pizzi, A., Ripete, M., Scisciani, V. and Turco, E. (2000). Quaternary faults and seismicity in the Umbro-Marchean Apennines (Central Italy): evidence from the 1997 Colfiorito earthquake. *Jour. of Geodyn*., 29, 245-264.

Calamita, F., Paltrinieri, W., Pelorosso, M., Scisciani, V., Tavarnelli, E. (2003a). Inherited mesozoic architecture of the Adria continental Palaeomargin in the Neogene central Apennines orogenic system, Italy. *Boll. Soc. Geol. It.*, 122, 307-318.

Calamita, F., Pelorosso, M. and Satolli, S. (2003b). Il ruolo dell'architettura del paleomargine mesozoico di Adria nel sistema orogenico del Gran Sasso d'Italia (Appennino centrale). *Boll. Soc. Geol. It.,* 122, 337-349.

Calamita, F., Pizzi, A., Ridolfi, M., Rusciadelli, G. and Scisciani, V. (1998). Il buttressing delle faglie sinsedimentarie pre-thrusting sulla strutturazione neogenica della catena: l'esempio della Montagna dei Fiori (Appennino Centrale esterno). *Boll. Soc. Geol. It.*, 117, 725-745.

Calamita, F., Scisciani, V., Adamoli, L., Ben M'Barek, M. Pelerosso, M. (2002). Il sistema a thrust del Gran Sasso D'Italia (Appennino Centrale). *Studi Geologici Camerti, nuova serie*, 1, 1-32.

Carmignani, L., and Kligfield, R. (1990). Crustal extension in the northern Apennines: the Transiction from comprenssion to extension in the Alpi Apuane core complex. *Tectonics,* 9, 1275-1303.

Casero, P., Roure, F., Endignoux, L., Moretti, I., Muller, C., Sage, L., and Vially, R. (1988). Neogene geodynamic evolution of the Southern Apennines. *Mem. Soc. Geol. It.,* 41, 109-120.

Finetti, I. R., Lentini, F., Carbone, S., Catalano, S., Del Ben, A. (1996). Il sistema Appennino meridionale-Arco Calabro-Sicilia nel Mediterraneo centrale: studio geologico-geofisico. *Boll. Soc. Geol. It*. 115, 529-559.

Finetti, I. R. and Del Ben, A. (2000). Ionian opening, crustal stratigraphy and tectono-dynamics of the Pelagian sea Region from new CROP seismic data. *Proccedings of the International Conference of the Tripoli; Libya*, 2000.

Gattacceca, J. and Speranza, F. (2002). Paleomagnetism of Jurassic to Miocene sediments from the Apenninic carbonate platform (southern Apennines, Italy): evidence for a 60° counterclockwise Miocene rotation. *Earth and Planetary Science Letters*, 201, 19-34.

Ghisetti, F. and Mezzani, L. (1990). Stili strutturali nei sistemi di sovrascorrimento della catena del Gran Sasso (Appennino Centrale). *Studi Geologici Camerti, vol. spec.* (1990), 37-50.

Ghisetti, F. and Vezzani, L. (1997). Interfering paths of deformation and development of arcs in the fold-and-thrust belt of the Central Apennines (Italy). *Tectonics*, 16, 523-536.

Guide Geologiche Regionali Vols 7 and 10. Società Geologica Italiana. BE-MA editrice.

Koopman, A. (1983). Detachment tectonics in the Central Apennines, Italy. *Geol.Ultraiectina*, 30, 155 pp.

Lavecchia, G. (1985). Il sovrascorrimento dei Monti Sibillini: analisi cinematica e strutturale. *Boll. Soc. Geol. It.*, 104, 161-194.

Lentini, F., Carbone, S., Di Stefano, A., Guarnieri. (2002). Stratigraphical and structural constraints in the Lucanian Apennines (Southern Italy): tools for reconstructing the geological evolution. *Journal of*

Volume n° 2 - from B16 to B33

Geodynamics, 34, 141-158.
Locardi, E. (1982). Individuazione di strutture sismogenetiche dall'esame dell'evoluzione vulcano-tettonica dell'Appennino e del Tirreno. *Mem. Soc. Geol. It*., 24, 569- 596.
Menardi Noguera, A. and Rea, G. (2000). Deep structure of the Campanian-Lucanian arc (Southern Apennine, Italy). *Tectonophysics*, 324, 239-265.
Mostardini, F., and Merlini, S. (1986). Appennino centro-meridionale: Sezioni geologiche e proposta di modello strutturale. *Mem. Soc. Geol. It*., 35, 177-202.
Parotto, M., Praturlon, A. (1975). Geological summary of the Central Apennines. *Quaderni de "La Ricerca Scientifica"*, 90, 257-306.
Patacca, E., Sartori, R. Scandone, P. (1990). Tyrrhenian basin and Apenninic arcs: kinematic relations since Late Tortonian times. *Mem. Soc. Geol. It.*, 45, 425-451.
Patacca, E., and Scandone, P. (1989). Post-Tortonian mountain building in the Apennines. The role of the passive sinking of a relic lithospheric slab. In: Boriano A., Bonafede M., Piccardo G.B. & Vai G. B. (Eds) – *The lithosfere in Italy. Atti Conv. Lincei*, 80, 157-176.
Patacca, E., Scandone, P., Tozzi, M. (2000). Il Profilo CROP-04. *Protecta, Dossier: Italia Profonda*, n. 10-12, Oct.-Dic. 2000, 49-52.
Vezzani, L., Casnedi, R. and Ghisetti, F. (1993). *Carta geologica dell'Abruzzo nord-orientale*. Selca, Firenze.

Back Cover:
Structural sketch of the Central Apennines. Itinerary and locations of figures related to 3 days field trip are indicated.

FIELD TRIP MAP

32nd INTERNATIONAL GEOLOGICAL CONGRESS

Edited by APAT